Dosis-abhängiger Einfluss von Lipopolysaccharid und oxidierten Phosphatidylcholinen auf endotheliale Funktionen

Inaugural-Dissertation

Zur Erlangung des Doktorgrades

der Mathematisch-Naturwissenschaftlichen Fakultät

der Heinrich-Heine-Universität Düsseldorf

vorgelegt von

Dennis Merk

aus Düsseldorf

Düsseldorf, Mai 2025

Aus dem Zentralinstitut für Klinische Chemie und Laboratoriumsdiagnostik der Heinrich-Heine-Universität Düsseldorf

Gedruckt mit der Genehmigung der

Mathematisch-Naturwissenschaftlichen Fakultät der

Heinrich-Heine-Universität Düsseldorf

Berichterstatter:

1. Univ.-Prof. Dr. rer nat Judith Haendeler

2. Prof. Dr. Dieter Willbold

Tag der mündlichen Prüfung: 21.05.2025

Erklärung

Ich versichere an Eides statt, dass die Dissertation von mir selbstständig und ohne unzulässige fremde Hilfe unter Beachtung der „Grundsätze zur Sicherung guter wissenschaftlicher Praxis an der Heinrich-Heine-Universität Düsseldorf“ erstellt worden ist.

(Dennis Merk)

Düsseldorf, Mai 2025

Inhaltsverzeichnis

1. Abkürzungsverzeichnis

Kürzel	Bezeichnung
NO	Stickstoffmonoxid (*engl. nitric oxide*)
eNOS	Endotheliale NO-Synthase
ROS	Reaktive Sauerstoffspezies (*engl. reactive oxygen species*)
NOS	NO-Synthase
nNOS	Neuronale NO-Synthase
iNOS	Induzierbare NO-Synthase
eNOS	Endotheliale NO-Synthase
LPS	Lipopolysaccharid
PRR	Mustererkennungsrezeptor (*engl. pattern recognition receptor*)
ICAM-1	Interzelluläres Adhäsionsmolekül-1 (*engl. intercellular adhesion molecule-1*)
VCAM-1	Vaskuläres Zelladhäsionsmolekül-1 (*engl. vascular cell adhesion molecule-1*)
IL-6	Interleukin-6
TNF-α	Tumornekrosefaktor-α
NOX	NADPH-Oxidase
NAFLD	Nichtalkoholische Fettleber (*engl. Non-alcoholic fatty liver disease*)
Trx-1	Thioredoxin-1
TLR	Toll-like Rezeptor
LBP	LPS-bindendes Protein
MD-2	Myeloisches Differenzierungsprotein 2
TIRAP	TIR-Domäne-beinhaltendes Adapter Protein (*engl. TIR domain-containing adapter protein*)
IRAK	IL-1 Rezeptor assoziierte Kinase
TRAF6	TNF-Rezeptor assoziierter Faktor 6
AP-1	Aktivator Protein-1
CREB	cAMP Antwort-Element bindendes Protein (*engl. cAMP response element binding protein*)
TRAM	TRIF-verwandtes Adaptermolekül (*engl. TRIF-related adapter molecule*)
TBK-1	TANK bindende Kinase 1
IKKε	IκB Kinase ε
IRF	Interferon regulierender Faktor
SIPS	Stress-induzierte frühzeitige Seneszenz (*engl. stress-induced premature senescence*)
SASP	Seneszenz-assoziierter sekretorischer Phänotyp
NASH	Nichtalkoholische Steatohepatitis
oxPC	Oxidierte Phosphatidylcholine
IgM	Immunglobulin M

scFv-E06	Variables Einzelstrangfragment von E06 (*engl. single-chain variable fragment of E06*)
qRT-PCR	Quantitative Polymerase-Kettenreaktion mit reverser Transkription (*engl. quantitative reverse transcription polymerase chain reaction*)
HRP	Meerrettich-Peroxidase (*engl. horseradish peroxidase*)
FPC	Fructose-, Palmitat- und Cholesterin-reiche Ernährung
APEX1	Apurinische/Apyrimidinische Endodeoxyribonuklease 1
APEX1 (1-20)	APEX1 Konstrukt bestehend aus den n-terminalen Aminosäuren 1-20
Detox	Detoxifiziertes Lipopolysachharid
DGE	Differentielle Genexpressionsanalyse
GSEA	Anreicherungsanalyse von Gensätzen (*engl. gene set enrichment analysis*)
IL1RL1	Interleukin 1 Rezeptor-ähnliches Protein 1 (*engl. interleukine 1 receptor like 1*)
PXDN	Peroxidasin
SELENOT	Selenoprotein T
ER	Endoplasmatisches Retikulum
sec	Selenocystein
$tRNA^{sec}$	Selenocystein-spezifische tRNA
SECIS	Selenocystein-Insertionssequenz (*engl. selenocystein insertion sequence*)
UTR	Untranslatierte Region
FLAG-SELENOT	Selenoprotein T Konstrukt mit n-Terminalem FLAG
HFD	Fettreiche Ernährung (*engl. high fat diet*)
Mito p27	Mitochondriales p27
EV	Leervektor (*engl. empty vector*)

2. Einleitung

2.1 Kardiovaskuläre Erkrankungen

Herzkreislauferkrankungen sind weltweit die Hauptursache von Morbidität und Mortalität und waren 2021 für 19,4 Millionen Tode verantwortlich (IHME, Global Burden of Disease (2024) – with minor processing by Our World in Data). Der Großteil der Herzkreislauferkrankungen resultiert aus Komplikationen im Zusammenhang mit Gefäßerkrankungen (Madamanchi et al. 2005). Zu diesen kardiovaskulären Erkrankungen gehören koronare Herzkrankheit, Schlaganfall, Bluthochdruck, Herzinsuffizienz, Atherosklerose und angeborene Herzerkrankungen (Widmer and Lerman 2014). Die wichtigsten Risikofaktoren für Herzkreislauferkrankungen sind Übergewicht, chronische Entzündung der Gefäße, Diabetes, Rauchen, ein sitzender und ungesunder Lebensstil, wie auch genetische Prädisposition (Dubois-Deruy et al. 2020,Higashi 2022). Weiterhin ist das Altern als unabhängiger Risikofaktor für kardiovaskuläre Erkrankungen hervorzuheben, da die Prävalenz dieser Erkrankungen mit dem Fortschreiten des Alters korreliert (Rodgers et al. 2019,Steenman and Lande 2017). Trotz verbesserter Diagnose, Behandlung und Prävention hat die Relevanz kardiovaskulärer Erkrankungen im Laufe der Jahre nicht abgenommen.

Interessanterweise spielt bei der Pathogenese von fast allen kardiovaskulären Erkrankungen die Fehlfunktion des Endothels, also der innersten Schicht aller Blutgefäße, eine ausschlaggebende Rolle. Diese sogenannte endotheliale Dysfunktion ist häufig auf erhöhten oxidativen Stress und verminderte Stickstoffmonoxid (NO)-Bioverfügbarkeit zurückzuführen (Widmer and Lerman 2014,Poredos 2002).

Bevor aber die endotheliale Dysfunktion, als Ursache der Entstehung und Progression kardiovaskulärer Erkrankungen, in den nachfolgenden Abschnitten erläutert wird, soll zunächst der Aufbau und die Funktion der Blutgefäße, insbesondere des Endothels, näher betrachtet werden.

2.2 Endothel

Das Gefäßsystem, bestehend aus Blut- und Lymphgefäßen, ist für den Transport von Flüssigkeit, Sauerstoff und Nährstoffen von essenzieller Bedeutung für den menschlichen Organismus. Die Blutgefäße sind in Körperkreislauf und Lungenkreislauf unterteilt. Im Körperkreislauf transportieren sie sauerstoffreiches Blut vom Herzen in die Peripherie und sauerstoffarmes Blut zurück zum Herzen. Im Lungenkreislauf wird das aus der Peripherie erhaltene sauerstoffarme Blut vom Herzen zur Lunge transportiert. Dort findet der Sauerstoffaustausch statt, wodurch sauerstoffreiches Blut zurück zum Herzen und anschließend der Peripherie transportiert wird. Der Aufbau der Gefäßwände variiert je nach Region und Funktion, kann generell aber in drei Schichten aufgeteilt werden. Die Tunica adventitia umgibt als äußerste Schicht die Blutgefäße und ist für deren Verankerung mit dem Gewebe zuständig. Die Tunica media, bestehend aus glatter Muskulatur und elastischem Bindegewebe, reguliert den Tonus der Ge-

fäße durch Vasokonstriktion und -dilatation. Die Tunica intima ist die innerste Schicht, bestehend aus einer einzelnen Schicht aus vaskulären Endothelzellen, die eine Barriere zwischen dem Blut und dem umliegenden Gewebe bilden. Diese innerste Endothelschicht besitzt, konträr zu ursprünglichen Überzeugungen, allerdings nicht nur eine Barrierefunktion, sondern ist zudem notwendig für die Regulierung des Stofftransports und der Aufrechterhaltung der vaskulären Homöostase (Kruger-Genge et al. 2019).

Durch die Sekretion von Faktoren kann das Endothel den vaskulären Tonus beeinflussen, sowie die Adhäsion von Leukozyten als auch die Entstehung von Entzündungen inhibieren. Die zugrundeliegende Integrität des gesunden Endothels verhindert außerdem die Aggregation von Thrombozyten und sorgt für einen funktionierenden Blutstrom (De Pablo-Moreno et al. 2022). Diese sekretorische Kapazität spiegelt die Befähigung des Endothels wider, sich selbst vor Schäden zu schützen, was besonders im Hinblick auf den direkten Kontakt des Endothels mit dem Blut relevant ist.

Berücksichtigt man die vielfältigen Funktionen des Endothels ist es nicht verwunderlich, dass eine Beeinträchtigung des Endothels bei der Entstehung und Progression von fast allen kardiovaskulären Erkrankungen beteiligt ist. Unter diesem Aspekt wird im nächsten Kapitel die endotheliale Dysfunktion näher betrachtet.

2.3 Endotheliale Dysfunktion

Endotheliale Dysfunktion beschreibt eine pathologische Fehlfunktion des Endothels welche durch ein Ungleichgewicht sowohl zwischen vasodilatatorischen und vasokonstriktorischen Faktoren als auch pro- und anti-koagulatorischen Substanzen auftritt. Weiterhin ist diese durch die Dysbalance zwischen pro- und anti-inflammatorischen Mediatoren und der verminderten Synthese und Bioverfügbarkeit von NO charakterisiert (Poredos 2002). Diese Eigenschaften beeinflussen die Homöostase negativ und führen zu einem Verlust der Endothel-Integrität.

Wichtige Faktoren bei der Entstehung und Progression der endothelialen Dysfunktion sind Verlust der Menge und/oder Aktivität der endothelialen NO-Synthase (eNOS), Aktivierung der Endothelzellen und die Beeinträchtigung der Redox-Homöostase, also dem Gleichgewicht zwischen Bildung und Abbau von reaktiven Sauerstoffspezies (*reactive oxygen species*, ROS) (Pober et al. 2009,Endemann and Schiffrin 2004,**Merk** et al. 2024).

NO wird von sogenannten NO-Synthasen (NOS) produziert, welche in die 3 Isoformen der neuronalen NOS (nNOS), der induzierbaren NOS (iNOS) und der eNOS unterteilt werden können. Diese NOS verwenden die Aminosäure L-Arginin und molekularen Sauerstoff als Substrate, woraus mithilfe von Co-Faktoren NO gebildet wird (Forstermann and Sessa 2012). Als konstitutiv exprimierte NOS reguliert die vorwiegend in Neuronen exprimierte nNOS den Blutdruck, die Relaxation von glatten Muskelzellen und die Vasodilatation. iNOS wird im Gegensatz dazu als Antwort auf Cytokine, Lipopolysaccharide (LPS) oder andere Wirkstoffe exprimiert,

wodurch große Mengen an NO generiert und sekretiert werden. Die auf Endothelzellen konstitutiv exprimierte eNOS kontrolliert, wie auch nNOS, den Blutdruck und die Vasodilatation, hat zudem aber auch gefäßschützende- und anti-atherosklerotische Funktionen (Forstermann and Sessa 2012,Alderton et al. 2001).

Im Endothel reguliert NO den vaskulären Tonus, indem es von Endothelzellen sekretiert wird und in die angrenzenden glatten Muskelzellen diffundiert. Das sekretierte NO bindet in diesen glatten Muskelzellen an die lösliche Guanylylzyklase wodurch zyklisches Guanosinmonophosphat vermehrt gebildet wird, welches die Anspannung der glatten Muskelzellen vermindert und damit zu Vasodilatation führt (Sandoo et al. 2010,Jones et al. 1999). Die zahlreichen Funktionen von NO, wie das Induzieren der Relaxation von glatten Muskelzellen, der verbesserten Adhäsion von Immunzellen und dem Schutz von endothelialen Vorgängerzellen, erklären dessen Notwendigkeit für die Homöostase der endothelialen Integrität und Permeabilität (Tousoulis et al. 2012,Aicher et al. 2003,Hossain et al. 2012).

Eine verminderte NO-Produktion, einhergehend mit dessen beeinträchtigter Bioverfügbarkeit, aufgrund von verminderter eNOS-Expression und Aktivität, ist ein häufiger Mediator der endothelialen Dysfunktion.

Die Aktivierung von Endothelzellen ist durch funktionelle und morphologische Veränderungen charakterisiert und kann durch verschiedene Stimuli wie bakterielle Endotoxine, inflammatorische Zytokine, oder sogenannte Mustererkennungsrezeptoren (*pattern recognition receptors*, PRRs) induziert werden. Sie geht mit der Expression von Zelloberflächen-Proteinen wie dem interzellulären Adhäsionsmolekül-1 (*intercellular adhesion molecule-1*, ICAM-1) oder dem vaskulären Zelladhäsionsmolekül-1 (*vascular cell adhesion molecule-1*, VCAM-1) einher. Diese Adhäsionsmoleküle erlauben die Rekrutierung und das Anbinden von Leukozyten an das Endothel, was die Diapedese, also die Transmigration der Leukozyten durch die Endothelzellschicht, ermöglicht (Pober *et al.* 2009). Die Aktivierung der Endothelzellen wird durch proinflammatorische Zytokine wie Interleukin-6 (IL-6) oder Tumornekrosefaktor α (TNF-α) induziert (Liao 2013). IL-6 und TNF-α sind multifunktionelle pro-inflammatorische Zytokine, welche bei der Antwort des Immunsystems auf Infektionen und Gewebeschäden produziert werden und an der Rekrutierung von Leukozyten beteiligt sind (Bruunsgaard et al. 2000,Tanaka et al. 2018). Eine andauernde Aktivierung der Endothelzellen und die daraus resultierende Adhäsion von Zellen zieht eine vermehrte Produktion und Sekretion von inflammatorischen Zytokinen, Chemokinen und ROS nach. Dies kann zu chronischer Inflammation führen, was als wichtiger Risikofaktor für die endotheliale Dysfunktion und den darauffolgenden kardiovaskuläre Erkrankungen, besonders in Assoziation mit der Alterung, gilt (Sanada et al. 2018). Weiterhin kann die Aktivierung zur Apoptose der Endothelzellen führen, wodurch die Integrität und Barrierefunktion des Endothels beeinträchtigt ist und die endotheliale Dysfunktion verstärkt wird (Theofilis et al. 2021).

ROS sind grundsätzlich für eine Vielzahl an biologischen Prozessen als Signalmoleküle notwendig. Sie werden sowohl in den Mitochondrien als Beiprodukte der Atmungskette als auch

durch die NADPH-Oxidasen (NOX), einer Enzym-Familie, welche auf die Produktion von ROS spezialisiert ist, gebildet (Sies and Jones 2020). ROS können jedoch auch Schäden sowohl an DNA, Proteinen oder Lipiden hervorrufen, was beispielsweise zur Bildung von oxidierten Lipiden führt, welche bei der Entstehung von Krankheiten, wie der nichtalkoholischen Fettleber (*non-alcoholic fatty liver disease*, NAFLD) eine Rolle spielen. Wie bereits erwähnt wird das ausgewogene Gleichgewicht zwischen Bildung und Abbau von ROS Redox-Homöostase genannt. Ein Ungleichgewicht führt zu zellulärem oxidativem Stress, welcher mit der Entstehung von endothelialer Dysfunktion assoziiert wird. Dieses Ungleichgewicht wird durch die Hochregulation von oxidativen Mechanismen, wie der vermehrten Aktivität der Atmungskette in den Mitochondrien oder einer verstärkten Expression der bereits erwähnten NOX-Enzymfamilie und der Herunterregulation ihrer Gegenspieler, den anti-oxidativen Mechanismen, wie beispielsweise dem Thioredoxin-1 (Trx-1)-System, welches in einem späteren Abschnitt erläutert wird, verursacht (Schulz et al. 2004).

Aus diesem Grund werden die Entstehung und die Auswirkungen von oxidativem Stress auf das Endothel im nächsten Abschnitt besonders aufgezeigt.

2.4 Oxidativer Stress

Zellulärer oxidativer Stress entsteht, sobald die Produktion von ROS die Kapazität der protektiven anti-oxidativen Systeme übersteigt (Man et al. 2020). Dieses Ungleichgewicht, hervorgerufen durch den Überschuss an ROS kann, wie bereits erwähnt, zu Schäden an zellulärer DNA, Lipiden und Proteinen führen. Die daraus resultierenden Fehlfunktionen können zu schwerwiegenden Störungen und Schädigungen der Zellen bis hin zu deren Zelltod führen (Fatehi-Hassanabad et al. 2010).

Generell sind ROS reaktive Zwischenprodukte von molekularem Sauerstoff. Zu den wichtigsten ROS gehören im Endothel Wasserstoffperoxid und Superoxid-Anion. Unter physiologischen Bedingungen fungieren ROS als sekundäre Botenstoffe in verschiedenen intrazellulären Signalwegen (Sies et al. 2017). Die wichtigsten ROS-produzierenden Systeme sind auch im Endothel die NOX und die Atmungskette der Mitochondrien, welche für die ATP-Produktion unabdingbar ist (Fatehi-Hassanabad *et al.* 2010,Li et al. 2014). Bei der mitochondrialen ATP-Produktion, welche in den Enzymkomplexen I bis V stattfindet, die an die Elektronentransportkette gekoppelt sind, treten konstant Elektronen aus wodurch ROS, vor allem durch die Komplexe I und III, gebildet werden (Miwa et al. 2003). Da ein Großteil der ROS in Mitochondrien produziert wird, wirken sich deren destruktiven Eigenschaften besonders auf diese als primäres Ziel aus (Balaban et al. 2005). Der daraus resultierende mitochondriale Schaden kann zu verminderter Funktion und Anzahl der Mitochondrien führen, was zu Nekrose und Apoptose der Zellen führt. Dieser Vorgang spielt besonders bei Erkrankungen, die mit fortschreitendem Alter assoziiert werden, eine wichtige Rolle (Raha and Robinson 2000).

Um überschüssige ROS zu eliminieren sind im Endothel mehrere anti-oxidative Enzyme und Systeme involviert, wie die Katalase, die Superoxid-Dismutasen, die Glutathion-Peroxidasen

oder das Trx-1-System (Chance et al. 1979). Im Endothel ist eines der wichtigsten anti-oxidativen Systeme das Trx-1-System. Trx-1 ist eine ubiquitär exprimierte Oxidoreduktase, welche oxidierte Proteine reduziert. Die beiden Cysteine in seinem aktiven Zentrum werden bei der Reduktion des Zielproteins zu dem Disulfid Cystin oxidiert, und können durch die Thioredoxin-Reduktase 1 wieder reduziert werden (Holmgren 2000).

Zu den Risikofaktoren, welche zur Entstehung von ROS beitragen gehören Diabetes mellitus, Rauchen, Alterung aber auch Entzündungen (Panth et al. 2016). Besonderes Augenmerk sollte hierbei auf die Entstehung von ROS und Entzündungen durch das bakterielle Endotoxin LPS gelegt werden, da dieses bei der Entstehung von endothelialer Dysfunktion eine große Rolle spielt. Die Wirkung von LPS auf das Endothel variiert je nach auftretender Konzentration. So führen niedrige LPS Konzentrationen zu chronischen Pathologien wie der endothelialen Seneszenz, welche in Kapitel 2.6 Chronische Entzündung, Alterung und Endothelzellseneszenz näher behandelt wird, während hohe LPS Konzentrationen akute Erkrankungen wie Sepsis oder septischer Schock hervorrufen (**Merk** *et al.* 2024,**Merk** et al. 2023).

Im darauffolgenden Kapitel werden in diesem Bezug zunächst die akuten Folgen von hohen Konzentrationen an LPS aufgezeigt.

2.5 Sepsis

Sepsis ist definiert als lebensgefährliche Organfunktionsstörung, die durch eine fehlregulierte Antwort des Organismus auf Infektionen verursacht wird (Singer et al. 2016). Sepsis und septischer Schock sind bei schwerkranken Patienten die Hauptursachen für Mortalität und für ca. 20% der Gesamttode auf der Welt verantwortlich. Es wird angenommen, dass Sepsis 2017 über 49 Millionen Individuen betroffen hat und für 11 Millionen Tode weltweit verantwortlich war (Sepsis (who.int) (Stand 21.September, 2024).

Trotz über 100 klinischer Studien gibt es, neben der Verwendung von Antibiotika und Vasopressoren, noch immer keine umfassende Therapiemöglichkeit, die von der FDA akzeptiert wurde, um den Ausgang der Sepsis drastisch zu verbessern (Guarino et al. 2023,Marshall 2014). Dies hängt zum größten Teil mit den komplexen, multifaktoriellen Antworten des Organismus auf die Erkrankung zusammen.

Sepsis beginnt mit einer Infektion, durch welche gramnegative Bakterien, wie *Escherichia coli* und *Pseudomonas aeruginosa,* in die Blutzirkulation gelangen (Mayr et al. 2014). Das als Bestandteil der äußeren Membran der Bakterien vorkommende LPS ist ein Endotoxin und generiert einen, für das menschliche Immunsystem, pro-inflammatorischen Stimulus, welcher sich sowohl lokal als auch systemisch auswirken kann. Es ist dabei bekannt, dass höhere LPS-Konzentrationen (1-2 mg) im Blutstrom tödlich sind (Boutagy et al. 2016). LPS besteht aus einem proximalen, sich wiederholenden Oligosaccharidkern, einem distalen O-Antigen, einem Glycan Polymer und einem hydrophoben Lipid-A Anker, bestehend aus einem Glucosamindisaccharid mit mehreren Fettsäuren (Page et al. 2022). Die Immunsystem-stimulierende Aktivität kommt hauptsächlich von der Lipid-A Einheit, welche in Menschen und Mäusen von Toll-like-

Rezeptoren (TLR) gebunden wird und die angeborene Immunantwort aktiviert (Molinaro et al. 2015).

TLR sind eine Familie aus transmembranen Glykoproteinen, welche auf Makrophagen, T-Zellen, B-Zellen aber auch Endothelzellen vorkommen (Duan et al. 2022,Vaure and Liu 2014). Sie binden verschiedene Moleküle wie LPS, Lipopeptide oder doppelsträngige DNA, was zu einer Umstrukturierung des Rezeptorkomplexes führt und die angeborene Immunantwort und Entzündung induziert (Molinaro *et al.* 2015). Der wichtigste TLR in Bezug auf LPS ist TLR4 (Poltorak et al. 1998). Die Lipid-A Einheit des LPS wird von dem sogenannten LPS-bindenden Protein (LBP) gebunden und zu CD14-Molekülen transportiert, welche den Weitertransport zum myeloischen Differenzierungsprotein 2 (MD-2) katalysieren (Ryu et al. 2017). Die homodimere Bildung eines Komplexes aus TLR4/MD2/LPS aktiviert sowohl den MyD88-abhängigen Signalweg, welcher auf der Plasmamembran induziert wird als auch den TRIF-abhängigen Signalweg, welcher in frühen Endosomen nach der Endozytose des Rezeptorkomplexes beginnt (Abbildung 1: LPS induzierter TLR4-Signalweg, (**Merk** *et al.* 2024)) (Zhang et al. 2022).

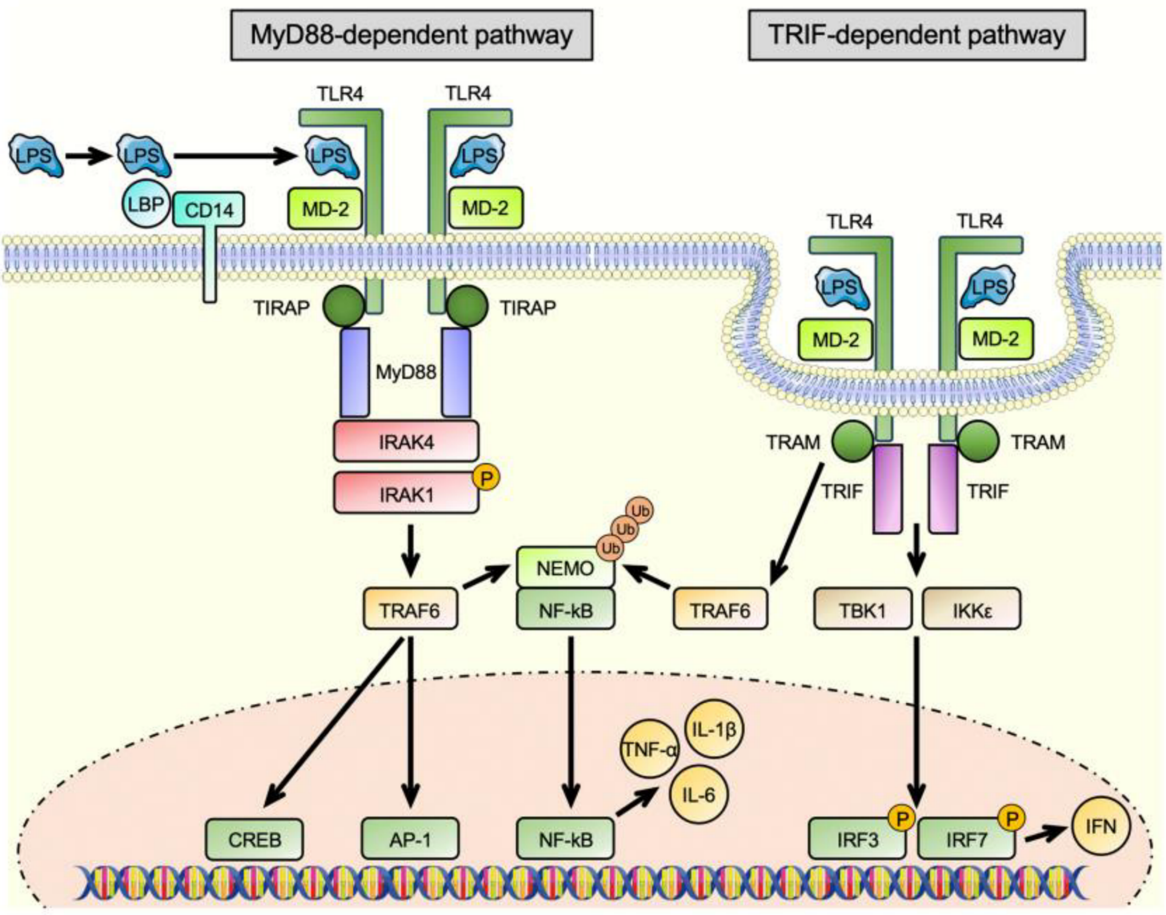

Abbildung 1: LPS-induzierter TLR4-Signalweg

Während des MyD88-abhängigen Signalwegs interagiert der membranständige TLR4-Rezeptor mit dem sogenannten TIR-Domäne-beinhaltenden Adapter Protein (*TIR domain-containing adapter protein,* TIRAP), was zur Rekrutierung von MyD88 führt und eine Signalkaskade initiiert. Diese Signalkaskade beinhaltet die Rekrutierung der beiden IL-1 Rezeptor assoziierten

Kinasen (IRAK) 1 und 4. IRAK4 phosphoryliert und aktiviert hierbei IRAK1, welche mit dem sogenannten TNF-Rezeptor assoziierten Faktor 6 (TRAF6) interagiert (Li et al. 2002,Arch et al. 1998). TRAF6 fungiert als Zytokin- und Stresssignalweg Mediator, welcher sowohl die Transkriptionsfaktoren Aktivator Protein-1 (AP-1) und cAMP Antwort-Element bindendes Protein (*cAMP response element binding protein*, CREB) aktiviert als auch die Translokation von NF-κB beeinflusst, wodurch pro-inflammatorische Mediatoren produziert werden (Shaywitz and Greenberg 1999,Zhao et al. 2017,Lu et al. 2022).

Nach der Dissoziation des membrangebundenen TLR4 von TIRAP und MyD88 durchläuft TLR4 eine Endozytose und bindet sowohl TRIF als auch das TRIF-verwandte Adaptermolekül (*TRIF-related adapter molecule*, TRAM). LPS induziert dabei die Bildung eines Komplexes aus TLR4 und TRAM und die nachfolgende Translokation in das Endosom (Tanimura et al. 2008). Dieser TRIF-abhängige Signalweg aktiviert die beiden Kinasen TANK bindende Kinase 1 (TBK1) und IκB Kinase ε (IKKε), welche die Transkriptionsfaktoren Interferon regulierender Faktor (IRF) 3 und 7 phosphorylieren, was zur Expression von Typ-1 Interferonen führt, welche die inflammatorische Antwort noch weiter verstärken (Zhang *et al.* 2022).

Unter physiologischen Umständen fungiert das Immunsystem als Schutz des Organismus vor Infektion. Wird jedoch die Kontrolle über die lokale Infektion verloren, wird die Infektion systemisch, was zu einer Hyperaktivität des Immunsystems führt. Der oxidative Stress wird dabei durch die von Immunzellen ausgeschütteten pro-inflammatorischen Zytokine und ROS verursacht. Die Folgen sind Zellschäden und Apoptose, wodurch die Integrität des Endothels beeinträchtigt wird und dessen Fehlfunktion ausgelöst werden kann, worauf Gewebe- und Organschäden folgen. Je nach Schwere dieser Schäden sind Organversagen und der Tod des Organismus die Folge (Virzi et al. 2022). Um diesen schweren Folgen der Sepsis Erkrankung zuvorzukommen, wären adjuvante Therapien mit dem Ziel die endotheliale Integrität zu bewahren hilfreich, wodurch das Auftreten eines septischen Schocks vermieden werden könnte.

Im Gegensatz zu den akuten Effekten von hohen Konzentrationen an LPS auf das Endothel führen niedrige LPS-Konzentrationen im Normalfall zu chronischen Komplikationen, welche im nächsten Kapitel näher beleuchtet werden.

2.6 Chronische Entzündung, Alterung und Endothelzellseneszenz

Chronische Entzündungen entstehen sobald Immunzellen am Ort einer Entzündung verweilen und deren ausgestoßene pro-inflammatorischen Zytokine und ROS das umliegende Gewebe beschädigen. Risikofaktoren für chronische Entzündung sind neben bakteriellen Ursachen wie LPS auch Rauchen, genetische Prädisposition, Alterung, Übergewicht und eine ungesunde Ernährung (Pahwa et al. 2024).

Im Gegensatz zu chronischen Entzündungen wie Morbus Crohn, welche mit bemerkbaren Symptomen einhergehen, wirken sich stille Entzündungen langfristig vorerst unbemerkt aus. Diese stillen Entzündungen gehen mit oxidativem Stress einher und können zur Akkumulierung von Zellschäden beitragen, was eine große Belastung für den Organismus darstellt

(Sanada *et al.* 2018). Weiterhin induziert dieser zelluläre Stress die Entstehung der Stress-induzierten Seneszenz, welche unter anderem auch durch DNA-Schäden (Gire et al. 2004), aktivierte Onkogene (Ferbeyre et al. 2002) oder sogenannte „low-dose" Endotoxämie (**Merk** *et al.* 2023) hervorgerufen wird.

Seneszenz beschreibt den irreversiblen Stillstand des Zellzyklus, wodurch die Proliferation der Zellen inhibiert wird, was mit Alterung in Verbindung gebracht wird. Seneszente Zellen unterscheiden sich sowohl morphologisch als auch funktionell von nicht-seneszenten Zellen. In Bezug auf das kardiovaskuläre System zeichnen sich beispielsweise seneszente Endothelzellen durch eine verminderte Produktion von NO, einer Veränderung der Expression und/oder Aktivität der eNOS und der verstärkten Adhäsion von Monozyten aus. Auf molekularer Ebene sind bei der Seneszenz außerdem die Zellzyklus-Inhibitoren p53 und p21 verstärkt exprimiert, was den Stillstand des Zellzyklus erklärt (Tian and Li 2014)

Neben der replikativen Seneszenz, welche *in vitro* auftritt und auf die Verkürzung der Telomere, aufgrund ausgeschöpfter Replikationskapazität, zurückgeführt wird (Hayflick 1965), spielt besonders die Stress-induzierte Seneszenz eine wichtige Rolle bei Alterungs-assoziierten Erkrankungen, die mit der endothelialen Dysfunktion in Zusammenhang stehen. Die Stress-induzierte frühzeitige Seneszenz (*stress-induced premature senescence*, SIPS) entsteht durch stille Entzündung und damit einhergehendem oxidativen Stress (Munoz-Espin and Serrano 2014).

Weiterhin wurde gezeigt, dass die Menge an pro-inflammatorischen Zytokinen wie IL-6 und TNF-α in älteren Individuen, im Vergleich zu jüngeren, konstitutiv erhöht ist (Singh and Newman 2011). Interessanterweise wurde festgestellt, dass die dadurch entstehende stille Entzündung weiterhin besteht, obwohl man die pro-inflammatorischen Stimuli, mithilfe von anti-inflammatorischen Wirkstoffen, zum Beispiel den Statinen, beseitigt (Tousoulis et al. 2014). Dies kann durch den Seneszenz-assoziierten sekretorischen Phänotyp (SASP) erklärt werden (Sanada *et al.* 2018). Dieser Phänotyp ist Teil der Seneszenz und ist durch die Sekretion von pro-inflammatorischen Faktoren und der Verursachung von oxidativem Stress charakterisiert (Coppe et al. 2008). Endothelzellen, die diesen Phänotyp ausbilden, stimulieren durch die Sekretion von pro-inflammatorischen Zytokinen umliegende Zellen dazu diesen Phänotyp auch auszubilden, was die Anzahl an seneszenten Endothelzellen erhöht. Durch Inhibierung der Entstehung und Ausbreitung der Endothelzellseneszenz könnte die Funktion von Endothelzellen beibehalten und die daraus resultierenden Komplikationen unterbunden werden.

Wie bereits erwähnt wirkt sich die Ernährung im Zusammenhang mit chronischer Entzündung maßgeblich auf die Funktionalität des Endothels aus (Pahwa *et al.* 2024). Dieser Effekt ist jedoch nicht nur auf das Endothel begrenzt, sondern kann auch andere Organe wie die Leber beeinträchtigen. In diesem Zusammenhang ist die Pathogenese der NAFLD besonders hervorzuheben, da es derzeit keine pharmakologischen Therapiemöglichkeiten oder nutzbare Biomarker für diese Erkrankung und deren Folgeerkrankungen gibt. Aus diesem Grund wurde in

der folgenden Studie auf die Pathogenese der NAFLD eingegangen und ein möglicher therapeutischer Ansatz zur Verhinderung der Progression dieser Erkrankung untersucht.

3. Eliminierung von oxidierten Phospholipiden durch AAV-vermittelten Gentransfer von scFv-E06 verhindert die Progression der hepatischen Steatose zur Fibrose

NAFLD ist charakterisiert durch die Akkumulation von Fett in der Leber und der Ausbildung einer hepatischen Steatose. NAFLD schließt mehrere Krankheitsstadien ein, ausgehend von nichtalkoholischer Steatohepatitis (NASH), über Fibrose bis hin zur Leberzirrhose. Der Mechanismus der Entstehung und der Progression von NAFLD ist komplex und von unterschiedlichen Faktoren abhängig. Zu diesen gehören Insulinresistenz, Übergewicht, Veränderung des Darmmikrobioms und Ernährung (Buzzetti et al. 2016). Die Akkumulation von Fett in der Leber in Form von Triglyzeriden geht mit dem Anstieg der Lipotoxizität einher. Dies führt zu hohen Leveln an freien Fettsäuren, Cholesterol und anderen Lipid-Stoffwechselprodukten. Die daraus resultierende Fehlfunktion der Mitochondrien und ROS-Produktion fördert die Entstehung von oxidativem Stress und amplifiziert die Progression der Krankheit (Cusi 2009). Eine anhaltende Verletzung der Leber führt zur Entstehung von NASH. NASH ist charakterisiert durch Inflammation und Aktivierung von hepatischen Sternzellen und der Möglichkeit zu hepatischer Fibrose fortzuschreiten (Schuster et al. 2018,Kisseleva and Brenner 2021). Fibrose ist definiert als reversible Vernarbungsreaktion, welche in fast allen Patienten mit chronischen Leberverletzungen vorkommt. Letztendlich kann die hepatische Fibrose zur Leberzirrhose fortschreiten, was mit Organkontraktion und Knotenbildung assoziiert ist (Friedman 2008). Die Leberzirrhose entsteht nach langanhaltender Inflammation, welche dazu führt, dass das gesunde Leberparenchym durch fibrotisches Gewebe ersetzt wird (Gines et al. 2021).

Der anhaltende oxidative Stress führt neben der Oxidation von LDL, welches Cholesterin zu Gewebe und Organen transportiert, auch zur Bildung von Lipidoxidationsprodukten wie den oxidierten Phosphatidylcholinen (oxPC) (Kadl et al. 2010), welche zelluläre Mechanismen, wie die Integrität des Endothels, die Migration und Aktivierung von Immunzellen und die zelluläre Apoptose, beeinflussen (Ke et al. 2019,Karki et al. 2018).

Die Verwendung des natürlichen Immunglobulin M (IgM) E06 ermöglicht es Plasma-Levels von oxPCs zu messen, da diese von E06 gebunden werden können (Tsimikas et al. 2006). Dies wurde durch die konstitutive transgene Expression eines Einzelstrangfragments von E06 (scFv-E06) in LDL-Rezeptor defizitären $Ldlr^{-/-}$ Mäusen nachgewiesen (Schreyer et al. 2002).

Obwohl die konstitutive Expression von scFv-E06, $Ldlr^{-/-}$ defizitäre Mäuse vor Ernährungs-induzierter hepatischer Steatose und der nachfolgenden NASH schützt (Sun et al. 2020), war es nicht bekannt ob die Eliminierung von oxPCs durch scFv-E06 der ausschlaggebende Faktor und zudem ausreichend ist, um diesen Effekt auszuüben. Deswegen wurde der Einfluss von scFv-E06 auf die verschiedenen Stadien der NAFLD mithilfe eines AAV8-scFv-E06 Konstrukts (Abbildung 2: Expressionsvektor AAV8-scFv-E06) untersucht, welches den Virus-vermittelten Gentransfer von scFv-E06 erlaubt. Für den Expressionsnachweis wurde sowohl ein myc- als auch ein 6xHIS-Tag verwendet (Upchurch,**… Merk** et al. 2022).

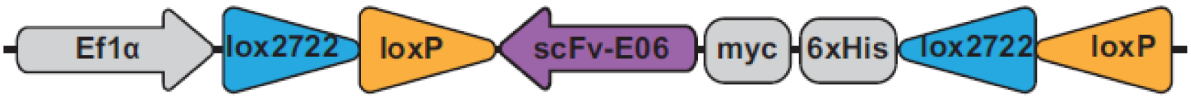

Abbildung 2: Expressionsvektor AAV8-scFv-E06. Dieser Expressionsvektor wurde für den Virus-vermittelten Gentransfer von scFv-E06 entwickelt. Für den Expressionsnachweis wurden sowohl ein myc- als auch 6xHIS-Tag implementiert.

Die Expression des myc-markierten scFv-E06 wurde in der Leber durch Western Blot und auf RNA-Ebene durch quantitative Polymerase-Kettenreaktion mit reverser Transkription (*quantitative reverse transcription polymerase chain reaction*, qRT-PCR) nachgewiesen. Durch die Verwendung eines kompetitiven HIS/myc sandwich ELISAs konnten zudem detektierbare Titer von scFv-E06 im Plasma nachgewiesen werden (Abbildung 3: Kompetitiver HIS/myc sandwich ELISA nach 6 Wochen). Hierzu wurden der myc- und 6xHIS-Tag des scFv-E06 Konstrukts utilisiert und eine HIS-Standardkurve, mithilfe eines HIS-Protein ELISA-Standard Stocks, generiert. Durch die Verwendung eines HIS-Antikörpers konnte scFv-E06 gebunden werden, welches jedoch mit dem HIS-Protein ELISA-Standard Stock konkurrierte. Da nur scFv-E06 ein myc-Tag besaß, kam es anschließend nur dort zur Bindung des sekundären myc-Antikörpers, an welchen Meerrettich-Peroxidase (*horseradish-peroxidase*, HRP) gebunden ist. Damit wurde gezeigt, dass scFv-E06 Protein nur in den AAV-scFv-E06 injizierten Mausplasmaproben nachweisbar war und nicht in den AAV8-GFP Kontrollproben (Upchurch,**… Merk** *et al.* 2022).

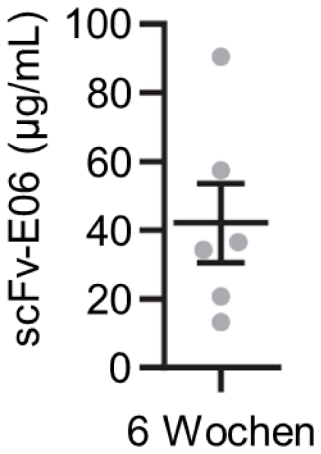

Abbildung 3: Kompetitiver HIS/myc sandwich ELISA nach 6 Wochen. Mäusen wurde 2 Wochen vor einer 6-wöchigen FPC-Ernährung entweder das AAV8-scFv-E06 Konstrukt oder eine AAV8-GFP Kontrolle über die Schwanzvene injiziert. scFv-E06 Konzentrationen wurden im Blutplasma mithilfe des kompetitiven HIS/myc sandwich ELISAs nachgewiesen. In den Kontrollproben konnte keine scFv-E06 Expression nachgewiesen werden.

Da das Vorhandensein von scFv-E06 die normale Physiologie der Mäuse nicht beeinflusste, konnte dieser Versuchsaufbau verwendet werden, um die Entfernung der oxPCs und deren Einfluss auf die Progression der NAFLD zu untersuchen.

Die Progression der NAFLD wurde über ein Fructose-, Palmitat- und Cholesterin-reiches (FPC) Ernährungsmodell dargestellt, welches ein bekanntes Modell zur Induktion von hepatischer Steatose ist (Wang et al. 2016). Die Expression von scFv-E06 eliminierte in diesem Modell ein-

zelne oxPC-Spezies im Plasma der Mäuse, was zur Verringerung von Leberschäden und Lipidakkumulation führte. Da oxPCs spezifisch von scFv-E06 gebunden werden, bestätigt die Verminderung der Leberschäden die Relevanz von oxPCs bei der Entwicklung und Progression von hepatischer Steatose (Upchurch,**… Merk** *et al.* 2022).

Der virus-vermittelte Gentransfer von scFv-E06 wurde weiterhin verwendet, um nach der Etablierung der hepatischen Steatose durch FPC-Ernährung therapeutisch einzugreifen und die Progression zur Fibrose zu verhindern. Der Expressionsnachweis des scFv-E06 wurde erneut durch Western Blot und ELISA nachgewiesen. Auch hier konnte, durch die Verwendung des zuvor beschriebenen kompetitiven HIS/myc sandwich ELISAs, scFv-E06 im Plasma nachgewiesen werden (Abbildung 4: Kompetitiver HIS/myc sandwich ELISA nach 20 Wochen). Die Expression von scFv-E06 führte zu verminderten Leberschäden und einer verbesserten Leberfunktion, wobei keine Änderungen an Fettleibigkeit und Insulinresistenz auftraten. Weiterhin konnte das Fortschreiten zur hepatischen Fibrose verhindert werden (Upchurch,**… Merk** *et al.* 2022).

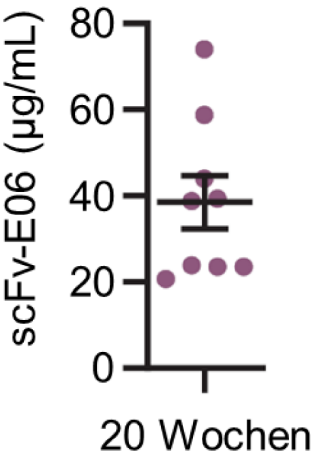

Abbildung 4: Kompetitiver HIS/myc sandwich ELISA nach 20 Wochen. Mäuse wurden einer 6-wöchigen FPC-Ernährung ausgesetzt und anschließend entweder das AAV8-scFv-E06 Konstrukt oder eine AAV8-GFP Kontrolle über die Schwanzvene injiziert. Nach weiteren 14 Wochen wurden die scFv-E06 Konzentrationen im Blutplasma mithilfe des kompetitiven HIS/myc sandwich ELISAs nachgewiesen. In den Kontrollproben konnte keine scFv-E06 Expression nachgewiesen werden.

Zur Untersuchung, welche oxPC-Spezies von scFv-E06 eliminiert werden, wurde die in silico Plattform LPPTiger in Kombination mit Massenspektrometrie verwendet. Dabei wurde die Spezifität von scFv-E06 nur gegenüber oxidierten Phospholipiden erfüllt, und einzelne oxPC-Spezies identifiziert. Diese oxPC-Spezies führten *in vitro* in Hepatozyten und Sternzellen zu metabolischen Veränderungen und beeinflussten die hepatische Genexpression. Dabei konnte gezeigt werden, dass Leberzellen oxPC-Spezies erkennen und auf diese reagieren, was ein Grund der Entstehung von pathologischen Veränderungen sein kann. Eine Intervention mit scFv-E06 konnte diese pathologischen Veränderungen verhindern und zu verminderter Fibrose und Inflammation in der Leber führen. Die Progression der etablierten hepatischen Steatose zu hepatischer Fibrose kann folglich durch die Expression von scFv-E06 unterbunden werden (Upchurch,**… Merk** *et al.* 2022).

Diese Untersuchungen haben gezeigt, dass die AAV8-vermittelte Expression von scFv-E06 in der Leber bestimmte Plasma oxPC-Spezies eliminiert. Diese oxPC-Spezies nehmen Einfluss auf die Genexpression von Leberzellen und verschieben den zellulären Mechanismus hin zu einem bioenergetisch-eingeschränkten Status. Die Intervention mit AAV8-scFv-E06 verhinderte in Mäusen mit etablierter hepatischer Steatose die Progression zu NASH und hepatischer Fibrose, durch die Verminderung der im Plasma vorkommenden oxPC-Spezies (Upchurch,**… Merk** *et al.* 2022).

Da verschiedene oxPCs zu unterschiedlichen Zeitpunkten der NAFLD Progression eliminiert werden, könnten diese als nicht-invasive Biomarker für die Bestimmung der Schwere der NAFLD verwendet werden. Außerdem könnte nach weiterführenden und erfolgreichen Untersuchungen der AAV8-vermittelte Gentransfer von scFv-E06 als therapeutische Ansatz genutzt werden, um die Initiierung von hepatischer Steatose und deren Progression zu Fibrose und Zirrhose zu verhindern (Upchurch,**… Merk** *et al.* 2022).

Wie bereits erwähnt stellen Entzündungen und damit einhergehender oxidativer Stress, ausgelöst durch inflammatorische Mediatoren, eine große Belastung für das Endothel und den gesamten Organismus dar. Aufgrund der Relevanz des Endotoxins LPS für die Entstehung von chronischen, aber auch akuten Erkrankungen, werden dessen Dosis-abhängige Effekte auf das Endothel in den nächsten Kapiteln genauer beschrieben.

4. Selenoprotein T schützt Endothelzellen vor LPS-induzierter Aktivierung und Apoptose

Die Entstehung und Progression von kardiovaskulären Erkrankungen ist eng mit der endothelialen Dysfunktion, hervorgerufen durch oxidativen Stress, verknüpft (Pober *et al.* 2009). Dieser oxidative Stress wird durch die anhaltende Aktivierung von Endothelzellen, der Sekretion von inflammatorischen Zytokinen und damit der Rekrutierung von Leukozyten hervorgerufen (siehe Kapitel 2.3 Endotheliale Dysfunktion). Da die Endothelzellen zu den ersten Zellen gehören, welche mit externen Pathogenen, wie dem Endotoxin LPS, im Blutkreislauf in Kontakt kommen, sind diese besonders dem Risiko für oxidativen Stress ausgesetzt. Endotheliale Dysfunktion, hervorgerufen durch hohe Konzentrationen an LPS im Blutstrom, wird als Beginn der nachfolgenden Gewebe- und Organschäden betrachtet und trägt zur Entstehung von akuten Erkrankungen wie Sepsis (siehe Kapitel 2.5 Sepsis) bei.

Therapien, welche den Verlust der Integrität des Endothels verhindern könnten, wären im Anbetracht dessen von großem Nutzen für Patienten. Interessanterweise kann LPS das Transkriptom von Endothelzellen beeinflussen, indem es die Transkription von Protein-kodierenden und nicht-kodierenden RNAs reguliert (Zhao et al. 2001,Ho et al. 2016). Dementsprechend ist die Tatsache, dass es keine RNA deep sequencing Daten gab, die den Effekt von LPS auf das Transkriptom von Endothelzellen aufzeigten, umso verwunderlicher. Eine solche detaillierte Untersuchung des Transkriptoms könnte Signalwege aufweisen, die bei der Entstehung von Sepsis relevant sind und neue therapeutische Ansätze für deren Behandlung aufzeigen. Weiterhin könnten Proteine, welche die LPS-induzierte Aktivierung und Apoptose von Endothelzellen inhibieren eine Möglichkeit darstellen, um das Endothel zu schützen und somit wichtige Aspekte der Sepsis-Pathogenese zu unterbinden. Demnach wurde der Einfluss von LPS auf das Transkriptom von Endothelzellen untersucht und nach Möglichkeiten gesucht die endotheliale Integrität zu erhalten.

4.1 APEX1 (1-20) als möglicher Therapieansatz

In früheren Arbeiten konnte gezeigt werden, dass die ersten 20 Aminosäuren der apurinischen/apyrimidinischen Endodeoxyribonuklease 1 (APEX1) ausreichend sind, um die H_2O_2-induzierte Apoptose zu verhindern (Dyballa-Rukes et al. 2017). APEX1 ist ein ubiquitär exprimiertes Protein, welches zum einen als apurinische/apyrimidinische Endonuklease DNA-Basen herausschneiden kann und damit an der Reparatur der DNA beteiligt ist, und zum anderen als Redox-Faktor fungiert. Durch die Herstellung verschiedener APEX1-Konstrukte konnte die Funktion der unterschiedlichen APEX1-Domänen untersucht werden. Es wurde gezeigt, dass der anti-apoptotische Effekt von APEX1 von den ersten 20 N-terminalen Aminosäuren abhängig ist, und dieser Effekt über Trx-1 vermittelt wird. Dafür wurde eine Variante des APEX1 konstruiert, welches nur die ersten 20 N-terminalen Aminosäuren beinhaltet (APEX1 (1-20) (Dyballa-Rukes *et al.* 2017)).

4.2 RNA deep sequencing Analyse

In Anbetracht der Fähigkeit von APEX1 (1-20) die Apoptose von Endothelzellen unter oxidativem Stress zu inhibieren, lag die Überlegung nahe, dass APEX1 (1-20) auch die LPS-induzierte Apoptose verhindern könnte. Aus diesem Grund wurden Endothelzellen, welche APEX1 (1-20) exprimieren, in einer RNA-Deep-Sequencing-Analyse untersucht, um Gene zu identifizieren, deren Expression durch APEX1 (1-20) beeinflusst wird. Die Verwendung eines lentiviralen Vektors erlaubte eine flächendeckende Expression von APEX1 (1-20) in allen zu untersuchenden Zellen, während ein Leervektor als Kontrolle eingesetzt wurde. Die so transduzierten Zellen wurden mit aktivem LPS behandelt, wobei detoxifiziertes LPS (Detox) als Kontrolle verwendet wurde. Detoxifiziertes LPS wurde durch alkalische Hydrolyse delipidiert, was dessen Toxizität um ein 10.000-faches vermindert. Eine differentielle Genexpressionsanalyse (DGE) zeigte, dass die moderate APEX1 (1-20) Expression nicht zu Veränderungen des Transkriptoms von Endothelzellen führte, was die Hypothese der Verwendung von APEX1 (1-20) als Therapeutikum weiter unterstützt, da hiermit größere Nebenwirkungen ausgeschlossen werden können (**Merk** et al. 2021). Um Gene zu untersuchen, die durch die Behandlung von Endothelzellen mit LPS signifikant reguliert werden, wurde eine Anreicherungsanalyse von Gensätzen (*gene set enrichment analysis*, GSEA) verwendet. LPS führte in den Kontrollzellen zu einer signifikanten Hochregulation der Expression von Genen, deren Genprodukte mit Entzündungen assoziiert werden (**Merk** *et al.* 2021). Es ist schon lange bekannt, dass TNFα-assoziierte Signalwege bei der Aktivierung und der Apoptose von Endothelzellen hochreguliert sind (Pober 2002,Dimmeler et al. 1996). Zellen, die mit LPS behandelt wurden und APEX1 (1-20) exprimieren zeigten keine Hochregulation von Genen die mit der Immunantwort zusammenhängen und interessanterweise auch eine Herunterregulation der zellulären Antwort auf TNFα. Außerdem wurde gezeigt, dass die Antwort auf LPS sich zwischen APEX1 (1-20) exprimierenden Zellen und Kontrollzellen klar unterschied. Diese Daten unterstützen die zuvor aufgestellte Hypothese, dass APEX1 (1-20) möglicherweise die Aktivierung und Apoptose von Endothelzellen verhindern kann, indem es die transkriptionelle Antwort auf LPS verändert (**Merk** *et al.* 2021).

4.3 Validierung der RNA deep sequencing Daten

Für die darauffolgenden funktionellen Untersuchungen wurden Gene untersucht, die durch die Behandlung mit LPS in Zellen die APEX1 (1-20) exprimieren hochreguliert werden, da diese Gene voraussichtlich protektive Effekte ausüben könnten. Die drei am stärksten regulierten Gene waren, wie in Abbildung 5: APEX1 (1-20) induziert spezifische Veränderungen des Transkriptoms in Endothelzellen als Antwort auf LPS-Behandlung. zu erkennen, Interleukin 1 Rezeptor-ähnliches Protein 1 (*interleukine 1 receptor like* 1, IL1RL1), Peroxidasin (PXDN) und Selenoprotein T (SELENOT) (**Merk** *et al.* 2021).

IL1RL1 ist Mitglied einer Familie von 10 unterschiedlichen, aber strukturell verwandten Rezeptoren, die verschiedene Funktionen ausüben, wie die Bindung von Liganden oder die Inhibierung von Signalen. Die Translation des IL1RL1 Gens generiert außerdem drei unterschiedliche

Splice-Varianten, welche zusätzlich je nach Einzel-Nukleotid-Polymorphismus ungleiche Signale weitergeben (Savenije et al. 2011). Dementsprechend ist IL1RL1 Teil eines komplexen Signal-Netzwerks. Der Eingriff in dieses Netzwerk könnte zu ungewollten Nebeneffekten führen oder kompensatorische Antworten hervorrufen, wodurch die therapeutische Anwendung zur Behandlung von LPS-induzierten Veränderungen stark beeinträchtigt sein könnte.

PXDN ist eine Häm-bindende Peroxidase, welche im Herzen und der Gefäßwand am höchsten exprimiert wird (Cheng et al. 2008). Das Protein wird schnell sekretiert (Cheng et al. 2011) und ist notwendig für die Bildung der vaskulären Basalmembran, indem es Sulfilimin-Bindungen bildet, welche das verstärkende fibrilläre Netzwerk in der extrazellulären Matrix ausbildet (Bhave et al. 2012). Außerdem wurde gezeigt, dass PXDN die Angiogenese verbessert und für das Überleben von Endothelzellen von essenzieller Bedeutung ist (Medfai et al. 2019,Lee et al. 2020). Diese protektiven Eigenschaften könnten bei der Verteidigung gegen LPS-induzierte Schäden von Nutzen sein, um die endotheliale Integrität zu schützen.

SELENOT ist ein Mitglied der Selenoprotein-Familie und gehört zu einem der 7 von 25 humanen Selenoproteinen, die im endoplasmatischen Retikulum (ER) lokalisiert sind (Pitts and Hoffmann 2018). Selenoproteine werden durch deren Inkorporation einer oder mehrerer Selenocystein-Reste in ihrem enzymatisch aktiven Zentrum charakterisiert (Mariotti et al. 2012). Die Notwendigkeit von SELENOT wird sowohl durch dessen starke evolutionäre Konservierung als auch der Tatsache, dass eine konstitutive Störung des SELENOT Gens bei der Embryonalgenese schon in frühen Stadien letal wirkt, aufgezeigt (Pothion et al. 2020,Boukhzar et al. 2016). SELENOT ist als ER-stämmiges Selenoprotein mit der ER-Membran assoziiert und spielt eine wichtige Rolle in der ER-Redox-Homöostase (Pothion *et al.* 2020). Wie bei allen anderen Selenoproteinen, hängt die Expression von SELENOT von der ausreichenden Nahrungsaufnahme von Selen ab, da dieses für dessen Generierung benötigt wird. Ein Defizit an Selen ist zwar selten, kann jedoch die Entstehung und Progression von Krankheiten verstärken (Holben and Smith 1999). Es wurde zudem gezeigt, dass eine reduzierte Expression von SELENOT in Hühnermägen nach 55 Tagen einer Selen-Mangel Ernährung auftrat, welche mit dem Auftreten von Stress-induzierten Verletzungen einherging (Huang et al. 2017). Diese Untersuchungen unterstützen die Annahme, dass ER-ständige Selenoproteine für die zelluläre Antwort auf Stress notwendig sind, was für den Schutz von Endothelzellen gegenüber LPS hilfreich sein könnte (Addinsall et al. 2018). Es wurde zudem gezeigt, dass die Selen-Serumlevel in Sepsis Patienten besonders vermindert sind (Alhazzani et al. 2013). Dieser Selenmangel geht mit verminderten *selenot* mRNA-Leveln einher. Eine Vorbehandlung mit Selen konnte der Hochregulation von Inflammation-assoziierten Genen, wie IL-6 und TNF-α, nach LPS-Behandlung, entgegenwirken (Wang et al. 2018). In den APEX1 (1-20) exprimierenden und LPS behandelten Zellen war SELENOT auf RNA-Level stark hochreguliert, was suggeriert, dass APEX1 (1-20) einen protektiven Einfluss ausüben könnte (**Merk** *et al.* 2021).

Mit dem therapeutischen Nutzen als Ziel, und da die protektiven Eigenschaften von PXDN im Gegensatz zu SELENOT im Endothel bereits untersucht wurden, wurden semi-quantitative

Real-Time PCRs für SELENOT durchgeführt, welche die RNA-Deep-Sequencing-Daten validierten (Abbildung 5: APEX1 (1-20) induziert spezifische Veränderungen des Transkriptoms in Endothelzellen als Antwort auf LPS-Behandlung).

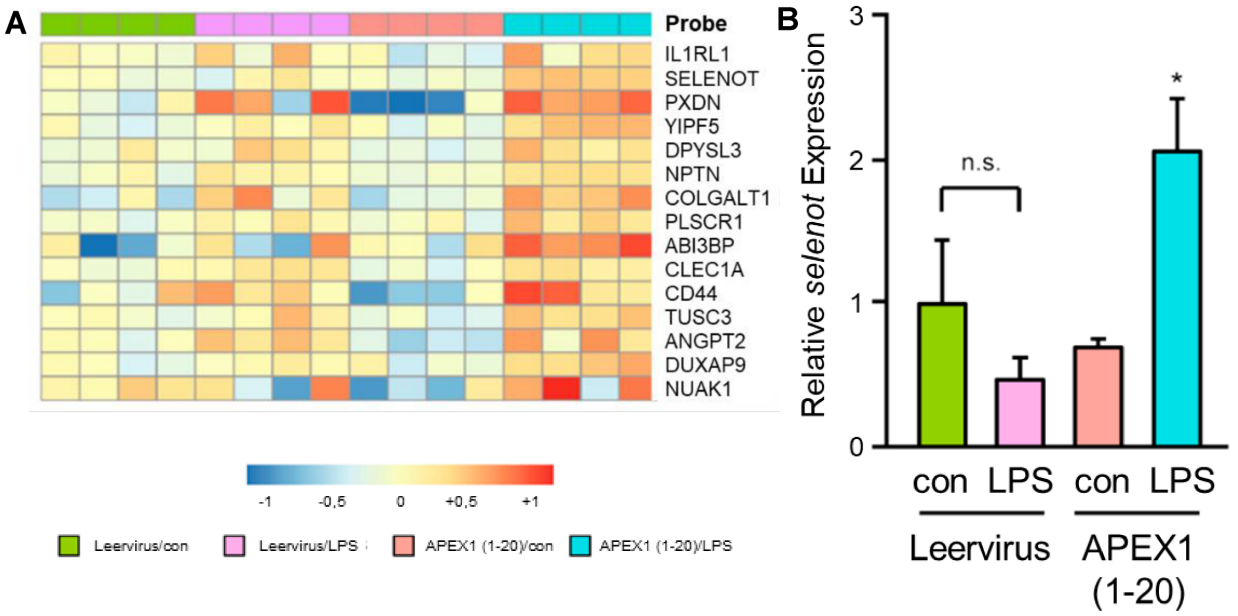

Abbildung 5: *APEX1 (1-20) induziert spezifische Veränderungen des Transkriptoms in Endothelzellen als Antwort auf LPS-Behandlung. Endothelzellen wurden mit einem lentiviralen Expressionsvektor für APEX1 (1-20) oder einer Leervirus-Kontrolle transduziert und mit 150 ng/mL detoxifiziertem (con) oder aktivem LPS (LPS) für 18h behandelt. (A) RNAs der transduzierten Zellen wurden in einem RNA deep sequencing untersucht. Gene die nach LPS-Behandlung nur in APEX1 (1-20) exprimierenden Zellen hochreguliert wurden, werden als Heatmap visualisiert. (B) Die relative SELENOT-Expression wurde mithilfe der semi-quantitativen real-time PCR untersucht, mit RPL32 als Referenzgen (Fehlerabweichung wird als ±SEM dargestellt. n = 4, p* < 0.05 vs. APEX1 (1-20)/con, n.s. = nicht signifikant, one-way ANOVA mit post-hoc Tukey LSD Test).*

4.4 Generierung und Validierung eines SELENOT Expressionsvektors

Für funktionelle Untersuchungen und um den Einfluss von SELENOT auf die Endothelzellfunktion nach LPS-Behandlung zu ermitteln, wurde ein Expressionsvektor generiert, welcher ein FLAG-Epitop-Tag beinhaltet, was die Identifikation des überexprimierten SELENOT ermöglicht. Das FLAG-Epitop-Tag besitzt den Vorteil, dass es aus einer limitierten Anzahl an Aminosäuren besteht, demnach klein ist und somit nicht bei der nativen Faltung der Proteine stört (Einhauer and Jungbauer 2001). Außerdem musste berücksichtigt werden, dass die Selenocystein (sec)-Reste bei der Bildung der Selenoproteine nicht post-translational modifiziert, sondern direkt bei deren Translation eingebaut werden. Dies geschieht, indem eines der Translations-Terminations-Codons (UGA) von der Selenocystein-spezifischen tRNA ($tRNA^{sec}$) gebunden wird und damit die Translations-Termination verhindert wird. Um diese Recodierung des UGA-Codons zu bewerkstelligen, wird eine Selenocystein-Insertionssequenz (*selenocysteine insertion sequence,* SECIS) in der 3‘-untranslatierten Region (UTR) des Transkripts benötigt. Diese bildet eine Haarnadelstruktur, welche sich zurückfaltet und die Rekrutierung des $tRNA^{sec}$ zum UGA-Codon mit Hilfe mehrerer Proteine ermöglicht (Tujebajeva et al. 2000). Fehlt diese SECIS, wird

die Translation am ersten UGA-Codon abgebrochen und ein unvollständiges Protein translatiert. Neben dem offenen Leseraster des SELENOT wurde demnach auch ein Teil des SELENOT 3'-UTR, einschließlich der SECIS, in den Expressionsvektor inkludiert (Abbildung 6: Inkorporation des Selenocysteins (A) und FLAG-SELENOT Expressionsvektor (B).).

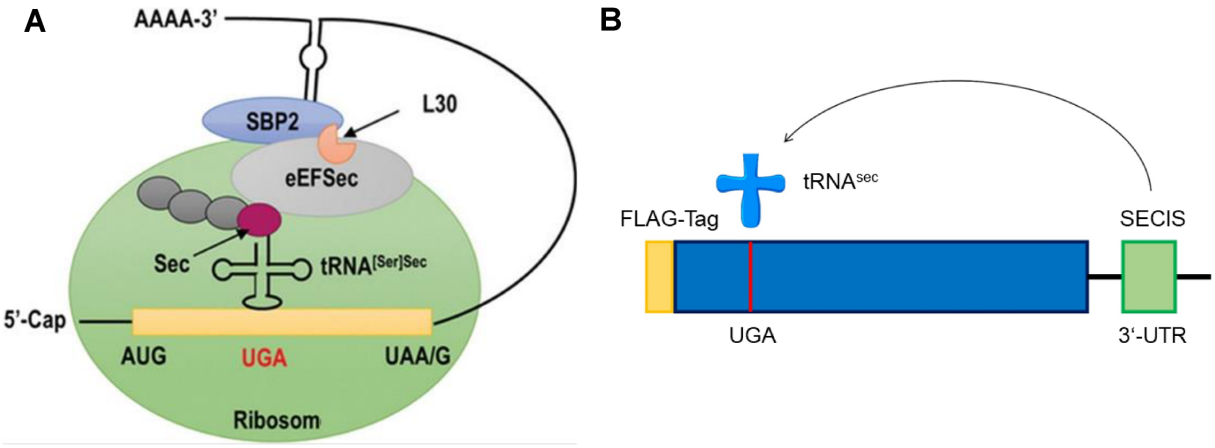

Pothion et al., Antioxidants & Redox Signaling, 2020

Abbildung 6: Inkorporation des Selenocysteins (A) und FLAG-SELENOT Expressionsvektor (B). (A) Das UGA-Stop-Codon wird recodiert und anstelle der Translationstermination kommt es zur Rekrutierung der Selenocystein-spezifischen tRNA (tRNA$^{(sec)}$) und Inkorporation von Selenocystein (Sec) in die wachsende Peptidkette. Dies wird durch die Haarnadelstruktur der SECIS innerhalb der 3'-UTR und die Rekrutierung des SECIS-bindenden Proteins (SBP) und des eukaryotischen Elongationsfaktors für Selenocystein-tRNA (eEFSec) ermöglicht. (B) Der Expressionsvektor für FLAG-SELENOT ermöglicht durch die Inkludierung der 3'-UTR und der SECIS die Inkorporation des Selenocysteins anstelle des UGA-Stop-Codons. Das FLAG-Tag ermöglicht den Expressionsnachweis.

Der Nachweis der erfolgreichen Expression wurde auf RNA-Ebene anhand einer reversen Transkriptase PCR sichergestellt. Auf dem Protein-Level wurde die Co-Lokalisation des SELENOT Proteins, mitsamt des N-terminalen FLAG-Epitop-Tag (FLAG-SELENOT), mit Calnexin, einem ER-ständigen Protein, welches bei der Faltung und der Qualitätskontrolle von Proteinen involviert ist, sichergestellt (**Merk** *et al.* 2021,Paskevicius et al. 2023).

4.5 SELENOT Überexpression verhindert LPS-induzierte Endothelzell-Aktivierung

Wie bereits erwähnt sind die Aktivierung und Apoptose von Endothelzellen wichtige Ursachen für das Auftreten der endothelialen Dysfunktion (siehe Kapitel 2.3 Endotheliale Dysfunktion). Eine Reduktion der Aktivierung der Endothelzellen induziert durch LPS würde das Endothel demnach vor der darauffolgenden Fehlfunktion besser schützen. Daher wurde der Effekt der SELENOT Überexpression auf die LPS-induzierte Endothelzell-Aktivierung untersucht. Immunfärbungen mit ICAM-1, welches als Marker für Endothelzell-Aktivierung gilt, zeigten, dass nach LPS-Behandlung, Zellen, die das Konstrukt FLAG-SELENOT exprimierten, signifikant weniger ICAM-1 exprimierten als Kontrollzellen (Abbildung 7: FLAG-SELENOT inhibiert die Aktivierung von Endothelzellen durch LPS). Dies zeigt, dass die SELENOT Überexpression die LPS-induzierte Aktivierung von Endothelzellen inhibiert und somit einen protektiven Effekt ausübt (**Merk** *et al.* 2021).

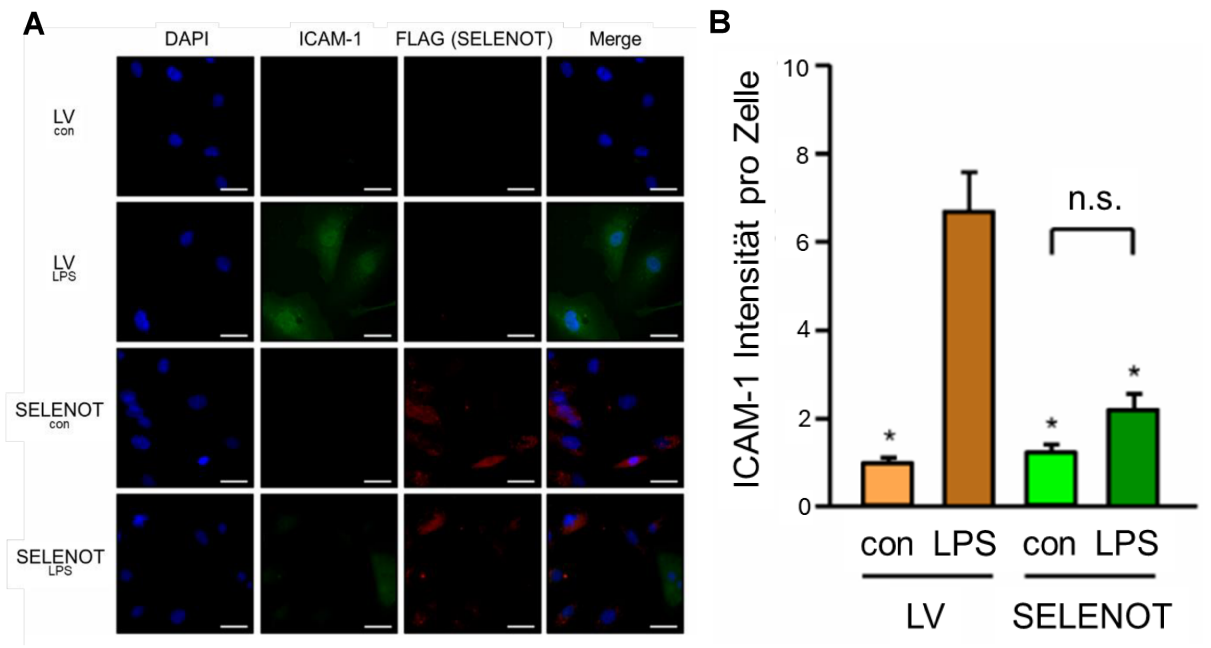

Abbildung 7: FLAG-SELENOT inhibiert die Aktivierung von Endothelzellen durch LPS. (A,B) Endothelzellen wurden mit dem FLAG-SELENOT Expressionsvektor (SELENOT) oder einem Leervektor (LV) transfiziert und mit 150 ng/mL detoxifiziertem (con) oder aktivem LPS (LPS) für 18 h behandelt. Mithilfe eines Antikörpers gegen ICAM-1 (grün) und eines anti-FLAG Antikörpers (rot) wurden ICAM-1 und SELENOT durch Immunfärbung detektiert. Die Detektion der Nuclei wurde durch DAPI ermöglicht. Der Merge-Kanal zeigt die Überlappung aller Kanäle. (A) Repräsentative Immunfärbung. (B) Quantifizierung der ICAM-1 Level. Die Intensität der grünen Fluoreszenz wurde mit Image J gemessen. Die Auswertung der mit FLAG-SELENOT transfizierten Zellen erfolgte nur mit den FLAG-SELENOT positiven Zellen (Fehlerabweichung wird als ±SEM dargestellt. n = 4, p < 0.05 vs. LV/LPS, n.s. = nicht signifikant, one-way ANOVA mit post-hoc Tukey LSD Test).*

Anschließend wurde der Effekt von SELENOT auf die LPS-induzierte Apoptose untersucht, da bekannt ist, dass LPS die Apoptose von Endothelzellen steigert (Haendeler et al. 1996). Hierfür wurde die Menge an gespaltener und somit aktiver Caspase 3 im Western Blot untersucht (Abbildung 8: FLAG-SELENOT inhibiert die Apoptose von Endothelzellen durch LPS). Wie bereits erwähnt sind Caspasen wichtige Vermittler für die zelluläre Apoptose. Die Bestimmung der Proteinmengen der aktiven Caspase 3 erlaubt es das Ausmaß der Apoptose nachzuweisen. Auch hier hatte die Überexpression von SELENOT eine signifikante Inhibierung der durch LPS induzierten gespaltenen Caspase 3 im Vergleich zur Kontrolle zur Folge. Dies unterstützt die Hypothese, dass SELENOT Endothelzellen vor LPS-induzierten Schäden schützt und somit der endothelialen Dysfunktion entgegenwirkt (**Merk** *et al.* 2021).

Diese Untersuchungen zeigten zum ersten Mal, anhand einer RNA-Deep-Sequencing-Analyse, die durch LPS-induzierten Veränderungen in primären humanen Endothelzellen. Außerdem wurde gezeigt, dass SELENOT in APEX1 (1-20) exprimierenden Zellen nach LPS-Behandlung hochreguliert ist und in diesem Kontext als wichtiger Mediator der protektiven Effekte von APEX1 (1-20) fungiert. Demnach könnten sowohl SELENOT als auch APEX1 (1-20) potenzielle adjuvante Therapeutika für die Behandlung von LPS-induzierten Erkrankungen sein (**Merk** *et al.* 2021).

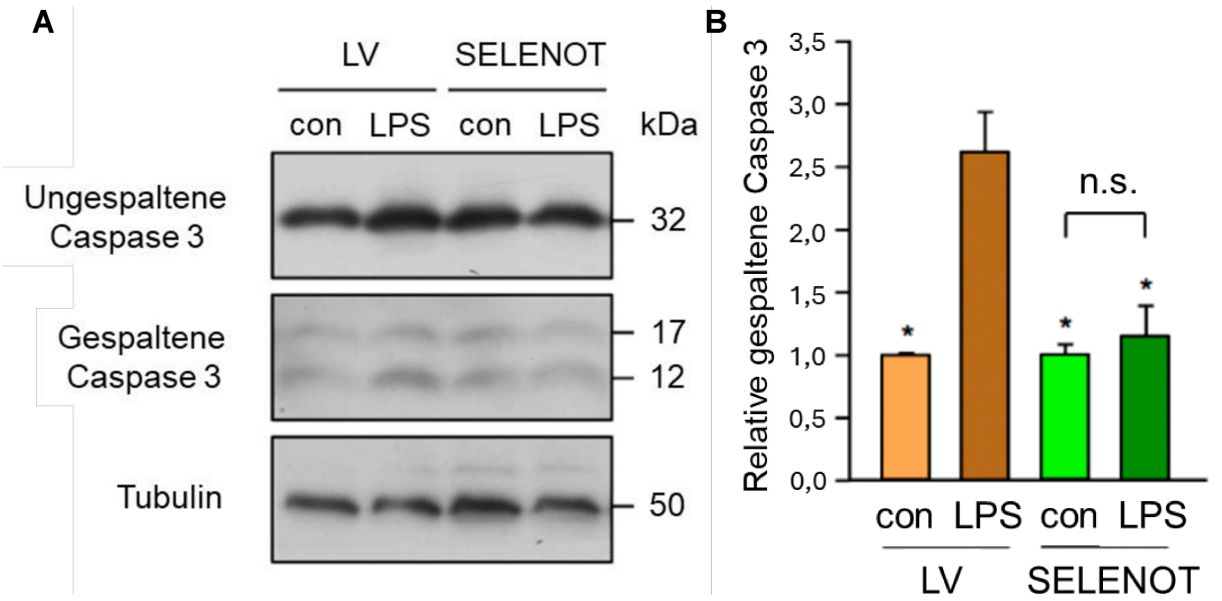

Abbildung 8: FLAG-SELENOT inhibiert die Apoptose von Endothelzellen durch LPS. (A,B) Endothelzellen wurden mit dem FLAG-SELENOT Expressionsvektor (SELENOT) oder einem Leervektor (LV) transfiziert und mit 150 ng/mL detoxifiziertem (con) oder aktivem LPS (LPS) für 18 h behandelt. Ungespaltene und gespaltene Capsase 3 wurden im Western Blot bestimmt, wobei Tubulin als Ladekontrolle fungierte. (A) Repräsentativer Western Blot. (B) Semi-quantitative Analyse der relativen gespaltenen Caspase 3 Mengen (Fehlerabweichung wird als ± SEM dargestellt. n = 4, p < 0.05 vs. LV/LPS, n.s. = nicht signifikant, one-way ANOVA mit post-hoc Tukey LSD Test).*

Im Gegensatz zur akuten Sepsis und dem septischen Schock, aufgrund von hohen Dosen an LPS, führen niedrigere LPS-Konzentration häufig zu chronischer Inflammation, welche im Zusammenhang mit Alterung und Herzkreislauf-Erkrankungen steht. Diese chronische Inflammation führt zu einem Anstieg an ROS, was die Entstehung von seneszenten Endothelzellen fördert und einen dramatischen, negativen Effekt auf Gewebefunktion und -Homöostase ausübt (Minamino et al. 2002). Die Untersuchung von molekularen Mechanismen, welche zur Stress-induzierten Seneszenz führen, könnte bei der Entwicklung von therapeutischen Strategien gegen alterungsbedingte Pathologien helfen. Im Normalfall bildet das intestinale Epithel des Darms eine Barriere gegen das Eindringen von LPS in den Blutstrom, wodurch nur geringe LPS-Konzentrationen im Blutplasma erreicht werden (Ghanim et al. 2009). Durch Faktoren wie Übergewicht, Alterung und ungesunde Ernährung kann die LPS-Plasma-Konzentration jedoch bis auf 1 ng/mL LPS ansteigen, was zur Entstehung einer sogenannten Niedrig-Dosis Endotoxämie führt (Opal et al. 2013). Der Effekt von dieser LPS-Konzentration wurde bisher nicht im Rahmen der Endothelzellseneszenz untersucht. Daher wird dies im nächsten Kapitel näher beleuchtet.

5. Koffein inhibiert Seneszenz ausgelöst durch niedrige LPS-Konzentrationen

5.1 Auswirkungen der Seneszenz auf Endothelzellen

Die zelluläre Seneszenz ist Teil des Alterungsprozesses und geht mit einer veränderten Funktion der Zellen einher. Seneszente Endothelzellen sind durch die Hochregulierung von Zellzyklus-Inhibitoren, wie p16 oder p21, einer gestörten Redox-Homöostase und einer eingeschränkten migratorischen Kapazität charakterisiert (Chen and Goligorsky 2006). Diese migratorische Kapazität ist von intakten Mitochondrien abhängig und ist ein Zeichen für die endotheliale Funktionalität (Spyridopoulos et al. 2008,Gonnissen et al. 2019). Es wurde weiterhin gezeigt, dass die Bioverfügbarkeit von NO in seneszenten Endothelzellen vermindert ist, was auf eine reduzierte, aktive Phosphorylierung sowie Proteinexpression der eNOS zurückzuführen ist (siehe Kapitel 2.6 Chronische Entzündung, Alterung und Endothelzellseneszenz) (Hoffmann et al. 2001). Die Funktionen von NO schließen die Instandhaltung der vaskulären Homöostase und die Regulierung des vaskulären Tonus ein, weswegen eine verminderte NO-Produktion schwerwiegende Folgen für das endotheliale Gleichgewicht hat (Tousoulis *et al.* 2012). Außerdem ist eine ausbalancierte Redox-Homöostase notwendig, um den Körper vor akkumulierenden Schäden zu bewahren, die durch oxidativen Stress verursacht werden. In diesem Zusammenhang ist das bereits beschriebene Thioredoxin-1 System von großer Bedeutung für das Endothel, da es oxidierte Proteine wieder reduziert und somit die Folgen, induziert durch oxidativen Stress, mindert (siehe Kapitel 2.4 Oxidativer Stress).

In vorangehenden Studien wurde in einem durch H_2O_2-induzierten Seneszenz-Modell gezeigt, dass die Menge an Trx-1 Protein in seneszenten Endothelzellen vermindert war (Goy et al. 2014). Der Abbau von Trx-1 erfolgt über die lysosomale Asparagin-Endopeptidase Cathepsin D und führt zur Induktion der Apoptose und der Gefährdung der endothelialen Integrität (Benes et al. 2008). Weiterhin konnte gezeigt werden, dass die permanente, lentivirale Trx-1 Expression die Seneszenz-Entstehung inhibiert (Goy *et al.* 2014). Dementsprechend ist die Entstehung der Seneszenz eng mit Veränderungen des Redox-Status in den Endothelzellen verknüpft (**Merk** *et al.* 2024). Im Zusammenhang mit einer Seneszenz-Entstehung darf der Einfluss der Ernährung und von äußeren Umweltfaktoren nicht unberücksichtigt bleiben. So wurde gezeigt, dass sowohl 100 mg/dL LDL als auch ultrafeine Kohlenstoffpartikel Seneszenz in primären Endothelzellen induzieren (Buchner et al. 2013). Wie bereits erwähnt können geringe LPS-Konzentrationen im Blutstrom, ausgelöst durch Faktoren wie ungesunde Ernährung, Übergewicht und Alterung, zur Bildung einer Niedrig-Dosis Endotoxämie führen (Opal *et al.* 2013). Diese wird durch den vermehrten Transport von LPS aus dem Darm in den Blutstrom induziert (Neves et al. 2013). Das Auftreten der Niedrig-Dosis Endotoxämie wird zudem von einem Anstieg an inflammatorischen Zytokinen begleitet, was die Entstehung von oxidativem Stress und Entzündungen indiziert, welche bei der Entstehung der Seneszenz eine grundlegende Rolle spielen (Cani et al. 2007). Die Induktion der Seneszenz führt zu verminderter mitochondrialer Funktion, was die ATP-Produktion und Migration einschränkt (Gonnissen *et al.*

2019). Mit diesem Wissen ist es vorstellbar, dass eine Therapie, welche den oxidativen Stress in Endothelzellen mindert, die Mitochondrien-Funktion und die migratorische Kapazität verbessert, der Seneszenzentstehung entgegenwirken könnte.

5.2 Effekt von Koffein

Es wurde bereits nachgewiesen, dass eine Kurzzeitbehandlung mit Koffein die migratorische Kapazität von Endothelzellen verbessert (Spyridopoulos *et al.* 2008). Koffein beinhaltet ein weites Spektrum an biologisch aktiven Molekülen, von denen bekannt ist, dass sie den Glukose- und Fettmetabolismus fördern, das Darmmikrobiom unterstützen oder oxidativen Stress vermindern können (Vitaglione et al. 2010,Jaquet et al. 2009,Correa et al. 2012). Es ist demnach nicht verwunderlich, dass die positiven Effekte von Koffein auf die Mortalitätsrate für unterschiedliche Herzkreislauf-Erkrankungen gezeigt werden konnten. Dieser Effekt war vor allem bei kardiovaskulären Erkrankungen, welche mit endothelialer Dysfunktion einhergehen, zu beobachten und das Ausmaß der schützenden Eigenschaften des Koffeins hing direkt mit dessen Dosis zusammen (Freedman et al. 2012). Der molekulare Mechanismus, über welchen Koffein wirkt, wurde in vorangehenden Studien aufgezeigt. Koffein verstärkt die Translokation von p27, einem Zellzyklus-Inhibitor, in die Mitochondrien, wodurch deren Funktion verbessert wird. Bewiesen wurde dies, da die Aktivität der Elektronentransportkette in Mäusen, die eine Koffeinbehandlung erhalten hatten, stark erhöht war. Dieser Effekt konnte nicht in p27-defizienten Mäusen beobachtet werden, woraus geschlossen werden kann, dass der Effekt von Koffein über die p27-Translokation in die Mitochondrien vermittelt wird (Ale-Agha et al. 2018).

5.3 Koffein verhindert LPS-induzierte Seneszenz in Endothelzellen

Wie bereits erwähnt konnte Seneszenz in Endothelzellen auch durch die Behandlung mit 100 mg/dL LDL induziert werden (Buchner *et al.* 2013). Es ist zudem bekannt, dass eine fettreiche Ernährung (*high fat diet*, HFD) die Entstehung von Diabetes, Insulin-Resistenz und den Anstieg an LDL zur Folge hat (Buren et al. 2021). Außerdem konnte gezeigt werden, dass diese Form der Ernährung zu bis zu 1 ng/mL LPS im Blutstrom führt (Cani *et al.* 2007). LPS kommt natürlich auf den gram-negativen Bakterien der Darmflora vor, wird aber auch durch die Nahrung aufgenommen. Es wurde nachgewiesen, dass unter physiologischen Bedingungen LPS im menschlichen Darm vorhanden ist, jedoch kleinere Mengen regelmäßig in den Blutkreislauf gelangen (**Merk** *et al.* 2024,Moreira et al. 2012). Eine HFD kann jedoch die Balance der Darmflora beeinträchtigen und zum Verlust der Darmintegrität und einem Anstieg an LPS im Blutkreislauf führen, was die Entstehung der Niedrig-Dosis Endotoxämie, auch metabolische Endotoxämie genannt, induziert (Mohr et al. 2022). Diese metabolische Endotoxämie geht mit einer systemischen Inflammation einher, welche neben Leukozyten auch Endothelzellen betrifft (Violi et al. 2023). Mit dem Wissen, dass hohe LDL-Konzentrationen einhergehend mit verminderter mitochondrialer Funktion und migratorischer Kapazität zur Induktion der Seneszenz führen (Gonnissen *et al.* 2019), wurde untersucht, ob die metabolische Endotoxämie mit 1 ng/mL LPS Seneszenz in Endothelzellen induzieren kann. Zudem sollte die Rolle von Koffein

in diesem Szenario beleuchtet werden. Hierfür wurden Endothelzellen zur Seneszenz-Induktion mit LPS (1 ng/mL) für 2 Wochen, jeden zweiten Tag behandelt. Als Kontrolle wurde detoxifiziertes LPS verwendet. Dies führte zum einen zum Anstieg von p21 und ROS und zum anderen zu verminderten Protein-Level von eNOS und Trx-1. Der Anstieg an ROS wurde durch die Messung von Dihydroethidium und mitoSOX bestimmt (Abbildung 9: Niedrig-Dosis Endotoxämie führt zu einem Anstieg an ROS). Gemeinsam mit den verminderten Trx-1 Protein-Leveln spricht dieser Befund für eine gestörte Redox-Balance und spiegelt den durch LPS-induzierten oxidativen Stress wider. Interessanterweise verändert LPS nicht die mRNA-Level an Trx-1, was dafürspricht, dass LPS zur Degradation des Proteins führt (**Merk** *et al.* 2023).

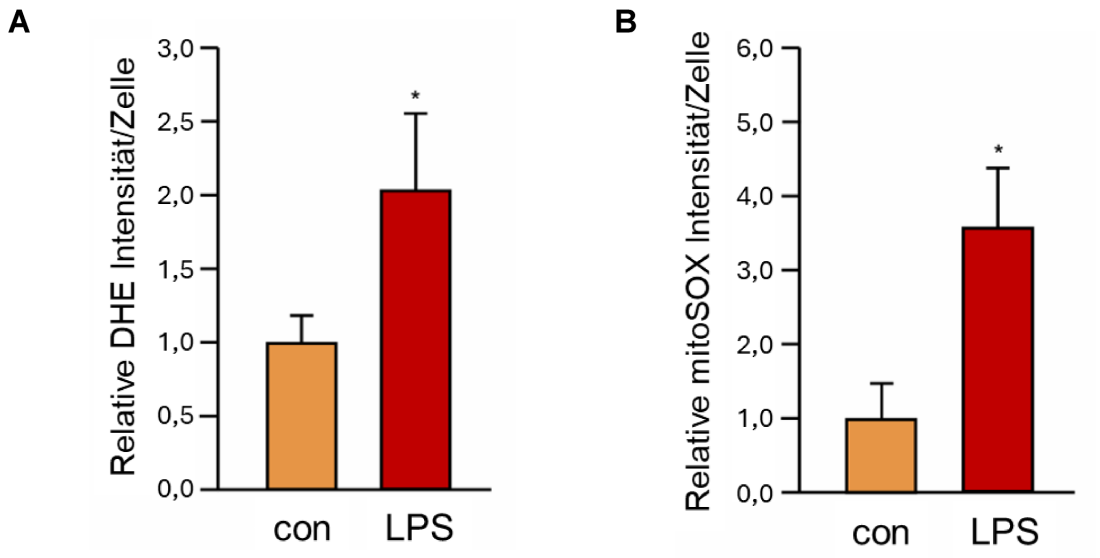

Abbildung 9: Niedrig-Dosis Endotoxämie führt zu einem Anstieg an ROS. Endothelzellen wurden mit 1 ng/mL detoxifiziertem (con) oder aktivem LPS (LPS) jeden zweiten Tag über einen Zeitraum von zwei Wochen behandelt. Die relativen (A) Dihydroethidium (DHE) oder (B) mitochondrialem Superoxid-Indikator (mitoSOX) Intensitäten wurden mit Image J gemessen und die Gesamt-Zellzahl zur Normalisierung verwendet (Fehlerabweichung wird als ± SEM dargestellt. n = 3, p < 0,05 vs. con, zweiseitiger gepaarter t-Test).*

Zur Untersuchung der Rolle von Koffein bei der Niedrig-Dosis Endotoxämie wurden die Zellen mit LPS und Koffein für 2 Wochen co-inkubiert. Die Koffein Co-Behandlung brachte die p21, eNOS und Trx-1 Protein-Level in den LPS-behandelten Zellen auf das der Detox-Kontrolle (Abbildung 10: Koffein inhibiert LPS-induzierte Seneszenz). Dies zeigt, dass Koffein die LPS-induzierte Seneszenz inhibieren und den zellulären Redox-Status wiederherstellen kann (**Merk** *et al.* 2023).

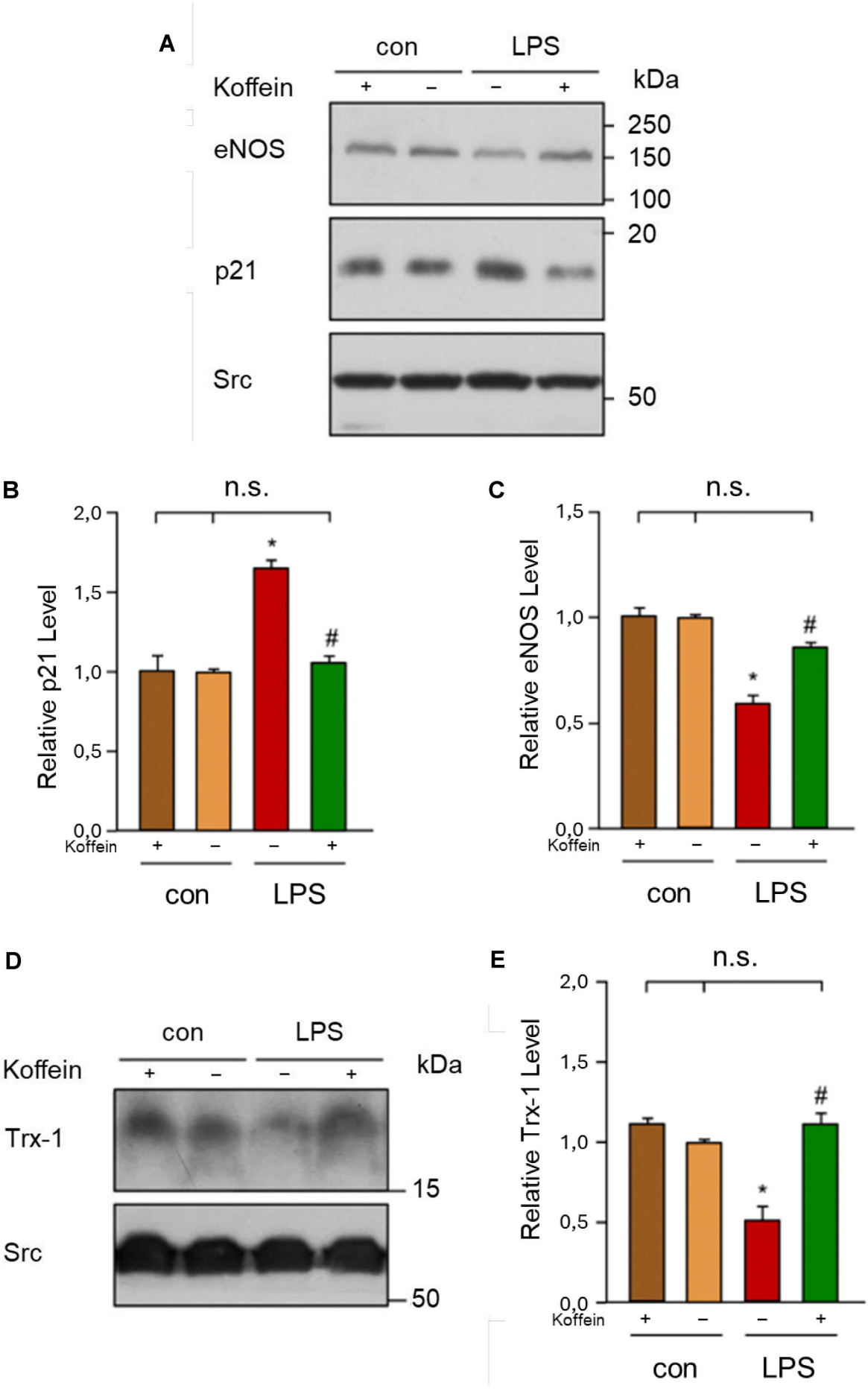
A
con
LPS
Koffein
+ – – +
kDa
eNOS
250
150
100
p21
20
Src
50
B
n.s.
Relative p21 Level
2,0
1,5
1,0
0,5
0,0
*
#
Koffein + – – +
con
LPS
C
n.s.
Relative eNOS Level
1,5
1,0
0,5
0,0
*
#
Koffein + – – +
con
LPS
D
con
LPS
Koffein
+ – – +
kDa
Trx-1
15
Src
50
E
n.s.
Relative Trx-1 Level
2,0
1,5
1,0
0,5
0,0
*
#
Koffein + – – +
con
LPS

Abbildung 10: Koffein inhibiert LPS-induzierte Seneszenz. (A-E) Endothelzellen wurden mit 1 ng/mL detoxifiziertem (con) oder aktivem LPS (LPS) und 10 µM Koffein jeden zweiten Tag über einen Zeitraum von zwei Wochen behandelt. Die Kontrollen mit detoxifiziertem LPS und die LPS-behandelten Gruppen erhielten Koffein (+) oder nicht (-). (A) Repräsentativer Western Blot für eNOS (oben), p21 (mitte), Src (unten). (B-C) Semi-quantitative Analyse der relativen p21 (B) und eNOS (C) Level (Fehlerabweichung wird als ± SEM dargestellt. n = 4, p < 0.05 vs. con, #p < 0,05 vs. LPS ohne Koffein, n.s. = nicht signifikant, one-way ANOVA mit post hoc Tukey LSD Test). (D) Repräsentativer Western Blot für Trx-1 (oben) und Src (unten). (E) Semi-quantitative Analyse der relativen Trx-1 Level (Fehlerabweichung wird als ± SEM dargestellt. n = 4, p* < 0.05 vs. con, #p < 0,05 vs. LPS ohne Koffein, n.s. = nicht signifikant, one-way ANOVA mit post hoc Tukey LSD Test).*

Die Verwendung eines sogenannten „scratch-wound Assays" erlaubte es die Migrations-Fähigkeit der Endothelzellen nach LPS und Koffeinbehandlung zu untersuchen. Dieser Assay weist die migratorische Kapazität der Endothelzellen nach und spiegelt die Endothelzell-Funktionalität wider. Die Behandlung mit LPS führte zu einer Migration der Endothelzellen, welche jedoch durch die Co-Behandlung mit Koffein wiederhergestellt werden konnte (Abbildung 11: Koffein wirkt der Einschränkung der migratorischen Kapazität nach LPS-induzierter Seneszenz entgegen).

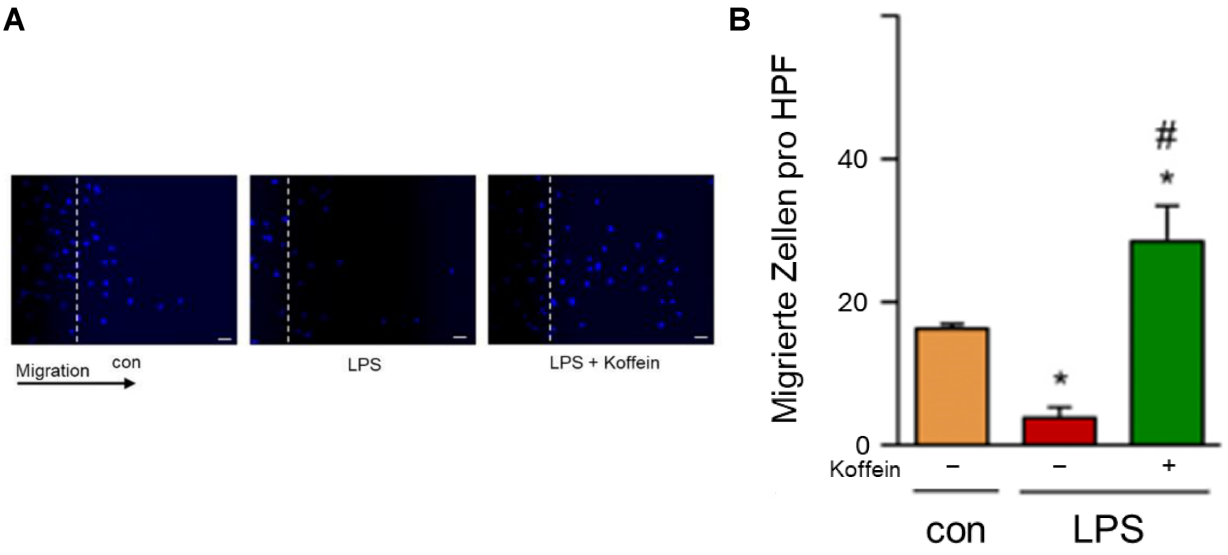

Abbildung 11: Koffein wirkt der Einschränkung der migratorischen Kapazität nach LPS-induzierter Seneszenz entgegen. (A,B) Endothelzellen wurden mit 1 ng/mL detoxifiziertem (con) oder aktivem LPS (LPS) und 10 µM Koffein jeden zweiten Tag über einen Zeitraum von zwei Wochen behandelt. Die LPS-behandelten Gruppen erhielten Koffein (+) oder nicht (-). (A) Repräsentative DAPI-Färbung (Skala = 50 µm). (B) Semi-quantitative Analyse der migrierten Zellen pro Hochenergiebereich (high power field, HPF) (Fehlerabweichung wird als ± SEM dargestellt. n = 4, p < 0,05 vs. con, #p < 0,05 vs. LPS ohne Koffein, one-way ANOVA mit post hoc Tukey LSD Test).*

Die Tatsache, dass Koffein die Migration von Endothelzellen durch die Translokation von p27 in die Mitochondrien verbessert, legt die Annahme nahe, dass der Seneszenz-inhibierende Effekt von Koffein über mitochondriales p27 (mito p27) vermittelt wird (**Merk** *et al.* 2023,Ale-Agha *et al.* 2018).

5.4 Permanente Expression von mitochondrialem p27 inhibiert die LPS-induzierte Seneszenz-Induktion

Um zu untersuchen, ob eine permanente Expression von mito p27 die LPS-induzierte Seneszenz inhibieren kann, wurde nur in Mitochondrien lokalisiertes p27 lentiviral in Endothelzellen

exprimiert und anschließend mit LPS behandelt. Diese ausschließliche Lokalisation in den Mitochondrien wurde durch das im Expressionsvektor vorhandene myc-Tag nachgewiesen. Außerdem führte die LPS-Behandlung weder zur Veränderung des mito p27 Transkripts noch des Protein-Levels (Abbildung 12: mito p27 Transkript- und Protein-Level werden nicht durch LPS beeinflusst.) (**Merk** *et al.* 2023).

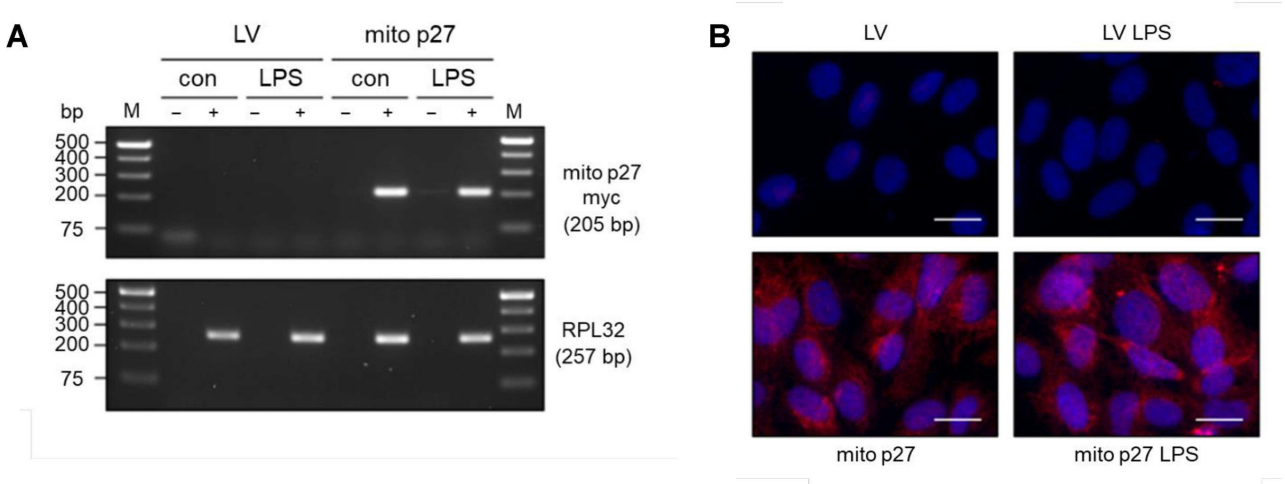

Abbildung 12: mito p27 Transkript- und Protein-Level werden nicht durch LPS beeinflusst. (A,B) Endothelzellen wurden mit einem lentiviralen Expressionsvektor für mitochondrielles p27 mit einem C-terminalen myc-Epitop-Tag (mito p27) oder einem entsprechenden Leervirus (LV) transduziert. Anschließend wurden diese mit 1 ng/mL detoxifiziertem (con) oder aktivem LPS (LPS) jeden zweiten Tag über einen Zeitraum von zwei Wochen behandelt. (A) Die Expression von mito p27 wurde durch eine reverse Transkriptions-PCR analysiert. Hierfür wurde RNA der transduzierten Zellen isoliert und cDNA synthetisiert wobei reverse Transkriptase beigefügt (+) wurde oder nicht enthalten (-) war. Die Amplifizierung erfolgte mit Primern, welche das mito p27 myc Transkript spezifisch detektierten, während RPL32 als Kontrolle diente. Die Amplifikationsprodukte wurden mithilfe einer Agarose-Gelelektrophorese aufgetrennt. Die zu erwartenden Produkte wurden identifiziert. DNA-Marker werden in den beiden äußeren Spuren geladen (M). (B) Repräsentative Immunfärbungen (Skala = 20 µm). Endothelzellen wurden mit einem Antikörper gegen das myc-Tag im mito p27 (rot) gefärbt. Zellkerne wurden mit DAPI (blau) gefärbt.

Die mito p27-Expression verringerte die durch LPS-induzierte p21 Hochregulierung und Trx-1 Herunterregulierung im Vergleich zu Leervektor (EV) transduzierten Zellen (Abbildung 13: mito p27 inhibiert die LPS-induzierte Entstehung der Seneszenz). Dies zeigt, dass die die Erhöhung der mitochondrialen Menge an p27 in Endothelzellen vor der LPS-induzierten Seneszenz-Entstehung schützen kann (**Merk** *et al.* 2023).

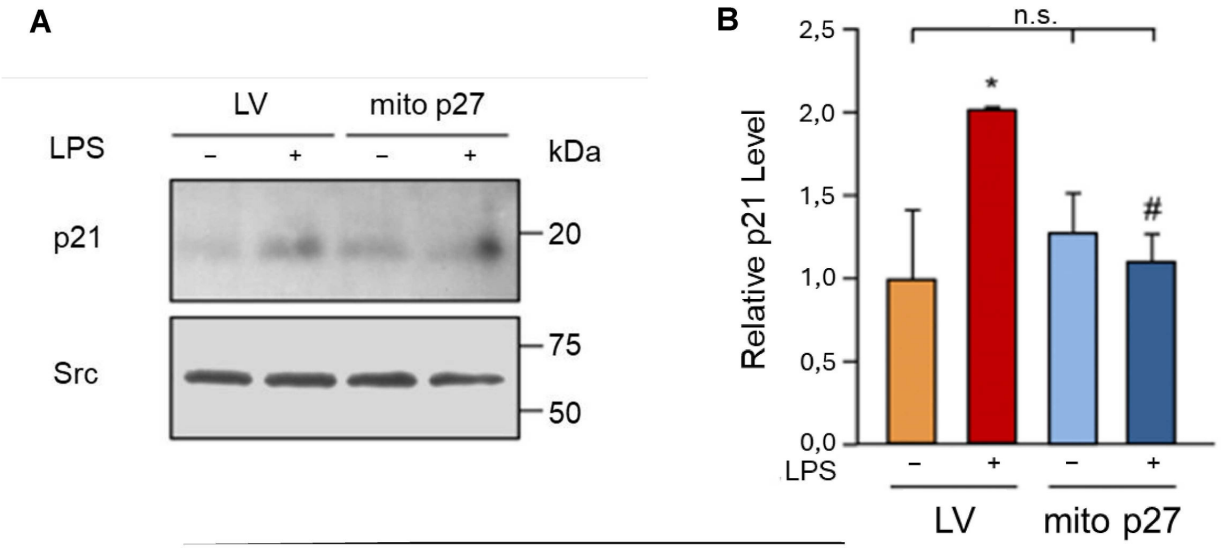

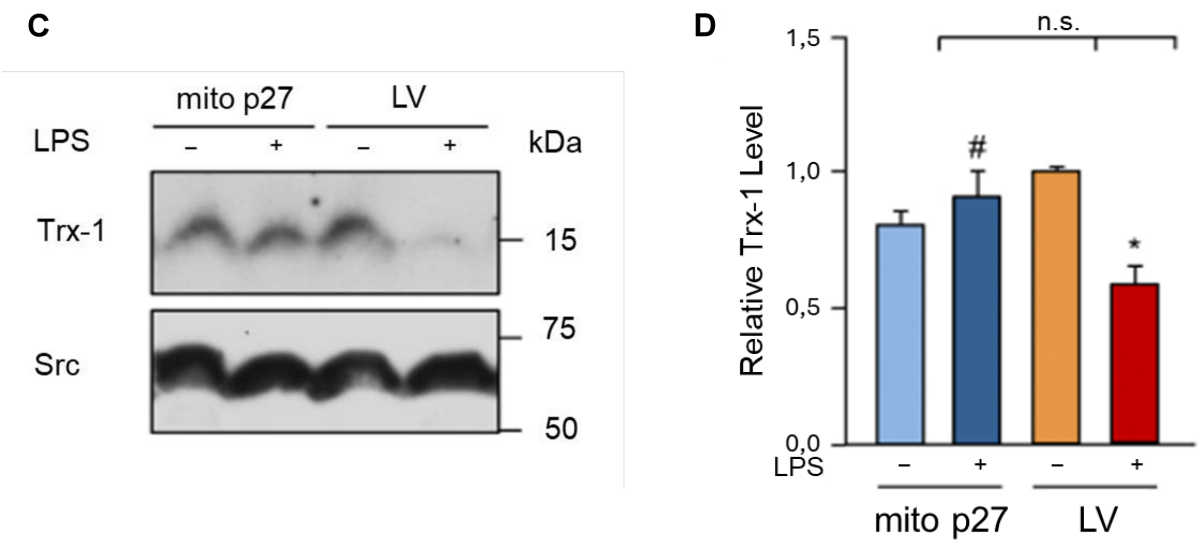

Abbildung 13: mito p27 inhibiert die LPS-induzierte Entstehung der Seneszenz. (A-D) Endothelzellen wurden mit einem lentiviralen Expressionsvektor für mitochondrielles p27 mit einem C-terminalen myc-Epitop-Tag (mito p27) oder einem entsprechenden Leervirus (LV) transduziert. Anschließend wurden diese mit 1 ng/mL detoxifiziertem (-) oder aktivem LPS (+) jeden zweiten Tag über einen Zeitraum von zwei Wochen behandelt. (A,B) p21 wurde durch Western Blots detektiert wobei Src als Ladekontrolle fungierte. (A) Repräsentativer Western Blot für p21 (oben) und Src (unten). (B) Semi-quantitative Analyse der relativen p21 Level (Fehlerabweichung wird als ±SEM dargestellt. n = 3, p < 0,05 vs. LV ohne LPS, #p < 0,05 vs. LV mit LPS, n.s. = nicht signifikant, one-way ANOVA mit post hoc Tukey LSD Test). (C,D) Trx-1 wurde durch Western Blots detektiert wobei Src als Ladekontrolle fungierte. (C) Repräsentativer Western Blot für Trx-1 (oben) und Src (unten). (D) Semi-quantitative Analyse der relativen Trx-1 Level (Fehlerabweichung wird als ±SEM dargestellt. n = 3, p* < 0,05 vs. LV ohne LPS, #p < 0,05 vs. LV mit LPS, n.s. = nicht signifikant, one-way ANOVA mit post hoc Tukey LSD Test).*

5.5 Koffein kann die LPS-induzierte Seneszenz in Endothelzellen umkehren

Da die Entstehung der Seneszenz ein fortlaufender Prozess während der Alterung ist, wäre ein therapeutischer Ansatz, der die endotheliale Seneszenz zumindest verzögert, von großem Nutzen. Um dies zu untersuchen wurde Seneszenz in Endothelzellen wie zuvor durch die Behandlung mit LPS induziert. Im Gegensatz zu den zuvor beschriebenen präventiven Co-Behandlungen mit Koffein, wurde Koffein nun nur ein einziges Mal in höherer Konzentration (50 µM) nach 12 Tagen der LPS-Behandlung zu den Endothelzellen gegeben, was einem therapeutischen Ansatz entspricht. Es wurde zuvor gezeigt, dass diese Menge an Koffein die Atmungskettenaktivität in den Mitochondrien und die migratorische Kapazität von Endothelzellen verbessert (Spyridopoulos *et al.* 2008,Ale-Agha *et al.* 2018). Außerdem wurde nachgewiesen, dass eine solche Menge an Koffein die Aktivität der Atmungskette in Herz-Mitochondrien von 24 Monate alten Mäusen verbessert und auf das Niveau von 6 Monate alten Mäusen bringt (Ale-Agha *et al.* 2018). Interessanterweise führte diese einzelne therapeutische Koffein-Behandlung zu verminderten p21 und erhöhten Trx-1 Leveln im Vergleich zu den LPS behandelten Proben. Dies beweist, dass eine einzelne Behandlung mit Koffein die LPS-induzierte Seneszenz-Entstehung verhindert oder zumindest verzögert und die Redox-Balance verbessert (Abbildung 14: Koffein kann die LPS-induzierte Seneszenz-Entstehung umkehren und Trx-1 Level wiederherstellen.) (**Merk** *et al.* 2023).

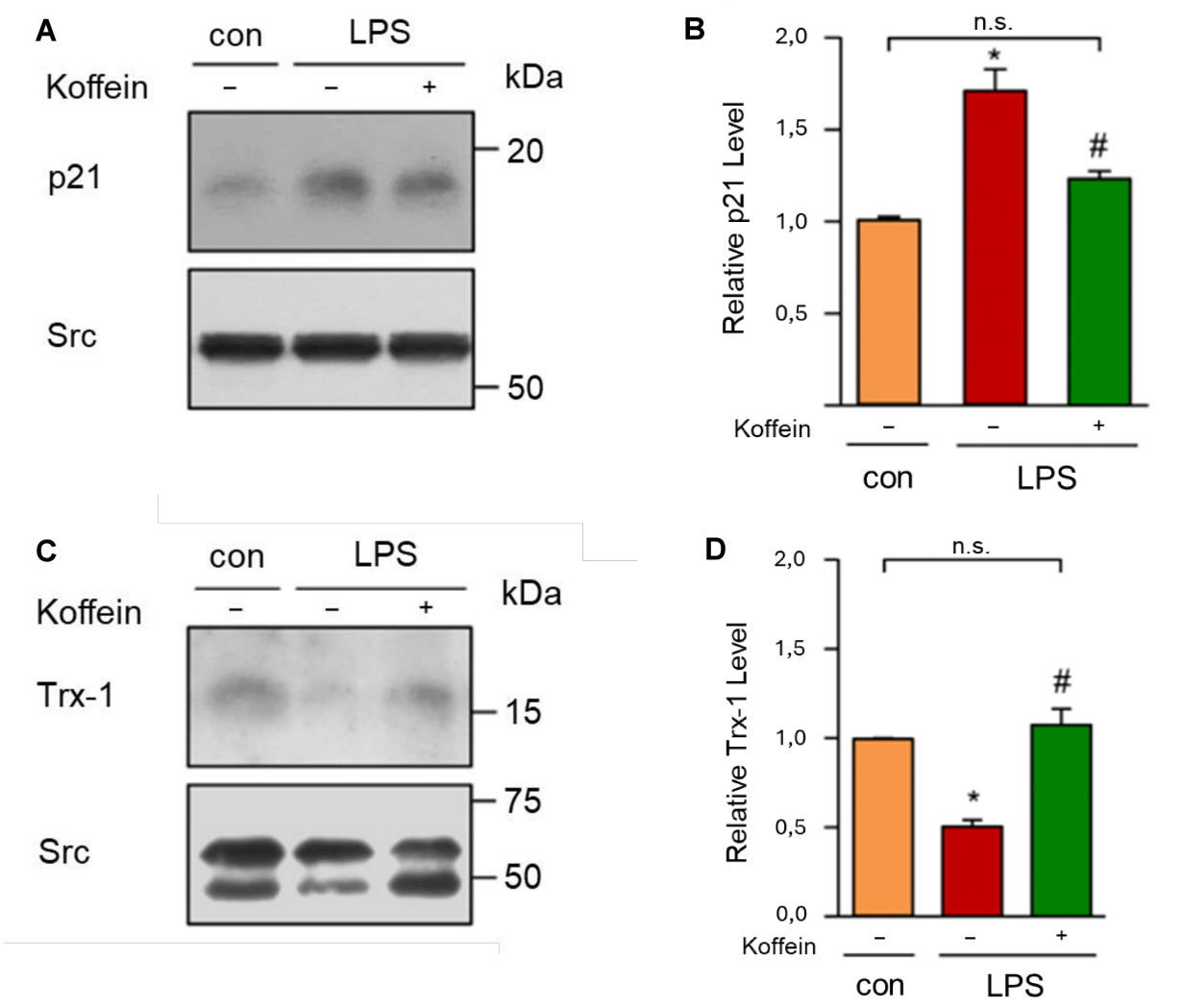

Abbildung 14: Koffein kann die LPS-induzierte Seneszenz-Entstehung umkehren und Trx-1 Level wiederherstellen. (A-D) Endothelzellen wurden mit 1 ng/mL detoxifiziertem (con) oder aktivem LPS (LPS) jeden zweiten Tag über einen Zeitraum von zwei Wochen behandelt. Am letzten Behandlungstag wurde eine einmalige Behandlung mit 50 µM Koffein durchgeführt. Die LPS-behandelten Zellen erhielten Koffein (+) oder nicht (-). (A,B) p21 wurde durch Western Blots detektiert wobei Src als Ladekontrolle fungierte. (A) Repräsentativer Western Blot für p21 (oben) und Src (unten). (B) Semi-quantitative Analyse der relativen p21 Level (Fehlerabweichung wird als ± SEM dargestellt. n = 5, p < 0,05 vs. con, #p < 0,05 vs. LPS ohne Koffein, n.s. = nicht signifikant, one-way ANOVA mit post hoc Tukey LSD Test). (C,D) Trx-1 wurde durch Western Blots detektiert wobei Src als Ladekontrolle fungierte. (C) Repräsentativer Western Blot für Trx-1 (oben) und Src (unten). (D) Semi-quantitative Analyse der relativen Trx-1 Level (Fehlerabweichung wird als ± SEM dargestellt. n = 4, p* < 0,05 vs. con, #p < 0,05 vs. LPS ohne Koffein, n.s. = nicht signifikant, one-way ANOVA mit post hoc Tukey LSD Test).*

Diese Untersuchungen zeigten zum ersten Mal, dass Koffein die LPS-induzierte Seneszenz-Entstehung verhindern oder zumindest verzögern kann. Dieser Effekt wurde erreicht, indem Koffein die Redox-Homöostase durch verminderte Degradierung von Trx-1 aufrechterhalten konnte. Da die Entstehung der Seneszenz zur Bildung der endothelialen Dysfunktion führen kann, welche in fast allen kardiovaskulären Erkrankungen eine wichtige Rolle spielt, könnte der Effekt von Koffein genutzt werden, um eine Seneszenz-Induktion und damit möglicherweise den Alterungsprozess hinauszuzögern (**Merk** *et al.* 2023).

6. Ausblick

Ziel dieser Doktorarbeit war es, den Einfluss der Ernährung und im speziellen von LPS auf die Funktionalität des Endothels zu untersuchen.

Im ersten Teil der Doktorarbeit wurde die Entstehung und Progression der NAFLD erforscht und die AAV8-vermittelte Expression von scFv-E06 als möglicher Therapieansatz untersucht. Hier konnte gezeigt werden, dass diese AAV8-vermittelte Expression von scFv-E06 in der Leber zur Eliminierung von bestimmten oxPC-Spezies führt (Upchurch,**… Merk** *et al.* 2022). Da oxPCs die Genexpression von Leberzellen verändern und den bioenergetischen Status beeinträchtigen, ist deren Eliminierung folglich ein möglicher therapeutischer Ansatz zur Inhibierung der NAFLD-Progression. Neben der Veränderung der Genexpression von Leberzellen könnten oxPCs zudem die Genexpression in Endothelzellen verändern. Untersuchungen der Regulation von Genen nach oxPC-Behandlung könnten mit Hilfe von RNA-deep sequencing weitere Gene aufdecken, welche zum Schutz von Endothelzellen hochreguliert werden und somit als Zielgene für therapeutische Ansätze identifiziert werden. Weiterhin könnten kardiovaskuläre Krankheiten, bei welchen durch oxidativen Stress die Oxidation von Lipiden erfolgt (Bsp. Atherosklerose), mithilfe der etablierten FPC-Ernährung untersucht werden (Zhong et al. 2019). Da diese oxidierten Lipide zur Inflammation beitragen, welche wie bereits gezeigt, auch zur Seneszenz von Endothelzellen führen kann, könnte dieses Modell zudem verwendet werden, um den Einfluss von ungesunder Ernährung auf Endothelzellseneszenz *in vivo* zu untersuchen. In einem darauffolgenden Schritt wäre hierbei der Effekt von scFv-E06 zur Prävention von Endothelzellseneszenz oder möglicherweise auch in einem therapeutischen Ansatz zur Umkehr der Seneszenz interessant.

Im zweiten Teil dieser Doktorarbeit wurden die Auswirkungen von LPS auf das Transkriptom von primären humanen Endothelzellen untersucht. Es konnte gezeigt werden, dass SELENOT als wichtiger Mediator der protektiven Effekte von APEX1 (1-20) fungiert und die Aktivierung und Apoptose von Endothelzellen inhibiert. Demnach könnten sowohl SELENOT als auch APEX1 (1-20) als potenzielle Therapieansätze für die Behandlung von LPS-induzierten Pathologien verwendet werden. Die weitere Untersuchung der SELENOT-vermittelten Effekte könnte Aufschluss auf die genauen molekularen Funktionen von SELENOT geben. In diesem Zusammenhang wurde von anderen Arbeitsgruppen ein SELENOT-Peptid synthetisiert, welches das Herz vor Ischämie und Reperfusions (I/R)-Schäden in Mäusen schützen kann. Auch in diesen Untersuchungen konnte der protektive Einfluss des SELENOT-Peptids auf die Verminderung von oxidativem Stress und der Inhibierung der Apoptose erzielt werden (Rocca et al. 2018). Dieses Peptid konnte außerdem in einer Zell-permeablen Form in einem Maus-Modell für Parkinson dopaminerge Neuronen schützen, was auch durch verminderten oxidativen Stress und Apoptose-Inhibierung gezeigt wurde (Alsharif et al. 2021). Da SELENOT in diesen unterschiedlichen Organen einen schützenden Effekt ausübt ist die Annahme naheliegend, dass dies auch im Endothel während Sepsis geschieht. Dies könnte durch Verwendung des SELENOT-Peptids untersucht werden.

Die Eigenschaft von APEX1 (1-20) Endothelzellen vor LPS-induzierter Aktivierung und Apoptose zu schützen, könnte, nachdem diese *ex vivo* nachgewiesen wurde, auch *in vivo* vorhanden sein. Tatsächlich führte eine Behandlung mit einem synthetisierten APEX1 (1-20) Peptid eine Stunde nach LPS-induzierter Endotoxämie in Mäusen zu einer verminderten Endothelzell-Aktivierung. Weiterhin könnte die Bestimmung der Apoptose in wie zuvor beschrieben behandelten Mäusen, durch Bestimmung der Protein-Level an gespaltener und damit aktiver Caspase 3, Hinweise auf die endotheliale Integrität und Dysfunktion geben. Nachfolgende Untersuchungen könnten somit den Einfluss des APEX1 (1-20) Peptids auf die Vermeidung der endothelialen Dysfunktion aufzeigen.

Im letzten Teil dieser Doktorarbeit wurden die Auswirkungen der Niedrig-Dosis Endotoxämie auf die Stress-induzierte frühzeitige Seneszenz in Endothelzellen und der protektive Effekt von Koffein untersucht. Tatsächlich induzierte die langfristige LPS-Behandlung die Entstehung der Endothelzellseneszenz, was zur Einschränkung der Endothelzellfunktion und deren migratorischen Kapazität führte. Sowohl die präventive als auch die therapeutische Behandlung mit Koffein verhinderte die Entstehung der Seneszenz, bzw. führte zu deren Rückbildung (**Merk** *et al.* 2023). Dieser Effekt wurde durch die Aufrechterhaltung der eNOS- und Trx-1 Level erreicht, was die migratorische Kapazität der Endothelzellen verbesserte und deren Redox-Homöostase aufrechterhielt. Der Mechanismus, durch welchen Koffein dies erreicht, ist weiterhin nicht erforscht. Der Verlust von Trx-1 und damit der Verlust des Redox-Gleichgewichtes geht in seneszenten Endothelzellen mit einer erhöhten Cathepsin D Aktivität einher. Es wurde gezeigt, dass die mitochondriale Atmungskette die lysosomale Funktion kontrolliert und eine Beeinträchtigung dieser zu einem Anstieg der lysosomalen Kompartimente führt (Baixauli et al. 2015). Dementsprechend könnte ein möglicher Mechanismus die Inhibierung der lysosomalen Aktivität sein, durch welchen Koffein die Trx-1 Level aufrechterhält bzw. wiederherstellt. Diese Annahme wird unterstützt durch die Tatsache, dass LPS sowohl in hohen als auch in niedrigen Dosen nicht zu einer Veränderung der mRNA-Level von Trx-1 führt, sondern die Degradierung auf Protein-Level geschehen muss (**Merk** *et al.* 2023). Weiterhin wäre der Einfluss von LPS auf Trx-2, das mitochondriale Analog von Trx-1, interessant. Im Unterschied zu Trx-1 besitzt Trx-2 keine zusätzlichen Cystein-Reste außerhalb des aktiven Zentrums. Dies hat den Vorteil, dass Trx-2 weniger anfällig für oxidativen Stress ist, da die Oxidation dieser Cystein-Reste die enzymatische Aktivität von Thioredoxin inhibiert (Holmgren and Lu 2010). Das aus Trx-2, der zugehörigen mitochondrialen Thioredoxin-Reduktase und der mitochondrialen Thioredoxin-Peroxidase (Peroxiredoxin III) bestehende System, gilt als wichtiges antioxidatives System in den Mitochondrien. Demnach ist es nicht verwunderlich, dass Trx-2 defiziente Zellen einen Anstieg an intrazellulären ROS aufweisen. Außerdem ist in diesen Zellen die Apoptose stark erhöht was dafürspricht, dass das Trx-2-Peroxiredoxin III-System in den Mitochondrien eine wichtige Rolle für den mitochondrialen Apoptose-Signalweg spielt (Tanaka et al. 2002). Zukünftig wäre somit interessant, ob dieser Effekt auch in den Mitochondrien von Endothelzellen auftaucht und die Überexpression den LPS-induzierten Veränderungen entgegenwirken könnte.

Zusammengefasst stellt die Akkumulierung von ROS und dem daraus resultierenden oxidativen Stress eine große Belastung für den menschlichen Organismus dar. Dies kann an chronischen Erkrankungen wie der NAFLD oder der Entstehung der Seneszenz, aber auch an akuten Pathologien wie Sepsis und septischem Schock, beobachtet werden. Therapiemöglichkeiten, welche die durch ROS-induzierten Schäden verhindern und somit zur Verbesserung der endothelialen Funktion und zur Inhibierung der jeweiligen Krankheitsprogression führen, sollten in zukünftigen Untersuchungen die Aufmerksamkeit zugesprochen bekommen, die sie verdienen.

7. Zusammenfassung

Herzkreislauferkrankungen sind die weltweit führende Ursache von Morbidität und Mortalität. Bei der Pathogenese dieser Erkrankungen spielt die Fehlfunktion des Endothels, der innersten Schicht aller Blutgefäße, eine kritische Rolle. Ziel dieser Arbeit war es Faktoren zu untersuchen, welche zur endothelialen Dysfunktion führen können und Therapiemöglichkeiten zu identifizieren, um dieser entgegenzuwirken. Dafür wurde der Einfluss hoher und niedriger LPS-Konzentrationen auf das Endothel untersucht, die sich im Rahmen einer Sepsis und durch ungesunde Ernährung ergeben. Bei der Entstehung der nicht-alkoholischen Fettleber-Erkrankung (NAFLD) wurde die AAV8-vermittelte Expression von scFv-E06 als möglicher Therapieansatz untersucht. Es konnte in einem Ernährungsmodell gezeigt werden, dass oxidierte Phosphatidylcholine (oxPC) das Entstehen und Fortschreiten der NAFLD fördern und zu einem dysregulierten mitochondrialen Metabolismus und zu veränderter Genexpression führen. Die Elimination dieser oxPC, durch die hepatische Expression von scFv-E06, konnte diese Auswirkungen als therapeutischen Ansatz verhindern. Im Weiteren konnte gezeigt werden, dass in primären Endothelzellen die Konzentrationen von Lipopolysaccharid (LPS), wie sie bei einer Sepsis im Blutstrom gemessen werden, zur Aktivierung und Apoptose führen – beides Merkmale der endothelialen Dysfunktion. In vorangehenden Studien wurde gezeigt, dass APEX1 Endothelzellen vor Apoptose schützt und dafür die ersten 20 Aminosäuren ausreichen. Daher wurden Gene mithilfe des RNA deep sequencing gesucht, welche durch LPS und APEX1 (1-20) hochreguliert wurden. In diesem Screen wurde Selenoprotein T (SELENOT) identifiziert und ein Expressionsvektor generiert, um dessen Einfluss auf die LPS-induzierte Aktivierung und Apoptose von Endothelzellen zu untersuchen. Die Expression von SELENOT führte dabei zur Verhinderung der negativen LPS-Effekte. Daher könnte eine Aktivierung und/oder Erhöhung von SELENOT zur Verhinderung der endothelialen Dysfunktion beitragen. Schließlich wurde der Einfluss von LPS in Konzentrationen, die mit fettreicher Ernährung im Blutstrom erzielt werden, auf die Seneszenz von Endothelzellen untersucht. Diese niedrigen LPS-Konzentrationen induzierten nach 14 Tagen Endothelzellseneszenz. Eine präventive Behandlung mit Koffein wirkte der Entstehung der Endothelzellseneszenz entgegen. Interessanterweise konnte auch eine therapeutische Behandlung mit Koffein nach Induktion der Seneszenz diese reduzieren. Dieser Effekt konnte auch durch die permanente Expression von mitochondrialem p27 als Downstream-Effektor von Koffein erzielt werden. Daher könnte Koffein ebenfalls zur Verbesserung der Endothelfunktion beitragen.

In dieser Arbeit konnten verschiedene Ursachen, die die endotheliale Dysfunktion induzieren, aufgezeigt werden, sowie einige zugrundeliegende Mechanismen identifiziert werden. Daraus könnten mögliche Ansätze zum Erhalt der Funktionen des Endothels abgeleitet werden.

8. Summary

Cardiovascular diseases are the leading cause of morbidity and mortality worldwide. The dysfunction of the endothelium, the innermost layer of all blood vessels, plays a critical role during their pathogenesis. The aim of this dissertation was to investigate factors that can lead to the development of endothelial dysfunction and to identify therapeutic options to counteract this. Therefore, the effect of high- and low-LPS concentrations on the endothelium, due to sepsis and unhealthy diet, was investigated. During the development of the non-alcoholic fatty liver disease (NAFLD) the AAV8-transmitted expression of scFv-E06 as a potential therapeutic approach was investigated. In a dietary model oxidized phosphatidylcholines (oxPCs) were found to promote the development and progression of NAFLD and lead to dysregulated mitochondrial metabolism and altered gene expression. This was inhibited by the elimination of oxPCs by hepatic expression of scFv-E06 as a therapeutic intervention. Furthermore, it was shown that concentrations of lipopolysaccharide (LPS) equal to those measured in the bloodstream of patients during sepsis lead to activation and apoptosis in primary endothelial cells – both characteristics of endothelial dysfunction. In previous studies it was shown that APEX1 protects endothelial cells from apoptosis and that the first 20 amino acids are sufficient for this effect. Therefore, RNA deep sequencing was used to identify genes which are upregulated by LPS and APEX1 (1-20). In this screening selenoprotein T (SELENOT) was revealed and an expression vector was generated to measure its effect on LPS-induced activation and apoptosis of endothelial cells. The expression of SELENOT inhibited the negative LPS-effects, which is why an increase in activity or elevation of SELENOT levels could prevent endothelial dysfunction. Finally, the effect of LPS concentrations measured in the bloodstream during high-fat diet was investigated in the view of endothelial senescence. These low LPS concentrations induced endothelial senescence after 14 days. Preventive treatment with caffeine inhibited the development of endothelial senescence. Interestingly, therapeutic treatment with caffeine also reduced the endothelial senescence after its induction. This effect was also observed by permanent expression of mitochondrial p27 as a downstream effector of caffeine. This leads to the suggestion that caffeine could also improve endothelial function.

In this dissertation different causes of endothelial dysfunction and their underlying mechanisms were identified. These could be used to find therapeutic approaches to improve the maintenance and functions of the endothelium.

9. Literaturverzeichnis

1. Madamanchi, N.R., Vendrov, A., and Runge, M.S. (2005). Oxidative stress and vascular disease. Arterioscler Thromb Vasc Biol *25*, 29-38. 10.1161/01.ATV.0000150649.39934.13.
2. Widmer, R.J., and Lerman, A. (2014). Endothelial dysfunction and cardiovascular disease. Glob Cardiol Sci Pract *2014*, 291-308. 10.5339/gcsp.2014.43.
3. Dubois-Deruy, E., Peugnet, V., Turkieh, A., and Pinet, F. (2020). Oxidative Stress in Cardiovascular Diseases. Antioxidants (Basel) *9*. 10.3390/antiox9090864.
4. Higashi, Y. (2022). Roles of Oxidative Stress and Inflammation in Vascular Endothelial Dysfunction-Related Disease. Antioxidants (Basel) *11*. 10.3390/antiox11101958.
5. Rodgers, J.L., Jones, J., Bolleddu, S.I., Vanthenapalli, S., Rodgers, L.E., Shah, K., Karia, K., and Panguluri, S.K. (2019). Cardiovascular Risks Associated with Gender and Aging. J Cardiovasc Dev Dis *6*. 10.3390/jcdd6020019.
6. Steenman, M., and Lande, G. (2017). Cardiac aging and heart disease in humans. Biophys Rev *9*, 131-137. 10.1007/s12551-017-0255-9.
7. Poredos, P. (2002). Endothelial dysfunction and cardiovascular disease. Pathophysiol Haemost Thromb *32*, 274-277. 10.1159/000073580.
8. Kruger-Genge, A., Blocki, A., Franke, R.P., and Jung, F. (2019). Vascular Endothelial Cell Biology: An Update. Int J Mol Sci *20*. 10.3390/ijms20184411.
9. Pober, J.S., Min, W., and Bradley, J.R. (2009). Mechanisms of endothelial dysfunction, injury, and death. Annu Rev Pathol *4*, 71-95. 10.1146/annurev.pathol.4.110807.092155.
10. Endemann, D.H., and Schiffrin, E.L. (2004). Endothelial dysfunction. J Am Soc Nephrol *15*, 1983-1992. 10.1097/01.ASN.0000132474.50966.DA.
11. Merk, D., Cox, F.F., Jakobs, P., Promel, S., Altschmied, J., and Haendeler, J. (2024). Dose-Dependent Effects of Lipopolysaccharide on the Endothelium-Sepsis versus Metabolic Endotoxemia-Induced Cellular Senescence. Antioxidants (Basel) *13*. 10.3390/antiox13040443.
12. Forstermann, U., and Sessa, W.C. (2012). Nitric oxide synthases: regulation and function. Eur Heart J *33*, 829-837, 837a-837d. 10.1093/eurheartj/ehr304.
13. Alderton, W.K., Cooper, C.E., and Knowles, R.G. (2001). Nitric oxide synthases: structure, function and inhibition. Biochem J *357*, 593-615. 10.1042/0264-6021:3570593.
14. Sandoo, A., van Zanten, J.J., Metsios, G.S., Carroll, D., and Kitas, G.D. (2010). The endothelium and its role in regulating vascular tone. Open Cardiovasc Med J *4*, 302-312. 10.2174/1874192401004010302.
15. Jones, K.A., Wong, G.Y., Jankowski, C.J., Akao, M., and Warner, D.O. (1999). cGMP modulation of Ca2+ sensitivity in airway smooth muscle. Am J Physiol *276*, L35-40. 10.1152/ajplung.1999.276.1.L35.
16. Tousoulis, D., Kampoli, A.M., Tentolouris, C., Papageorgiou, N., and Stefanadis, C. (2012). The role of nitric oxide on endothelial function. Curr Vasc Pharmacol *10*, 4-18. 10.2174/157016112798829760.
17. Aicher, A., Heeschen, C., Mildner-Rihm, C., Urbich, C., Ihling, C., Technau-Ihling, K., Zeiher, A.M., and Dimmeler, S. (2003). Essential role of endothelial nitric oxide synthase for mobilization of stem and progenitor cells. Nat Med *9*, 1370-1376. 10.1038/nm948.
18. Hossain, M., Qadri, S.M., and Liu, L. (2012). Inhibition of nitric oxide synthesis enhances leukocyte rolling and adhesion in human microvasculature. J Inflamm (Lond) *9*, 28. 10.1186/1476-9255-9-28.
19. Liao, J.K. (2013). Linking endothelial dysfunction with endothelial cell activation. J Clin Invest *123*, 540-541. 10.1172/JCI66843.
20. Bruunsgaard, H., Skinhoj, P., Pedersen, A.N., Schroll, M., and Pedersen, B.K. (2000). Ageing, tumour necrosis factor-alpha (TNF-alpha) and atherosclerosis. Clin Exp Immunol *121*, 255-260. 10.1046/j.1365-2249.2000.01281.x.

21. Tanaka, T., Narazaki, M., and Kishimoto, T. (2018). Interleukin (IL-6) Immunotherapy. Cold Spring Harb Perspect Biol *10*. 10.1101/cshperspect.a028456.
22. Sanada, F., Taniyama, Y., Muratsu, J., Otsu, R., Shimizu, H., Rakugi, H., and Morishita, R. (2018). Source of Chronic Inflammation in Aging. Front Cardiovasc Med *5*, 12. 10.3389/fcvm.2018.00012.
23. Theofilis, P., Sagris, M., Oikonomou, E., Antonopoulos, A.S., Siasos, G., Tsioufis, C., and Tousoulis, D. (2021). Inflammatory Mechanisms Contributing to Endothelial Dysfunction. Biomedicines *9*. 10.3390/biomedicines9070781.
24. Sies, H., and Jones, D.P. (2020). Reactive oxygen species (ROS) as pleiotropic physiological signalling agents. Nat Rev Mol Cell Biol *21*, 363-383. 10.1038/s41580-020-0230-3.
25. Schulz, E., Anter, E., and Keaney, J.F., Jr. (2004). Oxidative stress, antioxidants, and endothelial function. Curr Med Chem *11*, 1093-1104. 10.2174/0929867043365369.
26. Man, A.W.C., Li, H., and Xia, N. (2020). Impact of Lifestyles (Diet and Exercise) on Vascular Health: Oxidative Stress and Endothelial Function. Oxid Med Cell Longev *2020*, 1496462. 10.1155/2020/1496462.
27. Fatehi-Hassanabad, Z., Chan, C.B., and Furman, B.L. (2010). Reactive oxygen species and endothelial function in diabetes. Eur J Pharmacol *636*, 8-17. 10.1016/j.ejphar.2010.03.048.
28. Sies, H., Berndt, C., and Jones, D.P. (2017). Oxidative Stress. Annu Rev Biochem *86*, 715-748. 10.1146/annurev-biochem-061516-045037.
29. Li, H., Horke, S., and Forstermann, U. (2014). Vascular oxidative stress, nitric oxide and atherosclerosis. Atherosclerosis *237*, 208-219. 10.1016/j.atherosclerosis.2014.09.001.
30. Miwa, S., St-Pierre, J., Partridge, L., and Brand, M.D. (2003). Superoxide and hydrogen peroxide production by Drosophila mitochondria. Free Radic Biol Med *35*, 938-948. 10.1016/s0891-5849(03)00464-7.
31. Balaban, R.S., Nemoto, S., and Finkel, T. (2005). Mitochondria, oxidants, and aging. Cell *120*, 483-495. 10.1016/j.cell.2005.02.001.
32. Raha, S., and Robinson, B.H. (2000). Mitochondria, oxygen free radicals, disease and ageing. Trends Biochem Sci *25*, 502-508. 10.1016/s0968-0004(00)01674-1.
33. Chance, B., Schoener, B., Oshino, R., Itshak, F., and Nakase, Y. (1979). Oxidation-reduction ratio studies of mitochondria in freeze-trapped samples. NADH and flavoprotein fluorescence signals. J Biol Chem *254*, 4764-4771.
34. Holmgren, A. (2000). Antioxidant function of thioredoxin and glutaredoxin systems. Antioxid Redox Signal *2*, 811-820. 10.1089/ars.2000.2.4-811.
35. Panth, N., Paudel, K.R., and Parajuli, K. (2016). Reactive Oxygen Species: A Key Hallmark of Cardiovascular Disease. Adv Med *2016*, 9152732. 10.1155/2016/9152732.
36. Merk, D., Greulich, J., Vierkant, A., Cox, F., Eckermann, O., von Ameln, F., Dyballa-Rukes, N., Altschmied, J., Ale-Agha, N., Jakobs, P., and Haendeler, J. (2023). Caffeine Inhibits Oxidative Stress- and Low Dose Endotoxemia-Induced Senescence-Role of Thioredoxin-1. Antioxidants (Basel) *12*. 10.3390/antiox12061244.
37. Singer, M., Deutschman, C.S., Seymour, C.W., Shankar-Hari, M., Annane, D., Bauer, M., Bellomo, R., Bernard, G.R., Chiche, J.D., Coopersmith, C.M., et al. (2016). The Third International Consensus Definitions for Sepsis and Septic Shock (Sepsis-3). JAMA *315*, 801-810. 10.1001/jama.2016.0287.
38. Guarino, M., Perna, B., Cesaro, A.E., Maritati, M., Spampinato, M.D., Contini, C., and De Giorgio, R. (2023). 2023 Update on Sepsis and Septic Shock in Adult Patients: Management in the Emergency Department. J Clin Med *12*. 10.3390/jcm12093188.
39. Marshall, J.C. (2014). Why have clinical trials in sepsis failed? Trends Mol Med *20*, 195-203. 10.1016/j.molmed.2014.01.007.
40. Mayr, F.B., Yende, S., and Angus, D.C. (2014). Epidemiology of severe sepsis. Virulence *5*, 4-11. 10.4161/viru.27372.

41. Boutagy, N.E., McMillan, R.P., Frisard, M.I., and Hulver, M.W. (2016). Metabolic endotoxemia with obesity: Is it real and is it relevant? Biochimie *124*, 11-20. 10.1016/j.biochi.2015.06.020.
42. Page, M.J., Kell, D.B., and Pretorius, E. (2022). The Role of Lipopolysaccharide-Induced Cell Signalling in Chronic Inflammation. Chronic Stress (Thousand Oaks) *6*, 24705470221076390. 10.1177/24705470221076390.
43. Molinaro, A., Holst, O., Di Lorenzo, F., Callaghan, M., Nurisso, A., D'Errico, G., Zamyatina, A., Peri, F., Berisio, R., Jerala, R., et al. (2015). Chemistry of lipid A: at the heart of innate immunity. Chemistry *21*, 500-519. 10.1002/chem.201403923.
44. Duan, T., Du, Y., Xing, C., Wang, H.Y., and Wang, R.F. (2022). Toll-Like Receptor Signaling and Its Role in Cell-Mediated Immunity. Front Immunol *13*, 812774. 10.3389/fimmu.2022.812774.
45. Vaure, C., and Liu, Y. (2014). A comparative review of toll-like receptor 4 expression and functionality in different animal species. Front Immunol *5*, 316. 10.3389/fimmu.2014.00316.
46. Poltorak, A., He, X., Smirnova, I., Liu, M.Y., Van Huffel, C., Du, X., Birdwell, D., Alejos, E., Silva, M., Galanos, C., et al. (1998). Defective LPS signaling in C3H/HeJ and C57BL/10ScCr mice: mutations in Tlr4 gene. Science *282*, 2085-2088. 10.1126/science.282.5396.2085.
47. Ryu, J.K., Kim, S.J., Rah, S.H., Kang, J.I., Jung, H.E., Lee, D., Lee, H.K., Lee, J.O., Park, B.S., Yoon, T.Y., and Kim, H.M. (2017). Reconstruction of LPS Transfer Cascade Reveals Structural Determinants within LBP, CD14, and TLR4-MD2 for Efficient LPS Recognition and Transfer. Immunity *46*, 38-50. 10.1016/j.immuni.2016.11.007.
48. Zhang, Y., Liang, X., Bao, X., Xiao, W., and Chen, G. (2022). Toll-like receptor 4 (TLR4) inhibitors: Current research and prospective. Eur J Med Chem *235*, 114291. 10.1016/j.ejmech.2022.114291.
49. Li, S., Strelow, A., Fontana, E.J., and Wesche, H. (2002). IRAK-4: a novel member of the IRAK family with the properties of an IRAK-kinase. Proc Natl Acad Sci U S A *99*, 5567-5572. 10.1073/pnas.082100399.
50. Arch, R.H., Gedrich, R.W., and Thompson, C.B. (1998). Tumor necrosis factor receptor-associated factors (TRAFs) - a family of adaptor proteins that regulates life and death. Gene Dev *12*, 2821-2830. DOI 10.1101/gad.12.18.2821.
51. Shaywitz, A.J., and Greenberg, M.E. (1999). CREB: a stimulus-induced transcription factor activated by a diverse array of extracellular signals. Annu Rev Biochem *68*, 821-861. 10.1146/annurev.biochem.68.1.821.
52. Zhao, D., Kwon, S.H., Chun, Y.S., Gu, M.Y., and Yang, H.O. (2017). Anti-Neuroinflammatory Effects of Fucoxanthin via Inhibition of Akt/NF-kappaB and MAPKs/AP-1 Pathways and Activation of PKA/CREB Pathway in Lipopolysaccharide-Activated BV-2 Microglial Cells. Neurochem Res *42*, 667-677. 10.1007/s11064-016-2123-6.
53. Lu, Y., Li, B., Xu, A., Liang, X., Xu, T., Jin, H., Xie, Y., Wang, R., Liu, X., Gao, X., et al. (2022). NF-kappaB and AP-1 are required for the lipopolysaccharide-induced expression of MCP-1, CXCL1, and Cx43 in cultured rat dorsal spinal cord astrocytes. Front Mol Neurosci *15*, 859558. 10.3389/fnmol.2022.859558.
54. Tanimura, N., Saitoh, S., Matsumoto, F., Akashi-Takamura, S., and Miyake, K. (2008). Roles for LPS-dependent interaction and relocation of TLR4 and TRAM in TRIF-signaling. Biochem Biophys Res Commun *368*, 94-99. 10.1016/j.bbrc.2008.01.061.
55. Virzi, G.M., Mattiotti, M., de Cal, M., Ronco, C., Zanella, M., and De Rosa, S. (2022). Endotoxin in Sepsis: Methods for LPS Detection and the Use of Omics Techniques. Diagnostics (Basel) *13*. 10.3390/diagnostics13010079.
56. Pahwa, R., Goyal, A., and Jialal, I. (2024). Chronic Inflammation. In StatPearls.
57. Gire, V., Roux, P., Wynford-Thomas, D., Brondello, J.M., and Dulic, V. (2004). DNA damage checkpoint kinase Chk2 triggers replicative senescence. EMBO J *23*, 2554-2563. 10.1038/sj.emboj.7600259.

58. Ferbeyre, G., de Stanchina, E., Lin, A.W., Querido, E., McCurrach, M.E., Hannon, G.J., and Lowe, S.W. (2002). Oncogenic ras and p53 cooperate to induce cellular senescence. Mol Cell Biol *22*, 3497-3508. 10.1128/MCB.22.10.3497-3508.2002.
59. Tian, X.L., and Li, Y. (2014). Endothelial cell senescence and age-related vascular diseases. J Genet Genomics *41*, 485-495. 10.1016/j.jgg.2014.08.001.
60. Hayflick, L. (1965). The Limited in Vitro Lifetime of Human Diploid Cell Strains. Exp Cell Res *37*, 614-636. 10.1016/0014-4827(65)90211-9.
61. Munoz-Espin, D., and Serrano, M. (2014). Cellular senescence: from physiology to pathology. Nat Rev Mol Cell Biol *15*, 482-496. 10.1038/nrm3823.
62. Singh, T., and Newman, A.B. (2011). Inflammatory markers in population studies of aging. Ageing Res Rev *10*, 319-329. 10.1016/j.arr.2010.11.002.
63. Tousoulis, D., Psarros, C., Demosthenous, M., Patel, R., Antoniades, C., and Stefanadis, C. (2014). Innate and adaptive inflammation as a therapeutic target in vascular disease: the emerging role of statins. J Am Coll Cardiol *63*, 2491-2502. 10.1016/j.jacc.2014.01.054.
64. Coppe, J.P., Patil, C.K., Rodier, F., Sun, Y., Munoz, D.P., Goldstein, J., Nelson, P.S., Desprez, P.Y., and Campisi, J. (2008). Senescence-associated secretory phenotypes reveal cell-nonautonomous functions of oncogenic RAS and the p53 tumor suppressor. PLoS Biol *6*, 2853-2868. 10.1371/journal.pbio.0060301.
65. Buzzetti, E., Pinzani, M., and Tsochatzis, E.A. (2016). The multiple-hit pathogenesis of non-alcoholic fatty liver disease (NAFLD). Metabolism *65*, 1038-1048. 10.1016/j.metabol.2015.12.012.
66. Cusi, K. (2009). Role of insulin resistance and lipotoxicity in non-alcoholic steatohepatitis. Clin Liver Dis *13*, 545-563. 10.1016/j.cld.2009.07.009.
67. Schuster, S., Cabrera, D., Arrese, M., and Feldstein, A.E. (2018). Triggering and resolution of inflammation in NASH. Nat Rev Gastroenterol Hepatol *15*, 349-364. 10.1038/s41575-018-0009-6.
68. Kisseleva, T., and Brenner, D. (2021). Molecular and cellular mechanisms of liver fibrosis and its regression. Nat Rev Gastroenterol Hepatol *18*, 151-166. 10.1038/s41575-020-00372-7.
69. Friedman, S.L. (2008). Hepatic fibrosis -- overview. Toxicology *254*, 120-129. 10.1016/j.tox.2008.06.013.
70. Gines, P., Krag, A., Abraldes, J.G., Sola, E., Fabrellas, N., and Kamath, P.S. (2021). Liver cirrhosis. Lancet *398*, 1359-1376. 10.1016/S0140-6736(21)01374-X.
71. Kadl, A., Meher, A.K., Sharma, P.R., Lee, M.Y., Doran, A.C., Johnstone, S.R., Elliott, M.R., Gruber, F., Han, J., Chen, W., et al. (2010). Identification of a novel macrophage phenotype that develops in response to atherogenic phospholipids via Nrf2. Circ Res *107*, 737-746. 10.1161/CIRCRESAHA.109.215715.
72. Ke, Y., Karki, P., Kim, J., Son, S., Berdyshev, E., Bochkov, V.N., Birukova, A.A., and Birukov, K.G. (2019). Elevated truncated oxidized phospholipids as a factor exacerbating ALI in the aging lungs. FASEB J *33*, 3887-3900. 10.1096/fj.201800981R.
73. Karki, P., Meliton, A., Shah, A., Tian, Y., Ohmura, T., Sarich, N., Birukova, A.A., and Birukov, K.G. (2018). Role of truncated oxidized phospholipids in acute endothelial barrier dysfunction caused by particulate matter. PLoS One *13*, e0206251. 10.1371/journal.pone.0206251.
74. Tsimikas, S., Kiechl, S., Willeit, J., Mayr, M., Miller, E.R., Kronenberg, F., Xu, Q., Bergmark, C., Weger, S., Oberhollenzer, F., and Witztum, J.L. (2006). Oxidized phospholipids predict the presence and progression of carotid and femoral atherosclerosis and symptomatic cardiovascular disease: five-year prospective results from the Bruneck study. J Am Coll Cardiol *47*, 2219-2228. 10.1016/j.jacc.2006.03.001.
75. Schreyer, S.A., Vick, C., Lystig, T.C., Mystkowski, P., and LeBoeuf, R.C. (2002). LDL receptor but not apolipoprotein E deficiency increases diet-induced obesity and diabetes in mice. Am J Physiol Endocrinol Metab *282*, E207-214. 10.1152/ajpendo.2002.282.1.E207.

76. Sun, X., Seidman, J.S., Zhao, P., Troutman, T.D., Spann, N.J., Que, X., Zhou, F., Liao, Z., Pasillas, M., Yang, X., et al. (2020). Neutralization of Oxidized Phospholipids Ameliorates Non-alcoholic Steatohepatitis. Cell Metab *31*, 189-206 e188. 10.1016/j.cmet.2019.10.014.
77. Upchurch, C.M., Yeudall, S., Pavelec, C.M., Merk, D., Greulich, J., Manjegowda, M., Raghavan, S.S., Bochkis, I.M., Scott, M.M., Perez-Reyes, E., and Leitinger, N. (2022). Targeting oxidized phospholipids by AAV-based gene therapy in mice with established hepatic steatosis prevents progression to fibrosis. Sci Adv *8*, eabn0050. 10.1126/sciadv.abn0050.
78. Wang, X., Zheng, Z., Caviglia, J.M., Corey, K.E., Herfel, T.M., Cai, B., Masia, R., Chung, R.T., Lefkowitch, J.H., Schwabe, R.F., and Tabas, I. (2016). Hepatocyte TAZ/WWTR1 Promotes Inflammation and Fibrosis in Nonalcoholic Steatohepatitis. Cell Metab *24*, 848-862. 10.1016/j.cmet.2016.09.016.
79. Zhao, B., Bowden, R.A., Stavchansky, S.A., and Bowman, P.D. (2001). Human endothelial cell response to gram-negative lipopolysaccharide assessed with cDNA microarrays. Am J Physiol Cell Physiol *281*, C1587-1595. 10.1152/ajpcell.2001.281.5.C1587.
80. Ho, J., Chan, H., Wong, S.H., Wang, M.H., Yu, J., Xiao, Z., Liu, X., Choi, G., Leung, C.C., Wong, W.T., et al. (2016). The involvement of regulatory non-coding RNAs in sepsis: a systematic review. Crit Care *20*, 383. 10.1186/s13054-016-1555-3.
81. Dyballa-Rukes, N., Jakobs, P., Eckers, A., Ale-Agha, N., Serbulea, V., Aufenvenne, K., Zschauer, T.C., Rabanter, L.L., Jakob, S., von Ameln, F., et al. (2017). The Anti-Apoptotic Properties of APEX1 in the Endothelium Require the First 20 Amino Acids and Converge on Thioredoxin-1. Antioxid Redox Signal *26*, 616-629. 10.1089/ars.2016.6799.
82. Merk, D., Ptok, J., Jakobs, P., von Ameln, F., Greulich, J., Kluge, P., Semperowitsch, K., Eckermann, O., Schaal, H., Ale-Agha, N., et al. (2021). Selenoprotein T Protects Endothelial Cells against Lipopolysaccharide-Induced Activation and Apoptosis. Antioxidants (Basel) *10*. 10.3390/antiox10091427.
83. Pober, J.S. (2002). Endothelial activation: intracellular signaling pathways. Arthritis Res *4 Suppl 3*, S109-116. 10.1186/ar576.
84. Dimmeler, S., Haendeler, J., Rippmann, V., Nehls, M., and Zeiher, A.M. (1996). Shear stress inhibits apoptosis of human endothelial cells. FEBS Lett *399*, 71-74. 10.1016/s0014-5793(96)01289-6.
85. Savenije, O.E., Kerkhof, M., Reijmerink, N.E., Brunekreef, B., de Jongste, J.C., Smit, H.A., Wijga, A.H., Postma, D.S., and Koppelman, G.H. (2011). Interleukin-1 receptor-like 1 polymorphisms are associated with serum IL1RL1-a, eosinophils, and asthma in childhood. J Allergy Clin Immunol *127*, 750-756 e751-755. 10.1016/j.jaci.2010.12.014.
86. Cheng, G., Salerno, J.C., Cao, Z., Pagano, P.J., and Lambeth, J.D. (2008). Identification and characterization of VPO1, a new animal heme-containing peroxidase. Free Radic Biol Med *45*, 1682-1694. 10.1016/j.freeradbiomed.2008.09.009.
87. Cheng, G., Li, H., Cao, Z., Qiu, X., McCormick, S., Thannickal, V.J., and Nauseef, W.M. (2011). Vascular peroxidase-1 is rapidly secreted, circulates in plasma, and supports dityrosine cross-linking reactions. Free Radic Biol Med *51*, 1445-1453. 10.1016/j.freeradbiomed.2011.07.002.
88. Bhave, G., Cummings, C.F., Vanacore, R.M., Kumagai-Cresse, C., Ero-Tolliver, I.A., Rafi, M., Kang, J.S., Pedchenko, V., Fessler, L.I., Fessler, J.H., and Hudson, B.G. (2012). Peroxidasin forms sulfilimine chemical bonds using hypohalous acids in tissue genesis. Nat Chem Biol *8*, 784-790. 10.1038/nchembio.1038.
89. Medfai, H., Khalil, A., Rousseau, A., Nuyens, V., Paumann-Page, M., Sevcnikar, B., Furtmuller, P.G., Obinger, C., Moguilevsky, N., Peulen, O., et al. (2019). Human peroxidasin 1 promotes angiogenesis through ERK1/2, Akt, and FAK pathways. Cardiovasc Res *115*, 463-475. 10.1093/cvr/cvy179.
90. Lee, S.W., Kim, H.K., Naidansuren, P., Ham, K.A., Choi, H.S., Ahn, H.Y., Kim, M., Kang, D.H., Kang, S.W., and Joe, Y.A. (2020). Peroxidasin is essential for endothelial cell survival and growth

signaling by sulfilimine crosslink-dependent matrix assembly. FASEB J *34*, 10228-10241. 10.1096/fj.201902899R.

91. Pitts, M.W., and Hoffmann, P.R. (2018). Endoplasmic reticulum-resident selenoproteins as regulators of calcium signaling and homeostasis. Cell Calcium *70*, 76-86. 10.1016/j.ceca.2017.05.001.
92. Mariotti, M., Ridge, P.G., Zhang, Y., Lobanov, A.V., Pringle, T.H., Guigo, R., Hatfield, D.L., and Gladyshev, V.N. (2012). Composition and evolution of the vertebrate and mammalian selenoproteomes. PLoS One *7*, e33066. 10.1371/journal.pone.0033066.
93. Pothion, H., Jehan, C., Tostivint, H., Cartier, D., Bucharles, C., Falluel-Morel, A., Boukhzar, L., Anouar, Y., and Lihrmann, I. (2020). Selenoprotein T: An Essential Oxidoreductase Serving as a Guardian of Endoplasmic Reticulum Homeostasis. Antioxid Redox Signal *33*, 1257-1275. 10.1089/ars.2019.7931.
94. Boukhzar, L., Hamieh, A., Cartier, D., Tanguy, Y., Alsharif, I., Castex, M., Arabo, A., El Hajji, S., Bonnet, J.J., Errami, M., et al. (2016). Selenoprotein T Exerts an Essential Oxidoreductase Activity That Protects Dopaminergic Neurons in Mouse Models of Parkinson's Disease. Antioxid Redox Signal *24*, 557-574. 10.1089/ars.2015.6478.
95. Holben, D.H., and Smith, A.M. (1999). The diverse role of selenium within selenoproteins: a review. J Am Diet Assoc *99*, 836-843. 10.1016/S0002-8223(99)00198-4.
96. Huang, X., Sun, B., Zhang, J., Gao, Y., Li, G., and Chang, Y. (2017). Selenium Deficiency Induced Injury in Chicken Muscular Stomach by Downregulating Selenoproteins. Biol Trace Elem Res *179*, 277-283. 10.1007/s12011-017-0946-x.
97. Addinsall, A.B., Wright, C.R., Andrikopoulos, S., van der Poel, C., and Stupka, N. (2018). Emerging roles of endoplasmic reticulum-resident selenoproteins in the regulation of cellular stress responses and the implications for metabolic disease. Biochem J *475*, 1037-1057. 10.1042/BCJ20170920.
98. Alhazzani, W., Jacobi, J., Sindi, A., Hartog, C., Reinhart, K., Kokkoris, S., Gerlach, H., Andrews, P., Drabek, T., Manzanares, W., et al. (2013). The effect of selenium therapy on mortality in patients with sepsis syndrome: a systematic review and meta-analysis of randomized controlled trials. Crit Care Med *41*, 1555-1564. 10.1097/CCM.0b013e31828a24c6.
99. Wang, L., Jing, J., Yan, H., Tang, J., Jia, G., Liu, G., Chen, X., Tian, G., Cai, J., Shang, H., and Zhao, H. (2018). Selenium Pretreatment Alleviated LPS-Induced Immunological Stress Via Upregulation of Several Selenoprotein Encoding Genes in Murine RAW264.7 Cells. Biol Trace Elem Res *186*, 505-513. 10.1007/s12011-018-1333-y.
100. Einhauer, A., and Jungbauer, A. (2001). The FLAG peptide, a versatile fusion tag for the purification of recombinant proteins. J Biochem Biophys Methods *49*, 455-465. 10.1016/s0165-022x(01)00213-5.
101. Tujebajeva, R.M., Copeland, P.R., Xu, X.M., Carlson, B.A., Harney, J.W., Driscoll, D.M., Hatfield, D.L., and Berry, M.J. (2000). Decoding apparatus for eukaryotic selenocysteine insertion. EMBO Rep *1*, 158-163. 10.1093/embo-reports/kvd033.
102. Paskevicius, T., Farraj, R.A., Michalak, M., and Agellon, L.B. (2023). Calnexin, More Than Just a Molecular Chaperone. Cells *12*. 10.3390/cells12030403.
103. Haendeler, J., Messmer, U.K., Brune, B., Neugebauer, E., and Dimmeler, S. (1996). Endotoxic shock leads to apoptosis in vivo and reduces Bcl-2. Shock *6*, 405-409. 10.1097/00024382-199612000-00004.
104. Minamino, T., Miyauchi, H., Yoshida, T., Ishida, Y., Yoshida, H., and Komuro, I. (2002). Endothelial cell senescence in human atherosclerosis: role of telomere in endothelial dysfunction. Circulation *105*, 1541-1544. 10.1161/01.cir.0000013836.85741.17.
105. Ghanim, H., Abuaysheh, S., Sia, C.L., Korzeniewski, K., Chaudhuri, A., Fernandez-Real, J.M., and Dandona, P. (2009). Increase in plasma endotoxin concentrations and the expression of Toll-like receptors and suppressor of cytokine signaling-3 in mononuclear cells after a high-fat,

high-carbohydrate meal: implications for insulin resistance. Diabetes Care *32*, 2281-2287. 10.2337/dc09-0979.

106. Opal, S.M., Laterre, P.F., Francois, B., LaRosa, S.P., Angus, D.C., Mira, J.P., Wittebole, X., Dugernier, T., Perrotin, D., Tidswell, M., et al. (2013). Effect of eritoran, an antagonist of MD2-TLR4, on mortality in patients with severe sepsis: the ACCESS randomized trial. JAMA *309*, 1154-1162. 10.1001/jama.2013.2194.
107. Chen, J., and Goligorsky, M.S. (2006). Premature senescence of endothelial cells: Methusaleh's dilemma. Am J Physiol Heart Circ Physiol *290*, H1729-1739. 10.1152/ajpheart.01103.2005.
108. Spyridopoulos, I., Fichtlscherer, S., Popp, R., Toennes, S.W., Fisslthaler, B., Trepels, T., Zernecke, A., Liehn, E.A., Weber, C., Zeiher, A.M., et al. (2008). Caffeine enhances endothelial repair by an AMPK-dependent mechanism. Arterioscler Thromb Vasc Biol *28*, 1967-1974. 10.1161/ATVBAHA.108.174060.
109. Gonnissen, S., Ptok, J., Goy, C., Jander, K., Jakobs, P., Eckermann, O., Kaisers, W., von Ameln, F., Timm, J., Ale-Agha, N., et al. (2019). High Concentration of Low-Density Lipoprotein Results in Disturbances in Mitochondrial Transcription and Functionality in Endothelial Cells. Oxid Med Cell Longev *2019*, 7976382. 10.1155/2019/7976382.
110. Hoffmann, J., Haendeler, J., Aicher, A., Rossig, L., Vasa, M., Zeiher, A.M., and Dimmeler, S. (2001). Aging enhances the sensitivity of endothelial cells toward apoptotic stimuli: important role of nitric oxide. Circ Res *89*, 709-715. 10.1161/hh2001.097796.
111. Goy, C., Czypiorski, P., Altschmied, J., Jakob, S., Rabanter, L.L., Brewer, A.C., Ale-Agha, N., Dyballa-Rukes, N., Shah, A.M., and Haendeler, J. (2014). The imbalanced redox status in senescent endothelial cells is due to dysregulated Thioredoxin-1 and NADPH oxidase 4. Exp Gerontol *56*, 45-52. 10.1016/j.exger.2014.03.005.
112. Benes, P., Vetvicka, V., and Fusek, M. (2008). Cathepsin D--many functions of one aspartic protease. Crit Rev Oncol Hematol *68*, 12-28. 10.1016/j.critrevonc.2008.02.008.
113. Buchner, N., Ale-Agha, N., Jakob, S., Sydlik, U., Kunze, K., Unfried, K., Altschmied, J., and Haendeler, J. (2013). Unhealthy diet and ultrafine carbon black particles induce senescence and disease associated phenotypic changes. Exp Gerontol *48*, 8-16. 10.1016/j.exger.2012.03.017.
114. Neves, A.L., Coelho, J., Couto, L., Leite-Moreira, A., and Roncon-Albuquerque, R., Jr. (2013). Metabolic endotoxemia: a molecular link between obesity and cardiovascular risk. J Mol Endocrinol *51*, R51-64. 10.1530/JME-13-0079.
115. Cani, P.D., Amar, J., Iglesias, M.A., Poggi, M., Knauf, C., Bastelica, D., Neyrinck, A.M., Fava, F., Tuohy, K.M., Chabo, C., et al. (2007). Metabolic endotoxemia initiates obesity and insulin resistance. Diabetes *56*, 1761-1772. 10.2337/db06-1491.
116. Vitaglione, P., Morisco, F., Mazzone, G., Amoruso, D.C., Ribecco, M.T., Romano, A., Fogliano, V., Caporaso, N., and D'Argenio, G. (2010). Coffee reduces liver damage in a rat model of steatohepatitis: the underlying mechanisms and the role of polyphenols and melanoidins. Hepatology *52*, 1652-1661. 10.1002/hep.23902.
117. Jaquet, M., Rochat, I., Moulin, J., Cavin, C., and Bibiloni, R. (2009). Impact of coffee consumption on the gut microbiota: a human volunteer study. Int J Food Microbiol *130*, 117-121. 10.1016/j.ijfoodmicro.2009.01.011.
118. Correa, T.A., Monteiro, M.P., Mendes, T.M., Oliveira, D.M., Rogero, M.M., Benites, C.I., Vinagre, C.G., Mioto, B.M., Tarasoutchi, D., Tuda, V.L., et al. (2012). Medium light and medium roast paper-filtered coffee increased antioxidant capacity in healthy volunteers: results of a randomized trial. Plant Foods Hum Nutr *67*, 277-282. 10.1007/s11130-012-0297-x.
119. Freedman, N.D., Park, Y., Abnet, C.C., Hollenbeck, A.R., and Sinha, R. (2012). Association of coffee drinking with total and cause-specific mortality. N Engl J Med *366*, 1891-1904. 10.1056/NEJMoa1112010.
120. Ale-Agha, N., Goy, C., Jakobs, P., Spyridopoulos, I., Gonnissen, S., Dyballa-Rukes, N., Aufenvenne, K., von Ameln, F., Zurek, M., Spannbrucker, T., et al. (2018). CDKN1B/p27 is

localized in mitochondria and improves respiration-dependent processes in the cardiovascular system-New mode of action for caffeine. PLoS Biol *16*, e2004408. 10.1371/journal.pbio.2004408.

121. Buren, J., Ericsson, M., Damasceno, N.R.T., and Sjodin, A. (2021). A Ketogenic Low-Carbohydrate High-Fat Diet Increases LDL Cholesterol in Healthy, Young, Normal-Weight Women: A Randomized Controlled Feeding Trial. Nutrients *13*. 10.3390/nu13030814.
122. Moreira, A.P., Texeira, T.F., Ferreira, A.B., Peluzio Mdo, C., and Alfenas Rde, C. (2012). Influence of a high-fat diet on gut microbiota, intestinal permeability and metabolic endotoxaemia. Br J Nutr *108*, 801-809. 10.1017/S0007114512001213.
123. Mohr, A.E., Crawford, M., Jasbi, P., Fessler, S., and Sweazea, K.L. (2022). Lipopolysaccharide and the gut microbiota: considering structural variation. FEBS Lett *596*, 849-875. 10.1002/1873-3468.14328.
124. Violi, F., Cammisotto, V., Bartimoccia, S., Pignatelli, P., Carnevale, R., and Nocella, C. (2023). Gut-derived low-grade endotoxaemia, atherothrombosis and cardiovascular disease. Nat Rev Cardiol *20*, 24-37. 10.1038/s41569-022-00737-2.
125. Zhong, S., Li, L., Shen, X., Li, Q., Xu, W., Wang, X., Tao, Y., and Yin, H. (2019). An update on lipid oxidation and inflammation in cardiovascular diseases. Free Radic Biol Med *144*, 266-278. 10.1016/j.freeradbiomed.2019.03.036.
126. Rocca, C., Boukhzar, L., Granieri, M.C., Alsharif, I., Mazza, R., Lefranc, B., Tota, B., Leprince, J., Cerra, M.C., Anouar, Y., and Angelone, T. (2018). A selenoprotein T-derived peptide protects the heart against ischaemia/reperfusion injury through inhibition of apoptosis and oxidative stress. Acta Physiol (Oxf) *223*, e13067. 10.1111/apha.13067.
127. Alsharif, I., Boukhzar, L., Lefranc, B., Godefroy, D., Aury-Landas, J., Rego, J.D., Rego, J.D., Naudet, F., Arabo, A., Chagraoui, A., et al. (2021). Cell-penetrating, antioxidant SELENOT mimetic protects dopaminergic neurons and ameliorates motor dysfunction in Parkinson's disease animal models. Redox Biol *40*, 101839. 10.1016/j.redox.2020.101839.
128. Baixauli, F., Acin-Perez, R., Villarroya-Beltri, C., Mazzeo, C., Nunez-Andrade, N., Gabande-Rodriguez, E., Ledesma, M.D., Blazquez, A., Martin, M.A., Falcon-Perez, J.M., et al. (2015). Mitochondrial Respiration Controls Lysosomal Function during Inflammatory T Cell Responses. Cell Metab *22*, 485-498. 10.1016/j.cmet.2015.07.020.
129. Holmgren, A., and Lu, J. (2010). Thioredoxin and thioredoxin reductase: current research with special reference to human disease. Biochem Biophys Res Commun *396*, 120-124. 10.1016/j.bbrc.2010.03.083.
130. Tanaka, T., Hosoi, F., Yamaguchi-Iwai, Y., Nakamura, H., Masutani, H., Ueda, S., Nishiyama, A., Takeda, S., Wada, H., Spyrou, G., and Yodoi, J. (2002). Thioredoxin-2 (TRX-2) is an essential gene regulating mitochondria-dependent apoptosis. EMBO J *21*, 1695-1703. 10.1093/emboj/21.7.1695.

10. Eigene Veröffentlichungen

I. **Targeting oxidized phospholipids by AAV-based gene therapy in mice with established hepatic steatosis prevents progression to fibrosis.**
Sci Adv *8*, eabn0050. 10.1126/sciadv.abn0050.
Upchurch, C.M., Yeudall, S., Pavelec, C.M., **Merk, D.**, Greulich, J., Manjegowda, M., Raghavan, S.S., Bochkis, I.M., Scott, M.M., Perez-Reyes, E., and Leitinger, N. (2022).

II. **Selenoprotein T Protects Endothelial Cells against Lipopolysaccharide-Induced Activation and Apoptosis.**
Antioxidants (Basel) *10*. 10.3390/antiox10091427.
Merk, D., Ptok, J., Jakobs, P., von Ameln, F., Greulich, J., Kluge, P., Semperowitsch, K., Eckermann, O., Schaal, H., Ale-Agha, N., et al. (2021).

III. **Caffeine Inhibits Oxidative Stress- and Low Dose Endotoxemia-Induced Senescence-Role of Thioredoxin-1.**
Antioxidants (Basel) *12*. 10.3390/antiox12061244.
Merk, D., Greulich, J., Vierkant, A., Cox, F., Eckermann, O., von Ameln, F., Dyballa-Rukes, N., Altschmied, J., Ale-Agha, N., Jakobs, P., and Haendeler, J. (2023).

IV. **Dose-Dependent Effects of Lipopolysaccharide on the Endothelium-Sepsis versus Metabolic Endotoxemia-Induced Cellular Senescence.**
Antioxidants (Basel) *13*. 10.3390/antiox13040443.
Merk, D., Cox, F.F., Jakobs, P., Promel, S., Altschmied, J., and Haendeler, J. (2024).

Targeting oxidized phospholipids by AAV-based gene therapy in mice with established hepatic steatosis prevents progression to fibrosis.

Sci Adv *8*, eabn0050. 10.1126/sciadv.abn0050.

Upchurch, C.M., Yeudall, S., Pavelec, C.M., **Merk, D.**, Greulich, J., Manjegowda, M., Raghavan, S.S., Bochkis, I.M., Scott, M.M., Perez-Reyes, E., and Leitinger, N. (2022).

Publikation I

Beteiligung der Autoren:

Upchurch C.M.: Erstautor. Beteiligt an Planung und Umsetzung aller Versuche, Datenanalyse und entwerfen des Manuskripts.

Yeudall S.: Umsetzung von Experimenten in Leberzellen zur inflammatorischen Aktivierung und Signaltransduktion.

Pavelec C.M.: Durchführung von metabolischen Messungen im Seahorse-Analyzer und Analyse dieser Daten.

Merk D.: Messung von AAV8-scFv-E06 Konzentrationen im Plasma mithilfe von kompetitiven HIS/myc sandwich ELISAs.

Greulich J.: Durchführung von Immunoblots und Immunfluoreszenzfärbungen.

Manjegowda M.: Analyse der Daten aus RNA-sequencing und Chip-Experimenten.

Raghavan SS.: Clinical Scoring von Leberschnitten aus NASH-Tierversuchen.

Bochkis IM.: Durchführung von Chip-Experimenten und Datenanalysen.

Scott MM.: Erstellung des AAV8-scFv-E06 Expressionsvektor Konzepts gemeinsam mit E. Perez-Reyes.

Perez Reyes E.: Erstellung des AAV8-scFv-E06 Expressionsvektors Konzepts gemeinsam mit MM Scott und Produktion von AAV8-ScFv-E06 Viren.

Leitinger N.: Seniorautor. Erstellung des Studienkonzepts, Planung der Versuche und Finalisierung des Skripts.

Selenoprotein T Protects Endothelial Cells against Lipopolysaccharide-Induced Activation and Apoptosis.

Antioxidants (Basel) *10*. 10.3390/antiox10091427.

Merk, D., Ptok, J., Jakobs, P., von Ameln, F., Greulich, J., Kluge, P., Semperowitsch, K., Eckermann, O., Schaal, H., Ale-Agha, N., et al. (2021).

Publikation II

Beteiligung der Autoren:

Merk D.: Erstautor. Beteiligt an Planung und Umsetzung aller Versuche, Datenanalyse und entwerfen des Manuskripts.

Ptok J.: Erstautor. Beteiligt an Planung und Umsetzung des RNA-sequencing Analysen, Datenanalyse und entwerfen des Manuskripts.

Jakobs P.: Erstautor. Beteiligt an Planung und Umsetzung aller Versuche, Datenanalyse und entwerfen des Manuskripts.

von Ameln F.: Durchführung der real-time PCRs und Erstellung der Agarose-Gelbilder.

Greulich J.: Durchführung von Immunoblots.

Kluge P.: Durchführung der real-time PCRs und Erstellung der Agarose-Gelbilder.

Semperowitsch K.: Durchführung der lentiviralen APEX1 (1-20) Transduktionen und Isolation der RNA.

Eckermann O.: Durchführung der Produktion und Titration lentiviraler Partikel für deren Transduktion.

Schaal H.: Betreuung der RNA-sequencing Analysen und Auswertung der Daten.

Ale-Agha N.: Seniorautorin. Erstellung des Studienkonzepts, Planung der Versuche und Finalisierung des Skripts.

Altschmied J.: Seniorautor. Erstellung des Studienkonzepts, Planung der Versuche und Finalisierung des Skripts.

Haendeler J.: Seniorautorin. Erstellung des Studienkonzepts, Planung der Versuche und Finalisierung des Skripts.

Caffeine Inhibits Oxidative Stress- and Low Dose Endotoxemia-Induced Senescence-Role of Thioredoxin-1.

Antioxidants (Basel) *12*. 10.3390/antiox12061244.

Merk, D., Greulich, J., Vierkant, A., Cox, F., Eckermann, O., von Ameln, F., Dyballa-Rukes, N., Altschmied, J., Ale-Agha, N., Jakobs, P., and Haendeler, J. (2023).

Publikation III

Beteiligung der Autoren:

Merk D.: Erstautor. Beteiligt an Planung und Umsetzung aller Versuche, Datenanalyse und entwerfen des Manuskripts.

Greulich J.: Erstautor. Beteiligt an Planung und Umsetzung aller Versuche, Datenanalyse und entwerfen des Manuskripts.

Vierkant A.: Durchführung der Experimente zur Seneszenzinduktion durch H_2O_2 und Koffein.

Cox F.: Durchführung der Immunfluoreszenzfärbungen.

Eckermann O.: Durchführung der Produktion und Titration lentiviraler Partikel und deren Transduktion.

von Ameln F.: Durchführung der RNA-Isolierungen und PCRs.

Dyballa Rukes N.: Durchführung der Immunoblots.

Altschmied J.: Planung der Klonierung von Expressionsvektoren, Betreuung lentiviraler Transduktionen und Erstellung der Abbildungen.

Ale-Agha N.: Seniorautorin. Erstellung des Studienkonzepts, Planung der Versuche und Finalisierung des Skripts.

Jakobs P.: Seniorautor. Erstellung des Studienkonzepts, Planung der Versuche und Finalisierung des Skripts.

Haendeler J.: Seniorautorin. Erstellung des Studienkonzepts, Planung der Versuche und Finalisierung des Skripts.

Dose-Dependent Effects of Lipopolysaccharide on the Endothelium-Sepsis versus Metabolic Endotoxemia-Induced Cellular Senescence.

Antioxidants (Basel) *13*. 10.3390/antiox13040443.

Merk, D., Cox, F.F., Jakobs, P., Promel, S., Altschmied, J., and Haendeler, J. (2024).

Publikation IV

Beteiligung der Autoren:

Merk D.: Erstautor. Beteiligt an Planung und verfassen des Skripts.

Cox F.: Erstautorin. Beteiligt an Planung und verfassen des Skripts.

Jakobs P.: Beteiligt an Strukturierung und Erstellung der Abbildungen des Skripts.

Promel S.: Beteiligt an verfassen und Strukturierung des Skripts.

Altschmied J.: Seniorautor. Erstellung des Skript-Konzepts, der Abbildungen und der Finalisierung des Skripts.

Haendeler J.: Seniorautor. Erstellung des Skript-Konzepts, der Verfassung, Strukturierung und Finalisierung des Skripts.

11. Danksagung

Mit dem Abschluss dieser Dissertation findet eine sehr aufregende und lehrreiche Zeit ihr Ende. Mein besonderer Dank gilt allen voran Jojo Haendeler und Yogi Altschmied, welche mir die Möglichkeit gegeben haben ein Teil Ihrer Arbeitsgruppe zu werden und diese Dissertation unter Ihrer Führung zu vollenden. Ich habe mich während der gesamten Zeit hervorragend aufgehoben gefühlt und mir wurde immer das Gefühl vermittelt, dass ich mich bei Fragen und Problemen an Euch wenden kann. Eine bessere Betreuung kann man sich nicht wünschen! Die Lab-Meetings am Donnerstag vermisse ich schon jetzt.

Herrn Prof. Dr. Dieter Willbold danke ich für die Zeit und die Bereitschaft das Zweitgutachten zu übernehmen.

Weiterhin danke ich der gesamten Arbeitsgruppe für die großartige Zeit und die essenzielle Unterstützung für das Gelingen dieser Arbeit. Ich danke Jan, Fiona, Philipp, Nilo, Flo, Olaf, Nadine und Anne. Mit euch ist die Zeit im Labor und in den Büros immer wie im Flug vergangen. Danke Jan, Fiona und Anne für die angenehmen Pausen und den Schabernack den man ab und an gemeinsam angestellt hat. Danke Philipp für die persönliche Betreuung und die lustigen Abende und Feste, an welchen man den ein oder anderen Becher heben konnte. Danke Nilo und Nadine für eure quirlige und auflockernde Art, welche so manchen Laboralltag geschmückt hat. Danke Flo und Olaf für eure Geduld bei den Versuchen und eure uneingeschränkte Hilfsbereitschaft. Ich hoffe, dass ihr diese Zeit genauso wundervoll in Erinnerung behaltet wie ich.

Ich danke außerdem dem IRTG1902, welches mir die Durchführung der Promotion ermöglichte. Die regelmäßigen Meetings, Journal Clubs und Events haben mir immer viel Freude bereitet. Für die Koordination und die herzliche Betreuung möchte ich mich auch bei Dr. Sandra Berger bedanken, welche immer Ihr Bestes gegeben hat diese Events auf die Beine zu stellen.

Darüber hinaus war meine Zeit in den USA an der UVa eine bedeutende und bereichernde Erfahrung für mich. Ich danke Norbert Leitinger dafür, einen 6-monatigen Forschungsaufenthalt in seiner Arbeitsgruppe durchführen zu können und mein erstes Thanksgiving mit Ihm und seiner Familie feiern zu dürfen. Diese Zeit wurde neben den interessanten Experimenten besonders durch Scott Yeudall, Clint Upchurch und Caitlin Pavelec geprägt, welche mich direkt bei meiner Ankunft mit offenen Armen aufgenommen und in Ihre Gruppe involviert haben.

Außerdem danke ich meinen Freunden, dass sie mich über all die Jahre begleitet und mit mir unzählige einzigartige Erlebnisse geteilt haben. Ich danke weiterhin meiner Freundin Lisa, welche mir auch in stressigeren Situationen zur Seite stand. Durch dich werden schwierige Zeiten erträglich und schöne Zeiten noch schöner.

Zu guter Letzt danke ich meiner Familie für die großartige Unterstützung während meiner gesamten Studienzeit. Durch euren Rückhalt wurde all dies erst ermöglicht.

GENETICS

Targeting oxidized phospholipids by AAV-based gene therapy in mice with established hepatic steatosis prevents progression to fibrosis

Clint M. Upchurch[1], Scott Yeudall[1], Caitlin M. Pavelec[1,2], Dennis Merk[3], Jan Greulich[3,4], Mohan Manjegowda[1], Shyam S. Raghavan[5], Irina M. Bochkis[1], Michael M. Scott[1], Edward Perez-Reyes[1], Norbert Leitinger[1,2]*

Oxidized phosphatidylcholines (OxPCs) are implicated in chronic tissue damage. Hyperlipidemic LDL-R−−deficient mice transgenic for an OxPC-recognizing IgM fragment (scFv-E06) are protected against nonalcoholic fatty liver disease (NAFLD). To examine the effect of OxPC elimination at different stages of NAFLD progression, we used cre-dependent, adeno-associated virus serotype 8–mediated expression of the single-chain variable fragment of E06 (AAV8-scFv-E06) in hepatocytes of albumin-cre mice. AAV8-induced expression of scFv-E06 at the start of FPC diet protected mice from developing hepatic steatosis. Independently, expression of scFv-E06 in mice with established steatosis prevented the progression to hepatic fibrosis. Mass spectrometry–based oxophospho-lipidomics identified individual OxPC species that were reduced by scFv-E06 expression. In vitro, identified OxPC species dysregulated mitochondrial metabolism and gene expression in hepatocytes and hepatic stellate cells. We demonstrate that individual OxPC species independently affect disease initiation and progression from hepatic steatosis to steatohepatitis, and that AAV-mediated expression of scFv-E06 is an effective therapeutic intervention.

INTRODUCTION

Nonalcoholic fatty liver disease (NAFLD) is a multistage disease that affects approximately 30% of the global population (*1*, *2*). Hepatic steatosis is the hallmark of NAFLD, which, in a subset of patients, will progress into nonalcoholic steatohepatitis (NASH). Steatosis can arise as a result of caloric overload, which dysregulates hepatocyte bioenergetics and metabolism (*3*) and increases reactive oxygen species (*4*) and hepatic triglyceride accumulation (*5*, *6*), resulting in organ damage indicated by elevated plasma alanine aminotransferase (ALT) and aspartate aminotransferase (AST) (*4*, *7*–*11*). The culmination of multiple hepatic insults leads to the development of NASH, which is characterized by inflammation (*12*) and activation of hepatic stellate cells, ultimately leading to irreversible hepatic fibrosis (*12*–*17*). In the absence of U.S. Food and Drug Administration–approved pharmacological interventions and suitable biomarkers for NASH, there is an urgent need for new therapeutic and diagnostic tools (*18*).

Excess radical oxygen species generation in steatotic livers leads to the formation of lipid oxidation products, including oxidized phosphatidylcholines (OxPCs) (*19*–*22*). Free radical–driven and enzymatically driven oxidation of polyunsaturated fatty acids contained in phospholipids forms chemically unique classes of oxidized species whose location and chemical functionalization dictate the regulation of specific cellular responses, including endothelial barrier integrity (*23*–*27*); immune cell migration (*28*), activation (*19*, *20*), and metabolism (*29*); bone homeostasis (*30*); and regulated cell death (*31*, *32*). Consequently, OxPCs are thought to play a central role in acute pathologies such as sepsis (*21*) and lung injury (*23*, *24*, *33*), as well as in chronic diseases including those of the metabolic syndrome (*34*, *35*). Moreover, plasma levels of OxPCs, as measured by reactivity with E06, a natural immunoglobulin M (IgM) that binds oxidized phosphorylcholine (*36*), predict severity of human carotid and femoral atherosclerosis (*37*).

Recent work from the Witztum laboratory has demonstrated that constitutive transgenic expression of a single-chain variable fragment of E06 (scFv-E06) protects hypercholesterolemic *Ldlr*$^{-/-}$ mice from diet-induced hepatic steatosis and subsequent NASH (*35*, *37*, *38*). While these studies demonstrated that targeting OxPCs in general is sufficient to improve clinical outcomes in a mouse model of chronic disease, the identity of individual OxPC species that are eliminated by scFv-E06 in vivo remains unknown. Furthermore, it is unknown whether OxPC sequestration by scFv-E06 is sufficient to independently halt the progression to NASH and the transition to hepatic fibrosis, and it is necessary to identify the cellular targets and the pathological mechanisms by which OxPCs drive hepatic steatosis and fibrosis.

Here, we show that adeno-associated virus serotype 8–mediated hepatic expression of scFv-E06 (AAV8-E06) eliminates defined plasma OxPC species derived from oxidation of 1-palmitoyl-2-arachidonyl-*sn*-glycero-3-phosphocholine (PAPC) and 1-palmitoyl-2-linoleoyl-*sn*-glycero-3-phosphocholine (PLPC), which protects mice from diet-induced hepatic steatosis. Identified OxPC species regulate hepatocyte gene expression and shift cellular metabolism toward a bioenergetically impaired state, which results in reduced oxygen consumption and increased lipid droplet accumulation. Moreover, intervention with AAV8-scFv-E06 in mice with established hepatic steatosis prevents the progression to NASH and hepatic fibrosis. OxPC species that were reduced during the progression phase regulate hepatic stellate cell bioenergetics and gene expression. Together, we identify specific pathology-driving OxPC species in plasma that

[1]Department of Pharmacology, University of Virginia School of Medicine, Charlottesville, VA 22904, USA. [2]Robert M. Berne Cardiovascular Research Center, University of Virginia School of Medicine, Charlottesville, VA 22904, USA. [3]Environmentally-Induced Cardiovascular Degeneration, Clinical Chemistry and Laboratory Diagnostics, Medical Faculty, University Hospital and Heinrich-Heine University Düsseldorf, 40225 Düsseldorf, Germany. [4]IUF-Leibniz Research Institute for Environmental Medicine, 40225 Düsseldorf, Germany. [5]Department of Pathology, University of Virginia, Charlottesville, VA 22904, USA.
*Corresponding author. Email: nl2q@virginia.edu

may be used as noninvasive biomarkers to diagnose distinct stages of NAFLD, and we demonstrate efficacy of AAV8-mediated gene transfer of scFv-E06 as an intervention-based therapeutic measure that attenuates the initiation of hepatic steatosis and the progression to fibrotic steatohepatitis in mice.

RESULTS

AAV8-mediated gene transfer for cre recombinase–dependent expression of scFv-E06 in mice

Previous reports demonstrated that constitutive transgenic expression of scFv-E06 via the *Apoe* promoter protected *Ldlr*$^{-/-}$ mice fed a high-cholesterol diet from hepatic steatosis and ensuing steatohepatitis (*35*, *38*). To investigate the effect of scFv-E06 at different stages of disease progression and to establish a therapeutic approach using virus-mediated gene transfer of scFv-E06, we developed an AAV8 construct containing a myc- and 6xHis-tagged scFv-E06 flanked by double-inverse orientation flox sites (AAV8-scFv-E06) for cre-dependent expression (Fig. 1A). Speer6-ps1$^{Tg(Alb\text{-}cre)21Mgn}$/J (Alb-cre) mice, which express cre recombinase specifically in hepatocytes, were injected via tail vein with AAV8-scFv-E06 or a control AAV8 expressing green fluorescent protein (AAV8-GFP). Viral transduction resulted in incorporation of the scFv-E06 vector predominantly in the liver and, to some extent, in adipose tissue, kidney, and spleen, while it was not detected in the heart or lungs (Fig. 1B). Messenger RNA and protein expression of scFv-E06 was restricted to the liver, demonstrating that expression was dependent on cre recombinase (Fig. 1, C and D). scFv-E06 protein was secreted into the plasma with detectable levels as early as 10 days after AAV administration (Fig. 1J).

AAV8-mediated hepatic expression of scFv-E06 had no observable effect on total body weight, and liver, gonadal adipose tissue, heart, kidney, or spleen mass (fig. S1). There were also no differences in levels of ALT (Fig. 1E) and AST (Fig. 1F) in plasma, or esterified (Fig. 1G), free (Fig. 1H), and total cholesterol (Fig. 1I) in livers of mice given AAV8-scFv-E06 compared to AAV-GFP controls. Together, these data demonstrate that AAV8-mediated hepatic expression of scFv-E06 in mice leads to accumulation of scFv-E06 protein in the liver and plasma without inducing overt physiological changes.

Using a high fructose, palmitate, and cholesterol (FPC) diet supplemented with 4.2% sugar water (55/45 glucose/fructose), we establish a progressive model NAFLD defined by distinct stages of hepatic steatosis and subsequent inflammation and fibrosis (*39*). These stages were evident in histopathological assessment of livers from mice fed FPC diet compared to chow-fed controls (fig. S1, G to J). This allowed us to assess the impact of scFv-E06 expression at different stages of NAFLD progression.

AAV8-mediated expression of scFv-E06 protects mice from diet-induced hepatic steatosis and reduces oxidized phospholipids in plasma

To determine whether induced expression of scFv-E06 could be used as a therapeutic approach to prevent hepatic steatosis in mice, we inoculated Speer6-ps1$^{Tg(Alb\text{-}cre)21Mgn}$/J (Alb-cre) mice via tail vein with AAV8-scFv-E06 or AAV8-GFP 2 weeks before feeding mice FPC diet for 6 weeks to induce hepatic steatosis (Fig. 2A). After 6 weeks, we confirmed the expression of myc-tagged scFv-E06 in the liver by Western blot (Fig. 2B) and mRNA by quantitative reverse transcription polymerase chain reaction (qRT-PCR) in the liver (fig. S2A) and confirmed detectable titers of scFv-E06 in the plasma by enzyme-linked immunosorbent assay (ELISA) (Fig. 2C). scFv-E06–expressing mice exhibited no difference in weight gain compared to GFP-expressing mice over 6 weeks (fig. S2B); however, scFv-E06 expression reduced body fat percentage starting at 4 weeks on FPC diet (fig. S2C). FPC diet feeding increased liver and adipose mass; however, there was no difference in organ mass between GFP- and scFv-E06–expressing mice (fig. S2, D to I). Histological assessment

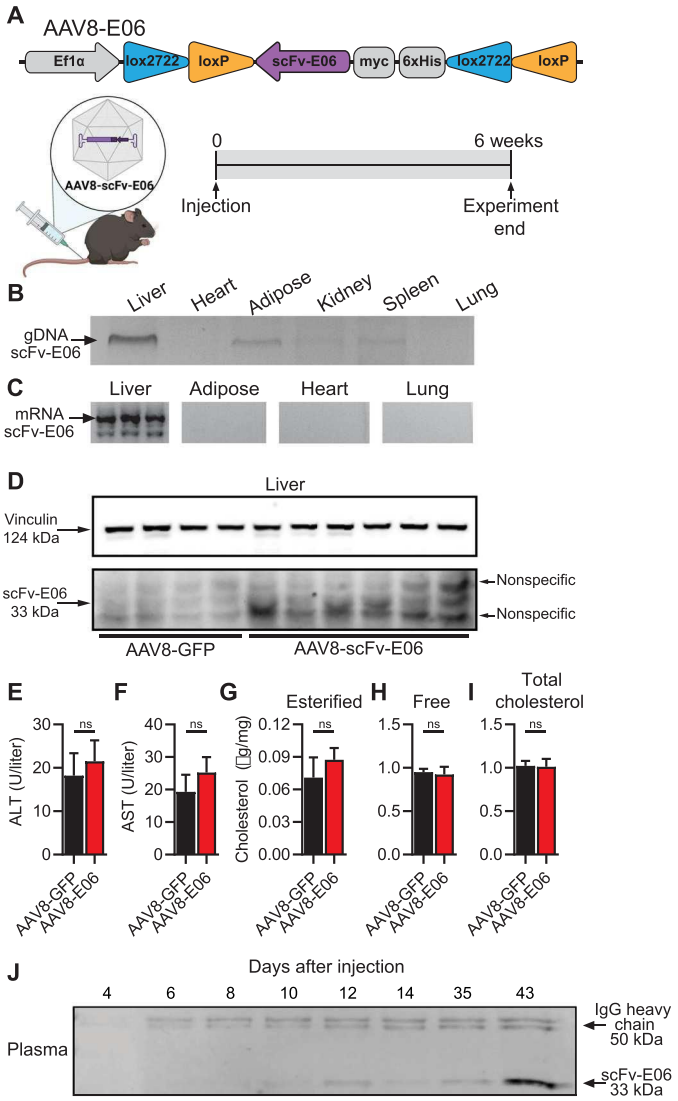

Fig. 1. Virus-mediated gene transfer for cre-dependent expression of scFv-E06 in a murine model. (**A**) Schematic of experimental design. Mice were injected via tail vein with AAV8-E06 or AAV-GFP and fed chow diet for 6 weeks (created with BioRender.com). Viral transduction of AAV8-scFv-E06 was assessed by (**B**) polymerase chain reaction (PCR) of genomic DNA and (**C**) reverse transcription PCR of mRNA. scFv-E06 expression in the (**D**) liver was confirmed via Western blotting 6 weeks after injection. Vinculin was used as a loading control. There were no significant changes in (**E**) ALT, (**F**) AST, and (**G**) esterified, (**H**) free, and (**I**) total liver cholesterol between scFv-E06– and GFP-expressing mice (AAV8-GFP, $n = 5$; AAV8-E06, $n = 6$). (**J**) scFv-E06 was detectable in plasma 12 days after injection and remained elevated after 6 weeks. Nonspecific IgG heavy chain staining was used as a loading control. ns, not significant.

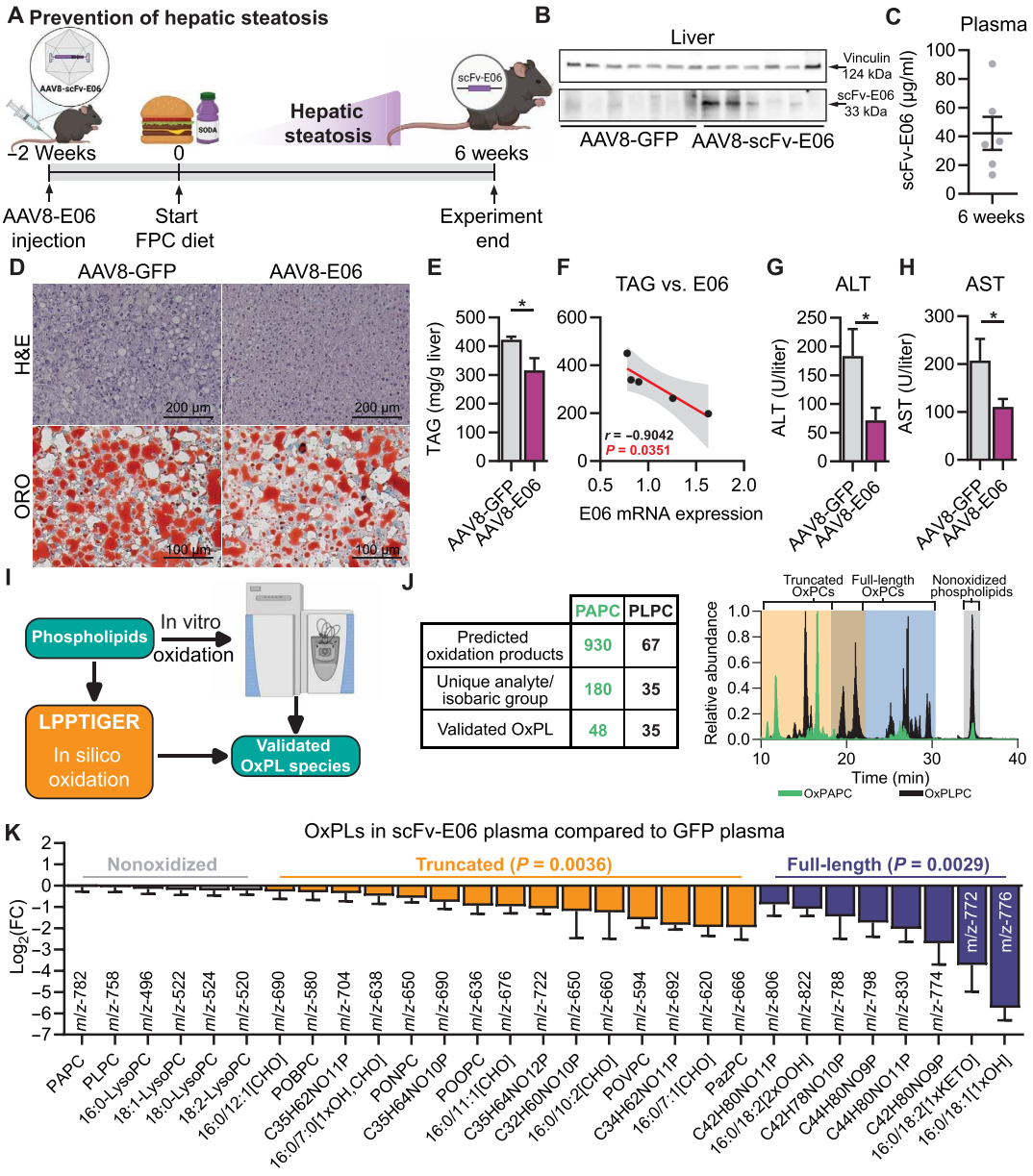

	PAPC	PLPC
Predicted oxidation products	930	67
Unique analyte/ isobaric group	180	35
Validated OxPL	48	35

Fig. 2. Virus-mediated hepatic expression of scFv-E06 prevented development of diet-induced hepatic steatosis. (**A**) Schematic of experimental design. Mice were injected via tail vein with AAV8-E06 or AAV8-GFP 2 weeks before the start of 6-week FPC diet challenge (created with BioRender.com). (**B**) scFv-E06 protein expression in mouse liver 8 weeks after injection. (**C**) scFv-E06 titer concentrations were estimated in plasma by competitive sandwich enzyme-linked immunosorbent assay (ELISA). (**D**) Hematoxylin and eosin (H&E) and Oil red O (ORO) staining revealed decreased hepatic lipid burden in mice expressing scFv-E06 and was confirmed by (**E**) quantification of hepatic triglycerides (GFP, $n = 6$; scFv-E06, $n = 5$). (**F**) Hepatic triglyceride concentrations negatively correlated with hepatic mRNA expression of scFv-E06 (scFv-E06, $n = 5$). scFv-E06 expression protected mice from diet-induced liver toxicity resulting in significantly lower (**G**) ALT and (**H**) AST (GFP, $n = 6$; scFv-E06, $n = 6$). (**I**) Schema demonstrating strategy for mass spectrometry method development and validation. (**J**) Forty-eight analytes/isobaric groups from PAPC and 35 analytes/isobaric groups from PLPC were validated. (**K**) Both truncated and full-length OxPC species were significantly reduced in mice expressing scFv-E06 (GFP, $n = 7$; scFv-E06, $n = 6$). Statistical significance was determined by two-way analysis of variance (ANOVA), Spearman's rank correlation, and Student's t test (*$P < 0.05$).

of liver sections by hematoxylin and eosin (H&E) or Oil red O staining revealed that treatment with AAV8-scFv-E06 reduced hepatic tissue damage and lipid accumulation compared to GFP controls (Fig. 2D). Hepatic triglyceride levels were significantly reduced in scFv-E06–expressing mice and negatively correlated with hepatic mRNA expression of scFv-E06 (Fig. 2, E and F). Moreover, plasma ALT (Fig. 2G) and AST (Fig. 2H) levels were significantly decreased in mice expressing scFv-E06, while alkaline phosphatase (ALP), cholesterol, low-density lipoprotein (LDL) and high-density lipoprotein (HDL) cholesterol, plasma triglycerides, albumin, and total protein were unchanged (fig. S2, J to R). These data demonstrate that AAV8-mediated expression of scFv-E06 protects mice from diet-induced hepatic lipid accumulation and liver damage.

Previously published studies have demonstrated that constitutive scFv-E06 expression reduced overall plasma reactivity with IgM E06 (*35*, *38*), indicative of reduced OxPC levels in plasma. However,

the identity of OxPC species that are reduced by scFv-E06 expression and the degree of reduction remain unknown.

To identify OxPC species that are affected by scFv-E06 in plasma, we used an in silico platform, LPPTiger (*40*), to predict structures of possible oxidation products that can be generated from oxidation of PAPC and PLPC. We then validated predicted OxPC species by electrospray ionization liquid chromatography–mass spectrometry (ESI–LC-MS) using air- or copper (I) chloride–oxidized PAPC (OxPAPC) and PLPC (OxPLPC) (fig. S3, A and B), which resulted in validation of 48 PAPC- and 35 PLPC-derived oxidized individual analytes or groups of isobaric compounds (Fig. 2, I and J). Next, we assessed the presence of validated compounds in the plasma of GFP- or scFv-E06–expressing mice after 6 weeks on FPC diet (fig. S3, C and D). We identified 23 individual OxPC species and isobaric groups containing OxPCs and 6 nonoxidized PC and lyso-PC species in mouse plasma. Levels of nonoxidized PCs and lyso-PCs were not different in GFP- and scFv-E06–expressing mice; however, all identified OxPC species, including truncated and full-length OxPCs, were markedly decreased in plasma of mice expressing scFv-E06 (Fig. 2K). A similar pattern was observed in the liver; however, the differences in OxPC species were less pronounced between the two groups (fig. S2S).

In the plasma, the truncated and full-length OxPCs that were substantially decreased in scFv-E06–expressing mice included several previously described biologically active compounds containing specific functional groups: Among decreased truncated OxPC species were γ-keto/hydroxy OxPCs [mass/charge ratio (*m/z*) 650] (*22*, *41*), the aldehyde-containing 1-palmitoyl-2-(5′-oxo-valeroyl)-*sn*-glycero-3-phosphocholine (POVPC; *m/z* 594) (*42*), the 4-carbon aldehyde 1-palmitoyl-2-(4′-oxo-butanoyl)-*sn*-glycero-3-phosphocholine (POBPC; *m/z* 580) (*43*), the 8-carbon aldehyde 1-palmitoyl-2-(8′-oxo-octanoyl)-*sn*-glycero-3-phosphocholine (POOPC; *m/z* 636), the 9-carbon aldehyde 1-palmitoyl-2-(9′-oxo-nonanoyl)-*sn*-glycero-3-phosphocholine (*m/z* 650) (*44*, *45*), and the carboxylic acid–containing 1-palmitoyl-2-azelaoyl-*sn*-glycero-3-phosphocholine (PazPC; *m/z* 666) (Fig. 2J) (*45*, *46*). Among the most substantially reduced full-length OxPC were 1-palmitoyl-2-((E)-8′-hydroxyoctadec-12′-enoyl)-*sn*-glycero-3-phosphocholine (HODE-PC; *m/z* 776), an isobaric group with an *m/z* of 798 containing 1-palmitoyl-2-((5E,8E,11E,14E)-4′-hydroxyicosa-5′,8′,11′,14′-tetraenoyl (HETE-PC) (*47*), and an isobaric group with an *m/z* of 830 containing isoprostane-PC (Fig. 2K) (*48*, *49*). The structures of the identified compounds with the corresponding *m/z* values are represented in table S1.

Together, these data demonstrate that AAV8-dependent hepatic expression of scFv-E06 results in its secretion into the plasma, decreased plasma levels of defined OxPC species, and protection from diet-induced hepatic. scFv-E06 showed specificity toward OxPCs, but not nonoxidized phospholipids, recognizing a variety of oxidation-specific functional groups that are associated with previously reported biological functions (*50*, *51*).

OxPCs regulate hepatocyte gene expression and mitochondrial bioenergetics

These data imply a role of OxPCs in the development of hepatic steatosis; however, it is unknown if hepatocytes recognize and respond to OxPCs. To investigate whether OxPCs regulate hepatocyte function, we treated a murine hepatocyte cell line (AML12) with a mixture of full-length and truncated OxPCs (OxPAPC) (*42*) for 4 hours and analyzed changes in gene expression by RNA sequencing (RNA-seq). OxPAPC regulated the expression of 1367 genes in AML12 hepatocytes [fold change > 1.5, false discovery rate (FDR) < 0.05], of which 782 were up-regulated and 585 were down-regulated compared to vehicle-treated cells (Fig. 3A and table S2). EnrichR (*52*, *53*) Gene Ontology (GO) pathway analysis revealed that OxPAPC induced pathways associated with oxidative stress, including the "NRF2-mediated oxidative stress response," the "unfolded protein response," and the "aryl hydrocarbon receptor signaling pathway," as well as the "superpathway of cholesterol biosynthesis" (fig. S4A), suggesting that OxPCs contribute to dysregulating cholesterol metabolism, a hallmark of NAFLD (*54*).

Since our data showed that levels of both truncated and full-length OxPCs were decreased by scFv-E06, we separated OxPAPC into two fractions enriched for either truncated or full-length OxPC species using a strong anionic solid phase exchange chromatography method that we previously described (*34*). Treatment of AML12 cells with truncated OxPCs resulted in regulation of 720 genes (427 up-regulated, 293 down-regulated), while full-length OxPCs regulated the expression of 259 (204 up-regulated, 55 down-regulated) genes (Fig. 3B). Of those, truncated OxPCs uniquely regulated 78 genes (30 up/45 down), while full-length OxPCs uniquely down-regulated 2 genes (Fig. 3B and table S2). Both truncated and full-length OxPAPC up-regulated genes associated with oxidative stress such as *Hmox1*, *Gsta1*, *Txnrd1*, *Hspa1a*, and *Hspa1b*, as well as *Ptgs2* (cyclooxygenase 2) (table S2). In addition, qRT-PCR confirmed that full-length OxPCs, truncated OxPCs, and OxPAPC up-regulated the expression of *Hmox1* (fig. S4D) and *Pgd* (fig. S4E), while only truncated OxPCs up-regulated *Acly* (fig. S4F), *Hmgcoas* (fig. S4G), and *Hmgcoar* (fig. S4H). GO Biological Pathway analysis revealed that, like OxPAPC, both truncated OxPCs and full-length OxPCs induced the "NRF2-mediated oxidative stress pathway"; however, only truncated OxPCs induced the "superpathway of cholesterol biosynthesis" (Fig. 3, D and E, and fig. S4A). Moreover, truncated OxPAPC down-regulated the expression of *Cav1* (caveolin 1), which has been shown to increase hepatic lipid droplet size in NAFLD (*55*–*57*), and up-regulated *Slc25a1*, which has recently been associated with hepatic steatosis and glucose intolerance by dysregulation of hepatocyte metabolism (*58*).

To investigate the effect of OxPCs on hepatocyte metabolism, we treated AML12 cells with OxPAPC or the fractions enriched for truncated or full-length OxPCs for 4 hours and measured oxygen consumption rate via extracellular flux analysis. Treatment with OxPAPC significantly decreased maximal oxygen consumption rate (Fig. 4A), which was mimicked by truncated OxPCs (Fig. 4B). Impaired oxygen consumption in hepatocytes is indicative of mitochondrial dysfunction that precedes the transition from steatosis to NASH (*9*, *59*). To investigate whether this metabolic dysregulation would lead to increased lipid accumulation, we treated AML12 hepatocytes with OxPAPC, truncated OxPCs, or full-length OxPCs for 48 hours and then stained cells with Nile red to quantify lipid droplet numbers and size (*60*). Consistent with the effects on hepatocyte mitochondrial function, OxPAPC (Fig. 4C) and truncated OxPCs (Fig. 4D) increased average lipid droplet size in cells compared to vehicle, while full-length OxPCs (Fig. 4E) did not alter lipid droplet size (Fig. 4F). However, both fractions increased the number of lipid droplets per cell compared to vehicle control (Fig. 4G).

Together, these data demonstrate that distinct OxPC species differently regulate hepatocyte gene expression and metabolic function in vitro. While both truncated and full-length OxPCs regulate

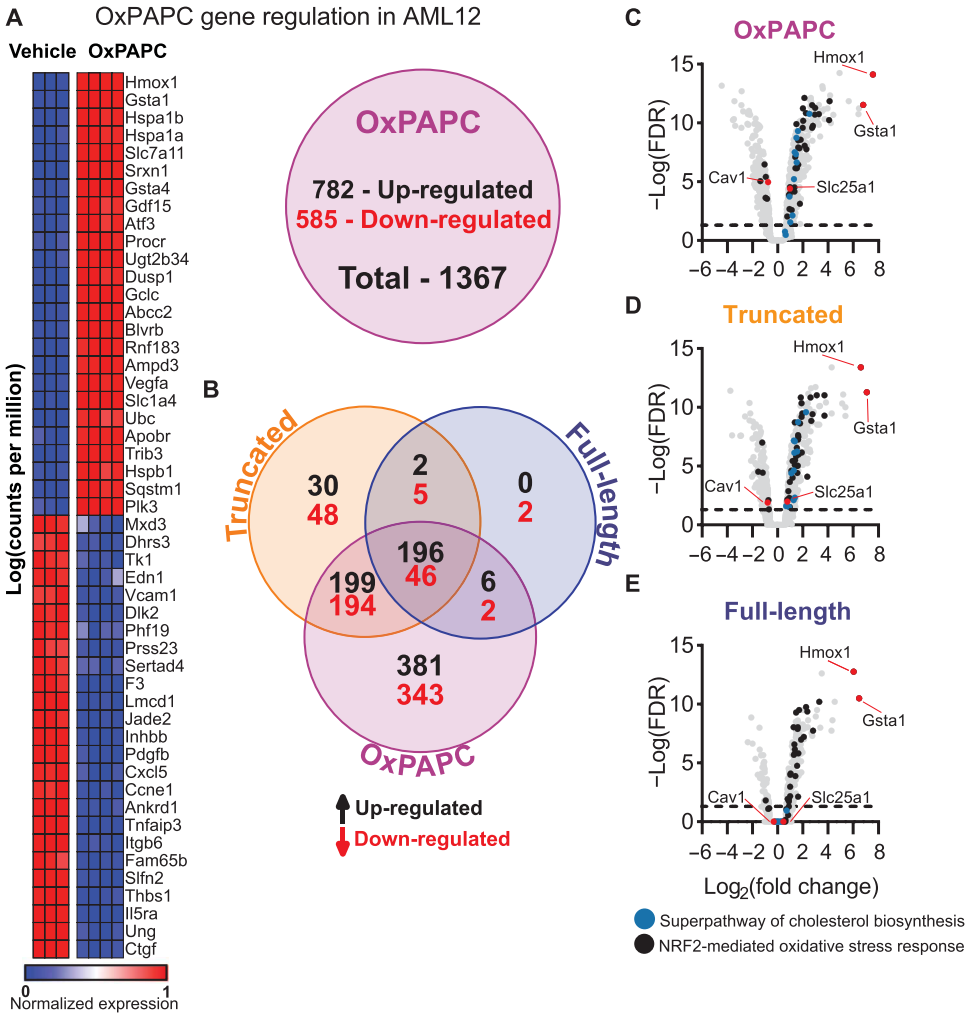

Fig. 3. Truncated OxPLs shift AML12 hepatocytes to an anabolic metabolic programming. AML12 hepatocytes were treated with OxPAPC (100 μg/ml) for 4 hours, and gene expression was measured via RNA-seq. (**A**) OxPAPC regulated 1367 genes (782 up-regulated/585 down-regulated, fold change > |1.5| and adjusted $P < 0.05$; vehicle, $n = 3$; OxPAPC; $n = 4$). (**B**) Truncated OxPLs uniquely regulated 78 genes (30 up-regulated/48 down-regulated) compared to 2 down-regulated genes in full-length OxPL and 724 (381 up-regulated/343 down-regulated) in OxPAPC treatment with 242 regulated by all three treatments (196 up-regulated/46 down-regulated) (fold change > |1.5| and adjusted $P < 0.05$, $n = 3$ to 4). Volcano plot analysis of (**C**) OxPAPC, (**D**) truncated OxPAPC, and (**E**) full-length OxPAPC revealed that *Hmox1* and *Gsta1* were the most highly up-regulated genes in all three treatments along with genes associated with the NRF2-mediated oxidative stress response. *Slc25a1* and *Cav1* were regulated in OxPAPC and truncated OxPL treatment, but not in full-length OxPL treatment. The same pattern was observed for genes associated with the superpathway of cholesterol biosynthesis. Statistical significance was determined by one-way ANOVA and Student's *t* test. Multiple comparisons were corrected by FDR or Dunnett's multiple comparison correction.

redox transcriptomic programming, only truncated OxPCs regulate anabolic gene programming, such as the superpathway of cholesterol biosynthesis, and inhibit mitochondrial oxygen consumption, resulting in increased lipid droplets.

scFv-E06 after development of hepatic steatosis halts disease progression to fibrosis

To test whether elimination of OxPCs through inducible expression of scFv-E06 during the transition from steatosis to NASH could halt the progression to fibrosis, we first fed age-matched Alb-cre mice an FPC diet for 6 weeks (Fig. 5A), which established hepatic steatosis without signs of fibrosis. Then, weight-randomized mice were injected with AAV8-scFv-E06 or AAV8-GFP via tail vein. To induce fibrosis, mice were fed FPC diet for an additional 14 weeks (Fig. 5A). Sustained scFv-E06 gene expression was confirmed in the liver (fig. S5A), and scFv-E06 protein was detected in the liver by Western blot and in the plasma by ELISA (Fig. 5, B and C) at the end of the experiment (20 weeks). As expected, FPC diet significantly elevated body mass and body fat percentage compared to chow control (fig. S5, B and C); however, there were no differences in body mass (fig. S5B); body fat percentage (fig. S5C); liver, adipose, lung, heart, kidney, and spleen mass (fig. S5, D to I); and fasting glucose and insulin tolerance between AAV8-scFv-E06– or AAV8-GFP–treated mice at 20 weeks (fig. S5, Q to S).

Notably, intervention with AAV8-scFv-E06 protected mice with established hepatic steatosis from further liver injury as evidenced by significantly reduced plasma AST (Fig. 5D), ALT (Fig. 5E), ALP (Fig. 5F), LDL:HDL ratio (fig. S5J), and cholesterol:HDL ratio

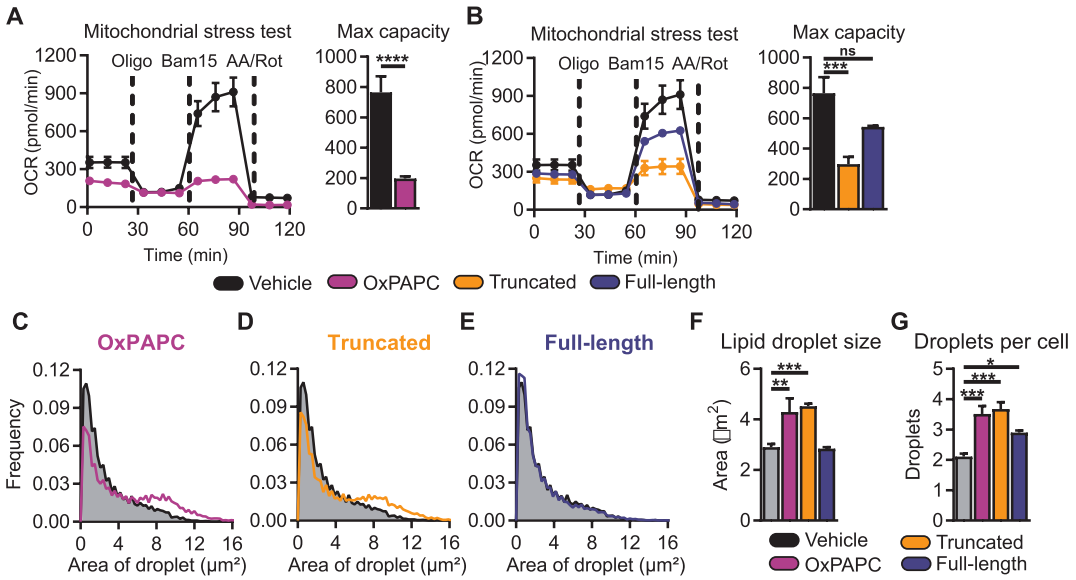

Fig. 4. Truncated oxidized phospholipids dysregulate hepatocyte metabolism resulting in lipid droplet accumulation. (**A**) Mitochondrial stress test analysis of AML12 murine hepatocytes treated with OxPAPC (100 μg/ml) for 4 hours significantly inhibited maximum oxygen consumption in hepatocytes ($n = 5$). (**B**) Truncated, but not full-length, OxPLs significantly inhibited maximum mitochondrial oxygen consumption rate ($n = 5$). AML12 cells were treated with (**C**) OxPAPC (100 μg/ml), (**D**) truncated OxPAPC, and (**E**) full-length OxPAPC for 48 hours. (**F**) Lipid droplet size and (**G**) number were significantly increased in AML12 cells treated with OxPAPC and truncated OxPLs. Full-length OxPLs increased droplet number per cell ($n = 4$, three fields of view per biological replicate). Statistical significance was determined by one-way ANOVA and Mann-Whitney *U* test. Multiple comparisons were corrected by FDR or Dunnett's multiple comparison correction (*$P < 0.05$, **$P < 0.01$, ***$P < 0.001$, and ****$P < 0.0001$). OCR, oxygen consumption rate.

(fig. S5K), indicating significantly improved liver function compared to control mice. Plasma cholesterol (fig. S5L), LDL (fig. S5M), HDL (fig. S5N), triglycerides (fig. S5O), and albumin (fig. S5P) were not changed by expression of scFv-E06. Total hepatic triglyceride levels were not affected by AAV8-E06 (Fig. 5G); however, histological analysis by H&E and Oil red O staining revealed a decrease in average lipid droplet size and a concomitant increase in lipid droplet number (Fig. 5, H and I) in the livers of mice expressing scFv-E06, a pattern of lipid droplet morphology suggestive of improved liver health (*6*).

To examine whether intervention with AAV8-scFv-E06 affects hepatic gene expression in mice with established steatosis during NASH progression, we performed RNA-seq in bulk liver tissue from mice that were treated with either AAV8-scFv-E06 or AAV8-GFP. Notably, 701 genes (154 up-regulated and 547 down-regulated in scFv-E06–expressing mice) were differentially expressed (fold change > 1.5, FDR < 0.05) between AAV8-scFv-E06– and AAV8-GFP–treated mice. EnrichR and GO Pathway Analysis for Biological Processes revealed that the most significantly down-regulated GO term in the scFv-E06–expressing group was "Extracellular Matrix Organization," indicating down-regulation of genes associated with matrix production and consequently hepatic fibrosis (Fig. 5J). In addition, "Regulation of Cell Migration," "PDGFR Signaling Pathway," "Cell Matrix Adhesion," and "Regulation of Macrophage Cytokine Production" were all down-regulated, suggesting a reduced fibrotic and inflammatory tone in the liver of mice expressing scFv-E06. Extracellular matrix protein (ECM) gene regulation was confirmed by qRT-PCR. Overall, expression of a panel of ECM proteins was significantly lower in livers of scFv-E06–expressing mice (fig. S6). To assess the extent of hepatic fibrosis in mice expressing scFv-E06, we quantified picrosirius red staining in livers after 20 weeks of FPC diet, which revealed a trend toward a decrease in positive staining in mice that received intervention with scFv-E06 (Fig. 5K). Liver hydroxyproline concentration was significantly increased in GFP-expressing mice fed FPC diet for 20 weeks compared to chow (Fig. 5L), and the FPC-induced increase in hydroxyproline was attenuated by intervention with scFv-E06 after 6 weeks on diet (Fig. 5M). Together, these data demonstrate that intervention with scFv-E06 in mice with established steatosis protects mice from further diet-induced liver damage and hepatic fibrosis.

Biologically active oxidized phospholipids are reduced by interventional expression of scFv-E06 during the progression to hepatic fibrosis

To identify OxPC species that are affected by intervention with AAV8-scFv-E06 in the plasma of mice during the progression to fibrosis, we performed LC-MS as described above, using the in silico–predicted and in vitro–validated compound list (Fig. 2, I and J). We identified 29 OxPC analytes or groups of isobaric compounds and 6 nonoxidized PCs in the plasma of mice with hepatic fibrosis (Fig. 6A). A similar but less pronounced reduction in OxPCs was observed in the liver of scFv-E06 mice compared to GFP controls (sup. Fig. 6B). In addition, there was a slight but statistically significant decrease in nonoxidized PCs in the scFv-E06 liver (fig. S6B). In the plasma, the majority of both truncated and full-length OxPCs were significantly decreased in scFv-E06–expressing mice and included several previously described biologically active compounds containing specific functional groups. Among decreased truncated OxPC species were the carboxylic acid–containing 1-palmitoyl-2-glutaryl-*sn*-glycero-3-phosphocholine (PGPC; *m/z* 610) as well as PazPC (*m/z* 666) (*45*, *46*), a group of γ-keto/hydroxy OxPCs [C32H60NO10P

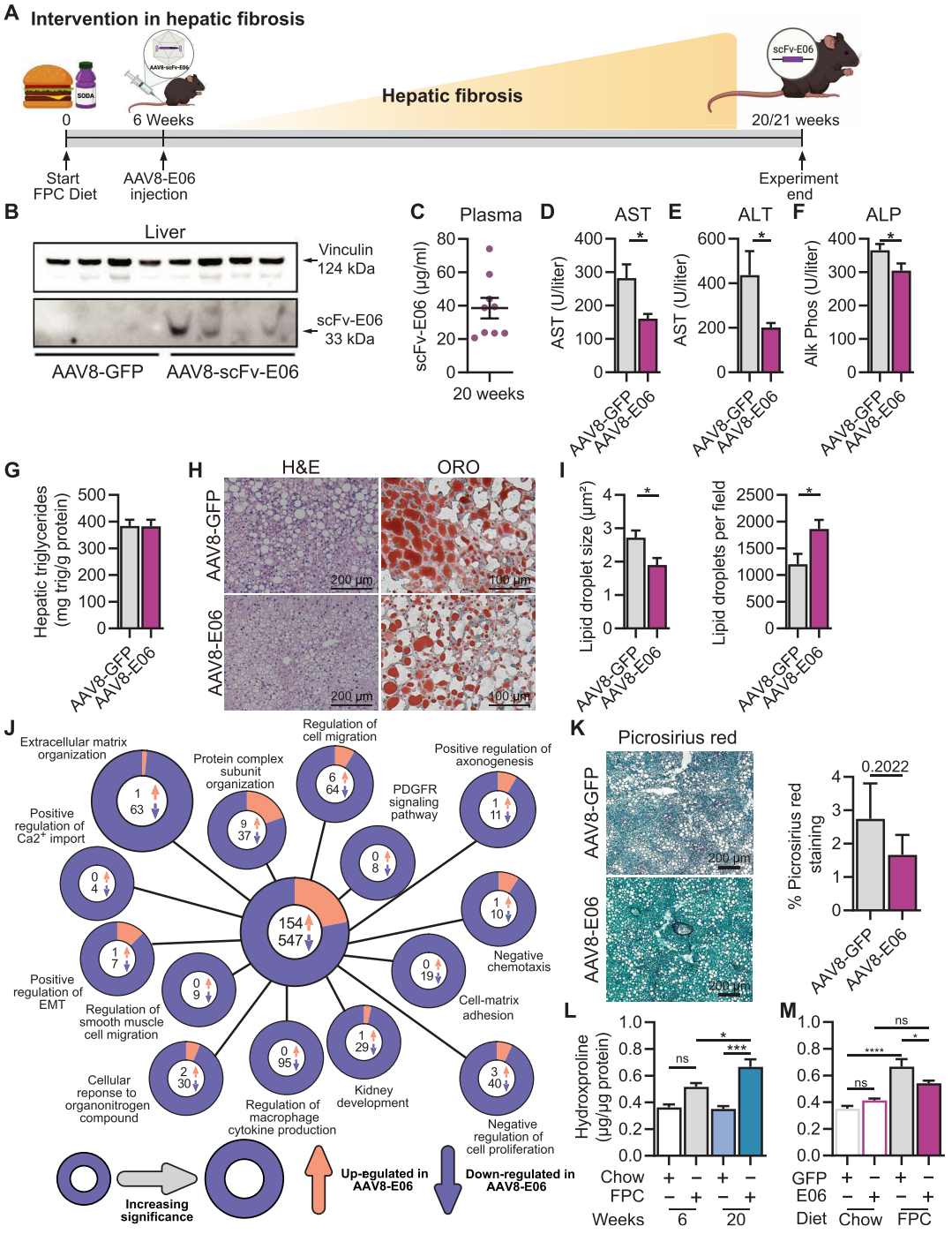

Fig. 5. Passive genetic immunization against oxidized phospholipids inhibits liver fibrogenesis. (**A**) Schematic of experimental design. Mice were challenged with FPC diet for 6 weeks. After 6 weeks, mice were injected with AAV8-GFP or AAV8-E06 and fed FPC diet for an additional 14 weeks (total: 20 weeks) (created with BioRender.com). (**B**) Expression of scFv-E06 in mouse liver 14 weeks after injection. (**C**) scFv-E06 titer concentrations were estimated in plasma by competitive sandwich ELISA. (**D**) Plasma AST, (**E**) ALT, and (**F**) ALP levels were decreased in mice expressing scFv-E06 ($n = 6$). (**G** and **H**) H&E and ORO staining revealed no difference in hepatic triglycerides with an (**I**) increased droplet size but reduced number in mice expressing scFv-E06 (GFP, $n = 6$; scFv-E06, $n = 6$; 15 fields of view per biological replicate). (**J**) Pathway analysis of differential gene expression in bulk liver tissue identified 701 genes (154 up-regulated/547 down-regulated) that were significantly regulated by scFv-E06 expression (GFP, $n = 3$; scFv-E06, $n = 3$; fold change > |1.5| and FDR < 0.05). Extracellular matrix organization was the most significantly down-regulated pathway in scFv-E06–expressing mice. (**K**) Representative picrosirius red staining of livers from mice expressing GFP or scFv-E06 after 20 weeks of FPC diet. (**L**) Hydroxyproline concentration was measured in liver tissue from mice fed chow or FPC diet for 6 or 20 weeks. (**M**) Liver hydroxyproline concentration was decreased in mice expressing scFv-E06 after 20 weeks on FPC diet compared to GFP-expressing controls. Quantification of picrosirius red confirmed reduced staining in scFv-E06 mice ($n = 4$). Statistical significance was determined by one-way ANOVA, two-way ANOVA, Spearman's correlation, and Student's *t* test with Dunnett's multiple comparisons correction (*$P < 0.05$). Statistical outliers were excluded using ROUT test with $Q = 2\%$.

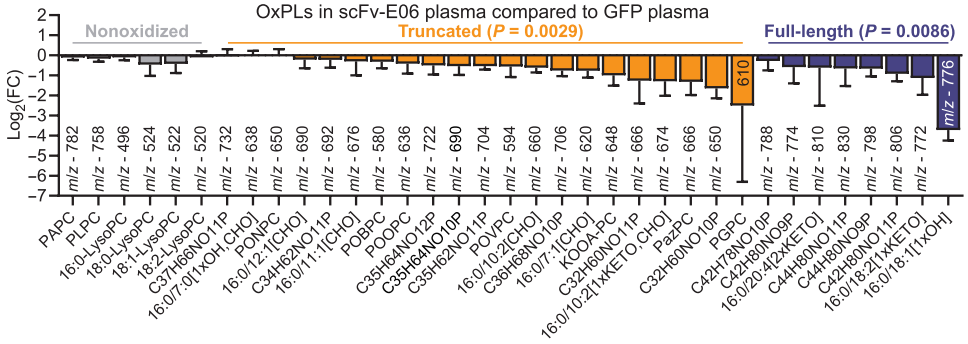

Fig. 6. scFv-E06 expression decreases plasma OxPL levels in mice with hepatic fibrosis. OxPL levels were measured in the plasma by LC-MS. Both truncated and full-length OxPLs were significantly reduced by scFv-E06 expression. Nonoxidized phospholipids were unaffected by scFv-E06 expression. Statistical significance was determined by two-way ANOVA. Multiple comparisons were corrected by FDR.

(isobaric group containing HOOA-PC), *m/z* 650]; HODA-PC [1-palmitoyl-2-(9-hydroxy-12-oxo-10E-dodecenoyl)-*sn*-glycero-3-phosphocholine] (*m/z* 706); KOOA-PC (*m/z* 648); C32H60NO11P (isobaric group containing HOdiA-PC) (*m/z* 666) (*22*, *41*), the aldehyde-containing POVPC (*m/z* 594) (*42*), POBPC (*m/z* 580) (*43*), and POOPC (*m/z* 636) (Fig. 6A) (*44*, *45*). Among the most substantially reduced full-length OxPCs were HOME-PC (*m/z* 776) and three isobaric species containing HODE-PC (*m/z* 774), an isobaric group with an *m/z* of 798, containing HETE-PC (*61*), and an isobaric group with an *m/z* of 830, containing isoprostane-PC (Fig. 6A) (*48*, *49*). The predicted structures of the identified compounds with corresponding *m/z* values are shown in table S3.

Selectivity of scFv-E06 for oxidized PCs was further illustrated by the fact that expression of scFv-E06 specifically decreased levels of truncated and full-length OxPC species, while none of the other lipid classes were significantly affected, as demonstrated by comparison of the overall plasma lipidome between scFv-E06– and GFP-expressing mice after either 6 (steatosis) or 20 (fibrosis) weeks of FPC feeding (fig. S7A). Comparing the OxPC profiles at the different stages of disease progression not only demonstrated that individual OxPC species are differentially affected by scFv-E06 but also indicated that levels of OxPCs may be selectively affected during disease progression.

To study the changes in the levels of the different OxPC classes during the progression from hepatic steatosis to fibrosis, we compared OxPC levels in control mice (expressing AAV8-GFP) that had been fed FPC diet for 6 and 20 weeks to their chow-fed counterparts. Of the nonoxidized species, PAPC and 16:0 LysoPC were decreased after 6, but not 20, weeks on diet, while PLPC and 18:0, 18:1, and 18:2 LysoPC were increased after both 6 and 20 weeks on FPC diet (Fig. 7A). Of the truncated OxPC species, levels of a subset of aldehyde-containing OxPCs, including POVPC, were lower at both 6 and 20 weeks, while carboxylic acid–containing and other aldehyde-containing OxPCs, including POBPC, were increased in response to FPC diet (Fig. 7A).

Full-length OxPC species were differentially regulated at different time points. At 6 weeks, levels of 16:0/18:1[1xOH] trended to be lower compared to chow but higher at 20 weeks. 16:0/18:2[1xKETO] was higher at 6 weeks compared to chow and lower at 20 weeks. Isobaric groups C44H80NO10P and C42H80NO9P, which contain HETE-PCs and HODE-PCs, were significantly higher at 20 weeks. Together, these data show that levels of plasma nonoxidized and individual OxPC species are differently regulated at defined stages of NAFLD progression.

Comparison of OxPCs that were affected by AAV8-scFv-E06 in the plasma of mice at the initiation of hepatic steatosis (Fig. 2K) and during the progression to hepatic fibrosis (Fig. 6A) revealed 28 OxPC species that were decreased in both settings, while 1 OxPC was uniquely identified in hepatic steatosis and 7 OxPC species were uniquely detected in mice with hepatic fibrosis (fig. S7B). Of the seven unique species identified in hepatic fibrosis, four were decreased by more than 50% by scFv-E06. These four species include two previously identified biologically active OxPCs: KOOA-PC and the isobaric group C32H60NO11P containing HOdiA-PC (*41*).

To elucidate at which stage of disease progression these identified OxPC species may exert pathologic activity, we took a closer look at the timeline of scFv-E06–mediated reduction of their plasma levels. The aldehyde-containing species POVPC, POOPC, and 16:0/7:1[CHO] were preferentially reduced by scFv-E06 after 6 weeks on FPC diet (Fig. 7B), implying a role in the initiation of hepatic steatosis. To test whether aldehyde-containing OxPCs affect hepatocyte lipid storage, we treated AML12 hepatocytes with POVPC for 48 hours and assessed lipid droplet size and number per cell. POVPC significantly increased the number and size of lipid droplets (Fig. 7C). On the other hand, carboxylic acid–containing OxPC species (PazPC and C35H62NO11P) were affected by scFv-E06 predominantly after 20 weeks of FPC diet (Fig. 7D), implying a role for these compounds in NAFLD progression to NASH. Treatment of AML12 cells with PGPC (a carboxylic acid–containing OxPC) significantly decreased maximum oxygen consumption rate (Fig. 7E) and increased lipid droplet size and number in a concentration-dependent manner (fig. S8, A and B). Of the γ-keto/hydroxy OxPC species, the levels of KOOA-PC and isobaric group C32H60NO10P (containing HOOA-PC) were reduced by scFv-E06 specifically at 20 weeks of FPC diet (Fig. 7F). Treatment of AML12 hepatocytes for 4 hours with 1-palmitoyl-2-(5-keto-6-octene-dioyl)-*sn*-glycero-3-phosphocholine (KOdiA-PC), a representative γ-keto/hydroxy OxPC, significantly decreased maximum oxygen consumption rate of hepatocytes in a concentration-dependent manner (Fig. 7G). These data show that identified truncated OxPC species that are reduced by scFv-E06 promote a hepatocyte phenotype in vitro that is observed in hepatic steatosis and steatohepatitis.

Hepatic stellate cells are the primary cell niche in the liver that produce fibrotic matrix in response to liver injury (*15*, *62*). To determine

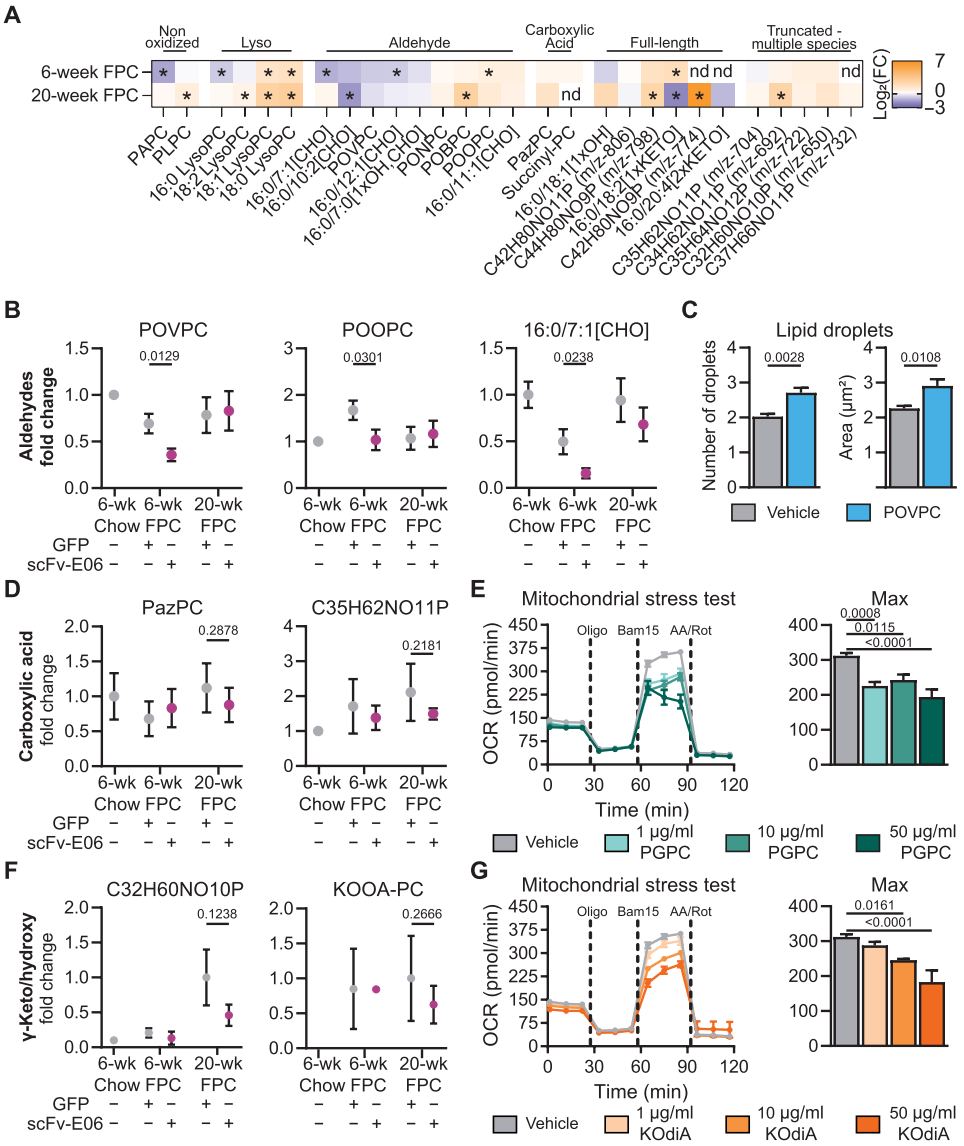

Fig. 7. Bioactive oxidized phospholipids are differentially regulated during hepatic steatosis and fibrosis. (**A**) Semiquantitative analysis of OxPL species normalized to their chow counterparts demonstrates a complex, pathology-specific pattern. (**B**) Aldehyde-containing OxPLs, POVPC (6-week Chow GFP, $n = 3$; 6-week FPC GFP, $n = 7$; 6-week FPC scFv-E06, $n = 6$; 20-week FPC GFP, $n = 10$; 20-week FPC scFv-E06, $n = 10$), POOPC (6-week Chow GFP, $n = 3$; 6-week FPC GFP, $n = 7$; 6-week FPC scFv-E06, $n = 6$; 20-week FPC GFP, $n = 10$; 20-week FPC scFv-E06, $n = 10$), and 16:0/7:1[CHO] (6-week Chow GFP, $n = 3$; 6-week FPC GFP, $n = 5$; 6-week FPC scFv-E06, $n = 5$; 20-week FPC GFP, $n = 7$; 20-week FPC scFv-E06, $n = 8$), were decreased by scFv-E06 expression at 6 weeks. (**C**) POVPC, a representative of the aldehyde class, increased lipid droplet size and number after 48 hours in AML12 hepatocytes ($n = 4$). (**D**) Carboxylic acid–containing OxPLs were decreased by scFv-E06 after 20 weeks on diet (6-week Chow GFP, $n = 3/1$; 6-week FPC GFP, $n = 7/4$; 6-week FPC scFv-E06, $n = 5/2$; 20-week FPC GFP, $n = 9/5$; 20-week FPC scFv-E06, $n = 9/6$). (**E**) PGPC, a representative of the carboxylic acid class, decreased maximum oxygen consumption of AML12 hepatocytes after 4 hours ($n = 8$; 50 µg/ml, $n = 6$). (**F**) γ-Keto/hydroxy–containing OxPLs were decreased after 20 weeks on diet (6-week Chow GFP, $n = 1/0$; 6-week FPC GFP, $n = 5/2$; 6-week FPC scFv-E06, $n = 2/1$; 20-week FPC GFP, $n = 9/2$; 20-week FPC scFv-E06, $n = 8/4$), and (**G**) KOdiA-PC, a class representative, decreased maximum oxygen consumption in AML12 hepatocytes in a dose-dependent manner ($n = 8$). Statistical significance was determined by Student's *t* test.

whether individual OxPC species that were targeted by scFv-E06 could activate hepatic stellate cells, we challenged LX-2 human hepatic stellate cells with OxPAPC, full-length OxPCs, truncated OxPCs, POVPC, or KOdiA-PC. Treatment of LX-2 hepatic stellate cells for 4 hours with KOdiA-PC, OxPAPC, or POVPC significantly decreased maximum oxygen consumption rate of hepatic stellate cells (fig. S8C).

Previously, *Hmox1* has been implicated in fibrotic activation of hepatic stellate cells (*63*). We found that truncated OxPCs and OxPAPC increased the expression of the NRF2-dependent genes *Hmox1* and *Gclm* in LX-2 human hepatic stellate cells (fig. S8D).

Together, these data demonstrate that expression of scFv-E06 decreases levels of individual OxPCs in plasma. FPC diet results in multivariate changes in the OxPC lipidome, which suggest complex

regulation of OxPC species in pathology. Identified OxPC species that were decreased by scFv-E06, including aldehyde-, carboxylic acid–, and γ-keto/hydroxy–containing OxPCs, regulate metabolism and gene expression in hepatocytes and hepatic stellate cells, suggesting that they are actively involved in the initiation and progression of hepatic steatosis and fibrosis (Fig. 8A).

DISCUSSION

Here, we examined a potential therapeutic application of AAV-mediated hepatic expression of the oxidized phospholipid-binding antibody fragment scFv-E06 for the prevention of the initiation of NAFLD and, independently, of the progression to NASH and hepatic fibrosis. We show that AAV8-mediated gene transfer of scFv-E06 is sufficient to express scFv-E06 in a cre-dependent manner in the liver, which by itself leads to secretion of scFv-E06 protein into the plasma. Expression of scFv-E06 in mice fed a chow diet did not alter normal mouse physiology, which provided an excellent tool to interrogate the effect of OxPCs on diet-induced NAFLD initiation and disease progression, without secondary effects on mouse physiology or development, while providing a way to regulate dosing and timing of expression. We demonstrated that hepatic expression of scFv-E06 before the start of FPC diet feeding resulted in a marked reduction in individual OxPC species in plasma, which was sufficient to protect mice from diet-induced hepatic steatosis. Given the efficacy of this model in eliminating plasma OxPCs and subsequent protection from diet-induced hepatic steatosis, we leveraged the flexibility of virus-mediated gene transfer to intervene therapeutically with scFv-E06 expression after the establishment of diet-induced hepatic steatosis. We showed that, in a clinically relevant intervention model, scFv-E06 expression prevented further diet-induced liver damage and hepatic fibrosis independent of obesity and insulin resistance. Separately, scFv-E06 expression was sufficient to reduce a variety of OxPC species in plasma. At present, it is unclear whether reduction of OxPCs is protective in NASH pathogenesis or simply a biomarker of the therapeutic effect of scFv-E06. Using mass spectrometry, we identified individual OxPC species that are decreased by expression of scFv-E06 in mice. Identified OxPC species induced gene expression and metabolic changes in hepatocytes and stellate cells in vitro. These data suggest that plasma OxPCs regulate liver function uniquely at different stages of disease progression. For instance, expression of scFv-E06 before the start of FPC diet protected mice from hepatic steatosis, while intervention with scFv-E06 after established steatosis did not reduce lipid burden in the liver. Despite no overall decrease in lipid burden, scFv-E06–expressing mice had smaller hepatic lipid droplets. This may suggest that OxPCs are involved in dysregulation of cellular lipid storage vital to initiation of hepatic steatosis but not maintenance of steatosis. Together, this suggests that lowering the concentration of identified plasma OxPC species is necessary for preventing hepatic steatosis and progression to fibrosis in a normolipidemic mouse model of diet-induced NAFLD without genetic lipodystrophy. Using this approach, we provide the first evidence that therapeutic intervention after the development of diet-induced steatosis with virus-induced scFv-E06 expression halts progression to hepatic fibrosis in a clinically relevant model of NAFLD.

The natural IgM E06 has been shown to recognize oxidized products of PAPC in vitro and has been used clinically to assess total plasma OxPC levels (*36*, *64*). However, individual OxPC species that are eliminated by E06 in vivo had not been identified. Our findings demonstrate that scFv-E06 recognizes a variety of OxPC species irrespective of the type of oxidative modification or *sn*-1 position acyl-chain length while not affecting plasma levels of nonoxidized lipids in vivo. Further research is necessary to investigate binding affinities and specificity of scFv-E06 among OxPC species and to demonstrate the potency of scFv-E06 as a potential therapeutic in the context of NAFLD and other oxidative stress–induced diseases.

Oxidized phospholipids have previously been shown to regulate numerous cellular functions and biological processes (*20*, *21*, *27*, *29*, *30*, *34*, *35*, *38*, *65*–*67*). We show that individual OxPCs that are targeted by scFv-E06 activate hepatocytes, resulting in up-regulation of the evolutionarily conserved NRF2-dependent antioxidant program and metabolic dysregulation. While both truncated

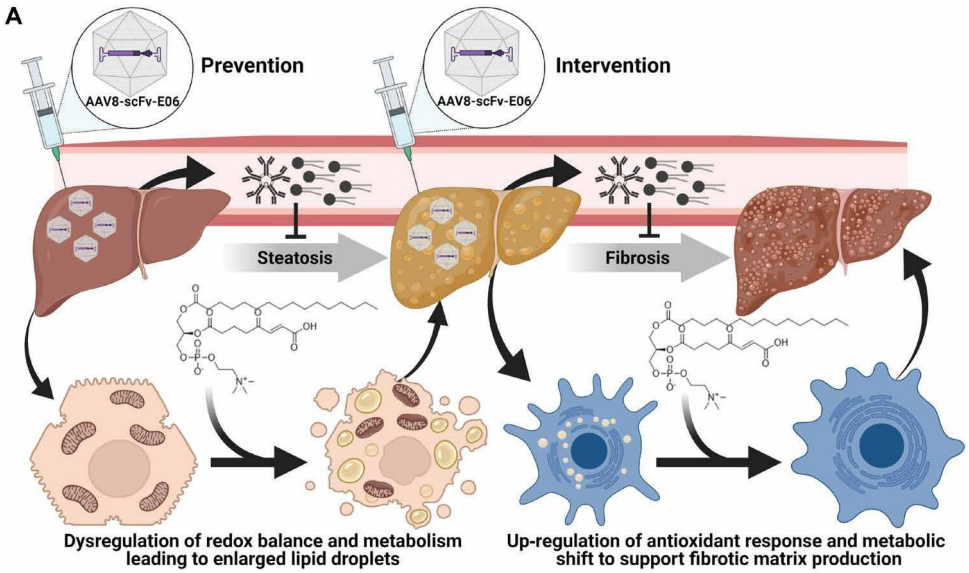

Fig. 8. scFv-E06 expression protects mice from hepatic steatosis, and intervention with viral expression of scFv-E06 halts disease progression. (Created with BioRender.com)

and full-length OxPCs up-regulated genes related to oxidative stress, only truncated OxPCs up-regulated prosteatotic anabolic pathways including cholesterol biosynthesis. Induction of de novo cholesterol synthesis leading to cholesterol accumulation has been shown to promote transition from hepatic steatosis to NASH (*68*) and may be one mechanism through which OxPCs promote disease progression. Furthermore, identified OxPCs inhibited mitochondrial oxygen consumption in hepatocytes, consistent with a switch to an anabolic cellular phenotype, and resulted in increased lipid droplet formation, a hallmark of hepatic steatosis (*6*). Together, our findings demonstrate that hepatocytes recognize and respond to OxPCs, and treatment of hepatocytes in vitro with truncated OxPCs phenocopies pathological alterations in mitochondrial bioenergetics and lipid droplet regulation seen during the development of hepatic steatosis. Differences in regulation of the transcriptome in mice expressing scFv-E06 compared to GFP during development of diet-induced hepatic steatosis may give key insights into the mechanisms by which OxPCs drive early metabolic changes in hepatocytes that promote disease initiation.

Levels of truncated OxPCs containing a γ-keto/hydroxy functional group were also reduced by scFv-E06 in vivo. Several biological functions have been described for these lipids (*22*, *41*); however, it is unknown if γ-keto/hydroxy–containing OxPCs play a role in NASH and hepatic fibrosis. Here, we show that KOdiA-PC inhibits mitochondrial oxygen consumption and extracellular acidification rate in hepatic stellate cells. In addition, truncated OxPCs induced expression of the NRF2-dependent genes *Hmox1* and *Gclm* in hepatic stellate cells. These data demonstrate that individual truncated OxPCs that are targeted by scFv-E06 regulate hepatic stellate cell bioenergetics and gene expression and may polarize the cells toward a redox-regulatory state.

Plasma levels of both truncated and full-length OxPC species were significantly reduced by scFv-E06 either at the initiation of hepatic steatosis or during the progression to hepatic fibrosis. These data demonstrate that scFv-E06 specifically recognizes individual oxidized phosphorylcholine phospholipids in vivo, without affecting levels of OxPCs or lyso-PCs, which builds on previous studies that have demonstrated similar specificity of E06 in vitro (*37*, *69*). We identified one unique OxPC species in the setting of hepatic steatosis and seven unique OxPC species in the setting of hepatic fibrosis that are targeted by scFv-E06. Identification of specific OxPC species that are eliminated by scFv-E06 during the different stages of disease progression suggests that plasma OxPCs could serve as noninvasive biomarkers of NAFLD severity. In human plasma, oxidized phospholipids are carried on LDLs and previous work has shown that the ratio of OxPCs to apoB-100 or apo(a) correlates with cardiovascular disease, calcific aortic valve disease, and aortic valve stenosis (*70*, *71*). These risk factors are assessed from lipoprotein-bound OxPCs. Our method assesses free or "unconjugated" OxPCs. Considering the pathologic role of OxPCs in NAFLD and the dearth of viable noninvasive biomarkers for NASH, analysis of individual unconjugated OxPC species may provide an additional diagnostic metric and possible alternative to more invasive techniques like liver biopsy.

In this study, we limited our analysis to validated OxPC species predicted by LPPTiger (*40*) and identified in air- and copper-oxidized PAPC and PLPC. Combining an in silico–based approach with in vitro validation allowed us to assess 83 validated analytes (individual lipid species and isobaric groups); however, this accounts for only a fraction of the possible oxidation species present in vivo. Given the numerous possible oxidative modifications that can arise as products of oxidation, many oxidized phospholipid species are isobaric requiring additional metrics to accurately distinguish individual species. In this study, we leverage both mass and chromatographic retention time to distinguish between OxPC species. Consequently, isobaric species with similar retention times were not uniquely identified. Future studies are necessary to identify unique fragmentation patterns for isobaric species that overlap chromatographically to confidently identify each species. In addition, expanding the OxPL panel to include not only other OxPC species but also phospholipids with other head groups, which have been shown to play critical roles in diverse biological processes ranging from thrombus formation (*72*) to ferroptosis (*31*) and apoptosis (*73*), is essential to understand how OxPLs regulate complex pathologies. Currently, our method is limited to semiquantitation of OxPL species because of the lack of deuterated and nondeuterated OxPL standards. Synthesis of OxPL standards is necessary to directly quantify the concentration of pathology-driving OxPLs in the plasma. In addition, our method measures OxPCs that can be isolated by liquid-liquid organic extraction, which likely reflects the free OxPC lipidome as it is likely that some electrophilic lipid species bind covalently with proteins. For example, POVPC has previously been shown to bind manganese superoxide dismutase (*35*).

We demonstrate that scFv-E06 expression lowers levels of OxPCs in the plasma, which are necessary for pathogenesis of both hepatic steatosis and fibrosis. Furthermore, although OxPC levels are lowered by scFv-E06 expression as measured by mass spectrometry, the mechanism through which this occurs remains unclear. We propose two possible mechanisms that will require further study: (i) elimination from the biological system by enzymatic activity or excretion or (ii) masking of OxPC inhibiting their biological effects. Distinguishing whether it is necessary to lower both plasma and liver OxPC species to inhibit disease progression as well as understanding the mechanism through which OxPC species are lowered by scFv-E06 expression will provide a deeper understanding of the role of OxPC species in NAFLD pathology and guide future therapeutic approaches.

In conclusion, our study establishes the translational potential of plasma OxPC elimination using AAV8-mediated gene transfer of scFv-E06 in a clinically relevant NAFLD model. This approach to target plasma OxPCs provides multimodal control over oxidized lipid-driven pathologies. Temporal and spatial regulation of scFv-E06 expression will allow for exploration of previously inaccessible OxPC-mediated biology and pathology. Last, assessment of plasma levels of individually identified, pathology-driving OxPC species during NAFLD initiation and progression may lead to the discovery of urgently needed noninvasive biomarkers.

MATERIALS AND METHODS

Study design

The objective of this study was to determine whether AAV8-induced expression of scFv-E06 was sufficient to prevent hepatic steatosis by decreasing plasma OxPCs, and further to intervene in progression from hepatic steatosis to hepatic fibrosis by decreasing plasma OxPCs. Group size was selected on the basis of similar studies previously reported in the literature. The number of mice included in all groups was selected before the start of study and not altered throughout the study. End points to assess hepatic steatosis (6 weeks on diet)

and hepatic fibrosis (20 weeks on FPC diet) were defined before the start of the study. Mice were randomized into each group based on body mass and excluded from analysis if they did not gain weight in response to FPC diet feeding. The study was blinded for the duration of FPC diet feeding and after for all subjective analyses. All animal experiments were approved by the University of Virginia's Animal Care and Use Committee (protocol #3444). For each analysis, statistical outliers were assessed using the robust regression and outlier removal method (ROUT) method ($Q = 5\%$). Outliers were excluded from final analysis and determination of statistical significance. All in vitro experiments were conducted, at minimum, in duplicate, and representative results were reported.

Generation of AAV8-scFV-E06

We developed a cre-dependent adeno-associated viral construct for expression of scFv-E06. The E06 coding region was synthesized by GenScript from the publicly available, published sequence (Piscataway, NJ, USA), containing a C-terminal myc- and His-tag and flanking 5′ Mlu I and 3′ Nhe I restriction sites. This DNA fragment was then cloned into the unique Nhe I–Asc I restriction sites of pAAV-EF1a-double floxed-hChR2(H134R)-EYFP-WPRE-HGHpA (gift from K. Deisseroth—Addgene, plasmid #20298). The subsequent construct contained the scFv-E06 fusion in the inverse orientation from the EF1a promoter. Cre recombinase expression then reverses the orientation of scFv-E06 and allows expression. AAV viral particles using serotype 8 were then prepared by the University of Pennsylvania Vector Core Facility.

Mice

B6.Cg-Speer6-ps1$^{Tg(Alb\text{-}cre)21Mgn}$/J (The Jackson Laboratory, 003574) (Alb-cre) were obtained from The Jackson Laboratory (Bar Harbor, ME) and housed in the Pinn vivarium at the University of Virginia Center for Comparative Medicine. Unless otherwise stated, animals were maintained in pathogen-free housing with a 12-hour light/dark cycle with ad libitum access to food and water. All animal experiments were approved by the University of Virginia's Animal Care and Use Committee (protocol #3444). To assess the impact of scFv-E06 on hepatic steatosis, 6-week-old mice were injected with either AAV8-GFP (UNC Vector Core) or AAV8-scFv-E06 [10^{11} genome copies/100 μl of sterile phosphate-buffered saline (PBS)]. Mice, 8 weeks of age, were fed a high FPC diet (Teklad TD.190142) supplemented with 4.2% glucose (Thermo Fisher Scientific, D12-500)/fructose (Thermo Fisher Scientific, L95-500) water (55%/45%, w/w) for 6 weeks. At the end of the experiment, mice were euthanized via CO_2 inhalation and cardiac puncture. To assess the impact of scFv-E06 expression on fibrosis and whether expression of scFv-E06 after the onset of hepatic steatosis could mitigate progression to hepatic fibrosis, mice, 6 weeks of age, were fed FPC diet for 6 weeks. After 6 weeks of feeding, mice were injected via tail vein with AAV8-GFP or AAV8-scFv-E06. Mice continued FPC diet for an additional 14 weeks, at which point they were euthanized via CO_2 inhalation. Control mice were fed chow diet (Teklad 7912).

Histology

PBS-perfused liver tissue was either fixed in 10% formalin (w/v) for 24 hours and transferred to 200 proof ethanol or cryopreserved in NEG-50 (Richard Allan Scientific, 6502) and stored at −80°C. Tissue samples were processed for histology at the Robert M. Berne Cardiovascular Research Center Histology Facility at the University of Virginia. Briefly, samples were embedded in paraffin, and 10-μm serial sections were stained with H&E, picrosirius red, or Oil red O. Images were collected using Olympus BX51 or Leica Thunder with a total internal reflection fluorescence microscope operating in bright field. Picrosirius red counterstained with Fast Green was quantified using ImageJ (*74*) to assess stained area in three sections from the liver tissue of each mouse. Positive staining was determined by thresholding while blinded after exclusion of perivascular collagen: Threshold settings were kept constant for all samples assessed.

Triglyceride assay

Hepatic triglyceride concentration was quantified using triglyceride colorimetric assay (Pointe Scientific, T7532500). Liver tissue (20 to 30 mg) was lysed in 400 μl of 0.6% NaCl using Qiagen TissueLyser II (30 Hz for 15 min). Samples were diluted 1:4 in 0.6% NaCl and mixed with 4.4 parts chloroform (EMD UN1888/Fisher Scientific, C607-1) and 2.2 parts methanol (Sigma-Aldrich, 646377-1 L). Samples were vortexed vigorously and centrifuged for 10 min at 3000*g* to accelerate phase separation. The organic phase (500 μl) of each sample was transferred to a new tube and dried under N_2 purge. The dried organic phase was resuspended in 200 μl of 95% ethanol (200 μl) (Fisher Scientific, 04-0355-223). Samples from mice on FPC diet were diluted 1:5 in 95% ethanol. Assay was conducted in triplicate according to the manufacturer's recommendations.

Plasma liver biomarkers

Whole blood was collected from mice after euthanasia via cardiac puncture and dispensed into heparin-coated plasma collection tubes (Becton Dickinson, 365985) and stored on ice. Plasma was separated via centrifugation at 2000*g* for 15 min at 4°C. Plasma was stored at −80°C. Plasma was diluted 1:1 in sterile 0.9% saline, and liver biomarkers were analyzed by UVA Clinical Laboratories.

Cell culture

AML12 murine hepatocytes (American Type Culture Collection, CRL-2254) were cultured in Dulbecco's modified Eagle's medium (DMEM):F12 supplemented with 10% fetal bovine serum (FBS) (R&D Systems, S12450/Atlanta Biologicals, S11150) and 1% Anti-Anti (Gibco, 15240-062) and grown at 37°C with 5% CO_2. Cells were passaged when they reached 90% confluency using 0.5% trypsin (Gibco, 15400-054). LX-2 human hepatic stellate cells (MilliporeSigma, SCC064) were cultured in DMEM supplemented with 2% FBS (R&D Systems,S12450/Atlanta Biologicals, S11150) and 1% penicillin-streptomycin (Gibco, 15140-122) and grown in DMEM (Gibco, 11965-092) at 37°C with 5% CO_2. Cells were passaged when they reached 90% confluency using 0.25% trypsin (Gibco, 25200-056). For all experiments using the LX-2 cell line, cells were cultured on Matrigel (83 μg/ml) (Fisher Scientific, CB-40230) for 24 hours in DMEM containing 1% penicillin-streptomycin before the start of the experiment.

Mitochondrial and glycolytic stress test

XF24 seahorse bioenergetics assay

AML12 hepatocytes (75,000 cells per well) were plated in complete medium in XF24 cell culture microplates (Agilent, 100777-004) and allowed to settle overnight. The following day, cells were treated for 4 hours with oxidized phospholipids (10 to 100 μg/ml) in DMEM:F12 supplemented as described. At the end of the experimental treatment, the medium was removed and replaced with assay appropriate

medium: mitochondrial stress test medium (Corning, 50-003-PB). Oxygen consumption was measured via mitochondrial stress test. The rate of PO_2 (partial pressure of oxygen) consumption was measured every 10 min for a 4-min interval preceded by a 3-min mixing and 3-min waiting interval. Oligomycin A (Sigma-Aldrich, 75351) (0.91 μM), BAM15 (Cayman Chemical Company 17811) (1.667 μM), antimycin A (Sigma-Aldrich, A8674) (7.692 μM), and rotenone (Sigma-Aldrich, R88751G) (7.692 μM) were used to interrogate basal, reserve, and maximum oxygen consumption capacity.

XFe96 seahorse bioenergetics assay

AML12 hepatocytes were plated (25,000 cells per well) in complete medium in XFe96 cell culture microplates (Agilent, 101085-004) and incubated for 1 hour at room temperature before settling overnight at 37°C. The following day, cells were treated for 4 hours with oxidized phospholipids (10 to 100 μg/ml) in DMEM:F12 supplemented as previously described. After treatment, the medium was removed and replaced with assay appropriate medium: mitochondrial stress test medium (Corning, 50-003-PB) and glycolytic stress test medium (Sigma-Aldrich, D5030) supplemented with 143 mM NaCl (Thermo Fisher Scientific, S671-3) and 2 mM L-glutamine (Gibco, 25030-081). Oxygen consumption was measured via mitochondrial stress test. The rate of PO_2 consumption was measured every 10 min for a 4-min interval for 30 min before sequential challenge with (i) oligomycin A (Sigma-Aldrich 75351) (1 μM), (ii) BAM15 (Cayman Chemical Company, 17811) (2 μM), and (iii) antimycin A (Sigma-Aldrich, A8674) (10 μM) and rotenone (Sigma-Aldrich, R88751G) (10 μM). PO_2 consumption was measured as described previously to analyze basal, reserve, and maximum oxygen consumption capacity. Glycolytic rate was measured via extracellular acidification rate. The rate of pH change was measured every 10 min for a 4-min interval for 30 min before sequential challenge with (i) glucose (Sigma-Aldrich, D9434) (20 mM), (ii) oligomycin A (Sigma-Aldrich, 75351) (1 μM), and (iii) 2-deoxyglucose (Sigma-Aldrich, D8375) (80 mM) to interrogate basal, reserve, and stressed glycolytic rate.

Quantitative real-time PCR

In vitro

RNA was isolated from cells lysed in RLT lysis buffer using the RNeasy Mini Kit (Qiagen 74106). The manufacturer's recommendations were followed for RNA isolation. RNA quantity and purity were analyzed by spectrometric analysis. cDNA was synthesized from 250 ng of total RNA using an iScript cDNA synthesis kit (Bio-Rad, 1708891) according to the manufacturer's recommendations. SensiMIX SYBR Green (Bioline, QT615-05) was used to quantify gene expression. Relative gene expression was calculated using the ΔΔCq method normalized to cyclophilin A in AML12 cells and *Hprt* in LX-2 cells.

Ex vivo

Liver tissue was stored at −80°C in RNAlater (Sigma-Aldrich, R0901) until analysis. Liver tissue was lysed using Qiagen TissueLyser II (30 Hz for 15 min) in RLT lysis buffer. The manufacturer's recommendations were followed for RNA isolation using the RNeasy Mini Kit. RNA quantity and purity were analyzed by spectrometric analysis (260/280, >1.8 and <2.2; 260/230, >1.8 and <2.2). cDNA was synthesized from 250 ng of total RNA using an iScript cDNA synthesis kit according to the manufacturer's recommendations. SensiMIX SYBR Green was used to quantify gene expression. Relative gene expression was calculated using the ΔΔCq method normalized to β-2-microglobulin. Primer sequences were generated using NCBI Primer Blast and span an exon-exon junction to ensure mRNA specificity and synthesized by Eurofins or Integrated DNA Technologies (table S4).

Air oxidation of PAPC

One milligram of PAPC (Avanti Polar Lipids, 850459C) was dried in a 13 × 100 borosilicate glass tube (Corning, 99445-13) with nitrogen, covered loosely with aluminum foil to allow gas exchange, and oxidized by exposure to air for 7 to 12 days to generate the oxidized phospholipid mixture, OxPAPC. Level of oxidation was monitored by LC-MS to maintain a consistent oxidation profile.

Copper oxidation of PLPC

Ten micrograms of PLPC (Avanti Polar Lipids, 850458) was transferred to a tube and dried under N_2. PLPC was resuspended in water containing CuCl (10.547 mM) and H_2O_2 (659 mM) and oxidized for 19 hours at 37°C to generate oxidized PLPC (OxPLPC). OxPLPC was extracted via liquid-liquid extraction using chloroform:methanol: water (1:1:1). Briefly, chloroform, methanol, and water were added to a glass tube. The extraction mixture was vortex vigorously and centrifuged at 805*g* for 10 min at 20°C. After centrifugation, the organic layer was transferred to a new a tube and dried under nitrogen. OxPLPC was resuspended in methanol.

Oxidized phospholipid quantification by LC-MS/MS

OxPL extraction from plasma

Plasma was collected from mice as described above and stored at −80°C in 50 μM butylated hydroxytoluene to prevent ex vivo oxidation. Twenty-five microliters of plasma was added to 1.975 ml of high-performance LC (HPLC) water (Tedia, WS2211-001) in a 13 × 100 borosilicate glass tube (Corning, 99445-13). Two milliliters of chloroform (EMD, UN1888/Fisher Scientific, C607-1) and 2 ml of methanol (Sigma-Aldrich, 646377-1L) containing 16.24 nM 1-palmitoyl-2-glutaryl-*sn*-glycerol-3-phosphocholine-*d*6 (Cayman Chemical, 25746) were added and vortexed vigorously. Samples were centrifuged at 805*g* (20°C) for 10 min to accelerate phase separation. The organic phase was transferred to a new tube, and 2 ml of chloroform was added to the original tube. The extraction was repeated twice more for a total of three times. Samples were dried under nitrogen and resuspended in 200 μl of methanol and vortexed vigorously. Samples were transferred to sample vials for LC-MS analysis.

OxPL extraction from liver

Liver tissue was collected from mice and stored at −80°C in 50 μM in butylated hydroxytoluene to prevent ex vivo oxidation. Liver tissue was homogenized using Qiagen TissueLyser II (30 Hz for 15 min) in water. Thirty-five milligrams of tissue was used for extraction as described previously (see the previous section). Samples were resuspended in 200 μl of HPLC butanol (PHARMCO-AAPER 13050-03).

In silico phospholipid oxidation and method development

LPPTiger (*40*) was used to predict possible oxidation products of PAPC and PLPC. Oxidation level was set to level 3. Maximum modification site was set to 8, max keto was set to 8, max peroxy was set to 3, and max epoxy was set to 3. Nine hundred eighty oxidation species were predicted for PAPC, and 67 oxidation species were predicted for PLPC. Isobaric species were combined as a single analyte recording corresponding to the chemical formula. After combining isobaric species, there were 180 potential analytes for PAPC and 35 potential analytes for PLPC. Predicted analytes were validated by mass [<5-ppm (parts per million) variance from predicted mass] using PAPC oxidized by air and PLPC oxidized by copper (I) chloride.

Lipid analysis

Oxidized phospholipids were measured using Thermo Fisher Scientific Q Exactive coupled with a Vanquish UHPLC. Samples were separated by reversed-phase chromatography using C18 Phenomenex 4.6 μm × 100 mm with 69% methanol–31% water with 10 mM ammonium acetate (mobile phase A) and 50% methanol–50% isopropanol with 10 mM ammonium acetate (mobile phase B) at a flow rate of 0.5 ml/min using the following gradient: 0 to 4 min 0% B, 4 to 6 min 0 to 17.5% B, 6 to 12 min 17.5% B, 12 to 14 min 17.5 to 25% B, 14 to 21 min 25% B, 21 to 24 min 25 to 60% B, 24 to 33 min 60% B, 33 to 36 min 60 to 65% B, 36 to 40 min 65% B, 40 to 43 min 65 to 0% B, and 43 to 50 min 0% B. Q Exactive was operated in positive mode using parallel reaction monitoring mode with an inclusion list and the following settings: MS^2 resolution, 17,500; automatic gain control (AGC) target, 1×10^5; maximum injection time (IT), 100 ms; isolation window, 1.0 *m/z*; normalized collision energy, 27. Analyte detection was limited to inclusion list within a specified retention window determined from in vitro OxPAPC and PLPC. Peaks corresponding to individual oxidized phospholipid species or isobaric groups were identified using Xcalibur (v4.1) QuanBrowser based on mass (<5-ppm variance from predicted mass) and validated retentions times. Peak areas were normalized to PGPC-*d*6. Biological replicates were excluded from analysis for an individual analyte if the analyte was not detected.

Lipidomics LC-MS and data analysis

The plasma lipidome was assessed using Thermo Fisher Scientific Q Exactive coupled with a Vanquish UHPLC. Samples were separated by reversed-phase chromatography using Thermo Scientific Acclaim 120 (C18 5 μm 120 Å 4.6 × 100 mm) with 50% acetonitrile, 50% water, and 0.1% formic acid with 10 mM ammonium formate (mobile phase A) and 88% isopropanol, 10% acetonitrile, 2% water, and 0.02% formic acid with 2 mM ammonium formate (mobile phase B) at a flow rate of 400 μl/min using the following gradient: 0 to 4 min 30 to 60% B, 4 to 10 min 60 to 80% B, 10 to 15 min 80 to 90% B, 15 to 24 min 90 to 100% B, 24 to 27 min 100% B, 27 to 27.1 min 100 to 30% B, 27.1 to 31 30% B. Q Exactive was operated in positive mode and collected spectra using full MS data-dependent MS^2 mode with an inclusion list containing analytes in Splash Lipidomix Mass Spec Standard (Avanti, 330707) using the following settings: full MS settings: resolution, 35,000; AGC target, 1×10^5, max IT, 128 ms; scan range, 200 to 1500 *m/z*; dd-MS^2 settings: resolution, 17,500; AGC target, 2×10^5; max IT, 64 ms, loop count, 5; normalized collision energy (NCE), 40. Data were analyzed using LipidSearch (version 4.1.16) with the following settings: search—database: Q Exactive, precursor tolerance, 5.0 ppm; product tolerance, 8.0 ppm; alignment—alignment method, mean; retention time tolerance, 0.25 min. Samples were normalized to the internal standard PGPC-*d*6 to control for extraction efficiency.

In vitro quantification of lipid droplet

AML12 cells were fixed with 4% paraformaldehyde (diluted from 16%, Alfa Aesar, 43368-9M) and stained with Hoechst blue (Invitrogen, 953557) and Nile red (Invitrogen, N1142). Two images (Zeiss Axiovert 200 with QICAM Fast 1394), one of 4′,6-diamidino-2-phenylindole (DAPI) and one of Nile red, were taken at three locations in each well. Lipid droplet size and quantity were calculated from epifluorescent widefield micrographs using an ImageJ plugin, MRI Lipid Droplets (*75*). Lipid droplets were identified as areas larger than five pixels. MRI Lipid Droplets ImageJ plugin was used to identify nuclei in DAPI staining and count total cell number.

In vitro and ex vivo RNA-seq

In vitro

AML12 hepatocytes (100,000 cells per well) were treated with OxPAPC (100 μg/ml), truncated OxPAPC (100 μg/m), and full-length OxPAPC (100 μg/ml) for 4 hours. RNA was isolated using the RNeasy Mini Kit (Qiagen 74106). RNA quantity and purity were analyzed by spectrometric analysis (260/280, >1.8 and <2.2; 260/230, >1.8 and <2.2; RNA integrity number ≥ 8). cDNA libraries were generated using the NEBNext Ultra II Directional RNA Library Prep Kit (New England Biosciences, E7760S). cDNA library fragment size was verified using Bioanalyzer 2100. Samples were sequenced by the UVA Genomics and Technology core with a read length of 75 base pairs (bp) and a target depth of 10 million reads using the Illumina NextSeq 500 Sequencing System.

Ex vivo

After dissection, liver tissue was stored at −80°C in RNAlater (Sigma-Aldrich, R0901) until use. Liver tissue was lysed using Qiagen TissueLyser II (30 Hz for 15 min) in RLT lysis buffer (Qiagen, 1015762). The manufacturer's recommendations were followed for RNA isolation using the RNeasy Mini Kit (Qiagen, 74106). RNA quantity and purity were analyzed by spectrometric analysis (260/280, >1.8 and <2.2; 260/230, >1.8 and <2.2). RNA was shipped to GeneWiz (South Plainfield, NJ). RNA was sequenced in a strand-specific manner with a read length of 150 bp and a target depth of 20 million to 30 million reads.

Data analysis

Reads were aligned using UVA Rivanna Supercluster using Spliced Transcripts Alignment to a Reference (STAR) (*76*). Reads were trimmed and aligned to the mouse reference genome (mm10) with either single- or pair-end alignment where appropriate. Aligned reads were counted, and differential gene expression was calculated if reads exceeded 1 read per million using EdgeR (*77*) and RStudio. Genes were considered differentially expressed if they deviated from the control condition by 50% with a *P* value less than 0.05 (in vitro) or 0.1 (in vivo). EnrichR (*53*) was used to identify pathways that were up- or down-regulated on the basis of differentially regulated genes.

Magnetic resonance imaging

Body composition analysis was performed by EchoMRI-100H on mice before the start of FPC diet feeding and weekly for the duration of feeding.

Western blot

Tissue

Tissues were lysed using Qiagen TissueLyser II (30 Hz for 15 min) in radioimmunoprecipitation assay (RIPA) lysis buffer containing cOmplete Mini protease inhibitors (Roche, 37439120) and phosphatase inhibitors (Sigma-Aldrich, P5726 and P0044). Protein concentration was quantified via Pierce BCA Protein Assay (Thermo Fisher Scientific, 23225). Total protein (25 to 75 μg) was separated by SDS–polyacrylamide gel electrophoresis (PAGE) (8 to 12%) and transferred to nitrocellulose or polyvinylidene difluoride membranes. Membranes were blocked with Intercept Blocking Buffer (LI-COR Biosciences, 927-70001) or 5% bovine serum albumin in tris-buffered saline (TBS) or 5% milk powder in TBS with 0.1% Tween 20 for 1 hour at room temperature. Membranes were

stained with goat anti-myc [horseradish peroxidase (HRP)] antibody (1:30,000; NovusBio, NB600-341) or rabbit anti-vinculin antibody (1:1000; CST, E1E9V) diluted in 1% milk powder in TBS with 0.1% Tween 20 overnight at 4°C. Next, membranes were washed in TBS containing 0.1% Tween 20, followed by incubation for 1 hour at room temperature with HRP-conjugated secondary antibodies (1:10,000 dilution in 1% milk in TBS with 0.1% Tween 20, CST), except for membranes incubated with the goat anti-myc [HRP] antibody. Membranes were washed in TBS containing 0.1% Tween 20 and imaged on the Odyssey Imager (LI-COR Biosciences) or incubated with ECL substrate (Thermo Scientific SuperSignal, 34580) for 5 min at room temperature and imaged using Amersham ImageQuant 800.

Plasma

Plasma was diluted in loading dye (150 μl/ml) and denatured at 95°C for 10 min. Heat-denatured samples were separated by SDS-PAGE gel and transferred to nitrocellulose membranes. Membranes were blocked with PBS Blocking Buffer (LI-COR Biosciences) and for 1 hour at room temperature and stained with a 1:1000 dilution of mouse anti-myc antibody (Millipore, 05-724) overnight at 4°C. The blot was washed three times for 15 min with PBS Blocking Buffer. The blot was stained with the secondary antibody IRDye 800CW Goat anti-Rabbit (1:10,000 in PBS) (LI-COR Biosciences, 926-32211) for 1 hour at room temperature followed by three washes with LI-COR PBS Blocking Buffer. The resulting blot was visualized using the Odyssey Imager (LI-COR Biosciences).

HIS/myc competitive sandwich ELISA

Ninety-six–well Nunc MaxiSorp flat-bottom plates (Thermo Fisher Scientific) were coated with rabbit anti HIS-Tag antibody (1:250 in 1× PBS; CST, 2365S) overnight at 4°C. Coated wells were then aspirated and washed three times with 1× PBS (~1-min soaking in between). After blocking for 1 hour at room temperature with 1× ELISA/Elispot Diluent (Invitrogen, 19045636) diluted in double-distilled water, wells were washed as previously described. Plasma samples were diluted 1:20 in double-distilled water and added into the wells. For the HIS-competitive standard curve, 2 μg of HIS-protein ELISA standard (stock, 50 μg/ml; Cayman Chemical, 0556338) was serially diluted in double-distilled water and E06 plasma sample was added (1:20). The E06 plasma standard curve was generated by serial dilution of plasma. A HIS-protein competitive standard curve was generated by serial dilution of HIS-tagged 4EBP1 (11.1 mg/ml). Blanks were incubated with 1× ELISA/Elispot Diluent. Plates were sealed and incubated overnight at 4°C. Following five washing steps, the detection antibody goat anti–c-Myc HRP-coupled (1:5000 in 1× ELISA/Elispot Diluent; Novus P26) was added to the plates and incubated for 1 hour at room temperature. After washing seven times, 1× TMB ELISA Substrate Solution (eBioscience Inc., E00008-1655) was pipetted into the wells and incubated for 35 min. Absorbance was measured using Plate Reader (BioTek) at 450 and 570 nm.

Glucose and insulin tolerance tests

Intraperitoneal glucose (GTT) and insulin tolerance tests (ITT) were performed on fasted mice at time points indicated. Mice were fasted for 6 hours, and body mass and basal blood glucose were measured via tail vein nick using a glucometer (CVS Health). For GTT, glucose (1 mg/g) in sterile water was administered by intraperitoneal injection, and blood glucose was recorded 15, 30, 45, 60, 90, and 120 min after injection. For ITT, Humulin R (100 U/ml, Lilly) was diluted in sterile 0.9% saline, 0.75 U/kg was administered by intraperitoneal injection, and blood glucose was recorded 15, 30, 45, 60, 90, and 120 min after injection.

Cholesterol assay

Hepatic cholesterol was assessed using the Amplex Red Cholesterol Assay Kit (Invitrogen, A12216). Liver tissue was weighed and lysed in 400 μl of RIPA lysis buffer (EMD Millipore 20-188) using TissueLyser II. The protein concentration of the lysate was determined by Pierce BCA Protein Assay (Thermo Fisher Scientific, 23225). Lysates were diluted (15 μg per reaction) and analyzed in triplicate for free, esterified, and total cholesterol according to the manufacturer's recommendations. Final hepatic cholesterol concentrations were reported as micrograms of cholesterol per milligram of liver protein.

Hydroxyproline assay

Liver tissue (20 to 30 mg) was lysed in 200 μl of HPLC water (Sigma-Aldrich, 270733) using TissueLyser II shaking at 30 Hz for 15 min. Lysates were centrifuged at 20,817*g* at 4°C for 15 min. Supernatants were collected, and protein concentration was assessed by Pierce BCA Protein Assay (Thermo Fisher Scientific, 23225). Five hundred micrograms of protein was diluted 1:1 in 37% HCl (12.1 M) to a final concentration of 1.89 mg/ml in ~6 M HCl. The lysates were incubated at 95°C for 20 hours. After 20 hours, samples were cooled to room temperature and centrifuged at 13,000*g* for 10 min. Supernatants were collected and diluted to 4 M HCl. Hydroxyproline content was assessed using QuickZyme Sensitive Tissue Hydroxyproline Assay (QuickZyme Biosciences QZBTISHYP1) according to the manufacturer's recommendations.

Statistical analysis

Statistical analysis was performed using GraphPad Prism 9. Data are represented as the mean ± SEM. Statistical tests were applied as described in the figure legends. Statistical outliers were identified using the ROUT method ($Q = 2$ or 5%) and excluded from analyses.

SUPPLEMENTARY MATERIALS

Supplementary material for this article is available at https://science.org/doi/10.1126/sciadv.abn0050

View/request a protocol for this paper from *Bio-protocol*.

REFERENCES AND NOTES

1. Z. M. Younossi, Non-alcoholic fatty liver disease—A global public health perspective. *J. Hepatol.* **70**, 531–544 (2019).
2. R. Loomba, A. J. Sanyal, The global NAFLD epidemic. *Nat. Rev. Gastroenterol. Hepatol.* **10**, 686–690 (2013).
3. K. K. Bence, M. J. Birnbaum, Metabolic drivers of non-alcoholic fatty liver disease. *Mol. Metab.* **50**, 101143 (2020).
4. Z. Chen, R. Tian, Z. She, J. Cai, H. Li, Role of oxidative stress in the pathogenesis of nonalcoholic fatty liver disease. *Free Radic. Biol. Med.* **152**, 116–141 (2020).
5. D. H. Ipsen, J. Lykkesfeldt, P. Tveden-Nyborg, Molecular mechanisms of hepatic lipid accumulation in non-alcoholic fatty liver disease. *Cell. Mol. Life Sci.* **75**, 3313–3327 (2018).
6. N. L. Gluchowski, M. Becuwe, T. C. Walther, R. V. Farese, Lipid droplets and liver disease: From basic biology to clinical implications. *Nat. Rev. Gastroenterol. Hepatol.* **14**, 343–355 (2017).
7. M. H. Wehmeyer, B. C. Zyriax, B. Jagemann, E. Roth, E. Windler, J. S. Z. Wiesch, A. W. Lohse, J. Kluwe, Nonalcoholic fatty liver disease is associated with excessive calorie intake rather than a distinctive dietary pattern. *Medicine (Baltimore)* **95**, e3887 (2016).
8. B. A. Neuschwander-Tetri, Hepatic lipotoxicity and the pathogenesis of nonalcoholic steatohepatitis: The central role of nontriglyceride fatty acid metabolites. *Hepatology* **52**, 774–788 (2010).

9. R. S. Rector, J. P. Thyfault, G. M. Uptergrove, E. M. Morris, S. P. Naples, S. J. Borengasser, C. R. Mikus, M. J. Laye, M. H. Laughlin, F. W. Booth, J. A. Ibdah, Mitochondrial dysfunction precedes insulin resistance and hepatic steatosis and contributes to the natural history of non-alcoholic fatty liver disease in an obese rodent model. *J. Hepatol.* **52**, 727–736 (2010).
10. Y. Wei, R. S. Rector, J. P. Thyfault, J. A. Ibdah, Nonalcoholic fatty liver disease and mitochondrial dysfunction. *World J. Gastroenterol.* **14**, 193–199 (2008).
11. F. Nassir, J. Ibdah, Role of mitochondria in nonalcoholic fatty liver disease. *Int. J. Mol. Sci.* **15**, 8713–8742 (2014).
12. S. Schuster, D. Cabrera, M. Arrese, A. E. Feldstein, Triggering and resolution of inflammation in NASH. *Nat. Rev. Gastroenterol. Hepatol.* **15**, 349–364 (2018).
13. T. Kisseleva, D. Brenner, Molecular and cellular mechanisms of liver fibrosis and its regression. *Nat. Rev. Gastroenterol. Hepatol.* **18**, 151–166 (2021).
14. S. Caldwell, Y. Ikura, D. Dias, K. Isomoto, A. Yabu, C. Moskaluk, P. Pramoonjago, W. Simmons, H. Scruggs, N. Rosenbaum, T. Wilkinson, P. Toms, C. K. Argo, A. M. S. Al-Osaimi, J. A. Redick, Hepatocellular ballooning in NASH. *J. Hepatol.* **53**, 719–723 (2010).
15. T. Tsuchida, S. L. Friedman, Mechanisms of hepatic stellate cell activation. *Nat. Rev. Gastroenterol. Hepatol.* **14**, 397–411 (2017).
16. K. Kazankov, S. M. D. Jørgensen, K. L. Thomsen, H. J. Møller, H. Vilstrup, J. George, D. Schuppan, H. Grønbæk, The role of macrophages in nonalcoholic fatty liver disease and nonalcoholic steatohepatitis. *Nat. Rev. Gastroenterol. Hepatol.* **16**, 145–159 (2019).
17. Y. Takahashi, T. Fukusato, Histopathology of nonalcoholic fatty liver disease/nonalcoholic steatohepatitis. *World J. Gastroenterol.* **20**, 15539–15548 (2014).
18. V. A. Piazzolla, A. Mangia, Noninvasive diagnosis of NAFLD and NASH. *Cell* **9**, 1005 (2020).
19. A. Kadl, A. K. Meher, P. R. Sharma, M. Y. Lee, A. C. Doran, S. R. Johnstone, M. R. Elliott, F. Gruber, J. Han, W. Chen, T. Kensler, K. S. Ravichandran, B. E. Isakson, B. R. Wamhoff, N. Leitinger, Identification of a novel macrophage phenotype that develops in response to atherogenic phospholipids via Nrf2. *Circ. Res.* **107**, 737–746 (2010).
20. A. Kadl, P. R. Sharma, W. Chen, R. Agrawal, A. K. Meher, S. Rudraiah, N. Grubbs, R. Sharma, N. Leitinger, Oxidized phospholipid-induced inflammation is mediated by Toll-like receptor 2. *Free Radic. Biol. Med.* **51**, 1903–1909 (2011).
21. V. N. Bochkov, A. Kadl, J. Huber, F. Gruber, B. R. Binder, N. Leitinger, Protective role of phospholipid oxidation products in endotoxin-induced tissue damage. *Nature* **419**, 77–81 (2002).
22. E. A. Podrez, E. Poliakov, Z. Shen, R. Zhang, Y. Deng, M. Sun, P. J. Finton, L. Shan, M. Febbraio, D. P. Hajjar, R. L. Silverstein, H. F. Hoff, R. G. Salomon, S. L. Hazen, A novel family of atherogenic oxidized phospholipids promotes macrophage foam cell formation via the scavenger receptor CD36 and is enriched in atherosclerotic lesions. *J. Biol. Chem.* **277**, 38517–38523 (2002).
23. Y. Ke, P. Karki, J. Kim, S. Son, E. Berdyshev, V. N. Bochkov, A. A. Birukova, K. G. Birukov, Elevated truncated oxidized phospholipids as a factor exacerbating ALI in the aging lungs. *FASEB J.* **33**, 3887–3900 (2019).
24. K. G. Birukov, P. Karki, Injured lung endothelium: Mechanisms of self-repair and agonist-assisted recovery (2017 Grover Conference Series). *Pulm. Circ.* **8**, 2045893217752660 (2018).
25. P. Karki, A. Meliton, A. Shah, Y. Tian, T. Ohmura, N. Sarich, A. A. Birukova, K. G. Birukov, Role of truncated oxidized phospholipids in acute endothelial barrier dysfunction caused by particulate matter. *PLOS ONE* **13**, e0206251 (2018).
26. K. G. Birukov, V. N. Bochkov, A. A. Birukova, K. Kawkitinarong, A. Rios, A. Leitner, A. D. Verin, G. M. Bokoch, N. Leitinger, J. G. Garcia, Epoxycyclopentenone-containing oxidized phospholipids restore endothelial barrier function via Cdc42 and Rac. *Circ. Res.* **95**, 892–901 (2004).
27. S. Nonas, I. Miller, K. Kawkitinarong, S. Chatchavalvanich, I. Gorshkova, V. N. Bochkov, N. Leitinger, V. Natarajan, J. G. N. Garcia, K. G. Birukov, Oxidized phospholipids reduce vascular leak and inflammation in rat model of acute lung injury. *Am. J. Respir. Crit. Care Med.* **173**, 1130–1138 (2006).
28. A. Kadl, E. Galkina, N. Leitinger, Induction of CCR2-dependent macrophage accumulation by oxidized phospholipids in the air-pouch model of inflammation. *Arthritis Rheum.* **60**, 1362–1371 (2009).
29. V. Serbulea, C. M. Upchurch, K. W. Ahern, G. Bories, P. Voigt, D. E. DeWeese, A. K. Meher, T. E. Harris, N. Leitinger, Macrophages sensing oxidized DAMPs reprogram their metabolism to support redox homeostasis and inflammation through a TLR2-Syk-ceramide dependent mechanism. *Mol. Metab.* **7**, 23–34 (2018).
30. E. Ambrogini, X. Que, S. Wang, F. Yamaguchi, R. S. Weinstein, S. Tsimikas, S. C. Manolagas, J. L. Witztum, R. L. Jilka, Oxidation-specific epitopes restrain bone formation. *Nat. Commun.* **9**, 2193 (2018).
31. V. E. Kagan, G. Mao, F. Qu, J. P. Angeli, S. Doll, C. S. Croix, H. H. Dar, B. Liu, V. A. Tyurin, V. B. Ritov, A. A. Kapralov, A. A. Amoscato, J. Jiang, T. Anthonymuthu, D. Mohammadyani, Q. Yang, B. Proneth, J. Klein-Seetharaman, S. Watkins, I. Bahar, J. Greenberger, R. K. Mallampalli, B. R. Stockwell, Y. Y. Tyurina, M. Conrad, H. Bayir, Oxidized arachidonic and adrenic PEs navigate cells to ferroptosis. *Nat. Chem. Biol.* **13**, 81–90 (2017).
32. T. M. Grigory, G. Borisenko, Macrophage recognition of externalized phosphatidylserine and phagocytosis of apoptotic Jurkat cells—Existence of a threshold. *Arch. Biochem. Biophys.* **413**, 41–52 (2003).
33. Y. Imai, K. Kuba, G. G. Neely, R. Yaghubian-Malhami, T. Perkmann, G. Van Loo, M. Ermolaeva, R. Veldhuizen, Y. H. C. Leung, H. Wang, H. Liu, Y. Sun, M. Pasparakis, M. Kopf, C. Mech, S. Bavari, J. S. M. Peiris, A. S. Slutsky, S. Akira, M. Hultqvist, R. Holmdahl, J. Nicholls, C. Jiang, C. J. Binder, J. M. Penninger, Identification of oxidative stress and toll-like receptor 4 signaling as a key pathway of acute lung injury. *Cell* **133**, 235–249 (2008).
34. V. Serbulea, C. M. Upchurch, M. S. Schappe, P. Voigt, D. E. DeWeese, B. N. Desai, A. K. Meher, N. Leitinger, Macrophage phenotype and bioenergetics are controlled by oxidized phospholipids identified in lean and obese adipose tissue. *Proc. Natl. Acad. Sci. U.S.A.* **115**, E6254–E6263 (2018).
35. X. Sun, J. S. Seidman, P. Zhao, T. D. Troutman, N. J. Spann, X. Que, F. Zhou, Z. Liao, M. Pasillas, X. Yang, J. A. Magida, T. Kisseleva, D. A. Brenner, M. Downes, R. M. Evans, A. R. Saltiel, S. Tsimikas, C. K. Glass, J. L. Witztum, Neutralization of oxidized phospholipids ameliorates non-alcoholic steatohepatitis. *Cell Metab.* **31**, 189–206.e8 (2020).
36. S. Tsimikas, S. Kiechl, J. Willeit, M. Mayr, E. R. Miller, F. Kronenberg, Q. Xu, C. Bergmark, S. Weger, F. Oberhollenzer, J. L. Witztum, Oxidized phospholipids predict the presence and progression of carotid and femoral atherosclerosis and symptomatic cardiovascular disease: Five-year prospective results from the Bruneck study. *J. Am. Coll. Cardiol.* **47**, 2219–2228 (2006).
37. S. Hörkkö, D. A. Bird, E. Miller, H. Itabe, N. Leitinger, G. Subbanagounder, J. A. Berliner, P. Friedman, E. A. Dennis, L. K. Curtiss, W. Palinski, J. L. Witztum, Monoclonal autoantibodies specific for oxidized phospholipids or oxidized phospholipid–protein adducts inhibit macrophage uptake of oxidized low-density lipoproteins. *J. Clin. Investig.* **103**, 117–128 (1999).
38. X. Que, M.-Y. Hung, C. Yeang, A. Gonen, T. A. Prohaska, X. Sun, C. Diehl, A. Määttä, D. E. Gaddis, K. Bowden, J. Pattison, J. G. Macdonald, S. Ylä-Herttuala, P. L. Mellon, C. C. Hedrick, K. Ley, Y. I. Miller, C. K. Glass, K. L. Peterson, C. J. Binder, S. Tsimikas, J. L. Witztum, Oxidized phospholipids are proinflammatory and proatherogenic in hypercholesterolaemic mice. *Nature* **558**, 301–306 (2018).
39. X. Wang, Z. Zheng, J. M. Caviglia, K. E. Corey, T. M. Herfel, B. Cai, R. Masia, R. T. Chung, J. H. Lefkowitch, R. F. Schwabe, I. Tabas, Hepatocyte TAZ/WWTR1 promotes inflammation and fibrosis in nonalcoholic steatohepatitis. *Cell Metab.* **24**, 848–862 (2016).
40. Z. Ni, G. Angelidou, R. Hoffmann, M. Fedorova, LPPtiger software for lipidome-specific prediction and identification of oxidized phospholipids from LC-MS datasets. *Sci. Rep.* **7**, 15138 (2017).
41. E. A. Podrez, E. Poliakov, Z. Shen, R. Zhang, Y. Deng, M. Sun, P. J. Finton, L. Shan, B. Gugiu, P. L. Fox, H. F. Hoff, R. G. Salomon, S. L. Hazen, Identification of a novel family of oxidized phospholipids that serve as ligands for the macrophage scavenger receptor CD36. *J. Biol. Chem.* **277**, 38503–38516 (2002).
42. A. D. Watson, N. Leitinger, M. Navab, K. F. Faull, S. Hörkkö, J. L. Witztum, W. Palinski, D. Schwenke, R. G. Salomon, W. Sha, G. Subbanagounder, A. M. Fogelman, J. A. Berliner, Structural identification by mass spectrometry of oxidized phospholipids in minimally oxidized low density lipoprotein that induce monocyte/endothelial interactions and evidence for their presence in vivo. *J. Biol. Chem.* **272**, 13597–13607 (1997).
43. M. Hiraoka, A. Abe, An increase of oxidized phospholipids and the role of macrophages in intraocular inflammation. *Investig. Opthalmol. Vis. Sci.* **61**, 23 (2020).
44. Z. Ahmed, A. Ravandi, G. F. Maguire, A. Emili, D. Draganov, B. N. La Du, A. Kuksis, P. W. Connelly, Multiple substrates for paraoxonase-1 during oxidation of phosphatidylcholine by peroxynitrite. *Biochem. Biophys. Res. Commun.* **290**, 391–396 (2002).
45. K. Sabatini, J. P. Mattila, F. M. Megli, P. K. Kinnunen, Characterization of two oxidatively modified phospholipids in mixed monolayers with DPPC. *Biophys. J.* **90**, 4488–4499 (2006).
46. J.-P. Mattila, K. Sabatini, P. K. J. Kinnunen, Interaction of Cytochrome c with 1-Palmitoyl-2-azelaoyl-sn-glycero-3-phosphocholine: Evidence for acyl chain reversal. *Langmuir* **24**, 4157–4160 (2008).
47. C. P. Thomas, L. T. Morgan, B. H. Maskrey, R. C. Murphy, H. Kühn, S. L. Hazen, A. H. Goodall, H. A. Hamali, P. W. Collins, V. B. O'Donnell, Phospholipid-esterified eicosanoids are generated in agonist-activated human platelets and enhance tissue factor-dependent thrombin generation. *J. Biol. Chem.* **285**, 6891–6903 (2010).
48. K. Kayganich-Harrison, D. Rose, R. Murphy, J. Morrow, L. Roberts, Collision-induced dissociation of F2-isoprostane-containing phospholipids. *J. Lipid Res.* **34**, 1229–1235 (1993).
49. A. D. Watson, G. Subbanagounder, D. S. Welsbie, K. F. Faull, M. Navab, M. E. Jung, A. M. Fogelman, J. A. Berliner, Structural identification of a novel pro-inflammatory epoxyisoprostane phospholipid in mildly oxidized low density lipoprotein. *J. Biol. Chem.* **274**, 24787–24798 (1999).
50. V. Bochkov, B. Gesslbauer, C. Mauerhofer, M. Philippova, P. Erne, O. V. Oskolkova, Pleiotropic effects of oxidized phospholipids. *Free Radic. Biol. Med.* **111**, 6–24 (2017).

51. V. N. Bochkov, O. V. Oskolkova, K. G. Birukov, A.-L. Levonen, C. J. Binder, J. Stöckl, Generation and biological activities of oxidized phospholipids. *Antioxid. Redox Signal.* **12**, 1009–1059 (2010).
52. M. V. Kuleshov, M. R. Jones, A. D. Rouillard, N. F. Fernandez, Q. Duan, Z. Wang, S. Koplev, S. L. Jenkins, K. M. Jagodnik, A. Lachmann, M. G. McDermott, C. D. Monteiro, G. W. Gundersen, A. Ma'ayan, Enrichr: A comprehensive gene set enrichment analysis web server 2016 update. *Nucleic Acids Res.* **44**, W90–W97 (2016).
53. E. Y. Chen, C. M. Tan, Y. Kou, Q. Duan, Z. Wang, G. Meirelles, N. R. Clark, A. Ma'Ayan, Enrichr: Interactive and collaborative HTML5 gene list enrichment analysis tool. *BMC Bioinformatics* **14**, 128 (2013).
54. H. K. Min, A. Kapoor, M. Fuchs, F. Mirshahi, H. Zhou, J. Maher, J. Kellum, R. Warnick, M. J. Contos, A. J. Sanyal, Increased hepatic synthesis and dysregulation of cholesterol metabolism is associated with the severity of nonalcoholic fatty liver disease. *Cell Metab.* **15**, 665–674 (2012).
55. W. Xue, J. Wang, W. Jiang, C. Shi, X. Wang, Y. Huang, C. Hu, Caveolin-1 alleviates lipid accumulation in NAFLD associated with promoting autophagy by inhibiting the Akt/mTOR pathway. *Eur. J. Pharmacol.* **871**, 172910 (2020).
56. M. Li, D. Chen, H. Huang, J. Wang, X. Wan, C. Xu, C. Li, H. Ma, C. Yu, Y. Li, Caveolin1 protects against diet induced hepatic lipid accumulation in mice. *PLOS ONE* **12**, e0178748 (2017).
57. M. Han, W. Pioronska, S. Wang, Z. C. Nwosu, C. Sticht, S. Wang, Y. Gao, M. P. Ebert, S. Dooley, C. Meyer, Hepatocyte caveolin-1 modulates metabolic gene profiles and functions in non-alcoholic fatty liver disease. *Cell Death Dis.* **11**, 104 (2020).
58. M. Tan, R. Mosaoa, G. T. Graham, A. Kasprzyk-Pawelec, S. Gadre, E. Parasido, O. Catalina-Rodriguez, P. Foley, G. Giaccone, A. Cheema, B. Kallakury, C. Albanese, C. Yi, M. L. Avantaggiati, Inhibition of the mitochondrial citrate carrier, Slc25a1, reverts steatosis, glucose intolerance, and inflammation in preclinical models of NAFLD/NASH. *Cell Death Differ.* **27**, 2143–2157 (2020).
59. M. Pérez-Carreras, P. Del Hoyo, M. A. Martín, J. C. Rubio, A. Martín, G. Castellano, F. Colina, J. Arenas, J. A. Solis-Herruzo, Defective hepatic mitochondrial respiratory chain in patients with nonalcoholic steatohepatitis. *Hepatology* **38**, 999–1007 (2003).
60. P. Greenspan, E. P. Mayer, S. D. Fowler, Nile red: A selective fluorescent stain for intracellular lipid droplets. *J. Cell Biol.* **100**, 965–973 (1985).
61. B. H. Maskrey, A. Bermúdez-Fajardo, A. H. Morgan, E. Stewart-Jones, V. Dioszeghy, G. W. Taylor, P. R. S. Baker, B. Coles, M. J. Coffey, H. Kühn, V. B. O'Donnell, Activated platelets and monocytes generate four hydroxyphosphatidylethanolamines via lipoxygenase. *J. Biol. Chem.* **282**, 20151–20163 (2007).
62. P. Trivedi, S. Wang, S. L. Friedman, The power of plasticity-metabolic regulation of hepatic stellate cells. *Cell Metab.* **33**, 242–257 (2021).
63. X. Liu, S. B. Rosenthal, N. Meshgin, J. Baglieri, S. G. Musallam, K. Diggle, K. Lam, R. Wu, S. Q. Pan, Y. Chen, K. Dorko, S. Presnell, C. Benner, M. Hosseini, H. Tsukamoto, D. Brenner, T. Kisseleva, Primary alcohol-activated human and mouse hepatic stellate cells share similarities in gene-expression profiles. *Hepatol. Commun.* **4**, 606–626 (2020).
64. P. X. Shaw, S. Hörkkö, M.-K. Chang, L. K. Curtiss, W. Palinski, G. J. Silverman, J. L. Witztum, Natural antibodies with the T15 idiotype may act in atherosclerosis, apoptotic clearance, and protective immunity. *J. Clin. Investig.* **105**, 1731–1740 (2000).
65. I. Zanoni, Y. Tan, M. Di Gioia, A. Broggi, J. Ruan, J. Shi, C. A. Donado, F. Shao, H. Wu, J. R. Springstead, J. C. Kagan, An endogenous caspase-11 ligand elicits interleukin-1 release from living dendritic cells. *Science* **352**, 1232–1236 (2016).
66. C. Erridge, S. Kennedy, C. M. Spickett, D. J. Webb, Oxidized phospholipid inhibition of toll-like receptor (TLR) signaling is restricted to TLR2 and TLR4: Roles for CD14, LPS-binding protein, and MD2 as targets for specificity of inhibition. *J. Biol. Chem.* **283**, 24748–24759 (2008).
67. L. Wang, Y. Chai, C. Li, H. Liu, W. Su, X. Liu, B. Yu, W. Lei, B. Yu, J. L. Crane, X. Cao, M. Wan, Oxidized phospholipids are ligands for LRP6. *Bone Res.* **6**, 22 (2018).
68. G. N. Ioannou, The role of cholesterol in the pathogenesis of NASH. *Trends Endocrinol. Metab.* **27**, 84–95 (2016).
69. P. Friedman, S. Horkko, D. Steinberg, J. L. Witztum, E. A. Dennis, Correlation of antiphospholipid antibody recognition with the structure of synthetic oxidized phospholipids. Importance of Schiff base formation and aldol condensation. *J. Biol. Chem.* **277**, 7010–7020 (2002).
70. K. L. Gillotte, S. Hörkkö, J. L. Witztum, D. Steinberg, Oxidized phospholipids, linked to apolipoprotein B of oxidized LDL, are ligands for macrophage scavenger receptors. *J. Lipid Res.* **41**, 824–833 (2000).
71. P. R. Kamstrup, M. Y. Hung, J. L. Witztum, S. Tsimikas, B. G. Nordestgaard, Oxidized phospholipids and risk of calcific aortic valve disease: The copenhagen general population study. *Arterioscler. Thromb. Vasc. Biol.* **37**, 1570–1578 (2017).
72. D. A. Slatter, C. L. Percy, K. Allen-Redpath, J. M. Gajsiewicz, N. J. Brooks, A. Clayton, V. J. Tyrrell, M. Rosas, S. N. Lauder, A. Watson, M. Dul, Y. Garcia-Diaz, M. Aldrovandi, M. Heurich, J. Hall, J. H. Morrissey, S. Lacroix-Desmazes, S. Delignat, P. V. Jenkins, P. W. Collins, V. B. O'Donnell, Enzymatically oxidized phospholipids restore thrombin generation in coagulation factor deficiencies. *JCI Insight* **3**, e98459 (2018).
73. V. E. Kagan, B. Gleiss, Y. Y. Tyurina, V. A. Tyurin, C. Elenström-Magnusson, S.-X. Liu, F. B. Serinkan, A. Arroyo, J. Chandra, S. Orrenius, B. Fadeel, A role for oxidative stress in apoptosis: Oxidation and externalization of phosphatidylserine is required for macrophage Clearance of cells undergoing fas-mediated apoptosis. *J. Immunol.* **169**, 487–499 (2002).
74. C. A. Schneider, W. S. Rasband, K. W. Eliceiri, NIH Image to ImageJ: 25 years of image analysis. *Nat. Methods* **9**, 671–675 (2012).
75. V. Bäcker, ImageJ macro tool sets of biological image analysis. *Proc. ImageJ User Dev. Conf. Luxembourg* **24**, 1–6 (2012).
76. A. Dobin, C. A. Davis, F. Schlesinger, J. Drenkow, C. Zaleski, S. Jha, P. Batut, M. Chaisson, T. R. Gingeras, STAR: Ultrafast universal RNA-seq aligner. *Bioinformatics* **29**, 15–21 (2013).
77. M. D. Robinson, D. J. Mccarthy, G. K. Smyth, edgeR: A Bioconductor package for differential expression analysis of digital gene expression data. *Bioinformatics* **26**, 139–140 (2010).

Acknowledgments: AAV8-scFv-E06 was synthesized by the Penn Vector Core. RNA-seq analysis was supported by the UVA Genome Analysis and Technology Core. We thank M. Bevard (UVA CVRC Histology Core) for her expertise and preparation of histological samples. RNA sequencing of in vitro OxPAPC-treated hepatocytes was performed in the Genome Analysis and Technology Core at UVA. We thank J. Gatesman (UVA Center for Comparative Medicine) for technical assistance with viral injections. **Funding:** This work was funded by NIH grants T32GM007055 (to C.M.U.), F30HL154554 (to S.Y.), T32GM007267 (to S.Y.), T32GM007055 (to S.Y.), T32HL007284 (to C.M.P.), , R01DK121055 (to I.M.B.), R01MH116694 (to M.M.S.), R01NS097726 (to E.P.-R.), and P01HL120840 (N.L.) and Deutsche Forschungsgemeinschaft IRTG 1902-2 (to D.M.) and IRTG 1902-1 (to J.G.). **Author contributions:** Conceptualization: C.M.U., M.M.S., E.P.-R., and N.L. Methodology: C.M.U., S.Y., C.M.P., D.M., J.G., M.M., I.M.B., M.M.S., E.P.-R., and N.L. Investigation: C.M.U., S.Y., C.M.P., M.M., D.M., J.G., and S.S.R. Visualization: C.M.U. and N.L. Funding acquisition: C.M.U., S.Y., C.M.P., I.M.B., M.M.S., and N.L. Project administration: N.L. Supervision: N.L. Writing—original draft: C.M.U. and N.L. Writing—review and editing: C.M.U., S.Y., C.M.P., M.M., I.M.B., M.M.S., E.P.-R., and N.L. **Competing interests:** C.M.U., N.L., E.P.-R., and M.M.S. have applied for a provisional patent on the application of AAV8-mediated transduction of scFv-E06 for use in a therapeutic capacity in chronic disease. The authors declare no other competing interests. **Data and materials availability:** All data needed to evaluate the conclusions in the paper are present in the paper and/or the Supplementary Materials. The plasmid used to generate the viral construct AAV8-scFv-E06 was provided to the authors via an MTA agreement with genOway. Requests for the plasmid should be submitted to N.L. or E.P.-R. Genomic data for this manuscript have been deposited in the NCBI Genomic Expression Omnibus (accession number: GSE202984—in vitro RNA-seq; GSE202982—in vivo RNA-seq).

Submitted 27 October 2021
Accepted 3 June 2022
Published 15 July 2022
10.1126/sciadv.abn0050

ScienceAdvances

Targeting oxidized phospholipids by AAV-based gene therapy in mice with established hepatic steatosis prevents progression to fibrosis

Clint M. Upchurch, Scott Yeudall, Caitlin M. Pavelec, Dennis Merk, Jan Greulich, Mohan Manjegowda, Shyam S. Raghavan, Irina M. Bochkis, Michael M. Scott, Edward Perez-Reyes, and Norbert Leitinger

Sci. Adv., **8** (28), eabn0050.
DOI: 10.1126/sciadv.abn0050

Science Advances (ISSN) is published by the American Association for the Advancement of Science. 1200 New York Avenue NW, Washington, DC 20005. The title *Science Advances* is a registered trademark of AAAS.

Science Advances
AAAS

Supplementary Materials for

Targeting oxidized phospholipids by AAV-based gene therapy in mice with established hepatic steatosis prevents progression to fibrosis

Clint M. Upchurch *et al.*

Corresponding author: Norbert Leitinger, nl2q@virginia.edu

Sci. Adv. **8**, eabn0050 (2022)
DOI: 10.1126/sciadv.abn0050

The PDF file includes:

Other Supplementary Material for this manuscript includes the following:

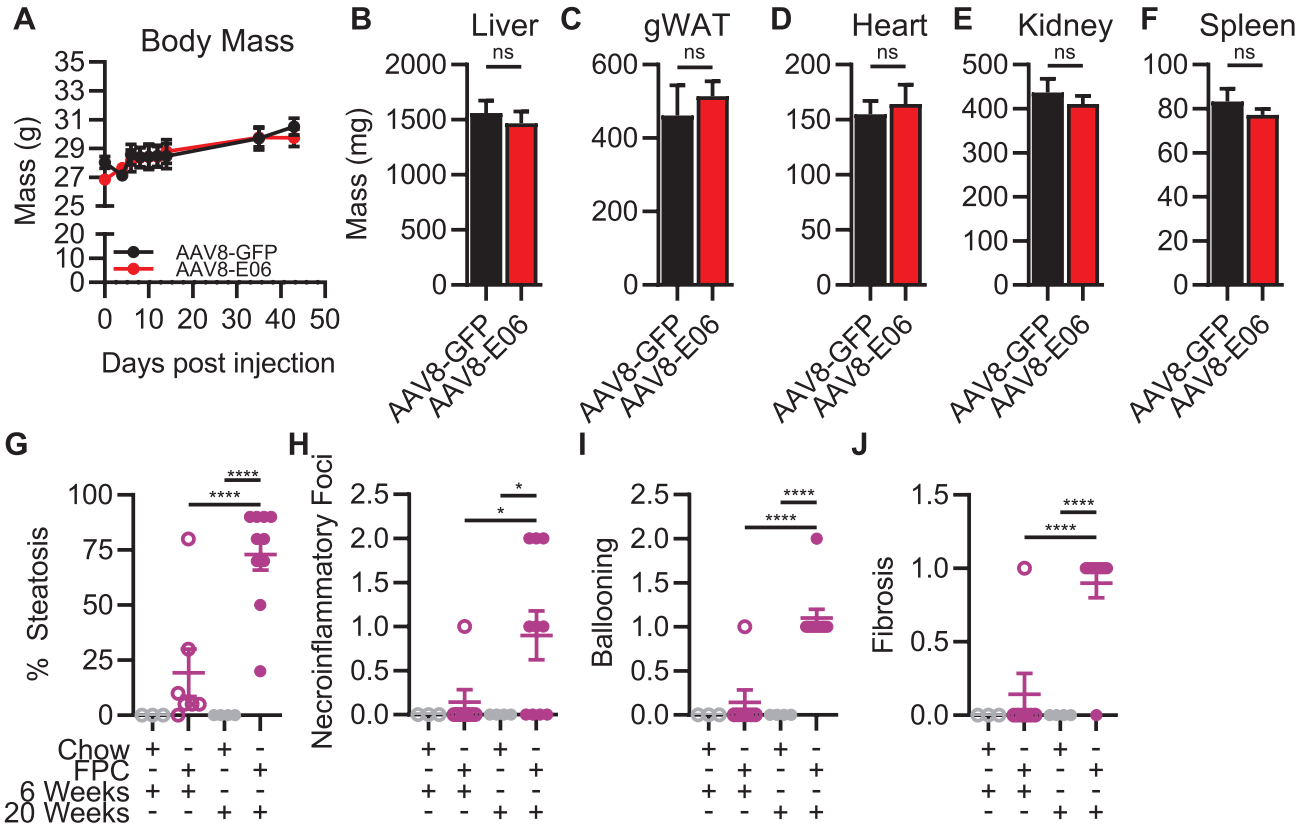
A
Body Mass
Mass (g)
Days post injection
AAV8-GFP
AAV8-E06
B
Liver
Mass (mg)
C
gWAT
D
Heart
E
Kidney
F
Spleen
ns
AAV8-GFP
AAV8-E06

G
% Steatosis
H
Necroinflammatory Foci
I
Ballooning
J
Fibrosis
****
*
Chow
FPC
6 Weeks
20 Weeks

Supplemental Figure 1. Adeno-associated virus serotype 8 scFv-E06 and FPC diet verification.

Mice were injected with either AAV8-GFP or AAV8-E06. There were no differences in **(A)** body mass, or mass of **(B)** liver, **(C)** gonadal white adipose tissue, **(D)** heart, **(E)** kidney, and **(F)** spleen (AAV8-GFP – n=5; AAV8-E06 – n=6). Mice injected with AAV8-GFP were fed chow or FPC diet for 6 or 20 weeks and histopathological assessment of **(G)** percent steatosis, **(H)** necroinflammatory foci, **(I)** hepatocellular ballooning, and **(J)** fibrosis was performed by a clinical pathologist. Statistical significance was determined by 2-way ANOVA (*=$p<0.05$, ****=$p<0.0001$).

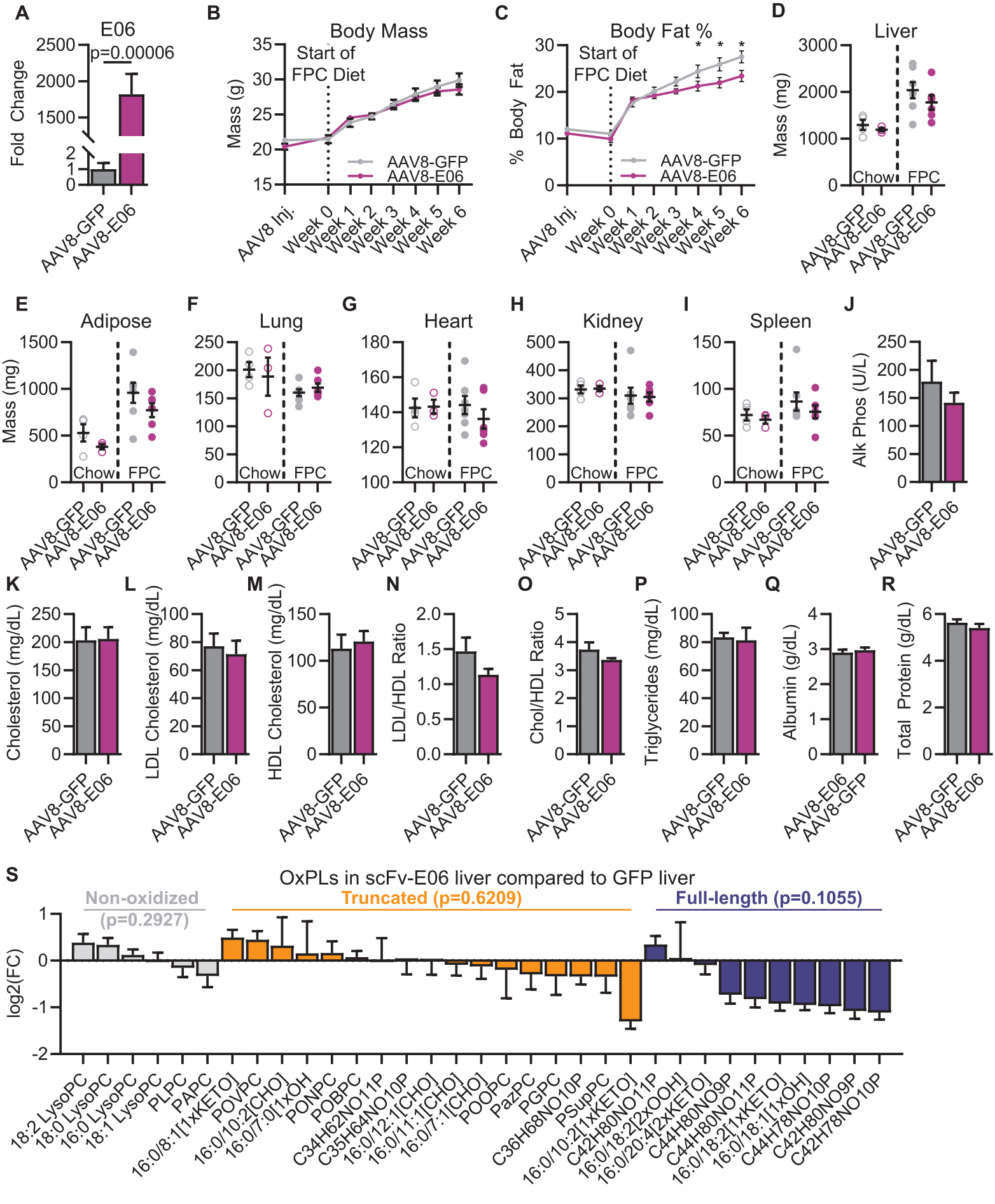
A
E06
p=0.00006
Fold Change
AAV8-GFP
AAV8-E06
B
Body Mass
Start of FPC Diet
Mass (g)
AAV8-GFP
AAV8-E06
AAV8 Inj.
Week 0
Week 1
Week 2
Week 3
Week 4
Week 5
Week 6
C
Body Fat %
Start of FPC Diet
% Body Fat
D
Liver
Mass (mg)
Chow
FPC
E
Adipose
F
Lung
G
Heart
H
Kidney
I
Spleen
J
Alk Phos (U/L)
K
Cholesterol (mg/dL)
L
LDL Cholesterol (mg/dL)
M
HDL Cholesterol (mg/dL)
N
LDL/HDL Ratio
O
Chol/HDL Ratio
P
Triglycerides (mg/dL)
Q
Albumin (g/dL)
R
Total Protein (g/dL)
S
OxPLs in scFv-E06 liver compared to GFP liver
Non-oxidized (p=0.2927)
Truncated (p=0.6209)
Full-length (p=0.1055)
log2(FC)
18:2 LysoPC
18:0 LysoPC
16:0 LysoPC
18:1 LysoPC
PLPC
PAPC
16:0/8:1[1xKETO]
POVPC
16:0/10:2[CHO]
16:0/7:0[1xOH
PONPC
POBPC
C34H62NO11P
C35H64NO10P
16:0/12:1[CHO]
16:0/11:1[CHO]
16:0/7:1[CHO]
POOPC
PazPC
PGPC
C36H68NO10P
PSupPC
16:0/10:2[1xKETO]
C42H80NO11P
16:0/18:2[2xOOH]
16:0/20:4[2xKETO]
C44H80NO9P
C44H80NO11P
16:0/18:2[1xKETO]
16:0/18:1[1xOH]
C44H78NO10P
C42H80NO9P
C42H78NO10P

Supplemental Figure 2. Characterization of mice treated with AAV8-scFv-E06 after six weeks of FPC diet.

Speer6-ps1$^{Tg(Alb\text{-}cre)21Mgn}$/J mice were injected with AAV8-GFP or AAV8-scFv-E06. Two weeks after injection, mice were fed FPC diet for six weeks (FPC AAV8-GFP, n=7; FPC AAV8-E06, n=6). **(A)** scFv-E06 mRNA expression was significantly increased in mice injected with AAV8-scFv-E06 (AAV8-GFP – n=6; AAV8-E06 – n=6). **(B)** Body mass (FPC AAV8-GFP, n=7; FPC AAV8-E06, n=6) and **(C)** body fat percentage (FPC AAV8-GFP, n=6; FPC AAV8-E06, n=6) were recorded weekly. While there was no difference in body mass, there was a significant decrease in body fat percentage between FPC diet-fed mice expressing scFv-E06 compared to mice expressing GFP after four weeks on diet. There was significant increase in body fat percentage between chow fed and FPC diet-fed mice after six weeks. After six weeks, mouse plasma was collected, and hepatic function and lipid profile were measured. (**D-I)** There were no significant differences in organ mass between AAV8-GFP and AAV8-scFv-E06 in either chow-fed or FPC-fed mice (FPC AAV8-GFP, n=7; FPC AAV8-E06, n=6). There was no significant difference in **(J)** alkaline phosphatase, **(K)** cholesterol, **(L)** LDL cholesterol, **(M)** HDL cholesterol, **(N)** LDL/HDL ratio, **(O)** cholesterol/HDL ratio, **(P)** triglycerides, **(Q)** albumin, and **(R)** total protein in the plasma of FPC diet-fed mice expressing scFv-E06 compared to GFP-expressing mice (AAV8-GFP – n=6; AAV8-E06 – n=6). **(S)** Truncated and full-length OxPCs extracted from liver tissue demonstrate a similar pattern to that observed in the plasma. Statistical significance was determined by 1-way and 2-way ANOVA and Student's T-test. Multiple comparisons were corrected by Dunnet or Tukey multiple comparisons correction (*=$p<0.05$, **=$p<0.01$, ***=$p<0.001$, ****=$p<0.0001$). Statistical outliers were excluded based on the ROUT test (Q=5%).

A

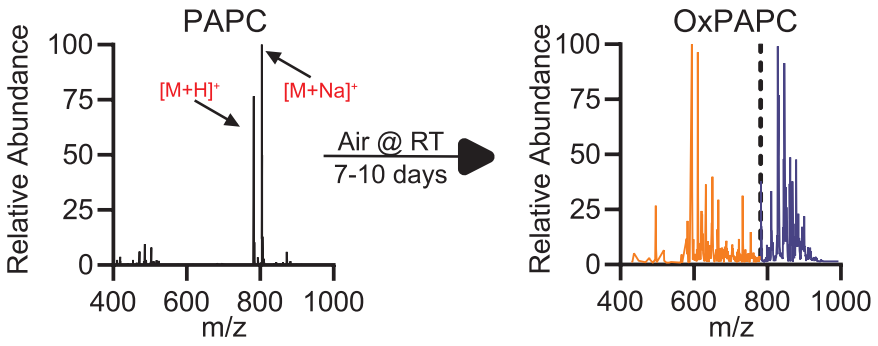

B

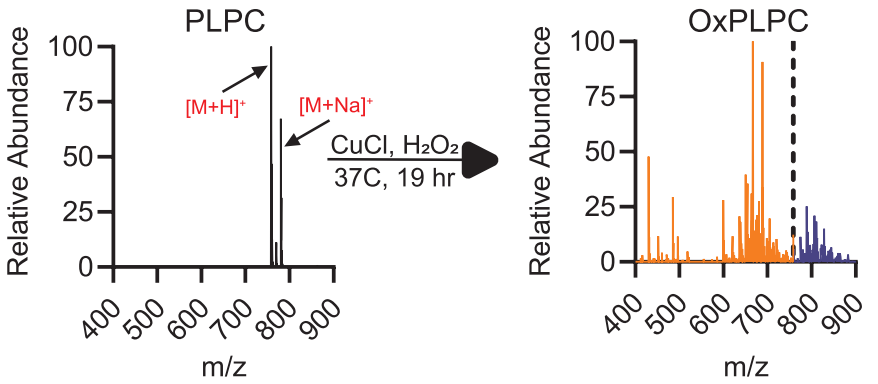

C

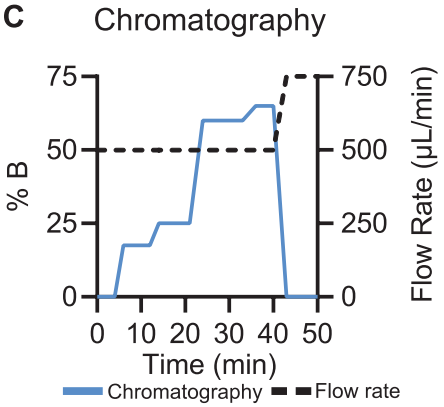

D

	Solvent A	Solvent B
Water	31%	---
Methanol	69%	50%
Isopropanol	---	50%
Ammonium acetate	10 mM	10 mM

Supplemental Figure 3. Oxidation and detection of oxidation products of PAPC and PLPC. Oxidized phospholipids were prepared for LCMS by *in vitro* oxidation. **(A)** PAPC was oxidized by air for 7-10 days. **(B)** PLPC was oxidized by Fenton-like copper reaction for 18 hours. **(C)** Schematic of chromatography for analysis mass spectrometric analysis of oxidized phospholipids. **(D)** Solvent system for separation of OxPL species by HPLC.

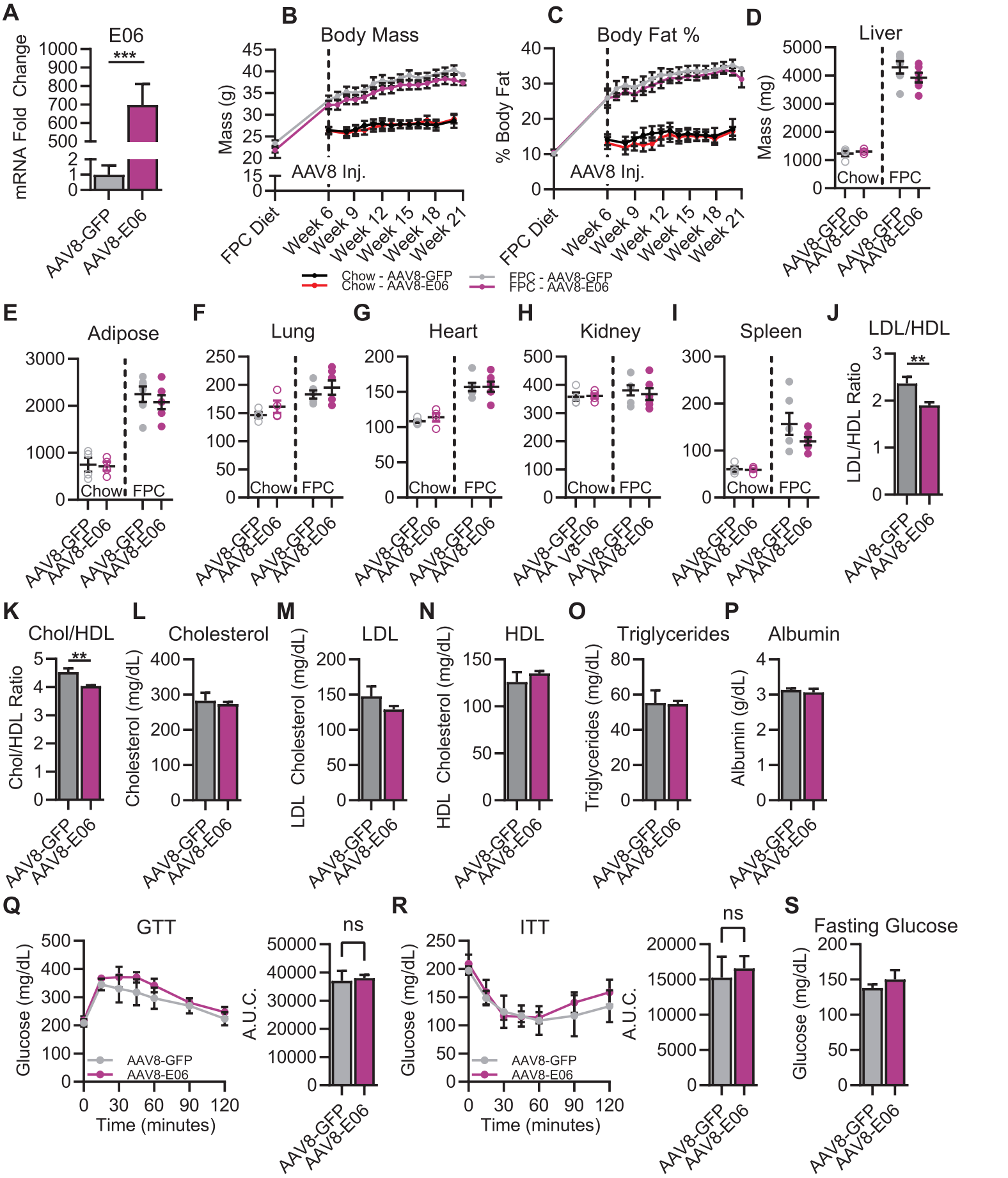
A
E06
***
mRNA Fold Change
AAV8-GFP
AAV8-E06
B
Body Mass
Mass (g)
AAV8 Inj.
FPC Diet
Week 6
Week 9
Week 12
Week 15
Week 18
Week 21
Chow - AAV8-GFP
Chow - AAV8-E06
FPC - AAV8-GFP
FPC - AAV8-E06
C
Body Fat %
% Body Fat
D
Liver
Mass (mg)
Chow
FPC
E
Adipose
F
Lung
G
Heart
H
Kidney
I
Spleen
J
LDL/HDL
LDL/HDL Ratio
**
K
Chol/HDL
Chol/HDL Ratio
L
Cholesterol
Cholesterol (mg/dL)
M
LDL
LDL Cholesterol (mg/dL)
N
HDL
HDL Cholesterol (mg/dL)
O
Triglycerides
Triglycerides (mg/dL)
P
Albumin
Albumin (g/dL)
Q
GTT
Glucose (mg/dL)
Time (minutes)
ns
A.U.C.
R
ITT
S
Fasting Glucose

Supplemental Figure 4. Gene ontology and gene expression of AML12 hepatocytes treated with truncated OxPAPC, full-length OxPAPC, and OxPAPC.

AML12 murine hepatocytes were treated with either OxPAPC, truncated OxPAPC, and full-length OxPAPC (100 μg/mL) for 4 hours and gene expression was measured via RNA-seq. GO Biological processes of upregulated genes (fold change > |1.5| and adjusted p-value < 0.05) identified by EnrichR for **(A)** OxPAPC, **(B)** truncated OxPAPC, and **(C)** full-length OxPAPC. Expression of **(D)** *Hmox1,* **(E)** *Pgd,* **(F)** *Acly,* **(G)** *Hmgcoas,* and **(H)** *Hmgcoar* in AML12 hepatocytes were confirmed by RT-qPCR (n=4). *Hmox1* and *Pgd* were regulated by all three oxidized phospholipid treatments; however, *Acly*, *Hmgcoas*, and *Hmgcoar* were exclusively upregulated by truncated OxPAPC. Statistical significance was determined by 1-way ANOVA. Multiple comparisons were corrected by Dunnet's multiple comparisons correction (*=p<0.05, **=p<0.01, ****=p<0.0001).

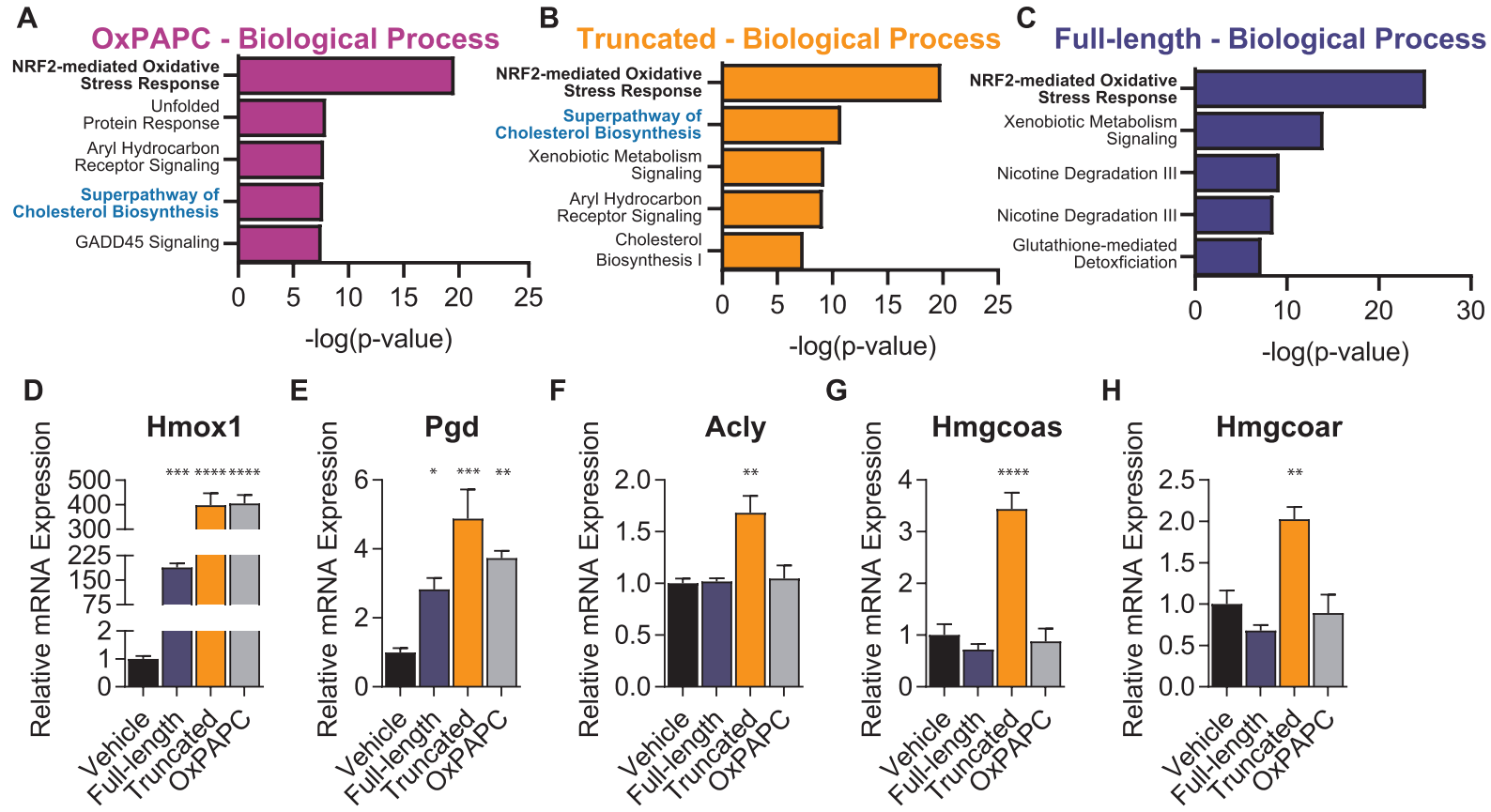
A
OxPAPC - Biological Process
NRF2-mediated Oxidative Stress Response
Unfolded Protein Response
Aryl Hydrocarbon Receptor Signaling
Superpathway of Cholesterol Biosynthesis
GADD45 Signaling
0 5 10 15 20 25
-log(p-value)
B
Truncated - Biological Process
NRF2-mediated Oxidative Stress Response
Superpathway of Cholesterol Biosynthesis
Xenobiotic Metabolism Signaling
Aryl Hydrocarbon Receptor Signaling
Cholesterol Biosynthesis I
0 5 10 15 20 25
-log(p-value)
C
Full-length - Biological Process
NRF2-mediated Oxidative Stress Response
Xenobiotic Metabolism Signaling
Nicotine Degradation III
Nicotine Degradation III
Glutathione-mediated Detoxficiation
0 10 20 30
-log(p-value)

D
Hmox1
Relative mRNA Expression
*** **** *****
500
400
300
225
150
75
2
1
0
Vehicle
Full-length
Truncated
OxPAPC
E
Pgd
Relative mRNA Expression
* *** **
6
4
2
0
Vehicle
Full-length
Truncated
OxPAPC
F
Acly
Relative mRNA Expression
**
2.0
1.5
1.0
0.5
0.0
Vehicle
Full-length
Truncated
OxPAPC
G
Hmgcoas
Relative mRNA Expression
****
4
3
2
1
0
Vehicle
Full-length
Truncated
OxPAPC
H
Hmgcoar
Relative mRNA Expression
**
2.5
2.0
1.5
1.0
0.5
0.0
Vehicle
Full-length
Truncated
OxPAPC

Supplemental Figure 5. Characterization of mice treated with AAV8-scFv-E06 after 20 weeks on FPC diet.

Speer6-ps1$^{Tg(Alb\text{-}cre)21Mgn}$/J mice were fed FPC or chow diet for six weeks. After six weeks mice were injected with either AAV8-GFP or AAV8-scFv-E06. Mice continued diet for a total of 20/21 weeks. **(A)** scFv-E06 gene expression was significantly increased in mice injected with AAV8-scFv-E06 ((FPC AAV8-GFP, n=5; FPC AAV8-E06, n=6). There were no significant differences in **(B)** body mass or **(C)** body fat percentage between GFP and scFv-E06 expressing mice on FPC or chow diet; however, there were a significant increase in both body mass and body fat percentage between diet groups (n=10). At the end of the experiment, plasma was collected, and hepatic function and lipid profile were measured. **(D-I)** There were no differences in organ mass between scFv-E06- and GFP-expressing mice fed chow or FPC diet (n=6). Ratios of **(J)** LDL/HDL and **(K)** Cholesterol/HDL in plasma were significantly reduced in mice expressing scFv-E06 compared to GFP after FPC diet feeding (n=6). **(L)** Cholesterol, **(M)** LDL, **(N)** HDL, **(O)** triglycerides, and **(P)** albumin levels in plasma were not significantly changed between scFv-E06 and GFP-expressing mice fed FPC diet (n=6). There were no differences in **(Q)** 6-hour fasted glucose and **(R)** insulin tolerance and **(S)** 18-hour fasting glucose in mice expressing GFP or scFv-E06 after 20 weeks FPC diet feeding (FPC AAV8-GFP, n=3; FPC AAV8-E06, n=4). Statistical significance was determined by 1-way and 2-way ANOVA and Student's T-test. Multiple comparisons were corrected by Dunnet or Tukey multiple comparisons correction (*=$p<0.05$, **=$p<0.01$, ****=$p<0.0001$).

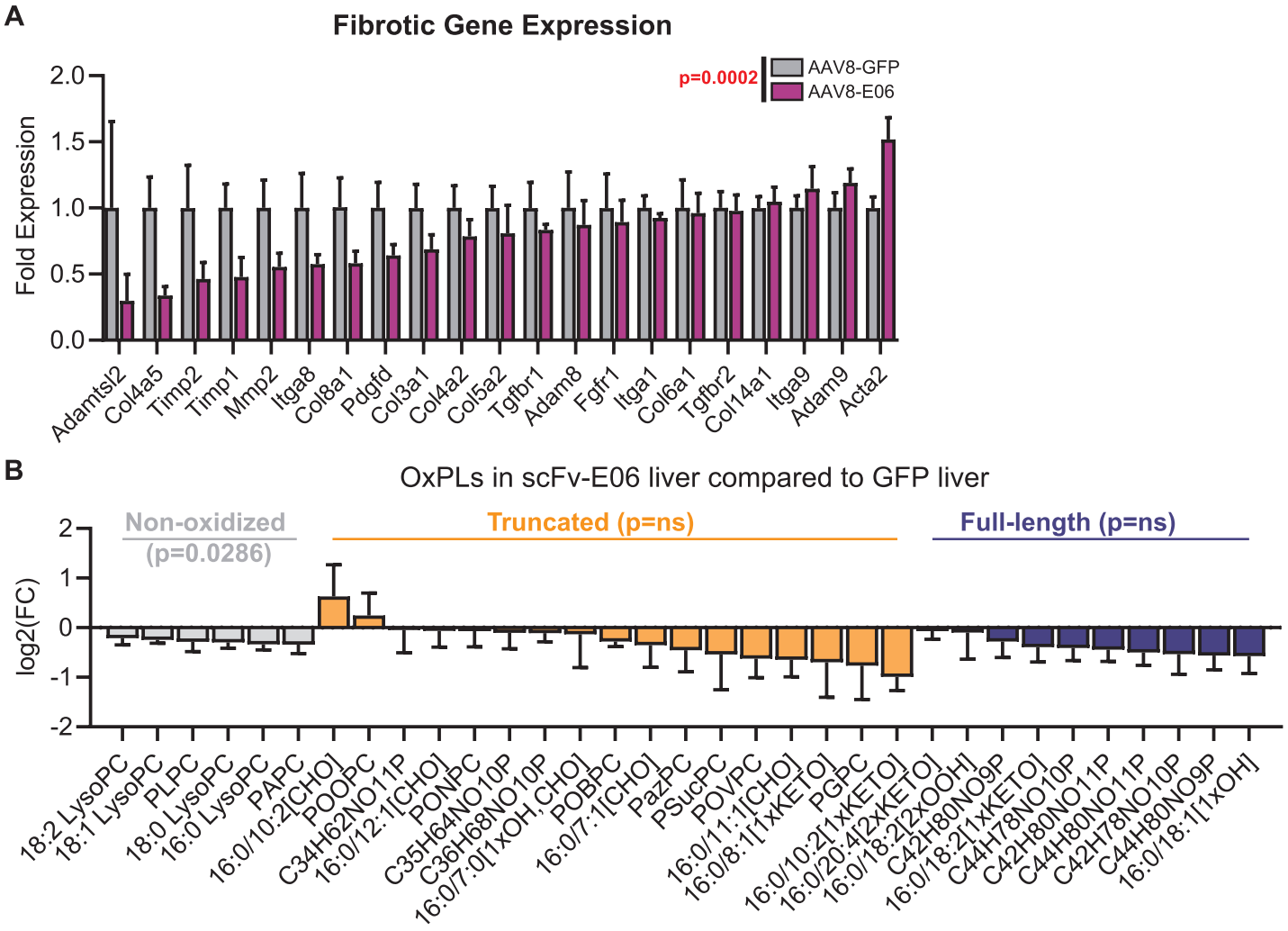
A
Fibrotic Gene Expression
p=0.0002
AAV8-GFP
AAV8-E06
Fold Expression
2.0
1.5
1.0
0.5
0.0
Adamtsl2
Col4a5
Timp2
Timp1
Mmp2
Itga8
Col8a1
Pdgfd
Col3a1
Col4a2
Col5a2
Tgfbr1
Adam8
Fgfr1
Itga1
Col6a1
Tgfbr2
Col14a1
Itga9
Adam9
Acta2

B
OxPLs in scFv-E06 liver compared to GFP liver
Non-oxidized
(p=0.0286)
Truncated (p=ns)
Full-length (p=ns)
log2(FC)
2
1
0
-1
-2
18:2 LysoPC
18:1 LysoPC
PLPC
18:0 LysoPC
16:0 LysoPC
PAPC
16:0/10:2[CHO]
POOPC
C34H62NO11P
16:0/12:1[CHO]
PONPC
C35H64NO10P
C36H68NO10P
16:0/7:0[1xOH,CHO]
POBPC
16:0/7:1[CHO]
PazPC
PSucPC
POVPC
16:0/11:1[CHO]
16:0/8:1[1xKETO]
PGPC
16:0/10:2[1xKETO]
16:0/20:4[2xKETO]
16:0/18:2[2xOOH]
C42H80NO9P
16:0/18:2[1xKETO]
C44H78NO10P
C42H80NO10P
C44H80NO11P
C42H78NO11P
C44H80NO10P
C42H78NO10P
C44H80NO9P
16:0/18:1[1xOH]

Supplemental Figure 6. Fibrotic gene expression in mice treated with AAV8-scFv-E06. **(A)** Hepatic gene expression of fibrogenic genes were confirmed by RT-qPCR (GFP – n=6, scFv – n=6). **(B)** Truncated and full-length OxPCs extracted from liver tissue demonstrate a similar pattern to that observed in the plasma, while non-oxidized phospholipids were significantly decreased. Statistical significance was determined by 2-way ANOVA with Dunnet's multiple comparisons correction. Statistical outliers were excluded with the ROUT test (Q=5%)

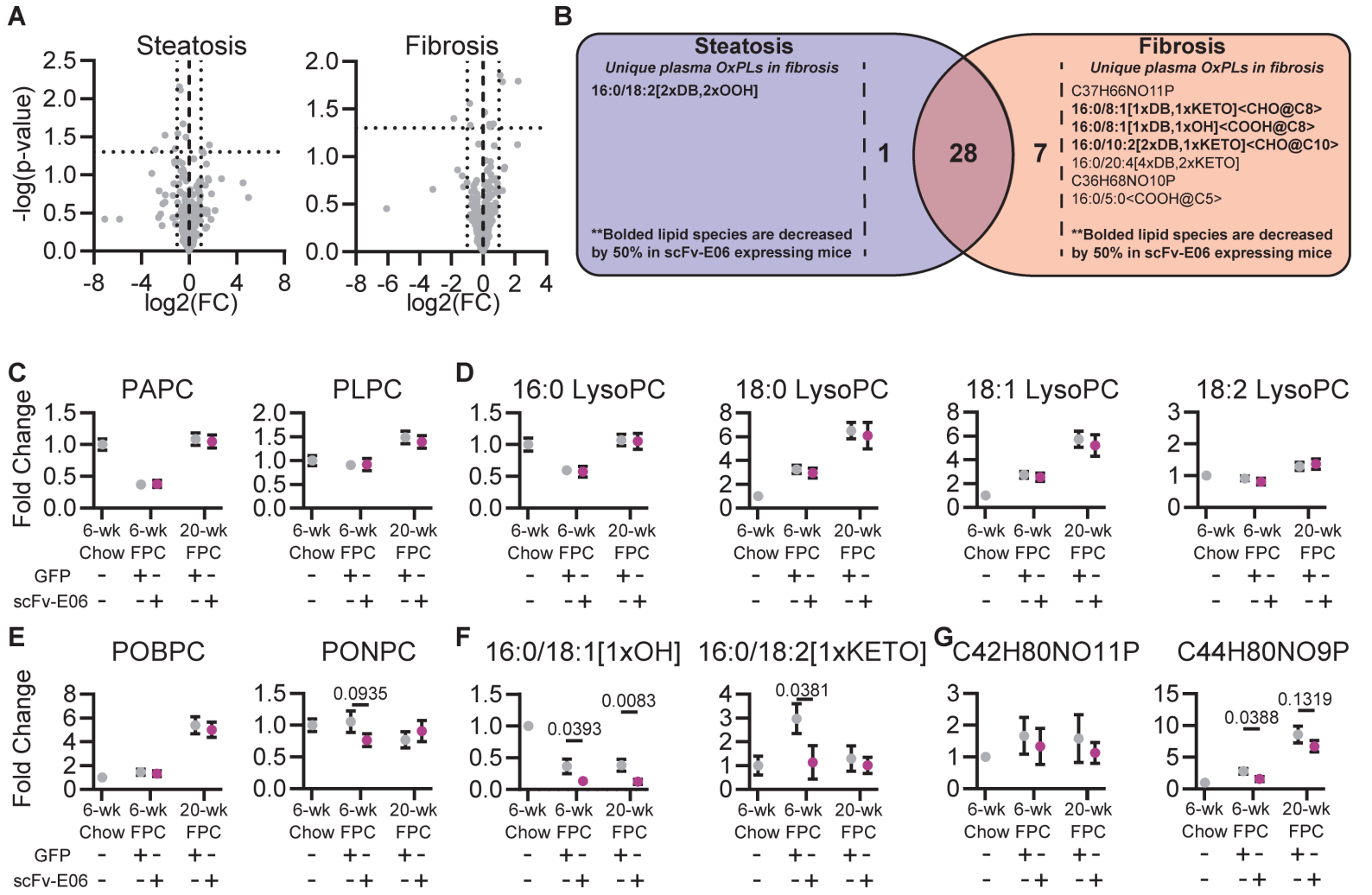
A
Steatosis
Fibrosis
-log(p-value)
log2(FC)
log2(FC)
B
Steatosis
Unique plasma OxPLs in fibrosis
16:0/18:2[2xDB,2xOOH]
**Bolded lipid species are decreased by 50% in scFv-E06 expressing mice
1
28
7
Fibrosis
Unique plasma OxPLs in fibrosis
C37H66NO11P
16:0/8:1[1xDB,1xKETO]<CHO@C8>
16:0/8:1[1xDB,1xOH]<COOH@C8>
16:0/10:2[2xDB,1xKETO]<CHO@C10>
16:0/20:4[4xDB,2xKETO]
C36H68NO10P
16:0/5:0<COOH@C5>
**Bolded lipid species are decreased by 50% in scFv-E06 expressing mice

C
PAPC
PLPC
D
16:0 LysoPC
18:0 LysoPC
18:1 LysoPC
18:2 LysoPC
Fold Change
6-wk Chow
6-wk FPC
20-wk FPC
GFP
scFv-E06

E
POBPC
PONPC
0.0935
F
16:0/18:1[1xOH]
16:0/18:2[1xKETO]
0.0393
0.0083
0.0381
G
C42H80NO11P
C44H80NO9P
0.0388
0.1319
Fold Change
6-wk Chow
6-wk FPC
20-wk FPC
GFP
scFv-E06

Supplemental Figure 7. Untargeted and targeted lipid analysis reveal a changing oxo-phospholipidome but no change in the overall lipidome.

The plasma lipidome of mice after **(A)** six (GFP – n=7, scFv-E06 – n=6) and twenty weeks (GFP – n=10, scFv-E06 – n=10) of FPC diet were unaffected by expression of scFv-E06. **(B)** Comparison of oxidized phospholipids species detected in steatosis and fibrosis revealed 1 unique plasma oxidized phospholipid in steatotic mice and 7 unique oxidized phospholipids in mice with hepatic fibrosis. **(C)** Non-oxidized phospholipids PAPC and PLPC were unaffected by expression of scFv-E06; though their levels were altered by FPC diet duration (6-wk Chow GFP – n=3, 6-wk FPC GFP – n=7, 6-wk FPC scFv-E06 – n=6, 20-wk FPC GFP – n=10, 20-wk FPC scFv-E06 – n=10). **(D)** 16:0 LysoPC (6-wk Chow GFP – n=3, 6-wk FPC GFP – n=7, 6-wk FPC scFv-E06 – n=6, 20-wk FPC GFP – n=10, 20-wk FPC scFv-E06 – n=10) decreased after 6-weeks of FPC diet feeding while 18:0, 18:1 (6-wk Chow GFP – n=3, 6-wk FPC GFP – n=7, 6-wk FPC scFv-E06 – n=6, 20-wk FPC GFP – n=7/6, 20-wk FPC scFv-E06 – n=7), and 18:2 LysoPC (6-wk Chow GFP – n=2, 6-wk FPC GFP – n=7, 6-wk FPC scFv-E06 – n=6, 20-wk FPC GFP – n=6, 20-wk FPC scFv-E06 – n=7) increased after 6 and 20 weeks on FPC diet compared to 6-week, chow-fed controls. **(E)** POBPC (6-wk Chow GFP – n=3, 6-wk FPC GFP – n=7, 6-wk FPC scFv-E06 – n=6, 20-wk FPC GFP – n=10, 20-wk FPC scFv-E06 – n=10) increased with longer duration FPC-feeding but was unaffected by scFv-E06, while PONPC (6-wk Chow GFP – n=3, 6-wk FPC GFP – n=7, 6-wk FPC scFv-E06 – n=6, 20-wk FPC GFP – n=10, 20-wk FPC scFv-E06 – n=10) was unaffected by feeding and scFv-E06 expression. **(F)** 16:0/18:1[1xOH] (6-wk Chow GFP – n=1, 6-wk FPC GFP – n=5, 6-wk FPC scFv-E06 – n=6, 20-wk FPC GFP – n=9, 20-wk FPC scFv-E06 – n=10) was decreased by expression of scFv-E06 at both 6-weeks and 20-weeks of FPC-diet feeding, while 16:0/18:2[1xKETO] was only decreased by scFv-E06 after six

weeks of feeding (6-wk Chow GFP – n=3, 6-wk FPC GFP – n=7, 6-wk FPC scFv-E06 – n=6, 20-wk FPC GFP – n=10, 20-wk FPC scFv-E06 – n=8). **(G)** The isobaric group C42H80NO11P (6-wk Chow GFP – n=3, 6-wk FPC GFP – n=7, 6-wk FPC scFv-E06 – n=6, 20-wk FPC GFP – n=10, 20-wk FPC scFv-E06 – n=10) was unaffected by diet and scFv-E06 expression while C44H80NO9P was increased after six and 20 weeks of FPC diet. scFv-E06 expression decreased levels of C44H80NO9P after 20 weeks of FPC diet (6-wk Chow GFP – n=3, 6-wk FPC GFP – n=7, 6-wk FPC scFv-E06 – n=6, 20-wk FPC GFP – n=10, 20-wk FPC scFv-E06 – n=10). Statistical significance was determined by 2-way ANOVA with Tukey multiple comparison correction or Student's t-test.

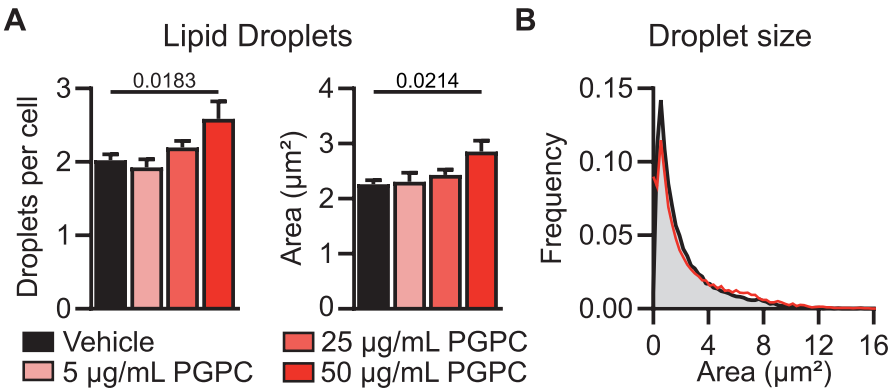
A
Lipid Droplets
Droplets per cell
0.0183
Area (μm²)
0.0214
Vehicle
5 μg/mL PGPC
25 μg/mL PGPC
50 μg/mL PGPC
B
Droplet size
Frequency
Area (μm²)

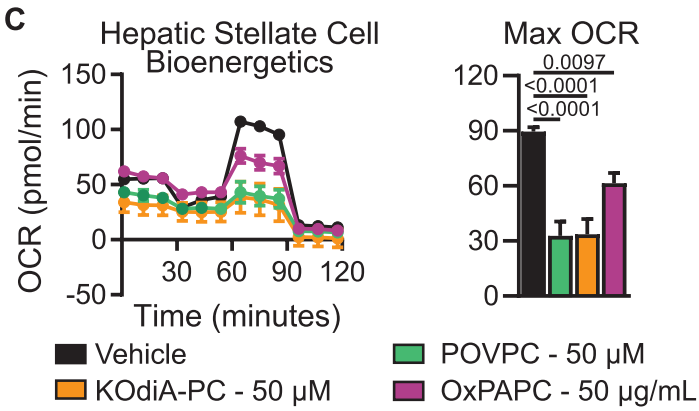
C
Hepatic Stellate Cell Bioenergetics
OCR (pmol/min)
Time (minutes)
Max OCR
0.0097
<0.0001
<0.0001
Vehicle
KOdiA-PC - 50 μM
POVPC - 50 μM
OxPAPC - 50 μg/mL

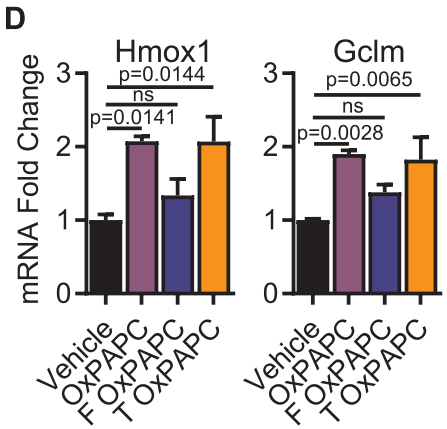
D
Hmox1
p=0.0144
ns
p=0.0141
Gclm
p=0.0065
ns
p=0.0028
mRNA Fold Change
Vehicle
OxPAPC
F OxPAPC
T OxPAPC

Supplemental Figure 8. Pathology-driving OxPCs regulate hepatocyte and hepatic stellate cell function *in vitro*.

AML12 hepatocytes treated with an increasing concentration of PGPC exhibited increased **(A)** lipid droplet number per cell and size resulting in a shift toward **(B)** a higher frequency of larger lipid droplets (n=4). **(C)** LX-2 hepatic stellate cell oxygen consumption rate was significantly decreased by POVPC, KOdiA-PC, and OxPAPC after 4 hours (Vehicle, n=6; POVPC, n=5; KOdiA-PC, n=5; OxPAPC, n=6), while **(D)** OxPAPC and truncated OxPAPC increased expression of *Hmox1* and *Gclm* after 4 hours (n=4). Statistical significance was determined by 1-way ANOVA with Dunnet's Multiple Comparison Correction or Student's t-test.

LPPTiger Nomenclature (previously identified species)	Parent Lipid	*m/z*	Formula	LPPTiger Predicted Structure(s)
1. PAPC	---	782	$C_{44}H_{80}NO_8P$	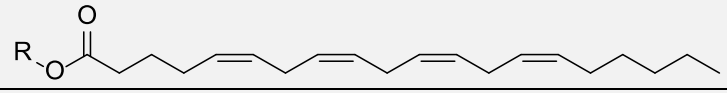
2. PLPC	---	758	$C_{42}H_{80}NO_8P$	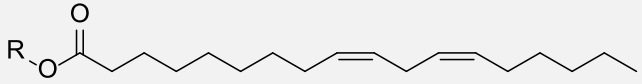
3. 16:0 LysoPC	---	496	$C_{24}H_{50}NO_7P$	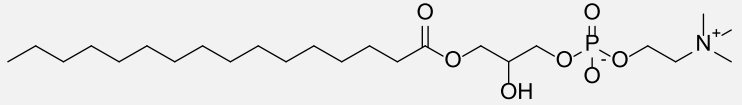
4. 18:1 LysoPC	---	522	$C_{26}H_{52}NO_7P$	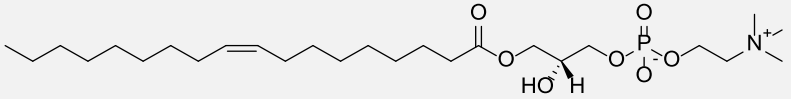
5. 18:2 LysoPC	---	520	$C_{26}H_{54}NO_7P$	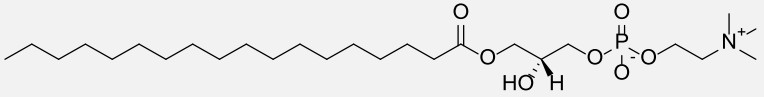
6. 18:0 LysoPC	---	524	$C_{26}H_{54}NO_7P$	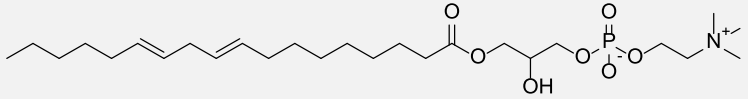
7. 16:0/12:1[CHO]	PLPC	690	$C_{36}H_{68}NO_9P$	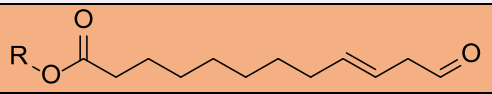
8. POBPC	PAPC	580	$C_{28}H_{54}NO_9P$	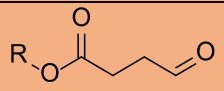
9. C35H62NO11P	PAPC	704	$C_{35}H_{62}NO_{11}P$	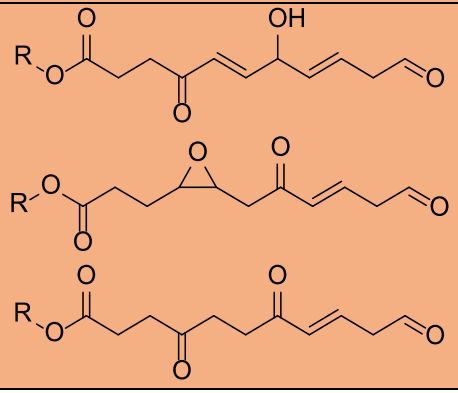

				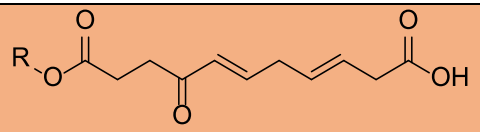
10. 16:0/7:0[1xOH,CHO]	PAPC	638	$C_{31}H_{60}NO_{10}P$	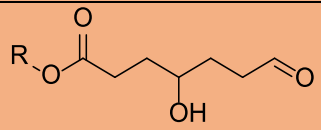
11. PONPC	PLPC	650	$C_{33}H_{64}NO_9P$	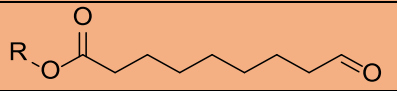
12. C35H64NO10P	PAPC	690	$C_{35}H_{64}NO_{10}P$	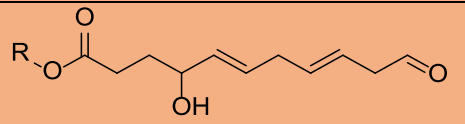 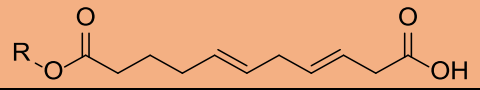
13. 16:0/11:1[CHO]	PLPC	676	$C_{35}H_{66}NO_9P$	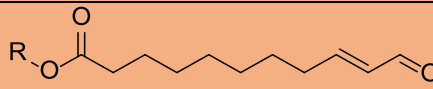
14. 16:0/8:0[CHO] (POOPC)	PLPC	636	$C_{32}H_{62}NO_9P$	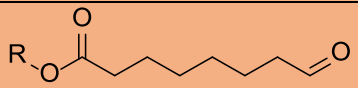
15. C35H64NO12P	PAPC	722	$C_{35}H_{64}NO_{12}P$	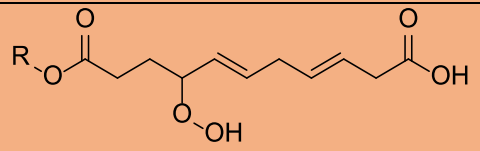 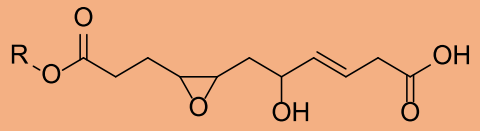 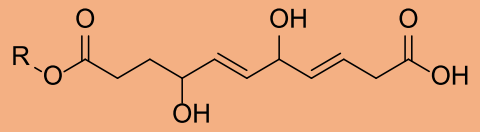 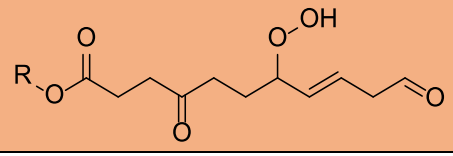

				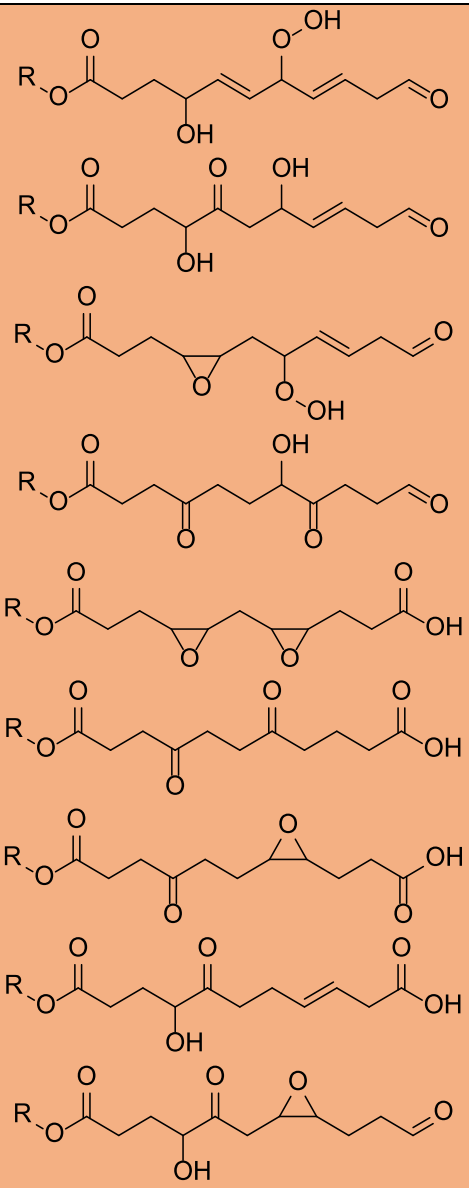
16. C32H60NO10P	PAPC	650	$C_{32}H_{60}NO_{10}P$	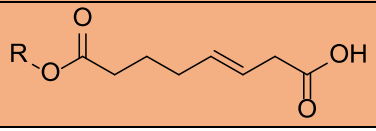

				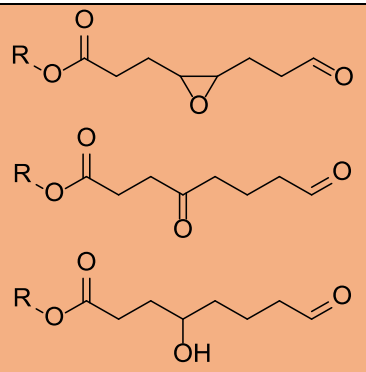
17. 16:0/10:2[CHO]	PAPC	660	$C_{34}H_{62}NO_9P$	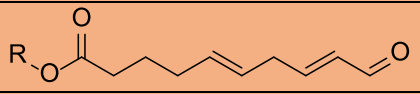
18. POVPC	PAPC	594	$C_{29}H56NO_9P$	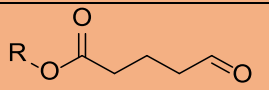
19. C34H62NO11P	PAPC	692	$C_{34}H_{62}NO_{11}P$	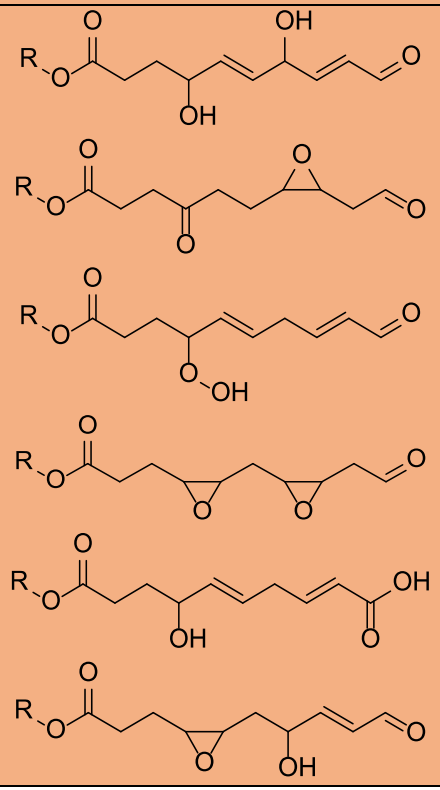

				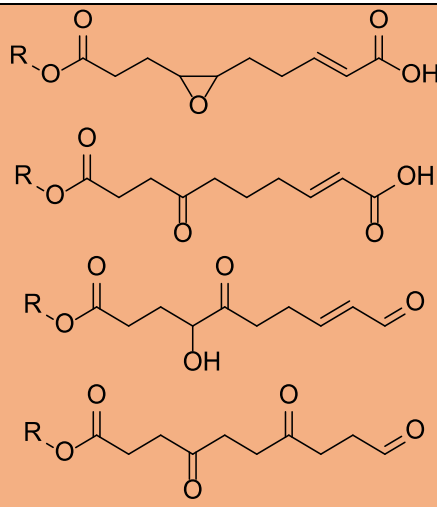
20. 16:0/7:1[CHO]	PAPC	620	$C_{31}H_{58}NO_9P$	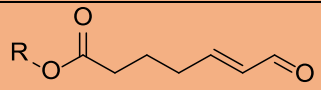
21. PazPC	PLPC	666	$C_{33}H_{64}NO_{10}P$	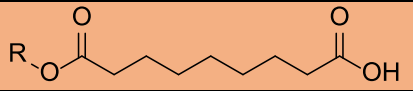
22. C42H80NO11P (HPODE-PC)	PLPC	806	$C_{42}H_{80}NO_{11}P$	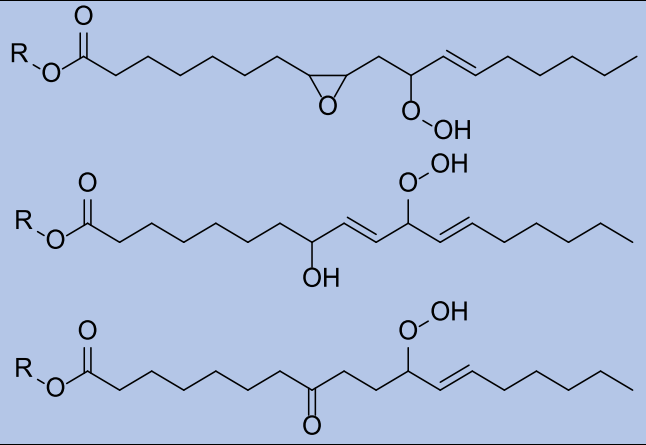
23. 16:0/18:2[2xOOH]	PLPC	822	$C_{42}H_{80}NO_{12}P$	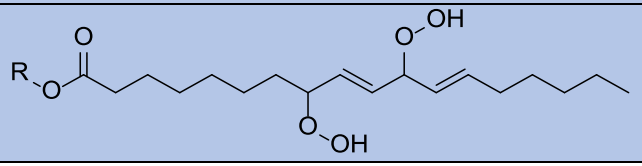

24. C42H78NO10P	PLPC	788	$C_{42}H_{78}NO_{10}P$	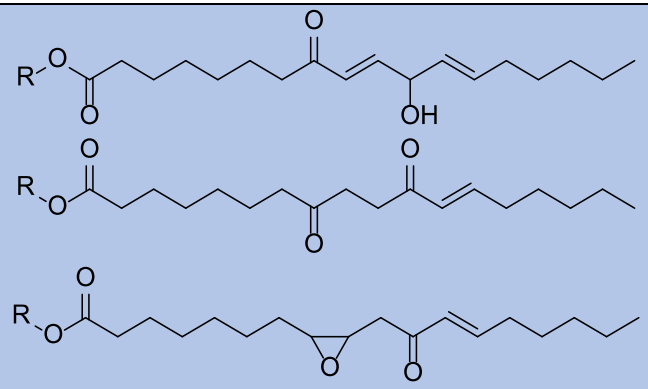
25. C44H80NO9P (HETE-PC)	PAPC	798	$C_{44}H_{80}NO_9P$	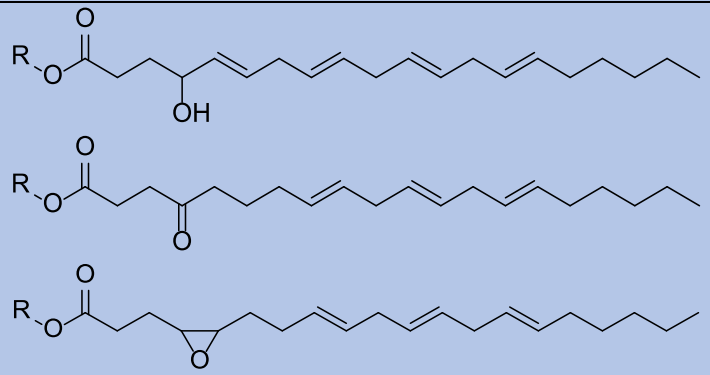
26. C44H80NO11P (Isoprostane-PC, Isoketal-PC)	PAPC	830	$C_{44}H_{80}NO_{11}P$	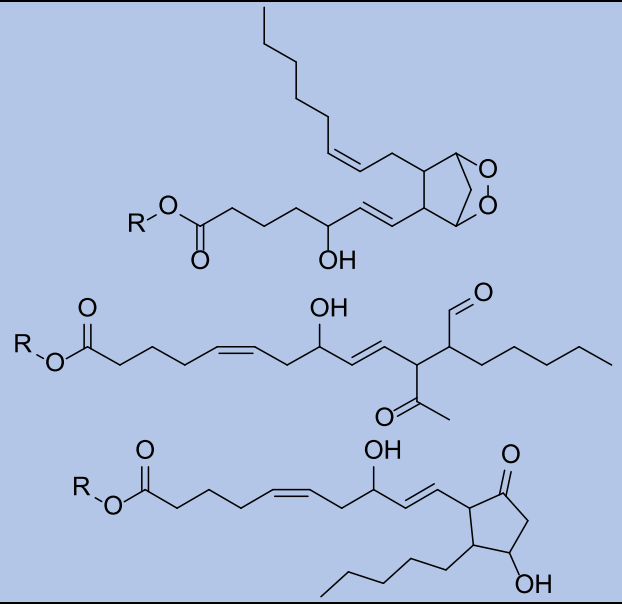

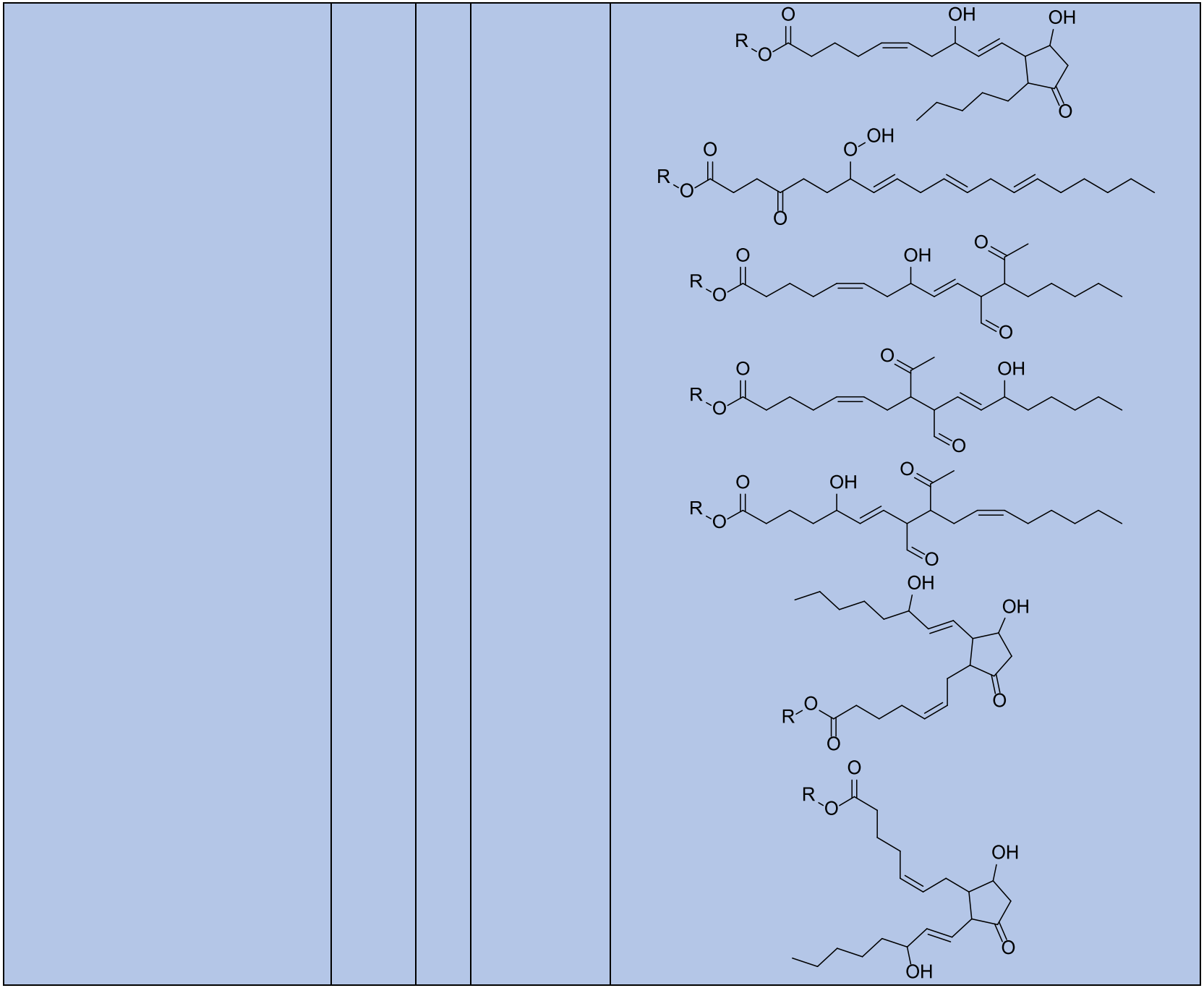
R
O
OH
OH
O
O
R
O
O
OH
O
O
R
O
O
OH
O
O
R
O
O
OH
O
O
R
O
O
OH
O
O
R
O
OH
OH
O
O
R
O
O
OH
O
OH

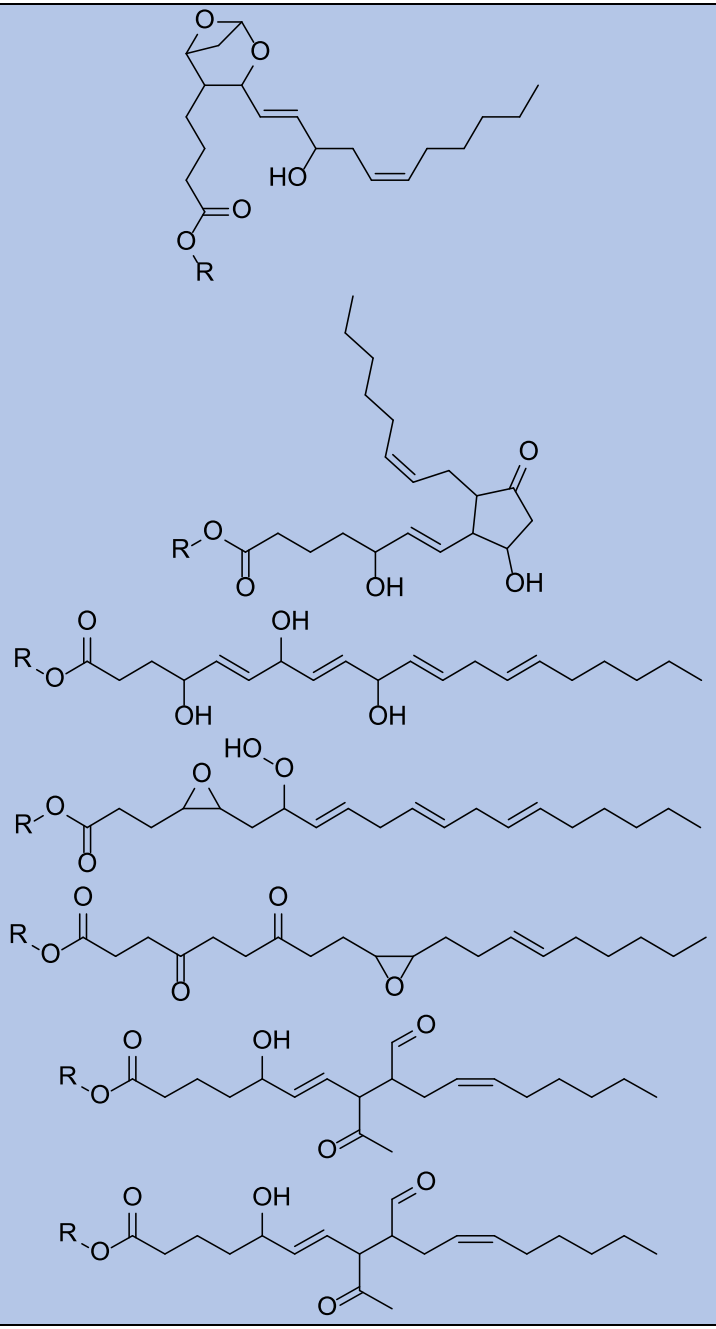
O
O
HO
O
O
R
O
R
O
O
OH
OH
O
R
O
O
OH
OH
OH
HO
O
R
O
O
O
O
R
O
O
O
O
O
R
O
OH
O
O
O
R
O
OH
O
O

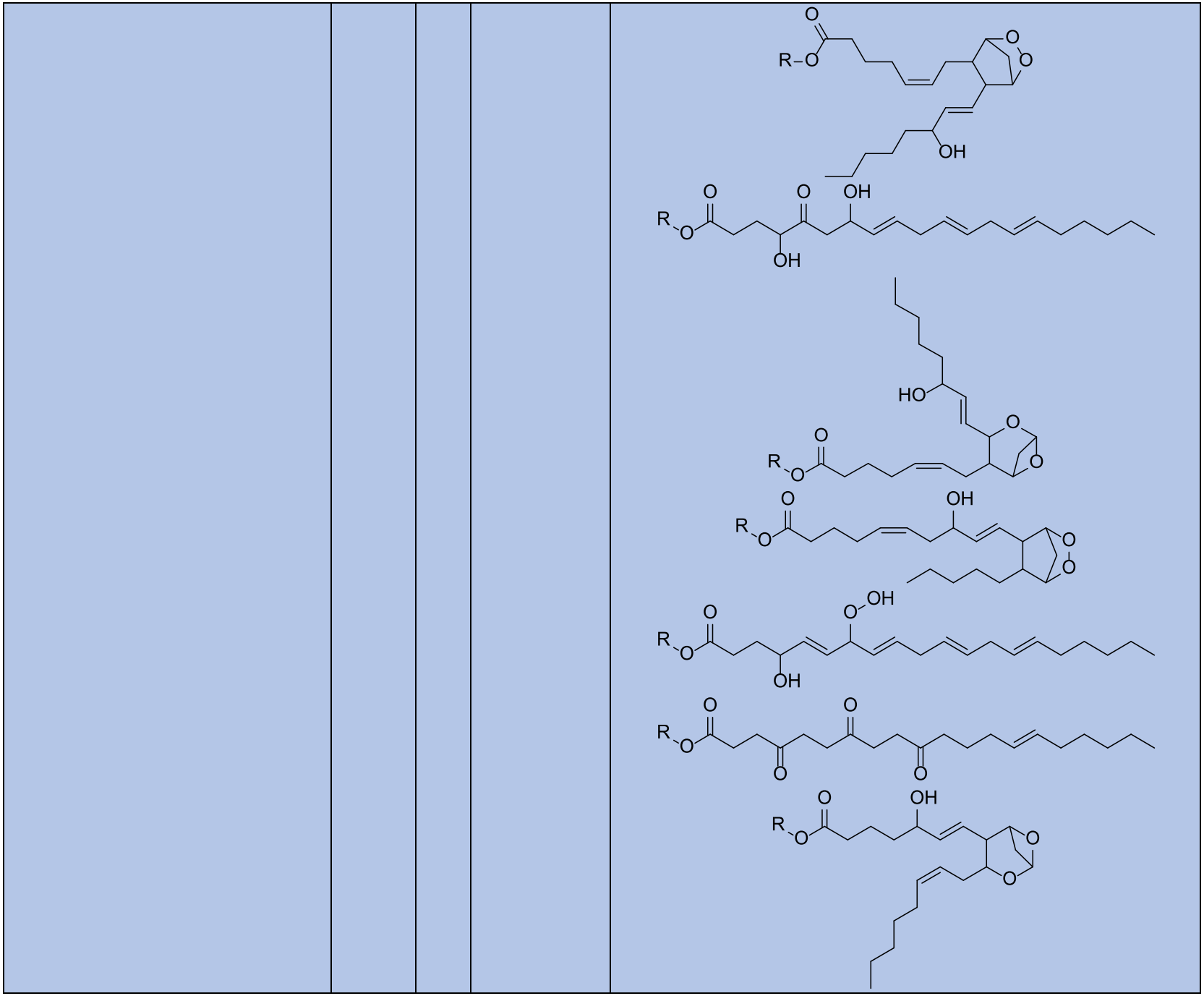
O
R–O
O
O
OH
O
O
OH
R
O
OH
HO
O
R
O
O
O
OH
R
O
O
OH
R
O
OH
O
R
O
O
O
O
O
OH
R
O
O

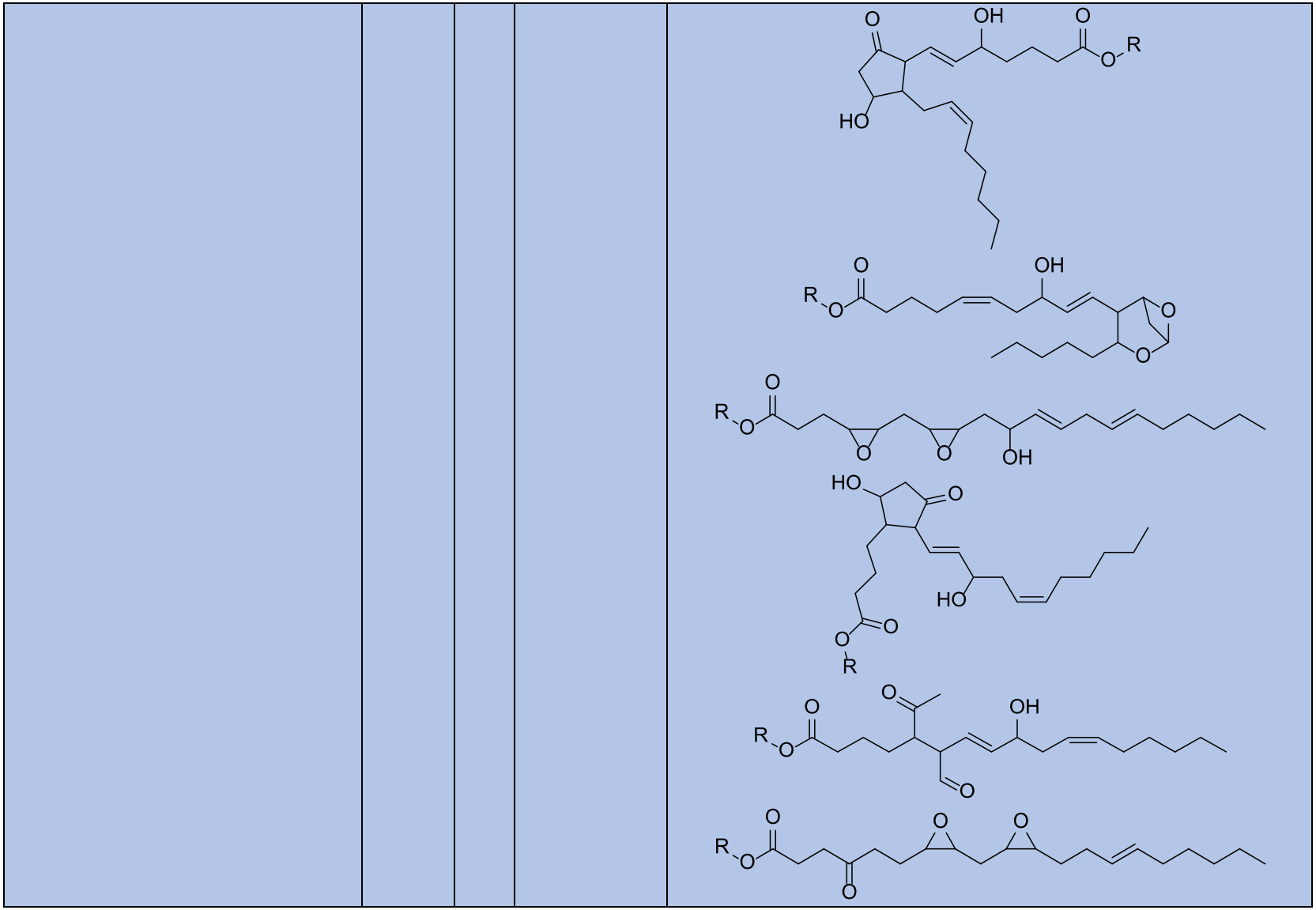
O
OH
O
R
HO
O
OH
R
O
O
O
R
O
O
O
OH
HO
O
HO
O
O
R
O
O
OH
R
O
O
O
O
R
O
O
O
O

				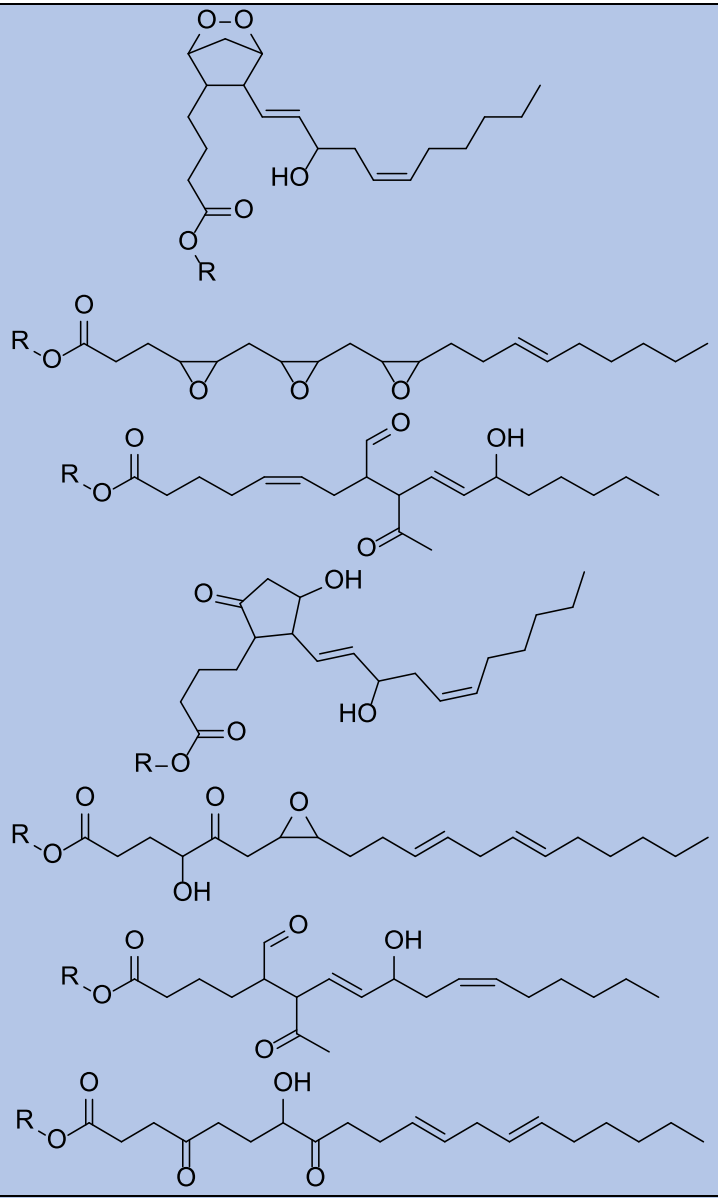
27. C42H80NO9P (HODE-PC)	PLPC	774	$C_{42}H_{80}NO_9P$	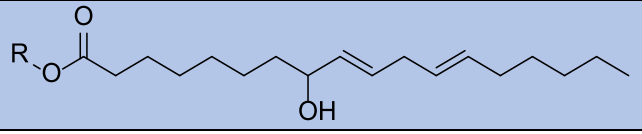

				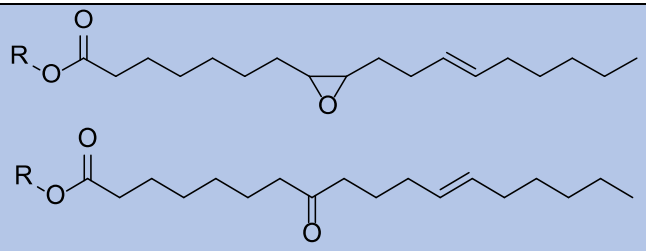
28. 16:0/18:2[2xDB,1xKETO] (KODE-PC)	PLPC	772	$C_{42}H_{78}NO_9P$	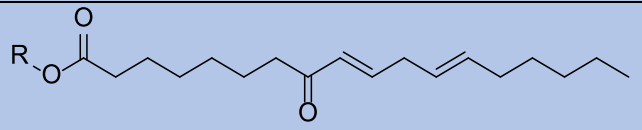
29. 16:0/18:1[1xDB,1xOH] (HOME-PC)	PLPC	776	$C_{42}H_{82}NO_9P$	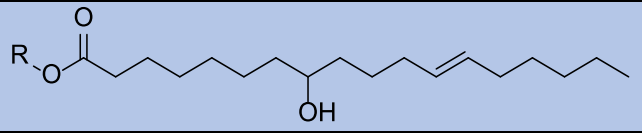

Supplemental Table 1. Oxidized phospholipids detected after development of hepatic steatosis. *In silico* predicted structures of oxidized phospholipids derived from PAPC or PLPC detected in mouse plasma after six weeks on FPC diet. CHO – aldehyde, COOH – carboxylic acid, OH – hydroxy, OOH – hydroperoxy, KETO – ketone, EPOXY – epoxide.

Gene Symbol	Trun-cated	Full-length	Ox-PAPC
1110002E22Rik	---	---	-1.06
1700011H14Rik	---	---	-0.83
1700066M21Rik	---	---	-0.74
1810011O10Rik	-1.11	---	---
2010111I01Rik	0.86	---	---
2310007B03Rik	---	---	-1.15
2310022B05Rik	---	---	-0.68
2410131K14Rik	0.77	---	0.86
2810417H13Rik	-0.77	---	-1.13
3010026O09Rik	---	---	-1.62
3110002H16Rik	---	---	0.72
3110043O21Rik	0.78	---	1.14
4921536K21Rik	---	---	1.63
4930427A07Rik	---	---	-0.82
4930430F08Rik	0.79	---	---
5031439G07Rik	---	---	0.75
5730508B09Rik	---	---	-0.97
9230110C19Rik	1.26	---	---
9330159F19Rik	---	---	0.97
9930012K11Rik	---	---	-0.95
AA415398	---	---	0.82
Aasdhppt	---	---	-0.75
Abca8b	2.50	1.43	2.74
Abcb6	2.03	1.35	1.77
Abcc1	1.90	1.58	2.02
Abcc2	3.72	2.81	4.08
Abcc4	1.53	1.37	1.71
Abcc5	1.03	---	1.04
Abcd4	---	---	0.87
Abhd4	1.36	1.03	1.64
Abhd5	---	---	0.92
Ablim1	-0.80	---	-0.77
Abr	1.05	---	1.20
Abtb1	1.24	---	1.02
Acan	-0.91	---	---
Acot2	1.01	---	1.38
Acox2	1.12	---	1.72
Acrbp	---	---	0.92
Actb	---	---	-0.67
Actg1	-0.72	---	-0.95
Actn1	-0.78	---	-0.72
Adamts1	-1.17	-1.36	---
Adamts6	-1.50	-1.58	-1.50
Adamts9	-1.73	-1.22	-1.73
Adap2	---	---	-1.26
Adgra2	-1.03	---	-0.81
Adgrg1	---	---	1.14
Adh7	2.75	1.86	1.86
Adprm	1.08	---	1.31
Adra1a	2.56	1.79	2.50
Adrm1	0.81	---	1.13
Afap1	---	---	0.85
Ahnak2	1.14	0.81	1.16
Ahr	-1.54	-0.92	-1.52
Ahsa1	0.79	---	0.84
Ahsa2	1.42	0.77	1.39
AI846148	---	---	0.88
Ajuba	---	---	-0.96
Akap1	---	---	-0.96
Akap12	-0.86	---	-0.99
Akap8l	0.79	---	1.05
Akr1c13	0.80	---	---
Akr1c14	2.30	1.37	1.73
Akr1c19	3.31	2.39	3.16
Akt1s1	---	---	0.78
Alas1	0.91	0.81	0.96
Aldh18a1	---	---	0.67
Aldh1a1	2.27	1.50	1.70
Aldh1l2	---	---	1.06
Aldh2	---	---	0.71
Aldh3a2	0.83	---	0.92
Aldoa	---	---	0.85
Alg6	---	---	-0.96
Als2	0.75	---	0.79
Amacr	---	---	-0.88
Ammecr1	---	---	-0.75
Amotl2	-0.86	---	-1.58
Ampd3	3.35	3.12	3.67
Anapc16	---	---	0.79
Angptl4	-0.97	---	-1.40
Angptl6	---	---	1.34
Ankle1	---	---	-1.24
Ankrd1	-2.23	-0.98	-2.75
Ankrd11	---	---	0.91
Ankrd12	---	---	1.05
Ankrd40	---	---	-0.63
Ankrd49	---	---	-0.80
Anln	-0.73	---	-0.91
Antxr2	-0.79	---	---
Anxa7	---	---	0.75
Aox1	2.67	2.07	2.79
Ap1ar	---	---	-0.76
Ap1s3	---	---	-0.84
Apba3	---	---	0.78
Apobr	2.59	1.14	3.37
Aqp9	1.84	---	2.08
Areg	---	---	1.37
Arhgap18	---	---	-0.82
Arhgap19	---	---	-1.35
Arhgap27	---	---	0.72
Arhgap8	-1.23	---	-1.22
Arhgef39	---	---	-1.01
Arid4b	---	---	0.70
Arid5a	---	---	1.36
Arih2	---	---	0.80
Arl4a	---	---	0.79
Arl4c	-1.13	-0.85	-1.65
Arl4d	1.19	---	---
Arl5b	---	---	0.93
Arl8a	---	---	0.95
Armcx3	---	---	0.96
Arrdc2	1.08	---	0.91
Arrdc3	0.66	---	---
Asns	0.69	---	0.78
Aspm	---	---	-1.38
Atad5	---	---	-1.02
Atf3	1.39	---	4.41
Atf4	---	---	1.11
Atf5	1.01	---	1.15
Atg12	---	---	0.65
Atg14	0.97	---	1.17
Atp10a	-1.01	---	---
Atp5sl	0.85	---	0.87
Atp6v0a1	---	---	1.09
Atp7a	---	---	0.79
Atxn1	---	---	-0.81
Atxn7l2	---	---	0.77
Aurkb	-0.73	---	-1.09
Avl9	---	---	0.82
B2m	---	---	0.73
B4galt7	---	---	0.75
B4gat1	---	---	-0.78
Bach1	1.63	1.01	1.98
Bag3	1.62	1.42	2.57
Bahcc1	-0.99	---	-1.36
Bahd1	---	---	0.65
Bbc3	---	---	0.86
Bbs12	---	---	-0.98

BC005537	0.71	---	0.92
BC025446	-0.88	---	-0.77
BC055324	---	---	-0.65
Bcar1	-1.31	---	-1.47
Bcl3	-0.86	---	---
Blcap	---	---	1.03
Blvrb	3.83	3.03	3.95
Bmf	---	---	-0.94
Bnip3	0.97	---	0.91
Bok	---	---	-1.16
Bora	-0.97	---	-1.31
Borcs5	---	---	-0.81
Brd2	---	---	0.89
Bsdc1	0.79	---	1.13
Btc	---	---	1.01
Bub1b	---	---	-0.88
C2cd4c	1.04	---	---
C2cd5	---	---	-0.80
Cachd1	2.24	1.67	2.61
Cacna1h	---	-1.03	-0.95
Cacnb2	-1.06	---	---
Cacybp	---	---	0.85
Cad	---	---	-0.83
Calcoco1	1.15	---	1.11
Calr3	2.88	2.24	2.91
Camkk1	---	---	-1.43
Camkk2	-0.89	---	-1.16
Camkmt	---	---	0.90
Capn5	-0.92	---	-0.74
Car15	---	---	1.41
Card10	-0.75	---	-1.45
Casc4	-0.97	---	---
Casp8ap2	---	---	-0.89
Cat	1.64	1.36	1.62
Cav1	-0.79	---	-0.76
Cav2	-0.88	---	-1.12
Cbr1	1.60	0.89	1.32
Cbx4	---	---	-0.81
Cbx6	---	---	-1.00
Cc2d2a	---	---	-0.86
Ccbe1	-1.42	---	-1.21
Ccdc117	0.83	---	0.75
Ccdc186	---	---	0.80
Ccdc28a	---	---	0.75
Ccdc71l	---	---	0.74
Ccdc88a	1.06	0.99	1.43
Ccdc92	---	---	0.79
Ccl2	-1.21	-1.12	-1.78

Ccna2	---	---	-0.99
Ccnb1	---	---	-1.05
Ccnb2	---	---	-0.84
Ccnd1	-0.96	---	-1.21
Ccnd3	-0.73	---	-0.93
Ccne1	-1.99	---	-2.41
Ccne2	-1.25	---	-1.64
Ccnf	---	---	-0.85
Ccng2	0.96	---	1.31
Ccsap	---	---	-1.36
Cd3eap	---	---	-1.11
Cd44	-0.88	---	---
Cd59a	0.94	---	1.06
Cd9	---	---	0.70
Cdc20	---	---	-0.87
Cdc25b	---	---	-0.74
Cdc25c	---	---	-0.91
Cdc42ep2	1.79	1.56	1.69
Cdc42ep5	---	---	0.93
Cdc6	-1.13	---	-1.35
Cdc7	-0.74	---	-0.99
Cdca2	---	---	-0.65
Cdca7	-1.22	---	-1.77
Cdca7l	---	---	-1.16
Cdk2	-0.75	---	-0.72
Cdk6	-0.84	---	-0.86
Cdkn1a	---	---	0.74
Cdkn2aipnl	---	---	-0.88
Cdkn2b	1.75	1.24	2.02
Cdkn2c	---	---	-0.79
Cdkn2d	---	---	-1.62
Cdr2l	---	---	0.95
Cds2	0.97	---	0.87
Cdt1	-0.87	---	-0.67
Cebpa	1.59	---	1.67
Cebpb	---	---	1.27
Cenpa	---	---	-1.10
Cenpf	---	---	-0.74
Cenpl	---	---	-0.78
Cep55	---	---	-0.85
Cep78	---	---	-0.71
Cep85l	---	---	1.61
Cep89	---	---	-0.69
Cfap43	-0.72	---	---
Cgn	---	---	-1.52
Cgnl1	1.48	1.15	1.53
Chac1	---	---	2.38
Chaf1b	-0.74	---	---

Chchd10	---	---	1.33
Chd2	---	---	1.12
Chka	-0.99	-0.76	-0.70
Chmp1b	---	---	0.73
Chn2	-0.86	---	---
Chordc1	0.97	0.82	1.06
Chpf2	2.13	1.39	2.03
Chrnb2	1.29	---	1.39
Chst15	---	---	-0.70
Cish	---	---	1.01
Ckap2	-0.77	---	-0.87
Clcf1	---	---	0.84
Clcn2	---	---	0.88
Clcn6	---	---	0.90
Cldn2	-0.80	---	-0.89
Clic4	---	---	0.93
Clip2	---	---	0.81
Clk1	---	---	0.82
Clk3	---	---	0.67
Clk4	---	---	0.80
Clmn	---	---	-0.79
Clspn	---	---	-0.73
Cnn2	-0.95	---	-1.18
Cnnm2	0.86	---	---
Cnot6	---	---	-0.68
Cnppd1	0.98	---	1.14
Cobl	---	---	0.93
Coil	---	---	-0.90
Col11a2	1.41	---	1.46
Col4a5	---	---	-0.80
Coro2a	---	---	1.01
Cotl1	---	---	-0.72
Cpeb2	---	---	1.13
Cpt1a	0.92	---	0.83
Cpt1b	---	---	0.87
Crb2	---	---	-1.19
Crebrf	---	---	0.90
Creg1	2.32	2.00	2.58
Creld1	0.90	---	---
Crem	0.84	---	1.41
Crim1	-0.72	---	-0.82
Crlf1	---	0.97	1.24
Crocc	---	---	-0.88
Crocc2	---	---	-1.12
Crtc1	1.05	0.94	1.34
Cryab	---	---	1.15
Csf1	---	---	0.73
Csnk1e	---	---	0.76

Csrnp2	0.72	---	0.80
Cstb	---	---	0.72
Ctdsp2	---	---	-0.67
Ctdspl	---	---	-0.90
Ctgf	-3.76	-2.09	-4.45
Cth	1.17	---	1.35
Ctns	---	---	0.97
Ctps	---	---	-1.04
Ctsb	---	---	0.65
Ctsd	0.92	---	1.07
Cxcl1	-1.26	---	---
Cxcl5	-1.53	-1.17	-2.39
Cyb5a	1.76	1.63	1.97
Cyb5r1	---	---	0.97
Cyld	---	---	-1.08
Cyp1a1	2.61	1.97	---
Cyp2j6	0.85	---	1.00
Cyp3a13	---	---	0.94
Cyp51	2.25	---	2.51
Cyr61	-1.36	---	-1.75
Cys1	---	---	1.17
D630003M21Rik	---	---	-1.42
D930048N14Rik	---	---	-1.10
Dact2	1.33	---	0.88
Dbt	---	---	-0.87
Dck	---	---	-0.84
Dcun1d3	---	---	1.01
Ddit3	1.60	---	2.82
Ddit4	0.98	---	2.10
Ddx11	---	---	-1.01
Ddx20	---	---	-0.88
Ddx41	---	---	-0.81
Ddx51	---	---	-0.72
Dedd2	2.46	1.48	2.77
Dennd4a	---	---	1.07
Depdc1a	---	---	-1.04
Depdc7	1.05	---	1.49
Deptor	1.06	---	0.91
Dgat2	---	---	1.09
Dhcr24	0.67	---	---
Dhodh	---	---	-0.86
Dhrs13	---	---	-1.09
Dhrs3	-1.34	-1.18	-1.91
Dhrs9	-1.26	---	---
Dimt1	-0.78	---	-1.08
Dip2b	---	---	0.81
Dkc1	-0.74	---	-0.80

Dlg5	---	---	0.99
Dlgap4	---	---	0.98
Dlk2	-1.04	---	-1.98
Dna2	-1.13	---	-1.22
Dnaja1	1.20	0.88	1.63
Dnaja4	1.51	0.99	2.74
Dnajb1	1.38	0.99	2.96
Dnajb2	1.47	0.84	1.41
Dnajb4	1.96	1.60	2.23
Dnajb9	---	---	1.48
Dnajc27	-1.16	---	-1.15
Dnase2a	1.46	1.19	1.40
Dnhd1	---	---	1.14
Dnph1	---	---	-1.00
Dock5	---	---	0.84
Dpp7	---	---	0.90
Dpy19l1	---	---	-0.97
Dsel	---	---	-0.79
Dtl	-1.29	---	-1.29
Dtx2	---	---	0.78
Dusp1	2.31	2.06	4.15
Dusp10	-0.79	---	-0.66
Dusp14	-1.07	---	-1.03
Dusp18	1.46	1.08	1.44
Dusp4	1.36	0.80	1.86
Dusp5	-1.21	---	---
Dusp6	---	---	0.98
Dusp7	-1.22	---	-0.84
Dut	---	---	-0.86
Dync1h1	---	---	0.77
Dync1li1	---	---	0.67
Dyrk1b	1.12	---	1.44
Dzip1l	---	---	-0.76
E2f6	0.96	0.89	1.08
E2f7	-0.88	---	-0.95
E2f8	-1.51	---	-1.61
E330009J07Rik	1.11	---	1.19
Eaf1	---	---	0.89
Ecm1	---	---	0.74
Ect2	-0.76	---	-1.03
Edn1	---	---	-1.95
Eea1	---	---	0.83
Eef2kmt	---	---	-0.71
Eepd1	-0.83	---	-1.18
Efcab8	---	---	0.95
Efnb1	1.00	---	1.22
Efnb2	-1.42	-0.68	-1.13

Egfr	-0.96	---	---
Egr1	-3.62	-2.38	---
Eid3	1.97	1.82	2.33
Eif2s2	---	---	0.83
Eif4ebp1	0.83	---	1.16
Elf1	---	---	1.01
Elmo1	---	---	0.97
Eml4	-0.86	---	-0.83
Emp1	-0.89	---	-0.80
Enc1	-1.22	---	-1.05
Endod1	---	---	-0.66
Engase	---	---	-1.29
Enpp1	-0.88	-0.84	-0.86
Enpp4	---	---	-0.83
Entpd5	1.52	1.07	1.46
Epb41	---	---	0.86
Epha7	---	---	-1.04
Ephx1	1.63	1.29	1.82
Eprs	---	---	0.73
Ercc6l	---	---	-0.80
Ereg	---	---	0.81
Eri1	---	---	-0.70
Eri2	---	---	-0.79
Ern1	---	---	1.00
Ero1l	---	---	0.77
Ero1lb	1.15	0.86	1.12
Errfi1	-1.20	-0.89	---
Esd	1.61	1.40	1.54
Espl1	---	---	-1.03
Esyt1	---	---	0.72
Etaa1	---	---	-0.97
Ets1	-0.84	---	-0.83
Exo1	-0.74	---	-1.01
Ext1	-0.78	---	-0.79
Eya2	---	---	1.14
Ezr	---	---	0.71
F2rl1	-1.35	---	-1.29
F3	-2.17	-0.89	-2.19
Faap100	-0.84	---	-0.98
Faap24	---	---	-0.84
Fadd	---	---	-0.83
Fads1	---	---	0.89
Fads2	0.99	---	1.23
Fam102a	---	---	1.09
Fam102b	-1.32	-0.87	-1.06
Fam118a	---	---	-0.78
Fam126a	---	---	0.74
Fam13a	2.35	1.44	2.43

Fam21	0.91	---	1.07
Fam214b	1.04	---	1.17
Fam219a	1.98	1.44	2.02
Fam63a	---	---	0.72
Fam64a	---	---	-1.08
Fam65b	-1.92	-1.29	-2.88
Fam73b	---	---	-0.76
Fam83d	---	---	-1.10
Fam83g	---	---	1.29
Fam83h	---	---	0.87
Fam84b	---	-0.83	---
Fanca	---	---	-0.80
Fancb	---	---	-0.92
Fancd2	---	---	-0.68
Fbxl20	0.77	---	0.76
Fbxo11	---	---	0.72
Fbxo30	1.01	---	1.11
Fbxo31	0.98	---	1.03
Fbxo32	1.06	---	0.89
Fbxo48	---	---	-1.23
Fbxo5	-1.08	---	-1.55
Fbxo9	1.06	0.82	0.82
Fchsd1	0.97	---	---
Fchsd2	-1.08	---	-1.09
Fdft1	1.32	---	1.44
Fech	---	0.79	0.80
Fen1	---	---	-0.93
Fermt1	-1.00	-0.75	-1.14
Fermt2	-0.73	---	-0.87
Fermt3	---	---	1.73
Fgd3	1.18	0.93	---
Fgf1	2.37	1.98	2.17
Fgfrl1	---	---	0.77
Fhdc1	---	---	1.10
Fhl2	-0.96	---	-1.22
Fhl3	-0.79	---	---
Fignl1	-0.71	---	-1.34
Fip1l1	---	---	0.74
Fjx1	---	---	-0.80
Flcn	---	---	0.77
Flrt2	-2.03	---	-1.72
Flrt3	---	---	0.91
Flywch1	1.13	---	1.00
Fndc4	---	---	-0.94
Fopnl	1.14	1.00	0.98
Fosl2	---	---	0.91
Foxj1	---	---	-1.10
Foxn3	---	---	1.02
Foxo3	---	---	0.88
Foxq1	1.74	1.46	1.45
Fpgt	0.78	---	---
Frmd4a	-0.85	---	---
Frmd6	-1.32	-0.80	-1.24
Fth1	1.66	1.64	2.14
Ftl1	1.37	0.89	1.52
Fxyd5	---	---	1.00
Fzd4	---	---	-0.90
Fzd7	1.09	0.75	1.06
G0s2	---	---	-1.12
G6pdx	0.79	---	1.23
Gaa	0.72	---	0.93
Gabarapl1	2.43	1.61	2.64
Gabpb2	---	---	-0.76
Gadd45a	1.68	---	2.29
Gadd45b	---	---	-1.32
Gart	---	---	-0.81
Gas2l3	---	---	-0.88
Gata3	---	---	1.52
Gba	---	---	0.73
Gbe1	1.44	0.91	1.60
Gch1	1.32	---	1.60
Gclc	3.72	3.31	4.12
Gclm	2.61	2.26	2.72
Gcnt2	---	---	0.76
Gcnt3	---	---	-0.91
Gdf11	---	---	0.89
Gdf15	1.93	1.48	4.41
Gemin4	---	---	-0.95
Gemin8	-1.11	---	-0.99
Ggta1	-0.71	---	-0.75
Ghdc	---	---	0.80
Ghitm	---	---	0.66
Gimd1	---	---	-0.79
Gjb1	1.21	1.18	1.59
Gjb3	-0.89	---	-1.55
Gla	0.95	---	1.11
Glis2	---	---	-0.92
Glmp	---	---	0.77
Glul	1.12	0.77	1.28
Glyat	2.50	2.01	2.81
Gm10073	---	---	1.23
Gm21949	---	---	-1.15
Gm21972	---	---	0.93
Gm42878	---	---	0.72
Gm42906	---	---	-1.22
Gm43518	---	---	-0.86
Gm43552	1.15	0.82	1.10
Gm45208	---	---	0.69
Gm7694	1.05	---	1.08
Gm8797	---	---	1.26
Gm9938	---	---	-0.94
Gmnn	---	---	-0.90
Gnal	---	---	0.77
Gpam	-0.77	---	-1.19
Gpcpd1	1.72	1.12	1.93
Gpd1l	---	---	-0.70
Gpi1	---	---	0.76
Gpr137b	0.81	0.88	1.12
Gpr180	---	---	-0.98
Gprc5a	-1.34	---	---
Gpt2	---	---	0.88
Gpx1	0.82	---	---
Gramd1a	---	---	0.79
Gramd3	---	---	0.96
Gramd4	-0.91	-0.71	-0.88
Grasp	---	---	0.80
Grik5	---	---	1.01
Grina	---	---	0.72
Grk6	---	---	-0.81
Grn	0.78	---	0.82
Gsg2	-0.99	---	-1.51
Gsr	1.36	1.26	1.48
Gss	2.37	1.60	2.38
Gsta1	7.09	6.46	6.79
Gsta3	3.11	2.35	2.96
Gsta4	5.13	4.49	4.69
Gstm1	1.91	1.55	2.28
Gsto1	---	---	0.77
Gstp1	2.35	1.63	1.76
Gtf2ird1	---	---	0.99
Gxylt2	-1.18	---	-1.13
H1f0	-1.11	---	-1.51
H2-DMa	1.39	---	1.40
Hap1	---	---	-0.90
Haus5	---	---	-1.07
Havcr1	-1.50	-0.92	-1.54
Hax1	---	---	0.87
Hbegf	-1.10	---	-0.90
Hbp1	0.97	---	1.24
Hdac4	---	---	0.74
Heatr3	---	---	-0.68
Heca	---	---	0.95
Hells	-1.38	---	-1.41
Herpud1	---	---	1.16

Hes1	-0.97	---	-1.41
Hfe	2.39	1.88	2.22
Hgs	---	---	0.87
Hhipl1	---	---	1.31
Hid1	---	---	1.39
Hist1h1c	1.16	---	1.05
Hist3h2a	0.96	---	0.81
Hivep2	-1.05	---	---
Hk2	-1.17	---	---
Hmga2	-0.84	---	---
Hmgcr	1.29	---	1.48
Hmgcs1	1.37	---	1.35
Hmmr	---	---	-0.87
Hmox1	6.60	6.03	7.55
Hnf1b	-1.02	---	---
Hnrnpr	---	---	-0.75
Homer3	0.97	0.71	1.13
Hook1	---	---	-0.76
Hpdl	---	---	-1.05
Hr	---	---	1.12
Hs3st3b1	1.17	---	---
Hsd17b7	---	---	0.87
Hsf2	---	---	0.81
Hsp90aa1	1.19	0.86	1.71
Hsp90ab1	0.81	---	1.21
Hspa1a	5.39	4.26	6.42
Hspa1b	5.38	4.36	6.45
Hspa2	---	---	0.80
Hspa4l	1.17	---	1.12
Hspa8	1.14	1.00	1.61
Hspb1	2.25	1.58	3.30
Hspb8	1.84	1.47	2.11
Hsph1	2.12	1.46	2.65
Htatip2	2.00	1.05	1.66
Htr1b	-1.25	---	-1.37
Hyal1	1.03	---	1.15
Hyal3	1.09	0.83	1.37
Icam1	-1.15	---	-0.85
Ick	1.64	1.52	2.04
Id2	-1.00	---	-1.45
Idh1	2.64	1.48	2.54
Idi1	1.27	---	0.98
Ier3	---	---	0.67
Iffo2	-0.72	---	-0.74
Ifi202b	0.85	---	1.47
Ifi203	---	---	1.03
Ifi47	---	---	-1.20
Ifit2	---	---	-1.44
Ifngr1	---	---	-0.74
Ifnlr1	---	---	-1.01
Igfbp3	-0.86	---	-0.67
Igip	---	---	-1.15
Igsf9	-0.90	---	-1.16
Igtp	1.52	1.24	1.33
Ikbkg	1.45	1.06	1.06
Ikzf2	---	---	-1.38
Il11	---	---	1.26
Il18rap	---	---	-1.01
Il1r1	---	---	-1.17
Il24	-2.11	---	-1.70
Il33	---	---	0.72
Il4ra	0.96	0.91	1.15
Il5ra	-2.91	-2.00	-3.48
Il7	---	---	0.99
Impact	1.41	1.00	1.75
Inhba	-1.43	---	-0.87
Inhbb	-1.15	---	-2.33
Inpp4b	-1.81	---	-1.21
Inpp5j	0.91	---	1.25
Insig1	2.28	---	3.06
Ipp	---	---	-0.93
Iqck	---	---	0.89
Iqgap3	-0.77	---	-0.89
Irs2	1.09	1.03	0.75
Itga3	-0.81	---	---
Itga6	---	---	-0.64
Itga7	1.33	1.09	1.84
Itgb6	-1.59	-1.04	-2.88
Itpripl1	---	---	-0.75
Itsn1	---	---	0.70
Jade2	-1.78	-1.07	-2.28
Jade3	0.85	---	1.07
Jag1	-1.18	-0.78	-1.12
Jmjd6	---	---	0.75
Jrk	---	---	-0.82
Jun	---	---	2.46
Junb	-1.18	---	-0.97
Jup	---	---	0.74
Kank3	---	---	-1.40
Kbtbd8	---	---	-1.19
Kcmf1	---	---	0.91
Kcnab1	---	---	-0.71
Kcnk5	---	---	-0.84
Kctd18	0.92	---	---
Kdm2a	---	---	0.83
Kdm3a	---	---	0.83
Kdm4a	0.83	---	0.89
Keap1	0.97	---	0.95
Kif11	---	---	-0.82
Kif14	---	---	-1.21
Kif15	---	---	-0.82
Kif18a	-0.81	---	-1.04
Kif1b	0.76	---	0.91
Kif20a	---	---	-0.63
Kif20b	---	---	-0.70
Kif21a	0.94	---	1.32
Kif23	---	---	-0.68
Kif24	---	---	-0.99
Kif2a	1.03	0.94	1.40
Kif2c	---	---	-0.71
Kif3c	0.83	---	1.10
Kif7	---	---	-1.21
Kifc3	---	---	-0.90
Kitl	1.07	0.83	0.85
Klc4	0.91	---	0.78
Klf11	0.89	---	1.17
Klf15	---	---	-1.62
Klf16	-0.95	---	-0.89
Klf4	---	---	1.43
Klf5	---	---	0.81
Klf6	---	---	0.69
Klf7	-0.99	---	-1.00
Klf9	---	---	1.02
Klhl15	---	---	0.73
Klhl21	---	---	0.74
Klhl24	1.46	---	1.58
Klhl26	---	---	0.79
Klhl5	---	---	-0.70
Krt7	---	---	-0.88
Krt80	-1.04	---	-1.83
Ksr1	1.26	0.97	1.19
L2hgdh	---	---	-0.68
L3mbtl2	---	---	-0.86
Lancl2	---	---	-0.63
Lancl3	1.28	1.24	1.13
Lasp1	---	---	-0.71
Layn	1.25	1.05	1.71
Lcmt2	---	---	-0.83
Ldlr	1.51	---	1.72
Lfng	---	---	-1.02
Lgals8	0.77	---	1.26
Lgalsl	---	---	-0.99
Lgr6	-1.36	---	-1.73
Lhfpl2	---	---	0.76

Lif	-1.20	---	-1.04
Lig1	-0.80	---	-0.87
Lin37	---	---	0.85
Lipe	0.95	---	1.03
Lmbr1l	---	---	0.72
Lmcd1	-1.96	-1.15	-2.26
Lmln	---	---	-1.45
Lmnb2	---	---	-0.86
Lonrf3	---	---	0.83
Lpar2	0.69	---	---
Lpcat1	-0.91	---	-1.37
Lpcat4	-0.84	---	-0.74
Lpin1	1.99	---	2.41
Lpin2	1.31	---	1.61
Lrig1	-0.76	---	-0.64
Lrp8	1.38	1.28	1.66
Lrr1	---	---	-1.20
Lrrc49	---	---	0.73
Lrrc8c	-1.21	---	---
Lrrc8d	---	---	0.97
Lrrfip2	---	---	0.94
Lrtm2	1.44	---	---
Lss	1.09	---	0.93
Lurap1l	---	---	-0.80
Ly75	---	---	-0.79
Ly96	---	---	1.27
Lyar	-0.76	---	---
Maff	---	---	1.07
Mafg	1.19	0.80	1.39
Mafk	---	---	0.96
Maml2	-0.96	---	---
Man2a1	---	---	0.68
Maoa	1.08	---	0.90
Map1b	---	---	1.44
Map1lc3b	1.13	---	1.34
Map2k6	-1.55	-0.95	-1.38
Map3k4	---	---	-0.69
Map4k4	---	---	0.78
Mapk9	0.78	---	0.96
Mapkapk5	---	---	0.72
Mars2	---	---	-1.09
Masp1	-0.92	---	-1.08
Mat2a	---	---	-0.97
Mb21d2	---	---	0.91
Mccc2	---	---	-0.90
Mcm2	-0.90	---	-0.87
Mcm3	-0.88	---	-0.91
Mcm4	-0.91	---	-0.90
Mcm6	---	---	-0.69
Mcoln1	---	---	0.73
Mdfic	---	---	0.65
Mdm1	---	---	-1.00
Mdm2	---	---	0.96
Mecom	-1.52	-1.07	-1.55
Mef2d	---	---	0.90
Melk	---	---	-0.79
Mettl21a	---	---	-0.83
Mettl7a1	1.85	1.46	1.76
Mettl7b	1.15	1.18	1.34
Mfsd6	0.90	---	1.25
Mgat3	---	---	-1.35
Mgea5	0.69	---	0.85
Mgst1	1.79	1.33	1.62
Mgst2	1.57	1.41	1.33
Mia3	---	---	0.68
Mib2	---	---	0.82
Mical2	-0.99	---	-0.81
Micall2	---	---	-0.85
Mid1ip1	---	---	-0.93
Mipol1	---	---	-0.70
Mkx	---	---	-1.02
Mlkl	0.85	0.80	1.14
Mllt11	1.13	1.31	2.20
Mlycd	---	---	-0.89
Mmachc	-1.16	---	-1.29
Mmp11	0.82	---	---
Mmp13	---	---	1.14
Mms22l	---	---	-0.83
Mndal	---	---	0.88
Mns1	---	---	-0.89
Mocos	2.53	1.75	2.86
Mocs1	1.11	---	1.23
Mogs	---	---	-1.09
Mplkip	---	---	-0.83
Mpp4	1.14	1.06	1.38
Mpzl3	---	---	0.83
Mras	---	---	0.91
Mrc1	-1.77	-1.04	-1.76
Mre11a	---	---	-0.68
Mrpl14	1.03	---	0.88
Mrps6	0.96	---	1.02
Msantd3	1.15	1.05	1.30
Msantd4	0.73	---	---
Msh6	-1.09	---	-1.53
Msmo1	1.54	---	1.51
Msrb3	---	---	-0.76
Mtcl1	-0.81	---	---
mt-Co1	---	---	1.06
Mthfd1	---	---	-0.71
Mthfr	1.19	---	1.31
Mtmr10	-1.72	-0.75	-1.70
Mtmr3	---	---	0.71
Mttp	---	---	0.88
Mturn	1.45	---	1.32
Mvd	0.92	---	---
Mxd1	---	---	0.95
Mxd3	-1.39	---	-1.89
Mxd4	0.73	---	---
Myc	-0.75	---	-0.63
Myo5c	0.75	---	0.72
N4bp3	---	---	-0.84
Naif1	---	---	0.82
Nampt	1.07	---	1.49
Nanos1	-1.19	---	-1.01
Napa	---	---	0.68
Napb	1.10	---	1.16
Napepld	---	---	-1.02
Narf	0.89	---	0.72
Nars	---	---	0.73
Nat6	1.05	---	1.29
Nbeal2	-0.78	---	-1.01
Ncaph	-0.68	---	-0.80
Ncbp2	---	---	-0.77
Ndel1	---	---	0.75
Ndrg1	1.60	0.85	2.41
Neil3	---	---	-0.81
Nek6	-0.84	---	-0.78
Net1	-0.95	---	-0.70
Neurl1b	---	---	-1.01
Neurl3	---	-1.06	---
Nfatc4	1.18	---	---
Nfe2l1	---	---	0.83
Nfkb2	-0.83	---	---
Nfkbia	-1.00	-0.77	---
Nfkbie	---	---	-0.75
Nfkbiz	-0.85	---	-1.05
Ngf	1.47	1.50	2.29
Nid1	0.95	1.26	1.36
Nif3l1	1.06	---	1.41
Noa1	---	---	-1.06
Nolc1	-0.73	---	---
Notch2	---	---	0.77
Npc1	---	---	0.91
Npcd	---	---	-0.99

Nploc4	---	---	0.94
Npnt	-0.93	---	-0.89
Nr1h4	-1.15	---	-1.29
Nr4a1	-1.21	---	---
Nrarp	---	---	-1.35
Nrep	0.98	---	---
Nrg1	-0.90	---	---
Nsdhl	1.29	---	1.28
Nsfl1c	---	---	0.69
Nuak1	---	---	-0.80
Nuak2	---	---	-1.44
Nub1	0.78	---	0.82
Nucks1	---	---	-0.67
Nudt12	0.95	---	---
Nuf2	-0.75	---	-1.03
Numbl	2.19	1.74	2.31
Nup107	---	---	-0.73
Nup210l	---	---	0.69
Nup37	---	---	-0.97
Nup85	---	---	-0.83
Nupl2	---	---	-1.10
Nupr1	1.55	---	2.14
Nusap1	---	---	-0.93
Nxt1	---	---	-0.83
Nyap1	---	---	1.09
Obfc1	-0.66	---	---
Oip5	---	---	-0.76
Olfr56	---	---	-1.19
Onecut1	---	---	-1.64
Osbpl9	---	---	0.69
Oser1	---	---	1.40
Osgin1	2.10	1.87	2.75
Otud4	-0.93	---	-0.79
P2ry1	---	---	-1.01
P4ha1	1.35	0.79	1.66
P4ha2	---	---	0.74
Pacsin2	---	---	0.72
Padi2	-0.81	---	-1.10
Pafah2	0.91	---	0.68
Pag1	-1.20	---	-1.35
Palld	-1.09	---	-0.85
Palmd	-0.96	---	-1.10
Pank1	---	---	-0.83
Papd5	---	---	0.74
Papd7	---	---	-0.66
Papss2	1.73	---	1.98
Parp1	---	---	-0.66
Parp8	-1.00	---	---
Parpbp	-0.79	---	-1.01
Pax3	---	---	0.97
Pbk	---	---	-1.19
Pcdh1	-0.79	---	---
Pcdh7	-1.60	-0.98	-1.41
Pcdh9	---	---	1.55
Pcsk9	1.50	---	1.35
Pcx	1.54	---	1.31
Pcyt2	0.84	---	0.74
Pdcd4	0.80	---	---
Pddc1	---	---	-0.83
Pde4b	---	1.38	1.09
Pdgfb	-1.72	-1.09	-2.37
Pdk4	1.35	---	1.12
Pdlim7	---	---	1.04
Pdss1	-0.77	---	-0.73
Pdxk	-1.02	-1.03	-1.36
Pex13	1.09	---	1.12
Pfas	---	---	-0.87
Pgd	2.41	1.99	2.39
Pgm2l1	0.91	---	0.77
Phf1	0.99	---	1.19
Phf10	---	---	1.04
Phf19	-1.62	-0.90	-2.02
Phlda1	---	0.84	1.67
Pif1	-0.91	---	-1.59
Pik3ap1	0.92	---	0.74
Pilra	-0.73	---	---
Pilrb1	-0.94	---	---
Pim3	---	---	-0.81
Pla2g4a	1.13	0.91	0.86
Plat	---	---	0.71
Plau	-1.47	---	-1.30
Plaur	---	---	0.85
Pld3	---	---	0.73
Plek2	-1.03	---	-0.80
Plekha2	---	---	-0.75
Plekha7	-0.98	---	-1.00
Plekho1	---	---	0.74
Plekho2	-0.73	---	---
Plk1	-0.72	---	-1.08
Plk3	1.50	1.29	3.27
Plk4	---	---	-0.72
Plod1	---	---	0.68
Plod2	1.32	0.82	1.84
Plscr2	---	---	-1.01
Plxnd1	-0.78	---	---
Pmaip1	---	---	0.77
Pmvk	1.37	---	1.17
Pnpla8	---	---	0.71
Pnrc1	1.07	---	1.81
Pold1	---	---	-0.83
Pole2	-1.01	---	-0.98
Polh	-0.81	---	-1.08
Por	---	---	0.74
Pou6f1	1.04	---	1.22
Ppard	1.09	1.02	1.73
Ppat	-0.76	---	-0.94
Ppl	-0.71	---	-0.96
Ppp1r13b	---	---	0.91
Ppp1r13l	---	---	-0.89
Ppp1r15a	1.17	---	2.72
Ppp1r3e	---	---	-0.87
Ppp3ca	---	---	0.89
Pqlc2	1.22	0.82	1.34
Prc1	---	---	-0.85
Prdm2	---	---	0.90
Prdx1	0.93	---	0.92
Prdx6	2.18	1.58	2.28
Prex2	---	---	-0.88
Prim1	---	---	-0.63
Prim2	-0.81	---	---
Prkci	-0.69	---	-0.84
Prob1	1.01	---	0.84
Procr	3.31	2.74	4.38
Prodh	---	---	-0.99
Prorsd1	---	---	-1.00
Proser2	1.75	1.65	2.02
Prox1	---	---	1.03
Prr13	1.16	1.05	1.67
Prss23	-1.24	-0.90	-2.03
Prx	---	---	0.83
Psap	0.84	---	0.79
Psmb3	---	---	1.00
Psmc6	---	---	0.74
Psmd11	0.90	0.78	1.12
Psmd4	---	---	0.79
Psmd5	0.90	0.72	0.84
Psme4	0.74	---	0.83
Psph	1.01	---	1.06
Ptger4	---	---	1.26
Ptgr1	1.42	---	1.11
Ptgs2	2.08	2.10	3.18
Ptprb	-0.90	---	-1.36
Ptrh2	---	---	-0.89
Purb	---	---	-0.71

Pvr	---	---	1.27
Pxmp2	-1.35	---	-1.31
Pxylp1	---	---	-1.24
Pycr1	---	---	0.73
Rab17	---	---	-1.05
Racgap1	---	---	-0.71
Rad18	---	---	-0.73
Rad23b	---	---	0.76
Rad51ap1	-0.73	---	-0.99
Radil	2.05	1.86	2.30
Raf1	---	---	0.76
Ralgps2	-0.84	---	-0.73
Ranbp6	---	---	-0.75
Rap2b	---	---	0.91
Raph1	---	---	1.32
Rasgrf2	-0.92	---	---
Rasgrp3	---	-0.86	-1.53
Rasl12	---	---	-0.84
Rassf6	1.37	1.18	1.50
Rassf8	0.78	---	0.69
Rbbp6	---	---	0.78
Rbm33	---	---	0.76
Rbpms2	---	---	0.80
Rccd1	---	---	-0.80
Rcl1	---	---	-0.66
Rdh10	---	---	-1.16
Recql	---	---	-0.91
Reep6	---	---	1.48
Relb	-1.21	-1.21	-1.04
Rem2	-1.20	---	-1.17
Reps1	---	---	0.90
Rfc3	-0.88	---	-0.71
Rfc5	-0.73	---	-0.92
Rgs17	---	---	0.83
Rgs20	-0.85	---	---
Rhbdd1	---	---	1.06
Rhbdf2	---	---	1.06
Rhob	---	---	0.89
Rhobtb3	---	---	-0.74
Rhpn2	1.10	0.86	1.14
Riok3	0.73	---	0.84
Rit1	1.46	0.90	1.48
Rmi2	-1.11	---	-1.08
Rnd1	-1.25	---	-0.75
Rnd2	1.09	---	1.04
Rnf115	---	---	0.95
Rnf145	-1.50	-0.76	-1.86
Rnf183	3.14	2.69	3.72
Rnf19b	---	---	1.05
Rnf39	-1.08	---	-1.42
Rnf41	---	---	0.68
Rock2	---	---	0.79
Ror1	-1.36	---	-1.39
Rora	1.38	---	2.18
Rorb	---	---	0.93
RP23-145I16.3	0.94	---	0.99
Rragd	1.36	---	1.28
Rrm1	---	---	-0.64
Rrm2	-0.75	---	-0.82
Rrp12	---	---	-0.93
Rrp1b	-1.06	---	-1.09
Rsrp1	---	---	0.75
Rtkn2	---	---	-1.10
Runx2	-1.10	---	-1.19
Rusc2	---	0.77	1.14
Rybp	---	---	0.95
Ryr3	---	---	1.78
S1pr2	-1.07	---	-1.12
Saraf	0.98	---	0.93
Sars	---	---	0.78
Sat1	---	---	1.13
Sbds	---	---	1.17
Sc5d	---	---	0.89
Scamp5	---	---	-1.00
Scarb1	0.85	---	0.89
Scd2	1.36	---	0.68
Schip1	---	---	-1.15
Scpep1	0.77	---	0.85
Sdpr	-0.84	---	-1.41
Sec24d	---	---	1.29
Sel1l3	0.92	---	1.28
Sema6c	1.06	---	---
Sept10	---	---	-0.73
Sepw1	1.19	---	---
Serinc3	---	---	0.86
Serpinb9	1.48	1.16	1.52
Serpinb9b	1.13	1.06	1.33
Serpind1	-1.63	---	-1.39
Serpinh1	---	---	0.74
Sertad2	---	---	0.80
Sertad3	0.91	---	0.97
Sertad4	-1.77	-1.21	-2.08
Sesn2	---	---	1.38
Sesn3	1.30	0.91	1.39
Sf1	---	---	0.71
Sfxn4	---	---	0.78
Sgk1	1.09	1.13	1.10
Sgk3	---	---	0.82
Sgtb	1.15	---	1.70
Sh3bgrl2	---	---	0.86
Sh3bp1	-1.07	---	-0.90
Sh3bp2	2.10	1.54	2.65
Sh3bp5	-0.72	---	-0.95
Sh3tc1	0.92	---	0.77
Shank2	---	---	-0.93
Shcbp1	---	---	-0.80
Shmt1	-0.89	---	-0.94
Siglecg	---	---	-0.98
Sim2	---	---	0.74
Six4	1.40	1.30	1.29
Six5	---	---	-1.03
Ska1	---	---	-0.84
Ska3	---	---	-0.84
Skp2	---	---	-0.83
Slbp	---	---	-0.80
Slc12a2	---	---	-0.78
Slc16a10	---	---	1.58
Slc16a13	1.05	---	0.82
Slc16a6	1.11	---	1.17
Slc19a2	---	---	0.77
Slc1a4	3.01	2.00	3.54
Slc20a1	---	---	1.09
Slc22a23	1.51	1.27	1.74
Slc22a4	1.91	1.51	2.07
Slc25a1	0.77	---	0.96
Slc25a12	---	---	-0.66
Slc25a15	---	---	-0.99
Slc25a27	---	---	1.04
Slc25a33	0.93	---	1.25
Slc25a45	---	---	1.00
Slc25a48	-1.01	---	-1.63
Slc27a6	-1.31	---	-1.13
Slc29a2	-1.45	---	-1.24
Slc2a1	0.97	0.77	1.72
Slc2a2	---	---	-1.47
Slc30a1	---	---	-1.05
Slc35b2	-0.97	---	-1.15
Slc35d1	---	---	0.95
Slc35e2	---	---	0.81
Slc35e4	---	---	0.96
Slc35g1	---	---	-0.71
Slc36a4	---	---	-0.77
Slc38a2	---	---	0.97

Slc38a3	1.20	1.08	1.16
Slc38a7	0.92	---	1.24
Slc39a4	0.83	---	1.11
Slc3a2	1.83	1.22	2.56
Slc40a1	1.81	1.45	1.46
Slc43a2	0.93	---	0.98
Slc48a1	2.55	2.42	3.04
Slc5a3	1.20	---	1.30
Slc5a6	---	---	-0.96
Slc6a8	---	---	0.65
Slc6a9	2.12	1.32	2.83
Slc7a1	---	---	0.97
Slc7a11	5.19	4.54	5.63
Slc7a5	---	---	0.80
Slc8b1	1.28	---	1.02
Slco3a1	---	---	-0.71
Slco4a1	-1.17	-1.06	-0.98
Slfn2	-2.96	-1.76	-3.38
Slfn9	-1.72	---	-1.77
Sltm	---	---	0.95
Slu7	---	---	0.68
Smad5	---	---	-0.64
Smad7	-0.84	---	-0.84
Smcr8	---	---	0.98
Smim14	0.83	---	0.88
Smim3	---	---	0.97
Smox	---	---	0.75
Smpd3	-0.85	---	-0.99
Smtn	-1.01	---	-0.66
Smtnl2	---	---	-0.85
Smyd4	1.18	0.80	0.80
Snai2	-1.35	---	---
Snca	2.05	1.25	2.21
Snx10	1.33	0.93	1.37
Snx30	0.80	---	1.13
Soat2	1.41	---	2.24
Socs5	-0.84	---	-0.93
Sod1	0.97	---	1.11
Sorbs2	---	---	-0.78
Sord	0.91	---	0.74
Sox13	-0.97	---	-1.00
Spata1	---	---	0.98
Spc25	---	---	-1.02
Spcs3	---	---	-0.88
Spns2	-0.99	---	-1.33
Spns3	---	---	-1.17
Spp1	-0.76	---	-0.67
Sppl2b	---	---	-0.79

Sprr1a	-1.57	---	---
Spry1	---	---	-0.78
Spry2	-0.85	---	-0.95
Spry4	---	---	0.95
Spsb4	-1.12	---	-1.82
Sqle	1.63	---	1.61
Sqrdl	2.25	1.72	2.06
Sqstm1	2.77	1.85	3.27
Srd5a1	-0.89	---	-0.99
Srebf2	---	---	0.78
Srf	-1.01	---	-1.17
Srgap3	-1.87	-1.39	-1.77
Srm	-0.86	---	-0.87
Srr	---	---	1.20
Srrm4	---	---	0.86
Srsf10	---	---	-0.73
Srxn1	4.29	3.51	4.90
Ss18l1	---	---	0.83
Ssbp2	-0.92	---	-0.77
St13	---	---	0.89
Stambpl1	-1.09	---	-0.73
Stard13	-0.82	---	-1.20
Stard4	1.19	---	0.91
Stard9	---	---	0.98
Stat1	---	---	-0.94
Stat2	0.86	---	0.79
Stip1	---	---	1.00
Stk10	0.75	---	1.26
Stk40	---	---	0.68
Stx3	---	---	0.78
Stxbp1	---	---	1.04
Stxbp6	---	---	-0.86
Styk1	0.86	---	0.85
Suv39h2	---	---	-0.75
Swap70	---	---	0.67
Swt1	---	---	0.99
Syvn1	---	---	0.73
Tacc2	1.23	0.72	1.39
Tada1	---	---	-0.75
Tada2a	-0.72	---	-0.72
Taf7	1.46	1.23	2.04
Taldo1	0.91	---	0.87
Tapbpl	0.85	---	0.78
Tbc1d1	-0.77	---	---
Tbc1d9	---	---	0.97
Tbce	---	---	0.67
Tbcel	1.05	0.81	1.15
Tbl2	---	---	-1.04

Tcf19	-1.23	---	-1.44
Tcp11l2	1.00	---	1.26
Tdrp	1.14	---	1.06
Tef	0.86	---	---
Tex9	-1.04	---	-0.92
Tfap2a	1.03	---	1.58
Tfe3	---	---	1.21
Tfrc	-1.90	-1.12	-1.62
Tgif2	---	---	-1.17
Tgoln1	---	---	0.69
Thbs1	-2.60	-1.32	-3.45
Them4	---	---	1.04
Thnsl1	---	---	-0.78
Thrb	1.79	1.67	2.08
Tiam2	-0.74	---	-0.69
Ticam1	---	---	1.00
Ticrr	---	---	-0.98
Tigit	-0.90	---	---
Timeless	-0.79	---	-1.03
Tipin	-1.02	---	-1.31
Tk1	-1.21	---	-1.93
Tkt	0.71	---	0.91
Tlk2	---	---	0.76
Tm4sf4	---	---	-1.40
Tmco4	---	---	1.04
Tmem117	2.23	1.53	2.38
Tmem171	-1.60	---	-1.10
Tmem18	---	---	-0.92
Tmem194b	---	---	-1.03
Tmem2	---	---	-0.73
Tmem216	---	---	-0.76
Tmem37	1.19	1.34	1.25
Tmem38a	---	---	0.93
Tmem41b	0.85	---	1.19
Tmem55a	0.87	---	0.91
Tmem57	---	---	0.76
Tmem63b	---	---	0.71
Tmie	1.62	1.23	1.19
Tmpo	---	---	-0.87
Tmppe	0.75	---	0.69
Tnc	-0.99	-0.78	---
Tnfaip2	-0.83	---	---
Tnfaip3	-2.24	-1.44	-2.86
Tnfrsf1a	---	---	0.84
Tnfsf9	---	---	1.15
Tnnc1	1.41	---	1.85
Tns1	---	---	-1.11
Tob1	---	---	1.12

Tob2	0.67	---	0.97
Tollip	---	---	0.85
Tom1	---	---	1.16
Tom1l1	---	---	0.75
Top2a	-0.69	---	-0.99
Tor1aip2	---	---	0.75
Tor4a	---	---	-0.68
Tox	---	---	0.85
Tpx2	---	---	-0.68
Trdmt1	---	---	-0.79
Trib1	-0.86	---	-0.79
Trib3	2.39	---	3.31
Trim16	---	0.88	1.35
Trim17	0.97	---	0.86
Trim36	---	---	1.40
Trim46	---	---	1.12
Trim59	---	---	-0.76
Trim6	0.92	---	1.08
Trio	---	---	0.88
Trip10	---	---	0.92
Trmt1l	---	---	0.85
Trmt2a	---	---	-0.78
Trnt1	---	---	-0.67
Trp53bp2	---	---	0.70
Trp53inp1	1.51	---	2.05
Trp53inp2	---	---	0.91
Tsc22d1	---	---	-0.78
Tsc22d2	---	---	0.94
Tsc22d3	0.97	---	1.16
Tsfm	---	---	-0.91
Tshz1	1.12	1.12	1.48
Tsku	1.61	1.83	1.60
Tspan8	---	---	-1.01
Tspyl2	0.99	---	1.38
Ttc26	---	---	-0.79
Ttc30b	---	---	-0.79
Ttc7	-0.82	---	-0.74
Ttk	---	---	-0.71
Tuba1a	---	---	1.22
Tuba4a	0.81	0.92	1.19
Tubb2a	1.64	1.09	2.01
Tubb2b	---	---	0.78
Tubb6	-0.87	---	-0.78
Txnrd1	1.90	1.71	2.00
Ubap1	0.87	---	1.36
Ubash3b	-1.14	---	-1.02
Ubb	1.21	1.10	2.20
Ubc	1.72	1.34	3.52

Ube2h	---	---	0.75
Ube2j1	---	---	0.69
Ube2o	1.02	---	1.22
Ube4b	---	---	0.79
Ubl3	0.80	0.78	0.80
Ubqln1	---	---	0.81
Ubr4	---	---	0.87
Ubr7	---	---	-1.13
Ubtd1	---	---	0.96
Ubxn4	1.17	0.95	1.39
Ubxn8	---	---	0.65
Ugdh	1.48	1.17	1.52
Ugt1a1	1.16	0.87	0.94
Ugt1a10	1.10	0.88	0.97
Ugt1a2	1.16	0.87	0.94
Ugt1a5	1.16	0.87	0.95
Ugt1a6a	1.10	0.85	0.93
Ugt1a6b	1.09	0.87	0.96
Ugt1a7c	1.10	0.88	0.97
Ugt1a8	1.10	0.88	0.97
Ugt1a9	1.10	0.88	0.97
Ugt2b34	4.29	3.39	4.22
Uhrf1	-1.04	---	-1.17
Ulk1	0.73	---	0.95
Ung	-3.05	-0.90	-3.56
Usp1	---	---	-0.82
Usp14	---	---	0.67
Usp20	0.91	---	---
Usp22	---	---	0.96
Usp35	1.27	---	1.24
Usp43	-1.03	---	-0.89
Uspl1	---	---	0.69
Uts2b	---	---	-1.56
Vamp1	1.04	---	1.04
Vash2	---	---	0.88
Vasn	1.03	0.77	1.36
Vcam1	-1.86	-1.42	-1.96
Vegfa	2.39	1.74	3.57
Vegfc	-0.99	-0.96	-0.82
Vgll3	-0.96	---	-1.14
Vil1	-1.09	---	-1.31
Vipas39	---	---	0.78
Vldlr	1.07	---	1.16
Vnn1	1.03	---	---
Vps18	1.08	---	1.08
Vps37b	0.85	---	1.63
Vstm5	-1.17	---	-0.92
Wbp2	---	---	0.70

Wbscr27	1.40	---	0.96
Wdhd1	-0.84	---	-1.13
Wdr35	---	---	-0.78
Wdr5b	---	---	-1.27
Wdr6	-0.77	---	-1.50
Wdr76	-0.80	---	-1.14
Wdr77	---	---	-0.70
Wdr81	1.15	---	0.99
Wee1	---	---	-0.92
Whamm	0.97	---	1.12
Wipi2	---	---	0.66
Wnt10a	-0.95	---	-1.22
Wnt4	1.50	1.15	1.33
Wnt7b	-1.42	-0.75	-1.41
Wrb	---	---	-0.99
Xkr9	2.05	1.30	2.05
Xpo1	---	---	0.72
Xpot	---	---	0.65
Xrcc2	---	---	-1.06
Xrcc6	---	---	-0.69
Xrcc6bp1	---	---	-0.92
Xxylt1	---	---	-0.86
Ypel2	---	---	1.10
Ypel5	2.39	1.44	2.61
Ywhag	0.94	---	1.27
Zadh2	0.82	0.69	0.70
Zbtb10	---	---	1.14
Zbtb12	---	---	-0.96
Zbtb2	---	---	1.09
Zbtb21	---	---	1.01
Zbtb37	---	---	-0.94
Zbtb45	---	---	-0.73
Zbtb7b	---	---	0.90
Zc2hc1c	1.16	---	0.92
Zdhhc18	1.52	1.28	1.65
Zeb2	---	---	0.98
Zfand2a	1.90	1.22	3.27
Zfand5	1.43	0.89	1.68
Zfp142	---	---	1.21
Zfp185	---	---	1.14
Zfp324	---	---	-1.46
Zfp36	---	---	1.91
Zfp365	1.19	---	1.23
Zfp367	-0.88	---	-1.06
Zfp385a	---	---	0.74
Zfp39	---	---	-1.02
Zfp395	---	---	-0.86
Zfp41	---	---	-0.82

Zfp418	---	---	0.99
Zfp516	---	---	0.91
Zfp617	---	---	0.72
Zfp651	---	---	-0.89
Zfp703	---	---	0.79
Zfp867	---	---	-0.93
Zfp874a	1.00	---	0.83
Zfp874b	1.04	---	1.36
Zfp945	---	---	0.96
Zfp958	---	---	-0.88
Zfp961	---	---	-0.76
Zfpm1	---	---	1.12
Zfpm2	-1.20	---	---
Zfyve1	0.84	---	1.06
Zgrf1	---	---	-1.07
Zhx3	-0.93	---	-1.09
Zik1	---	---	-1.24
Zmynd19	---	---	-0.74
Zrsr1	2.11	1.61	2.54
Zswim4	---	---	1.01
Zswim6	---	---	1.12
Zwint	0.94	0.82	1.15
Zyx	-1.14	---	---

Supplemental Table 2. Gene expression of AML12 hepatocytes treated with truncated OxPAPC, full-length OxPAPC, and OxPAPC. Gene expression represented as $\log_2$ of the fold change compared to vehicle. Genes regulated single treatment are highlighted in orange (truncated OxPAPC), blue (full-length OxPAPC), and purple (OxPAPC).

LPPTigr Nomenclature (previously known species)	Parent Lipid	*m/z*	Formula	LPPTigr Predicted Structure(s)
1. PAPC	---	782	$C_{44}H_{80}NO_8P$	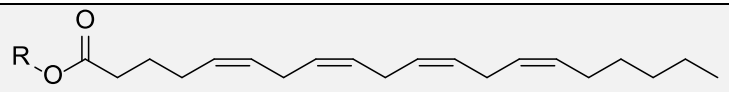
2. PLPC	---	758	$C_{42}H_{80}NO_8P$	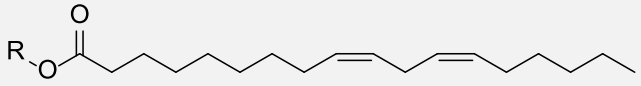
3. 16:0 LysoPC	---	496	$C_{24}H_{50}NO_7P$	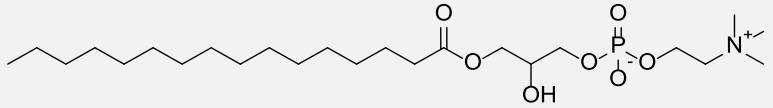
4. 18:0 LysoPC	---	524	$C_{26}H_{54}NO_7P$	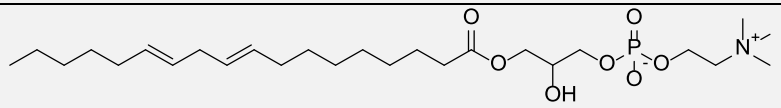
5. 18:1 LysoPC	---	522	$C_{26}H_{52}NO_7P$	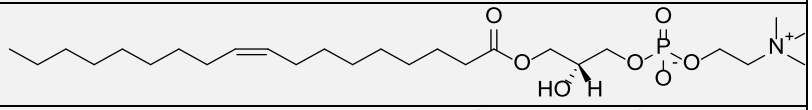
6. 18:2 LysoPC	---	520	$C_{26}H_{54}NO_7P$	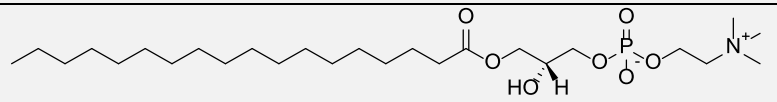
7. C37H66NO11P	PAPC	732	$C_{37}H_{66}NO_{11}P$	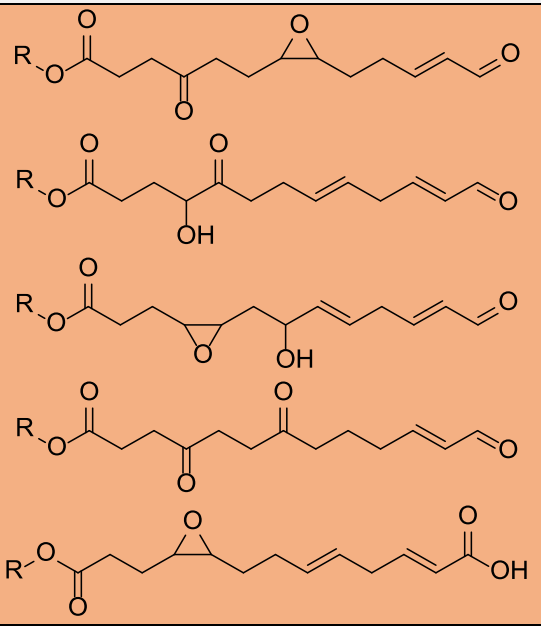

				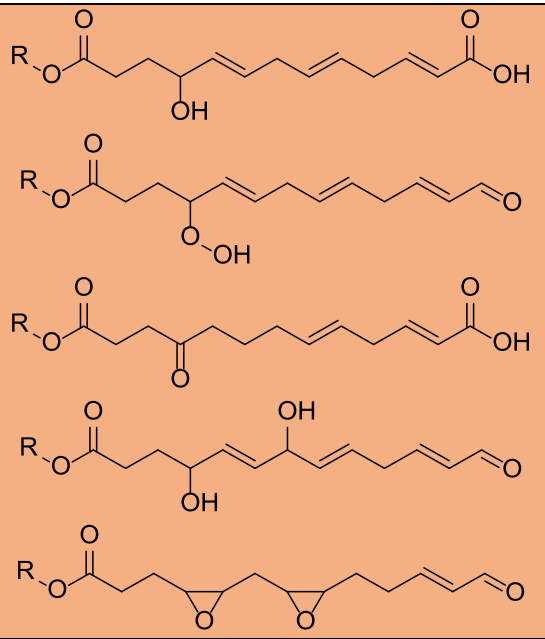
8. 16:0/7:0[1xOH,CHO]	PAPC	638	$C_{31}H_{60}NO_{10}P$	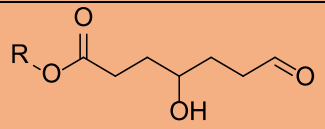
9. PONPC	PLPC	650	$C_{33}H_{64}NO_9P$	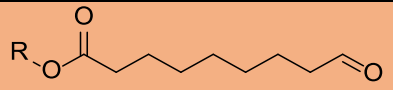
10. 16:0/12:1[CHO]	PLPC	690	$C_{36}H_{68}NO_9P$	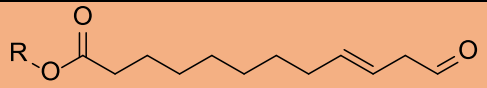
11. C34H62NO11P	PAPC	692	$C_{34}H_{62}NO_{11}P$	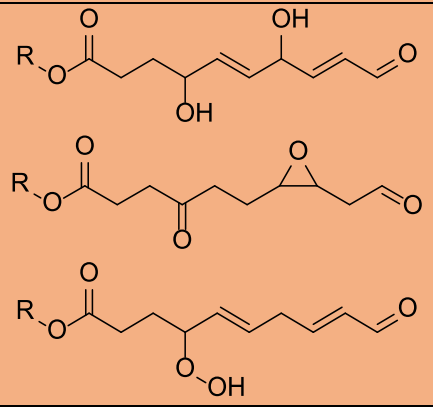

				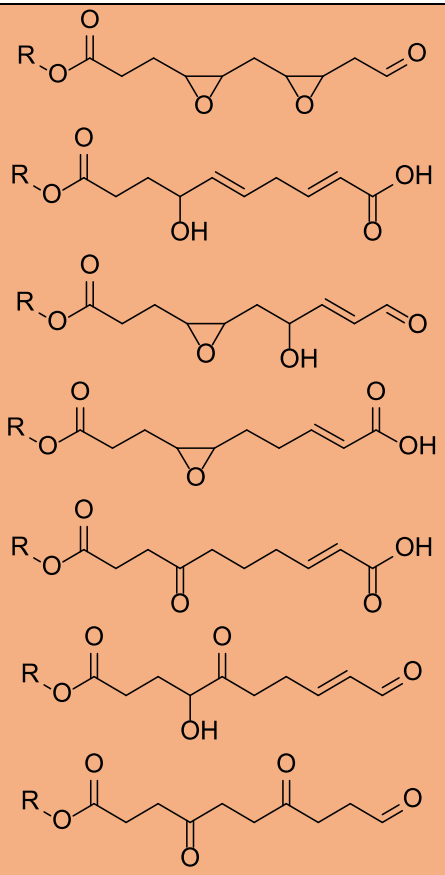
12. 16:0/11:1[CHO]	PLPC	676	$C_{35}H_{66}NO_9P$	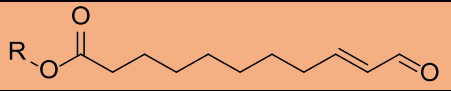
13. POBPC	PAPC	580	$C_{28}H_{54}NO_9P$	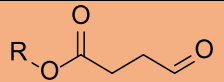
14. 16:0/8:0[CHO] (POOPC)	PLPC	636	$C_{32}H_{62}NO_9P$	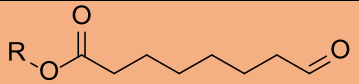
15. C35H64NO12P	PAPC	722	$C_{35}H_{64}NO_{12}P$	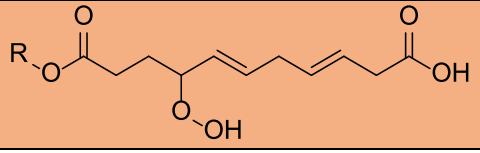

				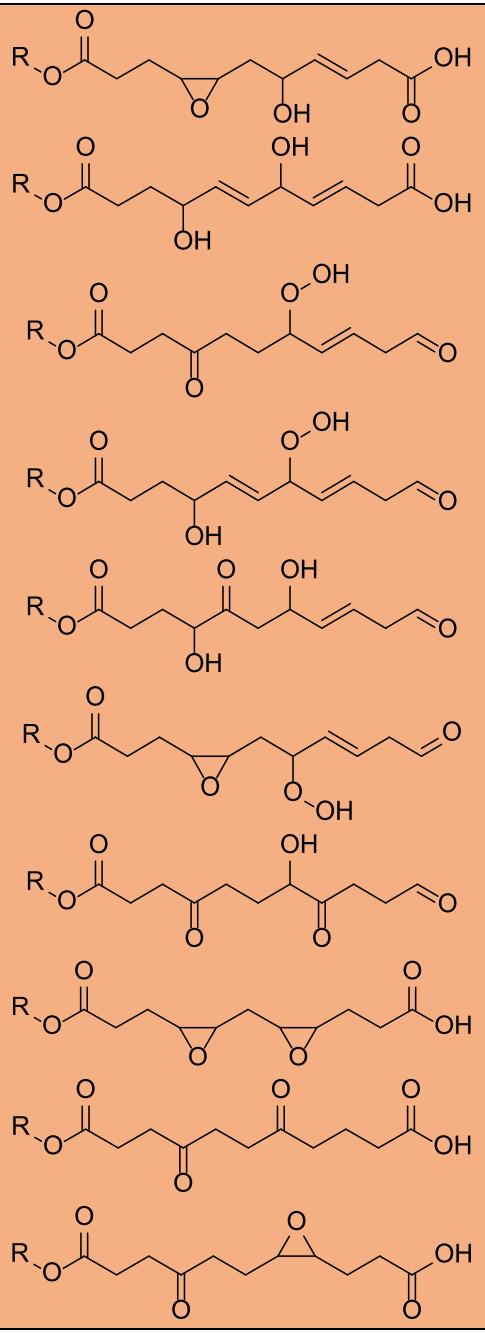

				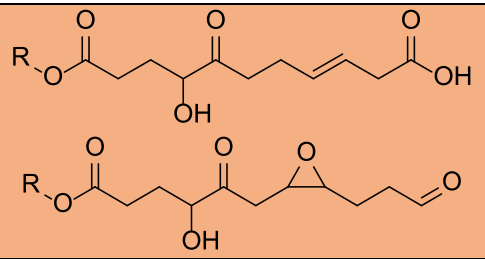
16. C35H64NO10P	PAPC	690	$C_{35}H_{64}NO_{10}P$	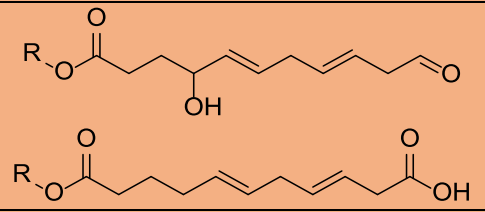
17. C35H62NO11P	PAPC	704	$C_{35}H_{62}NO_{11}P$	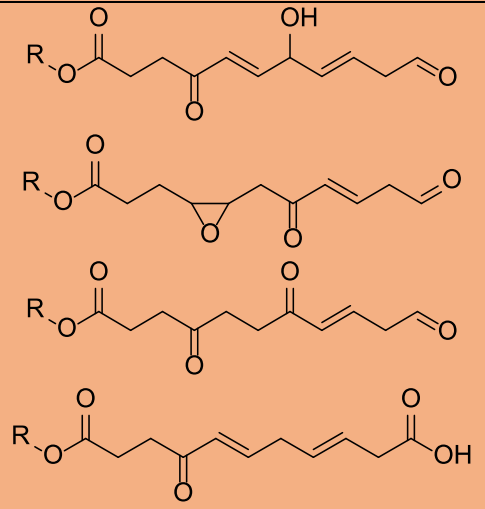
18. POVPC	PAPC	594	$C_{29}H_{56}NO_{9}P$	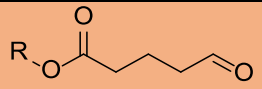
19. 16:0/10:2[CHO]	PAPC	660	$C_{34}H_{62}NO_{9}P$	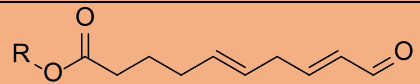
20. C36H68NO10P (HODA-PC)	PLPC	706	$C_{36}H_{68}NO_{10}P$	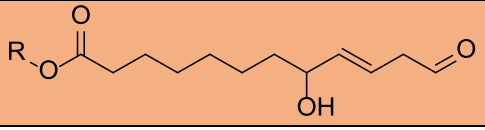

				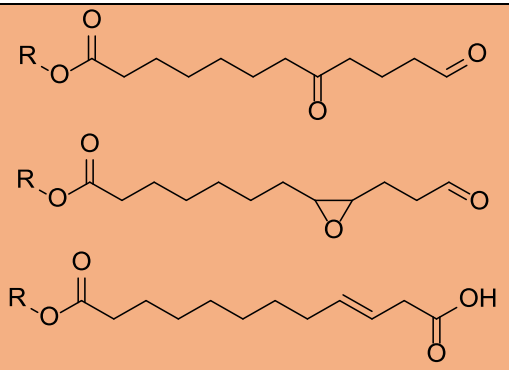
21. 16:0/7:1[CHO]	PAPC	620	$C_{31}H_{58}NO_9P$	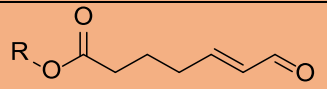
22. KOOA-PC	PAPC	648	$C_{32}H_{58}NO_{10}P$	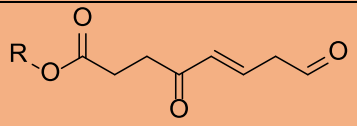
23. C32H60NO11P (HOdiA-PC)	PAPC	666	$C_{32}H_{60}NO_{11}P$	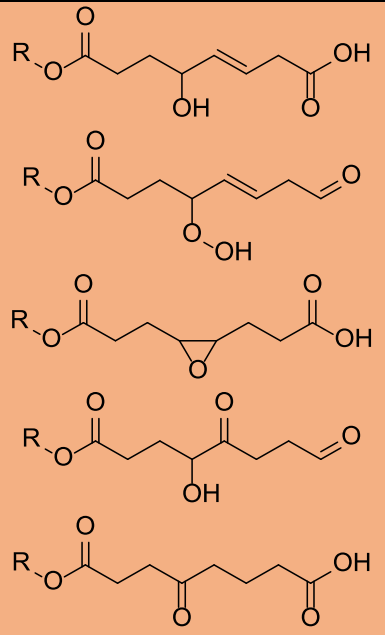
24. 16:0/10:2[1xKETO,CHO]	PAPC	674	$C_{34}H_{60}NO_{10}P$	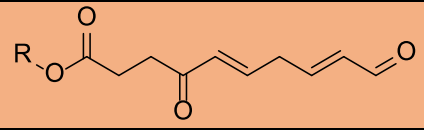

25. PazPC	PLPC	666	$C_{33}H_{64}NO_{10}P$	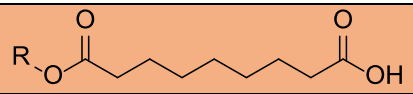
26. C32H60NO10P (HOOA-PC)	PAPC	650	$C_{32}H_{60}NO_{10}P$	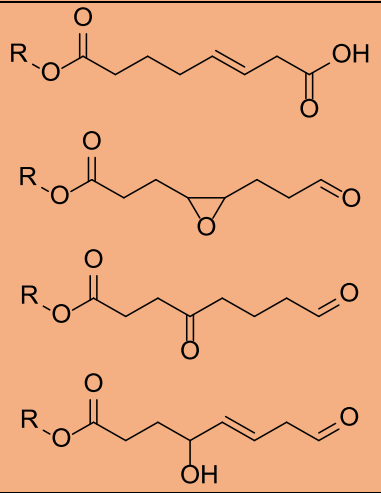
27. PGPC	PAPC	610	$C_{29}H_{56}NO_{10}P$	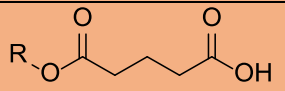
28. C42H78NO10P	PLPC	788	$C_{42}H_{78}NO_{10}P$	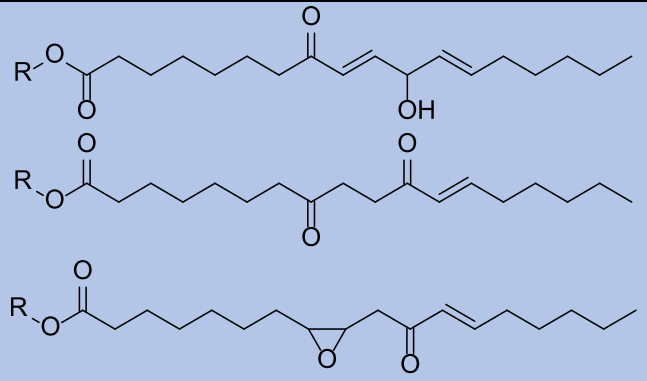
29. C42H80NO9P (HODE-PC)	PLPC	774	$C_{42}H_{80}NO_9P$	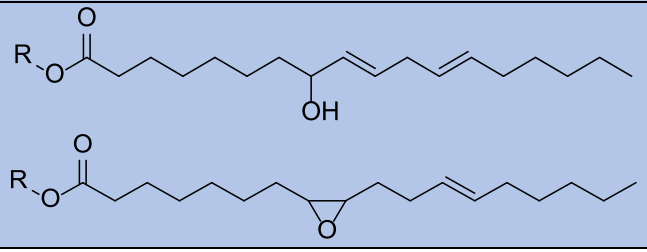

				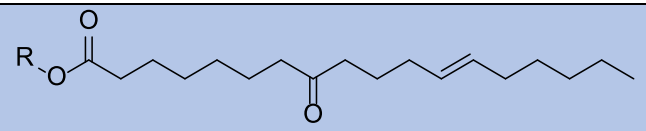
30. 16:0/20:4[2xKETO]	PAPC	810	$C_{44}H_{76}NO_{10}P$	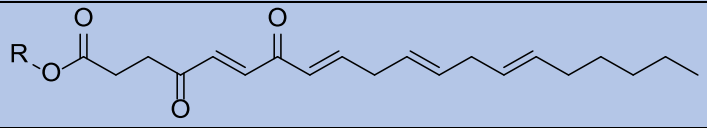
31. C44H80NO11P	PAPC	830	$C_{44}H_{80}NO_{11}P$	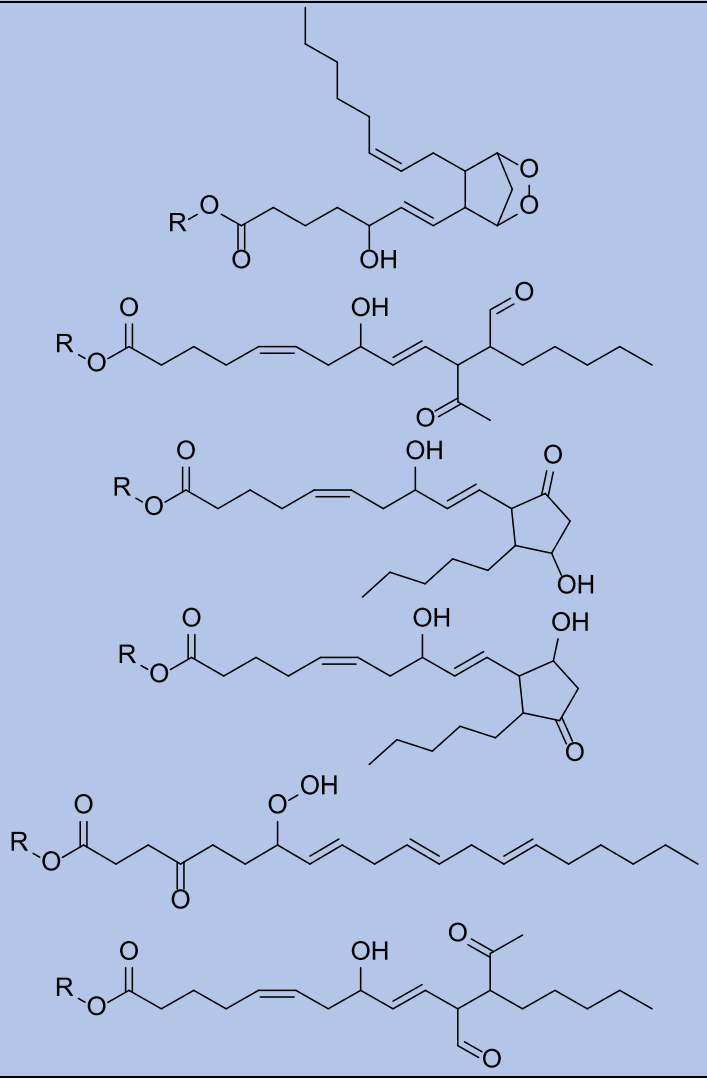

				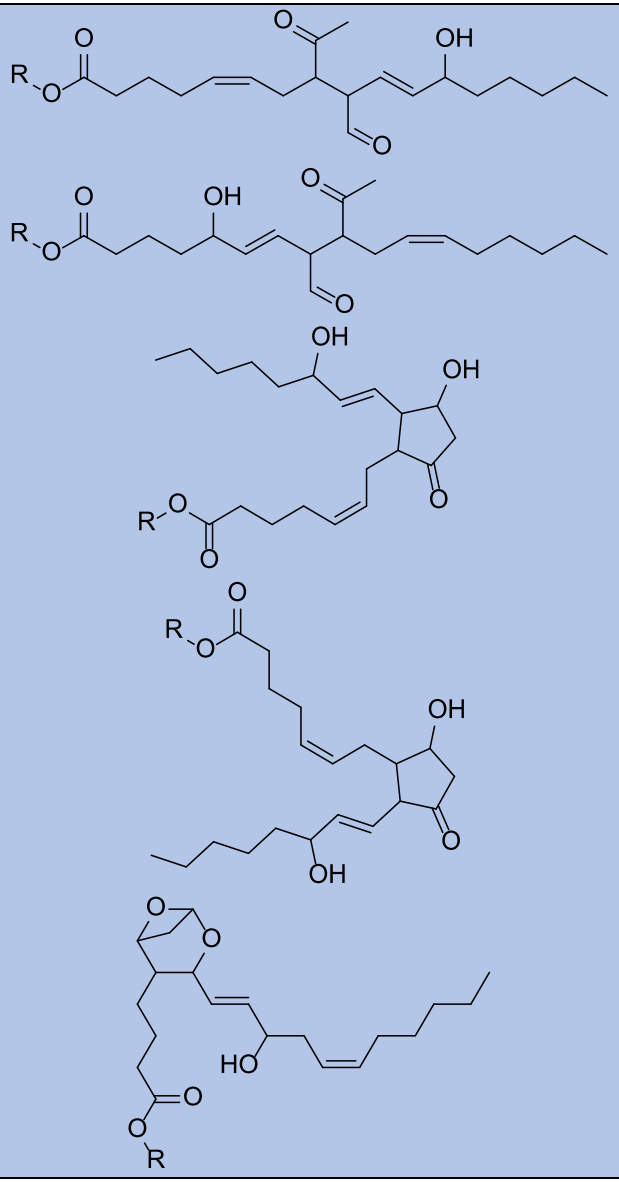

				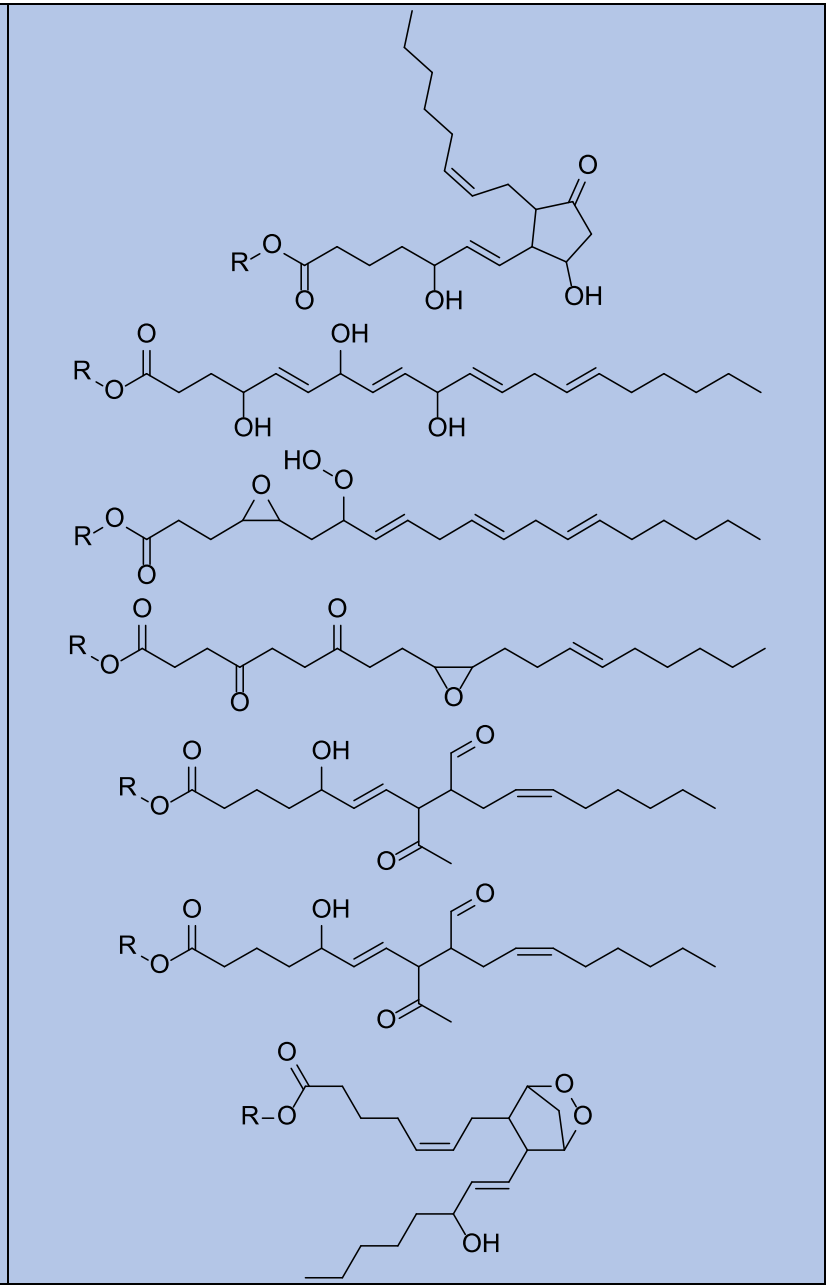

				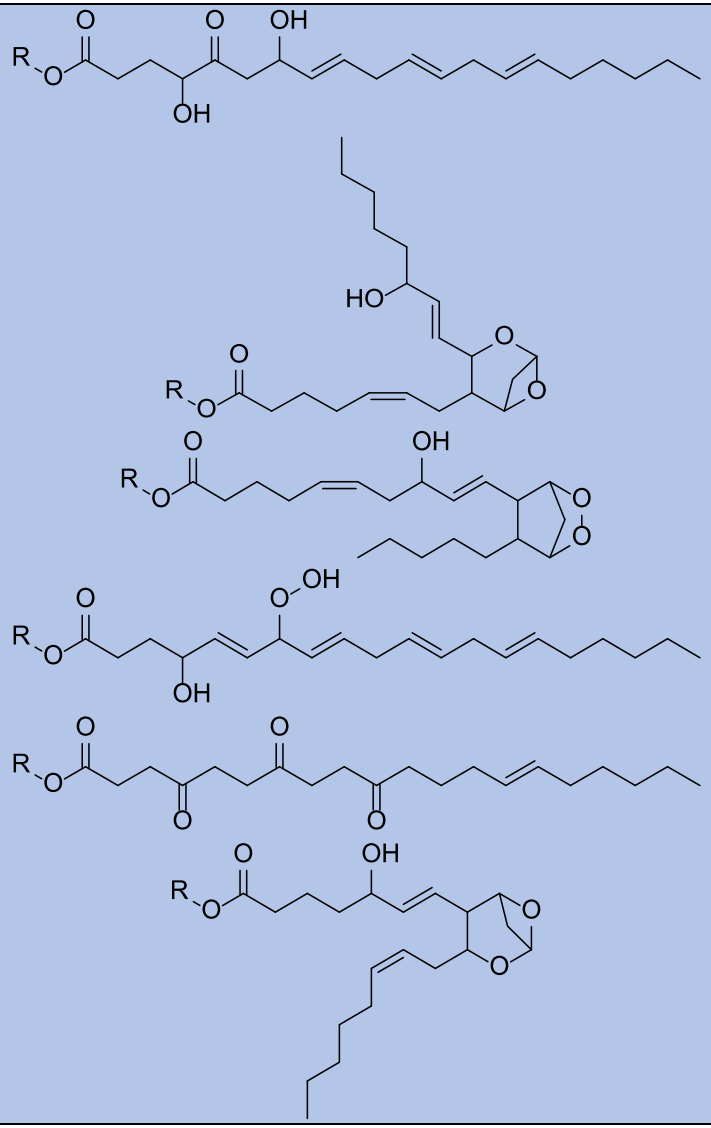

				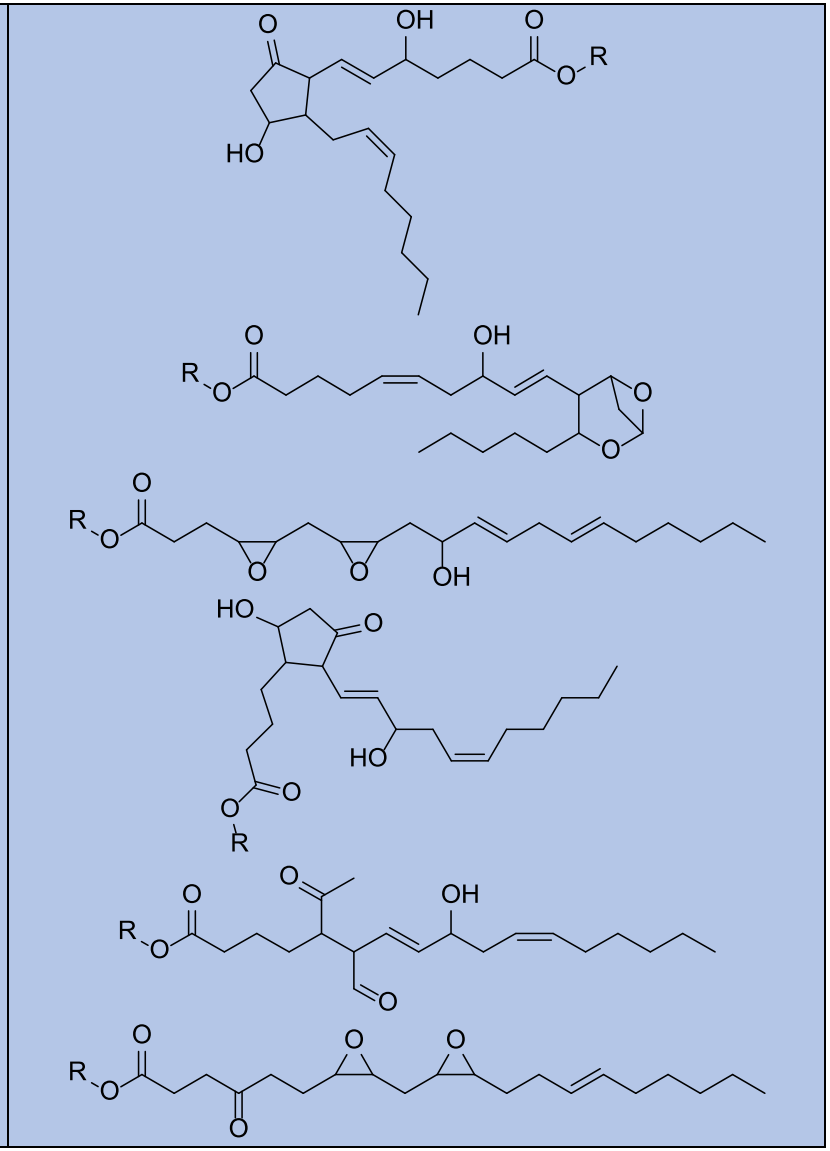

				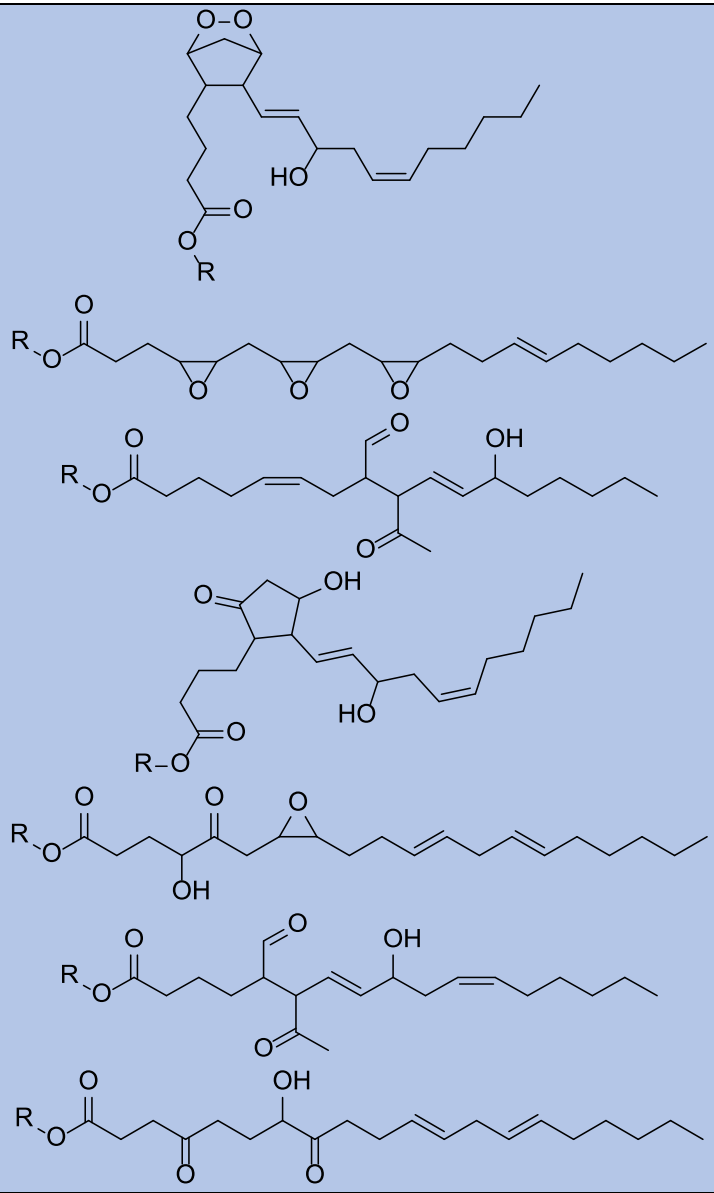
32. C44H80NO9P (HETE-PC)	PAPC	798	$C_{44}H_{80}NO_9P$	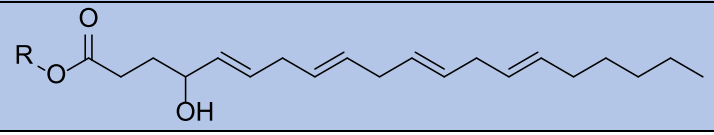

				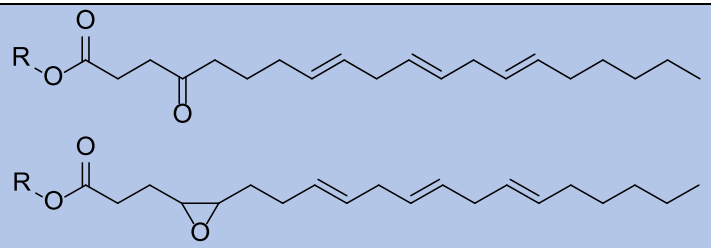
33. C42H80NO11P	PLPC	806	$C_{42}H_{80}NO_{11}P$	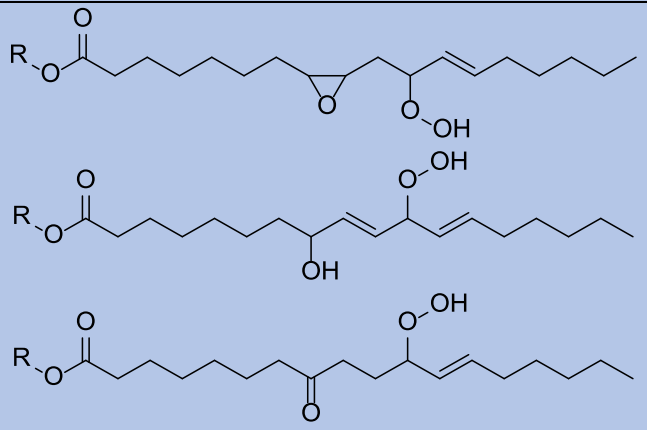
34. 16:0/18:2[1xKETO] (KODE-PC)	PLPC	772	$C_{42}H_{78}NO_9P$	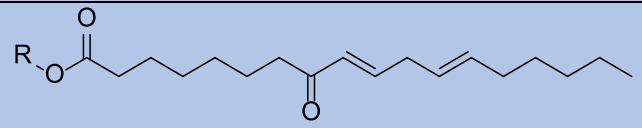
35. 16:0/18:1[1xOH] (HOME-PC)	PLPC	776	$C_{42}H_{82}NO_9P$	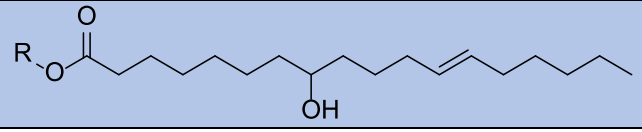

Supplemental Table 3. Oxidized phospholipids detected after development of hepatic fibrosis. *In silico* predicted structures of oxidized phospholipids derived from PAPC or PLPC detected in mouse plasma after twenty weeks on FPC diet. CHO – aldehyde, COOH – carboxylic acid, OH – hydroxy, OOH – hydroperoxy, KETO – ketone, EPOXY – epoxide.

Gene	Species	Primer orientation	Sequence
Hmox1	*Mus musculus*	Forward	ACAGCCCCACCAAGTTCAAA
		Reserve	TCTGCAGGGGCAGTATCTTG
Gclm	*Mus musculus*	Forward	TGGAGCAGCTGTATCAGTGG
		Reserve	AGAGCAGTTCTTTCGGGTCA
Pgd	*Mus musculus*	Forward	CTCCTCGACTCTGCTTCGTC
		Reserve	CGGCATCTTCTTGTCGTGTC
Acly	*Mus musculus*	Forward	TGATGGGAGAAGTTGGGAAG
		Reserve	ATCAGCTCGGGACTCAGAAA
Hmgcoas	*Mus musculus*	Forward	ACAAGCCTGACATGCTCTCC
		Reserve	TTCAGGAACATCCGAGCTAGA
Hmgcoar	*Mus musculus*	Forward	TCTTGTGGAATGCTCTGTGA
		Reserve	AAGCTCTAGGACCAGCGACA
Adamtsl2	*Mus musculus*	Forward	ATGTGAGCCCATTGGCTGTG
		Reserve	TCGGTACTTGACCACTGTGC
Timp2	*Mus musculus*	Forward	ATGGCAACCCCATCAAGAGG
		Reserve	TGGGACAGCGAGTGATCTTG
Timp1	*Mus musculus*	Forward	TCGGACCTGGTCATAAGGC
		Reserve	GTACGCCAGGGAACCAAGAA
Mmp2	*Mus musculus*	Forward	GTGTTCTTCGCAGGGAATGAG
		Reserve	GATGCTTCCAAACTTCACGCT
Itga8	*Mus musculus*	Forward	ACACGTTCCTCAAGAGAAAGAA
		Reserve	GGAGTGGCCCAAATAACCGA
Col15a1	*Mus musculus*	Forward	CTGTCCACTTTCCGAGCCTTT
		Reserve	AAAGCACTTGGCCCTTGAGA

Col8a1	*Mus musculus*	Forward	GGCAAAGAGTACCCACACCTACC
		Reserve	GACCTTGTTCTCCGCGCAAACTG
Col4a2	*Mus musculus*	Forward	TCGTTCAGCCAGGTTGCATT
		Reserve	AAAGCCCTTGAGCCCTTGTT
Col5a2	*Mus musculus*	Forward	TGGGGACTGATGGTACACCT
		Reserve	GGATCACCCGATTGTCCTCG
Adam8	*Mus musculus*	Forward	TGAACAAGCAGCGTCTACGA
		Reserve	CTGGGAGTGGTGAACTGGAC
Fgfr1	*Mus musculus*	Forward	TCCCTGTGGAAGTGGAGTCT
		Reserve	GCTACAGGCCTACGGTTTGG
Tgfbr1	*Mus musculus*	Forward	GGCGAAGGCATTACAGTGTT
		Reserve	TGGTGAATGACAGTGCGGTT
Itga9	*Mus musculus*	Forward	GCTCTCGCTGTAGCCCATC
		Reserve	ACCCACGAGGACCCAGC
Col6a1	*Mus musculus*	Forward	AGGGCTACAAGGAACCATGC
		Reserve	TTTCCTCGCTCCCCCTCATA
Tgfbr2	*Mus musculus*	Forward	CCAAGTCGGATGTGGAAATGG
		Reserve	TGTCGCAAGTGGACAGTCTC
Col14a1	*Mus musculus*	Forward	TGAAGCACCCACAGCCATAG
		Reserve	TCCAGGCACCATAACCACTTC
Itga1	*Mus musculus*	Forward	TCAGTGGAGAGCAGATCGGA
		Reserve	CCCACAGGGCTCATTCTTGT
Adam9	*Mus musculus*	Forward	GGGCCGACGTATAATGCAAAG
		Reserve	CAGGTGGCGGTCTGGAG
CypA	*Mus musculus*	Forward	CGATGACGAGCCCTTGG

		Reserve	TCTGCTGTCTTTGGAACTTTGTC
B2m	*Mus musculus*	Forward	ATTCACCCCCACTGAGACTG
		Reserve	TGCTATTTCTTTCTGCGTGC
Hmox1	*Homo sapiens*	Forward	AAGACTGCGTTCCTGCTCAAC
		Reserve	AAAGCCCTACAGCAACTGTCG
Gclm	*Homo sapiens*	Forward	GCGAGGAGCTTCATGATTGT
		Reserve	TGTGCAACTCCAAGGACTGA
Hprt	*Homo sapiens*	Forward	AGGCGAACCTCTCGGCTTTC
		Reserve	CAAGACGTTCAGTCCTGTCCATA
scFv-E06	*N/A*	Forward	GTACTGCTGCTCTGGGTTCC
		Reserve	CACTGGCCGTGCAACTAATG

Supplemental Table 4. Forward and reserve primer sequences for cDNA and genomic DNA amplification.

Data File S1. Source data.

antioxidants

Article

Selenoprotein T Protects Endothelial Cells against Lipopolysaccharide-Induced Activation and Apoptosis

Dennis Merk [1,†], Johannes Ptok [2,†], Philipp Jakobs [1,†], Florian von Ameln [3], Jan Greulich [3], Pia Kluge [1], Kathrin Semperowitsch [1], Olaf Eckermann [1,3], Heiner Schaal [2], Niloofar Ale-Agha [1,*], Joachim Altschmied [1,3,*] and Judith Haendeler [1,*]

1 Environmentally-Induced Cardiovascular Degeneration, Clinical Chemistry and Laboratory Diagnostics, Medical Faculty, University Hospital and Heinrich-Heine University Düsseldorf, 40225 Düsseldorf, Germany; dennis.merk@hhu.de (D.M.); philipp.jakobs@hhu.de (P.J.); pia.kluge@uni-potsdam.de (P.K.); semperina@gmail.com (K.S.); olaf.eckermann@hhu.de (O.E.)
2 Institute for Virology, Medical Faculty, University Hospital and Heinrich-Heine University Düsseldorf, 40225 Düsseldorf, Germany; Johannes.ptok@hhu.de (J.P.); schaal@uni-duesseldorf.de (H.S.)
3 Environmentally-Induced Cardiovascular Degeneration, Clinical Chemistry and Laboratory Diagnostics, Medical Faculty, University Hospital and Heinrich-Heine University Düsseldorf, Germany and IUF-Leibniz Research Institute for Environmental Medicine, 40225 Düsseldorf, Germany; florian.ameln@hhu.de (F.v.A.); jan.greulich@hhu.de (J.G.)
* Correspondence: aleagha@hhu.de (N.A.-A.); joalt001@hhu.de (J.A.); juhae001@hhu.de (J.H.); Tel.: +49-211-3389-291 (N.A.-A. & J.A. & J.H.); Fax: +49-211-3389-331 (N.A.-A. & J.A. & J.H.)
† D.M., J.P. and P.J. contributed equally to the work.

Abstract: Sepsis is an exaggerated immune response upon infection with lipopolysaccharide (LPS) as the main causative agent. LPS-induced activation and apoptosis of endothelial cells (EC) can lead to organ dysfunction and finally organ failure. We previously demonstrated that the first twenty amino acids of the Apurinic/Apyrimidinic Endodeoxyribonuclease 1 (APEX1) are sufficient to inhibit EC apoptosis. To identify genes whose regulation by LPS is affected by this N-terminal APEX1 peptide, EC were transduced with an expression vector for the APEX1 peptide or an empty control vector and treated with LPS. Following RNA deep sequencing, genes upregulated in LPS-treated EC expressing the APEX1 peptide were identified bioinformatically. Selected candidates were validated by semi-quantitative real time PCR, a promising one was Selenoprotein T (SELENOT). For functional analyses, an expression vector for SELENOT was generated. To study the effect of SELENOT expression on LPS-induced EC activation and apoptosis, the SELENOT vector was transfected in EC. Immunostaining showed that SELENOT was expressed and localized in the ER. EC transfected with the SELENOT plasmid showed no activation and reduced apoptosis induced by LPS. SELENOT as well as APEX1(1-20) can protect EC against activation and apoptosis and could provide new therapeutic approaches in the treatment of sepsis.

Keywords: APEX1(1-20); Selenoprotein T; lipopolysaccharide; endothelial cell activation; apoptosis

Citation: Merk, D.; Ptok, J.; Jakobs, P.; von Ameln, F.; Greulich, J.; Kluge, P.; Semperowitsch, K.; Eckermann, O.; Schaal, H.; Ale-Agha, N.; et al. Selenoprotein T Protects Endothelial Cells against Lipopolysaccharide-Induced Activation and Apoptosis. *Antioxidants* **2021**, *10*, 1427. https://doi.org/10.3390/antiox10091427

Academic Editor: Stanley Omaye

Received: 17 August 2021
Accepted: 3 September 2021
Published: 7 September 2021

1. Introduction

Sepsis can best be described as an overwhelming inflammatory condition, in which the body responds to an infection in a hyperactive, dysregulated way, which in turn results in life-threatening organ dysfunction and eventually septic shock. According to an estimate of the World Health Organization (WHO), sepsis affects more than 48 million people every year, potentially leading to 11 million deaths [1]. The basis for the pathophysiological responses in the context of sepsis is multifactorial. Therefore, except for the introduction of vasopressor agents 40 years ago, no new therapeutic principle for the treatment of sepsis has been developed until today.

Lipopolysaccharide (LPS) is an outer membrane component of Gram-negative bacteria. Most bacterial LPS molecules are thermostable and generate a pro-inflammatory stimulus

for the immune system in humans. LPS is a serologically reactive bacterial toxin, and 1 to 2 mg in the bloodstream can be lethal. LPS can enter the bloodstream through intestinal absorption of the LPS produced by gut bacteria. Moreover, gut lesions and diet rich in lipids boost the transport across membranes into the systemic circulation [2]. Therefore, at the cellular level, endothelial cells (EC) are directly affected by LPS, which triggers their activation and ultimately apoptosis, leading to vascular leakage. Thus, it is undisputable that the loss of endothelial cell integrity is a mainstay of septic shock [3]. Hence, therapies that could prevent endothelial cell leakage or even restore endothelial cell integrity would be of tremendous value for patients and would address medical needs. EC with LPS affect the endothelial transcriptome by regulating the levels of numerous transcripts, not only of protein coding RNAs, but also of non-coding RNAs such as microRNAs and long non-coding RNAs [4,5]. Having pointed this out, it is a mystery to us that we failed to find any RNA deep sequencing data on LPS-induced transcriptome changes in the endothelium in the established databases such as the Gene expression omnibus (GEO), the European nucleotide archive (ENA), Short Sequence Archive (SRA) or ArrayExpress. However, such an in-depth transcriptome profiling combined with pathway analyses could provide novel targets for the development of new therapeutic principles for the treatment of sepsis, especially for protecting the endothelium. Therefore, one aim of this study was to perform a deep sequencing analysis in LPS-treated primary EC.

Moreover, we have recently shown that the first 20 amino acids of the Apurinic/Apyrimidinic Endodeoxyribonuclease 1 (APEX1) are sufficient to inhibit H_2O_2-induced apoptosis [6]. As the underlying molecular mechanisms initiating apoptosis are independent of the trigger, we hypothesized that this N-terminal APEX1 peptide, APEX1(1-20), could also interfere with LPS-induced apoptosis. Therefore, we included cells expressing the APEX1(1-20) in our deep sequencing analysis to find potential therapeutic targets for sepsis, possibly regulated by this peptide.

2. Materials and Methods

2.1. Cultivation of Primary Human Endothelial Cells and HEK293

Primary human endothelial cells (EC) were obtained from LONZA (Cologne, Germany) and cultured as previously described [7]. In detail, EC were cultured in endothelial basal medium supplemented with 1 µg/mL hydrocortisone, 12 µg/mL bovine brain extract, 50 µg/mL gentamicin, 50 ng/mL amphotericin B, 10 ng/mL epidermal growth factor (LONZA, Cologne, Germany) and 10% fetal bovine serum until the third passage. After detachment with trypsin, cells were grown for at least 20 h. All experiments were performed with EC in passage 3. HEK293 were cultured in DMEM GlutaMAX™ supplemented with 10% heat-inactivated fetal bovine serum and 1% penicillin/streptomycin and then used for the production of lentiviruses.

2.2. Lentiviral Production and Transduction of EC

Generation of VSV-G pseudotyped lentiviral particles and transduction of EC were performed as previously described [8]. Lentiviral titers were determined with the QuickTiter™ Lentivirus Titer kit (Lentivirus-Associated HIV p24) (Biocat, Heidelberg, Germany). EC were transduced with a multiplicity of infection of approximately 20. The day after transduction the cells were washed three times, the medium replaced, and cells cultivated for another day before they were treated with 150 ng/mL LPS for 18 h.

2.3. Isolation of Total Cellular RNA

Cells were lysed using TRIzol® (Thermo Fisher Scientific, Dreieich, Germany) and RNA was isolated according to the manufacturer's instructions. RNAs were subjected to a second purification step using the RNeasy® Mini kit (Qiagen, Hilden, Germany). RNA concentrations were measured using a NanoDrop™ 2000c (Thermo Fisher Scientific, Dreieich, Germany), and RNA integrity and purity were determined by agarose gel electrophoresis.

2.4. RNA Sequencing and Bioinformatic Analysis

RNA sequencing data were obtained from quadruplicate total RNA samples. Total RNAs used for transcriptome analyses were quantified using the Qubit™ RNA HS Assay kit (Thermo Fisher Scientific, Dreieich, Germany) and quality was determined by capillary electrophoresis using the FragmentAnalyzer and the Total RNA Standard Sensitivity Assay (Agilent Technologies, Santa Clara, CA, USA). All samples in this study showed highest RNA Quality Numbers (RQN 10.0). Library construction and sequencing were performed at the Genomics and Transcriptomics Laboratory at the Biological Medical Research Centre (BMFZ) of the Heinrich-Heine University Düsseldorf. Library preparation was performed according to the manufacturer's protocol using the TruSeq Stranded mRNA Assay kit (Illumina, San Diego, CA, USA). Briefly, 500 ng total RNA was used for mRNA capturing, fragmentation, synthesis of cDNA, adapter ligation and library amplification. Bead purified libraries were normalized and finally sequenced on the HiSeq 3000 system (Illumina San Diego, CA, USA) with a read setup of 1 × 150 bp. The bcl2fastq2 (version 2.17.1.4) tool was used to convert the bcl files to fastq files as well for adapter trimming and demultiplexing. GC-content, base-calling quality, adapter content and read length were measured using the tool FASTQC by Andrews (http://www.bioinformatics.babraham.ac.uk/projects/fastqc/ accessed on 17 August 2021) and MultiQC [9]. Reads were then trimmed or discarded based on their base calling quality and adapter content with Trimmomatic version 0.36 [10]. Subsequently, with the help of the SortMeRNA algorithm version 2.1b [11], the extent of rRNA depletion was measured by mapping the reads to rRNA databases. For alignment and the following analyses, the human genomic reference sequence (GRCh38) and annotation data (release 101) were downloaded from Ensembl [12] and BioMart [13]. For splice site usage analysis, the reads were then aligned to the human reference genome using the two-pass mapping protocol of the STAR aligner (2.5.4b) [14]. With help of the SAMtools software package [15], uniquely mapped reads were selected for creation of a gap table, listing the coordinates of every gap found in the alignment of the reads and the number of overlapping reads. For DGE analysis with the R package DESeq2 version 1.18.1 [16], count matrices were generated using the software salmon version 0.9.1 [17]. Significantly enriched gene sets were calculated, using the R package GOseq [18]. Scripts used for this work are publicly available at https://github.com/caggtaagtat/SELENOT (accessed on 17 August 2021). FASTQ file preparation and alignment were accomplished using custom BASH shell scripts in the environment of the High Performing Cluster of the Heinrich-Heine University Düsseldorf.

2.5. cDNA Synthesis

Total cellular RNA was reverse transcribed using the QuantiTect Reverse Transcription kit (Qiagen, Hilden Germany) according to the manufacturer's instructions.

2.6. Polymerase Chain Reaction (PCR)

Endpoint PCRs were performed with MyTaq™ HS DNA Polymerase (Biocat, Heidelberg, Germany) according to manufacturer's recommendations in a Bio-Rad T100 Thermal Cycler (Bio-Rad, Feldkirchen Germany). Reaction products were resolved on standard agarose gels.

Relative transcript levels were determined by semi-quantitative real-time PCR using cDNA as a template and the primaQUANT 2x qPCR-SYBR-Green-MasterMix (Steinbrenner, Wiesenbach, Germany), the transcript for the ribosomal protein L32 (RPL32), served as a reference. The PCR reactions were performed in a Rotor-Gene Q instrument (Qiagen, Hilden, Germany). Relative expression was calculated by the ΔC_t method [19].

The sequences of all primer used for PCR are listed in Supplementary Table S1.

2.7. Plasmids

A lentiviral expression vector for the first twenty amino acids of APEX1 was constructed by transferring the coding sequence for APEX1(1-20) with a C-terminal myc-tag

from the previously published expression vector [6] into a lentiviral transfer vector, in which the transgene is expressed under the transcriptional control of the cytomegalovirus immediate early promoter/enhancer [8]. To generate an expression vector for human SELENOT with an N-terminal FLAG-tag, the SELENOT coding sequence together with the first 179 bp of the 3′-untranslated region of the human SELENOT gene containing the selenocysteine insertion sequence were amplified from a human EC cDNA using Q5® High-Fidelity DNA Polymerase (New England Biolabs, Frankfurt, Germany). This fragment was inserted into pFLAG-CMV-2 (Sigma-Aldrich, Deisenhofen, Germany) opened with Not I and Xba I using the Gibson Assembly® Cloning kit (New England Biolabs, Frankfurt, Germany) according to the manufacturer's protocol. The construct was verified by DNA sequencing. Cloning details and the complete plasmid sequence are available upon request.

2.8. Transient Transfection of EC

Transient transfections of EC with plasmid DNA were performed using Superfect (Qiagen, Hilden, Germany) as previously described [20,21]. In detail, EC were transfected on 6 cm culture dishes with 3 µg plasmid DNA and 22.5 µL Superfect, or in 6-well plates with 1.2 µg plasmid DNA and 12 µL Superfect per well.

2.9. Immunostaining of EC

EC were fixed and permeabilized as described previously [7]. Afterwards, cells were incubated with an anti-FLAG-tag antibody (1:100, DYKDDDDK Tag Antibody (clone 8H8L17), Abfinity™, Cat. No. 701629, Invitrogen, Darmstadt, Germany). As secondary antibody, a goat anti-rabbit highly cross-adsorbed antibody coupled to Alexa Fluor 594 (1:500, Cat. No. A-11012, Invitrogen, Darmstadt, Germany) was used. For ICAM1 staining, an Alexa Fluor 488-coupled primary antibody (1:50, ICAM1/CD54 (15.2), Cat. No. SC-107 AF488, Santa Cruz Biotechnology, Heidelberg, Germany) was used. The endoplasmic reticulum (ER) was stained with an anti-Calnexin (clone C5C9) Alexa Fluor 488-conjugate (1:25, Cat. No. 38552, Cell Signaling, Technology, Frankfurt, Germany). Nuclei were counterstained with 4′,6-diamidino-2-phenylindole (DAPI) (100 ng/mL, Sigma-Aldrich, Deisenhofen, Germany). Images were taken using Zeiss microscopes (Axio Observer D1 or Axio Imager M2, magnification 400-fold, oil).

2.10. Immunoblotting

Cells were detached from the culture surface with a rubber policeman, centrifuged at 800× *g*, resuspended in radioimmunoprecipitation assay (RIPA) buffer (50 mM Tris-HCl pH 8.0, 150 mM NaCl, 1% (*v*/*v*) IGEPAL®-CA630, 0.1% (*w*/*v*) SDS and 0.5% (*w*/*v*) Na-Deoxycholate) supplemented with 1/100 volume of a protease inhibitor cocktail (Bimake, Munich, Germany) and lysed for 30 min on ice. The lysates were centrifuged at 18,000× *g* and 4 °C for 15 min and the supernatant was transferred to a fresh tube. Lysate proteins were separated by sodium-dodecyl-sulfate polyacrylamide gel electrophoresis according to standard procedures and transferred onto polyvinylidene difluoride membranes. After blocking with 5% milk powder in TBS (200 mM Tris-HCl pH 8.0, 300 mM NaCl, 100 mM KCl) with 0.1% (*v*/*v*) Tween-20 for 1 h at room temperature, membranes were incubated with an antibody directed against Caspase 3 (1:300 for detection of cleaved Caspase 3, 1:500 for uncleaved Caspase 3, Cat. No. 9662, Cell Signaling Technology, Frankfurt, Germany) and an anti α-Tubulin antibody (clone (DM1A), 1:50,000, Cat. No. T9026, Sigma-Aldrich, Deisenhofen, Germany). Antibodies were incubated overnight at 4 °C. The following day, membranes were incubated with secondary antibodies coupled to horseradish peroxidase (ECL™ Anti-Rabbit or Anti-Mouse IgG, Horseradish Peroxidase linked whole antibody (from sheep), 1:5000; Cat. Nos. NA934V and NA931V, GE healthcare, Solingen, Germany). Detection was performed using ECL substrate (GE healthcare, Solingen, Germany) and X-ray films. Semi-quantitative analyses were performed on scanned X-ray films using Fiji [22].

2.11. Statistics

The number of experiments (n) given in the figure legends represents independent biological replicates, the data shown are mean ± SEM. Normal distribution for all data sets was confirmed by a Shapiro–Wilk test; homogeneity of variances (from means) between groups was verified by Levene's test. Multiple comparisons were performed using one-way ANOVA with post-hoc Tukey LSD test.

3. Results

3.1. APEX1(1-20) Induces Specific Transcriptome Changes in EC in Response to LPS

To identify APEX1(1-20)-mediated transcriptome differences in the response of EC to LPS we performed RNA deep sequencing. For this purpose, primary human EC were transduced with either a lentiviral vector leading to moderate expression of APEX1(1-20) or an empty vector, respectively. Cells were then treated with 150 ng/mL active LPS or detoxified LPS as control. RNA from these cells was used for RNA deep sequencing and analyzed for differential gene expression (DGE). To identify APEX1(1-20)-specific transcriptome changes in response to LPS, we analyzed which genes were specifically regulated by LPS in the APEX1(1-20) expressing cells, but not in the cells transduced with the empty vector.

PCA analysis revealed that all samples from the cells treated with detoxified LPS cluster together, no matter whether the cells expressed APEX1(1-20) or not. The same held true for the LPS-treated cells (Supplementary Figure S1), showing a clear effect of LPS on the cellular transcriptome.

DGE analysis revealed that the APEX1(1-20) transcript derived from the expression vector was only detectable in the cells transduced with this vector, but not in the cells transduced with the empty vector. More importantly, expression of APEX1(1-20) alone did not appear to affect the overall transcriptome as changes in the expression of only a very small number of genes were observed (Supplementary Table S2).

In addition to the DGE analysis, we performed a gene set enrichment analysis (GSEA) focusing on genes that were significantly regulated by LPS exclusively in either the cells transduced with the empty vector or the cells expressing APEX1(1-20). As expected, cells transduced with the empty vector showed a significant enrichment of upregulated genes belonging to gene ontology (GO) terms related to immune responses including the response to bacteria and tumor necrosis factor signaling (Supplementary Table S3). Interestingly, we did not observe these changes in the presence of APEX1(1-20), and, moreover, genes belonging to the GO term cellular response to tumor necrosis factor were significantly downregulated in LPS-treated cells expressing the APEX1 peptide (Supplementary Table S4). These data support the assumption that APEX1(1-20) might provide protection against endothelial cell activation and apoptosis via alteration of the transcriptional responses to LPS treatment.

In the DGE analysis, we found that after LPS treatment, 323 genes were significantly upregulated in cells transduced with the empty vector and 280 were downregulated. In contrast, in the cells expressing APEX1(1-20), only 177 genes were upregulated by LPS and 139 genes were downregulated (Figure 1A,B and Supplementary Tables S5 and S6). Thus, the expression of only roughly half as many genes appeared to be affected by the presence of APEX1(1-20).

Notably, we observed clearly different LPS responses in cells expressing APEX1(1-20) when compared to cells transduced with the empty vector (Figure 1C–F and Supplementary Tables S7–S10).

For functional studies, we focused on genes whose expression is upregulated by LPS only in cells expressing the small APEX1 peptide as the corresponding proteins might evoke APEX1(1-20)-dependent protective effects in EC, which could be of interest in a therapeutic setting.

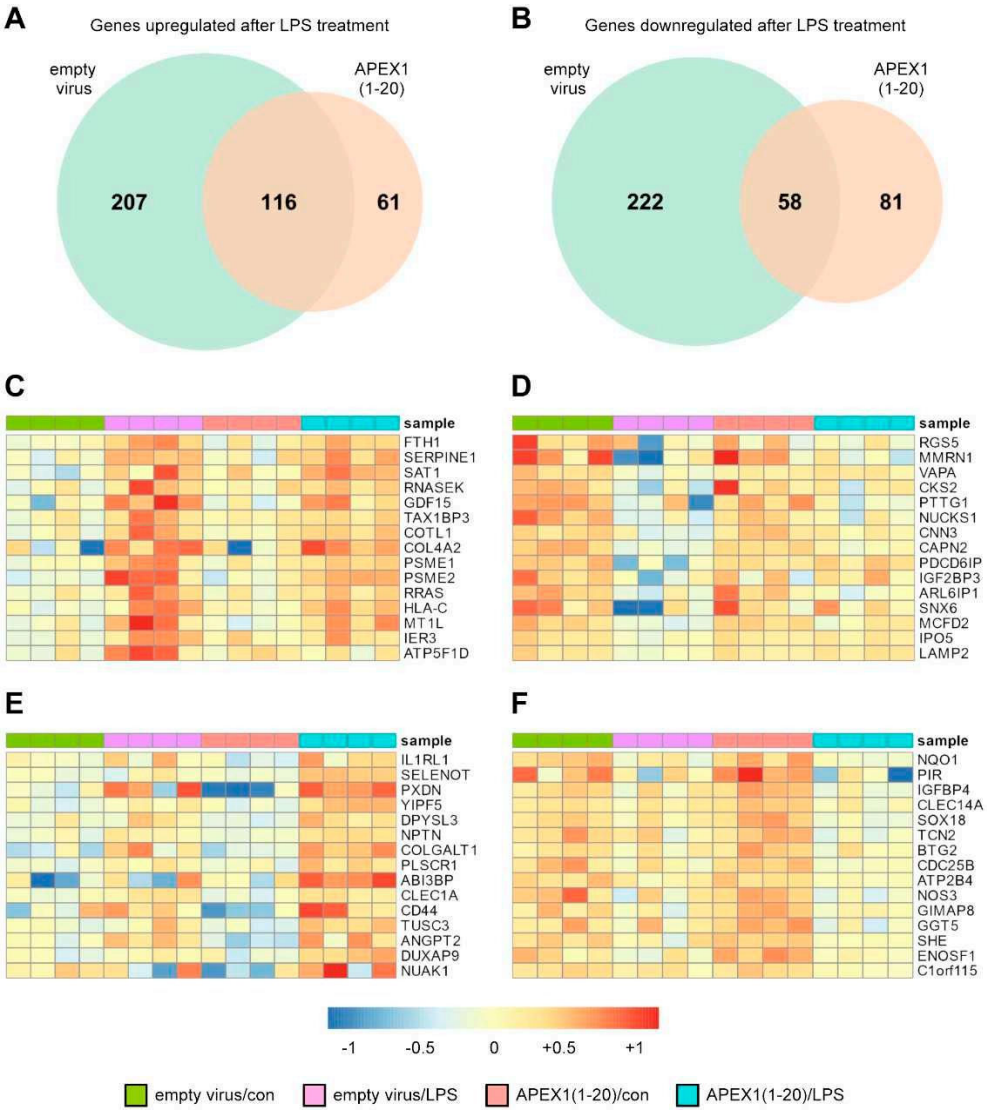

Figure 1. APEX1(1-20) induces specific transcriptome changes in EC in response to LPS. (**A**–**F**) EC were transduced with a lentiviral expression vector for APEX1(1-20) or an empty virus and treated with 150 ng/mL detoxified (con) or active LPS (LPS) for 18 h. RNAs from the transduced cells were subjected to RNA deep sequencing. Differential gene expression was calculated using the R package DESeq2. Wald test from DESeq2 was used to calculate the significance of the change in the expression. (**A**,**B**) Venn-diagrams for genes upregulated (**A**) or downregulated (**B**) after LPS treatment of empty virus transduced cells and cells expressing APEX1(1-20). (**C**–**F**) Heatmaps of genes significantly differentially expressed upon LPS treatment of cells transduced with the empty virus or cells expressing APEX1(1-20). Shown are the 15 top ranked genes from Supplementary Tables S7–S10. The color depicts the normalized expression relative to the respective mean in all samples. (**C**) Genes uniquely upregulated after LPS treatment of empty virus transduced cells. (**D**) Genes uniquely downregulated after LPS treatment of empty virus transduced cells. (**E**) Genes uniquely upregulated after LPS treatment of APEX1(1-20) expressing cells. (**F**) Genes uniquely downregulated after LPS treatment of APEX1(1-20) expressing cells.

3.2. Expression of PXDN and SELENOT Is Specifically Upregulated after LPS Treatment of EC Expressing APEX1(1-20)

As a prerequisite for functional studies, we first validated the regulation of the top-ranked candidates, which, according to the RNA sequencing data, should be expressed to levels allowing reliable detection and quantification.

IL1RL encodes an Interleukin 1 Receptor-like protein, which belongs to a family of ten distinct but structurally related receptors. These proteins serve either as ligand binding or accessory chains and some act as signaling inhibitors. Moreover, two members of this family are orphan receptors [23]. Therefore, IL1RL1 is part of a complex signaling network and one could easily envision that—due to this redundancy—interference with this network might be compensated or evoke unwanted side effects.

Peroxidasin (PXDN), originally described as Vascular Peroxidase 1, is a heme-containing peroxidase, which shows highest expression in the heart and the vascular wall [24]. The protein is rapidly secreted [25] and required for formation of the vascular basement membrane by reinforcing fibrillar network assembly in the extracellular matrix through formation of sulfilimine bonds [26]. It has recently been shown that PXDN promotes angiogenesis [27] and, furthermore, is essential for endothelial cell survival [28].

Selenoprotein T (SELENOT) is a member of the selenoprotein family, whose members are characterized by containing one or more selenocysteine residues, frequently in enzymatically active sites [29]. SELENOT is the most highly conserved selenoprotein throughout evolution [30], suggestive of an essential function, which is underscored by the early embryonic lethality of mice in which the *selenot* gene is constitutively disrupted [31]. SELENOT is one of 7 out of 25 human selenoproteins localized to the ER [32]. The expression of SELENOT, like all other selenoproteins, depends on dietary selenium as shown by a reduced expression in chicken stomach after 55 days on a selenium-deficient diet. Moreover, this regimen resulted in stress injuries [33]. In addition, SELENOT protects kidney cells against cisplatin-induced apoptosis [34]. These observations go along with the notion that ER-resident selenoproteins are critical in cellular stress responses [35].

For the reasons explained above, we did not follow up on IL1RL, but validated the regulation of PXDN and SELENOT by semi-quantitative real-time PCR (Figure 2).

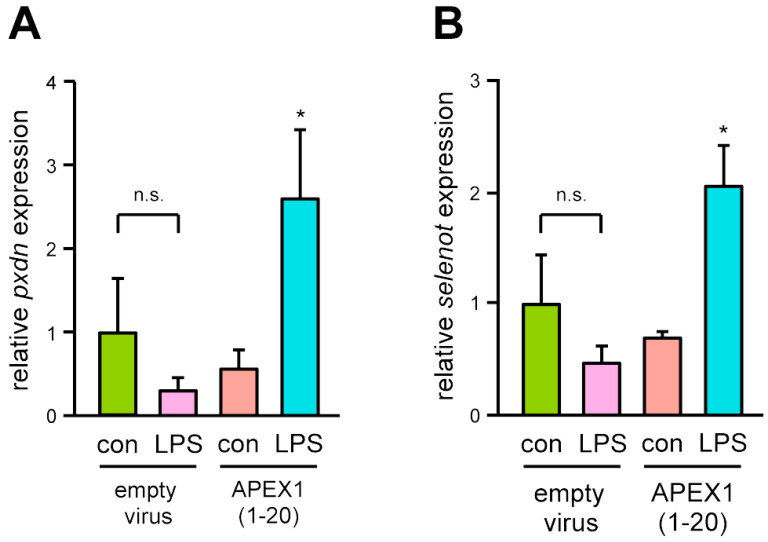

Figure 2. LPS induces upregulation of PXDN and SELENOT expression specifically in EC expressing APEX1(1-20). Transcript levels of PXDN (**A**) and SELENOT (**B**) in EC transduced with an empty virus or the expression vector for APEX1(1-20) and treated with 150 ng/mL detoxified (con) or active LPS (LPS) for 18 h were analyzed by semi-quantitative real-time PCR; RPL32 served as reference (data are mean ± SEM, $n = 4$, * $p < 0.05$ vs. APEX1(1-20)/con, n.s. = not significant, one-way ANOVA with post-hoc Tukey LSD test).

The real-time PCR analysis corroborated the deep sequencing data as for both genes, an upregulation of the transcript level by LPS was only observed in the cells expressing APEX1(1-20). Although PXDN has already been characterized with respect to protective functions in EC [28], these data provide independent proof for the validity of the experi-

mental approach. The second protein, SELENOT, for which no functions in endothelial activation and apoptosis have been described so far, was chosen for functional analyses.

3.3. Generation of a SELENOT Expression Vector and Intracellular Localization of the Overexpressed Protein

To study the impact of SELENOT on endothelial cell functions affected by LPS, we generated an expression vector, which contained a FLAG-epitope tag allowing the identification of the overexpressed protein. For the generation of this expression vector, an aspect unique to selenoproteins had to be taken into account. Selenocysteine (Sec) residues in selenoproteins are not the product of a post-translational modification, but are rather incorporated already during translation by using one of the translation termination codons, namely UGA, for binding of the selenocysteine tRNA ($tRNA^{Sec}$) to the mRNA. This translational recoding of the UGA codon involves a so-called selenocysteine insertion sequence (SECIS) in the 3′-untranslated region (UTR) of the transcript. The SECIS, which is not highly conserved on the sequence level, forms a stem-loop structure that is required for recruitment of the $tRNA^{Sec}$ to the UGA codon [36]. Consequently, the lack of a SECIS leads to premature translation termination, when the ribosome encounters the first UGA within the open reading frame. Therefore, we included—besides the SELENOT open reading frame—a portion of the SELENOT 3′-UTR including the SECIS in the expression vector.

We first analyzed the expression of FLAG-SELENOT after transient transfection of EC on the RNA level by reverse transcriptase PCR (Figure 3A). We then determined the intracellular localization of the overexpressed FLAG-SELENOT protein by immunofluorescence. As demonstrated by colocalization with the ER-resident protein Calnexin (Figure 3B), FLAG-SELENOT was localized in the ER.

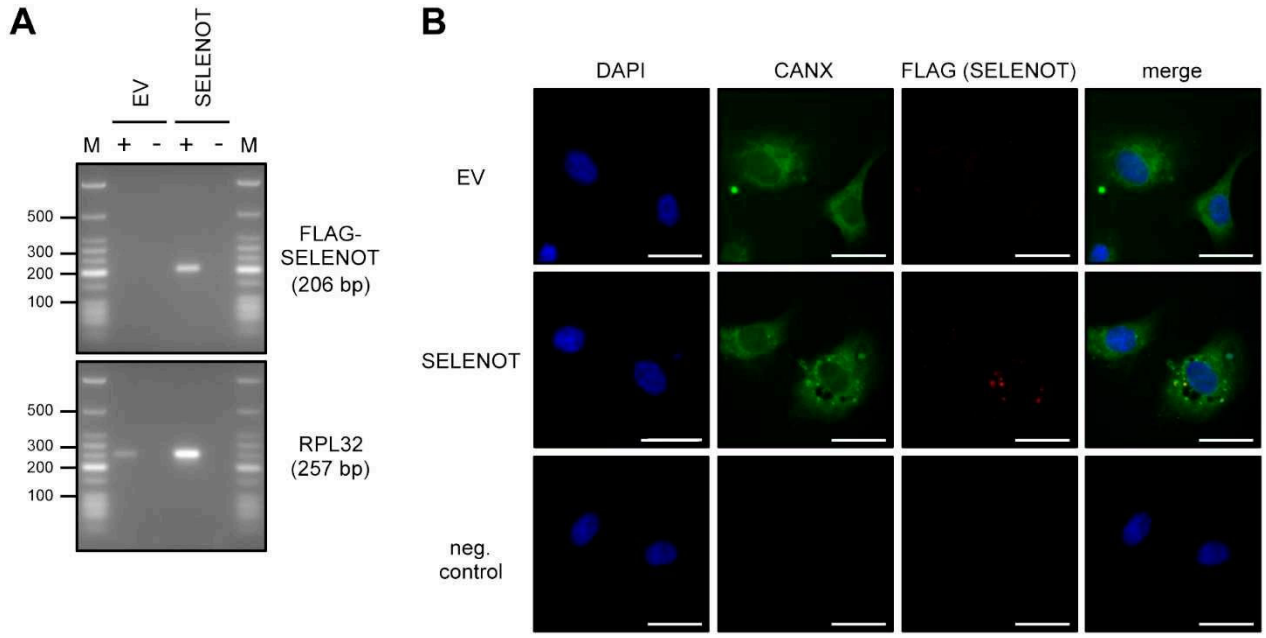

Figure 3. Overexpressed SELENOT is localized in the ER. (**A**,**B**) EC were transfected with the FLAG-SELENOT expression vector (SELENOT) or an empty vector (EV). Expression and localization of exogenously expressed SELENOT was verified on the RNA (**A**) and protein (**B**) level. (**A**) Expression of SELENOT was analyzed by reverse transcription polymerase chain reaction (RT-PCR). Therefore, RNA was isolated from the transfected cells and cDNA was synthesized in the presence (+) or absence (−) of reverse transcriptase. Amplification was performed with primers specifically detecting the FLAG-SELENOT fusion transcript, the housekeeping gene RPL32 served as control. Amplification products were resolved by agarose gel electrophoresis, the expected fragment sizes are specified, numbers on the left indicate selected DNA size markers (M). (**B**) Localization of FLAG-SELENOT was examined by immunostaining and fluorescence microscopy. Cells were stained with an antibody directed against Calnexin (CANX), a marker for the ER (green) and an anti-FLAG antibody (red). Nuclei were counterstained with DAPI (blue); merge is the overlay of all channels (scale bar = 30 µm).

3.4. SELENOT Overexpression Inhibits LPS-Induced Endothelial Cell Activation

Having demonstrated that FLAG-SELENOT is localized in the ER, we next investigated the effect of SELENOT on LPS-induced endothelial cell activation. Therefore, FLAG-SELENOT was expressed in EC as before. After treatment with 150 ng/mL LPS for 18 h, ICAM1—a marker for endothelial cell activation—was detected. As expected, LPS upregulated ICAM1 protein levels in empty vector transfected EC. This upregulation was completely inhibited in cells, in which SELENOT is overexpressed (Figure 4).

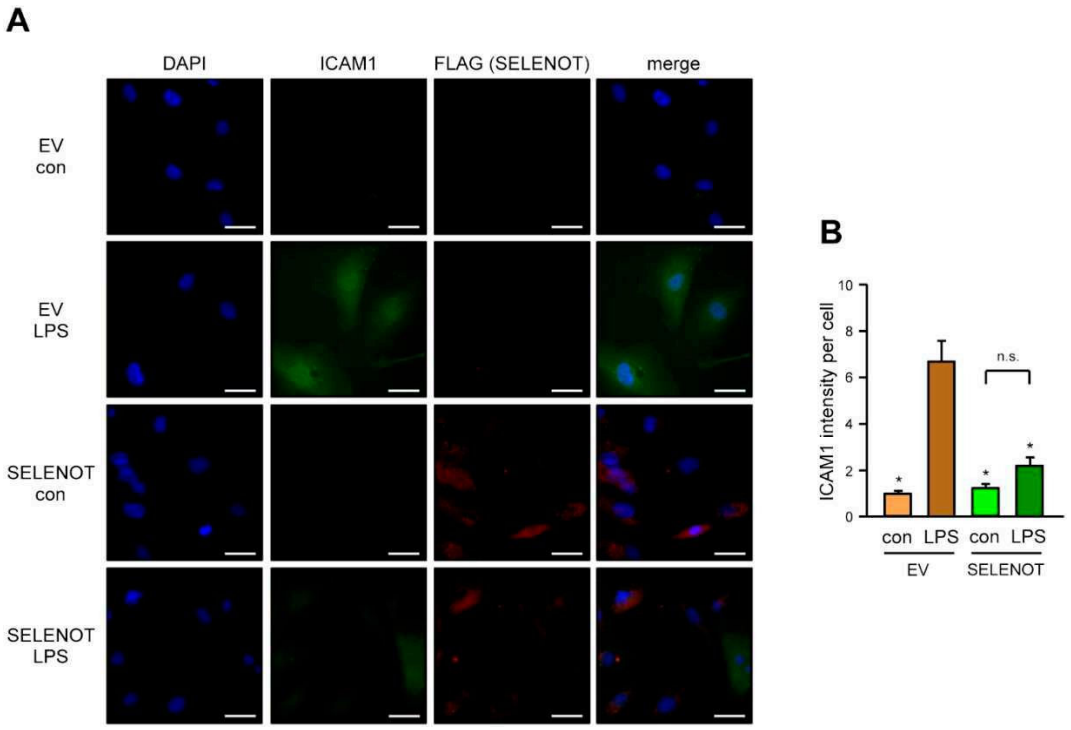

Figure 4. SELENOT suppresses LPS-induced upregulation of ICAM1. (**A**,**B**) EC were transfected with the FLAG-SELENOT expression vector (SELENOT) or an empty vector (EV) and treated with 150 ng/mL detoxified (con) or active LPS (LPS) for 18 h. FLAG-SELENOT and ICAM1 were detected by immunofluorescence. Cells were stained with an antibody directed ICAM1 (green) and an anti-FLAG antibody (red). Nuclei were counterstained with DAPI (blue); merge is the overlay of all channels. (**A**) Representative immunostaining (scale bar = 30 μm). (**B**) Quantitation of ICAM1 levels. The intensity of the green fluorescence per cell was measured using Fiji; in the cells transfected with the SELENOT expression vector, only FLAG-SELENOT positive cells were included (data are mean ± SEM, $n = 4$, * $p < 0.05$ vs. EV/LPS, n.s. = not significant, one-way ANOVA with post-hoc Tukey LSD test).

3.5. SELENOT Overexpression Inhibits LPS-Induced Endothelial Cell Apoptosis

Besides endothelial cell activation, LPS also induces apoptosis of EC [37]. Therefore, we determined Caspase 3 cleavage as a marker for apoptosis in EC. As for ICAM1, LPS increased Caspase 3 cleavage in cells not expressing SELENOT. On the contrary, overexpression of SELENOT completely blunted apoptosis induction by LPS (Figure 5).

In conclusion, SELENOT, which is upregulated by LPS in EC expressing APEX1(1-20), seems to be an important mediator of the protective effects of APEX1(1-20) and could thus be of interest as an adjuvant therapeutic agent in endotoxemia.

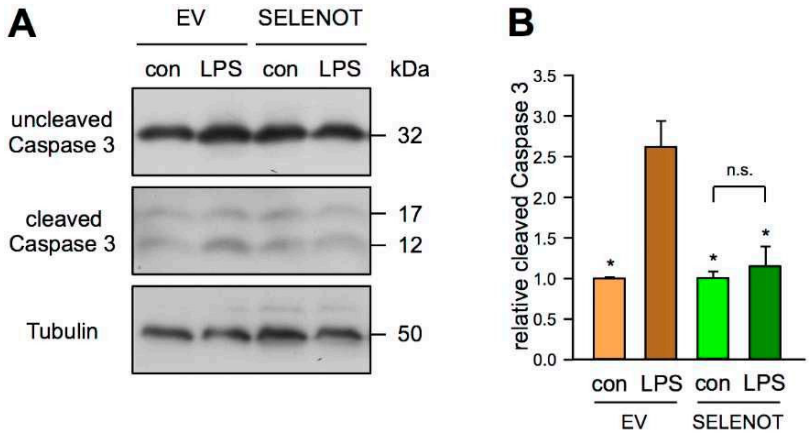

Figure 5. SELENOT suppresses apoptosis induction by LPS. (**A**,**B**) EC were transfected with the FLAG-SELENOT expression vector (SELENOT) or an empty vector (EV) and treated with 150 ng/mL detoxified (con) or active LPS (LPS) for 18 h. Uncleaved and cleaved Caspase 3 were detected by immunoblot, Tubulin served as loading control. (**A**) Representative immunoblot. (**B**) Semi-quantitative analysis of relative amounts of cleaved Caspase 3 (data are mean ± SEM, $n = 4$, * $p < 0.05$ vs. EV/LPS, n.s. = not significant, one-way ANOVA with post-hoc Tukey LSD test).

4. Discussion

The major findings of the present study are the first RNA deep sequencing analysis of LPS-induced changes in primary human EC and the identification of a protective role of APEX1(1-20) and SELENOT in LPS-induced endothelial cell activation and apoptosis.

With respect to the possibility of using an APEX1(1-20) peptide or a related small molecule as a therapeutic agent, it has to be noted that APEX1(1-20) does not change the transcriptome when compared to empty virus transduced cells. Thus, there is no evidence of potential side effects induced by APEX1(1-20) in the endothelium. As expected, LPS treatment induced typical pathways known in sepsis. Those upregulated genes upon LPS treatment in cells not expressing APEX1(1-20) are found, for example, under the GO terms cellular response to tumor necrosis factor, tumor necrosis factor-mediated signaling pathway, and plasma membrane (Supplementary Table S3). It has been known for years that tumor necrosis factor induces endothelial cell activation [38] and apoptosis [39]. Therefore, activation of those pathways is a typical answer of the endothelium to LPS, which in turn leads to loss of endothelial integrity and barrier function. Loss of endothelial cell integrity is a mainstay of septic shock [3], because LPS can enter the systemic circulation destroy endothelial cell integrity, thereby leading to multiple organ failure. Thus, an additional therapy protecting the integrity of the endothelium would be of tremendous interest. Interestingly, APEX1(1-20) leads to reduced responses of the tumor necrosis factor pathways (Supplementary Table S4). Hence, APEX1(1-20) or its downstream targets could be of interest as potential therapeutic options. Therefore, we specifically focused on those targets induced by APEX1(1-20) in the presence of LPS in EC to identify potential candidates. Indeed, we found SELENOT to be upregulated upon APEX1(1-20).

SELENOT is an ER-resident selenoprotein, which is associated with the ER membrane and required to maintain ER redox homeostasis. It is needed to cope with intracellular stress conditions and is one of the most important selenoproteins [30].

As mentioned before, the expression of all selenoproteins depends on selenium. However, there seems to be a hierarchy in the sensitivity of different selenoproteins with respect to selenium levels and SELENOT seems to respond more avidly to selenium depletion than several other proteins of this family [40]. It has been estimated that up to one in seven people worldwide have a low dietary selenium intake [41] and it is clear that proper endothelial functionality depends on an adequate selenium supply [42]. Even more interesting is the observation that selenium serum levels are dramatically reduced in critically ill patients with sepsis [43]. Therefore, selenium supplementation seems to be an obvious

supplementary treatment option for sepsis and possibly the protection of the endothelium in this disease. In this context, it is interesting to note that selenium pretreatment or supplementation alleviates some of the deleterious effects of LPS. In the murine macrophage cell line RAW264.7, LPS induced immunological stress as shown by the upregulation of multiple inflammation-related genes. This was accompanied by a reduction in the relative *selenot* mRNA level. Pretreatment with selenium partially rescued this downregulation and had only a very modest effect on the expression of the inflammation-related genes [44]. In mice, LPS-induced myocardial dysfunction, oxidative stress and apoptosis in the heart could be attenuated when the animals were put on a selenium-supplemented diet 2 weeks prior to LPS treatment [45]. Again, this pretreatment did not completely restore heart functionality or prevent oxidative stress and apoptosis induction evoked by LPS. Our experiments did not show a significant downregulation of *selenot* expression in LPS-treated EC, although there seems to be a trend in this direction. On the contrary, the cells expressing APEX1(1-20) showed an upregulation of *selenot* RNA levels of approximately threefold after LPS treatment. This clearly indicates that the small APEX1 peptide can convey a protective outcome, which is much stronger than the effects observed with selenium supplementation or pretreatment.

Up to now, the precise molecular functions of SELENOT have not been elucidated. Nevertheless, a peptide derived from SELENOT has already been used in animal models. Rocca et al. demonstrated that this SELENOT-derived peptide—including the active catalytic site corresponding to the sequence FQICVSUGYR—applied after ischemia and prior to reperfusion is able to protect the heart from ischemia/reperfusion injury. This protection was attributed to a reduction in oxidative stress and inhibition of apoptosis [46]. This is in accordance with our study presented here, in which we demonstrate that SELENOT completely inhibited LPS-induced activation and apoptosis in human primary EC.

The same peptide was applied in a cell-permeable form in a mouse model for Parkinson's disease, where it protected dopaminergic neurons. This effect was also associated with reduced oxidative stress and Caspase 3 activity [47].

Based on the protective effects of this SELENOT peptide in such different organs as the brain and the heart, it is conceivable that it could exert its protective functions also in the vasculature in the setting of sepsis.

Given the high numbers of patients and the up to 11 million deaths per year due to sepsis, a protection of the endothelium as an additional additive therapy could be of tremendous importance. The metabolic response to sepsis entails the rapid breakdown of intracellular reserves of proteins, carbohydrates and fat. This is accompanied by an increase in ER stress. An increase in SELENOT or application of a peptide could dampen this stress and maintain the ER homeostasis, counteracting the overshooting responses of the body to sepsis.

5. Conclusions

In conclusion, our data presented here suggest that APEX1(1-20) and SELENOT are promising therapeutic options for the treatment of sepsis to protect the endothelium and thus, to prevent endothelial cell leakage or even to restore endothelial cell integrity. This would be of tremendous value for patients and would potentially lower the numbers of septic shock, multiple organ failure and deaths.

Supplementary Materials: The following are available online at https://www.mdpi.com/article/10.3390/antiox10091427/s1, Figure S1: Principal component analysis, Table S1: Primer pairs used for endpoint PCR and semi-quantitative real-time PCR. Primer pairs used for endpoint PCR and semi-quantitative real-time PCR, Table S2: Differential gene expression analysis for genes regulated byexpression of APEX1(1-20), Table S3: Overrepresented GO terms in genes upregulated by LPS exclusively in cells not expressing APEX1(1-20), Table S4: Overrepresented GO terms in genes downregulated by LPS exclusively in cells expressing APEX1(1-20), Table S5: Differentially expressed genes upon LPS treatment of cells not expressing APEX1(1-20), Table S6: Differentially expressed genes upon LPS treatment of cells expressing APEX1(1-20), Table S7: Genes upregulated by LPS exclusively

in cells that do not express APEX1(1-20), Table S8: Genes downregulated by LPS exclusively in cells that do not express APEX1(1-20), Table S9: Genes upregulated by LPS exclusively in cells that express APEX1(1-20), Table S10: Genes downregulated by LPS exclusively in cells that express APEX1(1-20).

Author Contributions: Conceptualization, H.S., N.A.-A., J.A. and J.H.; Data curation, H.S., N.A.-A., J.A. and J.H.; Formal analysis, D.M., J.P., P.J. and P.K.; Funding acquisition, H.S. and J.A.; Investigation, D.M., J.P., P.J., F.v.A., J.G., P.K., K.S., O.E. and N.A.-A.; Methodology, D.M., J.P., P.J. and P.K.; Project administration, H.S., J.A. and J.H.; Resources, H.S., J.A. and J.H.; Supervision, P.J., H.S., N.A.-A., J.A. and J.H.; Validation, D.M., J.P., P.J. and P.K.; Visualization, D.M., J.P. and N.A.-A.; Writing—original draft, D.M. and J.P.; Writing—review and editing, H.S., N.A.-A., J.A. and J.H. All authors have read and agreed to the published version of the manuscript.

Funding: This research was funded by the Deutsche Forschungsgemeinschaft (DFG), IRTG1902-1 and IRTG1902-2 to J.A. and J.H. D.M., J.G. and K.S. are stipend holders of the IRTG1902. This research was also in part funded by Bayer Grant4Target (2019-08-2427) to J.H. and by intramural funding (9772727) of the University Hospital of the Heinrich-Heine University to H.S. and J.H.

Institutional Review Board Statement: Not applicable.

Informed Consent Statement: Not applicable.

Data Availability Statement: Data are contained within the article. The RNA sequencing data used to support the findings of this study have been deposited at ArrayExpress under accession number E-MTAB-10936 (https://www.ebi.ac.uk/arrayexpress/09/2021, accessed on 17 August 2021).

Acknowledgments: Computational support and infrastructure were provided by the Center for Information and Media Technology (ZIM) at the Heinrich-Heine University Düsseldorf.

Conflicts of Interest: The authors declare no conflict of interest.

References

1. Rudd, K.E.; Johnson, S.C.; Agesa, K.M.; Shackelford, K.A.; Tsoi, D.; Kievlan, D.R.; Colombara, D.V.; Ikuta, K.S.; Kissoon, N.; Finfer, S.; et al. Global, regional, and national sepsis incidence and mortality, 1990–2017: Analysis for the Global Burden of Disease Study. *Lancet* **2020**, *395*, 200–211. [CrossRef]
2. Boutagy, N.E.; McMillan, R.P.; Frisard, M.I.; Hulver, M.W. Metabolic endotoxemia with obesity: Is it real and is it relevant? *Biochimie* **2016**, *124*, 11–20. [CrossRef]
3. Joffre, J.; Hellman, J.; Ince, C.; Ait-Oufella, H. Endothelial Responses in Sepsis. *Am. J. Respir. Crit. Care Med.* **2020**, *202*, 361–370. [CrossRef]
4. Zhao, B.; Bowden, R.A.; Stavchansky, S.A.; Bowman, P.D. Human endothelial cell response to gram-negative lipopolysaccharide assessed with cDNA microarrays. *Am. J. Physiol. Cell Physiol.* **2001**, *281*, C1587–C1595. [CrossRef]
5. Ho, J.; Chan, H.; Wong, S.H.; Wang, M.H.; Yu, J.; Xiao, Z.; Liu, X.; Choi, G.; Leung, C.C.; Wong, W.T.; et al. The involvement of regulatory non-coding RNAs in sepsis: A systematic review. *Crit. Care* **2016**, *20*, 383. [CrossRef]
6. Dyballa-Rukes, N.; Jakobs, P.; Eckers, A.; Ale-Agha, N.; Serbulea, V.; Aufenvenne, K.; Zschauer, T.C.; Rabanter, L.L.; Jakob, S.; von Ameln, F.; et al. The Anti-Apoptotic Properties of APEX1 in the Endothelium Require the First 20 Amino Acids and Converge on Thioredoxin-1. *Antioxid. Redox Signal.* **2017**, *26*, 616–629. [CrossRef]
7. Ale-Agha, N.; Goy, C.; Jakobs, P.; Spyridopoulos, I.; Gonnissen, S.; Dyballa-Rukes, N.; Aufenvenne, K.; von Ameln, F.; Zurek, M.; Spannbrucker, T.; et al. CDKN1B/p27 is localized in mitochondria and improves respiration-dependent processes in the cardiovascular system-New mode of action for caffeine. *PLoS Biol.* **2018**, *16*, e2004408. [CrossRef]
8. Goy, C.; Czypiorski, P.; Altschmied, J.; Jakob, S.; Rabanter, L.L.; Brewer, A.C.; Ale-Agha, N.; Dyballa-Rukes, N.; Shah, A.M.; Haendeler, J. The imbalanced redox status in senescent endothelial cells is due to dysregulated Thioredoxin-1 and NADPH oxidase 4. *Exp. Gerontol.* **2014**, *56*, 45–52. [CrossRef]
9. Ewels, P.; Magnusson, M.; Lundin, S.; Käller, M. MultiQC: Summarize analysis results for multiple tools and samples in a single report. *Bioinformatics* **2016**, *32*, 3047–3048. [CrossRef]
10. Bolger, A.M.; Lohse, M.; Usadel, B. Trimmomatic: A flexible trimmer for Illumina sequence data. *Bioinformatics* **2014**, *30*, 2114–2120. [CrossRef]
11. Kopylova, E.; Noé, L.; Touzet, H. SortMeRNA: Fast and accurate filtering of ribosomal RNAs in metatranscriptomic data. *Bioinformatics* **2012**, *28*, 3211–3217. [CrossRef]
12. Yates, A.D.; Achuthan, P.; Akanni, W.; Allen, J.; Allen, J.; Alvarez-Jarreta, J.; Amode, M.R.; Armean, I.M.; Azov, A.G.; Bennett, R.; et al. Ensembl 2020. *Nucleic Acids Res.* **2020**, *48*, D682–D688. [CrossRef]
13. Durinck, S.; Moreau, Y.; Kasprzyk, A.; Davis, S.; De Moor, B.; Brazma, A.; Huber, W. BioMart and Bioconductor: A powerful link between biological databases and microarray data analysis. *Bioinformatics* **2005**, *21*, 3439–3440. [CrossRef]

14. Dobin, A.; Davis, C.A.; Schlesinger, F.; Drenkow, J.; Zaleski, C.; Jha, S.; Batut, P.; Chaisson, M.; Gingeras, T.R. STAR: Ultrafast universal RNA-seq aligner. *Bioinformatics* **2013**, *29*, 15–21. [CrossRef]
15. Li, H.; Handsaker, B.; Wysoker, A.; Fennell, T.; Ruan, J.; Homer, N.; Marth, G.; Abecasis, G.; Durbin, R. The Sequence Alignment/Map format and SAMtools. *Bioinformatics* **2009**, *25*, 2078–2079. [CrossRef]
16. Love, M.I.; Huber, W.; Anders, S. Moderated estimation of fold change and dispersion for RNA-seq data with DESeq2. *Genome Biol.* **2014**, *15*, 550. [CrossRef]
17. Patro, R.; Duggal, G.; Love, M.I.; Irizarry, R.A.; Kingsford, C. Salmon provides fast and bias-aware quantification of transcript expression. *Nat. Methods* **2017**, *14*, 417–419. [CrossRef] [PubMed]
18. Young, M.D.; Wakefield, M.J.; Smyth, G.K.; Oshlack, A. Gene ontology analysis for RNA-seq: Accounting for selection bias. *Genome Biol.* **2010**, *11*, R14. [CrossRef]
19. Pfaffl, M.W. A new mathematical model for relative quantification in real-time RT-PCR. *Nucleic Acids Res.* **2001**, *29*, e45. [CrossRef]
20. Jakob, S.; Schroeder, P.; Lukosz, M.; Büchner, N.; Spyridopoulos, I.; Altschmied, J.; Haendeler, J. Nuclear protein tyrosine phosphatase Shp-2 is one important negative regulator of nuclear export of telomerase reverse transcriptase. *J. Biol. Chem.* **2008**, *283*, 33155–33161. [CrossRef]
21. Schroeder, P.; Popp, R.; Wiegand, B.; Altschmied, J.; Haendeler, J. Nuclear redox-signaling is essential for apoptosis inhibition in endothelial cells–important role for nuclear thioredoxin-1. *Arterioscler. Thromb. Vasc. Biol.* **2007**, *27*, 2325–2331. [CrossRef] [PubMed]
22. Schindelin, J.; Arganda-Carreras, I.; Frise, E.; Kaynig, V.; Longair, M.; Pietzsch, T.; Preibisch, S.; Rueden, C.; Saalfeld, S.; Schmid, B.; et al. Fiji: An open-source platform for biological-image analysis. *Nat. Methods* **2012**, *9*, 676–682. [CrossRef]
23. Boraschi, D.; Italiani, P.; Weil, S.; Martin, M.U. The family of the interleukin-1 receptors. *Immunol. Rev.* **2018**, *281*, 197–232. [CrossRef]
24. Cheng, G.; Salerno, J.C.; Cao, Z.; Pagano, P.J.; Lambeth, J.D. Identification and characterization of VPO1, a new animal heme-containing peroxidase. *Free Radic. Biol. Med.* **2008**, *45*, 1682–1694. [CrossRef] [PubMed]
25. Cheng, G.; Li, H.; Cao, Z.; Qiu, X.; McCormick, S.; Thannickal, V.J.; Nauseef, W.M. Vascular peroxidase-1 is rapidly secreted, circulates in plasma, and supports dityrosine cross-linking reactions. *Free Radic. Biol. Med.* **2011**, *51*, 1445–1453. [CrossRef]
26. Bhave, G.; Cummings, C.F.; Vanacore, R.M.; Kumagai-Cresse, C.; Ero-Tolliver, I.A.; Rafi, M.; Kang, J.S.; Pedchenko, V.; Fessler, L.I.; Fessler, J.H.; et al. Peroxidasin forms sulfilimine chemical bonds using hypohalous acids in tissue genesis. *Nat. Chem. Biol.* **2012**, *8*, 784–790. [CrossRef]
27. Medfai, H.; Khalil, A.; Rousseau, A.; Nuyens, V.; Paumann-Page, M.; Sevcnikar, B.; Furtmüller, P.G.; Obinger, C.; Moguilevsky, N.; Peulen, O.; et al. Human peroxidasin 1 promotes angiogenesis through ERK1/2, Akt, and FAK pathways. *Cardiovasc. Res.* **2019**, *115*, 463–475. [CrossRef]
28. Lee, S.W.; Kim, H.K.; Naidansuren, P.; Ham, K.A.; Choi, H.S.; Ahn, H.Y.; Kim, M.; Kang, D.H.; Kang, S.W.; Joe, Y.A. Peroxidasin is essential for endothelial cell survival and growth signaling by sulfilimine crosslink-dependent matrix assembly. *FASEB J.* **2020**, *34*, 10228–10241. [CrossRef]
29. Mariotti, M.; Ridge, P.G.; Zhang, Y.; Lobanov, A.V.; Pringle, T.H.; Guigo, R.; Hatfield, D.L.; Gladyshev, V.N. Composition and evolution of the vertebrate and mammalian selenoproteomes. *PLoS ONE* **2012**, *7*, e33066. [CrossRef]
30. Pothion, H.; Jehan, C.; Tostivint, H.; Cartier, D.; Bucharles, C.; Falluel-Morel, A.; Boukhzar, L.; Anouar, Y.; Lihrmann, I. Selenoprotein T: An Essential Oxidoreductase Serving as a Guardian of Endoplasmic Reticulum Homeostasis. *Antioxid. Redox Signal.* **2020**, *33*, 1257–1275. [CrossRef]
31. Boukhzar, L.; Hamieh, A.; Cartier, D.; Tanguy, Y.; Alsharif, I.; Castex, M.; Arabo, A.; El Hajji, S.; Bonnet, J.J.; Errami, M.; et al. Selenoprotein T Exerts an Essential Oxidoreductase Activity That Protects Dopaminergic Neurons in Mouse Models of Parkinson's Disease. *Antioxid. Redox Signal.* **2016**, *24*, 557–574. [CrossRef] [PubMed]
32. Pitts, M.W.; Hoffmann, P.R. Endoplasmic reticulum-resident selenoproteins as regulators of calcium signaling and homeostasis. *Cell Calcium* **2018**, *70*, 76–86. [CrossRef]
33. Huang, X.; Sun, B.; Zhang, J.; Gao, Y.; Li, G.; Chang, Y. Selenium Deficiency Induced Injury in Chicken Muscular Stomach by Downregulating Selenoproteins. *Biol. Trace Elem. Res.* **2017**, *179*, 277–283. [CrossRef] [PubMed]
34. Huang, J.; Bao, D.; Lei, C.T.; Tang, H.; Zhang, C.Y.; Su, H.; Zhang, C. Selenoprotein T protects against cisplatin-induced acute kidney injury through suppression of oxidative stress and apoptosis. *FASEB J.* **2020**, *34*, 11983–11996. [CrossRef]
35. Addinsall, A.B.; Wright, C.R.; Andrikopoulos, S.; van der Poel, C.; Stupka, N. Emerging roles of endoplasmic reticulum-resident selenoproteins in the regulation of cellular stress responses and the implications for metabolic disease. *Biochem. J.* **2018**, *475*, 1037–1057. [CrossRef]
36. Tujebajeva, R.M.; Copeland, P.R.; Xu, X.M.; Carlson, B.A.; Harney, J.W.; Driscoll, D.M.; Hatfield, D.L.; Berry, M.J. Decoding apparatus for eukaryotic selenocysteine insertion. *EMBO Rep.* **2000**, *1*, 158–163. [CrossRef]
37. Haendeler, J.; Messmer, U.K.; Brüne, B.; Neugebauer, E.; Dimmeler, S. Endotoxic shock leads to apoptosis in vivo and reduces Bcl-2. *Shock* **1996**, *6*, 405–409. [CrossRef]
38. Pober, J.S. Endothelial activation: Intracellular signaling pathways. *Arthritis Res. Ther.* **2002**, *4* (Suppl. 3), S109–S116. [CrossRef]
39. Dimmeler, S.; Haendeler, J.; Rippmann, V.; Nehls, M.; Zeiher, A.M. Shear stress inhibits apoptosis of human endothelial cells. *FEBS Lett.* **1996**, *399*, 71–74. [CrossRef]

40. Carlson, B.A.; Xu, X.M.; Gladyshev, V.N.; Hatfield, D.L. Selective rescue of selenoprotein expression in mice lacking a highly specialized methyl group in selenocysteine tRNA. *J. Biol. Chem.* **2005**, *280*, 5542–5548. [CrossRef]
41. Jones, G.D.; Droz, B.; Greve, P.; Gottschalk, P.; Poffet, D.; McGrath, S.P.; Seneviratne, S.I.; Smith, P.; Winkel, L.H. Selenium deficiency risk predicted to increase under future climate change. *Proc. Natl. Acad. Sci. USA* **2017**, *114*, 2848–2853. [CrossRef] [PubMed]
42. Lopes Junior, E.; Leite, H.P.; Konstantyner, T. Selenium and selenoproteins: From endothelial cytoprotection to clinical outcomes. *Transl. Res.* **2019**, *208*, 85–104. [CrossRef]
43. Mertens, K.; Lowes, D.A.; Webster, N.R.; Talib, J.; Hall, L.; Davies, M.J.; Beattie, J.H.; Galley, H.F. Low zinc and selenium concentrations in sepsis are associated with oxidative damage and inflammation. *Br. J. Anaesth.* **2015**, *114*, 990–999. [CrossRef]
44. Wang, L.; Jing, J.; Yan, H.; Tang, J.; Jia, G.; Liu, G.; Chen, X.; Tian, G.; Cai, J.; Shang, H.; et al. Selenium Pretreatment Alleviated LPS-Induced Immunological Stress Via Upregulation of Several Selenoprotein Encoding Genes in Murine RAW264.7 Cells. *Biol. Trace Elem. Res.* **2018**, *186*, 505–513. [CrossRef] [PubMed]
45. Wang, X.; Yang, B.; Cao, H.L.; Wang, R.Y.; Lu, Z.Y.; Chi, R.F.; Li, B. Selenium Supplementation Protects Against Lipopolysaccharide-Induced Heart Injury via Sting Pathway in Mice. *Biol. Trace Elem. Res.* **2021**, *199*, 1885–1892. [CrossRef] [PubMed]
46. Rocca, C.; Boukhzar, L.; Granieri, M.C.; Alsharif, I.; Mazza, R.; Lefranc, B.; Tota, B.; Leprince, J.; Cerra, M.C.; Anouar, Y.; et al. A selenoprotein T-derived peptide protects the heart against ischaemia/reperfusion injury through inhibition of apoptosis and oxidative stress. *Acta Physiol.* **2018**, *223*, e13067. [CrossRef] [PubMed]
47. Alsharif, I.; Boukhzar, L.; Lefranc, B.; Godefroy, D.; Aury-Landas, J.; Rego, J.D.; Rego, J.D.; Naudet, F.; Arabo, A.; Chagraoui, A.; et al. Cell-penetrating, antioxidant SELENOT mimetic protects dopaminergic neurons and ameliorates motor dysfunction in Parkinson's disease animal models. *Redox Biol.* **2021**, *40*, 101839. [CrossRef]

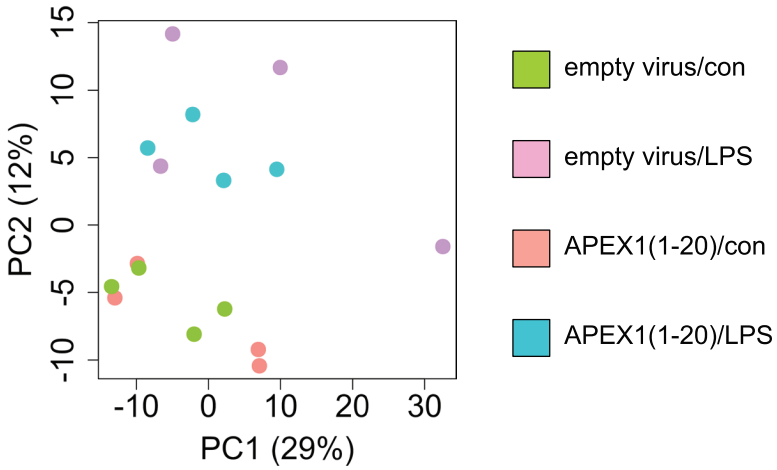

Supplementary figure S1: Principal component analysis. Endothelial cells were transduced with a lentiviral expression vector for APEX1(1-20) or an empty virus and treated with detoxified (con) or active LPS (LPS). and subjected to RNA deep sequencing.

Supplementary table S1: Primer pairs used for endpoint PCR and semi-quantitative real-time PCR.
Shown are the sequences of the primers in 5'→3' direction and the expected amplification products.

transcript	primer	sequence	amplification product
RPL32	hmRPL32 Ex02 for1	5'- GTGAAGCCCAAGATCGTCAA -3'	257 bp
	hmRPL32 Ex03 rev1	5'- TTGTTGCACATCAGCAGCAC -3'	
PXDN	hPXDN Ex20/21 for1	5'- CGGAAAATACCCAGTGTTGGGAG -3'	223 bp
	hPXDN Ex22 rev1	5'- TGGTGTTGTTGGCGTGAGATTC -3'	
SELENOT	hSELENOT Ex01 for	5'- GCGTGCCCAGCAAGAGATTA -3'	99bp
	hSELENOT Ex02 rev1	5'- ACTCCTCAAACACCCGCCTA -3'	
FLAG-SELENOT	FLAG for2	5'- CAAAGACGATGACGACAAGC -3'	206 bp
	hSELENOT Ex02 rev1	5'- ACTCCTCAAACACCCGCCTA -3'	

Supplementary Table S2: Differential gene expression analysis for genes regulated by expression of APEX1(1-20). DGE was calculated using the R package DESeq2 in samples of cells transduced with the lentivirus expressing APEX1(1-20) versus cells transduced with the empty virus both treated with detoxified LPS. The L2FC (Log 2-fold change) states the ave-rage difference in gene expression between the two cell populations. Positive L2FC values denote upregulation by APEX1(1-20) expression, negative values downregulation. Wald test from DESeq2 was used to calculate the significance of the change in the expression. The adjusted p-values take the number of tested genes into account, the threshold for the adjusted p-value was set to 0.05. APEX1(1-20)-myc represents the transcript originating from the APEX1(1-20) expression vector, which codes for a fusion between the APEX1 peptide and a myc epitope tag.

gene name	Ensembl gene ID	L2FC	p-value	adusted p-value
APEX1(1-20)-myc	NA	9,861	3,73E-40	2,92E-36
LRTOMT	ENSG00000184154	0,653	5,85E-11	3,06E-07
SRP9P1	ENSG00000180581	-26,509	5,11E-10	2,00E-06
AL358472.7	NA	21,631	2,86E-08	8,99E-05
CR354443.1	NA	-23,191	6,74E-08	1,51E-04
H3P6	ENSG00000235655	-22,915	6,69E-08	1,51E-04
KCNJ15	ENSG00000157551	-0,848	1,05E-06	2,06E-03
CAMSAP3	ENSG00000076826	1,139	7,29E-06	1,21E-02
GJA5	ENSG00000265107	0,484	7,73E-06	1,21E-02
GDF7	ENSG00000143869	0,397	9,76E-06	1,39E-02
CCL2	ENSG00000108691	0,324	1,80E-05	2,35E-02
HNRNPCP1	ENSG00000258900	17,502	4,12E-05	4,97E-02

Supplementary Table S3: Overrepresented GO terms in genes upregulated by LPS exclusively in cells not expressing APEX1(1-20). Gene set enrichment analysis (GSEA) was applied to genes from the DGE analysis, which were significantly upregulated by LPS exclusively in cells transduced with the empty virus GSEA was performed using R package goseq with a treshold on the adjusted p-values of 0.05. numDEInCat: number of differentially expressed genes belonging to the respective GO term; numInCat: number of genes related to the GO term.

GO ID	GO term	overrepresented p-value	adjusted p-value	numDEInCat	numInCat
GO:0005886	plasma membrane	8,50E-08	8,19E-05	101	2946
GO:0002479	antigen processing and presentation of exogenous peptide antigen via MHC class I, TAP-dependent	5,13E-06	2,95E-03	10	65
GO:0050852	T cell receptor signaling pathway	8,51E-06	4,63E-03	13	134
GO:0033209	tumor necrosis factor-mediated signaling pathway	9,82E-06	5,18E-03	12	102
GO:0019722	calcium-mediated signaling	1,05E-05	5,38E-03	8	49
GO:0002250	adaptive immune response	1,11E-05	5,45E-03	11	92
GO:0006959	humoral immune response	1,13E-05	5,45E-03	6	22
GO:0045766	positive regulation of angiogenesis	1,25E-05	5,86E-03	11	100
GO:0019955	cytokine binding	2,55E-05	1,16E-02	6	27
GO:0002486	antigen processing and presentation of endogenous peptide antigen via MHC class I via ER pathway, TAP-independent	3,90E-05	1,61E-02	3	3
GO:0046977	TAP binding	3,90E-05	1,61E-02	3	3
GO:0009395	phospholipid catabolic process	4,21E-05	1,69E-02	4	11
GO:0005604	basement membrane	4,36E-05	1,71E-02	8	71
GO:0016020	membrane	5,34E-05	2,00E-02	159	5600
GO:0016032	viral process	6,23E-05	2,29E-02	26	520
GO:0071356	cellular response to tumor necrosis factor	8,18E-05	2,87E-02	10	92
GO:1990111	spermatoproteasome complex	8,70E-05	2,99E-02	3	4
GO:0035455	response to interferon-alpha	9,63E-05	3,25E-02	4	10
GO:0010466	negative regulation of peptidase activity	1,07E-04	3,48E-02	7	46
GO:0030414	peptidase inhibitor activity	1,11E-04	3,49E-02	7	46
GO:0009617	response to bacterium	1,15E-04	3,49E-02	8	66
GO:0010951	negative regulation of endopeptidase activity	1,17E-04	3,49E-02	8	64
GO:0042270	protection from natural killer cell mediated cytotoxicity	1,18E-04	3,49E-02	3	4
GO:0001968	fibronectin binding	1,18E-04	3,49E-02	5	22
GO:0004867	serine-type endopeptidase inhibitor activity	1,40E-04	4,06E-02	6	37
GO:0019882	antigen processing and presentation	1,45E-04	4,15E-02	6	32

Supplementary Table S4: Overrepresented GO terms in genes downregulated by LPS exclusively in cells expressing APEX1(1-20). Gene set enrichment analysis (GSEA) was applied to genes from the DGE analysis, which were significantly downregulated by LPS exclusively in cells transduced with the lentivrus expressing APEX1(1-20). GSEA was performed using R package goseq with a treshold on the adjusted p-values of 0.05. numDEInCat: number of differentially expressed genes belonging to the respective GO term; numInCat: number of genes related to the GO term.

GO ID	GO term	overrepresented p-value	adjusted p-value	numDEInCat	numInCat
GO:0008217	regulation of blood pressure	4,11E-08	4,89E-04	7	38
GO:0005615	extracellular space	7,26E-08	4,89E-04	26	853
GO:0032355	response to estradiol	8,53E-08	4,89E-04	9	87
GO:0005576	extracellular region	2,65E-07	1,14E-03	32	1306
GO:0031994	insulin-like growth factor I binding	2,85E-06	9,81E-03	4	12
GO:0005887	integral component of plasma membrane	5,11E-06	1,46E-02	22	839
GO:0016324	apical plasma membrane	6,85E-06	1,56E-02	11	236
GO:0009612	response to mechanical stimulus	8,14E-06	1,56E-02	6	53
GO:0048247	lymphocyte chemotaxis	8,17E-06	1,56E-02	4	13
GO:0009986	cell surface	9,27E-06	1,59E-02	15	444
GO:0031526	brush border membrane	1,58E-05	2,46E-02	5	36
GO:0005113	patched binding	2,55E-05	3,37E-02	3	7
GO:0071356	cellular response to tumor necrosis factor	2,55E-05	3,37E-02	7	93
GO:0006874	cellular calcium ion homeostasis	3,35E-05	4,12E-02	6	69
GO:0002548	monocyte chemotaxis	4,05E-05	4,59E-02	4	20
GO:0031995	insulin-like growth factor II binding	4,27E-05	4,59E-02	3	8

Supplementary Table S5: Differentially expressed genes upon LPS treatment of cells not expressing APEX1(1-20). DGE calculated using the R package DESeq2 comparing samples of cells transduced with an empty virus and treated with active LPS versus treated with detoxified LPS. The L2FC (Log 2-fold change) states the average difference in gene expression between both treatments. Positive L2FC values denote upregulation by LPS treatment, negative values downregulation. Wald test from DESeq2 was used to calculate the significance of the change in the expression. The adjusted p-values take the number of tested genes into account, the threshold for the adjusted p-value was 0.05.

gene name	Ensembl gene ID	L2FC	p-value	adusted p-value
LAMC2	ENSG00000058085	2,175	1,73E-211	2,50E-207
EBI3	ENSG00000105246	2,426	1,30E-60	9,40E-57
CXCL6	ENSG00000124875	1,813	1,84E-58	8,86E-55
SOD2	ENSG00000112096	1,027	2,11E-57	7,64E-54
CCL2	ENSG00000108691	1,201	6,20E-57	1,79E-53
UBD	ENSG00000226898	2,737	4,26E-56	1,03E-52
CFB	ENSG00000242335	1,832	3,80E-54	7,85E-51
MMP10	ENSG00000166670	1,176	2,23E-52	4,04E-49
CTSS	ENSG00000163131	1,296	2,29E-41	3,69E-38
IL32	ENSG00000008517	1,326	5,27E-36	7,63E-33
CTSK	ENSG00000143387	1,404	1,42E-35	1,87E-32
POU2F2	ENSG00000028277	1,233	3,86E-35	4,65E-32
LTB	ENSG00000223448	1,341	2,37E-34	2,64E-31
S100A3	ENSG00000188015	2,189	1,39E-33	1,44E-30
IGFBP3	ENSG00000146674	-0,846	3,62E-31	3,49E-28
PAPLN	ENSG00000100767	1,617	2,35E-29	2,13E-26
HLA-B	ENSG00000206450	1,221	5,52E-25	4,70E-22
ISG20	ENSG00000172183	0,842	2,84E-24	2,29E-21
CXCL1	ENSG00000163739	1,075	6,17E-23	4,70E-20
CNTNAP1	ENSG00000108797	0,572	1,34E-22	9,73E-20
CXCL3	ENSG00000163734	0,929	2,43E-22	1,67E-19
PLA2G4C	ENSG00000105499	0,885	6,16E-22	4,05E-19
IFI27	ENSG00000275214	0,615	1,36E-21	8,58E-19
MX1	ENSG00000157601	1,110	1,53E-20	9,21E-18
ANO9	ENSG00000185101	4,656	2,14E-20	1,24E-17
CXCL5	ENSG00000163735	1,905	5,18E-20	2,88E-17
ICAM1	ENSG00000090339	0,723	1,24E-18	6,64E-16
PSMB9	ENSG00000243958	0,719	2,21E-16	1,14E-13
IL4I1	ENSG00000104951	0,729	1,24E-15	6,21E-13
CXCL2	ENSG00000081041	1,059	2,09E-14	1,01E-11
SLC7A2	ENSG00000003989	0,634	4,06E-14	1,89E-11
THSD4	ENSG00000187720	0,353	4,20E-14	1,90E-11
MAMDC2	ENSG00000278608	0,919	8,41E-14	3,69E-11
IFI6	ENSG00000126709	0,620	1,71E-13	7,28E-11
NEURL1B	ENSG00000214357	-0,767	1,85E-13	7,63E-11
TFPI2	ENSG00000105825	0,766	2,66E-13	1,07E-10
AC139530.2	NA	-30,000	9,87E-13	3,86E-10
TNFRSF9	ENSG00000049249	1,451	1,08E-12	4,10E-10
LAMP3	ENSG00000078081	0,608	4,93E-12	1,83E-09
UBE2L6	ENSG00000156587	0,403	1,16E-11	4,19E-09
OAS2	ENSG00000111335	1,100	2,43E-11	8,58E-09
PSMB8	ENSG00000230669	0,433	3,00E-11	1,03E-08
CCL20	ENSG00000115009	1,110	4,08E-11	1,37E-08
CYB5R2	ENSG00000166394	0,696	5,67E-11	1,86E-08
GPSM2	ENSG00000121957	-0,652	7,28E-11	2,34E-08

CTHRC1	ENSG00000164932	0,593	1,00E-10	3,15E-08
P2RX4	ENSG00000135124	0,371	1,44E-10	4,40E-08
TNC	ENSG00000041982	3,090	1,46E-10	4,40E-08
CXCL8	ENSG00000169429	0,851	1,77E-10	5,21E-08
STAP2	ENSG00000178078	0,498	2,27E-10	6,56E-08
CSF2	ENSG00000164400	1,656	3,48E-10	9,87E-08
ARHGDIG	ENSG00000242173	0,656	4,24E-10	1,17E-07
C2CD4A	ENSG00000198535	0,895	4,27E-10	1,17E-07
PRICKLE1	ENSG00000139174	-0,558	6,19E-10	1,66E-07
CAV1	ENSG00000105974	-0,380	7,33E-10	1,93E-07
CDKN3	ENSG00000100526	-0,614	8,83E-10	2,21E-07
KIF20A	ENSG00000112984	-0,583	8,86E-10	2,21E-07
METTL7A	ENSG00000185432	-0,478	8,64E-10	2,21E-07
CYP51A1	ENSG00000001630	-0,352	1,73E-09	4,24E-07
STARD10	ENSG00000214530	0,569	1,99E-09	4,79E-07
VWA1	ENSG00000179403	0,476	3,39E-09	8,05E-07
MX2	ENSG00000183486	2,548	3,69E-09	8,60E-07
APOL1	ENSG00000100342	0,388	5,39E-09	1,24E-06
TAPBP	ENSG00000206281	0,477	5,53E-09	1,25E-06
GP1BB	ENSG00000203618	-22,691	6,22E-09	1,38E-06
DHRS3	ENSG00000162496	0,429	6,82E-09	1,50E-06
CEBPD	ENSG00000221869	0,785	7,57E-09	1,63E-06
PLA1A	ENSG00000144837	1,472	7,81E-09	1,66E-06
WASF3	ENSG00000132970	-0,313	9,19E-09	1,93E-06
LYPD6	ENSG00000187123	0,469	1,20E-08	2,47E-06
CAPN2	ENSG00000162909	-0,289	1,47E-08	2,95E-06
HLA-A	ENSG00000227715	0,395	1,47E-08	2,95E-06
HMGCS1	ENSG00000112972	-0,427	1,83E-08	3,63E-06
BUB1	ENSG00000169679	-0,492	1,96E-08	3,83E-06
SELENOM	ENSG00000198832	0,545	1,98E-08	3,83E-06
F2RL1	ENSG00000164251	0,380	2,29E-08	4,36E-06
BST1	ENSG00000109743	0,394	2,56E-08	4,81E-06
PCK2	ENSG00000285241	0,426	2,61E-08	4,84E-06
TNFSF18	ENSG00000120337	-0,583	3,14E-08	5,75E-06
DENND2B	ENSG00000166444	0,984	3,20E-08	5,79E-06
AL451062.4	NA	-23,299	3,34E-08	5,98E-06
UBA7	ENSG00000182179	0,446	3,41E-08	6,02E-06
ALOX5AP	ENSG00000132965	1,587	3,68E-08	6,41E-06
DLGAP5	ENSG00000126787	-0,621	4,30E-08	7,41E-06
CRYBG1	ENSG00000112297	-0,333	4,95E-08	8,42E-06
PRSS12	ENSG00000164099	1,198	5,39E-08	9,07E-06
LIPG	ENSG00000101670	0,513	5,53E-08	9,19E-06
SLC15A3	ENSG00000110446	0,517	5,73E-08	9,43E-06
ICOSLG	ENSG00000160223	0,533	7,11E-08	1,16E-05
OAS1	ENSG00000089127	0,519	8,71E-08	1,40E-05
CCNB2	ENSG00000157456	-0,480	9,09E-08	1,45E-05
AL358472.7	NA	20,830	9,30E-08	1,46E-05
ACBD7	ENSG00000176244	-0,775	1,04E-07	1,62E-05
MEST	ENSG00000106484	-0,435	1,21E-07	1,86E-05
JAK3	ENSG00000105639	0,743	1,22E-07	1,86E-05
ALDH1A1	ENSG00000165092	-0,403	1,34E-07	2,02E-05
CRTAC1	ENSG00000095713	0,499	1,67E-07	2,49E-05
OCIAD2	ENSG00000145247	0,437	1,74E-07	2,56E-05

CD69	ENSG00000110848	0,949	1,88E-07	2,75E-05
MKI67	ENSG00000148773	-0,525	1,98E-07	2,87E-05
FSTL3	ENSG00000070404	0,444	2,37E-07	3,39E-05
ADAMTS18	ENSG00000140873	-0,551	2,60E-07	3,59E-05
CIT	ENSG00000122966	-0,468	2,53E-07	3,59E-05
TMEM120A	ENSG00000189077	0,427	2,59E-07	3,59E-05
TNFRSF4	ENSG00000186827	0,959	2,61E-07	3,59E-05
DHH	ENSG00000139549	-0,464	3,68E-07	5,02E-05
PRR11	ENSG00000068489	-0,326	3,87E-07	5,24E-05
SERPINA3	ENSG00000196136	2,440	4,12E-07	5,52E-05
KIF12	ENSG00000136883	0,697	6,16E-07	8,18E-05
PLCG2	ENSG00000197943	1,263	6,57E-07	8,65E-05
PSME2	ENSG00000284889	0,443	6,76E-07	8,81E-05
BDKRB2	ENSG00000168398	0,931	8,27E-07	1,07E-04
ACSS1	ENSG00000154930	0,279	8,67E-07	1,11E-04
MAP2K6	ENSG00000108984	-0,373	8,88E-07	1,13E-04
CCL15-CCL14	ENSG00000282521	-0,416	9,40E-07	1,18E-04
MMP19	ENSG00000123342	0,573	1,04E-06	1,29E-04
ACE	ENSG00000159640	-0,620	1,11E-06	1,37E-04
ZCCHC2	ENSG00000141664	-0,507	1,16E-06	1,42E-04
PAQR7	ENSG00000182749	0,277	1,18E-06	1,42E-04
RASA4B	ENSG00000170667	0,567	1,18E-06	1,42E-04
CCNB1	ENSG00000134057	-0,496	1,20E-06	1,43E-04
PLAAT4	ENSG00000133321	0,728	1,30E-06	1,54E-04
TAPBPL	ENSG00000139192	0,812	1,37E-06	1,61E-04
LYVE1	ENSG00000133800	-0,703	1,52E-06	1,78E-04
APOD	ENSG00000189058	0,469	1,76E-06	2,04E-04
ZC3H12A	ENSG00000163874	0,514	1,86E-06	2,14E-04
CEP55	ENSG00000138180	-0,538	1,94E-06	2,21E-04
ITGAV	ENSG00000138448	0,523	2,09E-06	2,37E-04
ARHGEF19	ENSG00000142632	0,356	2,35E-06	2,64E-04
MAP3K6	ENSG00000142733	0,371	2,50E-06	2,76E-04
SEMA3G	ENSG00000010319	0,417	2,49E-06	2,76E-04
POSTN	ENSG00000133110	-0,702	2,60E-06	2,85E-04
GXYLT2	ENSG00000172986	1,226	2,62E-06	2,85E-04
AC087632.2	NA	-1,660	3,01E-06	3,23E-04
ZDHHC13	ENSG00000177054	-0,297	3,01E-06	3,23E-04
NUCKS1	ENSG00000069275	-0,368	3,07E-06	3,27E-04
CKAP2	ENSG00000136108	-0,456	3,21E-06	3,39E-04
ALDH1A2	ENSG00000128918	-0,356	3,38E-06	3,55E-04
ZNF791	ENSG00000173875	-0,512	3,74E-06	3,90E-04
AKAP12	ENSG00000131016	0,272	4,09E-06	4,23E-04
MTMR10	ENSG00000277086	-0,375	4,67E-06	4,79E-04
AL109918.1	NA	-0,486	4,70E-06	4,80E-04
CERS1	ENSG00000223802	0,381	4,84E-06	4,90E-04
C11orf96	ENSG00000187479	0,453	5,27E-06	5,30E-04
PLCG1	ENSG00000124181	0,243	5,57E-06	5,56E-04
MYRIP	ENSG00000170011	-0,347	5,87E-06	5,81E-04
CXADR	ENSG00000154639	-0,411	6,06E-06	5,93E-04
RASA4	ENSG00000105808	0,440	6,03E-06	5,93E-04
INCENP	ENSG00000149503	-0,443	6,36E-06	6,18E-04
ELMOD1	ENSG00000110675	-0,476	6,88E-06	6,64E-04
KNL1	ENSG00000137812	-0,713	7,35E-06	6,93E-04

MSMP	ENSG00000215183	-0,370	7,33E-06	6,93E-04
SAMD14	ENSG00000167100	0,369	7,29E-06	6,93E-04
SDC4	ENSG00000124145	0,352	7,37E-06	6,93E-04
MCFD2	ENSG00000180398	-0,277	7,55E-06	7,05E-04
BST2	ENSG00000130303	0,315	7,71E-06	7,15E-04
MYZAP	ENSG00000263155	-0,413	8,20E-06	7,55E-04
CENPF	ENSG00000117724	-0,557	8,47E-06	7,76E-04
HMMR	ENSG00000072571	-0,747	8,70E-06	7,92E-04
TSPAN13	ENSG00000106537	0,390	9,00E-06	8,14E-04
ASAP1	ENSG00000153317	-0,339	9,46E-06	8,50E-04
PIGK	ENSG00000142892	-0,369	9,79E-06	8,75E-04
PRCP	ENSG00000137509	0,212	1,02E-05	9,10E-04
PDCD6IP	ENSG00000170248	-0,363	1,11E-05	9,81E-04
LRFN4	ENSG00000173621	0,375	1,13E-05	9,94E-04
ACAT2	ENSG00000120437	-0,299	1,15E-05	9,95E-04
FXYD6	ENSG00000137726	0,656	1,15E-05	9,95E-04
R3HDM1	ENSG00000048991	-0,468	1,16E-05	1,00E-03
TNFRSF14	ENSG00000273936	0,388	1,20E-05	1,03E-03
AC087721.2	NA	-0,375	1,31E-05	1,11E-03
KIT	ENSG00000157404	0,262	1,33E-05	1,13E-03
IL27RA	ENSG00000288185	0,362	1,36E-05	1,14E-03
NEK2	ENSG00000117650	-0,489	1,35E-05	1,14E-03
SYNJ2	ENSG00000078269	0,160	1,36E-05	1,14E-03
TMPO	ENSG00000120802	-0,320	1,40E-05	1,16E-03
DEPDC1B	ENSG00000035499	-0,341	1,45E-05	1,19E-03
SEMA7A	ENSG00000288455	0,515	1,46E-05	1,19E-03
IRF9	ENSG00000285048	0,498	1,55E-05	1,26E-03
MTMR11	ENSG00000014914	0,364	1,57E-05	1,27E-03
MGARP	ENSG00000137463	-0,476	1,62E-05	1,31E-03
KCNJ15	ENSG00000157551	-0,746	1,74E-05	1,39E-03
MGME1	ENSG00000125871	-0,250	1,79E-05	1,42E-03
BORA	ENSG00000136122	-0,605	1,87E-05	1,48E-03
CENPA	ENSG00000115163	-0,407	1,95E-05	1,53E-03
ERMP1	ENSG00000099219	-0,267	1,95E-05	1,53E-03
ITGB4	ENSG00000132470	-0,576	2,06E-05	1,61E-03
CBR3	ENSG00000159231	0,357	2,09E-05	1,62E-03
PPL	ENSG00000118898	-0,801	2,30E-05	1,77E-03
SPTLC1P1	ENSG00000230397	-0,705	2,49E-05	1,91E-03
HSPE1-MOB4	ENSG00000270757	-0,483	2,51E-05	1,91E-03
ASPM	ENSG00000066279	-0,784	2,55E-05	1,93E-03
COBLL1	ENSG00000082438	-0,381	2,60E-05	1,95E-03
ULBP2	ENSG00000131015	0,338	2,59E-05	1,95E-03
CX3CL1	ENSG00000006210	0,553	2,63E-05	1,96E-03
RAB14	ENSG00000119396	-0,247	2,72E-05	2,01E-03
TOP2A	ENSG00000131747	-0,435	2,73E-05	2,01E-03
AC091951.4	NA	2,510	3,21E-05	2,35E-03
DPP4	ENSG00000197635	-0,347	3,23E-05	2,35E-03
LAMB3	ENSG00000196878	0,446	3,26E-05	2,35E-03
NFKBIZ	ENSG00000144802	0,541	3,24E-05	2,35E-03
NUF2	ENSG00000143228	-0,646	3,24E-05	2,35E-03
ARL5A	ENSG00000162980	-0,701	3,35E-05	2,40E-03
ABCA8	ENSG00000141338	-0,677	3,54E-05	2,53E-03
DIAPH3	ENSG00000139734	-0,353	3,57E-05	2,53E-03

FAHD2CP	ENSG00000231584	0,381	3,69E-05	2,59E-03
FP565260.3	NA	0,391	3,68E-05	2,59E-03
PSMB10	ENSG00000205220	0,328	3,84E-05	2,68E-03
TMEM121	ENSG00000184986	0,381	3,87E-05	2,69E-03
IFITM1	ENSG00000185885	0,366	4,00E-05	2,77E-03
SYNJ1	ENSG00000159082	-0,312	4,26E-05	2,94E-03
EMCN	ENSG00000164035	-0,524	4,30E-05	2,95E-03
IFIT1	ENSG00000185745	0,820	4,33E-05	2,95E-03
CCL14	ENSG00000277236	-0,431	4,57E-05	3,11E-03
VAPA	ENSG00000101558	-0,205	4,75E-05	3,21E-03
ACKR4	ENSG00000129048	-0,562	4,85E-05	3,26E-03
HMGCR	ENSG00000113161	-0,321	4,93E-05	3,30E-03
APAF1	ENSG00000120868	-0,294	5,05E-05	3,35E-03
CLDN14	ENSG00000159261	0,877	5,05E-05	3,35E-03
FBXO32	ENSG00000156804	0,355	5,18E-05	3,42E-03
CSF3	ENSG00000108342	1,066	5,63E-05	3,71E-03
CENPE	ENSG00000138778	-0,750	5,78E-05	3,78E-03
CPLANE2	ENSG00000132881	0,390	5,88E-05	3,83E-03
CAMTA2	ENSG00000108509	0,290	6,00E-05	3,88E-03
SLC22A31	ENSG00000259803	0,695	6,00E-05	3,88E-03
IFI35	ENSG00000068079	0,380	6,14E-05	3,95E-03
ZNF365	ENSG00000138311	0,517	6,32E-05	4,05E-03
PSME1	ENSG00000284916	0,266	6,45E-05	4,11E-03
GDF15	ENSG00000130513	0,428	6,56E-05	4,16E-03
HIBCH	ENSG00000198130	-0,436	6,70E-05	4,24E-03
ACHE	ENSG00000087085	0,801	6,78E-05	4,26E-03
FTH1	ENSG00000167996	0,268	6,87E-05	4,30E-03
RPS6KL1	ENSG00000198208	0,352	6,97E-05	4,35E-03
PTK7	ENSG00000112655	0,269	7,23E-05	4,49E-03
TNFRSF6B	ENSG00000243509	0,338	7,31E-05	4,52E-03
C17orf107	ENSG00000205710	0,459	7,81E-05	4,81E-03
NECTIN3	ENSG00000177707	-0,470	8,03E-05	4,92E-03
RNASE1	ENSG00000129538	-0,276	8,27E-05	5,05E-03
AFF1	ENSG00000172493	-0,327	8,44E-05	5,05E-03
GLRX	ENSG00000173221	-0,240	8,45E-05	5,05E-03
GRASP	NA	0,197	8,45E-05	5,05E-03
LPCAT2	ENSG00000087253	-0,362	8,40E-05	5,05E-03
NFKBIA	ENSG00000100906	0,272	8,34E-05	5,05E-03
INSIG1	ENSG00000186480	-0,278	9,05E-05	5,37E-03
TMOD1	ENSG00000136842	0,496	9,02E-05	5,37E-03
B3GALT4	ENSG00000235155	0,398	9,28E-05	5,43E-03
CCNYL1	ENSG00000163249	-0,395	9,26E-05	5,43E-03
MFAP2	ENSG00000117122	0,276	9,30E-05	5,43E-03
SYNGR3	ENSG00000127561	0,367	9,20E-05	5,43E-03
HTR2B	ENSG00000135914	-0,426	9,46E-05	5,50E-03
ADAM12	ENSG00000148848	1,044	9,52E-05	5,51E-03
MEF2C	ENSG00000081189	-0,347	9,70E-05	5,59E-03
SAPCD2	ENSG00000186193	-0,377	9,74E-05	5,60E-03
MS4A6A	ENSG00000110077	0,466	9,89E-05	5,66E-03
PLTP	ENSG00000100979	0,355	9,95E-05	5,67E-03
CCNA2	ENSG00000145386	-0,400	1,01E-04	5,75E-03
DPP3	ENSG00000254986	0,281	1,02E-04	5,75E-03
P2RY6	ENSG00000171631	1,229	1,03E-04	5,79E-03

MAP6	ENSG00000171533	0,992	1,05E-04	5,88E-03
TCEAL7	ENSG00000182916	0,328	1,05E-04	5,88E-03
TGFBR3L	ENSG00000260001	0,467	1,12E-04	6,18E-03
TMEM132A	ENSG00000006118	0,351	1,11E-04	6,18E-03
WDFY3	ENSG00000163625	-0,381	1,12E-04	6,18E-03
EPSTI1	ENSG00000133106	0,802	1,13E-04	6,22E-03
RND1	ENSG00000172602	0,401	1,15E-04	6,28E-03
HLA-H	ENSG00000231904	0,356	1,15E-04	6,30E-03
MSMO1	ENSG00000052802	-0,536	1,16E-04	6,33E-03
RNMT	ENSG00000101654	-0,425	1,17E-04	6,33E-03
MPHOSPH9	ENSG00000051825	-0,464	1,19E-04	6,44E-03
RAB7B	ENSG00000276600	1,191	1,20E-04	6,46E-03
AMPH	ENSG00000078053	0,488	1,23E-04	6,61E-03
HAS2	ENSG00000170961	1,050	1,30E-04	6,88E-03
KIF4A	ENSG00000090889	-0,318	1,29E-04	6,88E-03
SNX22	ENSG00000157734	0,983	1,30E-04	6,88E-03
AQP1	ENSG00000240583	-1,028	1,33E-04	6,98E-03
H2AC6	ENSG00000180573	-0,697	1,33E-04	6,98E-03
CASP1	ENSG00000137752	0,488	1,34E-04	6,99E-03
COTL1	ENSG00000103187	0,280	1,35E-04	6,99E-03
GSDMD	ENSG00000278718	0,274	1,35E-04	6,99E-03
KIF14	ENSG00000118193	-0,564	1,35E-04	6,99E-03
QTRT2	ENSG00000151576	-0,279	1,34E-04	6,99E-03
EFCAB14	ENSG00000159658	-0,243	1,40E-04	7,20E-03
IER3	ENSG00000235030	0,270	1,40E-04	7,20E-03
RASD1	ENSG00000108551	0,316	1,49E-04	7,60E-03
AOX1	ENSG00000138356	0,614	1,55E-04	7,85E-03
FRY	ENSG00000073910	-0,171	1,55E-04	7,85E-03
NBPF10	ENSG00000271425	-0,326	1,55E-04	7,85E-03
STEAP1	ENSG00000164647	-0,346	1,56E-04	7,86E-03
SULT1B1	ENSG00000173597	-0,498	1,58E-04	7,96E-03
OIP5	ENSG00000104147	-0,352	1,61E-04	8,05E-03
ANKH	ENSG00000154122	0,290	1,63E-04	8,12E-03
TMEM54	ENSG00000121900	0,266	1,64E-04	8,15E-03
SLC1A4	ENSG00000115902	0,234	1,68E-04	8,33E-03
IL11	ENSG00000095752	0,997	1,69E-04	8,34E-03
CGNL1	ENSG00000128849	-0,198	1,73E-04	8,48E-03
NRG1	ENSG00000157168	-0,397	1,73E-04	8,48E-03
RBBP9	ENSG00000089050	-0,332	1,74E-04	8,48E-03
CKS2	ENSG00000123975	-0,336	1,83E-04	8,89E-03
HLA-C	ENSG00000206435	0,313	1,83E-04	8,89E-03
TNIP3	ENSG00000050730	1,038	1,84E-04	8,90E-03
ADAM32	ENSG00000275594	-1,239	1,85E-04	8,91E-03
MYO5A	ENSG00000197535	-0,276	1,85E-04	8,91E-03
ACER3	ENSG00000078124	-0,213	1,97E-04	9,46E-03
RELB	ENSG00000104856	0,353	2,00E-04	9,55E-03
GBP4	ENSG00000162654	0,310	2,02E-04	9,61E-03
RAB11FIP2	ENSG00000107560	-0,544	2,02E-04	9,61E-03
SURF1	ENSG00000280627	0,234	2,04E-04	9,64E-03
MYH10	ENSG00000133026	-0,217	2,09E-04	9,83E-03
PIMREG	ENSG00000129195	-0,446	2,09E-04	9,83E-03
IL1A	ENSG00000115008	0,507	2,18E-04	1,02E-02
GMPPA	ENSG00000144591	0,312	2,20E-04	1,03E-02

ARL6IP1	ENSG00000170540	-0,280	2,22E-04	1,03E-02
CNN3	ENSG00000117519	-0,234	2,24E-04	1,04E-02
GALNT18	ENSG00000110328	0,494	2,25E-04	1,04E-02
FNBP1	ENSG00000187239	-0,269	2,28E-04	1,05E-02
PARP10	ENSG00000178685	0,319	2,28E-04	1,05E-02
MLIP	ENSG00000146147	-0,301	2,45E-04	1,12E-02
TM4SF18	ENSG00000163762	-0,366	2,45E-04	1,12E-02
UBR4	ENSG00000127481	0,376	2,47E-04	1,12E-02
RMDN2	ENSG00000115841	-0,550	2,48E-04	1,13E-02
HOXB9	ENSG00000170689	0,395	2,52E-04	1,14E-02
ARSA	ENSG00000100299	0,292	2,55E-04	1,15E-02
SOCS3	ENSG00000184557	0,302	2,55E-04	1,15E-02
FBLN5	ENSG00000140092	0,404	2,58E-04	1,15E-02
TSPAN5	ENSG00000168785	-0,195	2,58E-04	1,15E-02
RSAD1	ENSG00000136444	0,197	2,64E-04	1,18E-02
ARHGAP11A	ENSG00000275568	-0,412	2,65E-04	1,18E-02
ATP5F1D	ENSG00000099624	0,341	2,66E-04	1,18E-02
NSD2	ENSG00000109685	-0,239	2,68E-04	1,18E-02
ISG15	ENSG00000187608	0,345	2,81E-04	1,23E-02
PBK	ENSG00000168078	-0,449	2,82E-04	1,23E-02
LATS2	ENSG00000150457	-0,211	2,83E-04	1,24E-02
AGRN	ENSG00000188157	0,368	2,93E-04	1,28E-02
TSSC4	ENSG00000184281	0,419	2,95E-04	1,28E-02
PMM1	ENSG00000100417	0,341	3,00E-04	1,30E-02
H2AC11	ENSG00000196787	-0,650	3,06E-04	1,32E-02
EML2	ENSG00000125746	0,311	3,14E-04	1,35E-02
PCDH1	ENSG00000156453	0,269	3,14E-04	1,35E-02
NCKAP5	ENSG00000176771	0,847	3,16E-04	1,35E-02
TSPAN11	ENSG00000110900	-0,360	3,21E-04	1,37E-02
CEP70	ENSG00000114107	-0,520	3,27E-04	1,39E-02
CKAP5	ENSG00000175216	-0,220	3,32E-04	1,40E-02
HSPB8	ENSG00000152137	0,347	3,31E-04	1,40E-02
AHNAK	ENSG00000124942	-0,388	3,34E-04	1,41E-02
CCM2L	ENSG00000101331	-0,325	3,38E-04	1,42E-02
DUSP4	ENSG00000120875	-0,269	3,41E-04	1,43E-02
SULT1E1	ENSG00000109193	-0,482	3,41E-04	1,43E-02
TCIRG1	ENSG00000110719	0,271	3,43E-04	1,43E-02
FXYD2	ENSG00000137731	0,734	3,45E-04	1,43E-02
UBN2	ENSG00000157741	-0,561	3,47E-04	1,44E-02
SPAG5	ENSG00000076382	-0,278	3,49E-04	1,44E-02
THBS2	ENSG00000186340	0,836	3,48E-04	1,44E-02
ZNF800	ENSG00000048405	-0,353	3,52E-04	1,45E-02
SGO2	ENSG00000163535	-0,656	3,64E-04	1,49E-02
GFPT2	ENSG00000131459	0,367	3,69E-04	1,51E-02
APLN	ENSG00000171388	-0,407	3,81E-04	1,55E-02
ARHGAP11B	ENSG00000274734	-0,429	3,86E-04	1,57E-02
JUNB	ENSG00000171223	0,259	3,87E-04	1,57E-02
BPGM	ENSG00000172331	0,259	3,89E-04	1,57E-02
CDH15	ENSG00000129910	0,509	3,90E-04	1,57E-02
MTMR7	ENSG00000003987	0,867	3,93E-04	1,58E-02
ST6GALNAC2	ENSG00000070731	0,756	3,98E-04	1,60E-02
AC241640.1	NA	-1,539	4,06E-04	1,62E-02
SFRP1	ENSG00000104332	-0,311	4,07E-04	1,62E-02

LIG1	ENSG00000105486	0,274	4,10E-04	1,63E-02
SLC7A7	ENSG00000155465	0,298	4,23E-04	1,68E-02
CXCR4	ENSG00000121966	0,237	4,25E-04	1,68E-02
GBGT1	ENSG00000148288	0,343	4,36E-04	1,72E-02
SESN3	ENSG00000149212	-0,641	4,37E-04	1,72E-02
MAPK1	ENSG00000100030	-0,294	4,38E-04	1,72E-02
AC079594.2	NA	-0,631	4,42E-04	1,73E-02
FMNL1	ENSG00000184922	0,395	4,45E-04	1,74E-02
HIVEP1	ENSG00000095951	-0,366	4,48E-04	1,74E-02
PLEKHN1	ENSG00000187583	0,492	4,49E-04	1,74E-02
RBL2	ENSG00000103479	-0,287	4,48E-04	1,74E-02
PTGS2	ENSG00000073756	0,553	4,55E-04	1,76E-02
WNK3	ENSG00000196632	-0,654	4,59E-04	1,77E-02
NMNAT2	ENSG00000157064	0,987	4,62E-04	1,77E-02
TMSB15A	ENSG00000158164	-0,521	4,64E-04	1,77E-02
WASF1	ENSG00000112290	-0,307	4,63E-04	1,77E-02
PTGES3L	ENSG00000267060	1,020	4,69E-04	1,79E-02
GMFG	ENSG00000130755	0,214	4,74E-04	1,80E-02
HP1BP3	ENSG00000127483	-0,314	4,79E-04	1,81E-02
SLC35C2	ENSG00000080189	0,269	4,88E-04	1,84E-02
SLC27A3	ENSG00000263163	0,380	4,93E-04	1,86E-02
CFAP69	ENSG00000105792	-0,585	4,96E-04	1,86E-02
ZBTB42	ENSG00000179627	0,284	4,98E-04	1,87E-02
CPAMD8	ENSG00000160111	0,499	5,08E-04	1,88E-02
MAP1LC3A	ENSG00000101460	0,328	5,06E-04	1,88E-02
MT1L	ENSG00000260549	0,355	5,05E-04	1,88E-02
SMAD5	ENSG00000113658	-0,472	5,07E-04	1,88E-02
SMG1P3	ENSG00000180747	-0,283	5,13E-04	1,90E-02
DAW1	ENSG00000123977	-0,338	5,15E-04	1,90E-02
SLC38A5	ENSG00000017483	0,391	5,18E-04	1,91E-02
ACBD4	ENSG00000181513	0,278	5,27E-04	1,93E-02
SUV39H2	ENSG00000152455	-0,517	5,28E-04	1,93E-02
CPA4	ENSG00000128510	-0,847	5,34E-04	1,94E-02
MROH6	ENSG00000277781	0,678	5,31E-04	1,94E-02
NFATC4	ENSG00000285485	0,371	5,35E-04	1,94E-02
TM7SF3	ENSG00000064115	-0,245	5,34E-04	1,94E-02
UPP1	ENSG00000183696	0,232	5,41E-04	1,96E-02
ADGRB2	ENSG00000121753	0,324	5,56E-04	2,01E-02
ATOH8	ENSG00000168874	0,364	5,61E-04	2,02E-02
KNSTRN	ENSG00000128944	-0,257	5,71E-04	2,04E-02
ODF3B	ENSG00000177989	0,753	5,69E-04	2,04E-02
SERPINB9	ENSG00000170542	0,176	5,69E-04	2,04E-02
PTP4A1	ENSG00000112245	-0,335	5,88E-04	2,09E-02
TMC6	ENSG00000141524	0,276	5,88E-04	2,09E-02
SPTA1	ENSG00000163554	-1,154	5,92E-04	2,10E-02
SENP1	ENSG00000079387	-0,270	5,95E-04	2,11E-02
PIK3CD	ENSG00000171608	0,296	6,11E-04	2,16E-02
SPHK1	ENSG00000176170	0,285	6,15E-04	2,16E-02
TSPAN8	ENSG00000127324	-0,637	6,15E-04	2,16E-02
CD34	ENSG00000174059	-0,226	6,22E-04	2,18E-02
PLAC8	ENSG00000145287	-0,413	6,26E-04	2,19E-02
E2F1	ENSG00000101412	0,419	6,32E-04	2,20E-02
AMOT	ENSG00000126016	-0,550	6,38E-04	2,22E-02

C2CD2	ENSG00000157617	-0,279	6,60E-04	2,28E-02
CST1	ENSG00000170373	0,592	6,60E-04	2,28E-02
SAT1	ENSG00000130066	0,334	6,60E-04	2,28E-02
EFNA2	ENSG00000099617	0,374	6,66E-04	2,30E-02
ANGEL2	ENSG00000174606	-0,371	6,77E-04	2,33E-02
MCM9	ENSG00000111877	-0,297	6,81E-04	2,33E-02
POLD1	ENSG00000062822	0,320	6,82E-04	2,33E-02
SH3TC2	ENSG00000169247	-0,555	6,88E-04	2,35E-02
PHACTR4	ENSG00000204138	-0,233	6,93E-04	2,36E-02
HNRNPLL	ENSG00000143889	-0,211	6,99E-04	2,37E-02
MYO5C	ENSG00000128833	-0,322	7,01E-04	2,37E-02
TREX1	ENSG00000213689	0,275	7,02E-04	2,37E-02
LPAR1	ENSG00000198121	-0,631	7,06E-04	2,38E-02
DNM1P47	ENSG00000259660	-0,477	7,12E-04	2,40E-02
ARHGAP17	ENSG00000288353	-0,465	7,24E-04	2,43E-02
FBXO15	ENSG00000141665	-1,172	7,23E-04	2,43E-02
MMRN1	ENSG00000138722	-0,492	7,26E-04	2,43E-02
TNFSF15	ENSG00000181634	0,218	7,37E-04	2,46E-02
OCLN	ENSG00000273814	-0,336	7,39E-04	2,46E-02
CDK19	ENSG00000155111	-0,377	7,45E-04	2,47E-02
GALT	ENSG00000213930	0,230	7,58E-04	2,51E-02
C2CD4B	ENSG00000205502	0,558	7,68E-04	2,54E-02
IFI44L	ENSG00000137959	0,720	7,78E-04	2,56E-02
CCDC28B	ENSG00000160050	0,254	7,83E-04	2,57E-02
ADM2	ENSG00000128165	0,487	7,92E-04	2,59E-02
GAS2L3	ENSG00000139354	-0,436	7,90E-04	2,59E-02
BATF3	ENSG00000123685	0,662	7,95E-04	2,60E-02
ARNTL	ENSG00000133794	-0,285	8,03E-04	2,61E-02
TPPP3	ENSG00000159713	0,496	8,03E-04	2,61E-02
IPO5	ENSG00000065150	-0,156	8,09E-04	2,63E-02
GPNMB	ENSG00000136235	-0,996	8,15E-04	2,64E-02
IL3RA	ENSG00000185291	0,238	8,30E-04	2,67E-02
PDE3A	ENSG00000172572	-0,239	8,29E-04	2,67E-02
SCUBE3	ENSG00000146197	-0,411	8,38E-04	2,69E-02
ADAMTS12	ENSG00000281690	-0,546	8,53E-04	2,74E-02
PIK3CG	ENSG00000105851	-0,918	8,54E-04	2,74E-02
THOC3	ENSG00000051596	-0,528	8,70E-04	2,78E-02
COL4A2	ENSG00000134871	0,432	8,84E-04	2,82E-02
BLOC1S3	ENSG00000189114	0,447	9,02E-04	2,87E-02
APOBEC3G	ENSG00000239713	0,249	9,11E-04	2,89E-02
DHX58	ENSG00000108771	0,330	9,19E-04	2,91E-02
SGO1	ENSG00000129810	-0,365	9,31E-04	2,94E-02
PIK3R3	ENSG00000117461	-0,301	9,33E-04	2,94E-02
MOBP	ENSG00000168314	0,777	9,37E-04	2,95E-02
RACGAP1	ENSG00000161800	-0,327	9,45E-04	2,97E-02
C19orf47	ENSG00000160392	0,357	9,56E-04	2,99E-02
DHCR7	ENSG00000172893	-0,348	9,60E-04	3,00E-02
FHL3	ENSG00000183386	0,276	9,60E-04	3,00E-02
MELTF	ENSG00000163975	0,373	9,63E-04	3,00E-02
CCNE1	ENSG00000105173	0,263	9,67E-04	3,00E-02
CFAP410	ENSG00000160226	0,304	9,90E-04	3,05E-02
LRRC3	ENSG00000160233	0,273	9,89E-04	3,05E-02
PTTG1	ENSG00000164611	-0,362	9,88E-04	3,05E-02

SLC26A4	ENSG00000091137	-0,719	9,91E-04	3,05E-02
NDE1	ENSG00000275911	-0,219	1,01E-03	3,10E-02
TNFRSF21	ENSG00000146072	0,172	1,01E-03	3,10E-02
MMP28	ENSG00000278843	-1,256	1,02E-03	3,11E-02
WASHC5	ENSG00000164961	-0,200	1,02E-03	3,11E-02
NUDT22	ENSG00000149761	0,284	1,03E-03	3,13E-02
SIPA1	ENSG00000213445	0,279	1,03E-03	3,13E-02
PPP3CA	ENSG00000138814	-0,232	1,04E-03	3,15E-02
MFSD3	ENSG00000167700	0,235	1,04E-03	3,15E-02
TYMP	ENSG00000025708	0,669	1,04E-03	3,16E-02
DNAH5	ENSG00000039139	0,375	1,05E-03	3,16E-02
AC005363.1	NA	6,479	1,06E-03	3,18E-02
IGF2BP3	ENSG00000136231	-0,313	1,06E-03	3,19E-02
FEM1B	ENSG00000169018	-0,299	1,07E-03	3,20E-02
RALB	ENSG00000144118	-0,165	1,07E-03	3,20E-02
ASPHD2	ENSG00000128203	0,209	1,08E-03	3,21E-02
GALNT12	ENSG00000119514	0,317	1,08E-03	3,21E-02
RPL23AP87	ENSG00000232938	2,313	1,08E-03	3,21E-02
COMMD3-BMI1	ENSG00000269897	-0,606	1,09E-03	3,22E-02
CDK20	ENSG00000156345	0,409	1,09E-03	3,22E-02
ACTL10	ENSG00000288649	0,358	1,11E-03	3,23E-02
AKT3	ENSG00000275199	-0,276	1,11E-03	3,23E-02
BEST1	ENSG00000167995	3,000	1,10E-03	3,23E-02
ITPKC	ENSG00000086544	0,230	1,11E-03	3,23E-02
LRG1	ENSG00000171236	0,915	1,10E-03	3,23E-02
TNRC18	ENSG00000182095	-0,235	1,10E-03	3,23E-02
VPS8	ENSG00000156931	-0,319	1,10E-03	3,23E-02
PRRC2B	ENSG00000288701	-0,252	1,11E-03	3,23E-02
CHST6	ENSG00000183196	0,461	1,14E-03	3,30E-02
CLDN10	ENSG00000134873	-0,387	1,16E-03	3,36E-02
ELK3	ENSG00000111145	-0,267	1,16E-03	3,36E-02
IGFBP1	ENSG00000146678	-0,548	1,16E-03	3,36E-02
TXNIP	ENSG00000265972	-0,485	1,16E-03	3,36E-02
GLCE	ENSG00000138604	-0,244	1,17E-03	3,37E-02
PLCD3	ENSG00000161714	-0,285	1,17E-03	3,37E-02
CHKB	ENSG00000100288	0,197	1,19E-03	3,40E-02
POLD4	ENSG00000175482	0,346	1,20E-03	3,42E-02
FCF1	ENSG00000119616	-0,213	1,21E-03	3,43E-02
SP110	ENSG00000135899	0,241	1,20E-03	3,43E-02
LGALS3BP	ENSG00000108679	0,620	1,21E-03	3,43E-02
OAS3	ENSG00000111331	0,322	1,23E-03	3,49E-02
PLEKHA4	ENSG00000105559	0,272	1,24E-03	3,51E-02
ASPHD1	ENSG00000174939	0,680	1,26E-03	3,55E-02
ITPRIPL1	ENSG00000198885	0,456	1,26E-03	3,55E-02
S1PR2	ENSG00000267534	0,346	1,26E-03	3,55E-02
SIRT3	ENSG00000142082	0,207	1,26E-03	3,55E-02
UBA6	ENSG00000033178	-0,346	1,27E-03	3,56E-02
AMDHD2	ENSG00000162066	0,275	1,27E-03	3,56E-02
AGFG1	ENSG00000173744	-0,166	1,29E-03	3,60E-02
DEPDC1	ENSG00000024526	-0,581	1,31E-03	3,66E-02
NCEH1	ENSG00000144959	-0,174	1,32E-03	3,69E-02
STEAP1B	ENSG00000105889	-0,254	1,33E-03	3,71E-02
RMND5A	ENSG00000153561	-0,187	1,35E-03	3,74E-02

APPBP2	ENSG00000062725	-0,365	1,36E-03	3,76E-02
MALL	ENSG00000144063	-0,226	1,36E-03	3,76E-02
MAP3K5	ENSG00000197442	-0,280	1,37E-03	3,78E-02
CCS	ENSG00000173992	0,222	1,38E-03	3,81E-02
SELP	ENSG00000174175	-0,676	1,39E-03	3,81E-02
P4HA2	ENSG00000072682	0,217	1,40E-03	3,84E-02
NUDT18	ENSG00000275074	0,274	1,41E-03	3,86E-02
DOCK4	ENSG00000128512	-0,288	1,43E-03	3,91E-02
SERPINE1	ENSG00000106366	0,263	1,43E-03	3,91E-02
CDC20	ENSG00000117399	-0,358	1,44E-03	3,91E-02
LAMP2	ENSG00000005893	-0,141	1,44E-03	3,91E-02
SAMHD1	ENSG00000101347	-0,369	1,45E-03	3,92E-02
FANCG	ENSG00000221829	0,345	1,45E-03	3,94E-02
KYNU	ENSG00000115919	0,782	1,46E-03	3,95E-02
RSC1A1	ENSG00000215695	-0,388	1,47E-03	3,96E-02
SNX6	ENSG00000129515	-0,454	1,47E-03	3,97E-02
DIS3L	ENSG00000166938	-0,276	1,48E-03	3,98E-02
FLI1	ENSG00000151702	-0,212	1,48E-03	3,98E-02
SMG1P1	ENSG00000237296	-0,304	1,50E-03	4,00E-02
C6orf136	ENSG00000224120	0,223	1,51E-03	4,04E-02
ANKRD55	ENSG00000164512	0,227	1,53E-03	4,07E-02
NUSAP1	ENSG00000137804	-0,257	1,54E-03	4,10E-02
MCTP2	ENSG00000140563	0,553	1,55E-03	4,12E-02
SMIM10	ENSG00000184785	-0,426	1,56E-03	4,12E-02
IRF7	ENSG00000276561	0,301	1,56E-03	4,14E-02
FBXW4	ENSG00000107829	0,228	1,57E-03	4,15E-02
PDXK	ENSG00000160209	0,284	1,60E-03	4,22E-02
SIK1B	ENSG00000275993	0,287	1,62E-03	4,26E-02
ALDH3A2	ENSG00000072210	-0,186	1,62E-03	4,27E-02
MICAL1	ENSG00000135596	0,209	1,63E-03	4,27E-02
RNASEK	ENSG00000219200	0,259	1,63E-03	4,27E-02
POGLUT3	ENSG00000178202	-0,247	1,64E-03	4,29E-02
PIF1	ENSG00000140451	-0,318	1,69E-03	4,39E-02
SQLE	ENSG00000104549	-0,304	1,69E-03	4,39E-02
AP000295.1	NA	-0,791	1,72E-03	4,42E-02
ARHGAP29	ENSG00000137962	-0,385	1,70E-03	4,42E-02
HSD3B7	ENSG00000099377	0,300	1,71E-03	4,42E-02
KAT2B	ENSG00000114166	-0,353	1,72E-03	4,42E-02
LZTFL1	ENSG00000163818	-0,296	1,71E-03	4,42E-02
PARPBP	ENSG00000185480	-0,421	1,72E-03	4,42E-02
RRAS	ENSG00000126458	0,247	1,72E-03	4,42E-02
TAX1BP3	ENSG00000213977	0,221	1,70E-03	4,42E-02
YAP1	ENSG00000137693	-0,249	1,73E-03	4,42E-02
CFLAR	ENSG00000003402	0,156	1,74E-03	4,44E-02
ZBTB21	ENSG00000173276	-0,333	1,74E-03	4,44E-02
NPAS2	ENSG00000170485	-0,270	1,75E-03	4,45E-02
SPIN2B	ENSG00000186787	-0,244	1,75E-03	4,45E-02
ARHGAP4	ENSG00000089820	0,214	1,77E-03	4,48E-02
GPD1L	ENSG00000152642	-0,209	1,77E-03	4,48E-02
MEF2A	ENSG00000068305	-0,344	1,79E-03	4,52E-02
RGS5	ENSG00000232995	-0,291	1,80E-03	4,54E-02
YPEL3	ENSG00000090238	0,217	1,80E-03	4,54E-02
PRRX1	ENSG00000116132	1,003	1,81E-03	4,54E-02

YIPF1	ENSG00000058799	0,223	1,84E-03	4,62E-02
PIEZO2	ENSG00000154864	-0,312	1,85E-03	4,64E-02
IL1R1	ENSG00000115594	-0,282	1,86E-03	4,65E-02
SAMD8	ENSG00000156671	-0,225	1,86E-03	4,66E-02
NUDT4B	ENSG00000177144	-0,160	1,89E-03	4,73E-02
SULF1	ENSG00000137573	-0,415	1,90E-03	4,73E-02
ADGRF3	ENSG00000173567	2,100	1,91E-03	4,75E-02
PGM2	ENSG00000169299	-0,220	1,91E-03	4,75E-02
MOV10	ENSG00000155363	0,221	1,93E-03	4,78E-02
C1S	ENSG00000182326	1,036	1,95E-03	4,83E-02
FAM114A1	ENSG00000197712	-0,168	1,96E-03	4,83E-02
KPNA1	ENSG00000114030	-0,182	1,96E-03	4,83E-02
SCLT1	ENSG00000151466	-0,365	1,98E-03	4,88E-02
MARCHF2	ENSG00000099785	0,189	1,99E-03	4,89E-02
CMKLR1	ENSG00000174600	-1,002	2,00E-03	4,91E-02
DARS2	ENSG00000117593	-0,281	2,01E-03	4,92E-02
B3GAT3	ENSG00000149541	0,247	2,02E-03	4,92E-02
CCDC190	ENSG00000185860	-0,264	2,02E-03	4,92E-02
CD109	ENSG00000156535	-0,318	2,02E-03	4,92E-02
SBNO2	ENSG00000278788	0,304	2,03E-03	4,92E-02
STYXL1	ENSG00000127952	0,217	2,01E-03	4,92E-02
CYSTM1	ENSG00000120306	0,205	2,04E-03	4,95E-02
VPS26A	ENSG00000122958	-0,298	2,05E-03	4,96E-02
PTK2	ENSG00000169398	-0,273	2,06E-03	4,98E-02
PRKAR2B	ENSG00000284096	-0,307	2,07E-03	4,99E-02
RBPMS2	ENSG00000166831	0,311	2,07E-03	4,99E-02
RGS4	ENSG00000117152	-0,258	2,08E-03	5,00E-02
TAP2	ENSG00000225967	0,212	2,08E-03	5,00E-02

Supplementary Table S6: Differentially expressed genes upon LPS treatment of cells expressing APEX1(1-20). DGE calculated using the R package DESeq2 comparing sam-ples of cells transduced with the lentivirus expressing APEX1(1-20) and treated with active LPS versus treated with detoxified LPS. The L2FC (Log 2-fold change) states the average difference in gene expression between both treatments. Positive L2FC values denote upregulation by LPS treatment, negative values downregulation. Wald test from DESeq2 was used to calculate the significance of the change in the expression. The adjusted p-values take the number of tested genes into account, the threshold for the adjusted p-value was 0.05.

gene name	Ensembl gene ID	L2FC	p-value	adusted p-value
LAMC2	ENSG00000058085	2,107	1,12E-198	1,76E-194
SOD2	ENSG00000112096	1,108	1,25E-66	9,84E-63
EBI3	ENSG00000105246	2,271	1,43E-53	7,47E-50
CXCL6	ENSG00000124875	1,655	1,16E-49	4,57E-46
MMP10	ENSG00000166670	1,106	1,31E-46	4,12E-43
CCL2	ENSG00000108691	1,060	7,21E-45	1,88E-41
CTSS	ENSG00000163131	1,287	6,43E-41	1,44E-37
CFB	ENSG00000242335	1,565	1,12E-40	2,21E-37
UBD	ENSG00000226898	2,203	9,00E-40	1,57E-36
CTSK	ENSG00000143387	1,417	1,61E-36	2,53E-33
POU2F2	ENSG00000028277	1,240	1,29E-35	1,83E-32
LTB	ENSG00000223448	1,169	9,43E-27	1,23E-23
IGFBP3	ENSG00000146674	-0,776	2,00E-26	2,42E-23
IL32	ENSG00000008517	1,115	5,74E-26	6,43E-23
CNTNAP1	ENSG00000108797	0,597	1,69E-24	1,77E-21
IFI27	ENSG00000275214	0,640	2,88E-23	2,82E-20
PAPLN	ENSG00000100767	1,408	9,10E-23	8,39E-20
ANO9	ENSG00000185101	4,416	3,91E-20	3,41E-17
ISG20	ENSG00000172183	0,752	1,23E-19	1,02E-16
S100A3	ENSG00000188015	1,601	7,48E-19	5,87E-16
CXCL1	ENSG00000163739	0,959	1,42E-18	1,06E-15
CXCL5	ENSG00000163735	1,745	1,40E-17	9,96E-15
METTL7A	ENSG00000185432	-0,636	3,12E-16	2,13E-13
AC091951.4	NA	4,960	5,48E-16	3,58E-13
THSD4	ENSG00000187720	0,378	6,63E-16	4,16E-13
NEURL1B	ENSG00000214357	-0,822	3,17E-15	1,91E-12
CXCL8	ENSG00000169429	1,039	6,64E-15	3,86E-12
MAMDC2	ENSG00000278608	0,926	2,34E-14	1,31E-11
CR354443.1	NA	32,453	2,78E-14	1,50E-11
CCL15-CCL14	ENSG00000282521	-0,637	6,52E-14	3,30E-11
FCF1P2	ENSG00000228638	-23,428	6,46E-14	3,30E-11
MX1	ENSG00000157601	0,881	1,11E-13	5,45E-11
SLC7A2	ENSG00000003989	0,614	2,48E-13	1,18E-10
H3P6	ENSG00000235655	30,910	2,90E-13	1,34E-10
PLA2G4C	ENSG00000105499	0,669	3,43E-13	1,54E-10
TBC1D3K	ENSG00000275153	-30,254	6,41E-13	2,79E-10
HLA-B	ENSG00000206450	0,830	2,21E-12	9,37E-10
AL451062.4	NA	-29,257	3,51E-12	1,45E-09
LYPD6	ENSG00000187123	0,545	2,51E-11	1,01E-08
ITGB4	ENSG00000132470	-0,899	3,01E-11	1,18E-08
AKAP12	ENSG00000131016	0,392	3,13E-11	1,20E-08
ACBD7	ENSG00000176244	-0,963	3,63E-11	1,34E-08
PXDN	ENSG00000130508	0,668	3,67E-11	1,34E-08
LAMP3	ENSG00000078081	0,580	3,98E-11	1,42E-08
IL4I1	ENSG00000104951	0,582	1,45E-10	5,05E-08

LIPG	ENSG00000101670	0,605	1,48E-10	5,05E-08
CTHRC1	ENSG00000164932	0,586	1,60E-10	5,34E-08
ICAM1	ENSG00000090339	0,518	2,53E-10	8,27E-08
ALOX5AP	ENSG00000132965	1,792	4,57E-10	1,46E-07
CD69	ENSG00000110848	1,109	8,28E-10	2,60E-07
CYB5R2	ENSG00000166394	0,651	9,12E-10	2,80E-07
KLF2	ENSG00000127528	-0,494	1,42E-09	4,28E-07
MMP19	ENSG00000123342	0,700	1,82E-09	5,29E-07
SRP9P1	ENSG00000180581	25,646	1,82E-09	5,29E-07
CD34	ENSG00000174059	-0,395	1,98E-09	5,66E-07
PSMB9	ENSG00000243958	0,523	2,11E-09	5,90E-07
CXCL2	ENSG00000081041	0,820	3,17E-09	8,72E-07
IFI6	ENSG00000126709	0,493	4,18E-09	1,13E-06
KIT	ENSG00000157404	0,351	5,37E-09	1,43E-06
PPL	ENSG00000118898	-1,098	6,56E-09	1,72E-06
TFPI2	ENSG00000105825	0,607	6,91E-09	1,78E-06
C2CD4A	ENSG00000198535	0,816	1,09E-08	2,76E-06
AP005018.2	NA	-23,882	1,38E-08	3,43E-06
CCL14	ENSG00000277236	-0,599	1,43E-08	3,51E-06
F2RL1	ENSG00000164251	0,378	2,81E-08	6,78E-06
RNASE1	ENSG00000129538	-0,388	3,16E-08	7,52E-06
ALDH1A1	ENSG00000165092	-0,420	3,70E-08	8,66E-06
NID2	ENSG00000087303	0,901	4,00E-08	9,23E-06
NFKBIZ	ENSG00000144802	0,715	4,07E-08	9,25E-06
P2RX4	ENSG00000135124	0,313	6,22E-08	1,39E-05
SOX18	ENSG00000203883	-0,314	7,70E-08	1,70E-05
AQP1	ENSG00000240583	-1,437	9,16E-08	2,00E-05
CCNE1	ENSG00000105173	0,424	1,00E-07	2,16E-05
CXCL3	ENSG00000163734	0,498	1,33E-07	2,81E-05
CCL20	ENSG00000115009	0,878	1,41E-07	2,94E-05
ITGAV	ENSG00000138448	0,580	1,45E-07	2,99E-05
ACE	ENSG00000159640	-0,668	1,56E-07	3,18E-05
LYVE1	ENSG00000133800	-0,766	1,64E-07	3,29E-05
TNFRSF9	ENSG00000049249	1,044	2,28E-07	4,53E-05
STAP2	ENSG00000178078	0,406	2,37E-07	4,65E-05
PRICKLE1	ENSG00000139174	-0,462	2,88E-07	5,57E-05
OAS3	ENSG00000111331	0,509	3,18E-07	6,08E-05
ANGPT2	ENSG00000091879	0,361	4,34E-07	8,20E-05
BST1	ENSG00000109743	0,352	5,75E-07	1,07E-04
IL1A	ENSG00000115008	0,680	6,75E-07	1,25E-04
MEST	ENSG00000106484	-0,406	7,83E-07	1,43E-04
CCM2L	ENSG00000101331	-0,448	8,16E-07	1,47E-04
IFIT1	ENSG00000185745	0,962	9,22E-07	1,64E-04
CRACR2B	ENSG00000177685	-0,419	9,45E-07	1,65E-04
OAS1	ENSG00000089127	0,474	9,42E-07	1,65E-04
INHBB	ENSG00000163083	-0,814	9,82E-07	1,69E-04
PAPPA2	ENSG00000116183	1,562	9,88E-07	1,69E-04
TXNIP	ENSG00000265972	-0,730	1,01E-06	1,70E-04
GJA4	ENSG00000187513	-0,568	1,05E-06	1,75E-04
IGFBP4	ENSG00000141753	-0,294	1,18E-06	1,95E-04
TNFSF15	ENSG00000181634	0,311	1,38E-06	2,25E-04
ADAMTS18	ENSG00000140873	-0,514	1,55E-06	2,50E-04
FRY	ENSG00000073910	-0,217	1,61E-06	2,58E-04

PLCD3	ENSG00000161714	-0,419	1,81E-06	2,87E-04
IL7R	ENSG00000168685	0,419	1,89E-06	2,96E-04
TNC	ENSG00000041982	2,315	1,99E-06	3,09E-04
SYNJ2	ENSG00000078269	0,174	2,09E-06	3,21E-04
MSMP	ENSG00000215183	-0,386	3,03E-06	4,62E-04
GMFG	ENSG00000130755	0,286	3,12E-06	4,70E-04
OCIAD2	ENSG00000145247	0,388	3,39E-06	5,07E-04
TMEM120A	ENSG00000189077	0,384	3,56E-06	5,27E-04
CSF2	ENSG00000164400	1,186	3,78E-06	5,54E-04
CREB5	ENSG00000146592	0,326	4,06E-06	5,89E-04
EPSTI1	ENSG00000133106	0,947	4,15E-06	5,93E-04
KIF20A	ENSG00000112984	-0,438	4,16E-06	5,93E-04
PRIM1	ENSG00000198056	0,506	4,50E-06	6,36E-04
TMEM184A	ENSG00000164855	1,991	4,78E-06	6,69E-04
OAS2	ENSG00000111335	0,745	5,53E-06	7,67E-04
CAV1	ENSG00000105974	-0,277	7,04E-06	9,64E-04
NRROS	ENSG00000174004	-0,303	7,06E-06	9,64E-04
TNIP3	ENSG00000050730	1,239	7,28E-06	9,85E-04
ADAMTS15	ENSG00000166106	-1,383	7,59E-06	1,02E-03
TAPBP	ENSG00000206281	0,364	8,63E-06	1,15E-03
ABCG2	ENSG00000118777	-0,578	9,42E-06	1,24E-03
NLRC3	ENSG00000167984	0,376	9,48E-06	1,24E-03
LRRC75A	ENSG00000181350	-0,393	1,00E-05	1,30E-03
PRSS12	ENSG00000164099	0,973	1,02E-05	1,32E-03
IFI44L	ENSG00000137959	0,935	1,18E-05	1,51E-03
EGLN3	ENSG00000129521	-1,171	1,28E-05	1,62E-03
TSPAN11	ENSG00000110900	-0,436	1,33E-05	1,67E-03
QPCT	ENSG00000115828	0,564	1,38E-05	1,72E-03
TNFRSF4	ENSG00000186827	0,805	1,41E-05	1,75E-03
COL1A2	ENSG00000164692	-0,415	1,53E-05	1,87E-03
CCNB2	ENSG00000157456	-0,387	1,64E-05	1,98E-03
EXO1	ENSG00000174371	0,511	1,64E-05	1,98E-03
CFLAR	ENSG00000003402	0,213	1,90E-05	2,27E-03
ZNF365	ENSG00000138311	0,547	2,07E-05	2,47E-03
ALDH1A2	ENSG00000128918	-0,324	2,29E-05	2,68E-03
GALNT18	ENSG00000110328	0,563	2,28E-05	2,68E-03
APLN	ENSG00000171388	-0,484	2,33E-05	2,71E-03
HMGCS1	ENSG00000112972	-0,321	2,41E-05	2,78E-03
ARHGDIG	ENSG00000242173	0,442	2,47E-05	2,83E-03
ZC3H12A	ENSG00000163874	0,454	2,53E-05	2,87E-03
ZNF467	ENSG00000181444	-0,453	3,02E-05	3,40E-03
SELENOT	ENSG00000198843	0,254	3,21E-05	3,59E-03
ACAT2	ENSG00000120437	-0,283	3,27E-05	3,61E-03
GPX3	ENSG00000211445	-0,573	3,27E-05	3,61E-03
GGT5	ENSG00000099998	-0,353	3,35E-05	3,66E-03
HLA-A	ENSG00000227715	0,289	3,36E-05	3,66E-03
SEMA7A	ENSG00000288455	0,486	3,81E-05	4,13E-03
YIPF5	ENSG00000145817	0,269	3,90E-05	4,19E-03
ASS1	ENSG00000130707	-0,446	4,11E-05	4,39E-03
MGARP	ENSG00000137463	-0,451	4,35E-05	4,61E-03
FP565260.3	NA	0,386	4,38E-05	4,61E-03
MALL	ENSG00000144063	-0,288	4,47E-05	4,67E-03
MRAP2	ENSG00000135324	-0,384	4,63E-05	4,81E-03

IL1RL1	ENSG00000115602	0,254	4,78E-05	4,90E-03
RAMP2	ENSG00000131477	-0,465	4,75E-05	4,90E-03
CD44	ENSG00000026508	0,503	5,20E-05	5,30E-03
LRTOMT	ENSG00000184154	-0,402	5,45E-05	5,51E-03
AC005520.3	NA	-1,051	5,60E-05	5,63E-03
CSF3	ENSG00000108342	1,064	5,92E-05	5,91E-03
FBXO32	ENSG00000156804	0,351	6,03E-05	5,99E-03
DHH	ENSG00000139549	-0,365	6,08E-05	5,99E-03
RALB	ENSG00000144118	-0,201	6,25E-05	6,13E-03
HPSE	ENSG00000173083	0,245	6,31E-05	6,15E-03
LGALS3BP	ENSG00000108679	0,760	6,40E-05	6,19E-03
TUSC3	ENSG00000104723	0,294	6,43E-05	6,19E-03
SH3BP1	ENSG00000100092	0,715	6,69E-05	6,40E-03
SMIM3	ENSG00000256235	-0,424	6,75E-05	6,42E-03
NPTN	ENSG00000156642	0,193	6,88E-05	6,51E-03
ABLIM2	ENSG00000163995	-1,741	8,11E-05	7,58E-03
MYRIP	ENSG00000170011	-0,301	8,15E-05	7,58E-03
TCF15	ENSG00000125878	-0,467	8,17E-05	7,58E-03
C4B	ENSG00000224639	-1,377	8,74E-05	7,99E-03
CASP1	ENSG00000137752	0,501	8,76E-05	7,99E-03
KIF12	ENSG00000136883	0,542	8,73E-05	7,99E-03
SERPINA3	ENSG00000196136	1,848	8,87E-05	8,05E-03
COLGALT1	ENSG00000130309	0,367	9,66E-05	8,71E-03
AFF3	ENSG00000144218	1,033	1,05E-04	9,24E-03
EIF3CL	ENSG00000205609	-0,720	1,04E-04	9,24E-03
ERMP1	ENSG00000099219	-0,243	1,04E-04	9,24E-03
HLA-H	ENSG00000231904	0,357	1,05E-04	9,24E-03
SPACA6	ENSG00000182310	-0,405	1,04E-04	9,24E-03
CCNB1	ENSG00000134057	-0,396	1,06E-04	9,27E-03
MYZAP	ENSG00000263155	-0,356	1,19E-04	1,03E-02
C20orf204	ENSG00000196421	-0,498	1,21E-04	1,04E-02
CGNL1	ENSG00000128849	-0,203	1,21E-04	1,04E-02
SLC6A15	ENSG00000072041	0,655	1,22E-04	1,04E-02
DHRS3	ENSG00000162496	0,284	1,24E-04	1,05E-02
OASL	ENSG00000135114	1,044	1,24E-04	1,05E-02
DNAH5	ENSG00000039139	0,437	1,26E-04	1,05E-02
FBLN2	ENSG00000163520	-0,677	1,26E-04	1,05E-02
AOX1	ENSG00000138356	0,620	1,39E-04	1,15E-02
ICOSLG	ENSG00000160223	0,377	1,40E-04	1,15E-02
LHX6	ENSG00000106852	-0,471	1,41E-04	1,15E-02
SLIT3	ENSG00000184347	0,552	1,42E-04	1,16E-02
AC019117.4	NA	8,471	1,44E-04	1,17E-02
MAP3K6	ENSG00000142733	0,299	1,49E-04	1,20E-02
ABI3BP	ENSG00000154175	0,365	1,52E-04	1,22E-02
KYNU	ENSG00000115919	0,927	1,53E-04	1,22E-02
SAPCD2	ENSG00000186193	-0,366	1,52E-04	1,22E-02
MTMR7	ENSG00000003987	0,923	1,53E-04	1,22E-02
GIMAP1	ENSG00000213203	-0,265	1,60E-04	1,26E-02
NQO1	ENSG00000181019	-0,281	1,60E-04	1,26E-02
CASKIN1	ENSG00000167971	-2,314	1,67E-04	1,30E-02
CA4	ENSG00000167434	-1,172	1,76E-04	1,37E-02
LY75-CD302	ENSG00000248672	0,547	1,79E-04	1,38E-02
AC244260.1	NA	8,622	1,92E-04	1,48E-02

CDH4	ENSG00000280641	-0,476	1,93E-04	1,48E-02
GALNT12	ENSG00000119514	0,363	1,95E-04	1,49E-02
PCK2	ENSG00000285241	0,283	2,15E-04	1,63E-02
ABCC2	ENSG00000023839	-0,663	2,17E-04	1,63E-02
CAMSAP3	ENSG00000076826	-0,935	2,17E-04	1,63E-02
GUCY1A1	ENSG00000164116	-0,911	2,21E-04	1,65E-02
MAP3K14	ENSG00000282637	-0,384	2,28E-04	1,70E-02
ALDH1L2	ENSG00000136010	0,311	2,30E-04	1,70E-02
IFI44	ENSG00000137965	0,499	2,32E-04	1,71E-02
BCAM	ENSG00000187244	-0,275	2,37E-04	1,74E-02
TCF7	ENSG00000081059	0,391	2,44E-04	1,78E-02
SCNN1B	ENSG00000168447	-2,117	2,45E-04	1,78E-02
CHRNA1	ENSG00000138435	0,426	2,48E-04	1,79E-02
PLAAT4	ENSG00000133321	0,548	2,56E-04	1,84E-02
CYP1A1	ENSG00000140465	-0,508	2,66E-04	1,91E-02
PRCP	ENSG00000137509	0,175	2,71E-04	1,93E-02
NOS3	ENSG00000164867	-0,330	2,80E-04	1,99E-02
CLEC14A	ENSG00000176435	-0,190	2,82E-04	1,99E-02
IFI35	ENSG00000068079	0,344	2,86E-04	2,01E-02
PTGS2	ENSG00000073756	0,572	2,92E-04	2,05E-02
POSTN	ENSG00000133110	-0,539	3,01E-04	2,10E-02
DUXAP9	ENSG00000225210	0,284	3,07E-04	2,13E-02
MYPN	ENSG00000138347	0,620	3,15E-04	2,17E-02
PIR	ENSG00000087842	-0,566	3,27E-04	2,25E-02
AK4	ENSG00000162433	0,170	3,35E-04	2,29E-02
IFT122	ENSG00000163913	-0,270	3,36E-04	2,29E-02
P2RY6	ENSG00000171631	1,128	3,53E-04	2,40E-02
DPYSL3	ENSG00000113657	0,257	3,60E-04	2,43E-02
ATP2B4	ENSG00000058668	-0,175	3,69E-04	2,48E-02
GK	ENSG00000198814	0,285	3,79E-04	2,52E-02
SELENOM	ENSG00000198832	0,345	3,78E-04	2,52E-02
ZNF219	ENSG00000165804	-0,385	3,80E-04	2,52E-02
PIEZO2	ENSG00000154864	-0,355	3,88E-04	2,57E-02
STC1	ENSG00000159167	-0,462	3,91E-04	2,58E-02
APOD	ENSG00000189058	0,347	4,06E-04	2,64E-02
ATAD2	ENSG00000156802	0,366	4,10E-04	2,64E-02
BUB1	ENSG00000169679	-0,310	4,11E-04	2,64E-02
GPNMB	ENSG00000136235	-1,050	4,09E-04	2,64E-02
NOS1	ENSG00000089250	-2,260	4,09E-04	2,64E-02
PCDH1	ENSG00000156453	0,264	4,06E-04	2,64E-02
DLL1	ENSG00000275555	-0,370	4,21E-04	2,69E-02
ENOSF1	ENSG00000132199	-0,301	4,25E-04	2,71E-02
TMOD1	ENSG00000136842	0,445	4,30E-04	2,72E-02
TSPAN8	ENSG00000127324	-0,646	4,30E-04	2,72E-02
CLEC3B	ENSG00000163815	-1,195	4,35E-04	2,74E-02
SLCO2A1	ENSG00000174640	-0,674	4,36E-04	2,74E-02
PLA2G5	ENSG00000127472	1,414	4,50E-04	2,80E-02
RASSF10	ENSG00000189431	-1,470	4,49E-04	2,80E-02
AMPD3	ENSG00000133805	0,780	4,55E-04	2,81E-02
LRP12	ENSG00000147650	0,252	4,54E-04	2,81E-02
CHAF1A	ENSG00000167670	0,466	4,61E-04	2,83E-02
PRRT2	ENSG00000167371	2,229	4,61E-04	2,83E-02
HSPB6	ENSG00000004776	-0,351	4,65E-04	2,83E-02

WNT9A	ENSG00000143816	-0,439	4,66E-04	2,83E-02
CACHD1	ENSG00000158966	0,277	4,80E-04	2,91E-02
GSTM2	ENSG00000213366	-0,342	4,84E-04	2,92E-02
CD36	ENSG00000135218	-0,760	4,87E-04	2,93E-02
TNFSF18	ENSG00000120337	-0,366	5,05E-04	3,02E-02
CST1	ENSG00000170373	0,610	5,07E-04	3,02E-02
KCNN4	ENSG00000104783	-0,792	5,12E-04	3,04E-02
SHE	ENSG00000169291	-0,219	5,15E-04	3,05E-02
DUSP4	ENSG00000120875	-0,261	5,23E-04	3,09E-02
CENPBD1	ENSG00000177946	0,199	5,36E-04	3,14E-02
TM7SF2	ENSG00000149809	-0,335	5,35E-04	3,14E-02
HSPB8	ENSG00000152137	0,334	5,44E-04	3,18E-02
IGFBP1	ENSG00000146678	-0,582	5,65E-04	3,27E-02
UBE2L6	ENSG00000156587	0,205	5,64E-04	3,27E-02
SYT7	ENSG00000011347	-0,953	5,70E-04	3,29E-02
SLC15A3	ENSG00000110446	0,327	5,73E-04	3,29E-02
ZFPM2	ENSG00000169946	0,369	5,92E-04	3,39E-02
CDC20	ENSG00000117399	-0,386	6,03E-04	3,44E-02
ANKRD44	ENSG00000065413	-0,767	6,07E-04	3,45E-02
NTSR1	ENSG00000101188	-0,347	6,10E-04	3,46E-02
DNAH11	ENSG00000105877	0,366	6,21E-04	3,50E-02
CLSPN	ENSG00000092853	0,378	6,31E-04	3,55E-02
FAM221A	ENSG00000188732	-0,310	6,40E-04	3,55E-02
PIK3R3	ENSG00000117461	-0,311	6,35E-04	3,55E-02
PLSCR1	ENSG00000188313	0,208	6,38E-04	3,55E-02
RTN4RL1	ENSG00000185924	-2,401	6,39E-04	3,55E-02
BDKRB2	ENSG00000168398	0,651	6,48E-04	3,55E-02
CDC25B	ENSG00000101224	-0,240	6,46E-04	3,55E-02
MOBP	ENSG00000168314	0,795	6,44E-04	3,55E-02
NFIA	ENSG00000162599	-0,403	6,63E-04	3,63E-02
GIMAP8	ENSG00000171115	-0,227	6,76E-04	3,68E-02
PARD6A	ENSG00000102981	-0,362	6,88E-04	3,74E-02
ADGRF3	ENSG00000173567	2,256	7,00E-04	3,78E-02
PSMB8	ENSG00000230669	0,220	7,14E-04	3,85E-02
CCL23	ENSG00000276114	-0,826	7,24E-04	3,88E-02
RASGRF2	ENSG00000113319	0,347	7,24E-04	3,88E-02
C1orf115	ENSG00000162817	-0,180	7,31E-04	3,90E-02
NUAK1	ENSG00000074590	0,442	7,38E-04	3,93E-02
AUNIP	ENSG00000127423	0,412	7,58E-04	4,00E-02
FSTL3	ENSG00000070404	0,289	7,58E-04	4,00E-02
ARSK	ENSG00000164291	0,211	7,70E-04	4,04E-02
MXD3	ENSG00000213347	-0,387	7,69E-04	4,04E-02
CLEC1A	ENSG00000150048	0,182	7,77E-04	4,06E-02
HTR2B	ENSG00000135914	-0,366	8,16E-04	4,25E-02
BTD	ENSG00000169814	-0,185	8,29E-04	4,29E-02
TCN2	ENSG00000185339	-0,295	8,26E-04	4,29E-02
TSPAN5	ENSG00000168785	-0,178	8,41E-04	4,34E-02
CIT	ENSG00000122966	-0,302	8,70E-04	4,48E-02
ZDHHC13	ENSG00000177054	-0,211	8,97E-04	4,60E-02
ACKR4	ENSG00000129048	-0,454	9,16E-04	4,63E-02
ARL14EPL	ENSG00000268223	-0,995	9,21E-04	4,63E-02
MATN2	ENSG00000132561	-0,529	9,21E-04	4,63E-02
PDE1C	ENSG00000154678	0,280	9,17E-04	4,63E-02

RGS2	ENSG00000116741	0,398	9,15E-04	4,63E-02
SULF1	ENSG00000137573	-0,443	9,12E-04	4,63E-02
CYP51A1	ENSG00000001630	-0,193	9,28E-04	4,65E-02
ARHGEF26	ENSG00000277101	0,351	9,35E-04	4,67E-02
TUBB2B	ENSG00000137285	0,445	9,73E-04	4,84E-02
BTG2	ENSG00000159388	-0,190	9,94E-04	4,93E-02

Supplementary Table S7: Genes upregulated by LPS exclusively in cells that do not express APEX1(1-20). To identify genes upregulated by LPS specifically in cells transduced with the empty virus, but not in cells expressing moderate levels of APEX1(1- 20), the results of the DGE analysis of both cells populations after treatment with detoxified (con) or active LPS (LPS) were combined. The L2FC (Log 2-fold change) states the average difference in gene expression between both treatments, positive values denote upregulation by LPS treatment. Wald test from DESeq2 was used to calculate the significance of the change in the expression. The adjusted p-values take the number of tested genes into account, the threshold for the adjusted p-value was 0.05. Mean expression levels per sample group are stated in transcripts per million (TPM), calculated during quasi-mapping with the tool salmon. The list is sorted by gene expression.

gene name	L2FC	adjusted p-value	mean TPM empty virus con	mean TPM empty virus LPS	mean TPM APEX1(1-20) con	mean TPM APEX1(1-20) LPS
FTH1	0,268	4,30E-03	4639,36	5565,16	4723,13	5429,98
SERPINE1	0,263	3,91E-02	2753,76	3306,84	2860,91	3352,05
SAT1	0,334	2,28E-02	372,10	468,58	420,02	491,31
RNASEK	0,259	4,27E-02	302,79	362,46	319,66	347,36
GDF15	0,428	4,16E-03	181,22	243,01	186,96	225,56
TAX1BP3	0,221	4,42E-02	166,16	193,15	174,50	184,39
COTL1	0,280	6,99E-03	165,55	200,62	173,08	192,33
COL4A2	0,432	2,82E-02	148,83	198,87	156,04	201,24
PSME1	0,266	4,11E-03	147,10	176,17	153,10	168,61
PSME2	0,443	8,81E-05	134,36	181,67	140,36	171,61
RRAS	0,247	4,42E-02	128,19	152,15	131,01	143,27
HLA-C	0,313	8,89E-03	120,68	149,68	127,87	149,23
MT1L	0,355	1,88E-02	119,01	151,73	116,61	144,39
IER3	0,270	7,20E-03	100,45	120,93	107,70	115,41
ATP5F1D	0,341	1,18E-02	92,26	116,67	100,23	97,38
MFAP2	0,276	5,43E-03	70,80	85,75	75,64	78,59
CYSTM1	0,205	4,95E-02	68,11	78,37	68,82	69,97
SPHK1	0,285	2,16E-02	64,57	78,63	65,73	71,53
PDXK	0,284	4,22E-02	63,89	77,58	69,04	72,86
STYXL1	0,217	4,92E-02	55,70	64,54	53,68	57,32
BPGM	0,259	1,57E-02	47,34	56,61	48,03	56,46
PLCG1	0,243	5,56E-04	46,66	55,06	50,10	50,59
NFKBIA	0,272	5,05E-03	44,13	53,19	48,70	53,45
P4HA2	0,217	3,84E-02	41,12	47,65	40,49	44,88
ISG15	0,345	1,23E-02	40,32	51,21	43,32	50,22
SERPINB9	0,176	2,04E-02	40,12	45,26	43,72	46,50
DPP3	0,281	5,75E-03	39,09	47,59	39,50	45,15
CXCR4	0,237	1,68E-02	37,57	44,12	36,06	41,30
TSPAN13	0,390	8,14E-04	36,14	47,46	38,66	43,40
BST2	0,315	7,15E-04	35,86	44,46	37,59	42,84
SIPA1	0,279	3,13E-02	32,32	39,17	34,52	35,80
TMEM132A	0,351	6,18E-03	31,27	39,93	34,67	35,67
POLD4	0,346	3,42E-02	28,60	36,48	29,78	31,91
UPP1	0,232	1,96E-02	28,15	32,94	27,23	31,38
GMPPA	0,312	1,03E-02	28,14	34,92	28,84	32,19
PSMB10	0,328	2,68E-03	27,59	34,55	28,71	32,02
YPEL3	0,217	4,54E-02	26,38	30,64	29,57	28,61
GSDMD	0,274	6,99E-03	25,96	31,39	27,55	29,02
FHL3	0,276	3,00E-02	25,68	31,13	27,18	29,16
PLTP	0,355	5,67E-03	25,47	32,76	27,27	31,30
MARCHF2	0,189	4,89E-02	23,89	27,20	26,73	24,84
TMEM54	0,266	8,15E-03	23,67	28,40	25,16	25,07
NUDT22	0,284	3,13E-02	22,84	27,79	24,16	24,80
TNFRSF21	0,172	3,10E-02	22,78	25,62	24,02	26,02
UBR4	0,376	1,12E-02	22,72	29,57	22,32	25,97

ANKH	0,290	8,12E-03	22,47	27,49	22,50	24,26
GRASP	0,197	5,05E-03	22,21	25,48	23,13	23,42
AGRN	0,368	1,28E-02	21,33	27,78	21,89	26,02
MOV10	0,221	4,78E-02	20,49	23,73	21,01	20,55
FBLN5	0,404	1,15E-02	19,17	25,33	21,56	26,50
TSSC4	0,419	1,28E-02	18,98	25,48	19,43	19,63
TCIRG1	0,271	1,43E-02	18,05	21,85	19,29	20,30
EML2	0,311	1,35E-02	17,59	21,82	19,57	18,49
SURF1	0,234	9,64E-03	17,51	20,53	18,53	18,21
RSAD1	0,197	1,18E-02	16,94	19,36	17,55	18,60
CCS	0,222	3,81E-02	16,90	19,69	17,92	17,70
GBGT1	0,343	1,72E-02	16,83	21,36	17,33	19,51
SLC35C2	0,269	1,84E-02	16,83	20,30	17,60	18,66
CHKB	0,197	3,40E-02	16,68	19,04	17,40	17,25
LIG1	0,274	1,63E-02	16,52	19,88	15,96	18,60
SDC4	0,352	6,93E-04	16,38	20,79	17,77	19,54
STARD10	0,569	4,79E-07	16,35	24,40	18,98	22,60
SLC38A5	0,391	1,91E-02	16,17	21,13	18,27	19,16
MAP1LC3A	0,328	1,88E-02	15,91	19,99	17,73	18,79
LRFN4	0,375	9,94E-04	15,46	19,96	17,12	17,34
APOL1	0,388	1,24E-06	14,89	19,46	17,09	18,97
CAMTA2	0,290	3,88E-03	14,70	17,96	13,71	15,09
CRTAC1	0,499	2,49E-05	14,63	20,56	15,89	19,72
YIPF1	0,223	4,62E-02	14,38	16,72	14,35	15,65
MICAL1	0,209	4,27E-02	14,02	16,23	14,04	15,16
TNFRSF6B	0,338	4,52E-03	13,87	17,58	14,85	15,80
JUNB	0,259	1,57E-02	13,62	16,41	14,14	15,42
SBNO2	0,304	4,92E-02	13,55	16,80	14,23	16,14
NFATC4	0,371	1,94E-02	13,55	17,33	16,04	14,90
C6orf136	0,223	4,04E-02	13,28	15,48	12,90	13,51
POLD1	0,320	2,33E-02	12,27	15,26	12,21	14,22
B3GAT3	0,247	4,92E-02	12,23	14,49	12,50	13,71
GALT	0,230	2,51E-02	12,15	14,22	13,09	13,54
PTK7	0,269	4,49E-03	12,13	14,54	12,75	13,40
CCDC28B	0,254	2,57E-02	11,16	13,29	11,61	12,56
TAP2	0,212	5,00E-02	10,59	12,21	10,79	11,33
TNFRSF14	0,388	1,03E-03	10,32	13,55	11,52	13,07
IFITM1	0,366	2,77E-03	10,28	13,27	11,68	13,46
TMC6	0,276	2,09E-02	9,99	12,12	10,48	11,78
CBR3	0,357	1,62E-03	9,82	12,53	10,15	11,75
FBXW4	0,228	4,15E-02	9,73	11,36	10,21	10,78
FANCG	0,345	3,94E-02	9,48	12,03	9,66	10,17
SLC7A7	0,298	1,68E-02	9,01	11,09	9,71	10,53
ITPKC	0,230	3,23E-02	8,88	10,40	9,02	9,99
MFSD3	0,235	3,15E-02	8,42	9,89	8,93	8,74
SP110	0,241	3,43E-02	8,34	9,85	8,64	9,84
IRF9	0,498	1,26E-03	8,34	11,68	8,74	10,84
SIRT3	0,207	3,55E-02	8,30	9,56	8,63	8,25
UBA7	0,446	6,02E-06	7,69	10,51	8,69	10,17
TREX1	0,275	2,37E-02	7,35	8,84	7,15	8,25
IL3RA	0,238	2,67E-02	7,32	8,63	8,49	8,64
PARP10	0,319	1,05E-02	7,31	9,12	7,17	8,69
SLC27A3	0,380	1,86E-02	7,02	9,15	7,23	8,06

ULBP2	0,338	1,95E-03	6,99	8,81	7,68	8,43
C19orf47	0,357	2,99E-02	6,93	8,83	7,20	8,14
ARHGAP4	0,214	4,48E-02	6,92	8,02	7,26	6,77
RELB	0,353	9,55E-03	6,79	8,68	7,33	7,87
MS4A6A	0,466	5,66E-03	6,75	9,31	6,92	8,42
LAMB3	0,446	2,35E-03	6,66	9,08	6,82	7,85
SOCS3	0,302	1,15E-02	6,29	7,77	6,34	7,05
AMDHD2	0,275	3,56E-02	6,18	7,50	6,51	7,01
ARSA	0,292	1,15E-02	6,12	7,50	6,64	7,17
TCEAL7	0,328	5,88E-03	6,06	7,61	7,03	7,48
PMM1	0,341	1,30E-02	5,47	6,91	5,80	6,62
RPS6KL1	0,352	4,35E-03	5,18	6,57	6,25	6,57
APOBEC3G	0,249	2,89E-02	5,17	6,13	5,50	6,00
SAMD14	0,369	6,93E-04	5,09	6,59	5,72	6,44
E2F1	0,419	2,20E-02	5,08	6,74	5,14	6,70
RND1	0,401	6,28E-03	4,89	6,53	5,96	7,31
MTMR11	0,364	1,27E-03	4,50	5,80	4,61	5,11
PLCG2	1,263	8,65E-05	4,47	10,93	6,94	9,00
GFPT2	0,367	1,51E-02	4,46	5,74	4,86	6,11
PAQR7	0,277	1,42E-04	4,36	5,28	4,58	4,75
BLOC1S3	0,447	2,87E-02	4,25	5,83	5,33	4,58
NUDT18	0,274	3,86E-02	4,17	5,03	4,43	4,75
RASD1	0,316	7,60E-03	4,10	5,11	4,04	4,80
ANKRD55	0,227	4,07E-02	3,96	4,62	4,03	4,54
CERS1	0,381	4,90E-04	3,71	4,83	3,84	4,15
PLEKHA4	0,272	3,51E-02	3,61	4,37	3,79	4,16
TAPBPL	0,812	1,61E-04	3,35	5,70	4,36	4,51
SLC1A4	0,234	8,33E-03	3,22	3,78	3,42	3,70
CPLANE2	0,390	3,83E-03	3,18	4,17	3,23	3,57
SEMA3G	0,417	2,76E-04	3,17	4,24	3,57	4,37
CFAP410	0,304	3,05E-02	3,16	3,91	3,60	3,41
GBP4	0,310	9,61E-03	3,06	3,80	3,21	3,55
ACBD4	0,278	1,93E-02	2,93	3,55	3,31	3,18
CEBPD	0,785	1,63E-06	2,89	5,00	3,62	4,84
ACSS1	0,279	1,11E-04	2,85	3,45	2,97	3,29
RASA4	0,440	5,93E-04	2,80	3,81	3,00	3,68
IL27RA	0,362	1,14E-03	2,67	3,43	2,87	3,38
AMPH	0,488	6,61E-03	2,65	3,70	3,11	4,11
IRF7	0,301	4,14E-02	2,59	3,20	2,64	3,21
ASPHD2	0,209	3,21E-02	2,57	2,97	2,85	3,03
DENND2B	0,984	5,79E-06	2,56	4,92	3,05	3,49
PIK3CD	0,296	2,16E-02	2,54	3,14	2,75	3,18
SIK1B	0,287	4,26E-02	2,53	3,07	2,62	2,94
TMEM121	0,381	2,69E-03	2,44	3,17	2,82	2,99
C2CD4B	0,558	2,54E-02	2,43	3,57	2,65	3,46
TYMP	0,669	3,16E-02	2,16	3,43	3,14	3,38
FAHD2CP	0,381	2,59E-03	2,10	2,73	2,39	2,42
DHX58	0,330	2,91E-02	2,01	2,53	2,18	2,56
C11orf96	0,453	5,30E-04	1,98	2,72	2,22	2,34
VWA1	0,476	8,05E-07	1,95	2,71	2,18	2,54
RBPMS2	0,311	4,99E-02	1,84	2,28	1,97	2,08
SYNGR3	0,367	5,43E-03	1,82	2,36	2,02	2,27
ATOH8	0,364	2,02E-02	1,80	2,32	1,95	2,21

ARHGEF19	0,356	2,64E-04	1,59	2,04	1,71	1,88
TGFBR3L	0,467	6,18E-03	1,51	2,09	1,60	1,69
LRRC3	0,273	3,05E-02	1,31	1,58	1,35	1,52
RASA4B	0,567	1,42E-04	1,29	1,90	1,43	1,79
ZBTB42	0,284	1,87E-02	1,28	1,55	1,37	1,51
HSD3B7	0,300	4,42E-02	1,21	1,50	1,34	1,44
ITPRIPL1	0,456	3,55E-02	1,08	1,48	1,41	1,49
B3GALT4	0,398	5,43E-03	0,99	1,30	1,03	1,16
CX3CL1	0,553	1,96E-03	0,93	1,37	1,30	1,38
FMNL1	0,395	1,74E-02	0,93	1,23	1,10	1,15
AC005363.1	6,479	3,18E-02	0,89	3,89	2,74	2,46
ASPHD1	0,680	3,55E-02	0,87	1,41	1,44	1,44
CPAMD8	0,499	1,88E-02	0,77	1,10	0,82	0,96
FXYD6	0,656	9,95E-04	0,75	1,19	0,96	1,14
ODF3B	0,753	2,04E-02	0,74	1,25	0,82	1,21
MROH6	0,678	1,94E-02	0,69	1,10	1,10	0,90
ADM2	0,487	2,59E-02	0,65	0,91	0,65	0,81
FXYD2	0,734	1,43E-02	0,63	1,04	0,67	0,79
BATF3	0,662	2,60E-02	0,63	0,99	0,73	0,85
SLC22A31	0,695	3,88E-03	0,58	0,93	0,79	0,87
MELTF	0,373	3,00E-02	0,55	0,71	0,61	0,69
PLEKHN1	0,492	1,74E-02	0,54	0,76	0,52	0,70
TPPP3	0,496	2,61E-02	0,54	0,75	0,51	0,70
CDK20	0,409	3,22E-02	0,53	0,71	0,58	0,63
ACTL10	0,358	3,23E-02	0,50	0,64	0,54	0,56
HOXB9	0,395	1,14E-02	0,49	0,65	0,48	0,58
ADGRB2	0,324	2,01E-02	0,47	0,59	0,50	0,57
MCTP2	0,553	4,12E-02	0,44	0,64	0,58	0,53
ST6GALNAC2	0,756	1,60E-02	0,37	0,63	0,46	0,53
CDH15	0,509	1,57E-02	0,36	0,52	0,40	0,51
EFNA2	0,374	2,30E-02	0,34	0,44	0,39	0,39
JAK3	0,743	1,86E-05	0,33	0,56	0,40	0,55
C17orf107	0,459	4,81E-03	0,32	0,43	0,35	0,44
S1PR2	0,346	3,55E-02	0,29	0,37	0,33	0,37
NCKAP5	0,847	1,35E-02	0,27	0,49	0,33	0,50
NMNAT2	0,987	1,77E-02	0,21	0,41	0,27	0,35
PRRX1	1,003	4,54E-02	0,18	0,35	0,25	0,39
GXYLT2	1,226	2,85E-04	0,16	0,38	0,22	0,39
CLDN14	0,877	3,35E-03	0,15	0,28	0,20	0,25
CHST6	0,461	3,30E-02	0,15	0,21	0,15	0,21
SNX22	0,983	6,88E-03	0,14	0,29	0,16	0,18
ACHE	0,801	4,26E-03	0,13	0,23	0,14	0,22
IL11	0,997	8,34E-03	0,10	0,21	0,12	0,18
PTGES3L	1,020	1,79E-02	0,10	0,20	0,15	0,16
PLA1A	1,472	1,66E-06	0,10	0,27	0,14	0,24
C1S	1,036	4,83E-02	0,09	0,17	0,15	0,20
BEST1	3,000	3,23E-02	0,08	0,53	0,13	0,17
THBS2	0,836	1,44E-02	0,08	0,14	0,13	0,14
HAS2	1,050	6,88E-03	0,07	0,15	0,08	0,14
LRG1	0,915	3,23E-02	0,07	0,13	0,11	0,13
MAP6	0,992	5,88E-03	0,07	0,14	0,08	0,09
RAB7B	1,191	6,46E-03	0,05	0,12	0,08	0,10
RPL23AP87	2,313	3,21E-02	0,04	0,13	0,10	0,09

ADAM12	1,044	5,51E-03	0,04	0,08	0,04	0,07
MX2	2,548	8,60E-07	0,02	0,13	0,08	0,13
AL358472.7	20,830	1,46E-05	0,00	0,08	0,15	0,14

Supplementary Table S8: Genes downregulated by LPS exclusively in cells that do not express APEX1(1-20). To identify genes downregulated by LPS specifically in cells transduced with the empty virus, but not in cells expressing moderate levels of APEX1(1-20), the results of the DGE analysis of both cells populations after treatment with detoxified (con) or active LPS (LPS) were combined. The L2FC (Log 2-fold change) states the average difference in gene expression between both treatments, negative values denote downregulation by LPS treatment. Wald test from DESeq2 was used to calculate the significance of the change in the expression. The adjusted p-values take the number of tested genes into account, the threshold for the adjusted p-value was 0.05. Mean expression levels per sample group are stated in transcripts per million (TPM), calculated during quasi-mapping with the tool salmon. The list is sorted by gene expression.

gene name	L2FC	adjusted p-value	mean TPM empty virus con	mean TPM empty virus LPS	mean TPM APEX1(1-20) con	mean TPM APEX1(1-20) LPS
RGS5	-0,291	4,54E-02	1386,54	1138,17	1251,47	1178,35
MMRN1	-0,492	2,43E-02	888,40	637,40	859,18	699,02
VAPA	-0,205	3,21E-03	313,94	271,48	297,11	303,08
CKS2	-0,336	8,89E-03	287,78	228,74	288,97	258,79
PTTG1	-0,362	3,05E-02	285,06	221,31	276,16	228,63
NUCKS1	-0,368	3,27E-04	284,56	220,50	261,59	233,58
CNN3	-0,234	1,04E-02	273,16	231,87	274,05	257,51
CAPN2	-0,289	2,95E-06	260,46	212,68	252,84	228,05
PDCD6IP	-0,363	9,81E-04	189,22	147,31	181,29	183,72
IGF2BP3	-0,313	3,19E-02	182,15	146,90	163,66	171,08
ARL6IP1	-0,280	1,03E-02	162,45	133,86	160,85	137,37
SNX6	-0,454	3,97E-02	159,65	118,82	151,27	147,95
MCFD2	-0,277	7,05E-04	157,06	129,31	155,90	143,20
IPO5	-0,156	2,63E-02	149,62	133,94	146,54	145,32
LAMP2	-0,141	3,91E-02	147,87	133,68	145,02	147,45
PTK2	-0,273	4,98E-02	145,61	121,03	138,06	135,72
ARHGAP29	-0,385	4,42E-02	141,45	109,71	132,43	135,02
HP1BP3	-0,314	1,81E-02	139,47	112,32	131,88	120,54
RGS4	-0,258	5,00E-02	114,80	95,98	117,02	111,04
PRRC2B	-0,252	3,23E-02	112,97	94,70	107,19	104,11
CKAP5	-0,220	1,40E-02	107,89	92,55	102,33	94,75
VPS26A	-0,298	4,96E-02	107,19	87,14	98,37	102,76
TM7SF3	-0,245	1,94E-02	106,30	89,77	104,10	90,06
AHNAK	-0,388	1,41E-02	101,72	77,57	93,38	81,88
THOC3	-0,528	2,78E-02	101,44	70,86	81,58	81,55
NUDT4B	-0,160	4,73E-02	92,42	82,58	90,47	93,70
FAM114A1	-0,168	4,83E-02	92,21	81,82	91,47	90,41
ELK3	-0,267	3,36E-02	91,79	76,37	93,11	78,44
FLI1	-0,212	3,98E-02	90,93	78,68	90,90	82,08
MAPK1	-0,294	1,72E-02	88,64	72,59	86,09	85,87
SULT1B1	-0,498	7,96E-03	86,27	62,34	85,35	79,53
RAB14	-0,247	2,01E-03	85,29	71,61	83,80	80,96
DLGAP5	-0,621	7,41E-06	84,10	55,05	72,73	62,97
KPNA1	-0,182	4,83E-02	80,12	70,56	80,77	79,17
TMPO	-0,320	1,16E-03	79,02	63,21	73,14	75,58
AGFG1	-0,166	3,60E-02	78,64	69,89	77,52	78,78
PRR11	-0,326	5,24E-05	74,01	58,87	71,40	62,27
ARHGAP17	-0,465	2,43E-02	71,96	53,09	76,26	67,74
PTP4A1	-0,335	2,09E-02	71,32	56,77	71,78	69,82
AKT3	-0,276	3,23E-02	71,04	58,58	66,66	64,85
STEAP1B	-0,254	3,71E-02	70,66	59,27	73,25	67,94
FCF1	-0,213	3,43E-02	69,65	59,97	67,01	66,79
PGM2	-0,220	4,75E-02	67,65	58,03	64,30	59,35
NSD2	-0,239	1,18E-02	67,24	56,91	65,10	62,85
TOP2A	-0,435	2,01E-03	67,10	49,88	58,96	54,26

GLCE	-0,244	3,37E-02	66,72	56,47	67,09	61,35
EMCN	-0,524	2,95E-03	65,39	45,79	65,19	55,42
STEAP1	-0,346	7,86E-03	65,27	51,70	64,46	60,41
CD109	-0,318	4,92E-02	63,96	51,58	63,33	60,06
PRKAR2B	-0,307	4,99E-02	62,84	50,99	58,45	55,49
MYO5A	-0,276	8,91E-03	61,34	50,76	56,95	55,68
MSMO1	-0,536	6,33E-03	61,34	42,78	64,09	49,27
CDKN3	-0,614	2,21E-07	60,40	40,00	55,86	45,06
DOCK4	-0,288	3,91E-02	56,86	46,75	51,87	53,14
NPAS2	-0,270	4,45E-02	56,84	47,48	55,26	51,55
ASAP1	-0,339	8,50E-04	56,74	45,02	56,96	51,04
CKAP2	-0,456	3,39E-04	55,75	40,66	49,92	48,53
SPTLC1P1	-0,705	1,91E-03	54,20	33,52	41,77	47,38
UBA6	-0,346	3,56E-02	52,07	41,00	44,69	50,22
HNRNPLL	-0,211	2,37E-02	51,91	44,76	50,54	49,68
TM4SF18	-0,366	1,12E-02	51,79	40,24	51,66	46,59
PIGK	-0,369	8,75E-04	51,64	40,01	46,42	47,87
NDE1	-0,219	3,10E-02	49,68	42,66	48,99	43,31
CCNA2	-0,400	5,75E-03	48,48	36,81	47,63	40,45
MYH10	-0,217	9,83E-03	48,08	41,28	50,00	46,94
WDFY3	-0,381	6,18E-03	47,37	36,63	43,32	43,83
ARHGAP11A	-0,412	1,18E-02	46,93	35,56	40,52	42,96
R3HDM1	-0,468	1,00E-03	46,32	33,74	44,19	42,73
KNSTRN	-0,257	2,04E-02	45,96	38,50	43,46	40,62
CEP55	-0,538	2,21E-04	45,55	31,76	40,39	35,62
PBK	-0,449	1,23E-02	45,20	33,75	41,98	40,13
ARL5A	-0,701	2,40E-03	42,77	27,15	36,22	42,71
SQLE	-0,304	4,39E-02	42,63	34,49	42,79	37,29
CCNYL1	-0,395	5,43E-03	42,60	32,58	42,60	38,88
DHCR7	-0,348	3,00E-02	42,48	33,78	41,52	38,78
NRG1	-0,397	8,48E-03	42,39	31,95	35,24	34,48
NUSAP1	-0,257	4,10E-02	41,51	34,85	39,71	36,20
GLRX	-0,240	5,05E-03	41,14	34,71	39,91	36,15
NUF2	-0,646	2,35E-03	39,75	25,91	35,09	30,36
INSIG1	-0,278	5,37E-03	37,34	30,79	38,85	33,24
DARS2	-0,281	4,92E-02	37,20	30,55	34,90	34,55
SMAD5	-0,472	1,88E-02	36,84	26,75	32,33	33,09
ALDH3A2	-0,186	4,27E-02	36,02	31,66	37,27	34,20
EFCAB14	-0,243	7,20E-03	35,82	30,23	34,90	34,58
LPCAT2	-0,362	5,05E-03	35,25	27,55	35,88	32,97
SULT1E1	-0,482	1,43E-02	34,24	24,97	35,22	29,34
WASHC5	-0,200	3,11E-02	34,07	29,64	32,50	32,76
HMMR	-0,747	7,92E-04	33,34	20,52	27,10	24,57
MKI67	-0,525	2,87E-05	33,20	23,00	30,42	26,99
RACGAP1	-0,327	2,97E-02	32,94	26,26	30,63	28,43
POGLUT3	-0,247	4,29E-02	32,88	27,71	32,13	32,03
HIBCH	-0,436	4,24E-03	32,79	24,29	29,19	28,38
CENPF	-0,557	7,76E-04	32,77	22,82	24,86	24,63
PPP3CA	-0,232	3,15E-02	32,64	27,74	30,29	30,65
PHACTR4	-0,233	2,36E-02	31,22	26,47	30,90	27,69
NCEH1	-0,174	3,69E-02	31,00	27,51	29,64	29,31
SAMHD1	-0,369	3,92E-02	30,58	23,65	26,32	30,88
ACER3	-0,213	9,46E-03	28,85	24,84	27,65	28,00

YAP1	-0,249	4,42E-02	28,09	23,68	27,82	24,13
RBL2	-0,287	1,74E-02	28,00	22,97	27,75	25,92
MEF2A	-0,344	4,52E-02	25,86	20,49	26,06	24,22
DIAPH3	-0,353	2,53E-03	25,40	19,87	24,43	23,94
QTRT2	-0,279	6,99E-03	23,60	19,39	23,54	22,84
MLIP	-0,301	1,12E-02	23,51	19,05	21,92	19,99
MTMR10	-0,375	4,79E-04	23,37	17,98	25,88	21,54
INCENP	-0,443	6,18E-04	23,10	17,10	21,45	22,00
MPHOSPH9	-0,464	6,44E-03	23,10	16,83	19,80	20,44
SUV39H2	-0,517	1,93E-02	23,08	16,34	20,77	22,76
DEPDC1	-0,581	3,66E-02	22,60	15,59	20,95	18,12
FEM1B	-0,299	3,20E-02	22,23	18,09	20,12	20,75
CENPA	-0,407	1,53E-03	22,03	16,54	20,40	17,89
NEK2	-0,489	1,14E-03	22,02	15,84	19,40	16,29
ASPM	-0,784	1,93E-03	21,79	12,83	18,01	15,52
HMGCR	-0,321	3,30E-03	21,56	17,27	21,49	18,02
AFF1	-0,327	5,05E-03	21,49	17,22	20,68	20,16
SPAG5	-0,278	1,44E-02	21,35	17,53	20,53	18,15
VPS8	-0,319	3,23E-02	21,08	16,88	19,50	18,19
GPSM2	-0,652	2,34E-08	20,91	13,27	19,09	15,31
NECTIN3	-0,470	4,92E-03	20,80	15,17	19,88	18,09
RMND5A	-0,187	3,74E-02	20,62	18,11	19,45	20,02
WASF3	-0,313	1,93E-06	20,17	16,22	20,19	17,88
FNBP1	-0,269	1,05E-02	19,95	16,55	20,06	18,57
AC087721.2	-0,375	1,11E-03	19,71	15,18	18,38	16,98
RNMT	-0,425	6,33E-03	18,73	14,07	17,75	17,81
DAW1	-0,338	1,90E-02	18,59	14,68	18,49	15,57
APPBP2	-0,365	3,76E-02	18,50	14,48	17,97	17,14
LATS2	-0,211	1,24E-02	18,14	15,67	17,89	16,95
HSPE1-MOB4	-0,483	1,91E-03	18,08	12,83	14,01	17,11
TNRC18	-0,235	3,23E-02	17,96	15,27	16,98	16,51
COBLL1	-0,381	1,95E-03	17,94	13,75	18,11	18,74
KIF4A	-0,318	6,88E-03	17,68	14,14	16,63	14,60
ANGEL2	-0,371	2,33E-02	16,97	13,21	16,56	15,22
MEF2C	-0,347	5,59E-03	16,44	12,92	14,48	14,42
CEP70	-0,520	1,39E-02	16,00	11,25	14,09	12,74
GAS2L3	-0,436	2,59E-02	15,94	11,94	14,95	13,15
C2CD2	-0,279	2,28E-02	15,93	13,14	16,95	14,32
PIMREG	-0,446	9,83E-03	15,83	11,56	15,40	12,08
KNL1	-0,713	6,93E-04	15,79	9,70	13,00	12,47
ZNF800	-0,353	1,45E-02	15,76	12,34	15,31	14,62
LZTFL1	-0,296	4,42E-02	15,70	12,77	15,16	14,56
WASF1	-0,307	1,77E-02	14,78	11,94	15,34	14,30
PARPBP	-0,421	4,42E-02	14,56	11,09	13,45	13,05
SGO2	-0,656	1,49E-02	14,22	9,35	12,05	10,84
DEPDC1B	-0,341	1,19E-03	13,96	11,04	13,50	12,07
SENP1	-0,270	2,11E-02	13,76	11,38	12,95	13,53
RBBP9	-0,332	8,48E-03	13,73	10,93	14,11	13,07
COMMD3-BMI1	-0,606	3,22E-02	13,41	8,90	10,52	14,74
DIS3L	-0,276	3,98E-02	13,08	10,84	12,61	11,80
OIP5	-0,352	8,05E-03	12,74	9,96	12,37	10,39
CRYBG1	-0,333	8,42E-06	12,65	10,01	11,88	11,12
MGME1	-0,250	1,42E-03	12,53	10,52	12,16	11,54

ZCCHC2	-0,507	1,42E-04	12,17	8,65	11,66	9,51
SAMD8	-0,225	4,66E-02	12,12	10,39	12,15	11,68
CENPE	-0,750	3,78E-03	12,09	7,32	8,56	8,59
APAF1	-0,294	3,35E-03	10,95	8,93	10,43	10,60
SCLT1	-0,365	4,88E-02	10,30	8,06	9,18	8,74
SGO1	-0,365	2,94E-02	10,21	7,94	9,42	8,92
SMG1P3	-0,283	1,90E-02	9,83	8,09	9,21	8,92
BORA	-0,605	1,48E-03	9,52	6,33	8,54	7,95
GPD1L	-0,209	4,48E-02	9,38	8,12	9,50	8,38
SMG1P1	-0,304	4,00E-02	9,06	7,37	8,81	8,74
AC241640.1	-1,539	1,62E-02	8,80	3,10	10,71	4,34
ZNF791	-0,512	3,90E-04	8,68	6,12	8,47	8,46
PDE3A	-0,239	2,67E-02	8,68	7,37	8,38	7,77
HIVEP1	-0,366	1,74E-02	8,05	6,25	7,82	7,46
PLAC8	-0,413	2,19E-02	7,95	5,97	7,64	5,83
DPP4	-0,347	2,35E-03	7,75	6,08	7,84	6,65
CCDC190	-0,264	4,92E-02	7,46	6,19	7,29	6,82
IL1R1	-0,282	4,65E-02	7,25	6,00	7,21	7,81
KIF14	-0,564	6,99E-03	6,75	4,64	5,68	5,25
CXADR	-0,411	5,93E-04	6,35	4,78	5,87	5,17
MAP3K5	-0,280	3,78E-02	6,08	5,00	5,82	5,62
SYNJ1	-0,312	2,94E-03	6,07	4,89	5,73	5,43
TMSB15A	-0,521	1,77E-02	5,77	4,02	5,31	4,62
SFRP1	-0,311	1,62E-02	5,72	4,60	5,47	5,14
CDK19	-0,377	2,47E-02	5,68	4,36	5,76	4,81
ZBTB21	-0,333	4,44E-02	5,66	4,49	5,06	4,70
AP000295.1	-0,791	4,42E-02	5,60	3,52	5,37	5,08
MAP2K6	-0,373	1,13E-04	5,41	4,17	4,89	4,17
SPIN2B	-0,244	4,45E-02	5,22	4,40	5,07	4,63
RAB11FIP2	-0,544	9,61E-03	5,03	3,47	4,19	4,91
PIF1	-0,318	4,39E-02	5,01	4,02	4,92	4,13
MCM9	-0,297	2,33E-02	5,00	4,07	4,95	4,26
OCLN	-0,336	2,46E-02	4,99	3,94	5,14	4,58
RSC1A1	-0,388	3,96E-02	4,95	3,84	4,36	4,90
PIK3CG	-0,918	2,74E-02	4,87	2,59	3,73	3,36
KAT2B	-0,353	4,42E-02	4,34	3,43	4,45	3,95
ARNTL	-0,285	2,61E-02	4,25	3,48	3,91	3,68
ARHGAP11B	-0,429	1,57E-02	3,88	2,91	3,64	3,51
ELMOD1	-0,476	6,64E-04	3,50	2,52	3,34	2,71
ABCA8	-0,677	2,53E-03	3,31	2,07	3,08	2,19
MMP28	-1,256	3,11E-02	2,82	1,09	1,94	2,33
MYO5C	-0,322	2,37E-02	2,76	2,20	2,83	2,46
AL109918.1	-0,486	4,80E-04	2,58	1,85	2,46	2,03
UBN2	-0,561	1,44E-02	2,39	1,62	1,92	1,96
AC079594.2	-0,631	1,73E-02	2,29	1,48	1,89	2,29
SESN3	-0,641	1,72E-02	1,87	1,23	1,74	1,40
SMIM10	-0,426	4,12E-02	1,87	1,39	1,72	1,62
NBPF10	-0,326	7,85E-03	1,84	1,46	1,61	1,56
AC087632.2	-1,660	3,23E-04	1,79	0,53	1,83	1,71
CFAP69	-0,585	1,86E-02	1,66	1,12	1,54	1,45
RMDN2	-0,550	1,13E-02	1,65	1,14	1,48	1,52
H2AC6	-0,697	6,98E-03	1,58	0,98	1,56	1,14
SELP	-0,676	3,81E-02	1,48	0,93	1,36	0,99

CLDN10	-0,387	3,36E-02	1,16	0,89	1,25	0,96
SH3TC2	-0,555	2,35E-02	0,92	0,62	0,84	0,67
AMOT	-0,550	2,22E-02	0,72	0,49	0,64	0,53
ADAMTS12	-0,546	2,74E-02	0,71	0,49	0,67	0,62
CPA4	-0,847	1,94E-02	0,66	0,37	0,50	0,41
KCNJ15	-0,746	1,39E-03	0,61	0,36	0,34	0,37
WNK3	-0,654	1,77E-02	0,60	0,38	0,54	0,48
ADAM32	-1,239	8,91E-03	0,58	0,23	0,47	0,32
LPAR1	-0,631	2,38E-02	0,52	0,34	0,55	0,37
AC139530.2	-30,000	3,86E-10	0,41	0,00	0,28	0,21
H2AC11	-0,650	1,32E-02	0,34	0,22	0,33	0,22
SLC26A4	-0,719	3,05E-02	0,34	0,21	0,33	0,22
SCUBE3	-0,411	2,69E-02	0,25	0,19	0,26	0,20
GP1BB	-22,691	1,38E-06	0,23	0,00	0,34	0,21
SPTA1	-1,154	2,10E-02	0,17	0,08	0,11	0,10
FBXO15	-1,172	2,43E-02	0,16	0,07	0,14	0,11
CMKLR1	-1,002	4,91E-02	0,13	0,07	0,10	0,07
DNM1P47	-0,477	2,40E-02	0,12	0,09	0,10	0,10

Supplementary Table S9: Genes upregulated by LPS exclusively in cells that express APEX1(1-20). To identify genes upregulated by LPS specifically in cells expressing moderate levels of APEX1(1-20), but not in cells transduced with the empty virus, the results of the DGE analysis of both cells populations after treatment with detoxified (control) or active LPS (LPS) were com-bined. The L2FC (Log 2-fold change) states the average difference in gene expression between both treatments, positive values denote upregulation by LPS treatment. Wald test from DESeq2 was used to calculate the significance of the change in the expression. The adjusted p-values take the number of tested genes into account, the threshold for the adjusted p-value was 0.05. Mean expression levels per sample group are stated in transcripts per million (TPM), calculated during quasi-mapping with the tool salmon. The list is sorted by gene expression.

gene name	L2FC	adjusted p-value	mean TPM empty virus con	mean TPM empty virus LPS	mean TPM APEX1(1-20) con	mean TPM APEX1(1-20) LPS
IL1RL1	0,254	4,90E-03	186,63	200,07	175,35	209,27
SELENOT	0,254	3,59E-03	139,92	144,17	139,26	165,99
PXDN	0,668	1,34E-08	130,73	158,35	107,72	171,11
YIPF5	0,269	4,19E-03	85,82	92,90	86,53	104,21
DPYSL3	0,257	2,43E-02	88,43	94,98	83,51	99,79
NPTN	0,193	6,51E-03	67,85	72,68	67,70	77,38
COLGALT1	0,367	8,71E-03	55,94	68,32	56,83	73,29
PLSCR1	0,208	3,55E-02	49,76	53,82	50,49	58,32
ABI3BP	0,365	1,22E-02	42,83	48,38	48,73	62,49
CLEC1A	0,182	4,06E-02	49,73	54,56	48,64	55,20
CD44	0,503	5,30E-03	54,57	62,30	47,62	68,26
TUSC3	0,294	6,19E-03	41,13	44,21	39,24	48,10
ANGPT2	0,361	8,20E-05	38,50	43,80	34,41	44,26
DUXAP9	0,284	2,13E-02	18,14	19,50	18,29	22,28
NUAK1	0,442	3,93E-02	21,46	20,17	17,49	23,93
QPCT	0,564	1,72E-03	19,62	20,56	16,30	24,34
ATAD2	0,366	2,64E-02	14,35	15,01	13,40	17,11
IFI44	0,499	1,71E-02	12,54	15,99	12,14	17,09
HPSE	0,245	6,15E-03	10,00	11,08	9,86	11,67
PRIM1	0,506	6,36E-04	12,13	12,56	9,75	13,82
AK4	0,170	2,29E-02	9,80	10,28	9,68	10,88
CHAF1A	0,466	2,83E-02	9,93	11,66	9,48	13,05
NID2	0,901	9,23E-06	12,01	15,22	8,98	16,73
LRP12	0,252	2,81E-02	8,67	9,31	8,70	10,36
RGS2	0,398	4,63E-02	9,44	10,39	8,45	11,13
ARSK	0,211	4,04E-02	8,45	8,43	8,09	9,35
GK	0,285	2,52E-02	7,60	8,71	7,35	8,95
ZFPM2	0,369	3,39E-02	7,57	8,13	6,70	8,72
IL7R	0,419	2,96E-04	6,01	6,97	5,92	7,92
CLSPN	0,378	3,55E-02	5,33	6,04	5,66	7,33
EXO1	0,511	1,98E-03	5,92	6,37	5,28	7,53
CENPBD1	0,199	3,14E-02	4,71	4,52	4,22	4,85
CREB5	0,326	5,89E-04	2,77	3,01	2,82	3,52
PDE1C	0,280	4,63E-02	2,55	3,03	2,57	3,12
DNAH11	0,366	3,50E-02	2,47	2,47	2,19	2,81
AUNIP	0,412	4,00E-02	1,93	2,39	1,88	2,50
ALDH1L2	0,311	1,70E-02	2,04	2,30	1,85	2,29
LY75-CD302	0,547	1,38E-02	2,12	1,73	1,78	2,57
CACHD1	0,277	2,91E-02	1,81	2,00	1,76	2,13
SH3BP1	0,715	6,40E-03	1,32	1,89	1,40	2,31
CHRNA1	0,426	1,79E-02	1,13	1,44	1,26	1,69
TUBB2B	0,445	4,84E-02	1,12	1,35	1,08	1,47
TCF7	0,391	1,78E-02	1,07	1,19	1,05	1,38
NLRC3	0,376	1,24E-03	0,86	1,03	0,83	1,08
ARHGEF26	0,351	4,67E-02	0,63	0,64	0,58	0,74

RASGRF2	0,347	3,88E-02	0,57	0,71	0,56	0,71
SLC6A15	0,655	1,04E-02	0,37	0,53	0,40	0,64
AMPD3	0,780	2,81E-02	0,38	0,39	0,37	0,66
SLIT3	0,552	1,16E-02	0,23	0,31	0,25	0,36
AFF3	1,033	9,24E-03	0,30	0,35	0,23	0,46
PRRT2	2,229	2,83E-02	0,18	0,23	0,17	1,00
MYPN	0,620	2,17E-02	0,11	0,15	0,09	0,14
OASL	1,044	1,05E-02	0,07	0,09	0,08	0,17
PAPPA2	1,562	1,69E-04	0,06	0,09	0,04	0,12
PLA2G5	1,414	2,80E-02	0,02	0,08	0,03	0,08
TMEM184A	1,991	6,69E-04	0,04	0,05	0,02	0,06
AC019117.4	8,471	1,17E-02	0,47	0,18	0,00	0,26
CR354443.1	32,453	1,50E-11	0,08	0,18	0,00	0,20
H3P6	30,910	1,34E-10	1,80	3,13	0,00	13,28
SRP9P1	25,646	5,29E-07	20,60	15,67	0,00	8,97
AC244260.1	8,622	1,48E-02	0,10	0,20	0,00	0,21

Supplementary Table S10: Genes downregulated by LPS exclusively in cells that express APEX1(1-20). To identify genes downregulated by LPS specifically in cells expressing moderate levels of APEX1(1-20), but not in cells transduced with the empty virus, the results of the DGE analysis of both cells populations after treatment with detoxified (con) or active LPS (LPS) were combined. The L2FC (Log 2-fold change) states the average difference in gene expression between both treatments, negative values denote downregulation by LPS treatment. Wald test from DESeq2 was used to calculate the significance of the change in the expression. The adjusted p-values take the number of tested genes into account, the threshold for the adjusted p-value was 0.05. Mean expression levels per sample group are stated in transcripts per million (TPM), calculated during quasi-mapping with the tool salmon. The list is sorted by gene expression.

gene name	L2FC	adjusted p-value	mean TPM empty virus con	mean TPM empty virus LPS	mean TPM APEX1(1-20) con	mean TPM APEX1(1-20) LPS
NQO1	-0,281	1,26E-02	511,43	442,40	520,05	427,72
PIR	-0,566	2,25E-02	239,69	198,51	259,77	176,08
IGFBP4	-0,294	1,95E-04	187,16	172,64	197,36	160,86
CLEC14A	-0,190	1,99E-02	174,69	168,66	185,74	162,74
SOX18	-0,314	1,70E-05	54,38	50,61	57,60	46,31
TCN2	-0,295	4,29E-02	35,46	32,01	35,93	29,35
BTG2	-0,190	4,93E-02	30,69	28,95	32,58	28,57
CDC25B	-0,240	3,55E-02	28,01	24,68	28,15	23,83
ATP2B4	-0,175	2,48E-02	26,61	24,37	26,48	23,44
NOS3	-0,330	1,99E-02	25,85	21,96	25,64	20,42
GIMAP8	-0,227	3,68E-02	22,98	20,67	24,54	20,96
GGT5	-0,353	3,66E-03	22,00	20,89	24,12	18,92
SHE	-0,219	3,05E-02	22,25	20,13	22,92	19,69
ENOSF1	-0,301	2,71E-02	20,15	17,83	22,46	18,19
C1orf115	-0,180	3,90E-02	20,75	19,57	20,95	18,48
GJA4	-0,568	1,75E-04	14,65	12,07	19,24	12,98
KLF2	-0,494	4,28E-07	13,78	14,54	16,08	11,40
BTD	-0,185	4,29E-02	14,47	12,87	14,48	12,75
RAMP2	-0,465	4,90E-03	11,52	10,04	14,27	10,32
GIMAP1	-0,265	1,26E-02	11,67	11,04	12,66	10,53
BCAM	-0,275	1,74E-02	11,25	10,30	11,90	9,84
ABCG2	-0,578	1,24E-03	9,23	7,10	11,11	7,46
CYP1A1	-0,508	1,91E-02	10,46	8,05	10,60	7,45
IFT122	-0,270	2,29E-02	9,27	8,45	10,30	8,58
NFIA	-0,403	3,63E-02	7,98	7,49	9,43	7,14
MXD3	-0,387	4,04E-02	7,99	6,69	8,09	6,15
TM7SF2	-0,335	3,14E-02	6,80	6,27	6,85	5,42
ZNF467	-0,453	3,40E-03	5,68	4,91	6,20	4,54
HSPB6	-0,351	2,83E-02	4,44	4,25	5,03	3,95
MRAP2	-0,384	4,81E-03	3,70	3,13	4,15	3,17
ZNF219	-0,385	2,52E-02	3,65	2,93	3,90	2,98
SPACA6	-0,405	9,24E-03	3,56	3,10	3,69	2,80
LRTOMT	-0,402	5,51E-03	2,33	2,41	3,68	2,78
ANKRD44	-0,767	3,45E-02	2,23	2,28	3,61	2,12
GPX3	-0,573	3,61E-03	2,36	2,07	3,17	2,13
ASS1	-0,446	4,39E-03	2,43	2,14	2,98	2,19
GSTM2	-0,342	2,92E-02	2,59	2,20	2,86	2,26
MAP3K14	-0,384	1,70E-02	2,62	2,14	2,78	2,13
NRROS	-0,303	9,64E-04	2,48	2,40	2,65	2,15
STC1	-0,462	2,58E-02	2,79	2,23	2,33	1,69
FAM221A	-0,310	3,55E-02	2,04	1,88	2,23	1,80
CRACR2B	-0,419	1,65E-04	1,73	1,72	1,98	1,48
PARD6A	-0,362	3,74E-02	1,79	1,69	1,86	1,44
SLCO2A1	-0,674	2,74E-02	1,48	1,32	1,82	1,15
LRRC75A	-0,393	1,30E-03	1,45	1,25	1,58	1,20

GUCY1A1	-0,911	1,65E-02	1,09	0,83	1,55	0,84
SMIM3	-0,424	6,42E-03	1,27	1,14	1,40	1,05
NTSR1	-0,347	3,46E-02	1,41	1,20	1,33	1,05
C20orf204	-0,498	1,04E-02	1,08	0,97	1,17	0,83
TCF15	-0,467	7,58E-03	1,05	0,97	1,13	0,82
LHX6	-0,471	1,15E-02	1,04	0,83	1,05	0,76
FCF1P2	-23,428	3,30E-11	1,19	1,42	1,05	0,00
AP005018.2	-23,882	3,43E-06	0,91	1,50	1,03	0,00
CCL23	-0,826	3,88E-02	0,99	0,74	1,02	0,57
COL1A2	-0,415	1,87E-03	0,77	0,64	1,01	0,76
CASKIN1	-2,314	1,30E-02	0,36	0,10	0,91	0,29
WNT9A	-0,439	2,83E-02	0,74	0,63	0,85	0,63
MATN2	-0,529	4,63E-02	0,58	0,43	0,76	0,53
DLL1	-0,370	2,69E-02	0,63	0,58	0,70	0,54
C4B	-1,377	7,99E-03	0,51	0,53	0,67	0,25
CD36	-0,760	2,93E-02	0,49	0,31	0,58	0,34
EIF3CL	-0,720	9,24E-03	0,43	0,30	0,54	0,32
FBLN2	-0,677	1,05E-02	0,44	0,32	0,51	0,32
ABCC2	-0,663	1,63E-02	0,38	0,36	0,50	0,32
CA4	-1,172	1,37E-02	0,28	0,19	0,41	0,19
EGLN3	-1,171	1,62E-03	0,31	0,25	0,38	0,17
ARL14EPL	-0,995	4,63E-02	0,29	0,23	0,38	0,19
CDH4	-0,476	1,48E-02	0,33	0,26	0,37	0,26
INHBB	-0,814	1,69E-04	0,22	0,18	0,30	0,17
CLEC3B	-1,195	2,74E-02	0,17	0,11	0,28	0,12
AC005520.3	-1,051	5,63E-03	0,25	0,19	0,26	0,14
KCNN4	-0,792	3,04E-02	0,20	0,17	0,24	0,14
ABLIM2	-1,741	7,58E-03	0,17	0,13	0,24	0,07
CAMSAP3	-0,935	1,63E-02	0,07	0,08	0,17	0,09
SYT7	-0,953	3,29E-02	0,15	0,10	0,16	0,08
TBC1D3K	-30,254	2,79E-10	0,06	0,08	0,08	0,00
RASSF10	-1,470	2,80E-02	0,03	0,02	0,06	0,02
SCNN1B	-2,117	1,78E-02	0,04	0,03	0,04	0,01
ADAMTS15	-1,383	1,02E-03	0,03	0,02	0,04	0,02
NOS1	-2,260	2,64E-02	0,00	0,00	0,02	0,00
RTN4RL1	-2,401	3,55E-02	0,01	0,01	0,01	0,00

antioxidants

MDPI

Article

Caffeine Inhibits Oxidative Stress- and Low Dose Endotoxemia-Induced Senescence—Role of Thioredoxin-1

Dennis Merk [1,†], Jan Greulich [2,†], Annika Vierkant [2], Fiona Cox [1,3], Olaf Eckermann [1,2], Florian von Ameln [2], Nadine Dyballa-Rukes [1,2], Joachim Altschmied [2,4], Niloofar Ale-Agha [1,4,*], Philipp Jakobs [1,*] and Judith Haendeler [1,4,*]

[1] Cardiovascular Degeneration, Haendeler Group, Clinical Chemistry and Laboratory Diagnostics, Medical Faculty, University Hospital, Heinrich-Heine University Duesseldorf, 40225 Duesseldorf, Germany; dennis.merk@hhu.de (D.M.); fiona.cox@hhu.de (F.C.); olaf.eckermann@hhu.de (O.E.); nadine.dyballa@hhu.de (N.D.-R.)

[2] Cardiovascular Degeneration, Altschmied Group, Clinical Chemistry and Laboratory Diagnostics, Medical Faculty, University Hospital, Heinrich-Heine University Duesseldorf, 40225 Duesseldorf, Germany; jan.greulich@hhu.de (J.G.); annika.vierkant@hhu.de (A.V.); florian.ameln@hhu.de (F.v.A.); joalt001@hhu.de (J.A.)

[3] Institute for Translational Pharmacology, Medical Faculty, University Hospital, Heinrich-Heine University Duesseldorf, 40225 Duesseldorf, Germany

[4] CARID, Cardiovascular Research Institute Düsseldorf, Medical Faculty, University Hospital, Heinrich-Heine University Duesseldorf, 40225 Duesseldorf, Germany

* Correspondence: niale001@hhu.de (N.A.-A.); philipp.jakobs@hhu.de (P.J.); juhae001@hhu.de (J.H.); Tel.: +49-211-8112200 (N.A.-A.); +49-211-8112207 (P.J.); +49-211-8112008 (J.H.)

† These authors contributed equally to this work.

Abstract: The maintenance of Thioredoxin-1 (Trx-1) levels, and thus of cellular redox homeostasis, is vital for endothelial cells (ECs) to prevent senescence induction. One hallmark of EC functionality, their migratory capacity, which depends on intact mitochondria, is reduced in senescence. Caffeine improves the migratory capacity and mitochondrial functionality of ECs. However, the impact of caffeine on EC senescence has never been investigated. Moreover, a high-fat diet, which can induce EC senescence, results in approximately 1 ng/mL lipopolysaccharide (LPS) in the blood. Therefore, we investigated if low dose endotoxemia induces EC senescence and concomitantly reduces Trx-1 levels, and if caffeine prevents or even reverses senescence. We show that caffeine precludes H_2O_2-triggered senescence induction by maintaining endothelial NO synthase (eNOS) levels and preventing the elevation of p21. Notably, 1 ng/mL LPS also increases p21 levels and reduces eNOS and Trx-1 amounts. These effects are completely blocked by co-treatment with caffeine. This prevention of senescence induction is similarly accomplished by the permanent expression of mitochondrial p27, a downstream effector of caffeine. Most importantly, after senescence induction by LPS, a single bolus of caffeine inhibits the increase in p21. This treatment also blocks Trx-1 degradation, suggesting that the reversion of senescence is intimately associated with a normalized redox balance.

Keywords: caffeine; endothelial cells (EC); lipopolysaccharide; senescence; Thioredoxin-1

Citation: Merk, D.; Greulich, J.; Vierkant, A.; Cox, F.; Eckermann, O.; von Ameln, F.; Dyballa-Rukes, N.; Altschmied, J.; Ale-Agha, N.; Jakobs, P.; et al. Caffeine Inhibits Oxidative Stress- and Low Dose Endotoxemia-Induced Senescence—Role of Thioredoxin-1. *Antioxidants* **2023**, *12*, 1244. https://doi.org/10.3390/antiox12061244

Academic Editors: José Godoy and Luciana Azevedo

Received: 21 April 2023
Revised: 2 June 2023
Accepted: 6 June 2023
Published: 9 June 2023

1. Introduction

During the aging process and in a variety of diseases, there is an increase in reactive oxygen species (ROS, e.g., O_2^- and H_2O_2), which can lead to senescent endothelial cells (ECs) in humans [1]. Thioredoxin-1 (Trx-1) is a ubiquitously expressed oxidoreductase, which reduces ROS in concert with peroxiredoxins. Trx-1 also interacts with several proteins in different compartments of the cell and thereby modulates their functions [2,3]. In ECs, Trx-1 is one of the most important anti-oxidative proteins [4,5]. In a previous study, we demonstrated in an oxidative-stress-induced senescence model (using H_2O_2) that the amount of Trx-1 protein is decreased in those senescent ECs and that the levels

of the ROS-generating enzyme NADPH oxidase 4 are elevated, suggesting that disturbed redox homeostasis is linked to senescence induction. Along these lines, senescence induction could be blocked by the permanent expression of Trx-1 [6], demonstrating a causal relationship between the loss of Trx-1 and the appearance of cellular senescence.

Moreover, we were able to show that—in addition to ROS—100 mg/dL low-density lipoprotein (LDL) as well as ultrafine carbon nanoparticles also induce senescence in primary ECs [7].

One important feature of EC functionality is their ability to migrate, which is compromised in senescent ECs [7,8]. We found that the migratory capacity of ECs depends on intact mitochondria [8,9]. Moreover, short-term treatment with caffeine in concentrations up to 50 µM, which corresponds to 4–6 cups of coffee per day [9,10], improves the migratory capacity of ECs [9]. Interestingly, positive effects of caffeine in these doses were also shown in several cohort studies, in which an association was found between coffee consumption and a reduced mortality rate for several diseases affecting the cardiovascular system, most of which are associated with endothelial dysfunction. In these studies, the number of deaths from heart and respiratory diseases, stroke, and type II diabetes correlated negatively with coffee consumption, and the mortality risk was reduced by consumption of 4–6 cups a day compared to lower intake [11]. Altogether, these data suggest that caffeine could sustain EC functionality by counteracting processes leading to their dysfunction, which is a hallmark of senescent cells.

Recently, we unraveled the molecular mechanism explaining the protective role of caffeine. We demonstrated that caffeine increased the translocation of p27, a cell cycle inhibitor, into the mitochondria, leading to improved mitochondrial functionality. In p27-deficient mice, electron transport chain activity was reduced compared to their wild-type littermates and could not be improved with caffeine. This clearly demonstrated that the caffeine effects are mediated through an increase in mitochondrial p27. In addition, we found that caffeine was able to increase the functionality of mitochondria isolated from 24-month-old mice to the level of 6-month-old animals [12] and thus reverse the aging-associated functional decline of these organelles.

So far, we have shown that the maintenance of Trx-1 protein levels, and thus cellular redox homeostasis, has important beneficial effects on ECs by preventing senescence induction. Moreover, caffeine treatment results in functional improvements. However, the effects of caffeine on EC senescence have never been investigated. Furthermore, a high-fat diet has been shown to result in approximately 1 ng/mL lipopolysaccharide (LPS) in the blood [13]. Our finding that a simulated high-fat diet with elevated LDL levels induces EC senescence [7] suggests that low dose LPS might have a similar effect, although this has so far not been analyzed. Therefore, we investigated if low dose endotoxemia can induce EC senescence and concomitantly reduce Trx-1 levels, and if caffeine can counteract induction or even reverse senescence.

2. Materials and Methods

2.1. Cell Culture

Primary human ECs were supplied by LONZA (Cologne, Germany), and human embryonic kidney cells (HEK293T) were supplied by Invitrogen (Darmstadt, Germany). ECs and HEK293T were cultured as previously described [14,15]. In detail, ECs were cultured in endothelial basal medium supplemented with 50 ng/mL amphotericin B, 1 µg/mL hydrocortisone, 50 µg/mL gentamicin, 12 µg/mL bovine brain extract, 10 ng/mL epidermal growth factor (LONZA, Cologne, Germany), and 10% fetal bovine serum until the third passage was reached. Cells were grown for at least 20 h after detachment with trypsin. HEK293T cells were cultured in DMEM GlutaMAX™ (Invitrogen, Darmstadt, Germany) supplemented with 10% heat-inactivated fetal bovine serum and 1% penicillin/streptomycin.

2.2. Lentiviral Production and Transduction

VSV-G pseudotyped lentiviral particles were generated as previously described [6]. In detail, HEK293T cells were co-transfected with a transfer vector and expression vectors for the VSV-G envelope protein and lentiviral Gag/Pol, using the Calcium Phosphate Transfection Kit (Invitrogen, Darmstadt, Germany) according to the manufacturer's instructions. Viral particles containing supernatant were collected over three days, then filtered through a 0.45 µm PVDF membrane (Millipore, Burlington, MA, USA) and concentrated using Vivacell 100 ultrafiltration units with a PES membrane and a 100,000 MW cutoff (Sartorius, Goettingen, Germany). Concentrated virus particles were stored in aliquots at −80 °C. Viral titer was determined with the QuickTiter Lentivirus Titer Kit (Lentivirus-Associated HIV p24) (Cell Biolabs, San Diego, CA, USA). ECs were transduced with lentiviral expression vectors for mitochondrial p27 [12] with a multiplicity of infection of 50. The cells were washed 3 times 24 h after transduction.

2.3. Transient Transfection of ECs

Transient transfections of ECs with plasmid DNA were performed using Effectene (Qiagen, Hilden, Germany). In detail, ECs were transfected on 6 cm culture dishes with 2.5 µg plasmid DNA, 20 µL enhancer, and 25 µL Effectene in 150 µL buffer, with the subsequent addition of 1 mL cell culture medium.

2.4. Migration Assay

Migration was quantitated with a scratch wound assay, as previously described [12]. In detail, wounds were set by scraping cell monolayers with a sterile disposable rubber policeman. For that purpose, ECs were cultivated on 6 cm dishes, which were labeled with a trace line before setting the wound. After applying them to the injury, non-attached cells were removed by gentle washing with culture medium. Quantification of EC migration from the edge of the injured monolayer was performed by staining the cells with 500 ng/mL 4′,6-diamidino-2-phenylindole (DAPI) (Carl Roth, Karlsruhe, Germany) in PBS after the cells were fixed with 4% paraformaldehyde for 15 min at room temperature. Microscopic pictures were taken using an Axio Observer Z (Zeiss, Jena, Germany) using a 200× magnification. The cells which had invaded the wound from the trace line were automatically counted using the particle analysis feature of Image J 1.52a after watershed separation of overlapping nuclei.

2.5. Immunoblotting

Immunoblotting was performed as previously described [16]. In detail, cells were detached from the culture surface with a rubber policeman, centrifuged at 800× *g*, and washed twice with ice-cold PBS. After final centrifugation at 800× *g* and removal of the supernatant, cells were resuspended in radioimmunoprecipitation assay (RIPA) buffer (50 mM Tris-HCl pH 8.0, 150 mM NaCl, 1% (*v*/*v*) IGEPAL®-CA630, 0.1% (*w*/*v*) SDS, and 0.5% (*w*/*v*) Na-Deoxycholate) supplemented with 1/100 volume of a protease inhibitor cocktail and phosphatase inhibitor cocktail (Bimake, Munich, Germany) and lysed for 30 min on ice. Then, the lysates were centrifuged at 18,000× *g* and 4 °C for 15 min and the supernatant was transferred to a fresh tube. Proteins were separated by sodium dodecyl sulfate–polyacrylamide gel electrophoresis according to standard procedures. After the transfer of the proteins onto polyvinylidene difluoride membranes and blocking with 5% milk powder in TBS (200 mM Tris-HCl pH 8.0, 300 mM NaCl, and 100 mM KCl) with 0.1% (*v*/*v*) Tween-20 (TBS-T) for 1 h at room temperature, membranes were incubated with antibodies directed against GAPDH (1:50.000), Trx-1 (1:500), eNOS (1:500) (all three from Abcam, Cambridge, UK), p21 (1:500), and Src (1:1000) (both from Cell Signaling Technologies, Frankfurt, Germany). Antibodies were incubated overnight at 4 °C. The following day, membranes were washed three times with TBS-T and incubated with secondary antibodies coupled to horseradish peroxidase (ECL anti-rabbit or anti-mouse IgG, horseradish-peroxidase-linked whole antibody (from sheep) (1:5000) (Cytiva, Marlborough,

MA, USA). Detection was performed using ECL substrate (Cytiva, Marlborough, MA, USA) and X-ray films. Semi-quantitative analyses were performed on scanned X-ray films using Image J [17].

2.6. Immunostaining of ECs

Immunostaining of ECs was performed as previously described [12]. In detail, cells were fixed with 4% formaldehyde for 15 min and were blocked and permeabilized for 15 min at room temperature with 3% (*v*/*v*) normal goat serum (Sigma-Aldrich, Deisenhofen, Germany) diluted in PBS containing 0.3% (*v*/*v*) Triton X-100. Afterward, the cells were incubated with primary antibodies against a myc-tag or p21 (all from Cell Signaling Technologies, Frankfurt, Germany), each 1:100, overnight at 4 °C. The antibody against TIM23 (BD BioSciences, Heidelberg, Germany) was diluted 1:150 and incubated overnight at 4 °C. Subsequently, cells were washed three times with PBS and incubated with an Alexa Fluor® 594 coupled anti-mouse or anti-rabbit secondary antibody (1:500) (Santa Cruz Biotechnology, Heidelberg, Germany) for 1 h at room temperature. Nuclei were counterstained with DAPI (500 ng/mL) (Carl Roth, Karlsruhe, Germany) in PBS for 5 min at room temperature and the cells were mounted with ProLong™ Diamond Antifade Mountant (Invitrogen, Darmstadt, Germany). Images were taken using Zeiss microscopes (Axio Observer Z or Axio Imager M2, Zeiss, Jena, Germany) using a 400× or 200× magnification. Pixel intensities were measured with Image J [17].

2.7. Measurement of Intracellular ROS by Fluorescence Microscopy

ROS levels were quantitatively assessed using dihydroethidine (DHE) and MitoSOX™-Red, and mitochondria were co-stained with MitoTracker® Green FM (all purchased from Molecular Probes, Eugene, OR, USA). Cells were washed with endothelial basal medium and incubated with either 10 µM DHE or 5 µM MitoSOX™-Red combined with 100 nM MitoTracker® Green FM for 30 min at 37 °C. Afterward, cells were washed twice with endothelial basal medium, and images were taken with an Axio Observer Z (Zeiss, Jena, Germany) using a 200× magnification. Fluorescence intensity was calculated with Image J and normalized to the cell number.

2.8. Total Cellular RNA Isolation

Total cellular RNA was isolated as previously described [18]. In detail, TRIzol (Thermo Fisher Scientific, Dreieich, Germany) was used to extract total RNA from ECs according to the manufacturer's instructions. Further purification of RNA was achieved by using the RNeasy® Mini kit (Qiagen, Hilden, Germany) and concentrations were measured using a NanoDropTM 2000c (Thermo Fisher Scientific, Dreieich, Germany). RNA integrity and purity were analyzed by agarose gel electrophoresis.

2.9. cDNA Synthesis

cDNA was synthesized as previously described [18]. In detail, total cellular RNA was reverse transcribed using the QuantiTect Reverse Transcription kit (Qiagen, Hilden Germany) according to the manufacturer's instructions. For the verification of the expression of transgenes after lentiviral transduction, cDNA was synthesized with or, as a control for residual genomic DNA containing proviral genomes, without reverse transcriptase.

2.10. Polymerase Chain Reaction (PCR)

Endpoint PCRs were performed with MyTaq™ HS DNA Polymerase (Biocat, Heidelberg, Germany) and primers for RPL32 (hm RPL32 Ex02 for1 5′-GTGAAGCCCAAGATCGTCAA-3′ and hm RPL32 Ex03 rev1 5′-TTGTTGCACATCAGCAGCAC-3′) and mito p27 (hCDKN1B Ex01 for1 5′-GGTTAGCGGAGCAATGCG-3′ and myc-tag rev2 5′-TCCTCTTCTGAGATGA GTTTTTGTTC-3′) according to manufacturer's recommen-dations in a Bio-Rad T100 Thermal Cycler (BioRad, Feldkirchen Germany). The reaction products were visualized on standard agarose gels.

Semi-quantitative real-time PCRs were used to determine the relative transcript levels of Trx-1 with corresponding primers (hm TXN1 Ex01 for1 5′-TGGTGAAGCAGATCGAGAGC-3′ and hm TXN1 Ex03/04 rev1 5′-ACATCCTGACAGTCATCCACAT-3′), cDNA as a template, and the primaQUANT 2x qPCR SYBR-Green-MasterMix (Steinbrenner, Wiesenbach, Germany) in a Rotor-Gene Q instrument (Qiagen, Hilden, Germany). Relative expression was calculated by the ΔC_t method with RPL32 as a reference [19].

2.11. Statistics

The number of experiments (n) represents independent biological replicates. The data presented are mean ± SEM. Normal distribution was confirmed by the Shapiro–Wilk test and homogeneity of variances (from means) was verified by Levene's test. Since all data sets represented normal distribution, the multiple comparisons were performed using one-way ANOVA with the post hoc Tukey LSD test. Pairwise comparisons were performed with a paired Student's *t*-test on the raw data.

3. Results

3.1. Caffeine Prevents Stress-Induced Senescence in Endothelial Cells

In previous work, we demonstrated that stress-induced senescence of ECs entails an increase in the cell cycle inhibitor p21 and a decrease in the levels of eNOS, the enzyme constitutively producing NO to preserve the NO bioavailability and functionality of ECs. Moreover, the amount of Trx-1, which is essential for cellular redox homeostasis, was decreased and the migratory capacity of ECs was compromised. Lentiviral re-expression of Trx-1 in this model inhibited senescence induction, underscoring the importance of Trx-1 [6]. We also demonstrated that 100 mg/dL LDL induces EC senescence, reduces mitochondrial functionality, including ATP production, and impairs migration [8]. Interestingly, caffeine induces EC migration [9], enhances mitochondrial functionality in old mouse hearts, and improves the outcomes after myocardial infarction in prediabetic mice [12]. Thus, one could speculate that caffeine could be beneficial in stress-induced senescence in ECs.

To investigate the role of caffeine in stress-induced senescence in ECs, we used an established model [6]. In detail, we treated primary human ECs with 50 µM H_2O_2 and 10 µM caffeine every two days for two weeks (Figure 1A). As expected and previously published [6], H_2O_2-treatment-induced senescence in ECs was shown by an increase in p21. Interestingly, this effect was completely blocked by the co-treatment, while caffeine alone did not affect the p21 levels (Figure 1B,C,E). As a second marker of EC senescence, we investigated the levels of eNOS in this model. Repetitive treatment with H_2O_2 led to a significant decrease in eNOS protein levels, as observed previously [6]. However, the additional treatment with caffeine prevented the H_2O_2-induced loss of eNOS. As for p21, caffeine alone had no effect on eNOS protein levels (Figure 1B,D).

3.2. Caffeine Counteracts Low Dose Endotoxemia-Induced Senescence in Endothelial Cells

After having shown that caffeine is able to inhibit H_2O_2-induced senescence in ECs, we wanted to use a potentially more relevant inducer of EC senescence. In our hands, senescence could also be induced with 100 mg/dL LDL [7]. As it had been demonstrated that a high-fat diet, which leads to diabetes and insulin resistance, results in up to 1 ng/mL LPS in the blood [13], we next investigated if low dose endotoxemia can also induce senescence in ECs, and if this could be prevented with caffeine. Therefore, we treated human ECs repetitively with 1 ng/mL LPS every second day for a total of two weeks and co-incubated those cells with 10 µM caffeine (Figure 2A). As a control, we used LPS from the same *E. coli* serotype that had been partially delipidated by alkaline hydrolysis. This detoxified LPS has an endotoxin level about 10,000 times lower than the parent LPS. In this setting, we demonstrate here for the first time that 1 ng/mL LPS is able to induce a senescent phenotype in ECs, as shown by an increase in p21 (Figure 2B,C,E,F). Moreover, we found that this dose of LPS induces ROS (Supplementary Figure S1). Co-treatment with caffeine prevented this upregulation of p21 (Figure 2B,C,E,F), while caffeine alone had no effect. Next, we analyzed

whether LPS also affects eNOS levels. Repetitive low doses of LPS reduced the amount of eNOS significantly (Figure 2B,D) and this effect was inhibited by caffeine. As before, caffeine alone had no effect on eNOS protein levels. Next, we determined the levels of Trx-1 as an indicator of the cellular redox status. LPS significantly reduced the amount of Trx-1 (Figure 2G,H) comparable to the reduction shown with H_2O_2 in our previous study [6]. On the mRNA level, neither H_2O_2 nor LPS affected Trx-1 (Supplementary Figure S2), indicating that low dose endotoxemia—like oxidative stress—induces the degradation of the protein. Interestingly, co-treatment with caffeine completely restored Trx-1 protein levels (Figure 2G,H). As a functional cellular read-out, we determined the migratory capacity of ECs under this low dose endotoxemia by performing scratch wound assays. The LPS treatment dramatically reduced migration, and this detrimental effect was blocked by caffeine treatment (Figure 2I,J). We had previously shown that caffeine enhances the import of p27 into mitochondria and that the pro-migratory effect of caffeine in ECs completely depends on mitochondrial p27 [12]. Thus, it was tempting to speculate that the protective effects of caffeine in LPS-induced senescence are mediated through mitochondrial p27.

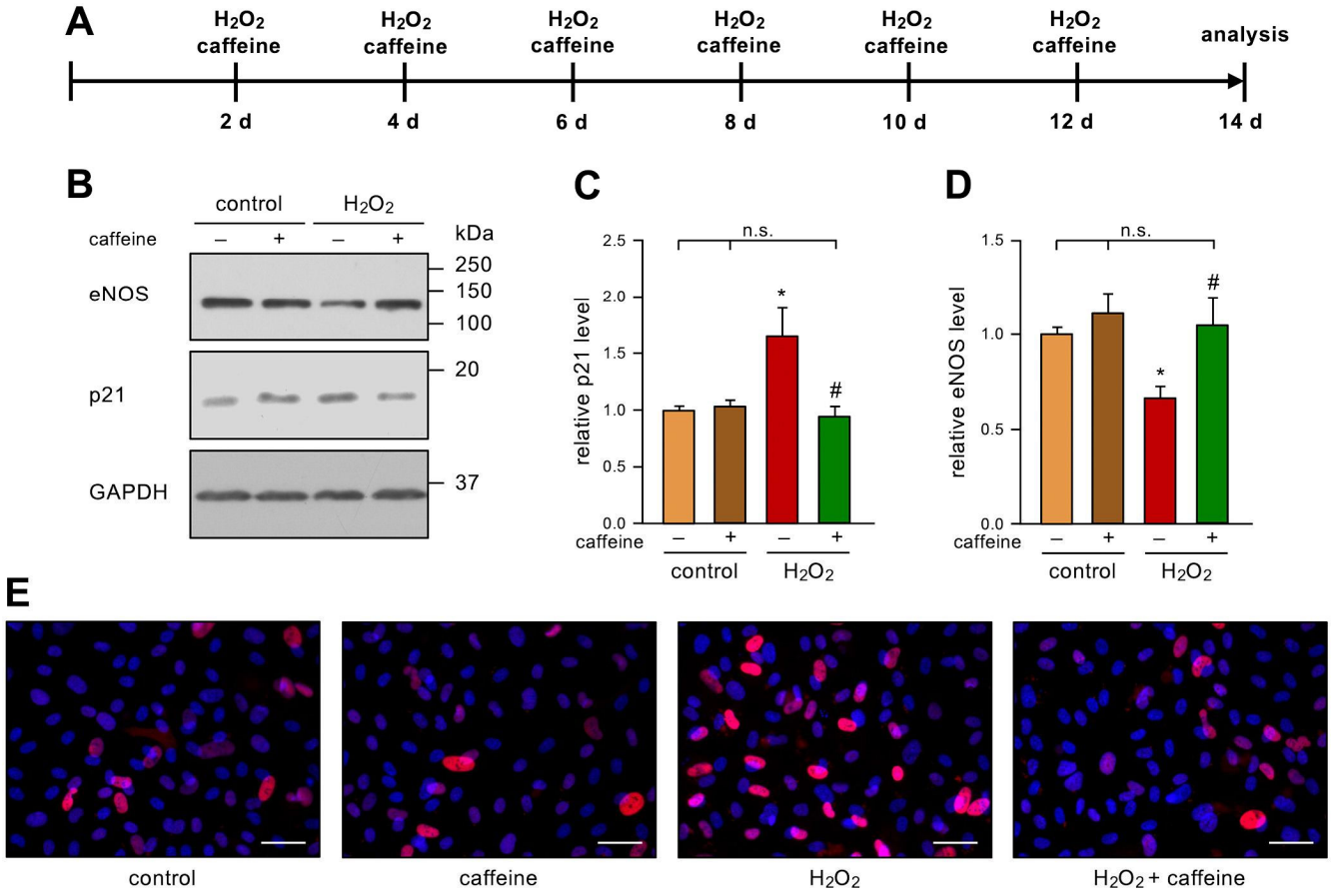

Figure 1. Caffeine prevents H_2O_2-induced senescence. (**A**–**E**) ECs were treated with 50 µM H_2O_2 and 10 µM caffeine every second day for two weeks. (**A**) Schematic representation of the treatment. (**B**–**D**) p21 and eNOS were detected by immunoblot, and GAPDH served as loading control. The untreated controls and the H_2O_2-treated group received caffeine (+) or not (−), as indicated. (**B**) Representative immunoblots for p21 (middle panel), eNOS (upper panel), and GAPDH (lower panel). (**C**,**D**) Semi-quantitative analysis of relative amounts of p21 (**C**) and eNOS (**D**) (data are mean ± SEM, n = 5, * $p < 0.05$ vs. control, # $p < 0.05$ vs. H_2O_2 without caffeine, n.s. = not significant, and one-way ANOVA with post hoc Tukey LSD test). (**E**) p21 was detected by fluorescence microscopy. ECs were stained with an anti-p21 antibody (red) and nuclei were counterstained with DAPI (blue). Shown is a representative immunostaining (scale bar = 50 µm).

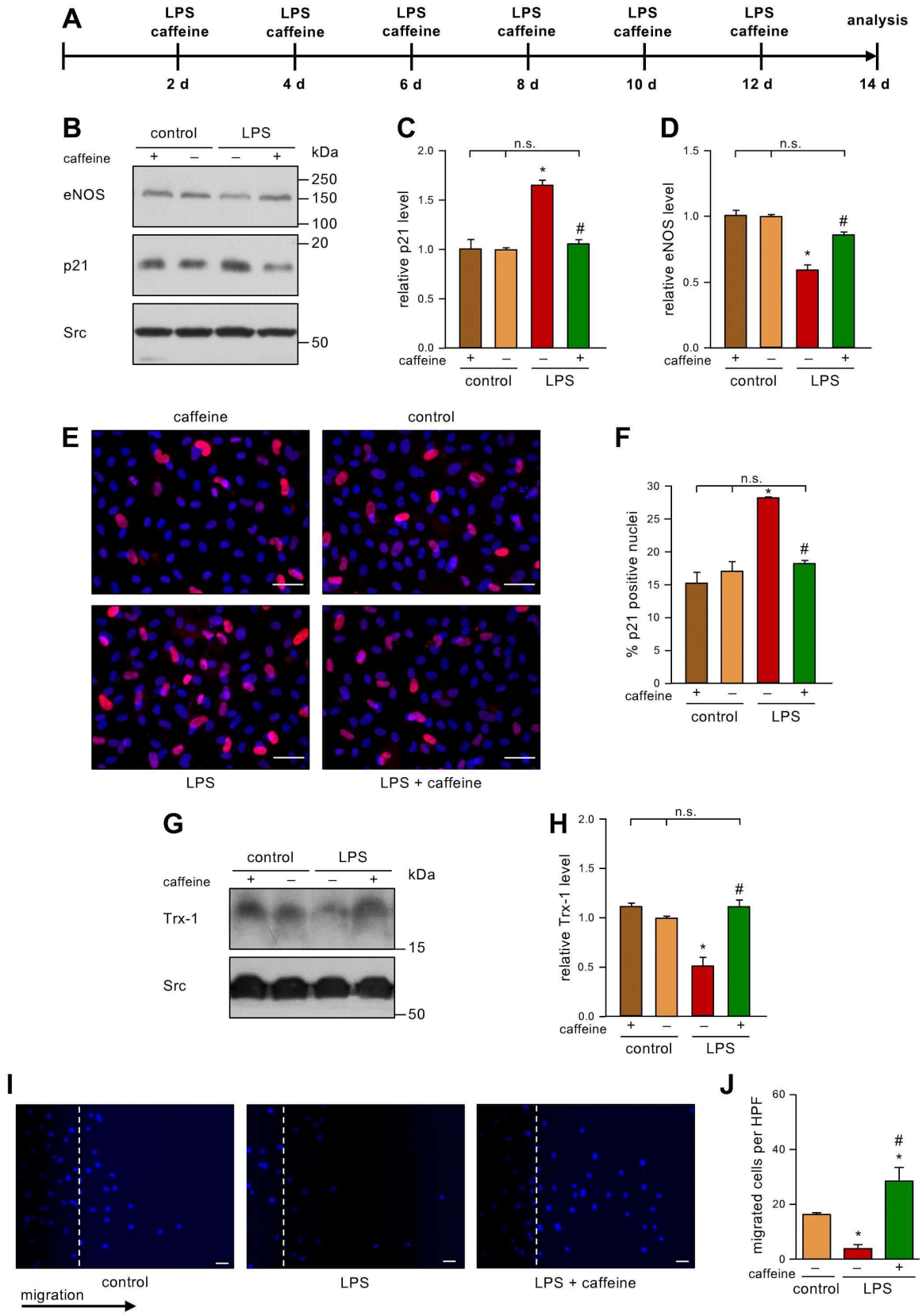

Figure 2. Caffeine counteracts LPS-induced senescence, maintains Trx-1 levels, and increases migratory capacity. (**A**–**J**) ECs were treated with 1 ng/mL detoxified (control) or active LPS (LPS) and 10 µM caffeine every second day for two weeks. (**A**) Schematic representation of the treatment. (**B**–**J**) The controls treated with detoxified LPS and the LPS-treated group received caffeine (+) or not

(−), as indicated. (**B**–**D**) p21 and eNOS were detected by immunoblot, and Src served as a loading control. (**B**) Representative immunoblots for p21 (middle panel), eNOS (upper panel), and Src (lower panel). (**C**,**D**) Semi-quantitative analysis of the relative amounts of p21 (**C**) and eNOS (**D**) (data are mean ± SEM, n = 4, *$p < 0.05$ vs. control, $^{\#}$ $p < 0.05$ vs. LPS without caffeine, n.s. = not significant, and one-way ANOVA with post hoc Tukey LSD test). (**E**,**F**) p21 was detected by fluorescence microscopy. Cells were stained with an anti-p21 antibody (red) and nuclei were counterstained with DAPI (blue). (**E**) Representative immunostainings (scale bar = 50 µm). (**F**) Image J analyses of the percentage of p21 positive nuclei (data are mean ± SEM, n = 4, * $p < 0.05$ vs. control, $^{\#}$ $p < 0.05$ vs. LPS without caffeine, n.s. = not significant, and one-way ANOVA with post hoc Tukey LSD test). (**G**,**H**) Trx-1 was detected by immunoblot and Src served as a loading control. (**G**) Representative immunoblots for Trx-1 (upper panel) and Src (lower panel). (**H**) Semi-quantitative analysis of the relative amounts of Trx-1 (data are mean ± SEM, n = 4, * $p < 0.05$ vs. control, $^{\#}$ $p < 0.05$ vs. LPS without caffeine, n.s. = not significant, and one-way ANOVA with post hoc Tukey LSD test). (**I**,**J**) Migratory capacity was detected by scratch wound assays. Cell nuclei were stained with DAPI. (**I**) Representative DAPI staining (scale bar = 50 µm). (**J**) Semi-quantitative analysis of migrated cells per high-power field (HPF) (data are mean ± SEM, n = 4, * $p < 0.05$ vs. control, $^{\#}$ $p < 0.05$ vs. LPS without caffeine, and one-way ANOVA with post hoc Tukey LSD test).

3.3. Permanent Expression of Mitochondrial p27 in Endothelial Cells Inhibits Senescence Induction by Low dose Endotoxemia

To investigate the impact of permanently elevated levels of mitochondrial p27 on LPS-induced EC senescence, we expressed mitochondrially-targeted p27 (mito p27) with a lentiviral vector [12] before repetitive treatment with LPS. After first confirming exclusive mitochondrial localization (Figure 3A), we showed that LPS treatment affected neither the transcript (Figure 3B) nor the protein levels (Figure 3C) of the lentivirally expressed mitochondrial p27. Next, we measured p21 protein levels by immunoblotting. In the control group transduced with an empty virus, the levels of p21 protein were elevated by LPS treatment. The transduction with the lentiviral mito p27 expression vector did not change p21 protein levels in cells not treated with LPS. Even more interestingly, p21 levels were not increased after repetitive LPS treatment when mitochondrial p27 levels were sustained (Figure 3D,E). Similar results were found by p21 immunostaining (Figure 3F,G). Along the same lines, Trx-1 protein levels were reduced by LPS treatment in the control group, yet transduction with a lentiviral mito p27 expression vector blocked LPS-induced Trx-1 degradation (Figure 3H,I). These data clearly demonstrate a protective effect of mitochondrial p27 as a downstream effector of caffeine in senescence induction in ECs, possibly by maintaining cellular redox homeostasis.

3.4. Caffeine Can Reverse Low dose endotoxemia-Induced Senescence in Endothelial Cells

Finally, we were interested in a therapeutic approach, to address the question of whether caffeine can reverse an already established senescent cellular phenotype. Therefore, we first induced senescence by LPS treatment as before and gave a single bolus of 50 µM caffeine after 12 days of LPS treatment (Figure 4A). This dose was chosen since we had already demonstrated that this concentration induces EC migration as a read-out for proper functionality. Moreover, 0.1% caffeine given with the drinking water resulted in a similar serum concentration in mice [9] and this regimen improved the respiratory chain activity in the heart mitochondria of 24-month-old mice to the level observed in mitochondria from 6-month-old animals [12]. As shown before, LPS treatment led to elevated p21 levels, and, interestingly, the single treatment with caffeine was sufficient to inhibit this increase in p21 (Figure 4B,C). These results were confirmed by immunostaining for p21 (Figure 4D,E). Similar to the results shown for the preventive treatment with caffeine (Figure 2G,H), the single treatment with caffeine blocked Trx-1 degradation induced by LPS (Figure 4F,G), suggesting that the reversion of senescence is intimately associated with a normalized redox balance.

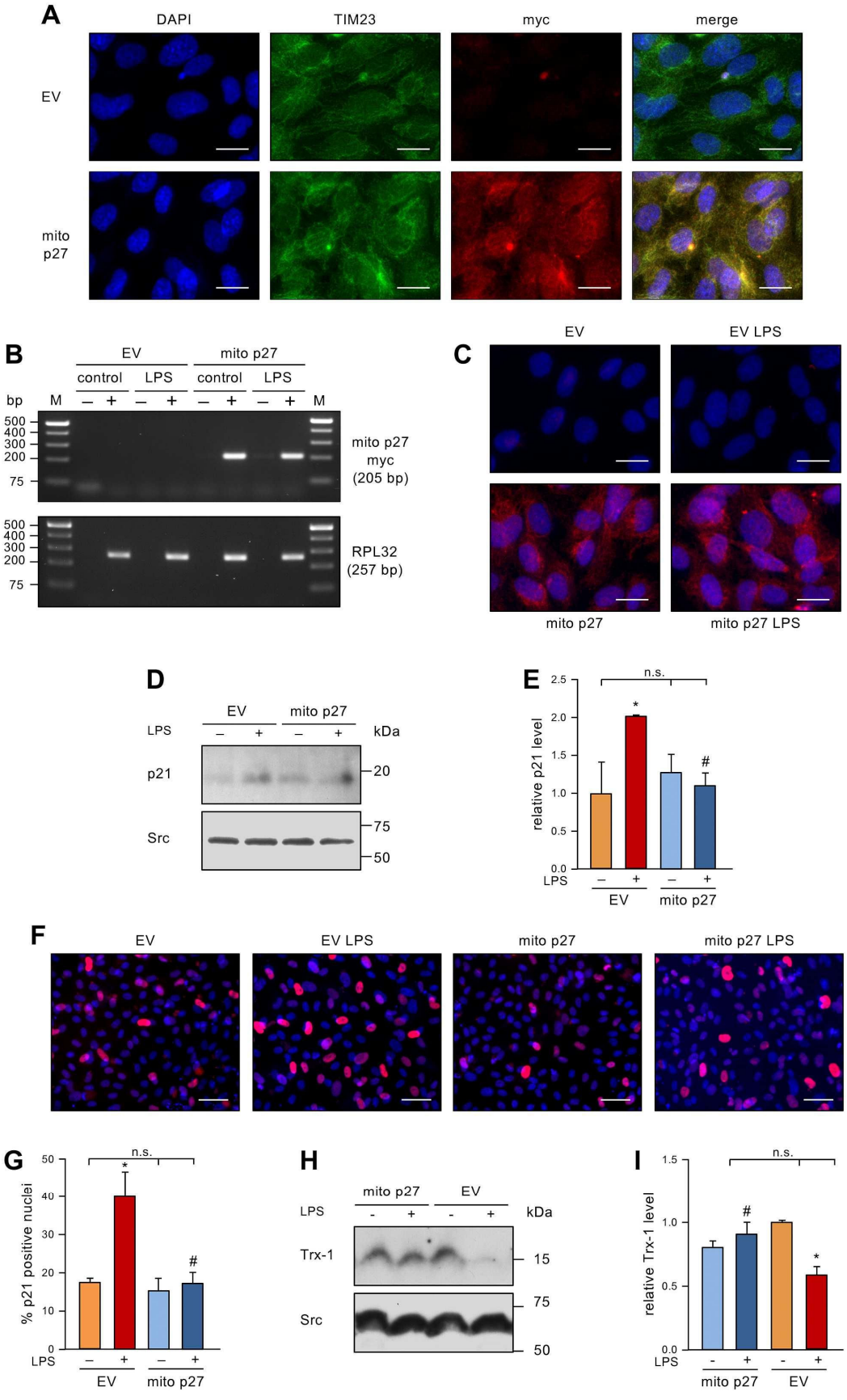

Figure 3. Mitochondrial p27 counteracts LPS-induced senescence and maintains Trx-1 levels. (**A**) ECs were transduced with a lentiviral expression vector for mitochondrially targeted p27 with a C-terminal

myc epitope tag (mito p27) or a corresponding empty virus (EV) and after two weeks localization of mito p27 was examined by fluorescence microscopy. ECs were stained with antibodies directed against the myc-tag on mito p27 (red) and the translocase of inner mitochondrial membrane 23 (TIM23, green), and the nuclei were counterstained with DAPI (blue); shown are representative immunostainings (scale bar = 20 μm). (**B**–**I**) ECs were transduced with a lentiviral expression vector for mitochondrially targeted p27 with a C-terminal myc epitope tag (mito p27) or a corresponding empty virus (EV) and subsequently treated with 1 ng/mL detoxified (control/−) or active LPS (LPS/+) every second day for two weeks. (**B**) Expression of mito p27 was analyzed by reverse transcription polymerase chain reaction. For that purpose, RNA was isolated from the transduced cells, and cDNA was synthesized in the presence (+) or absence (−) of reverse transcriptase. Amplification was performed with primers specifically detecting the mito p27 myc transcript, while the housekeeping gene RPL32 served as control. Amplification products were resolved by agarose gel electrophoresis; the expected fragment sizes are specified, and the numbers on the left indicate DNA size markers (M). (**C**–**E**) p21 was detected by immunoblot and immunostaining. (**C**) ECs were stained with an anti-myc antibody (red), and nuclei were counterstained with DAPI (blue); shown are representative immunostainings (scale bar = 20 μm). (**D**,**E**) p21 was detected by immunoblot and Src served as a loading control. (**D**) Representative immunoblots for p21 (upper panel) and Src (lower panel). (**E**) Semi-quantitative analysis of relative amounts of p21 (data are mean ± SEM, n = 3, * $p < 0.05$ vs. EV without LPS, $^{\#}$ $p < 0.05$ vs. EV + LPS, n.s. = not significant, and one-way ANOVA with post hoc Tukey LSD test). (**F**,**G**) p21 was detected by immunostaining and fluorescence microscopy. Cells were stained with an anti-p21 antibody (red), and nuclei were counterstained with DAPI (blue). (**F**) Representative immunostainings (scale bar = 50 μm). (**G**) Image J analyses of the percentage of p21 positive nuclei (data are mean ± SEM, n = 3, * $p < 0.05$ vs. EV without LPS, $^{\#}$ $p < 0.05$ vs. EV + LPS, n.s. = not significant, and one-way ANOVA with post hoc Tukey LSD test). (**H**,**I**) Trx-1 was detected by immunoblot and Src served as a loading control. (**H**) Representative immunoblots for Trx-1 (upper panel) and Src (lower panel). (**I**) Semi-quantitative analysis of the relative amounts of Trx-1 (data are mean ± SEM, n = 3, * $p < 0.05$ vs. EV without LPS, $^{\#}$ $p < 0.05$ vs. EV + LPS, n.s. = not significant, and one-way ANOVA with post hoc Tukey LSD test).

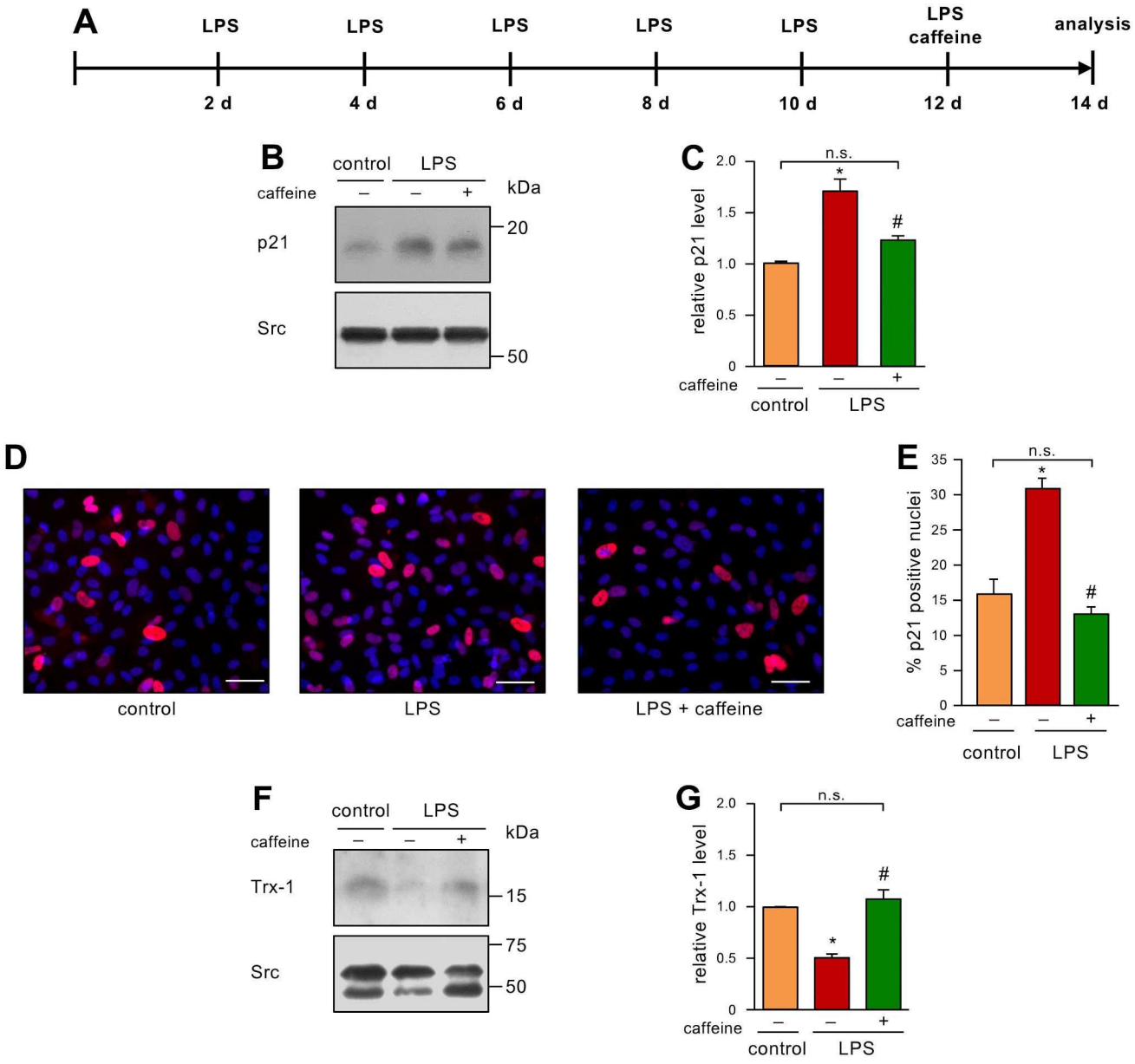

Figure 4. A single caffeine bolus reverses LPS-induced senescence and restores Trx-1 levels. (**A**–**G**) ECs were treated with 1 ng/mL detoxified (control) or active LPS (LPS) every second day for two weeks with a single bolus of 50 μM caffeine on the last treatment day. (**A**) Schematic representation of the treatment. (**B**–**G**) The LPS-treated group received caffeine (+) or not (−), as indicated. (**B**,**C**) p21 was detected by immunoblot and Src served as a loading control. (**B**) Representative immunoblots for p21 (upper panel) and Src (lower panel). (**C**) Semi-quantitative analysis of relative amounts of p21 (data are mean ± SEM, n = 5, * $p < 0.05$ vs. control, # $p < 0.05$ vs. LPS without caffeine, n.s. = not significant, and one-way ANOVA with post hoc Tukey LSD test). (**D**,**E**) p21 was detected by immunostaining and fluorescence microscopy. Cells were stained with an anti-p21 antibody (red), and nuclei were counterstained with DAPI (blue). (**D**) Representative immunostainings (scale bar = 50 μm). (**E**) Image J analyses of the percentage of p21 positive nuclei (data are mean ± SEM, n = 4, * $p < 0.05$ vs. control, # $p < 0.05$ vs. LPS without caffeine, n.s. = not significant, and one-way ANOVA with post hoc Tukey LSD test). (**F**,**G**) Trx-1 was detected by immunoblot and Src served as a loading control. (**F**) Representative immunoblots for Trx-1 (upper panel) and Src (lower panel). (**G**) Semi-quantitative analysis of relative amounts of Trx-1 (data are mean ± SEM, n = 4, * $p < 0.05$ vs. control, # $p < 0.05$ vs. LPS without caffeine, n.s. = not significant, and one-way ANOVA with post hoc Tukey LSD test).

4. Discussion

The major findings of the present study are the prevention and, even more importantly, the reversion of low dose endotoxemia-induced EC senescence by caffeine. Here we show for the first time that caffeine precludes senescence in ECs by preventing the loss of Trx-1 and eNOS, proteins vital for cellular redox homeostasis and NO bioavailability, respectively, and thereby, for the proper functionality of ECs. Moreover, we established a model for senescence induction by repetitive treatment with LPS in a low concentration. Indeed, in this low dose endotoxemia model, co-incubation with caffeine prevented the occurrence of senescence. Even more important, in a therapeutic setting, a single bolus of caffeine given on day 12 of senescence induction by LPS reversed senescence and the loss of Trx-1 protein.

Our data demonstrate that treatment of primary human ECs with 1 ng/mL LPS results in the onset of senescence and loss of EC functionality. This LPS concentration was chosen as several studies in mice and humans demonstrated that a high-fat diet leads to an increase in LPS levels in the blood. In mice, feeding a high-fat diet for 4 weeks increased the plasma LPS concentrations up to three times to a concentration of approximately 1.2 ng/mL [13]. Similarly, in healthy humans, a high fat, high carbohydrate meal resulted in elevated LPS levels in the blood when compared with humans consuming a high fiber and fruit meal [20]. The consumption of Western-type calorie rich diets combined with chronic overnutrition and a sedentary lifestyle represents a rising public health problem, as this often results in, for instance, type 2 diabetes and atherosclerosis. Given the fact that a high-fat diet leads to low dose endotoxemia, it is tempting to speculate that the senescent ECs found in human atherosclerotic plaques [1] are induced by increased LPS in the blood, as our findings here demonstrate that this low dose endotoxemia induces senescence in human ECs.

Senescence and aging are associated with mitochondrial dysfunction [21]. Here, we show that low dose endotoxemia reduces the migratory capacity of ECs. As previous studies demonstrated that the migration of ECs depends on intact mitochondria [9] and functional oxidative phosphorylation [8], one could assume that LPS treatment impairs electron transport chain activity and, thereby, diminishes migratory capacity. This would be in line with the findings of Deshpande et al. demonstrating that induction of senescence by constitutive active Rac1 results in increased mitochondrial ROS and decreased electron transport chain activity in ECs [22]. Similarly, we demonstrated that treatment of ECs with 100 mg/dL LDL results in senescence induction [7] and in a loss of mitochondrial ATP production [8]. Thus, mitochondrial functionality and EC senescence are intimately interwoven. Therefore, a substance that improves mitochondrial functions and, thus, endothelial functionality would be of great interest to prevent or delay endothelial dysfunction.

We have shown that caffeine in serum concentrations, which are reached after consumption of 4–6 cups of coffee, increases the migratory capacity of human ECs [9,10]. A few years ago, we unraveled the mechanisms underlying the promigratory effect of caffeine. We demonstrated that caffeine induces the translocation of p27 into the mitochondria and that the migratory capacity of ECs—also after stimulation with caffeine—is completely dependent on mitochondrial p27. Caffeine in the drinking water improved the respiratory chain activity in the hearts of wild-type mice, but not in p27-deficient littermates. More importantly, caffeine was able to increase the electron transport chain activity in the hearts of 24-month-old animals to the levels measured in adult, 6-month-old mice, suggesting an anti-aging effect of caffeine [12]. Here, we demonstrate that caffeine indeed inhibits senescence induction in ECs, possibly by improving mitochondrial functionality as the permanent expression of mitochondrially targeted p27 had the same effect. Caffeine also counteracted the loss of Trx-1 and, moreover, even when given in a therapeutic setting, i.e., after senescence induction by LPS, restored Trx-1 levels.

Since the maintenance of Trx-1 protein levels is important for preserving redox homeostasis as well as the ability to store NO in ECs, it is interesting to note that H_2O_2- as well as low dose LPS-induced senescence lead to the degradation of Trx-1 and increase in ROS ([6] and Supplementary Figure S1, respectively). Thus, one has to assume that disturbed redox homeostasis is a hallmark of senescence induction in ECs and thus, of

endothelial dysfunction. Since caffeine is able to restore Trx-1 levels and inhibit senescence, it would be interesting to understand how caffeine is capable of doing so. The loss of Trx-1 in senescent ECs goes along with the elevated activity of cathepsin D [6], the major lysosomal protease, which is responsible for Trx-1 degradation [23,24]. As it is known that mitochondrial respiration controls lysosomal function and that impairment of respiration leads to an increase in the lysosomal compartment [25], it is tempting to speculate that caffeine reduces lysosomal activity. This is beyond the scope of this study but will be investigated in the future. However, it has to be noted that low dose endotoxemia, but also the treatment of ECs with 150 ng/mL LPS for 24 h does not change Trx-1 mRNA levels (Supplementary Figure S2 and [18]). Those data suggest that it is not the downregulation of Trx-1 expression, but rather enhanced degradation that leads to the decrease in Trx-1 levels in senescent ECs. Having shown that treatment with low dose LPS led to a degradation of Trx-1, and that caffeine, which improves mitochondrial functionality [12], counteracts Trx-1 degradation, it would be interesting to investigate if LPS and caffeine have similar effects on Thioredoxin-2, the mitochondrial Thioredoxin, in a future study.

5. Conclusions

In conclusions, the observation that caffeine interferes with senescence induction in ECs, which would lead to endothelial dysfunction that is observed in nearly all cardiovascular diseases [26], might at least partially explain the beneficial effects of moderate coffee consumption on mortality risk in elderly people [11,27].

Supplementary Materials: The following supporting information can be downloaded at: https://www.mdpi.com/article/10.3390/antiox12061244/s1, Figure S1: Low dose endotoxemia increases ROS levels; Figure S2: Senescence induction does not change the Trx-1 transcript level.

Author Contributions: Conceptualization, D.M., N.A.-A., P.J., and J.H.; formal analysis, D.M., A.V., F.C., O.E., F.v.A., and N.D.-R.; investigation, J.G. and J.H.; methodology, J.G., F.C., O.E., and F.v.A.; software, F.v.A.; supervision, J.H.; validation, O.E., J.A., N.A.-A., and J.H.; writing—original draft, J.A., P.J., and J.H. All authors have read and agreed to the published version of the manuscript.

Funding: This study was in part funded by the Deutsche Forschungsgemeinschaft (DFG), IRTG1902-2 to J.A. and J.H.; D.M., J.G. and A.V. are stipend holders of IRTG1902-2. This study was also in part funded by Bayer Grant4Target (2019-08-2427) to J.H. and by intramural funding (9772727) of the University Hospital of the Heinrich-Heine University to J.H.

Institutional Review Board Statement: Not applicable.

Informed Consent Statement: Not applicable.

Data Availability Statement: Data are contained within the article. All further information will be provided by the corresponding authors upon request.

Conflicts of Interest: The authors declare no conflict of interest. The funders had no role in the design of the study; in the collection, analyses, or interpretation of data; in the writing of the manuscript; or in the decision to publish the results.

References

1. Minamino, T.; Miyauchi, H.; Yoshida, T.; Ishida, Y.; Yoshida, H.; Komuro, I. Endothelial cell senescence in human atherosclerosis: Role of telomere in endothelial dysfunction. *Circulation* **2002**, *105*, 1541–1544. [CrossRef] [PubMed]
2. Holmgren, A. Antioxidant function of thioredoxin and glutaredoxin systems. *Antioxid. Redox Signal.* **2000**, *2*, 811–820. [CrossRef]
3. Zschauer, T.C.; Matsushima, S.; Altschmied, J.; Shao, D.; Sadoshima, J.; Haendeler, J. Interacting with thioredoxin-1--disease or no disease? *Antioxid. Redox Signal.* **2013**, *18*, 1053–1062. [CrossRef]
4. Altschmied, J.; Haendeler, J. Thioredoxin-1 and endothelial cell aging: Role in cardiovascular diseases. *Antioxid. Redox Signal.* **2009**, *11*, 1733–1740. [CrossRef]
5. Haendeler, J. Thioredoxin-1 and posttranslational modifications. *Antioxid. Redox Signal.* **2006**, *8*, 1723–1728. [CrossRef]
6. Goy, C.; Czypiorski, P.; Altschmied, J.; Jakob, S.; Rabanter, L.L.; Brewer, A.C.; Ale-Agha, N.; Dyballa-Rukes, N.; Shah, A.M.; Haendeler, J. The imbalanced redox status in senescent endothelial cells is due to dysregulated Thioredoxin-1 and NADPH oxidase 4. *Exp. Gerontol.* **2014**, *56*, 45–52. [CrossRef]

7. Buchner, N.; Ale-Agha, N.; Jakob, S.; Sydlik, U.; Kunze, K.; Unfried, K.; Altschmied, J.; Haendeler, J. Unhealthy diet and ultrafine carbon black particles induce senescence and disease associated phenotypic changes. *Exp. Gerontol.* **2013**, *48*, 8–16. [CrossRef]
8. Gonnissen, S.; Ptok, J.; Goy, C.; Jander, K.; Jakobs, P.; Eckermann, O.; Kaisers, W.; von Ameln, F.; Timm, J.; Ale-Agha, N.; et al. High Concentration of Low-Density Lipoprotein Results in Disturbances in Mitochondrial Transcription and Functionality in Endothelial Cells. *Oxid. Med. Cell Longev.* **2019**, *2019*, 7976382. [CrossRef]
9. Spyridopoulos, I.; Fichtlscherer, S.; Popp, R.; Toennes, S.W.; Fisslthaler, B.; Trepels, T.; Zernecke, A.; Liehn, E.A.; Weber, C.; Zeiher, A.M.; et al. Caffeine enhances endothelial repair by an AMPK-dependent mechanism. *Arter. Thromb. Vasc. Biol.* **2008**, *28*, 1967–1974. [CrossRef] [PubMed]
10. Ohmichi, T.; Kasai, T.; Shinomoto, M.; Matsuura, J.; Koizumi, T.; Kitani-Morii, F.; Tatebe, H.; Sasaki, H.; Mizuno, T.; Tokuda, T. Quantification of Blood Caffeine Levels in Patients With Parkinson's Disease and Multiple System Atrophy by Caffeine ELISA. *Front. Neurol.* **2020**, *11*, 580127. [CrossRef] [PubMed]
11. Freedman, N.D.; Park, Y.; Abnet, C.C.; Hollenbeck, A.R.; Sinha, R. Association of coffee drinking with total and cause-specific mortality. *N Engl. J. Med.* **2012**, *366*, 1891–1904. [CrossRef]
12. Ale-Agha, N.; Goy, C.; Jakobs, P.; Spyridopoulos, I.; Gonnissen, S.; Dyballa-Rukes, N.; Aufenvenne, K.; von Ameln, F.; Zurek, M.; Spannbrucker, T.; et al. CDKN1B/p27 is localized in mitochondria and improves respiration-dependent processes in the cardiovascular system-New mode of action for caffeine. *PLoS Biol.* **2018**, *16*, e2004408. [CrossRef]
13. Cani, P.D.; Amar, J.; Iglesias, M.A.; Poggi, M.; Knauf, C.; Bastelica, D.; Neyrinck, A.M.; Fava, F.; Tuohy, K.M.; Chabo, C.; et al. Metabolic endotoxemia initiates obesity and insulin resistance. *Diabetes* **2007**, *56*, 1761–1772. [CrossRef] [PubMed]
14. Haendeler, J.; Hoffmann, J.; Tischler, V.; Berk, B.C.; Zeiher, A.M.; Dimmeler, S. Redox regulatory and anti-apoptotic functions of thioredoxin depend on S-nitrosylation at cysteine 69. *Nat. Cell Biol.* **2002**, *4*, 743–749. [CrossRef]
15. Jakob, S.; Schroeder, P.; Lukosz, M.; Buchner, N.; Spyridopoulos, I.; Altschmied, J.; Haendeler, J. Nuclear protein tyrosine phosphatase Shp-2 is one important negative regulator of nuclear export of telomerase reverse transcriptase. *J. Biol. Chem.* **2008**, *283*, 33155–33161. [CrossRef] [PubMed]
16. Jander, K.; Greulich, J.; Gonnissen, S.; Ale-Agha, N.; Goy, C.; Jakobs, P.; Farrokh, S.; Marziano, C.; Sonkusare, S.K.; Haendeler, J.; et al. Extra-Nuclear Functions of the Transcription Factor Grainyhead-Like 3 in the Endothelium-Interaction with Endothelial Nitric Oxide Synthase. *Antioxidants* **2021**, *10*, 428. [CrossRef] [PubMed]
17. Schindelin, J.; Arganda-Carreras, I.; Frise, E.; Kaynig, V.; Longair, M.; Pietzsch, T.; Preibisch, S.; Rueden, C.; Saalfeld, S.; Schmid, B.; et al. Fiji: An open-source platform for biological-image analysis. *Nat. Methods* **2012**, *9*, 676–682. [CrossRef] [PubMed]
18. Merk, D.; Ptok, J.; Jakobs, P.; von Ameln, F.; Greulich, J.; Kluge, P.; Semperowitsch, K.; Eckermann, O.; Schaal, H.; Ale-Agha, N.; et al. Selenoprotein T Protects Endothelial Cells against Lipopolysaccharide-Induced Activation and Apoptosis. *Antioxidants* **2021**, *10*, 1427. [CrossRef]
19. Pfaffl, M.W. A new mathematical model for relative quantification in real-time RT-PCR. *Nucleic. Acids Res.* **2001**, *29*, e45. [CrossRef]
20. Ghanim, H.; Abuaysheh, S.; Sia, C.L.; Korzeniewski, K.; Chaudhuri, A.; Fernandez-Real, J.M.; Dandona, P. Increase in plasma endotoxin concentrations and the expression of Toll-like receptors and suppressor of cytokine signaling-3 in mononuclear cells after a high-fat, high-carbohydrate meal: Implications for insulin resistance. *Diabetes Care* **2009**, *32*, 2281–2287. [CrossRef]
21. Lopez-Otin, C.; Blasco, M.A.; Partridge, L.; Serrano, M.; Kroemer, G. The hallmarks of aging. *Cell* **2013**, *153*, 1194–1217. [CrossRef] [PubMed]
22. Deshpande, S.S.; Qi, B.; Park, Y.C.; Irani, K. Constitutive activation of rac1 results in mitochondrial oxidative stress and induces premature endothelial cell senescence. *Arterioscler. Thromb. Vasc. Biol.* **2003**, *23*, e1–e6. [CrossRef] [PubMed]
23. Dyballa-Rukes, N.; Jakobs, P.; Eckers, A.; Ale-Agha, N.; Serbulea, V.; Aufenvenne, K.; Zschauer, T.C.; Rabanter, L.L.; Jakob, S.; von Ameln, F.; et al. The Anti-Apoptotic Properties of APEX1 in the Endothelium Require the First 20 Amino Acids and Converge on Thioredoxin-1. *Antioxid. Redox Signal.* **2017**, *26*, 616–629. [CrossRef] [PubMed]
24. Haendeler, J.; Popp, R.; Goy, C.; Tischler, V.; Zeiher, A.M.; Dimmeler, S. Cathepsin D and H_2O_2 stimulate degradation of thioredoxin-1: Implication for endothelial cell apoptosis. *J. Biol. Chem.* **2005**, *280*, 42945–42951. [CrossRef]
25. Baixauli, F.; Acin-Perez, R.; Villarroya-Beltri, C.; Mazzeo, C.; Nunez-Andrade, N.; Gabande-Rodriguez, E.; Ledesma, M.D.; Blazquez, A.; Martin, M.A.; Falcon-Perez, J.M.; et al. Mitochondrial Respiration Controls Lysosomal Function during Inflammatory T Cell Responses. *Cell Metab.* **2015**, *22*, 485–498. [CrossRef]
26. Cai, H.; Harrison, D.G. Endothelial dysfunction in cardiovascular diseases: The role of oxidant stress. *Circ Res* **2000**, *87*, 840–844. [CrossRef]
27. Greenberg, J.A.; Chow, G.; Ziegelstein, R.C. Caffeinated coffee consumption, cardiovascular disease, and heart valve disease in the elderly (from the Framingham Study). *Am. J. Cardiol.* **2008**, *102*, 1502–1508. [CrossRef]

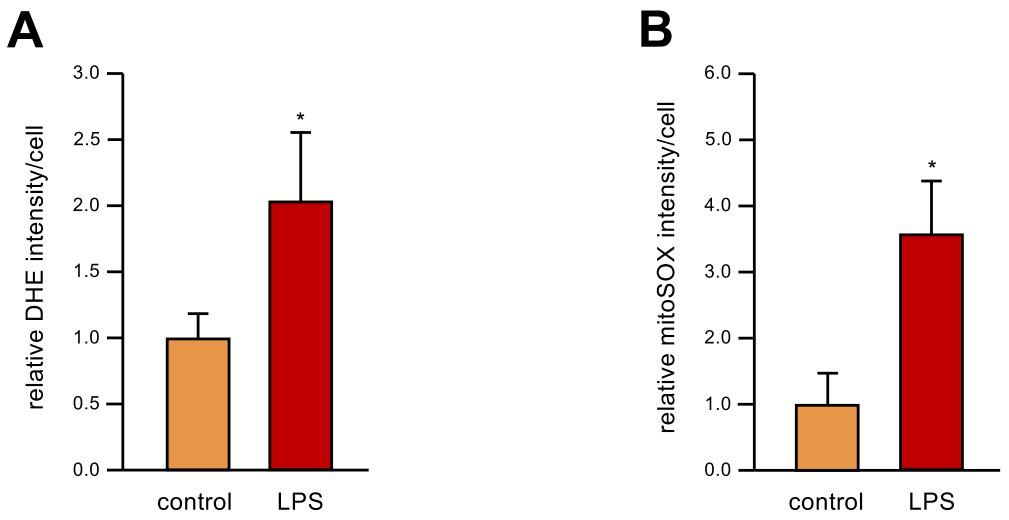

Supplementary figure S1: Low dose endotoxemia increases ROS levels. EC were treated with 1 ng/mL detoxified (control) or active LPS (LPS) every second day for two weeks. Rela-tive DHE (A) or mitoSOX (B) intensities were analyzed by Image J using total cell count for normalization (data are mean ± SEM, n = 3, *p < 0.05 vs control, two sided paired t-Test).

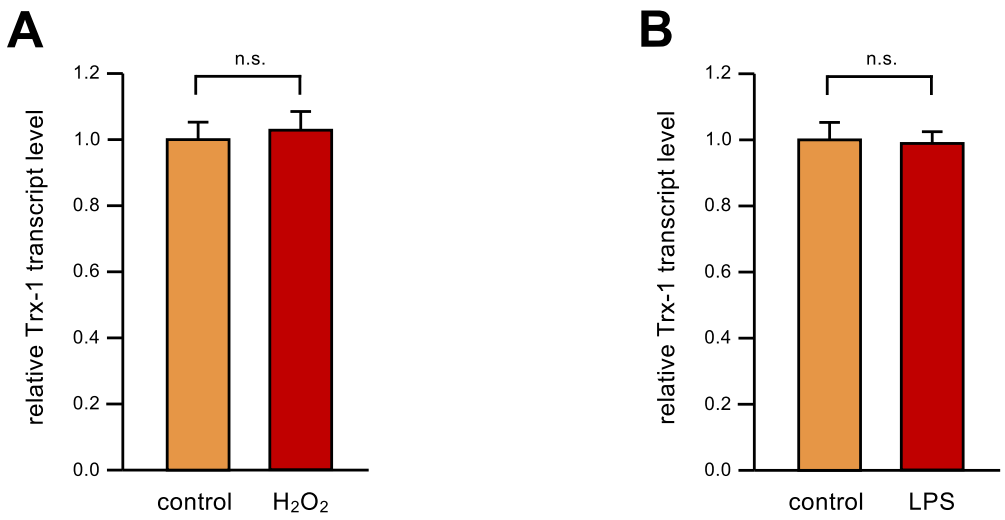

Supplementary figure S 2: Senescence induction does not change the Trx-1 transcript level. (A) EC were treated with 50 µM H_2O_2 every day for two weeks or left untreated (control). (B) In a low dose endotoxemia model, EC were treated with 1 ng/mL detoxified (control) or active LPS (LPS) every second day for two weeks. (A, B) Trx-1 transcript levels were ana-lyzed by semi-quantitative real-time PCR using RPL32 for normalization (data are mean ± SEM, n = 6, n.s. = not significant, two sided paired t-Test).

antioxidants

MDPI

Review

Dose-Dependent Effects of Lipopolysaccharide on the Endothelium—Sepsis versus Metabolic Endotoxemia-Induced Cellular Senescence

Dennis Merk [1,†], Fiona Frederike Cox [1,2,†], Philipp Jakobs [1], Simone Prömel [3], Joachim Altschmied [1,4,*] and Judith Haendeler [1,4,*]

[1] Environmentally-Induced Cardiovascular Degeneration, Clinical Chemistry and Laboratory Diagnostics, Medical Faculty, University Hospital and Heinrich-Heine-University, 40225 Düsseldorf, Germany; dennis.merk@hhu.de (D.M.); fiona.cox@hhu.de (F.F.C.); philipp.jakobs@hhu.de (P.J.)
[2] Medical Faculty, Institute for Translational Pharmacology, University Hospital and Heinrich-Heine-University, 40225 Düsseldorf, Germany
[3] Department of Biology, Institute of Cell Biology, Heinrich-Heine-University, 40225 Düsseldorf, Germany; proemel@hhu.de
[4] Medical Faculty, Cardiovascular Research Institute Düsseldorf, CARID, University Hospital and Heinrich-Heine-University Düsseldorf, 40225 Düsseldorf, Germany
* Correspondence: joalt001@hhu.de (J.A.); juhae001@hhu.de (J.H.); Tel.: +49-211-8112008 (J.A. & J.H.)
† These authors contributed equally to this work.

Abstract: The endothelium, the innermost cell layer of blood vessels, is not only a physical barrier between the bloodstream and the surrounding tissues but has also essential functions in vascular homeostasis. Therefore, it is not surprising that endothelial dysfunction is associated with most cardiovascular diseases. The functionality of the endothelium is compromised by endotoxemia, the presence of bacterial endotoxins in the bloodstream with the main endotoxin lipopolysaccharide (LPS). Therefore, this review will focus on the effects of LPS on the endothelium. Depending on the LPS concentration, the outcomes are either sepsis or, at lower concentrations, so-called low-dose or metabolic endotoxemia. Sepsis, a life-threatening condition evoked by hyperactivation of the immune response, includes breakdown of the endothelial barrier resulting in failure of multiple organs. A deeper understanding of the underlying mechanisms in the endothelium might help pave the way to new therapeutic options in sepsis treatment to prevent endothelial leakage and fatal septic shock. Low-dose endotoxemia or metabolic endotoxemia results in chronic inflammation leading to endothelial cell senescence, which entails endothelial dysfunction and thus plays a critical role in cardiovascular diseases. The identification of compounds counteracting senescence induction in endothelial cells might therefore help in delaying the onset or progression of age-related pathologies. Interestingly, two natural plant-derived substances, caffeine and curcumin, have shown potential in preventing endothelial cell senescence.

Keywords: endothelial cells; high-dose endotoxemia; lipopolysaccharide; low-dose endotoxemia; stress-induced endothelial cell senescence

Citation: Merk, D.; Cox, F.F.; Jakobs, P.; Prömel, S.; Altschmied, J.; Haendeler, J. Dose-Dependent Effects of Lipopolysaccharide on the Endothelium—Sepsis versus Metabolic Endotoxemia-Induced Cellular Senescence. *Antioxidants* **2024**, *13*, 443. https://doi.org/10.3390/antiox13040443

Academic Editor: Yuri Korystov

Received: 19 February 2024
Revised: 3 April 2024
Accepted: 8 April 2024
Published: 9 April 2024

1. Cardiovascular Diseases and Endothelial Dysfunction

Cardiovascular diseases (CVDs) are the leading cause of morbidity and mortality in the world and were responsible for 17.9 million deaths in 2019 (https://www.who.int/news-room/fact-sheets/detail/cardiovascular-diseases-(cvds) (accessed on 7 February 2024). Their development and progression are intimately linked to endothelial dysfunction caused by factors such as oxidative stress. The vascular endothelium consists of a monolayer of endothelial cells, which constitutes the inner lining of all blood vessels. Endothelial cells are attached to the basal lamina, which acts as a scaffold, with pericytes and smooth muscle cells situated on the outside. The endothelium thereby forms a barrier between the

bloodstream and the surrounding tissue and maintains vascular homeostasis. It secretes multiple factors that influence coagulation, vascular tone, adhesion of leukocytes, and inflammation, underscoring the importance of the endothelium for vascular homeostasis [1]. Endothelial cells are also important for the exchange of nutrients and molecules between the blood and the surrounding tissue. Their functionality requires energy to maintain a healthy endothelium [2].

Endothelial dysfunction is defined as the failure of endothelial cells to carry out their normal functions and is a consequence of their excessive activation and apoptosis [3]. The activation is induced by proinflammatory cytokines, including Tumor Necrosis Factor (TNF)-α and Interleukin-6 (IL-6) [4]. It is characterized by the expression of cell-surface adhesion molecules, such as Intercellular Adhesion Molecule 1 (ICAM1) or Vascular Cell Adhesion Molecule 1 (VCAM1). These adhesion molecules facilitate the recruitment and attachment of leukocytes to the endothelium, leading to increased endothelial leakiness, allowing diapedesis—the transmigration of leukocytes through the endothelial cell layer [3]. Prolonged endothelial cell activation and the unrestricted secretion of inflammatory cytokines by leukocytes favor endothelial cell apoptosis. Apoptosis is executed by caspases, which cleave proteins critical for cell survival [5]. Tight control of apoptosis is a prerequisite for maintaining a healthy endothelium, especially because endothelial cells are the first cells exposed to invading pathogens. Their dysfunction is a precursor to tissue and organ damage and is a major contributor to certain lethal pathologies, e.g., sepsis. Thus, the next two chapters will introduce the mechanisms in sepsis/high-dose endotoxemia with a specific focus on the endothelium.

2. Sepsis

Sepsis and septic shock are the leading cause of mortality in critically ill patients, accounting for approximately 20% of all-cause deaths globally. It was estimated that sepsis had affected 49 million individuals and was related to 11 million deaths worldwide in 2017 [6]. Sepsis is defined as a life-threatening organ dysfunction caused by a dysregulated host response to infection [7]. Its pathogenesis includes various steps, such as infection, hyperactivation of the immune system, endothelial dysfunction leading to loss of barrier integrity, followed by tissue damage, and finally, multi-organ failure and death [8] (Figure 1).

Infection with gram-negative bacteria, including *Escherichia coli* and *Pseudomonas aeruginosa*, is the prevailing cause of severe sepsis in humans [9]. Under normal circumstances, the innate immune system reacts to local infections and protects the organism from further damage. However, the hyperactivity of the immune response in sepsis occurs when the host loses control of the local containment of an infection, such that it becomes systemic. This leads to the production of proinflammatory cytokines, reactive oxygen species (ROS), and cellular injury, mediated by the recognition of pathogens by pattern recognition receptors (PRRs) [10,11]. Those PRRs, which are expressed on the surface of immune and phagocytic cells, and also on some non-immune cells, recognize pathogen-associated molecular patterns (PAMPs) that are expressed on both harmless and pathogenic microbes [11]. During tissue damage, intracellular components are released, which are recognized as damage-associated molecular patterns (DAMPs), and activate the immune system in concert with PAMPs [12].

The most important PAMP in the context of sepsis is lipopolysaccharide (LPS), an outer membrane component of gram-negative bacteria. LPS consists of a proximal oligosaccharide core, the distal O antigen, a glycan polymer, and a lipid A hydrophobic anchor—a glucosamine disaccharide decorated with multiple fatty acids [13]. Its immunostimulatory activity is mostly derived from the lipid A moiety, which in humans and mice binds to toll-like receptors (TLRs) and thereby activates the innate immune response [14]. LPS can exert its effect either locally or, after entering the blood circulation, systemically. LPS also affects the endothelial cell transcriptome by regulating transcripts of protein coding and non-coding RNAs [15]. Endothelial cells treated with LPS showed a significant increase in

upregulated genes with gene ontology (GO) terms related to immune response to bacteria and TNF signaling [16]. Moreover, LPS concentrations above approximately 500 pg/mL are known to be lethal. This was shown in a study with 253 patients at the onset of severe sepsis and/or septic shock, where the median endotoxin concentration in the plasma was 300 pg/mL. More importantly, in survivors over a 28-day period, the mean level at study entry was 230 pg/mL, while it was 515 pg/mL in non-survivors [17].

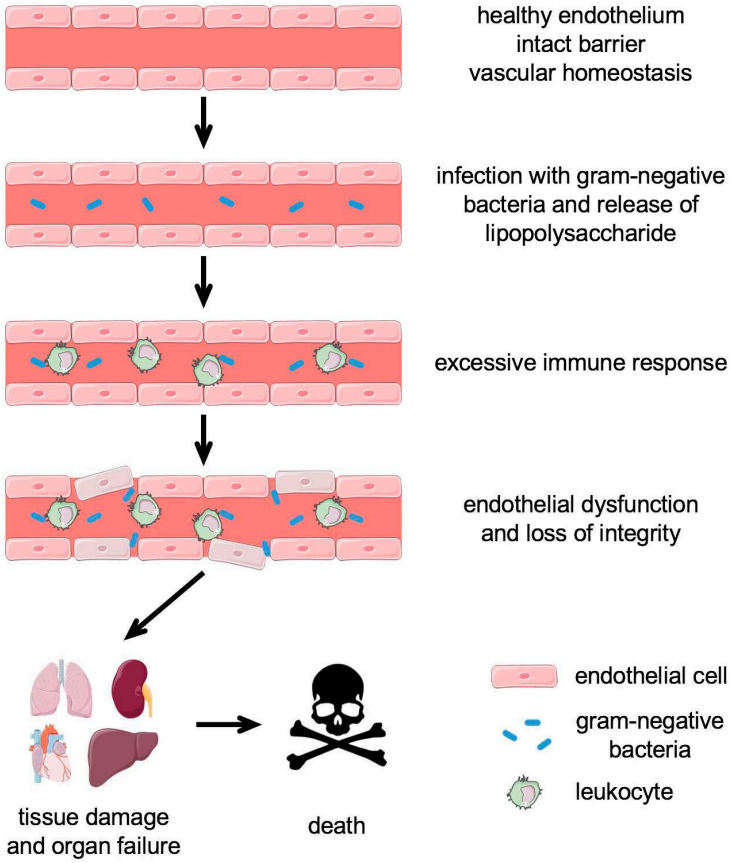

Figure 1. Sepsis progression. Under physiological conditions, the endothelium is an intact barrier between the bloodstream and surrounding tissues and maintains vascular homeostasis. Upon systemic infection with gram-negative bacteria, lipopolysaccharide is released, leading to the activation of endothelial cells. The excessive secretion of cytokines by recruited leukocytes leads to the breakdown of the endothelial barrier. This results in tissue damage and organ failure and can ultimately lead to death.

Although TLR signaling is well described (see chapter 3), LPS effects are more complex and multifaceted, and the underlying mechanisms are far from understood. This explains why there are still no FDA-approved treatment options available that improve sepsis survival, despite significant advancements in therapeutic management and over 100 therapeutic trials [18,19]. Further exploration of the endothelial cell response to LPS and possible interference with the negative effects might provide clues for new targets for adjuvant therapies aimed at protecting the endothelium against damage and preventing the breakdown of the endothelial barrier.

3. Toll-like Receptors

TLRs are a family of transmembrane glycoproteins, which, in humans, is comprised of 10 members. They are located on macrophages, T-cells, B-cells, dendritic cells, and also non-immune cells, like endothelial cells [20,21]. They recognize and bind to a wide range of different molecules, including microbial components, such as LPS, lipopeptides, or

double-stranded RNA, via a horseshoe-shaped ligand binding domain built from leucine-rich repeats [22]. The binding of ligands induces a rearrangement of the receptor complex and induces the innate immune response and inflammation [14]. They detect different microbial components, such as LPS, lipopeptides, or double-stranded RNA, and induce the innate immune response and inflammation [14]. The most important TLR in LPS signaling is TLR4 [23]. According to the publicly available databases Genecards [24], Human Protein Atlas [25], and GTEx Portal [26], its transcript is present in nearly all human tissues. TLR4 can not only be found on blood cells but also on the cell surface of endothelial cells [27], smooth muscle cells [28], skeletal muscle cells [29], cardiac myocytes [30], and cells of the central nervous system [31]. The lipid A moiety of LPS is recognized and first bound by lipopolysaccharide-binding protein (LBP) and transferred to CD14 molecules. Membrane-bound CD14 (mCD14) is a glycosylphosphatidylinositol (GPI)-anchored protein located on the surface of myeloid–lineage cells like monocytes, macrophages, and dendritic cells [32]. After binding to CD14, LPS is subsequently transferred to Myeloid Differentiation Protein 2 (MD-2), and this transfer is catalyzed by CD14 [33]. MD-2 is essential for the activation of TLR4 by LPS, which was shown by the lack of response of macrophages derived from MD-2 knockout mice after LPS treatment [34]. In addition to mCD14, a soluble form of CD14 (sCD14), which lacks the GPI anchor, exists, which is also released from non-myeloid cells, including hepatocytes, adipocytes, and intestinal epithelial cells [35]. It is produced by shedding or secretion and is found in serum of normal individuals [36]. It has long been known that sCD14 can make CD14-negative cells like epithelial and endothelial cells responsive to LPS stimulation [37,38]. This is achieved by the high-affinity binding of LPS to sCD14 and the transport of this complex through the bloodstream. Soluble CD14 can then transfer LPS to MD-2 as efficiently as mCD14 [33], such that this reaction can also take place on cells devoid of CD14 themselves [39,40]. At this step, a complex of TLR4/MD2/LPS is formed, which builds a homodimer and triggers two consecutive pathways: (1) The MyD88-dependent pathway, which is induced in the plasma membrane, and (2) the TRIF-dependent pathway, which starts in early endosomes after the endocytosis of the receptor complex [41] (Figure 2).

During the MyD88-dependent pathway, the membrane-anchored TLR4 receptor interacts with the TIR domain-containing adapter protein (TIRAP) and recruits MyD88, triggering a signaling cascade. This cascade includes the recruitment of IL-1 Receptor Associated Kinases (IRAKs) 1 and 4. IRAK4 was shown to phosphorylate and thereby activates IRAK1 upon stimulation [42]. Following phosphorylation, IRAK1 associates with TNF Receptor Associated Factor 6 (TRAF6), which is a mediator of cytokine signaling and stress response pathways [43]. These include the activation of the transcription factors cAMP Response Element Binding Protein (CREB) and Activator Protein-1 (AP-1) [44–46]. TRAF6 also promotes the polyubiquitination of NEMO, an inhibitor of nuclear factor-κB (NF-κB) nuclear translocation. This triggers the degradation of NEMO, allowing nuclear entry of NF-κB, which then initiates the production of pro-inflammatory mediators, such as IL-6, IL-1β, and TNF-α, leading to an even further enhanced inflammatory response [41]. Following the dissociation of membrane-bound TLR4 from TIRAP and MyD88, TLR4 undergoes endocytosis and binds TIR Domain Containing Adaptor Molecule 1 (TRIF) and TRIF-Related Adapter Molecule (TRAM). It was shown that TRAM recruits TRIF to the plasma membrane and acts as a bridging adaptor, enabling the interaction of TRIF with TLR4 [47]. LPS promotes the complex building of TLR4 and TRAM and their following translocation into the endosome [48]. The LPS-induced internalization of TLR4 is controlled by CD14, whose importance is highlighted by the increased localization of TRAM to regions enriched with CD14 [49]. Endocytosis terminates the MyD88-dependent signaling, and endosome maturation as well as lysosomal degradation of TLR4 define the extent of the TRIF-dependent signaling [50]. TRIF-dependent signaling activates two kinases, TANK Binding Kinase 1 (TBK1) and IκB Kinase ε (IKKε), which phosphorylate the transcription factors Interferon Regulatory Factor (IRF) 3 and 7, leading to the expression of type I inter-

ferons, enhancing the inflammatory response even further [41]. In addition, TRAM also interacts with TRAF6, supporting NF-κB activation through the degradation of NEMO [51].

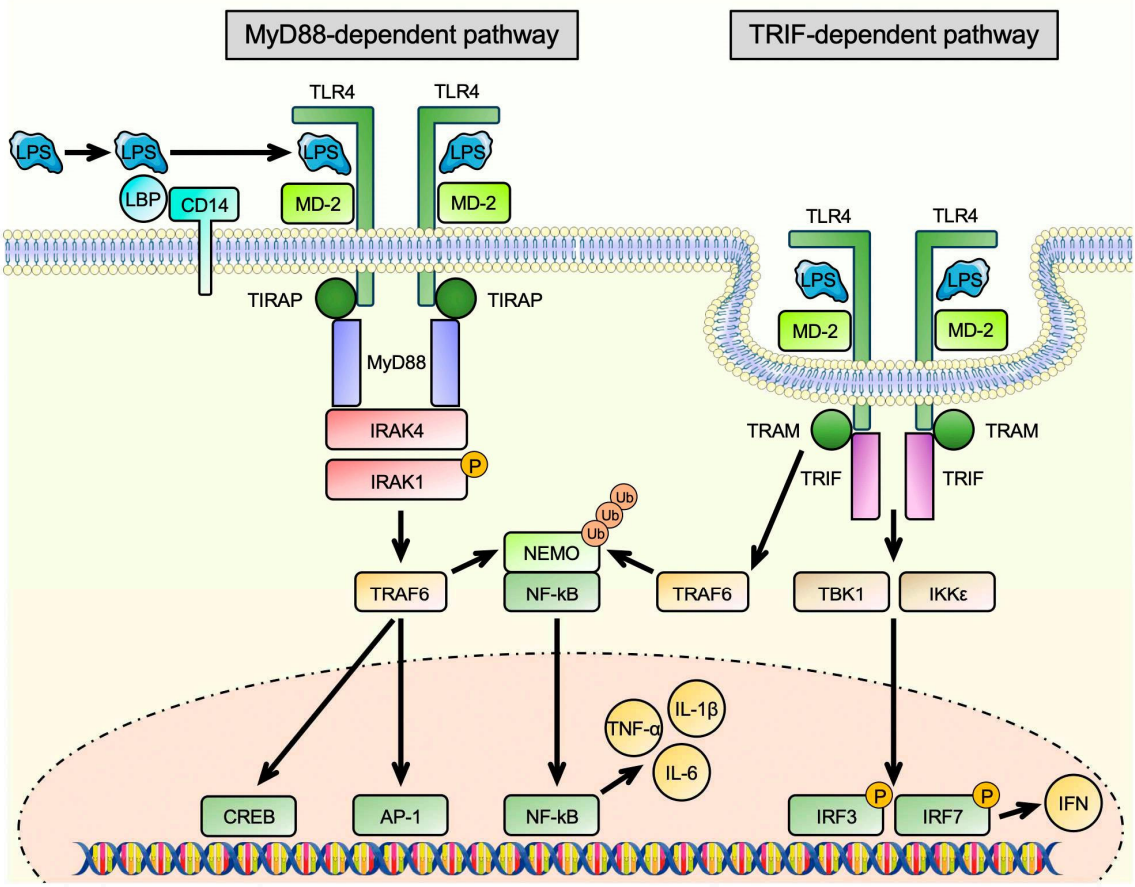

Figure 2. Lipopolysaccharide-induced Toll-like Receptor 4 signaling. After entering the circulation, lipopolysaccharide (LPS) is bound by Lipopolysaccharide-Binding Protein (LBP) and—facilitated by CD14—transferred to Myeloid Differentiation Protein 2 (MD-2). Together, LPS and MD-2 form a complex with Toll-like Receptor 4 (TLR4), which homodimerizes. This triggers two distinct, consecutive pathways: (1) the MyD88-dependent pathway and the (2) TRIF-dependent pathway. First, TLR4 interacts with the TIR Domain Containing Adapter Protein (TIRAP), which recruits MyD88. Following its association with the complex, IL-1 Receptor Associated Kinase 4 (IRAK4) phosphorylates IRAK1, which in turn couples to TNF Receptor Associated Factor 6 (TRAF6). TRAF6 activates the transcription factors cAMP Response Element Binding Protein (CREB) and Activator Protein-1 (AP-1) and promotes polyubiquitination of NEMO, an inhibitor of nuclear factor-κB (NF-κB) nuclear translocation. Its degradation allows nuclear entry of NF-κB and the expression of pro-inflammatory cytokines, such as IL-6, IL-1β, and TNF-α. In the second step, TLR4 dissociates from TIRAP and MyD88 and undergoes endocytosis. Now, the TRIF-Related Adapter Molecule (TRAM) enables binding of the TIR Domain Containing Adaptor Molecule 1 (TRIF). TRIF-dependent signaling activates two kinases, TANK Binding Kinase 1 (TBK1) and IκB Kinase ε (IKKε), which phosphorylate the transcription factors Interferon Regulatory Factor (IRF) 3 and 7, leading to the expression of type I interferons (IFN), enhancing the inflammatory response even further. In addition, TRAM also interacts with TRAF6, supporting NF-κB activation through the degradation of NEMO.

However, it has to be mentioned that the LPS signal cannot only be transmitted via TLR4. An intracellular inflammasome complex, which acts as a molecular signaling platform in the cytoplasm, has been found to recognize LPS intracellularly and activate a human caspase-4/murine caspase-11-dependent pathway that leads to increase in IL-1β and IL-18 and is sufficient to induce pyroptosis [52–54]. TLR4 is dispensable for this re-

sponse, as demonstrated in TLR4-deficient mice, which were primed with a TLR3 agonist to activate caspase 11 and were as susceptible to LPS-triggered sepsis as wildtype animals [52]. After these initial studies, which used LPS-loaded macrophages, it was later demonstrated that outer membrane vesicles produced by gram-negative bacteria can deliver LPS into the cytosol and trigger caspase-11-dependent effector responses in vitro and in vivo [55].

Additionally, it was shown that the shape of LPS can vary, activating different TLRs; for example, TLR2 [56]. This is highlighted by the alternative formation of specific TLR receptor clusters in response to different bacterial products [57]. Moreover, the potency of LPS varies, with the hexa-acylated and phosphorylated LPS of *Escherichia coli* being one of the most potent species, whereas under-acylated, dephosphorylated LPS species have weaker pro-inflammatory activity [58]. This also contributes to the aforementioned structural diversity among LPS and influences its functionality [59].

Since TLR4 is the dominant PRR in LPS signaling, it seems reasonable to inhibit TLR-4. However, Eritoran, an analog of lipid A and TLR4 antagonist, which inhibits LPS-triggered TLR4 signaling [60], did not result in reduced 28-day mortality in a phase III clinical trial [17].

Septic patients also exhibit overwhelming oxidative stress, which results from the uncontrolled production of reactive oxygen and nitrogen species from activated immune cells. This explains why antioxidant therapies, using vitamin C, selenium, or N-acetylcysteine, were investigated in sepsis models [61]. However, they did not show any positive effects in humans [11].

In contrast to the acute effects of high-dose LPS on the vasculature, the effects of low-dose LPS are usually chronic and related to stress-induced senescence and aging, with aging being a major risk factor for the development of CVDs. In the following chapters of the review, we focus on endothelial senescence, its induction by low-dose endotoxemia, the role of the gut microbiome, and highlight the potential of natural dietary compounds to counteract senescence induction.

4. Stress-Induced Senescence in the Endothelium

Stress-induced cellular senescence is a phenomenon that occurs in response to various stressors including oxidative stress, xenobiotics [62], or low-dose endotoxemia [63] and goes along with increased intracellular ROS production. It can have detrimental effects on tissue function and homeostasis, and thus, it plays a significant role in age-related dysfunction of the vascular system and the development of cardiovascular diseases. Cells undergoing senescence sometimes exhibit a senescence-associated secretory phenotype (SASP) [64,65]. The SASP-associated inflammatory molecules expressed by vascular cells in atherosclerotic lesions and LPS-induced cellular senescence exaggerate the pathogenesis of CVDs [66]. Understanding the molecular mechanisms underlying stress-induced senescence may provide valuable insights for the development of therapeutic strategies aimed at ameliorating age-related pathologies.

In an oxidative stress-induced senescence model in primary human endothelial cells, Goy et al. showed that senescent endothelial cells have decreased levels of the antioxidative enzyme Thioredoxin-1 (Trx-1), while the levels of the ROS-producing NADPH Oxidase 4 (NOX4) were elevated [67]. In mice overexpressing NOX4 specifically in the endothelium, in which ROS levels are increased [68], the protein levels of Trx-1 negatively correlated with the expression of NOX4, providing an explanation for the disturbed redox balance in senescent endothelial cells [67] (Figure 3). The importance of redox homeostasis was emphasized by the finding that senescence induction could be inhibited by permanent Trx-1 expression [67]. Induction of endothelial cell senescence with other stimuli was demonstrated by different studies, in which ultrafine carbon nanoparticles [69], low density lipoprotein (LDL) [69–71], or concentrations of LPS found in low-dose endotoxemia [63] were used.

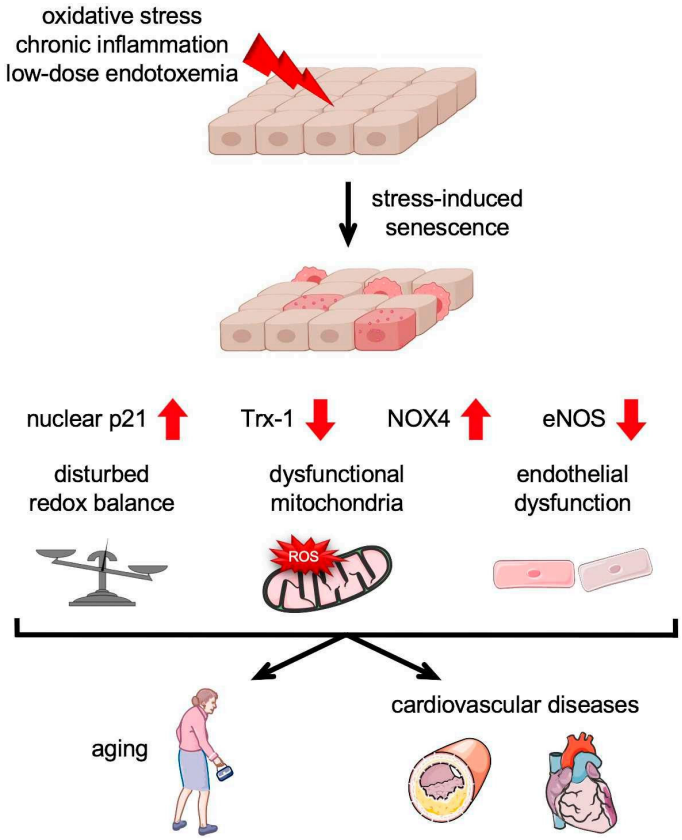

Figure 3. Stress-induced endothelial cell senescence. Endothelial cell senescence is triggered by various stressors including oxidative stress, chronic inflammation, and low-dose endotoxemia. Senescence encompasses an increase in nuclear p21 and NADPH Oxidase 4 (NOX4) with a concomitant decrease of the antioxidative enzyme Thioredoxin-1 (Trx-1) and endothelial NO Synthase (eNOS). This results in a disturbed redox balance and mitochondrial dysfunction along with increased production of reactive oxygen species (ROS) by these organelles, collectively leading to endothelial dysfunction, which contributes to aging and age-associated cardiovascular diseases.

Cellular senescence in general is inter alia characterized by the upregulation of senescence-associated beta-Galactosidase, an increase in nuclear p21, and a disturbed redox balance. An additional, specific hallmark of endothelial cell senescence is a decreased production of NO. NO is a key vasodilator that has also been observed to be reduced in endothelial dysfunction [72]. The loss of NO is due to downregulation of endothelial NO Synthase (eNOS), whose levels also decline with age. Moreover, there is less activity of the enzyme, caused by reduced levels of the essential cofactor tetrahydrobiopterin (BH_4) and the substrate L-arginine [72,73] (Figure 3).

One source of intracellular ROS in senescent cells, among others, is dysfunctional mitochondria [74]. Mitochondrial dysfunction is induced by altered mitochondrial structure due to reduced fusion and fission events, and mitochondrial DNA damage occurs during endothelial cell aging [75]. It is characterized by a reduced respiratory chain capacity per mitochondrion, a reduced mitochondrial membrane potential, and an increased production of ROS. It can lead to senescence and is simultaneously exacerbated by the initiation and maintenance of the senescent phenotype (Figure 3).

5. Low-Dose or Metabolic Endotoxemia—Role of the Gut Microbiome and the Endothelium

LPS is present—among other places—in the gastrointestinal tract, where it is ingested through the diet or on the gram-negative bacteria that are naturally present in the gut microbiota. It has been estimated that the human gut is populated with approximately

10^{14} commensal microorganisms, with the majority of them being present in the colon [76]. These include gram-negative bacteria, making them the major source of LPS in the intestinal lumen. Normally, the intestinal epithelium provides an effective barrier against LPS penetration into the bloodstream, such that the median plasma levels are below 15 pg/mL [77–80]. Consequently, an LPS concentration above 20 pg/mL in the circulation is considered a so-called low-dose endotoxemia, which is set apart from sepsis, where the plasma concentration of LPS is much higher [17].

Various factors, including an unhealthy diet, obesity, diet-induced changes in microbial diversity, and aging, increase the transfer of LPS from the gut to the bloodstream [81–83] (Figure 4). This results in low-dose endotoxemia, which—for the reasons explained below—is also called metabolic endotoxemia.

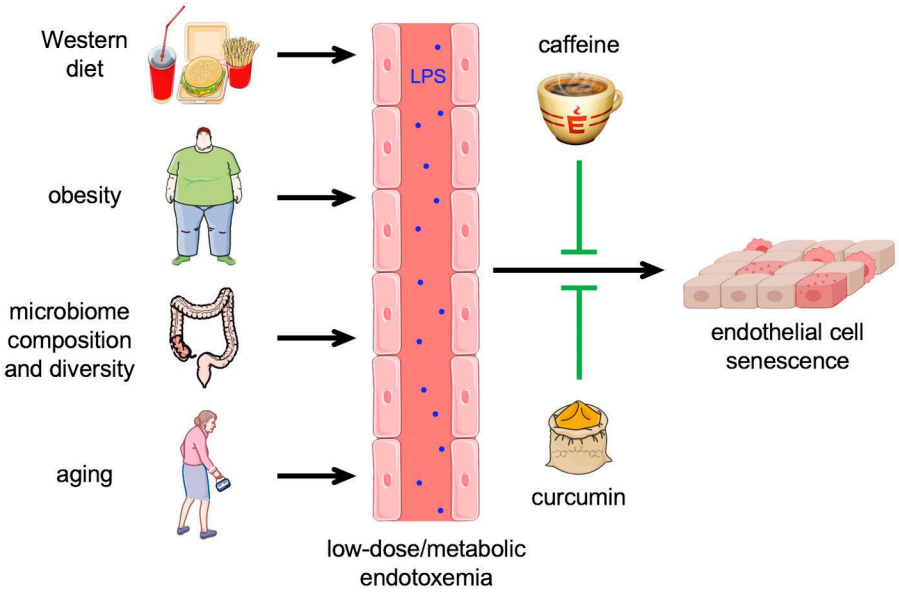

Figure 4. Low-dose endotoxemia-induced endothelial senescence. Under physiological conditions, very small amounts of lipopolysaccharide (LPS) from the intestinal lumen are released into the bloodstream. Various factors, e.g., Western diet, obesity, changes in gut microbiome composition and diversity, and aging, increase the transfer of LPS from the gut to the circulation, resulting in so-called low-dose or metabolic endotoxemia, which leads to endothelial cell senescence. This senescence induction by LPS can be prevented by caffeine and possibly also by curcumin.

It has been shown that unbalanced, hyperlipidic meals have a short-term effect on LPS plasma levels, leading to a post-prandial increase already within one hour after a high-fat meal or drink [80,84–86]. This rapid increase suggests that dietary lipids facilitate the transfer of LPS from the gut to the bloodstream, and there is evidence that chylomicrons could contribute to the adsorption and transport of LPS [86–88].

However, these effects are only transient; an unhealthy diet, on the contrary, leads to a persistent increase in blood LPS levels, which was first demonstrated in rodent models. 4 weeks of a high-fat diet in mice persistently increased the plasma LPS concentration, which usually fluctuates diurnally with the feeding cycles, reaching the highest levels at the end of the feeding period, approximately threefold. As the same effect was obtained by subcutaneous infusion of LPS and the increase in plasma LPS was 10 to 50 times lower than in sepsis, the term metabolic endotoxemia was coined for this phenomenon. In both settings, the increase in circulating LPS was paralleled by the upregulation of inflammatory cytokines, indicating that metabolic endotoxemia entails a low-grade inflammation [89]. An increase in plasma LPS was also observed in mice on high-glucose or high-fructose diets [90] and rats on Western [91] and high-fat/high-sugar diets [92], respectively. Furthermore, metabolic endotoxemia was associated with obesity and insulin resistance [89,90], both be-

ing risk factors for the development of cardiovascular diseases. Interestingly, endotoxemia seems to induce these phenomena [89].

Unhealthy diets also induce changes in the gut microbiome [89,90], which seem to be at least in part responsible for the observed metabolic alterations, as dietary interventions that positively affect the composition of the microbiota or treatment with antibiotics can revert some of the effects [93,94]. In that respect, it is noteworthy that not simply the sheer number of gut microorganisms but rather the composition of the microbiome and, thus, the source of LPS is critical for the outcome. While hexa-acylated *E. coli*-derived LPS promotes dysglycemia and inflammation, lower acylated LPS from another bacterial species does not evoke these effects. Moreover, it can even antagonize the dysglycemia caused by *E. coli* LPS in lean mice and improve insulin sensitivity in obese animals [95]. In summary, these data show that diet-induced metabolic endotoxemia is tightly linked to gut microbiome dysbiosis.

Although animal models allow for experimental manipulations not possible in humans, similar correlations and effects have been observed in epidemiological studies and some small-scale clinical trials. A study based on a dietary survey revealed an association between energy intake and endotoxemia in healthy men, and it was suspected that fat is the critical component for the transfer of LPS into the bloodstream [96]. A correlation between dietary habits and metabolic endotoxemia has also been inferred from another study, in which healthy food choices have been associated with lower serum LPS activity [97]. Direct experimental proof for the impact of an unhealthy diet on serum LPS levels was obtained in crossover studies with healthy subjects. Similar to mice, a meal rich in saturated fats induced a post-prandial increase in LPS in the blood [98]. Also, the long-term effects could be recapitulated by demonstrating an increase in plasma endotoxin activity of over 70% after a 4-week Western diet, which returned to baseline after a washout period and another 4 weeks on a prudent diet [99]. Interestingly, experimental endotoxemia in humans induced insulin resistance [100], similar to what has been observed in mice, again underscoring that low-dose endotoxemia leads to metabolic states that increase the risk for cardiovascular diseases.

As in mice, unhealthy diets also have a major impact on the human gut microbiome. Work in humanized gnotobiotic mice, i.e., germ-free animals transplanted with human fecal microbial communities, elegantly showed that a Western diet shifts the gut microbiome already within a day. Interestingly, mice colonized with microbiota from obese Western diet-fed humanized donors developed adiposity [101], similar to what has been described for animals on a 4-week high-fat diet. A correlation between dietary patterns and changes in gut microbiome composition has also been directly demonstrated in humans. Interestingly, controlled consumption of a high-fat/low-fiber or low-fat/high-fiber diet induced alterations already within 24 h, the same time frame as in the gnotobiotic mice [102]. Diet can not only change the ratio between different bacterial species in the gut microbiome, but also has a profound effect on its complexity, which is directly connected to metabolic and inflammatory parameters. A microbiome analysis of nearly 300 non-obese and obese subjects revealed that lower bacterial richness goes along with adiposity, insulin resistance, and more pronounced inflammation [103]. The same observations were made in a parallel study, which additionally demonstrated that weight loss and weight stabilization interventions in obese and overweight individuals can increase microbiome diversity and improve clinical phenotypes [104].

The connection between the intestinal microbiome and chronic diseases or risk factors for their development is also reflected in the elderly. The analysis of fecal microbiota in elderly subjects revealed major changes, which are related to clinical parameters like inflammatory markers and frailty [105,106]. Notably, although a part of these alterations in the microbiome is due to lifestyle, there also seem to be intrinsic changes in the gut microbiota during the aging process, which has been shown in rodent models [107] as well as in humans [108]. An unfavorable composition of the microbiome impairs the barrier function of the gut epithelium, leading to increased transfer of LPS into the bloodstream [109]. Actually,

a nearly two-fold increase in plasma LPS levels, and thus metabolic endotoxemia, was demonstrated in aged subjects free of chronic age-related diseases and physical disabilities, when compared to young individuals [29].

As described before, metabolic endotoxemia entails a systemic low-grade inflammation and thereby affects several cell types, also including those in the vasculature, e.g., leukocytes, platelets, and endothelial cells. Therefore, low-grade endotoxemia increases the risk for cardiovascular diseases [79,110]. One of the most critical targets for this metabolic endotoxemia-associated low-grade inflammation is the endothelium, as it plays a central role in vascular homeostasis, such that its dysfunction is associated with nearly all cardiovascular diseases. In fact, a low-grade systemic inflammation triggered by infusion of 2 ng/kg LPS in humans was paralleled by a significant decrease in peripheral endothelial progenitor cells, which are important for the repair of endothelial injuries [111]. However, not only these progenitor cells are affected by metabolic endotoxemia but also mature endothelial cells in the vascular wall. While treatment of primary human endothelial cells with 150 ng/mL of LPS led to activation and apoptosis [16], exposure to 1 ng/mL over a period of 2 weeks induced cellular senescence similarly to treatment with low doses of H_2O_2 [63], clearly demonstrating dose-dependent effects of LPS on the endothelium. The induction of endothelial cell senescence by low-dose endotoxemia also explains the association between metabolic endotoxemia and cardiovascular diseases.

Based on the notion that senescence impairs mitochondrial functionality, which is also essential for endothelial cells, it seems attractive to use compounds that positively affect the mitochondria to counteract senescence induction. One such compound is caffeine, a widely consumed drug found in coffee, tea, soft drinks, and chocolate. Large epidemiological studies have demonstrated an association between habitual caffeine intake and a decrease in mortality, including death as consequence of cardiovascular disorders [112,113]. We have previously shown that the consumption of four cups of coffee translates into caffeine serum concentrations of approximately 30 µM [114]. These physiological concentrations improved the migration of endothelial progenitor cells and mature endothelial cells and repair after vascular injury [114]. Moreover, in mice, they improved outcomes after myocardial infarction [115]. This positive effect is due to increased translocation of p27 into the mitochondria and improved electron transport chain activity. Moreover, caffeine reduced age-associated decline in mitochondrial functionality [115].

Another interesting natural compound in this context could be curcumin. This polyphenol is the main active ingredient in the root of *Curcuma longa*, which has been used as a medicinal plant in Asia for over 4000 years. Multiple studies have shown a protective effect of curcumin in cardiovascular diseases (for review, see [116]).

While there is some evidence that curcumin and caffeine play a role in the reduction of the effects of endotoxemia, information on detailed mechanisms underlying these are sparse to date. As these dietary factors have to pass through the digestive tract, one could assume that they interact with and have an impact on the gut microbiome. Some studies hint towards curcumin altering the gut microbiome composition with an increase in beneficial versus pathogenic bacteria (for review, see [117]). Based on the above-discussed impact of the microbiome on plasma LPS levels, it can be speculated that this effect might reduce LPS concentrations in the circulation. Although caffeine can alter the gut microbiome and thereby ameliorate the metabolic syndrome in obese mice [118], this is only very indirect evidence that it might also affect plasma LPS levels, as metabolic syndrome is associated with metabolic endotoxemia.

However, the direct effects of curcumin and caffeine on the endothelium have been investigated in some more detail and will be discussed in the following chapter.

6. Impact of Curcumin and Caffeine on High-Dose and Metabolic Endotoxemia with Respect to the Endothelium

As outlined above, upon leakage of the gut, LPS enters the circulation, which in high doses leads to so-called “leaky vessels”, resulting in circulatory and organ failure, finally

leading to death within hours or days in mice and humans. The role of curcumin and caffeine treatment in high-dose endotoxemia/sepsis with respect to the endothelium has barely been investigated.

With respect to curcumin, the expression of ICAM-1 was inhibited ex vivo and in vivo in mice, resulting in reduced adhesion of neutrophils and monocytes/macrophages to the endothelium [119]. In rats, curcumin infusion preserved endothelial barrier function in a high-dose LPS model [120]. Of note, these studies only investigated the preventive effects of the compound, as it was administered prior to LPS infusion or treatment. In 2022, the first double-blinded placebo controlled clinical trial with curcumin supplementation in critically ill sepsis patients was performed. Although, the curcumin supplementation was only for 10 days in 20 patients and 20 placebo controls, curcumin significantly improved inflammatory markers, such as Interleukin-1beta, and reduced markers of endothelial activation including ICAM-1. Moreover, it decreased the sepsis-related organ failure assessment score and the duration of mechanical ventilation [121]. Thus, one could assume that curcumin supplementation could improve endothelial functionality in sepsis and may lead to reduced mortality. However, further trials are needed to assess the potential of curcumin with respect to endothelial function and mortality in sepsis patients.

For caffeine, there are currently no studies available that investigate its impact on the endothelium in high-dose endotoxemia/sepsis.

As described before, low-dose endotoxemia entails endothelial cell senescence. However, the impact of curcumin on metabolic endotoxemia and endothelial cell senescence has not been investigated directly. Nevertheless, there is circumstantial evidence for potential protective effects. Curcumin improved the barrier function in two colon carcinoma cell lines [122], suggesting that it might reduce LPS transfer from the gut to the circulation and thus prevent systemic inflammation, one of the consequences of metabolic endotoxemia. A direct impact of curcumin on inflammation in a disease setting characterized by metabolic endotoxemia has been shown by the reduction of inflammatory cytokine levels in subjects with metabolic syndrome in a randomized controlled trial [123]. In this study, a daily dose of 1 g curcumin was administered over a period of 8 weeks; however, the curcumin concentrations in the blood were not measured. Several studies have measured the serum concentration after administration of crude curcumin ranging from 1 to 3200 ng/mL depending on dose (2 to 12 g) and subject physiology (for review, see [124]). Moreover, short-term treatment of human endothelial cells with curcumin induced stabilization and nuclear translocation of the transcription factor Nrf-2 and enhanced expression of antioxidative defense systems, including Thioredoxin-1 and Superoxide Dismutase 2 [125,126] (Figure 5). This could also be relevant in the context of endothelial cell senescence, which is associated with increased ROS production but has not been studied so far.

In contrast, caffeine effects have been investigated not only in healthy endothelial cells and with respect to vascular repair after injury but also in low-dose endotoxemia-induced endothelial senescence, which was counteracted by caffeine. This was shown by the treatment of endothelial cells with caffeine during senescence induction with low-dose LPS. The co-incubation with both substances blocked the upregulation of nuclear p21, a general senescence marker. Moreover, it also conserved endothelial functionality by maintaining the levels of Trx-1 and eNOS and preserving the migratory capacity of endothelial cells. Mechanistically, this is again due to the translocation of p27 into the mitochondria, as permanent expression of mitochondrially targeted p27 also blocked senescence induction (Figure 5). Interestingly, the same effects were observed when caffeine was applied to already senescent endothelial cells [63]. These data suggest that caffeine can reverse or at least delay endothelial cell senescence induced by metabolic endotoxemia and might, therefore, be an additional protective dietary factor in the context of aging.

This last section highlights that caffeine and curcumin—natural food components—could offer options to combat the negative senescence-inducing effects of low-dose or metabolic endotoxemia.

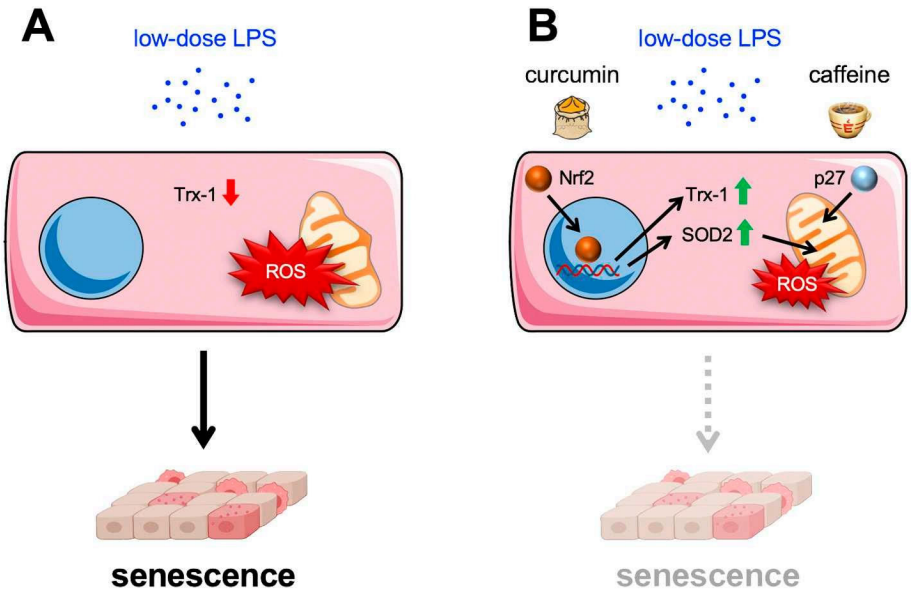

Figure 5. Curcumin and caffeine inhibit low-dose endotoxemia-induced endothelial senescence. (**A**) Low doses of lipopolysaccharide (LPS) in the circulation induce senescence in endothelial cells, which goes along with reduced levels of Thioredoxin-1 (Trx-1), one of the major antioxidative systems, reduced mitochondrial functionality, and increased ROS production. (**B**) Curcumin and caffeine inhibit senescence induction by low-dose endotoxemia through different mechanisms. Curcumin induces stabilization and nuclear translocation, resulting in enhanced expression of Trx-1 and Superoxide Dismutase 2 (SOD2) and reduced ROS production. Caffeine induces the translocation of p27 into the mitochondria, thereby maintaining their functionality.

7. Conclusions

In conclusion, dependent on the concentration of LPS in the blood, high-dose or low-dose endotoxemia is induced. High-dose endotoxemia, also called sepsis, often leads to septic shock, endothelial cell death, organ failure, and death. In contrast, low-dose or metabolic endotoxemia leads to chronic inflammation, which results in endothelial cell senescence. Two natural compounds, caffeine and curcumin, seem to inhibit or at least delay low-dose endotoxemia-induced endothelial cell senescence. Thus, natural compounds may have the potential to protect against the negative senescence-inducing effects of metabolic endotoxemia.

Author Contributions: Conceptualization, P.J., S.P., J.A. and J.H.; writing—original draft preparation, D.M., F.F.C., J.A. and J.H.; writing—review and editing, F.F.C., P.J., S.P., J.A. and J.H.; visualization, P.J. and J.A.; supervision, J.A. and J.H.; funding acquisition, S.P. and J.H. All authors have read and agreed to the published version of the manuscript.

Funding: This research was funded in part by Bayer Grant4Target (2019-08-2427) to J.H. and by intramural funding (9772888) of the University Hospital of the Heinrich-Heine-University to S.P. and J.H.

Institutional Review Board Statement: Not applicable.

Informed Consent Statement: Not applicable.

Data Availability Statement: Not applicable.

Acknowledgments: Single graphical elements for figures were taken from Servier Medical Art (smart.servier.com accessed on 2 April 2024), which is licensed under a Creative Commons Attribution 3.0 Unported License.

Conflicts of Interest: The authors declare no conflicts of interest.

References

1. Gao, J.; Pan, X.; Li, G.; Chatterjee, E.; Xiao, J. Physical Exercise Protects Against Endothelial Dysfunction in Cardiovascular and Metabolic Diseases. *J. Cardiovasc. Transl. Res.* **2022**, *15*, 604–620. [CrossRef]
2. Hadi, H.A.; Carr, C.S.; Al Suwaidi, J. Endothelial dysfunction: Cardiovascular risk factors, therapy, and outcome. *Vasc. Health Risk Manag.* **2005**, *1*, 183–198.
3. Pober, J.S.; Min, W.; Bradley, J.R. Mechanisms of endothelial dysfunction, injury, and death. *Annu. Rev. Pathol.* **2009**, *4*, 71–95. [CrossRef]
4. Liao, J.K. Linking endothelial dysfunction with endothelial cell activation. *J. Clin. Investig.* **2013**, *123*, 540–541. [CrossRef]
5. Boatright, K.M.; Salvesen, G.S. Mechanisms of caspase activation. *Curr. Opin. Cell Biol.* **2003**, *15*, 725–731. [CrossRef]
6. World Health Organization. *Global Report on the Epidemiology and Burden of Sepsis: Current Evidence, Identifying Gaps and Future Directions*; World Health Organization: Geneva, Switzerland, 2020; p. 55.
7. Singer, M.; Deutschman, C.S.; Seymour, C.W.; Shankar-Hari, M.; Annane, D.; Bauer, M.; Bellomo, R.; Bernard, G.R.; Chiche, J.D.; Coopersmith, C.M.; et al. The Third International Consensus Definitions for Sepsis and Septic Shock (Sepsis-3). *JAMA* **2016**, *315*, 801–810. [CrossRef]
8. Virzi, G.M.; Mattiotti, M.; de Cal, M.; Ronco, C.; Zanella, M.; De Rosa, S. Endotoxin in Sepsis: Methods for LPS Detection and the Use of Omics Techniques. *Diagnostics* **2022**, *13*, 79. [CrossRef]
9. Mayr, F.B.; Yende, S.; Angus, D.C. Epidemiology of severe sepsis. *Virulence* **2014**, *5*, 4–11. [CrossRef]
10. Dauphinee, S.M.; Karsan, A. Lipopolysaccharide signaling in endothelial cells. *Lab. Investig.* **2006**, *86*, 9–22. [CrossRef]
11. Delano, M.J.; Ward, P.A. The immune system's role in sepsis progression, resolution, and long-term outcome. *Immunol. Rev.* **2016**, *274*, 330–353. [CrossRef]
12. Medzhitov, R.; Janeway, C., Jr. Innate immunity. *N. Engl. J. Med.* **2000**, *343*, 338–344. [CrossRef]
13. Page, M.J.; Kell, D.B.; Pretorius, E. The Role of Lipopolysaccharide-Induced Cell Signalling in Chronic Inflammation. *Chronic Stress* **2022**, *6*, 24705470221076390. [CrossRef]
14. Molinaro, A.; Holst, O.; Di Lorenzo, F.; Callaghan, M.; Nurisso, A.; D'Errico, G.; Zamyatina, A.; Peri, F.; Berisio, R.; Jerala, R.; et al. Chemistry of lipid A: At the heart of innate immunity. *Chemistry* **2015**, *21*, 500–519. [CrossRef]
15. Ho, J.; Chan, H.; Wong, S.H.; Wang, M.H.; Yu, J.; Xiao, Z.; Liu, X.; Choi, G.; Leung, C.C.; Wong, W.T.; et al. The involvement of regulatory non-coding RNAs in sepsis: A systematic review. *Crit. Care* **2016**, *20*, 383. [CrossRef]
16. Merk, D.; Ptok, J.; Jakobs, P.; von Ameln, F.; Greulich, J.; Kluge, P.; Semperowitsch, K.; Eckermann, O.; Schaal, H.; Ale-Agha, N.; et al. Selenoprotein T Protects Endothelial Cells against Lipopolysaccharide-Induced Activation and Apoptosis. *Antioxidants* **2021**, *10*, 1427. [CrossRef]
17. Opal, S.M.; Laterre, P.F.; Francois, B.; LaRosa, S.P.; Angus, D.C.; Mira, J.P.; Wittebole, X.; Dugernier, T.; Perrotin, D.; Tidswell, M.; et al. Effect of eritoran, an antagonist of MD2-TLR4, on mortality in patients with severe sepsis: The ACCESS randomized trial. *JAMA* **2013**, *309*, 1154–1162. [CrossRef]
18. Marshall, J.C. Why have clinical trials in sepsis failed? *Trends Mol. Med.* **2014**, *20*, 195–203. [CrossRef]
19. Guarino, M.; Perna, B.; Cesaro, A.E.; Maritati, M.; Spampinato, M.D.; Contini, C.; De Giorgio, R. 2023 Update on Sepsis and Septic Shock in Adult Patients: Management in the Emergency Department. *J. Clin. Med.* **2023**, *12*, 3188. [CrossRef]
20. Duan, T.; Du, Y.; Xing, C.; Wang, H.Y.; Wang, R.F. Toll-Like Receptor Signaling and Its Role in Cell-Mediated Immunity. *Front. Immunol.* **2022**, *13*, 812774. [CrossRef]
21. Vaure, C.; Liu, Y. A comparative review of toll-like receptor 4 expression and functionality in different animal species. *Front. Immunol.* **2014**, *5*, 316. [CrossRef]
22. Gay, N.J.; Gangloff, M. Structure and function of Toll receptors and their ligands. *Annu. Rev. Biochem.* **2007**, *76*, 141–165. [CrossRef]
23. Poltorak, A.; He, X.; Smirnova, I.; Liu, M.Y.; Van Huffel, C.; Du, X.; Birdwell, D.; Alejos, E.; Silva, M.; Galanos, C.; et al. Defective LPS signaling in C3H/HeJ and C57BL/10ScCr mice: Mutations in Tlr4 gene. *Science* **1998**, *282*, 2085–2088. [CrossRef]
24. Stelzer, G.; Rosen, N.; Plaschkes, I.; Zimmerman, S.; Twik, M.; Fishilevich, S.; Stein, T.I.; Nudel, R.; Lieder, I.; Mazor, Y.; et al. The GeneCards Suite: From Gene Data Mining to Disease Genome Sequence Analyses. *Curr. Protoc. Bioinform.* **2016**, *54*, 1.30.1–1.30.33. [CrossRef]
25. Uhlen, M.; Fagerberg, L.; Hallstrom, B.M.; Lindskog, C.; Oksvold, P.; Mardinoglu, A.; Sivertsson, A.; Kampf, C.; Sjostedt, E.; Asplund, A.; et al. Tissue-based map of the human proteome. *Science* **2015**, *347*, 1260419. [CrossRef]
26. Consortium, G.T. The Genotype-Tissue Expression (GTEx) project. *Nat. Genet.* **2013**, *45*, 580–585. [CrossRef]
27. Taylor, K.R.; Trowbridge, J.M.; Rudisill, J.A.; Termeer, C.C.; Simon, J.C.; Gallo, R.L. Hyaluronan fragments stimulate endothelial recognition of injury through TLR4. *J. Biol. Chem.* **2004**, *279*, 17079–17084. [CrossRef]
28. Sasu, S.; LaVerda, D.; Qureshi, N.; Golenbock, D.T.; Beasley, D. Chlamydia pneumoniae and chlamydial heat shock protein 60 stimulate proliferation of human vascular smooth muscle cells via toll-like receptor 4 and p44/p42 mitogen-activated protein kinase activation. *Circ. Res.* **2001**, *89*, 244–250. [CrossRef]
29. Ghosh, S.; Lertwattanarak, R.; Garduno Jde, J.; Galeana, J.J.; Li, J.; Zamarripa, F.; Lancaster, J.L.; Mohan, S.; Hussey, S.; Musi, N. Elevated muscle TLR4 expression and metabolic endotoxemia in human aging. *J. Gerontol. A Biol. Sci. Med. Sci.* **2015**, *70*, 232–246. [CrossRef]
30. Frantz, S.; Kobzik, L.; Kim, Y.D.; Fukazawa, R.; Medzhitov, R.; Lee, R.T.; Kelly, R.A. Toll4 (TLR4) expression in cardiac myocytes in normal and failing myocardium. *J. Clin. Investig.* **1999**, *104*, 271–280. [CrossRef]

31. Kielian, T. Toll-like receptors in central nervous system glial inflammation and homeostasis. *J. Neurosci. Res.* **2006**, *83*, 711–730. [CrossRef]
32. Plociennikowska, A.; Hromada-Judycka, A.; Borzecka, K.; Kwiatkowska, K. Co-operation of TLR4 and raft proteins in LPS-induced pro-inflammatory signaling. *Cell Mol. Life Sci.* **2015**, *72*, 557–581. [CrossRef]
33. Ryu, J.K.; Kim, S.J.; Rah, S.H.; Kang, J.I.; Jung, H.E.; Lee, D.; Lee, H.K.; Lee, J.O.; Park, B.S.; Yoon, T.Y.; et al. Reconstruction of LPS Transfer Cascade Reveals Structural Determinants within LBP, CD14, and TLR4-MD2 for Efficient LPS Recognition and Transfer. *Immunity* **2017**, *46*, 38–50. [CrossRef]
34. Meng, J.; Gong, M.; Bjorkbacka, H.; Golenbock, D.T. Genome-wide expression profiling and mutagenesis studies reveal that lipopolysaccharide responsiveness appears to be absolutely dependent on TLR4 and MD-2 expression and is dependent upon intermolecular ionic interactions. *J. Immunol.* **2011**, *187*, 3683–3693. [CrossRef]
35. Funda, D.P.; Tuckova, L.; Farre, M.A.; Iwase, T.; Moro, I.; Tlaskalova-Hogenova, H. CD14 is expressed and released as soluble CD14 by human intestinal epithelial cells in vitro: Lipopolysaccharide activation of epithelial cells revisited. *Infect. Immun.* **2001**, *69*, 3772–3781. [CrossRef]
36. Haziot, A.; Chen, S.; Ferrero, E.; Low, M.G.; Silber, R.; Goyert, S.M. The monocyte differentiation antigen, CD14, is anchored to the cell membrane by a phosphatidylinositol linkage. *J. Immunol.* **1988**, *141*, 547–552. [CrossRef]
37. Frey, E.A.; Miller, D.S.; Jahr, T.G.; Sundan, A.; Bazil, V.; Espevik, T.; Finlay, B.B.; Wright, S.D. Soluble CD14 participates in the response of cells to lipopolysaccharide. *J. Exp. Med.* **1992**, *176*, 1665–1671. [CrossRef]
38. Pugin, J.; Schurer-Maly, C.C.; Leturcq, D.; Moriarty, A.; Ulevitch, R.J.; Tobias, P.S. Lipopolysaccharide activation of human endothelial and epithelial cells is mediated by lipopolysaccharide-binding protein and soluble CD14. *Proc. Natl. Acad. Sci. USA* **1993**, *90*, 2744–2748. [CrossRef]
39. Golenbock, D.T.; Bach, R.R.; Lichenstein, H.; Juan, T.S.; Tadavarthy, A.; Moldow, C.F. Soluble CD14 promotes LPS activation of CD14-deficient PNH monocytes and endothelial cells. *J. Lab. Clin. Med.* **1995**, *125*, 662–671.
40. Haziot, A.; Rong, G.W.; Silver, J.; Goyert, S.M. Recombinant soluble CD14 mediates the activation of endothelial cells by lipopolysaccharide. *J. Immunol.* **1993**, *151*, 1500–1507. [CrossRef]
41. Zhang, Y.; Liang, X.; Bao, X.; Xiao, W.; Chen, G. Toll-like receptor 4 (TLR4) inhibitors: Current research and prospective. *Eur. J. Med. Chem.* **2022**, *235*, 114291. [CrossRef]
42. Li, S.; Strelow, A.; Fontana, E.J.; Wesche, H. IRAK-4: A novel member of the IRAK family with the properties of an IRAK-kinase. *Proc. Natl. Acad. Sci. USA* **2002**, *99*, 5567–5572. [CrossRef]
43. Arch, R.H.; Gedrich, R.W.; Thompson, C.B. Tumor necrosis factor receptor-associated factors (TRAFs)—A family of adapter proteins that regulates life and death. *Genes. Dev.* **1998**, *12*, 2821–2830. [CrossRef]
44. Shaywitz, A.J.; Greenberg, M.E. CREB: A stimulus-induced transcription factor activated by a diverse array of extracellular signals. *Annu. Rev. Biochem.* **1999**, *68*, 821–861. [CrossRef]
45. Zhao, D.; Kwon, S.H.; Chun, Y.S.; Gu, M.Y.; Yang, H.O. Anti-Neuroinflammatory Effects of Fucoxanthin via Inhibition of Akt/NF-kappaB and MAPKs/AP-1 Pathways and Activation of PKA/CREB Pathway in Lipopolysaccharide-Activated BV-2 Microglial Cells. *Neurochem. Res.* **2017**, *42*, 667–677. [CrossRef]
46. Lu, Y.; Li, B.; Xu, A.; Liang, X.; Xu, T.; Jin, H.; Xie, Y.; Wang, R.; Liu, X.; Gao, X.; et al. NF-kappaB and AP-1 are required for the lipopolysaccharide-induced expression of MCP-1, CXCL1, and Cx43 in cultured rat dorsal spinal cord astrocytes. *Front. Mol. Neurosci.* **2022**, *15*, 859558. [CrossRef]
47. Marongiu, L.; Gornati, L.; Artuso, I.; Zanoni, I.; Granucci, F. Below the surface: The inner lives of TLR4 and TLR9. *J. Leukoc. Biol.* **2019**, *106*, 147–160. [CrossRef]
48. Tanimura, N.; Saitoh, S.; Matsumoto, F.; Akashi-Takamura, S.; Miyake, K. Roles for LPS-dependent interaction and relocation of TLR4 and TRAM in TRIF-signaling. *Biochem. Biophys. Res. Commun.* **2008**, *368*, 94–99. [CrossRef]
49. Jiang, Z.; Georgel, P.; Du, X.; Shamel, L.; Sovath, S.; Mudd, S.; Huber, M.; Kalis, C.; Keck, S.; Galanos, C.; et al. CD14 is required for MyD88-independent LPS signaling. *Nat. Immunol.* **2005**, *6*, 565–570. [CrossRef]
50. Ciesielska, A.; Matyjek, M.; Kwiatkowska, K. TLR4 and CD14 trafficking and its influence on LPS-induced pro-inflammatory signaling. *Cell Mol. Life Sci.* **2021**, *78*, 1233–1261. [CrossRef]
51. Verstak, B.; Stack, J.; Ve, T.; Mangan, M.; Hjerrild, K.; Jeon, J.; Stahl, R.; Latz, E.; Gay, N.; Kobe, B.; et al. The TLR signaling adaptor TRAM interacts with TRAF6 to mediate activation of the inflammatory response by TLR4. *J. Leukoc. Biol.* **2014**, *96*, 427–436. [CrossRef]
52. Kayagaki, N.; Wong, M.T.; Stowe, I.B.; Ramani, S.R.; Gonzalez, L.C.; Akashi-Takamura, S.; Miyake, K.; Zhang, J.; Lee, W.P.; Muszynski, A.; et al. Noncanonical inflammasome activation by intracellular LPS independent of TLR4. *Science* **2013**, *341*, 1246–1249. [CrossRef]
53. Hagar, J.A.; Powell, D.A.; Aachoui, Y.; Ernst, R.K.; Miao, E.A. Cytoplasmic LPS activates caspase-11: Implications in TLR4-independent endotoxic shock. *Science* **2013**, *341*, 1250–1253. [CrossRef]
54. Molloy, S. Host response: LPS goes non-canonical. *Nat. Rev. Microbiol.* **2013**, *11*, 599. [CrossRef]
55. Vanaja, S.K.; Russo, A.J.; Behl, B.; Banerjee, I.; Yankova, M.; Deshmukh, S.D.; Rathinam, V.A.K. Bacterial Outer Membrane Vesicles Mediate Cytosolic Localization of LPS and Caspase-11 Activation. *Cell* **2016**, *165*, 1106–1119. [CrossRef]

56. Hirschfeld, M.; Weis, J.J.; Toshchakov, V.; Salkowski, C.A.; Cody, M.J.; Ward, D.C.; Qureshi, N.; Michalek, S.M.; Vogel, S.N. Signaling by toll-like receptor 2 and 4 agonists results in differential gene expression in murine macrophages. *Infect. Immun.* **2001**, *69*, 1477–1482. [CrossRef]
57. Palsson-McDermott, E.M.; O'Neill, L.A. Signal transduction by the lipopolysaccharide receptor, Toll-like receptor-4. *Immunology* **2004**, *113*, 153–162. [CrossRef]
58. Steimle, A.; Autenrieth, I.B.; Frick, J.S. Structure and function: Lipid A modifications in commensals and pathogens. *Int. J. Med. Microbiol.* **2016**, *306*, 290–301. [CrossRef]
59. Mohr, A.E.; Crawford, M.; Jasbi, P.; Fessler, S.; Sweazea, K.L. Lipopolysaccharide and the gut microbiota: Considering structural variation. *FEBS Lett.* **2022**, *596*, 849–875. [CrossRef]
60. Barochia, A.; Solomon, S.; Cui, X.; Natanson, C.; Eichacker, P.Q. Eritoran tetrasodium (E5564) treatment for sepsis: Review of preclinical and clinical studies. *Expert. Opin. Drug Metab. Toxicol.* **2011**, *7*, 479–494. [CrossRef]
61. Abelli, J.; Mendez-Valdes, G.; Gomez-Hevia, F.; Bragato, M.C.; Chichiarelli, S.; Saso, L.; Rodrigo, R. Potential Antioxidant Multitherapy against Complications Occurring in Sepsis. *Biomedicines* **2022**, *10*, 3088. [CrossRef]
62. Liang, Y.; Liang, N.; Yin, L.; Xiao, F. Cellular and molecular mechanisms of xenobiotics-induced premature senescence. *Toxicol. Res.* **2020**, *9*, 669–675. [CrossRef]
63. Merk, D.; Greulich, J.; Vierkant, A.; Cox, F.; Eckermann, O.; von Ameln, F.; Dyballa-Rukes, N.; Altschmied, J.; Ale-Agha, N.; Jakobs, P.; et al. Caffeine Inhibits Oxidative Stress- and Low Dose Endotoxemia-Induced Senescence-Role of Thioredoxin-1. *Antioxidants* **2023**, *12*, 1244. [CrossRef]
64. Coppé, J.P.; Patil, C.K.; Rodier, F.; Sun, Y.; Muñoz, D.P.; Goldstein, J.; Nelson, P.S.; Desprez, P.Y.; Campisi, J. Senescence-associated secretory phenotypes reveal cell-nonautonomous functions of oncogenic RAS and the p53 tumor suppressor. *PLoS Biol.* **2008**, *6*, 2853–2868. [CrossRef]
65. Andreo-López, M.C.; Contreras-Bolívar, V.; Muñoz-Torres, M.; García-Fontana, B.; García-Fontana, C. Influence of the Mediterranean Diet on Healthy Aging. *Int. J. Mol. Sci.* **2023**, *24*, 4491. [CrossRef]
66. Suzuki, K.; Susaki, E.A.; Nagaoka, I. Lipopolysaccharides and Cellular Senescence: Involvement in Atherosclerosis. *Int. J. Mol. Sci.* **2022**, *23*, 11148. [CrossRef]
67. Goy, C.; Czypiorski, P.; Altschmied, J.; Jakob, S.; Rabanter, L.L.; Brewer, A.C.; Ale-Agha, N.; Dyballa-Rukes, N.; Shah, A.M.; Haendeler, J. The imbalanced redox status in senescent endothelial cells is due to dysregulated Thioredoxin-1 and NADPH oxidase 4. *Exp. Gerontol.* **2014**, *56*, 45–52. [CrossRef]
68. Ray, R.; Murdoch, C.E.; Wang, M.; Santos, C.X.; Zhang, M.; Alom-Ruiz, S.; Anilkumar, N.; Ouattara, A.; Cave, A.C.; Walker, S.J.; et al. Endothelial Nox4 NADPH oxidase enhances vasodilatation and reduces blood pressure in vivo. *Arter. Thromb. Vasc. Biol.* **2011**, *31*, 1368–1376. [CrossRef]
69. Büchner, N.; Ale-Agha, N.; Jakob, S.; Sydlik, U.; Kunze, K.; Unfried, K.; Altschmied, J.; Haendeler, J. Unhealthy diet and ultrafine carbon black particles induce senescence and disease associated phenotypic changes. *Exp. Gerontol.* **2013**, *48*, 8–16. [CrossRef]
70. Oh, S.T.; Park, H.; Yoon, H.J.; Yang, S.Y. Erratum to "Long-Term Treatment of Native LDL Induces Senescence of Cultured Human Endothelial Cells". *Oxid. Med. Cell Longev.* **2017**, *2017*, 4576985. [CrossRef]
71. Gonnissen, S.; Ptok, J.; Goy, C.; Jander, K.; Jakobs, P.; Eckermann, O.; Kaisers, W.; von Ameln, F.; Timm, J.; Ale-Agha, N.; et al. High Concentration of Low-Density Lipoprotein Results in Disturbances in Mitochondrial Transcription and Functionality in Endothelial Cells. *Oxid. Med. Cell Longev.* **2019**, *2019*, 7976382. [CrossRef]
72. Han, Y.; Kim, S.Y. Endothelial senescence in vascular diseases: Current understanding and future opportunities in senotherapeutics. *Exp. Mol. Med.* **2023**, *55*, 1–12. [CrossRef]
73. Förstermann, U.; Münzel, T. Endothelial nitric oxide synthase in vascular disease: From marvel to menace. *Circulation* **2006**, *113*, 1708–1714. [CrossRef]
74. Dodig, S.; Čepelak, I.; Pavić, I. Hallmarks of senescence and aging. *Biochem. Med.* **2019**, *29*, 030501. [CrossRef]
75. Jendrach, M.; Pohl, S.; Vöth, M.; Kowald, A.; Hammerstein, P.; Bereiter-Hahn, J. Morpho-dynamic changes of mitochondria during ageing of human endothelial cells. *Mech. Ageing Dev.* **2005**, *126*, 813–821. [CrossRef]
76. Berg, R.D. The indigenous gastrointestinal microflora. *Trends Microbiol.* **1996**, *4*, 430–435. [CrossRef]
77. Carnevale, R.; Sciarretta, S.; Valenti, V.; di Nonno, F.; Calvieri, C.; Nocella, C.; Frati, G.; Forte, M.; d'Amati, G.; Pignataro, M.G.; et al. Low-grade endotoxaemia enhances artery thrombus growth via Toll-like receptor 4: Implication for myocardial infarction. *Eur. Heart J.* **2020**, *41*, 3156–3165. [CrossRef]
78. Oliva, A.; Cammisotto, V.; Cangemi, R.; Ferro, D.; Miele, M.C.; De Angelis, M.; Cancelli, F.; Pignatelli, P.; Venditti, M.; Pugliese, F.; et al. Low-Grade Endotoxemia and Thrombosis in COVID-19. *Clin. Transl. Gastroenterol.* **2021**, *12*, e00348. [CrossRef]
79. Wiedermann, C.J.; Kiechl, S.; Dunzendorfer, S.; Schratzberger, P.; Egger, G.; Oberhollenzer, F.; Willeit, J. Association of endotoxemia with carotid atherosclerosis and cardiovascular disease: Prospective results from the Bruneck Study. *J. Am. Coll. Cardiol.* **1999**, *34*, 1975–1981. [CrossRef]
80. Ghanim, H.; Abuaysheh, S.; Sia, C.L.; Korzeniewski, K.; Chaudhuri, A.; Fernandez-Real, J.M.; Dandona, P. Increase in Plasma Endotoxin Concentrations and the Expression of Toll-Like Receptors and Suppressor of Cytokine Signaling-3 in Mononuclear Cells After a High-Fat, High-Carbohydrate Meal: Implications for insulin resistance. *Diabetes Care* **2009**, *32*, 2281–2287. [CrossRef]
81. Boutagy, N.E.; McMillan, R.P.; Frisard, M.I.; Hulver, M.W. Metabolic endotoxemia with obesity: Is it real and is it relevant? *Biochimie* **2016**, *124*, 11–20. [CrossRef]

82. Neves, A.L.; Coelho, J.; Couto, L.; Leite-Moreira, A.; Roncon-Albuquerque, R., Jr. Metabolic endotoxemia: A molecular link between obesity and cardiovascular risk. *J. Mol. Endocrinol.* **2013**, *51*, R51–R64. [CrossRef]
83. Erlanson-Albertsson, C.; Stenkula, K.G. The Importance of Food for Endotoxemia and an Inflammatory Response. *Int. J. Mol. Sci.* **2021**, *22*, 9562. [CrossRef]
84. Deopurkar, R.; Ghanim, H.; Friedman, J.; Abuaysheh, S.; Sia, C.L.; Mohanty, P.; Viswanathan, P.; Chaudhuri, A.; Dandona, P. Differential effects of cream, glucose, and orange juice on inflammation, endotoxin, and the expression of Toll-like receptor-4 and suppressor of cytokine signaling-3. *Diabetes Care* **2010**, *33*, 991–997. [CrossRef]
85. Erridge, C.; Attina, T.; Spickett, C.M.; Webb, D.J. A high-fat meal induces low-grade endotoxemia: Evidence of a novel mechanism of postprandial inflammation. *Am. J. Clin. Nutr.* **2007**, *86*, 1286–1292. [CrossRef]
86. Laugerette, F.; Vors, C.; Geloen, A.; Chauvin, M.A.; Soulage, C.; Lambert-Porcheron, S.; Peretti, N.; Alligier, M.; Burcelin, R.; Laville, M.; et al. Emulsified lipids increase endotoxemia: Possible role in early postprandial low-grade inflammation. *J. Nutr. Biochem.* **2011**, *22*, 53–59. [CrossRef]
87. Ghoshal, S.; Witta, J.; Zhong, J.; de Villiers, W.; Eckhardt, E. Chylomicrons promote intestinal absorption of lipopolysaccharides. *J. Lipid Res.* **2009**, *50*, 90–97. [CrossRef]
88. Tomassen, M.M.M.; Govers, C.; Vos, A.P.; de Wit, N.J.W. Dietary fat induced chylomicron-mediated LPS translocation in a bicameral Caco-2cell model. *Lipids Health Dis.* **2023**, *22*, 4. [CrossRef]
89. Cani, P.D.; Amar, J.; Iglesias, M.A.; Poggi, M.; Knauf, C.; Bastelica, D.; Neyrinck, A.M.; Fava, F.; Tuohy, K.M.; Chabo, C.; et al. Metabolic endotoxemia initiates obesity and insulin resistance. *Diabetes* **2007**, *56*, 1761–1772. [CrossRef]
90. Do, M.H.; Lee, E.; Oh, M.-J.; Kim, Y.; Park, H.-Y. High-Glucose or -Fructose Diet Cause Changes of the Gut Microbiota and Metabolic Disorders in Mice without Body Weight Change. *Nutrients* **2018**, *10*, 761. [CrossRef]
91. Guerville, M.; Leroy, A.; Sinquin, A.; Laugerette, F.; Michalski, M.C.; Boudry, G. Western-diet consumption induces alteration of barrier function mechanisms in the ileum that correlates with metabolic endotoxemia in rats. *Am. J. Physiol. Endocrinol. Metab.* **2017**, *313*, E107–E120. [CrossRef]
92. Zhou, X.; Han, D.; Xu, R.; Li, S.; Wu, H.; Qu, C.; Wang, F.; Wang, X.; Zhao, Y. A model of metabolic syndrome and related diseases with intestinal endotoxemia in rats fed a high fat and high sucrose diet. *PLoS ONE* **2014**, *9*, e115148. [CrossRef]
93. Cani, P.D.; Bibiloni, R.; Knauf, C.; Waget, A.; Neyrinck, A.M.; Delzenne, N.M.; Burcelin, R. Changes in gut microbiota control metabolic endotoxemia-induced inflammation in high-fat diet-induced obesity and diabetes in mice. *Diabetes* **2008**, *57*, 1470–1481. [CrossRef]
94. Cani, P.D.; Neyrinck, A.M.; Fava, F.; Knauf, C.; Burcelin, R.G.; Tuohy, K.M.; Gibson, G.R.; Delzenne, N.M. Selective increases of bifidobacteria in gut microflora improve high-fat-diet-induced diabetes in mice through a mechanism associated with endotoxaemia. *Diabetologia* **2007**, *50*, 2374–2383. [CrossRef]
95. Anhe, F.F.; Barra, N.G.; Cavallari, J.F.; Henriksbo, B.D.; Schertzer, J.D. Metabolic endotoxemia is dictated by the type of lipopolysaccharide. *Cell Rep.* **2021**, *36*, 109691. [CrossRef]
96. Amar, J.; Burcelin, R.; Ruidavets, J.B.; Cani, P.D.; Fauvel, J.; Alessi, M.C.; Chamontin, B.; Ferrieres, J. Energy intake is associated with endotoxemia in apparently healthy men. *Am. J. Clin. Nutr.* **2008**, *87*, 1219–1223. [CrossRef]
97. Ahola, A.J.; Lassenius, M.I.; Forsblom, C.; Harjutsalo, V.; Lehto, M.; Groop, P.H. Dietary patterns reflecting healthy food choices are associated with lower serum LPS activity. *Sci. Rep.* **2017**, *7*, 6511. [CrossRef]
98. Lyte, J.M.; Gabler, N.K.; Hollis, J.H. Postprandial serum endotoxin in healthy humans is modulated by dietary fat in a randomized, controlled, cross-over study. *Lipids Health Dis.* **2016**, *15*, 186. [CrossRef]
99. Pendyala, S.; Walker, J.M.; Holt, P.R. A High-Fat Diet Is Associated With Endotoxemia That Originates From the Gut. *Gastroenterology* **2012**, *142*, 1100–1101.e2. [CrossRef]
100. Mehta, N.N.; McGillicuddy, F.C.; Anderson, P.D.; Hinkle, C.C.; Shah, R.; Pruscino, L.; Tabita-Martinez, J.; Sellers, K.F.; Rickels, M.R.; Reilly, M.P. Experimental endotoxemia induces adipose inflammation and insulin resistance in humans. *Diabetes* **2010**, *59*, 172–181. [CrossRef]
101. Turnbaugh, P.J.; Ridaura, V.K.; Faith, J.J.; Rey, F.E.; Knight, R.; Gordon, J.I. The effect of diet on the human gut microbiome: A metagenomic analysis in humanized gnotobiotic mice. *Sci. Transl. Med.* **2009**, *1*, 6ra14. [CrossRef]
102. Wu, G.D.; Chen, J.; Hoffmann, C.; Bittinger, K.; Chen, Y.Y.; Keilbaugh, S.A.; Bewtra, M.; Knights, D.; Walters, W.A.; Knight, R.; et al. Linking long-term dietary patterns with gut microbial enterotypes. *Science* **2011**, *334*, 105–108. [CrossRef]
103. Le Chatelier, E.; Nielsen, T.; Qin, J.; Prifti, E.; Hildebrand, F.; Falony, G.; Almeida, M.; Arumugam, M.; Batto, J.M.; Kennedy, S.; et al. Richness of human gut microbiome correlates with metabolic markers. *Nature* **2013**, *500*, 541–546. [CrossRef]
104. Cotillard, A.; Kennedy, S.P.; Kong, L.C.; Prifti, E.; Pons, N.; Le Chatelier, E.; Almeida, M.; Quinquis, B.; Levenez, F.; Galleron, N.; et al. Dietary intervention impact on gut microbial gene richness. *Nature* **2013**, *500*, 585–588. [CrossRef]
105. Claesson, M.J.; Jeffery, I.B.; Conde, S.; Power, S.E.; O'Connor, E.M.; Cusack, S.; Harris, H.M.; Coakley, M.; Lakshminarayanan, B.; O'Sullivan, O.; et al. Gut microbiota composition correlates with diet and health in the elderly. *Nature* **2012**, *488*, 178–184. [CrossRef]
106. Jeffery, I.B.; Lynch, D.B.; O'Toole, P.W. Composition and temporal stability of the gut microbiota in older persons. *ISME J.* **2016**, *10*, 170–182. [CrossRef]
107. Langille, M.G.; Meehan, C.J.; Koenig, J.E.; Dhanani, A.S.; Rose, R.A.; Howlett, S.E.; Beiko, R.G. Microbial shifts in the aging mouse gut. *Microbiome* **2014**, *2*, 50. [CrossRef]

108. Xu, C.; Zhu, H.; Qiu, P. Aging progression of human gut microbiota. *BMC Microbiol.* **2019**, *19*, 236. [CrossRef]
109. Ghosh, S.S.; Wang, J.; Yannie, P.J.; Ghosh, S. Intestinal Barrier Dysfunction, LPS Translocation, and Disease Development. *J. Endocr. Soc.* **2020**, *4*, bvz039. [CrossRef]
110. Violi, F.; Cammisotto, V.; Bartimoccia, S.; Pignatelli, P.; Carnevale, R.; Nocella, C. Gut-derived low-grade endotoxaemia, atherothrombosis and cardiovascular disease. *Nat. Rev. Cardiol.* **2023**, *20*, 24–37. [CrossRef]
111. Mayr, F.B.; Spiel, A.O.; Leitner, J.M.; Firbas, C.; Sieghart, W.; Jilma, B. Effects of low dose endotoxemia on endothelial progenitor cells in humans. *Atherosclerosis* **2007**, *195*, e202–e206. [CrossRef]
112. Freedman, N.D.; Park, Y.; Abnet, C.C.; Hollenbeck, A.R.; Sinha, R. Association of coffee drinking with total and cause-specific mortality. *N. Engl. J. Med.* **2012**, *366*, 1891–1904. [CrossRef]
113. Gunter, M.J.; Murphy, N.; Cross, A.J.; Dossus, L.; Dartois, L.; Fagherazzi, G.; Kaaks, R.; Kuhn, T.; Boeing, H.; Aleksandrova, K.; et al. Coffee Drinking and Mortality in 10 European Countries: A Multinational Cohort Study. *Ann. Intern. Med.* **2017**, *167*, 236–247. [CrossRef]
114. Spyridopoulos, I.; Fichtlscherer, S.; Popp, R.; Toennes, S.W.; Fisslthaler, B.; Trepels, T.; Zernecke, A.; Liehn, E.A.; Weber, C.; Zeiher, A.M.; et al. Caffeine enhances endothelial repair by an AMPK-dependent mechanism. *Arter. Thromb. Vasc. Biol.* **2008**, *28*, 1967–1974. [CrossRef]
115. Ale-Agha, N.; Goy, C.; Jakobs, P.; Spyridopoulos, I.; Gonnissen, S.; Dyballa-Rukes, N.; Aufenvenne, K.; von Ameln, F.; Zurek, M.; Spannbrucker, T.; et al. CDKN1B/p27 is localized in mitochondria and improves respiration-dependent processes in the cardiovascular system-New mode of action for caffeine. *PLoS Biol.* **2018**, *16*, e2004408. [CrossRef]
116. Cox, F.F.; Misiou, A.; Vierkant, A.; Ale-Agha, N.; Grandoch, M.; Haendeler, J.; Altschmied, J. Protective Effects of Curcumin in Cardiovascular Diseases-Impact on Oxidative Stress and Mitochondria. *Cells* **2022**, *11*, 342. [CrossRef]
117. Scazzocchio, B.; Minghetti, L.; D'Archivio, M. Interaction between Gut Microbiota and Curcumin: A New Key of Understanding for the Health Effects of Curcumin. *Nutrients* **2020**, *12*, 2499. [CrossRef]
118. Chen, L.; Wang, X.J.; Chen, J.X.; Yang, J.C.; Ling, L.; Cai, X.B.; Chen, Y.S. Caffeine ameliorates the metabolic syndrome in diet-induced obese mice through regulating the gut microbiota and serum metabolism. *Diabetol. Metab. Syndr.* **2023**, *15*, 37. [CrossRef]
119. Olszanecki, R.; Gebska, A.; Korbut, R. The role of haem oxygenase-1 in the decrease of endothelial intercellular adhesion molecule-1 expression by curcumin. *Basic. Clin. Pharmacol. Toxicol.* **2007**, *101*, 411–415. [CrossRef]
120. Nugent, W.H.; Carr, D.A.; Friedman, J.; Song, B.K. Novel transdermal curcumin therapeutic preserves endothelial barrier function in a high-dose LPS rat model. *Artif. Cells Nanomed. Biotechnol.* **2023**, *51*, 33–40. [CrossRef]
121. Karimi, A.; Naeini, F.; Niazkar, H.R.; Tutunchi, H.; Musazadeh, V.; Mahmoodpoor, A.; Asghariazar, V.; Mobasseri, M.; Tarighat-Esfanjani, A. Nano-curcumin supplementation in critically ill patients with sepsis: A randomized clinical trial investigating the inflammatory biomarkers, oxidative stress indices, endothelial function, clinical outcomes and nutritional status. *Food Funct.* **2022**, *13*, 6596–6612. [CrossRef]
122. Wang, J.; Ghosh, S.S.; Ghosh, S. Curcumin improves intestinal barrier function: Modulation of intracellular signaling, and organization of tight junctions. *Am. J. Physiol. Cell Physiol.* **2017**, *312*, C438–C445. [CrossRef]
123. Panahi, Y.; Hosseini, M.S.; Khalili, N.; Naimi, E.; Simental-Mendia, L.E.; Majeed, M.; Sahebkar, A. Effects of curcumin on serum cytokine concentrations in subjects with metabolic syndrome: A post-hoc analysis of a randomized controlled trial. *Biomed. Pharmacother.* **2016**, *82*, 578–582. [CrossRef]
124. Dei Cas, M.; Ghidoni, R. Dietary Curcumin: Correlation between Bioavailability and Health Potential. *Nutrients* **2019**, *11*, 2147. [CrossRef]
125. Lukosz, M.; Jakob, S.; Buchner, N.; Zschauer, T.C.; Altschmied, J.; Haendeler, J. Nuclear redox signaling. *Antioxid. Redox Signal* **2010**, *12*, 713–742. [CrossRef]
126. Brinkmann, V.; Romeo, M.; Larigot, L.; Hemmers, A.; Tschage, L.; Kleinjohann, J.; Schiavi, A.; Steinwachs, S.; Esser, C.; Menzel, R.; et al. Aryl Hydrocarbon Receptor-Dependent and -Independent Pathways Mediate Curcumin Anti-Aging Effects. *Antioxidants* **2022**, *11*, 613. [CrossRef]